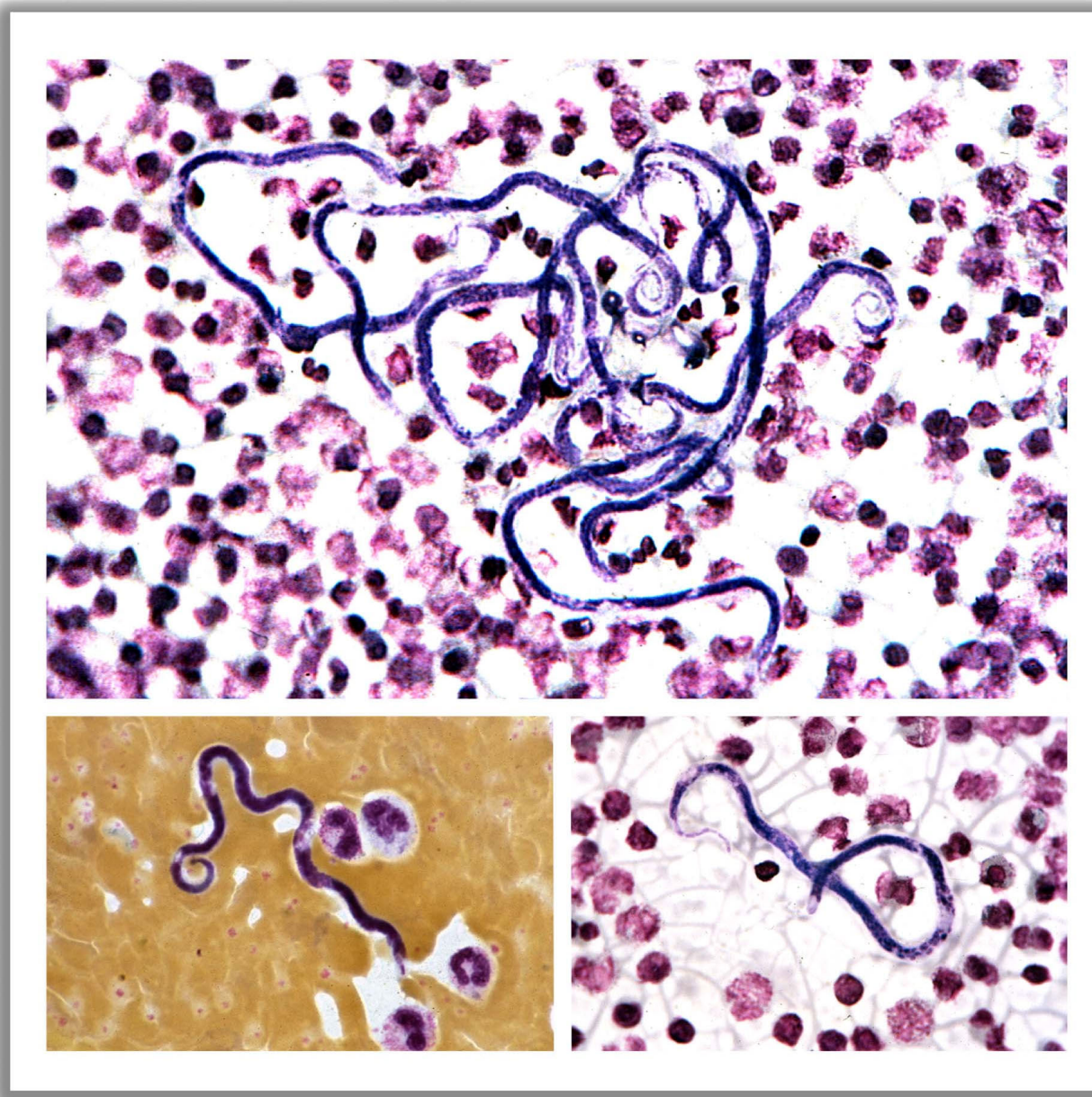




haematologica

Journal of The Ferrata Storti Foundation



ISSN 0390-6078

Volume 106

JUNE

2021 - 6

www.haematologica.org

haematologica

Looking for a definitive source
of information in hematology?

Haematologica is an Open Access
journal: all articles are completely
free of charge

Haematologica

is listed on *PubMed*, *PubMedCentral*,
DOAJ, *Scopus* and many other
online directories

5000 / amount of articles read daily
4300 / amount of PDFs downloaded daily

2.20 / gigabytes transferred daily

WWW.HAEMATOLOGICA.ORG

Editor-in-Chief

Jacob M. Rowe (Haifa)

Deputy Editors

Carlo Balduini (Pavia), Jerry Radich (Seattle)

Managing Director

Antonio Majocchi (Pavia)

Associate Editors

Hélène Cavé (Paris), Monika Engelhardt (Freiburg), Steve Lane (Brisbane), Pier Mannuccio Mannucci (Milan), Pavan Reddy (Ann Arbor), David C. Rees (London), Francesco Rodeghiero (Vicenza), Gilles Salles (New York), Kerry Savage (Vancouver), Aaron Schimmer (Toronto), Richard F. Schlenk (Heidelberg), Sonali Smith (Chicago)

Assistant Editors

Britta Dorst (English Editor), Catherine Klersy (Statistical Consultant), Rachel Stenner (English Editor)

Editorial Board

Walter Ageno (Varese), Sarit Assouline (Montreal), Andrea Bacigalupo (Roma), Taman Bakchoul (Tübingen), Pablo Bartolucci (Créteil), Katherine Borden (Montreal), Marco Cattaneo (Milan), Corey Cutler (Boston), Kate Cwynarski (London), Mary Eapen (Milwaukee), Francesca Gay (Torino), Ajay Gopal (Seattle), Alex Herrera (Duarte), Shai Izraeli (Ramat Gan), Martin Kaiser (London), Marina Konopleva (Houston), Johanna A. Kremer Hovinga (Bern), Nicolaus Kröger (Hamburg), Austin Kulasekararaj (London), Shaji Kumar (Rochester), Ann LaCasce (Boston), Anthony R. Mato (New York), Neha Mehta-Shah (St. Louis), Alison Moskowitz (New York), Yishai Ofran (Haifa), Farhad Ravandi (Houston), John W. Semple (Lund), Liran Shlush (Toronto), Sara Tasian (Philadelphia), Pieter van Vlieberghe (Ghent), Ofir Wolach (Haifa), Loic Ysebaert (Toulouse)

Editorial Office

Simona Giri (Production & Marketing Manager), Lorella Ripari (Peer Review Manager), Paola Cariati (Senior Graphic Designer), Igor Eboli Poletti (Senior Graphic Designer), Marta Fossati (Peer Review), Diana Serena Ravera (Peer Review)

Affiliated Scientific Societies

SIE (Italian Society of Hematology, www.siematologia.it)

SIES (Italian Society of Experimental Hematology, www.siesonline.it)

Information for readers, authors and subscribers

Haematologica (print edition, pISSN 0390-6078, eISSN 1592-8721) publishes peer-reviewed papers on all areas of experimental and clinical hematology. The journal is owned by a non-profit organization, the Ferrata Storti Foundation, and serves the scientific community following the recommendations of the World Association of Medical Editors (www.wame.org) and the International Committee of Medical Journal Editors (www.icmje.org).

Haematologica publishes editorials, research articles, review articles, guideline articles and letters. Manuscripts should be prepared according to our guidelines (www.haematologica.org/information-for-authors), and the Uniform Requirements for Manuscripts Submitted to Biomedical Journals, prepared by the International Committee of Medical Journal Editors (www.icmje.org).

Manuscripts should be submitted online at <http://www.haematologica.org/>.

Conflict of interests. According to the International Committee of Medical Journal Editors (<http://www.icmje.org/#conflicts>), “Public trust in the peer review process and the credibility of published articles depend in part on how well conflict of interest is handled during writing, peer review, and editorial decision making”. The ad hoc journal’s policy is reported in detail online (www.haematologica.org/content/policies).

Transfer of Copyright and Permission to Reproduce Parts of Published Papers. Authors will grant copyright of their articles to the Ferrata Storti Foundation. No formal permission will be required to reproduce parts (tables or illustrations) of published papers, provided the source is quoted appropriately and reproduction has no commercial intent. Reproductions with commercial intent will require written permission and payment of royalties.

Detailed information about subscriptions is available online at www.haematologica.org. Haematologica is an open access journal. Access to the online journal is free. Use of the Haematologica App (available on the App Store and on Google Play) is free.

For subscriptions to the printed issue of the journal, please contact: Haematologica Office, via Giuseppe Belli 4, 27100 Pavia, Italy (phone +39.0382.27129, fax +39.0382.394705, E-mail: info@haematologica.org).

Rates of the International edition for the year 2021 are as following:

	<i>Institutional</i>	<i>Personal</i>
<i>Print edition</i>	Euro 700	Euro 170

Advertisements. Contact the Advertising Manager, Haematologica Office, via Giuseppe Belli 4, 27100 Pavia, Italy (phone +39.0382.27129, fax +39.0382.394705, e-mail: marketing@haematologica.org).

Disclaimer. Whilst every effort is made by the publishers and the editorial board to see that no inaccurate or misleading data, opinion or statement appears in this journal, they wish to make it clear that the data and opinions appearing in the articles or advertisements herein are the responsibility of the contributor or advisor concerned. Accordingly, the publisher, the editorial board and their respective employees, officers and agents accept no liability whatsoever for the consequences of any inaccurate or misleading data, opinion or statement. Whilst all due care is taken to ensure that drug doses and other quantities are presented accurately, readers are advised that new methods and techniques involving drug usage, and described within this journal, should only be followed in conjunction with the drug manufacturer’s own published literature.

Direttore responsabile: Prof. Carlo Balduini; Autorizzazione del Tribunale di Pavia n. 63 del 5 marzo 1955.
Printing: Press Up, zona Via Cassia Km 36, 300 Zona Ind.le Settevene - 01036 Nepi (VT)



Associated with USPI, Unione Stampa Periodica Italiana.

Premiato per l'alto valore culturale dal Ministero dei Beni Culturali ed Ambientali

Table of Contents

Volume 106, Issue 6: June 2021

About the Cover

1511 Images from the Haematologica Atlas of Hematologic Cytology: filariasis
Antonello Malfitano and Rosangela Invernizzi
<https://doi.org/10.3324/haematol.2021.278713>

Editorials

1512 The doctor prescribed a fat-free diet for stem cell mobilization
Orit Kollet
<https://doi.org/10.3324/haematol.2020.278239>

1514 Philadelphia chromosome-like acute lymphoblastic leukemia. Still a pending matter
Josep-Maria Ribera et al.
<https://doi.org/10.3324/haematol.2020.270645>

1516 Granulocyte colony-stimulating factor acts on lymphoid-biased, short-term hematopoietic stem cells
Yulin Chen and K. Lenhard Rudolph
<https://doi.org/10.3324/haematol.2020.271205>

Review Articles

1519 The Hsp70 chaperone system: distinct roles in erythrocyte formation and maintenance
Yasith Mathangasinghe et al.
<https://doi.org/10.3324/haematol.2019.233056>

1535 Chronic organ injuries in children with sickle cell disease
Slimane Allali et al.
<https://doi.org/10.3324/haematol.2020.271353>

Articles

Acute Lymphoblastic Leukemia

1545 Oncorequisite role of an aldehyde dehydrogenase in the pathogenesis of T-cell acute lymphoblastic leukemia
Chujing Zhang et al.
<https://doi.org/10.3324/haematol.2019.245639>

1559 Philadelphia-like acute lymphoblastic leukemia is associated with minimal residual disease persistence and poor outcome. First report of the minimal residual disease-oriented GIMEMA LAL1913
Sabina Chiaretti et al.
<https://doi.org/10.3324/haematol.2020.247973>

Acute Myeloid Leukemia

1569 RUNX1-EVI1 disrupts lineage determination and the cell cycle by interfering with RUNX1 and EVI1 driven gene regulatory networks
Sophie G. Kellaway et al.
<https://doi.org/10.3324/haematol.2019.241885>

Bone Marrow Failure

1581 A frequent nonsense mutation in exon 1 across certain HLA-A and HLA-B alleles in leukocytes of patients with acquired aplastic anemia
Hiroki Mizumaki et al.
<https://doi.org/10.3324/haematol.2020.247809>

Bone Marrow Transplantation

1591 Post-transplant cyclophosphamide *versus* anti-thymocyte globulin for graft-*versus*-host disease prevention in haploidentical transplantation for adult acute lymphoblastic leukemia
Arnon Nagler et al.
<https://doi.org/10.3324/haematol.2020.247296>

1599 Allogeneic hematopoietic cell transplantation with non-myeloablative conditioning for patients with hematologic malignancies: improved outcomes over two decades
Jason P. Cooper et al.
<https://doi.org/10.3324/haematol.2020.248187>

Chronic Lymphocytic Leukemia

1608 Prognostic significance of translocations in the presence of mutated IGHV and of cytogenetic complexity at diagnosis of chronic lymphocytic leukemia
Nyla A. Heerema et al.
<https://doi.org/10.3324/haematol.2018.212571>

Coagulation & its Disorders

1616 Fibrinogen interaction with complement C3: a potential therapeutic target to reduce thrombosis risk
Rhodri J. King et al.
<https://doi.org/10.3324/haematol.2019.239558>

1624 Deciphering the Ets-1/2-mediated transcriptional regulation of *F8* gene identifies a minimal *F8* promoter for hemophilia A gene therapy
Rosella Fama et al.
<https://doi.org/10.3324/haematol.2019.239202>

1636 miR-146a is a pivotal regulator of neutrophil extracellular trap formation promoting thrombosis
Ana B. Arroyo et al.
<https://doi.org/10.3324/haematol.2019.240226>

Hematopoiesis

1647 Granulocyte colony-stimulating factor directly acts on mouse lymphoid-biased but not myeloid-biased hematopoietic stem cells
Miner Xie et al.
<https://doi.org/10.3324/haematol.2019.239251>

1659 Natural estrogens enhance the engraftment of human hematopoietic stem and progenitor cells in immunodeficient mice
Sara Fañanas-Baquero et al.
<https://doi.org/10.3324/haematol.2019.233924>

1671 Mobilization efficiency is critically regulated by fat via marrow PPARs
Tomohide Suzuki et al.
<https://doi.org/10.3324/haematol.2020.265751>

Hodgkin Lymphoma

1684 Whole-slide image analysis of the tumor microenvironment identifies low B-cell content as a predictor of adverse outcome in patients with advanced-stage classical Hodgkin lymphoma treated with BEACOPP
Ron Daniel Jachimowicz et al.
<https://doi.org/10.3324/haematol.2019.243287>

Non-Hodgkin Lymphoma

1693 Whole exome sequencing reveals *NOTCH1* mutations in anaplastic large cell lymphoma and points to Notch both as a key pathway and a potential therapeutic target
Hugo Larose et al.
<https://doi.org/10.3324/haematol.2019.238766>

1705 Brentuximab vedotin in combination with rituximab, cyclophosphamide, doxorubicin, and prednisone as frontline treatment for patients with CD30-positive B-cell lymphomas
Jakub Svoboda et al.
<https://doi.org/10.3324/haematol.2019.238675>

1714 Molecular profiling reveals a hypoxia signature in breast implant-associated anaplastic large cell lymphoma
Naoki Oishi et al.
<https://doi.org/10.3324/haematol.2019.245860>

Plasma Cell Disorders

1725 Subcutaneous daratumumab in patients with relapsed or refractory multiple myeloma: part 2 of the open-label, multicenter, dose-escalation phase Ib study (PAVO)
Jesus San-Miguel et al.
<https://doi.org/10.3324/haematol.2019.243790>

Letters to the Editor

1733 The survival impact of maintenance lenalidomide: an analysis of real-world data from the Canadian Myeloma Research Group national database
Hannah M. Cherniawsky et al.
<https://doi.org/10.3324/haematol.2020.259093>

1737 No association between *ECSIT* germline mutations and hemophagocytic lymphohistiocytosis in natural killer/T-cell lymphoma
Shin Yeu Ong et al.
<https://doi.org/10.3324/haematol.2020.269209>

1740 Pituitary iron and factors predictive of fertility status in transfusion-dependent thalassemia
Sylvia T. Singer et al.
<https://doi.org/10.3324/haematol.2020.252726>

1745 Antimicrobial resistance is a risk factor for mortality in adults with sickle cell disease
Andrew Srisuwananukorn et al.
<https://doi.org/10.3324/haematol.2020.267872>

1749 Rapid decline in estimated glomerular filtration rate in sickle cell anemia: results of a multicenter pooled analysis
Kenneth I. Ataga et al.
<https://doi.org/10.3324/haematol.2020.267419>

1754 Serum monoclonal component in chronic lymphocytic leukemia: baseline correlations and prognostic impact
Pablo Mozas et al.
<https://doi.org/10.3324/haematol.2020.263228>

1758 Homozygous Southeast Asian ovalocytosis in five live-born neonates
Amanda A. Lavinya et al.
<https://doi.org/10.3324/haematol.2020.268581>

1762 Structural aberrations are associated with poor survival in patients with clonal cytopenia of undetermined significance
Stine U. Mikkelsen et al.
<https://doi.org/10.3324/haematol.2020.263319>

1767 Minimal residual disease monitoring in acute myeloid leukemia with non-A/B/D *NPM1* mutations by digital polymerase chain reaction: feasibility and clinical use
Auriane Lesieur et al.
<https://doi.org/10.3324/haematol.2020.260133>

1770 Genome wide association study of silent cerebral infarction in sickle cell disease (HbSS and HbSC)
John N. Brewin et al.
<https://doi.org/10.3324/haematol.2020.265827>

1774 MK2 is a therapeutic target for high-risk multiple myeloma
Chunyan Gu et al.
<https://doi.org/10.3324/haematol.2017.182121>

Comment

1778 Breast dose matters
Renee M. Moadel et al.
<https://doi.org/10.3324/haematol.2019.219584>

The origin of a name that reflects Europe's cultural roots.

Ancient Greek

αἷμα [haima] = blood
αἷματος [haimatos] = of blood
λόγος [logos] = reasoning

Scientific Latin

haematologicus (adjective) = related to blood

Scientific Latin

haematologica (adjective, plural and neuter, used as a noun) = hematological subjects

Modern English

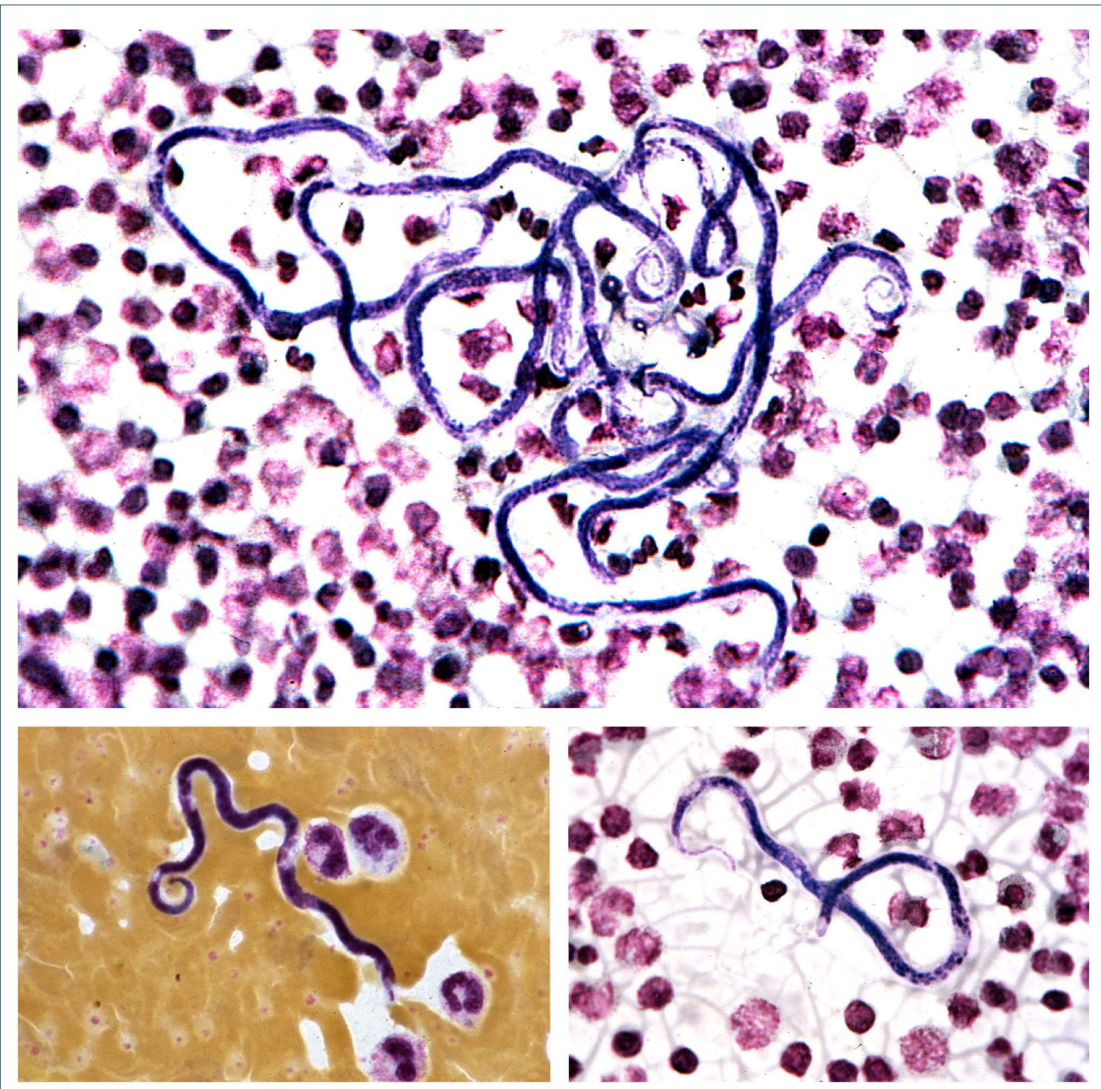
The oldest hematology journal,
publishing the newest research results.
2019 JCR impact factor = 7.116

Images from the Haematologica Atlas of Hematologic Cytology: filariasis

Antonello Malfitano¹ and Rosangela Invernizzi²¹IRCCS Policlinico San Matteo Foundation and ²University of Pavia, Pavia, Italy

E-mail: ROSANGELA INVERNIZZI - rosangela.invernizzi@unipv.it

doi:10.3324/haematol.2021.278713



Microfilariae, i.e. the larval stage of *Filaria* spp., may be found in the peripheral blood after white blood cell concentration by centrifugation and, occasionally, also in bone marrow preparations and other fine-needle aspirates. Morphological findings differ according to the species and form the basis for diagnosis. In buffy coat smears, *Loa loa* microfilariae appear as primitive serpentine-shaped organisms containing many nuclei with a head space, a sheath unstained with Giemsa and the tapering of the tail (top image). In the lower left image, a thick film shows the size of a *Loa loa* microfilaria in relation to white blood cells and the coiled tail; note also the row of nuclei through the whole body of the parasite right to the end of the tail (bottom right image).¹ Eosinophilia is often an associated feature.

Reference

1. Malfitano A, Invernizzi R. Parasitic and fungal diseases. Haematologica. 2020; 105(Suppl. 1):29-39.

The doctor prescribed a fat-free diet for stem cell mobilization

Orit Kollet,¹ Eman Khatib-Massalha^{1,2} and Tsvee Lapidot¹¹Department of Immunology, Weizmann Institute of Science, Rehovot, Israel and ²University of Cambridge, Department of Haematology, Cambridge, UK.

E-mail: TSVEE LAPIDOT - tsvee.lapidot@weizmann.ac.il

doi:10.3324/haematol.2020.278239

Mobilized hematopoietic stem and progenitor cells (HSPC) are widely utilized for clinical stem cell transplantation. HSPC mobilization by the cytokine granulocyte colony-stimulating factor (G-CSF) had been used clinically for several decades. Nevertheless, the underlying mechanisms and the factors leading to large variations in mobilization yields in healthy donors are poorly understood. In this issue of *Haematologica*, Suzuki and colleagues¹ shed light on the effect of dietary fat content on G-CSF-stimulated mobilization, deciphering the regulatory role of $\omega 3$ -polyunsaturated fatty acids (PUFA) processed by bone marrow (BM) neutrophils (and to a lesser extent by other cell types) as part of the mobilization process in mice. The authors show that G-CSF-mediated activation of peroxisome proliferator-activated receptor (PPAR) δ signaling first requires cues from the sympathetic nervous system via $\beta 1/2$ -adrenergic receptors in BM neutrophils, which in turn increases PPAR δ expression and activity. However, PPAR δ is a negative regulator of HSPC mobilization. A shrewd approach to bypass this negative regulation was to feed mice for a brief period with a fat-free diet. As a result of the low $\omega 3$ -PUFA content in this diet, the lack of $\omega 3$ -PUFA/PPAR δ activation decreased transcription of the negative regulator angiopoietin-like protein 4 (Angptl4), which in turn increased BM vascular permeability and facilitated enhanced HSPC mobilization. This simple, albeit novel approach could be easily assessed in order to address the problem of poor clinical HSPC mobilization in some healthy donors. However, BM neutrophils are not the only players in the complex multifaceted process of HSPC mobilization. Hence, the intriguing study by Suzuki *et al.*, in addition to its novelty regarding the machinery activated in BM neutrophils

during HSPC mobilization, opens new research directions regarding HSPC cell-intrinsic signaling.

Signals driving HSPC retention in the BM *versus* their egress to the blood are tightly balanced during steady-state homeostasis in order to facilitate blood and immune-cell production on demand along with preservation of the undifferentiated HSPC BM reservoir. Thus, physiological HSPC egress to the blood is dynamically modulated by homeostatic light/dark cycles and circadian rhythms involving $\beta 1/2$ -adrenergic receptor signaling² as well as BM blood vessel permeability and hormone/cytokine secretion.³ These signals in mice balance the daily rhythms of BM HSPC differentiation³ and egress during daylight to replenish the blood.² Melatonin secretion at night reduces BM vessel-permeability and egress, exerting anti-inflammatory effects, which reprogram stem cell self-renewal.³ Pro-inflammatory signals enforced by bacteria-mimicking lipopolysaccharide challenge and by G-CSF treatment in mice modulate this balance, skewing it towards differentiation and mobilization, to address the urgent need for immune-competent cells. The negative-regulatory function of Angptl4 seems to be part of the balance machinery addressing the need to preserve BM HSPC from exhaustion and hematopoietic failure. G-CSF is known to evoke pro-inflammatory stimuli in the BM, involving signals from the nervous system, which exert dramatic changes in myeloid cells, osteolineage cells,⁴ bone metabolism,⁵ and blood vessel permeability.⁶ HSPC also respond to G-CSF-induced signals, showing robust metabolic changes,^{7,8} which prepare them for the dynamic state, essential for making the active journey to the blood.

An interesting question is whether HSPC "sense" changes in BM lipid mediators during daily light/dark cycles and following

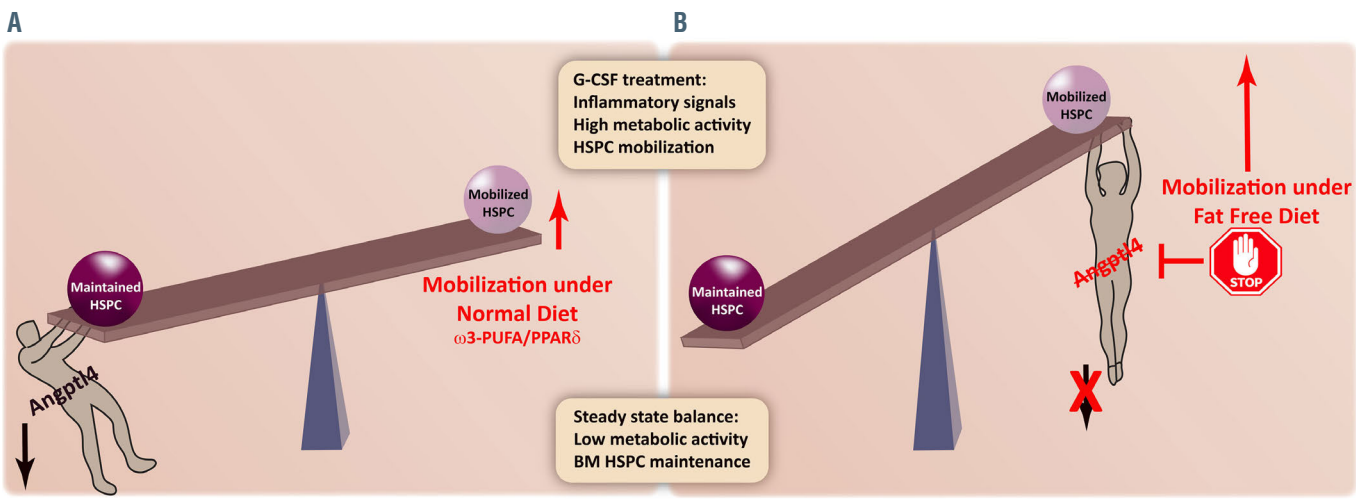


Figure 1. Fatty acid content of the diet affects granulocyte colony-stimulating factor-induced mobilization of hematopoietic stem and progenitor cells. In addition to signaling in bone marrow neutrophils, as reported by Suzuki *et al.*,¹ the fatty acid content of the diet may also affect granulocyte colony-stimulating factor (G-CSF)-induced mobilization via cell-intrinsic signaling in hematopoietic stem and progenitor cells (HSPC). (A) G-CSF-induced mobilization under normal diet provides fatty acids including the key $\omega 3$ -PUFA that activates PPAR δ /Angptl4 signaling in order to balance and maintain bone marrow HSPC despite the pro-inflammatory cues. (B) G-CSF-induced mobilization under a fat-free diet deprived of the key $\omega 3$ -PUFA, prevents the activation of PPAR δ /Angptl4 inhibitory signaling that yields higher rates of HSPC mobilization.

G-CSF stimuli. Furthermore, what signaling do these mediators induce in HSPC and particularly, do they involve changes in reactive oxygen species levels, as well as in Angptl4 expression and activity? Some hints come from several reports. HSPC bear the lipolytic machinery (phospholipase C- β 2) to control pharmacological (G-CSF and AMD3100) HSPC mobilization.⁹ Angiopoietin-like proteins 1-7 play multiple roles in the regulation of hematopoietic stem cell activity including quiescence, expansion, self-renewal, and homing.¹⁰ A major candidate for such future studies could be Angptl4. In humans, ANGPTL4 maintains the *in vivo* repopulating capacity of CD34⁺ cord blood HSPC.¹¹ In mice, the PML-PPAR δ -FAO pathway influences reactive oxygen species generation and stem cell division. Depletion of PPAR δ , which serves as a fatty acid nutrient sensor, reduced stem cell quiescence, and their repopulating potential since it controls asymmetric divisions that are essential for HSC maintenance.¹² Interestingly, Angptl4 is upregulated in the BM under inflammatory conditions induced by bacterial lipopolysaccharide challenges, leading to increased secretion of G-CSF and Angptl4 from BM stromal cells, which also expand BM myeloid progenitors.¹³ Thus, Angptl4 in HSPC balances the cells' response to pro-inflammatory effects in order to preserve their BM maintenance and long-term function. Suzuki *et al.* suggest that temporal attenuation of Angptl4 upregulation may further increase the efficiency of G-CSF-induced mobilization (Figure 1).

Another physiological life condition is aging, which is associated with stress and pro-inflammatory cues, an increase in marrow vascular permeability, adipocytes, and a decrease in hematopoietic cellularity. Adipocytes accumulate in the BM during obesity and aging, and notably also following a high-fat diet in mice. This change in the ratio of adipocytes/hematopoietic cells reprograms mesenchymal stem cells towards adipogenic rather than osteogenic differentiation, which reduces the rates of bone regeneration and hematopoiesis recovery.¹⁴ In addition to pro-inflammatory signals, in humans G-CSF also induces a pro-coagulant state and increased thrombin activity.¹⁵ The efficiency of G-CSF-induced mobilization in healthy donors for clinical HSPC transplantation can be predicted by the surface expression levels of the major coagulation- and inflammation-related thrombin receptor, protease activated receptor 1 (PAR1) on mature peripheral blood leukocytes and CD34⁺ HSPC before mobilization is conducted.¹⁶ Importantly, this surface PAR1 expression also predicts HSPC repopulating potential in transplanted patients and PAR1 signaling in mice is essential for steady-state egress and for directional *in vitro* migration of HSPC to a gradient of the major stem cell chemokine CXCL12.^{16,17} It would be of great interest in future studies to elucidate a potential cross-talk between these two axes, the coagulation and inflammation-related thrombin/PAR1/nitric oxide axis and ω 3-PUFA/PPAR δ /Angptl4 signaling, with the purpose of improving G-CSF-induced mobilization.

The manuscript by Suzuki *et al.* provides important insights into the signaling pathways activated in BM neu-

trophils by G-CSF stimuli, and the cross-talk with the lipid content in the BM as a major driving force for the intensity of HSPC mobilization from the BM into the blood.

Disclosures

No conflicts of interest to disclose.

Contributions

OK, EKM and TL wrote the commentary together.

References

1. Suzuki T. Mobilization efficiency is critically regulated by fat via marrow PPAR δ . *Haematologica*. 2021;106(6):1671-1683.
2. Mendez-Ferrer S, Lucas D, Battista M, Frenette PS. Haematopoietic stem cell release is regulated by circadian oscillations. *Nature*. 2008;452(7186):442-447.
3. Golan K, Kumari A, Kollet O, et al. Daily onset of light and darkness differentially controls hematopoietic stem cell differentiation and maintenance. *Cell Stem Cell*. 2018;23(4):572-585.e7.
4. Katayama Y, Battista M, Kao WM, et al. Signals from the sympathetic nervous system regulate hematopoietic stem cell egress from bone marrow. *Cell*. 2006;124(2):407-421.
5. Wakahashi K, Katayama Y. Bone: a key aspect to understand phenomena in clinical hematatology. *J Bone Miner Metab*. 2020;38(2):145-150.
6. Khatib-Massalha E, Bhattacharya S, Massalha H, et al. Lactate released by inflammatory bone marrow neutrophils induces their mobilization via endothelial GPR81 signaling. *Nat Commun*. 2020;11(1):3547.
7. Ludin A, Gur-Cohen S, Golan K, et al. Reactive oxygen species regulate hematopoietic stem cell self-renewal, migration and development, as well as their bone marrow microenvironment. *Antioxid Redox Signal*. 2014;21(11):1605-1619.
8. Lenkiewicz AM, Adamiak M, Thapa A, et al. The Nlrp3 inflammasome orchestrates mobilization of bone marrow-residing stem cells into peripheral blood. *Stem Cell Rev Rep*. 2019;15(3):391-403.
9. Adamiak M, Poniewierska-Baran A, Borkowska S, et al. Evidence that a lipolytic enzyme--hematopoietic-specific phospholipase C- β 2--promotes mobilization of hematopoietic stem cells by decreasing their lipid raft-mediated bone marrow retention and increasing the promobilizing effects of granulocytes. *Leukemia*. 2016;30(4):919-928.
10. Kadomatsu T, Oike Y. Roles of angiopoietin-like proteins in regulation of stem cell activity. *J Biochem*. 2019;165(4):309-315.
11. Blank U, Ehrnstrom B, Heinz N, et al. Angptl4 maintains *in vivo* repopulation capacity of CD34⁺ human cord blood cells. *Eur J Haematol*. 2012;89(3):198-205.
12. Ito K, Carracedo A, Weiss D, et al. A PML-PPAR δ pathway for fatty acid oxidation regulates hematopoietic stem cell maintenance. *Nat Med*. 2012;18(9):1350-1358.
13. Schumacher A, Denecke B, Braunschweig T, et al. Angptl4 is upregulated under inflammatory conditions in the bone marrow of mice, expands myeloid progenitors, and accelerates reconstitution of platelets after myelosuppressive therapy. *J Hematol Oncol*. 2015;8:64.
14. Ambrosi TH, Scialdone A, Graja A, et al. Adipocyte accumulation in the bone marrow during obesity and aging impairs stem cell-based hematopoietic and bone regeneration. *Cell Stem Cell*. 2017;20(6):771-784.e6.
15. LeBlanc R, Roy J, Demers C, Vu L, Cantin G. A prospective study of G-CSF effects on hemostasis in allogeneic blood stem cell donors. *Bone Marrow Transplant*. 1999;23(10):991-996.
16. Nevo N, Zuckerman T, Gur-Cohen S, et al. PAR1 expression predicts clinical G-CSF CD34(+) HSPC mobilization and repopulation potential in transplanted patients. *Hemisphere*. 2019;3(5):e288.
17. Gur-Cohen S, Itkin T, Chakrabarty S, et al. PAR1 signaling regulates the retention and recruitment of EPCR-expressing bone marrow hematopoietic stem cells. *Nat Med*. 2015;21(11):1307-1317.

Philadelphia chromosome-like acute lymphoblastic leukemia. Still a pending matter

Josep-Maria Ribera

Clinical Hematology Department, ICO-Hospital Germans Trias i Pujol, Josep Carreras Research Institute, Badalona and Universitat Autònoma de Barcelona, Spain

E-mail: JOSEP-MARIA RIBERA - jribera@iconcologia.net

doi:10.3324/haematol.2020.270645

New genetic abnormalities affecting risk assessment and patient stratification have been reported in B-cell precursor (BCP) acute lymphoblastic leukemia (ALL) defining novel subtypes. Some of these subtypes have been included in the most recent World Health Organization classification.¹ Almost 10 years ago, two independent studies identified a subset of pediatric ALL characterized by a specific gene expression profile similar to that of Philadelphia (Ph) chromosome-positive ALL.^{2,3} This novel ALL subtype, called Ph-like ALL or *BCR-ABL1*-like ALL, is a frequent ALL subtype that comprises up to 15% of pediatric BCP-ALL. Its incidence reaches 25% in adolescents and young adults and 20% in adults and it is generally recognized as being associated with a poor prognosis at any age.⁴

Ph-like ALL is characterized by multiple genetic aberrations that converge on tyrosine kinase and cytokine receptor signaling pathways.⁵ According to the signaling pathway involved several subgroups have been defined. These include *CRLF2* rearrangements or mutations, fusions involving *ABL*-class genes, *Ras* signaling pathways and other less common fusions. Alterations in the *CRLF2* gene are the most frequent and result in overexpression of this gene and an increase of *CRLF2* protein expression. Aberrant *CRLF2* expression frequently co-occurs with *JAK* activating mutations or other mutations deregulating *JAK/STAT* signaling (e.g., *IL7R* mutations). Deregulation of *JAK/STAT* signaling may also be due to *JAK2* or *EPOR* rearrangements or additional alterations

activating other *JAK/STAT* signaling genes. In turn, the subgroup of *ABL*-class fusions involving *ABL1*, *ABL2*, *CSF1R* and *PDGFRB* accounts for 15-20% of Ph-like ALL cases.

Since kinase-activating alterations are frequent in Ph-like ALL and most converge on clinically actionable signaling, there is great interest in the early identification of Ph-like patients, with the aim of improving the prognosis with the use of tyrosine kinase inhibitors (TKI). However, identification of Ph-like ALL is currently challenging, and appropriate assays are not yet available for use as routine diagnostic approaches.⁶

In this issue of *Haematologica*, Chiaretti *et al.* screened 88 BCP-ALL cases negative for the major fusion genes (*BCR-ABL1*, *ETV6-RUNX1*, *TCF3-PBX1* and *KMT2A*) enrolled in the pediatric-inspired, measurable residual disease (MRD)-driven GIMEMA LAL1913 front-line protocol for adults with Ph-negative ALL in order to assess response to the treatment and prognosis.⁷ Twenty-eight of these 88 cases (31.8%) showed the Ph-like phenotype. Screening for Ph-like ALL was performed successfully using the "BCR/ABL1-like predictor" developed by the GIMEMA Group.⁸ This model is based on the identification of nine genes specifically overexpressed by adult Ph-like ALL cases and uses their expression values together with *CRLF2* transcript quantification by real time quantitative polymerase chain reaction to build this predictive tool. This study showed that Ph-like patients had a lower complete response rate, event-free survival and disease-

Table 1. Clinical trials either specific for Philadelphia chromosome-like acute lymphoblastic leukemia (Ph-like ALL patients) or including patients with Ph-like ALL*.

NCT number	Group	Schedule	Phase	N patients planned or enrolled	Age (yrs)	Status
02883049	COG	Dasatinib Ruxolitinib	3	5,956	1-30	Active, not recruiting
02723994	COG	Ruxolitinib	2	170	1-21	Recruiting
03117751	SJCRH	Dasatinib Ruxolitinib	2/3	1,000	1-18	Recruiting
02420717	MDACC	Dasatinib Ruxolitinib	2	92	≥10	Active, not recruiting
03571321	University of Chicago	Ruxolitinib	1	15	18-39	Recruiting
03643276	AIEOP/BFM	Bortezomib Blinatumomab	3	5,000	≤17	Recruiting
02716233	Assistance Publique - Hôpitaux de Paris	Imatinib	3	1,578	1-18	Recruiting
03007147	COG EsPhALL	Imatinib	3	700	2-21	Recruiting
03564470	Nanfang Hospital Guangzhou	Chidamide Dasatinib	2	120	14-55	Unknown

*Clinicaltrials.gov accessed on November 28, 2020. COG: Children's Oncology Group; SJCRH: Saint Jude Childrens Research Hospital; MDACC: MD Anderson Cancer Center; AIEOP: Associazione Italiana di Ematologia e Oncologia Pediatrica; BFM: Berlin-Frankfurt-Münster; EsPhALL: European PhALL Consortium; yrs: years.

free survival, as well as greater MRD persistence when treated with a pediatric-oriented and MRD-driven adult ALL protocol, thus reinforcing the contention that early recognition of Ph-like ALL is crucial to refine risk-stratification and optimize therapeutic strategies. While some conflicting results on the prognosis of Ph-like ALL have been reported in pediatric patients, the results of this study are concordant with those of other studies performed in adults, uniformly showing a poor prognosis for this ALL subtype.^{4,9,10} An important finding of this study is the correlation between the Ph-like phenotype and the poor MRD clearance at all the time points analyzed, but especially at week 10 of the protocol, a time point used for the decision to proceed or not to hematopoietic stem cell transplantation (HSCT) in this trial. In fact, the Ph-like profile proved to be the only risk factor for MRD positivity at this time point. This finding is relevant since half of the patients were considered *a priori* as standard risk according to their features at baseline. In addition, Ph-like ALL patients from this trial showed inferior cytologic complete response after induction therapy (a feature not shown in all studies)¹¹ indicating that better induction therapies are needed for these patients. This study also suggests that HSCT is beneficial in these cases and should be pursued at the earliest opportunity in order to increase event-free survival.

It seems clear that apart from early recognition, the management of Ph-like ALL patients should be optimized, and many efforts are currently addressed to improve the results of therapy. These efforts are mainly focused on the incorporation of targeted therapies and immunotherapy to the chemotherapy schedules. TKI inhibitors (e.g., imatinib, dasatinib and ruxolitinib), histone deacetylase inhibitors (e.g., chidamide) and bispecific monoclonal antibodies (e.g., blinatumomab) are the compounds most frequently evaluated in clinical trials (Table 1). However, there is scarce information available on the results of these approaches. As an example, a recent retrospective report by Tanasi *et al.* showed that the introduction of TKI frontline during consolidation improved MRD-negative status and was associated with a 3-year OS of 77% in a small series of 24 adult patients.¹²

Clinical trials are limited in Ph-like ALL. Regarding pediatric trials, in the ongoing trials of the Children's Oncology Group (COG) (clinicaltrials.gov. Identifier: NCT028830499 and in the Total Therapy XVII trial of the Saint Jude Children's Research Hospital [SJCRH] clinicaltrials.gov. Identifier: NCT03117751),¹³ patients with National Cancer Institute (NCI) high-risk characteristics or poor early MRD response, who are positive for *ABL* class fusions and *JAK* pathway mutations, receive dasatinib and ruxolitinib, respectively, together with conventional frontline chemotherapy from consolidation until the end of maintenance therapy. The COG ALL1521 trial (clinicaltrials.gov. Identifier: NCT02723994) is investigating the benefit of adding ruxolitinib to backbone COG based NCI high-risk chemotherapy for patients with CRLF2-rearranged ALL. In the study by the European ALLTogether consortium, patients with *ABL*-class fusions at diagnosis receive TKI on top of chemotherapy from day 15 of induction; HSCT is indicated in cases with poor MRD response. In the French

CALL-F01 protocol (clinicaltrials.gov. Identifier: NCT02716233), RNA sequencing is performed in all B-other ALL in case of induction failure or MRD positivity. Imatinib is given in combination with chemotherapy in the high-risk group, and HSCT is indicated in poor responders. The early introduction of TKI in addition to chemotherapy in *ABL*-class positive BCP-ALL is planned to be evaluated within an intercontinental collaborative trial (clinicaltrials.gov. Identifier: NCT03007147) involving the COG and EsPhALL (European PhALL Consortium) groups.

Clinical trials for AYA and adult patients are even more limited. Phase I/II trials conducted at the MD Anderson Cancer Center are testing dasatinib or low doses of ruxolitinib in combination with hyper-CVAD (cyclophosphamide, vincristine, doxorubicin, and dexamethasone) in relapsed/refractory ALL and *ABL*-class fusions or *CRLF2/JAK* mutations, respectively. Interim data analysis has demonstrated the safety of these combinations with limited efficacy.⁹ A recent phase I trial at the University of Chicago and other institutions is studying ruxolitinib in combination with the pediatric-inspired CALBG (Cancer and Acute Leukemia Group B) 10408 chemotherapy regimen in adolescents with newly diagnosed Ph-like ALL harboring *CRLF2/JAK* alterations, with a planned phase II expansion study if safety is demonstrated.

Regarding the election of TKI, there is no clear evidence of the superiority of dasatinib over imatinib for Ph-like ALL cases with *ABL*-class fusions. This comparison is especially difficult given that the doses of these TKI differ among trials. Other TKI, such as nilotinib, bosutinib and ponatinib, are still being investigated as phase I and II trials in pediatric cancers. Since the combination of TKI and immunotherapy with blinatumomab has proven feasible and effective in patients with Ph-positive ALL,¹⁴ this approach should be explored in patients with Ph-like ALL together with reduced-intensity chemotherapy and HSCT.^{15,16}

There are challenges in the diagnosis of Ph-like ALL before using targeted therapy in frontline treatment. Diagnostic technologies such as RNA sequencing and similar strategies should be implemented in a timely fashion for all "B-other ALL", but to date appropriate assays are not yet available as widely recognized diagnostic approaches.¹⁷⁻¹⁹ Furthermore, although *ABL*-class and *JAK*-pathway alterations account for most Ph-like ALL cases, there are also several alterations involving kinases that are not inhibited by either TKI or *JAK* inhibitors. For this subgroup of Ph-like cases without known targetable lesions innovative therapies such as immunotherapy could be useful to reduce the MRD level before MRD-guided HSCT.²⁰ Nonetheless, all these efforts will undoubtedly require collaborative international approaches to conduct successful studies.

Disclosures

No conflicts of interest to disclose.

Funding

J-MR is supported in part by grant 2017 SGR288 (GRC) Generalitat de Catalunya and an unrestricted grant from "La Caixa" Foundation.

References

- Arber DA, Orazi A, Hasserjian R, et al. The 2016 revision to the World Health Organization classification of myeloid neoplasms and acute leukemia. *Blood*. 2016;127(20):2391-405.
- Den Boer ML, van Slegtenhorst M, De Menezes RX, et al. A subtype of childhood acute lymphoblastic leukaemia with poor treatment outcome: a genome-wide classification study. *Lancet Oncol*. 2009;10(2):125-34.
- Mullighan CG, Su X, Zhang J, et al. Deletion of IKZF1 and prognosis in acute lymphoblastic leukemia. *N Engl J Med*. 2009;360(5):470-80.
- Roberts KG, Gu Z, Payne-Turner D, et al. High frequency and poor outcome of Philadelphia chromosome-like acute lymphoblastic leukemia in adults. *J Clin Oncol*. 2017;35(4):394-401.
- Tasian SK, Loh ML, Hunger SP. Philadelphia chromosome-like acute lymphoblastic leukemia. *Blood*. 2017;130(19):2064-2072.
- Boer JM, Marchante JR, Evans WE, et al. BCR-ABL1-like cases in pediatric acute lymphoblastic leukemia: a comparison between DCOG/Erasmus MC and COG/St. Jude signatures. *Haematologica*. 2015;100(9):e354-7.
- Chiaretti S, Messina M, Della Starza I, et al. BCR-ABL1-like is associated with MRD persistence and poor outcome. First report of the MRD-oriented GIMEMA 1913. *Haematologica*. 2020. doi: 10.3324/haematol.2020.247973
- Chiaretti S, Messina M, Grammatico S, et al. Rapid identification of BCR/ABL1-like acute lymphoblastic leukaemia patients using a predictive statistical model based on quantitative real time-polymerase chain reaction: clinical, prognostic and therapeutic implications. *Br J Haematol*. 2018;181(5):642-652.
- Jain N, Roberts KG, Jabbour E, et al. Ph-like acute lymphoblastic leukemia: a high-risk subtype in adults. *Blood*. 2017;129(5):572-581.
- Stock W, Luger SM, Advani AS, et al. A pediatric regimen for older adolescents and young adults with acute lymphoblastic leukemia: results of CALGB 10403. *Blood*. 2019;133(14):1548-1559.
- Herold T, Schneider S, Metzeler KH, et al. Adults with Philadelphia chromosome-like acute lymphoblastic leukemia frequently have IGH-CRLF2 and JAK2 mutations, persistence of minimal residual disease and poor prognosis. *Haematologica*. 2017;102(1):130-138.
- Tanasi I, Ba I, Sirvent N, et al. Efficacy of tyrosine kinase inhibitors in Ph-like acute lymphoblastic leukemia harboring ABL-class rearrangements. *Blood*. 2019;134(16):1351-1355.
- Pui CH, Roberts KG, Yang JJ, Mullighan CG. Philadelphia chromosome-like acute lymphoblastic leukemia. *Clin Lymphoma Myeloma Leuk*. 2017;17(8):464-470.
- Foa R, Bassan R, Vitale A, et al. Dasatinib-Blinatumomab for Ph-Positive Acute Lymphoblastic Leukemia in Adults. *N Engl J Med*. 2020;383(17):1613-1623.
- Harvey RC, Tasian SK. Clinical diagnostics, and treatment strategies for Philadelphia chromosome-like acute lymphoblastic leukemia. *Blood Adv*. 2020;4(1):218-228.
- Cario G, Leoni V, Conter V, Baruchel A, Schrappe M, Biondi A. BCR-ABL1-like acute lymphoblastic leukemia in childhood and targeted therapy. *Haematologica*. 2020;105(9):207019.
- Brown LM, Lonsdale A, Zhu A, et al. The application of RNA sequencing for the diagnosis and genomic classification of pediatric acute lymphoblastic leukemia. *Blood Adv*. 2020;4(5):930-942.
- Anagnostou T, Knudson RA, Pearce KE, et al. Clinical utility of fluorescence *in situ* hybridization-based diagnosis of BCR-ABL1 like (Philadelphia chromosome like) B-acute lymphoblastic leukemia. *Am J Hematol*. 2020;95(3):e68-E72.
- Sánchez R, Ribera J, Morgades M, et al. A novel targeted RNA-Seq panel identifies a subset of adult patients with acute lymphoblastic leukemia with BCR-ABL1-like characteristics. *Blood Cancer J*. 2020;10(4):43. doi: 10.1038/s41408-020-0308-3.
- El Fakih R, Savani B, Mohty M, Aljurf M. Hematopoietic cell transplant consideration for Philadelphia chromosome-like acute lymphoblastic leukemia patients. *Biol Blood Marrow Transplant*. 2020;26(1):e16-e20.

Granulocyte colony-stimulating factor acts on lymphoid-biased, short-term hematopoietic stem cells

Yulin Chen and K. Lenhard Rudolph

Leibniz Institute on Aging - Fritz Lipmann Institute (FLI), Research Group on Stem Cell Aging, Jena and Medical Faculty, University Hospital Jena (UKJ), Jena, Germany

E-mail: K. LENHARD RUDOLPH - lenhard.rudolph@leibniz-fli.de

doi:10.3324/haematol.2020.271205

Granulocyte colony-stimulating factor (G-CSF) is a cytokine that increases myelopoiesis,¹ impairs lymphopoiesis by inhibiting committed progenitor cells,^{2,3} and enhances hematopoietic stem cell (HSC) mobilization.⁴ The direct effects of G-CSF on purified subpopulation of HSC remained to be delineated. In this issue of *Haematologica*, Xie *et al.*⁵ investigate the influence of G-CSF on proliferation and the repopulating potential of myeloid-biased, long-term HSC (CD201⁺CD150⁺CD48⁺CD41⁺CD34⁺KSL) and lymphoid-biased, short-term HSC (CD201⁺CD150⁺CD48⁺CD41⁺CD34⁺KSL).

Understanding the direct influences of G-CSF on HSC could improve our understanding of HSC responses to an increase in G-CSF level caused by inflammation.⁶ The study by Xie *et al.* shows that G-CSF acts directly on lymphoid-biased, short-term HSC but not on myeloid-biased HSC. Interestingly, G-CSF cooperates with stem cell factor in driving the expansion of lymphoid-biased, short-term HSC in culture and in maintaining the *in vivo* repopulating potential of such cultures. These findings suggest that G-CSF-mediated effects on lymphoid-biased, short-term HSC may contribute to the previously noted

enhancement of early lymphopoiesis of bone marrow stem and progenitor cells after exposure to G-CSF.⁷ In contrast, however, G-CSF is also known to instruct bone marrow stromal cells to suppress the function of committed progenitors of B-lymphopoiesis.² The functional relevance of the G-CSF-mediated priming of early lymphoid progenitor cells and lymphoid-biased HSC^{5,7} in association with G-CSF-mediated impairment in the progression of lymphopoiesis from committed progenitor cells² should be delineated in future studies.

The primary role of G-CSF is currently seen in activation of myelopoiesis to strengthen myeloid immune responses, such as the recruitment of neutrophils during bacterial lung infections.⁸ However, the simultaneous priming of early lymphoid progenitor cells and lymphoid-biased HSC by G-CSF may also be important to ensure prompt reactivation of lymphopoiesis after the initial induction of myeloid cell-driven immune responses. The sequential coordination of such immune actions by G-CSF seems to be an interesting area of future research.

Understanding direct influences of G-CSF on HSC could also be relevant for our understanding of HSC

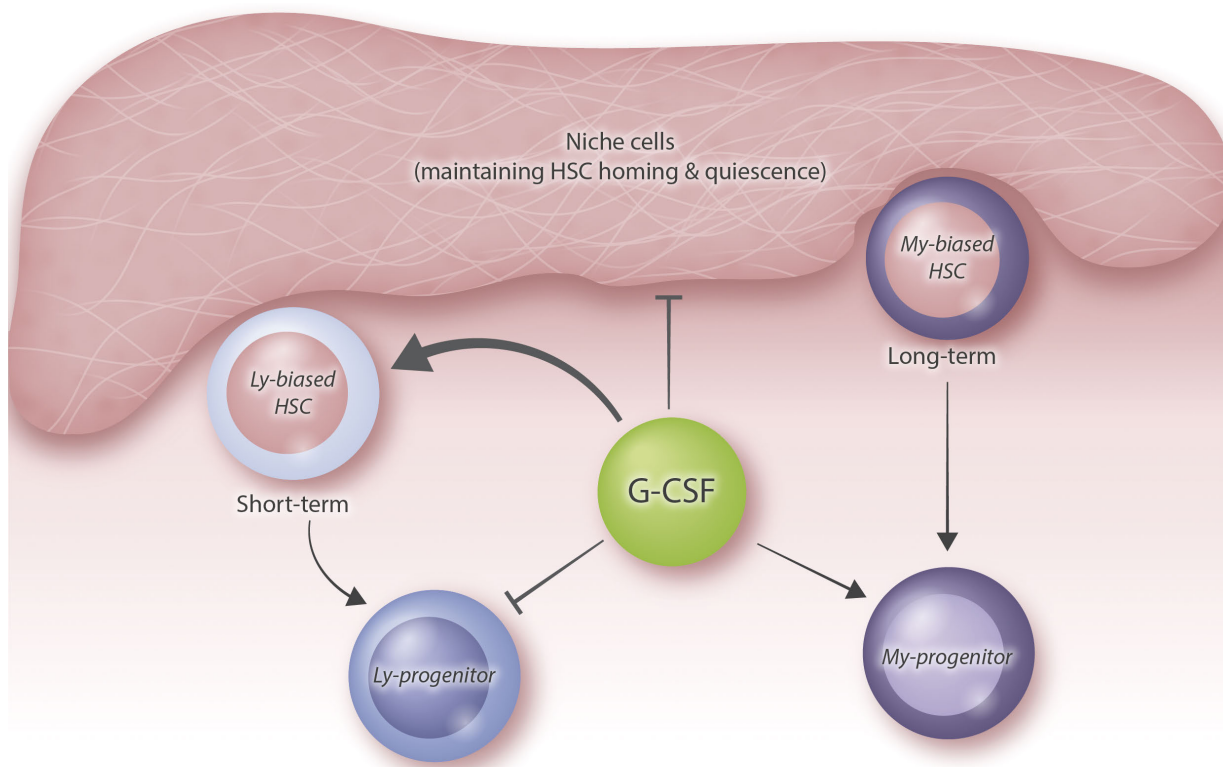


Figure 1. Granulocyte colony-stimulating factor influences the balance of myelopoiesis and lymphopoiesis. Granulocyte colony-stimulating factor (G-CSF) leads to mobilization of hematopoietic stem cells (HSC) by disrupting the function and maintenance of specific niche cells. G-CSF enhances expansion of lymphoid (Ly)-biased, short-term HSC in culture and maintains their *in vivo* repopulating potential. In contrast, G-CSF does not have a direct effect on purified myeloid (My)-biased, long-term HSC. Apart from regulating HSC, G-CSF can also increase myelopoiesis and impair lymphopoiesis by regulating committed progenitor cells.

aging. During mouse aging, the number of myeloid-biased HSC increases more than 10-fold, whereas the number of lymphoid-biased HSC shows only a mild (2-fold) increase.^{9,10} Xie *et al.* revealed that G-CSF improves the maintenance of lymphoid-biased HSC in culture, but does not have direct effects on myeloid-biased HSC. Whether G-CSF could contribute to the *in vivo* maintenance of lymphoid-biased HSC remains to be seen. Interestingly, in humans, G-CSF levels in the serum were reported to decrease during aging and this decrease was pronounced in patients with Alzheimer disease.¹¹ The findings of Xie *et al.* suggest that aging-associated declines in G-CSF level could contribute to the relative reduction in the self-renewal of lymphoid-biased HSC *versus* myeloid-biased HSC during aging. It would be interesting to investigate whether G-CSF has similar effects on human lymphoid-biased HSC as those on murine HSC described by Xie *et al.* However, the discrimination between different subtypes of HSC (lymphoid *vs.* myeloid-biased) has not yet been established in humans.

In addition, it would be of great interest to analyze the influence of other aging-related factors on G-CSF levels and HSC aging. Telomere dysfunction occurs as a consequence of telomere shortening and represents one of the hallmarks of aging. Telomere shortening induces cellular senescence and a strong increase in the secretion of pro-inflammatory cytokines by senescent cells - referred to as the senescence-associated secretory phenotype (SASP).¹² Of note, senescent cells also show strong increases in the secretion of G-CSF.¹³ An accumulation of senescent cells

have been described to occur in various tissues of primates, including humans, during aging.¹⁴⁻¹⁶ Interestingly, genetic studies on telomerase knockout mice revealed that G-CSF increases in blood serum as a consequence of telomere dysfunction, which led to impairments in lymphopoiesis and myeloid-skewed hematopoiesis.¹⁷ This phenotype is very similar to that present in aging humans, which is also characterized by increases in myeloid relative to lymphoid cells in the blood.¹⁸ While studies on human serum showed decreases in G-CSF during aging, future studies should investigate whether the accumulation of senescent cells in bone marrow tissue may lead to increases in G-CSF levels in the micro-milieu of HSC and lymphoid progenitor cells. If G-CSF does indeed contribute to the reduction in lymphopoiesis during aging, this could be related to the inhibitory effect of G-CSF on committed lymphoid progenitor cells.²

A direct influence of G-CSF on HSC could also be relevant for the clinical usage of G-CSF. It has been shown that macrophage colony-stimulating factor acts directly on HSC to enhance myeloid differentiation, which has positive effects in protecting HSC-transplanted mice from *Aspergillus* infection.¹⁹ Two of the main applications of G-CSF are to ameliorate chemotherapy-induced neutropenia and to mobilize HSC to be used for mobilized peripheral blood (MPB) transplantation. G-CSF leads to the mobilization of HSC by disrupting the function and maintenance of specific niche cells.²⁰ It remains to be determined whether direct effects of G-CSF on lymphoid-biased HSC would influence the mobilization of

sub-populations of HSC. If so, the method of mobilization could have an impact on transplantation results. In breast cancer patients who need a transplant of autologous MPB as part of their anticancer therapy, the transplantation of purified HSC improved the survival outcomes compared to those receiving non-purified MPB (<https://doi.org/10.1016/j.bbmt.2011.07.009>). It remains to be seen whether direct effects of G-CSF on HSC may influence transplantation outcomes.

In brief, the study by Xie *et al.* provides very interesting new data indicating that G-CSF can act directly on lymphoid-biased but not on myeloid biased HSC. This finding may have implications for our understanding of immune responses, HSC aging, and bone marrow transplantation therapies.

Disclosures

No conflicts of interest to disclose.

Contributions

YC and KLR wrote the editorial together.

Acknowledgments

This work was funded by the German Research Foundation (DFG) within the CRC "PolyTarget" (SFB 1278, Project B01) and by the Federal Ministry of Research and Education (BMBF) within the HaematoOPT project (031A424D).

References

1. Liongue C, Hall CJ, O'Connell BA, Crosier P, Ward AC. Zebrafish granulocyte colony-stimulating factor receptor signaling promotes myelopoiesis and myeloid cell migration. *Blood*. 2009;113(11):2535-2546.
2. Day RB, Bhattacharya D, Nagasawa T, Link DC. Granulocyte colony-stimulating factor reprograms bone marrow stromal cells to actively suppress B lymphopoiesis in mice. *Blood*. 2015;125(20):3114-3117.
3. Ingrid GW, Bendall LJ, Forristal CE, et al. B-lymphopoiesis is stopped by mobilizing doses of G-CSF and is rescued by overexpression of the anti-apoptotic protein Bcl2. *Haematologica*. 2013;98(3):325-333.
4. Petit I, Szyper-Kravitz M, Nagler A, et al. G-CSF induces stem cell mobilization by decreasing bone marrow SDF-1 and up-regulating CXCR4. *Nat Immunol*. 2002;3(7):687-694.
5. Xie M, Zhang S, Dong F, et al. Granulocyte colony-stimulating factor directly acts on mouse lymphoid-biased but not myeloid-biased hematopoietic stem cells. *Haematologica*. 2021;106(6):1647-1658.
6. Kawakami M, Tsutsumi H, Kumakawa T, et al. Levels of serum granulocyte colony-stimulating factor in patients with infections. *Blood*. 1990;76(10):1962-1964.
7. Hirayama F, Shih JP, Awgulewitsch A, Warr GW, Clark SC, Ogawa M. Clonal proliferation of murine lymphohemopoietic progenitors in culture. *Proc Natl Acad Sci U S A*. 1992;89(13):5907-5911.
8. Ye P, Rodriguez FH, Kanaly S, et al. Requirement of interleukin 17 receptor signaling for lung Cxcr chemokine and granulocyte colony-stimulating factor expression, neutrophil recruitment, and host defense. *J Exp Med*. 2001;194(4):519-528.
9. Muller-Sieburg C, Sieburg HB. Stem cell aging: survival of the laziest? *Cell Cycle*. 2008;7(24):3798-3804.
10. Wang J, Morita Y, Han B, Niemann S, Löffler B, Rudolph KL. Per2 induction limits lymphoid-biased haematopoietic stem cells and lymphopoiesis in the context of DNA damage and ageing. *Nat Cell Biol*. 2016;18(5):480-490.
11. Laske C, Stellos K, Stransky E, Leyhe T, Gawaz M. Decreased plasma levels of granulocyte-colony stimulating factor (G-CSF) in patients with early Alzheimer's disease. *J Alzheimers Dis*. 2009;17(1):115-123.
12. Salminen A, Kauppinen A, Kaarniranta K. Emerging role of NF-κB signaling in the induction of senescence-associated secretory phenotype (SASP). *Cell Signal*. 2012;24(4):885-845.
13. Xu M, Tcheknoria T, Ding H, et al. JAK inhibition alleviates the cellular senescence-associated secretory phenotype and frailty in old age. *Proc Natl Acad Sci U S A*. 2015;112(46):E6301-6310.
14. Herbig U, Ferreira M, Condel L, Carey D, Sedivy JM. Cellular senescence in aging primates. *Science*. 2006;311(5765):1257.
15. Iida ML, McClusky WG, Dodde V, et al. Survey of senescent cell markers with age in human tissues. *Aging* (Albany NY). 2020;12(5):4052-4066.
16. Dimri GP, Lee X, Basile G, et al. A biomarker that identifies senescent human cells in culture and in aging skin in vivo. *Proc Natl Acad Sci U S A*. 1995;92(20):9363-9367.
17. Ju Z, Jiang H, Jaworski M, et al. Telomere dysfunction induces environmental alterations limiting hematopoietic stem cell function and engraftment. *Nat Med*. 2007;13(6):742-747.
18. Pang WW, Price EA, Sahoo D, et al. Human bone marrow hematopoietic stem cells are increased in frequency and myeloid-biased with age. *Proc Natl Acad Sci U S A*. 2011;108(50):20012-20017.
19. Kandalla PK, Sarrazin S, Molawi K, et al. M-CSF improves protection against bacterial and fungal infections after hematopoietic stem/progenitor cell transplantation. *J Exp Med*. 2016;213(11):2269-2279.
20. Winkler IG, Sims NA, Pettit AR, et al. Bone marrow macrophages maintain hematopoietic stem cell (HSC) niches and their depletion mobilizes HSCs. *Blood*. 2010;116(23):4815-4828.

The Hsp70 chaperone system: distinct roles in erythrocyte formation and maintenance



Ferrata Storti Foundation

Yasith Mathangasinghe,¹ Bruno Fauvet,² Stephen M. Jane,^{3,4} Pierre Goloubinoff² and Nadinath B. Nillegoda¹

¹Australian Regenerative Medicine Institute, Monash University, Clayton, Victoria, Australia;

²Department of Plant Molecular Biology, Lausanne University, Lausanne, Switzerland;

³Central Clinical School, Monash University, Prahran, Victoria, Australia and ⁴Department of Hematology, Alfred Hospital, Monash University, Prahran, Victoria, Australia

ABSTRACT

Haematologica 2021
Volume 106(6):1519-1534

Erythropoiesis is a tightly regulated cell differentiation process in which specialized oxygen- and carbon dioxide-carrying red blood cells are generated in vertebrates. Extensive reorganization and depletion of the erythroblast proteome leading to the deterioration of general cellular protein quality control pathways and rapid hemoglobin biogenesis rates could generate misfolded/aggregated proteins and trigger proteotoxic stresses during erythropoiesis. Such cytotoxic conditions could prevent proper cell differentiation resulting in premature apoptosis of erythroblasts (ineffective erythropoiesis). The heat shock protein 70 (Hsp70) molecular chaperone system supports a plethora of functions that help maintain cellular protein homeostasis (proteostasis) and promote red blood cell differentiation and survival. Recent findings show that abnormalities in the expression, localization and function of the members of this chaperone system are linked to ineffective erythropoiesis in multiple hematological diseases in humans. In this review, we present latest advances in our understanding of the distinct functions of this chaperone system in differentiating erythroblasts and terminally differentiated mature erythrocytes. We present new insights into the protein repair-only function(s) of the Hsp70 system, perhaps to minimize protein degradation in mature erythrocytes to warrant their optimal function and survival in the vasculature under healthy conditions. The work also discusses the modulatory roles of this chaperone system in a wide range of hematological diseases and the therapeutic gain of targeting Hsp70.

Introduction

Cells are highly vulnerable to proteotoxic stresses during widespread remodeling of proteomes that typically accompany cell differentiation. Under such challenging conditions, molecular chaperones that constitute an essential part of cellular protein quality control (PQC) pathways, help maintain proteostasis by decreasing protein misfolding and aggregation, and promote cell viability.^{1,2} In response to cell differentiation, considerable rearrangements in cellular chaperomes have been detected,^{2,3} but the functional consequences of such changes largely remain enigmatic. In particular, the heat shock protein 70 (Hsp70) chaperone system is maintained at high levels during red blood cell differentiation.³⁻⁵ Emerging data demonstrate that Hsp70 machineries have distinct functions ranging from modulating cell signaling to PQC activities at different stages of erythropoiesis. These multi-faceted roles of the Hsp70 chaperone include maintaining erythroid progenitors, assessing fitness of progenitors prior to initiating lineage specific terminal cell differentiation, supporting hemoglobin (Hb) biogenesis, counteracting proteotoxicities and preventing premature apoptosis of differentiating erythroblasts, and promoting viability of terminally differentiated erythrocytes via protein repair. Hence, the dysfunction of this chaperone system is invariably associated with ineffective erythropoiesis, which leads to chronic anemia in several hematological diseases in humans.

Correspondence:

NADINATH B. NILLEGODA
nadinath.nillegoda@monash.edu

Received: July 29, 2019.

Accepted: September 25, 2020.

Pre-published: April 8, 2021.

<https://doi.org/10.3324/haematol.2019.233056>

© 2021 Ferrata Storti Foundation

Material published in *Haematologica* is covered by copyright. All rights are reserved to the Ferrata Storti Foundation. Use of published material is allowed under the following terms and conditions: <https://creativecommons.org/licenses/by-nc/4.0/legalcode>. Copies of published material are allowed for personal or internal use. Sharing published material for non-commercial purposes is subject to the following conditions: <https://creativecommons.org/licenses/by-nc/4.0/legalcode>, sect. 3. Reproducing and sharing published material for commercial purposes is not allowed without permission in writing from the publisher.



Formation of red blood cells

Erythropoiesis is a vital process throughout vertebrate life, which helps maintain adequate tissue oxygenation under physiological and nonphysiological states (e.g., hypoxia, hemorrhage or other anemic conditions). This cell differentiation event leads to the generation of highly specialized erythrocytes that function as dedicated oxygen and carbon dioxide transporting cells across the body. Erythrocytes have a finite lifespan (approximately 120 days in humans) in the circulatory system before they are recycled mainly in the spleen by macrophages.⁶ These cells, therefore, must be continuously and rapidly replaced in vertebrates. About two million new erythrocytes per second are generated in adult humans⁷ via proliferation and differentiation of a self-renewing population of pluripotent hematopoietic stem cells (HSC) located in the yolk sac, liver, spleen (antenatal) or bone marrow (postnatal) that give rise to early erythroid progenitors.⁶ During erythropoiesis, these progenitors undergo a red cell lineage specific terminal differentiation program to generate mature erythrocytes.

Erythrocyte production is tightly regulated by a set of hormones. For example, glucocorticoids regulate both the proliferation and differentiation of early erythroid progenitors known as early burst forming unit-erythroid (BFU-E) cells.⁸ The proliferation and differentiation of subsequent erythroid progenitors including late stage BFU-E and colony forming unit-erythroid (CFU-E) cells occur after the stimulation by erythropoietin (EPO), a glycoprotein cytokine secreted by the kidneys.⁹ EPO stimulation is vital for the induction of GATA-binding factor 1 (GATA-1) transcription factor, the master regulator of erythropoiesis. GATA-1 together with the transcription factor STAT5, promote further erythroblast proliferation¹⁰ and turn on the gene activation and repression program, which drives the multistep terminal differentiation process of these cells.¹¹ In mammals, erythropoiesis can be resolved into six morphologically distinct cell stages that result from a series of mitotic cell divisions (Figure 1A). These stages include: (i) proerythroblast, (ii) basophilic erythroblast, (iii) polychromatophilic erythroblast, (IV) orthochromatophilic erythroblast, (V) reticulocyte, and (VI) mature erythrocyte. During terminal differentiation, the erythroblasts decrease in cell size, condense chromatin, reorganize and reduce cellular proteome and membranes, and eliminate organelles, thereby making space for the rapidly increasing levels of Hb, the oxygen-trafficking protein complex. The most striking morphological change occurs in orthochromatophilic erythroblasts that eject nuclei to form reticulocytes in the bone marrow (Figure 1A). These reticulocytes loose ribosomes and the bulk of RNA molecules, and develop into Hb packed mature erythrocytes that have a characteristic biconcave disk-like shape with a flattened center.

The mature erythrocytes contain a remarkably high concentration of Hb molecules (approximately 29.5 pg/cell),¹² which represents approximately 98% of the proteome.¹³ Hb is a tetrameric globular protein made up of four globin protein subunits/chains, each containing a heme group, which reversibly binds to oxygen and carbon dioxide. The adult human hemoglobin (HbA) is made from two 141 amino acid-long α -globin chains and two 146 amino acid-long β -globin chains ($\alpha_2\beta_2$) (Figure 1B). Under physiological conditions, HbA makes up

>97% of the Hb constituent in adult humans. The remaining Hb contains fetal Hb (HbF; $\alpha_2\gamma_2$) and HbA2 ($\alpha_2\delta_2$), two isotypes generated by switching the β globin chain with either γ or δ globin chains.⁶

Proteotoxic stresses associated with erythropoiesis

Proteostasis is maintained by balancing the cellular pathways that facilitate protein synthesis, folding, assembly, trafficking, and degradation under varying environmental and metabolic conditions.¹ Even under normal growth conditions, cells experience a continuous influx of misfolded proteins generated from various protein biogenesis mistakes such as errors in transcription, translation and folding. Additionally, most proteins are at risk of misfolding due to the marginal stability of their native conformations.¹⁴ Cells have evolved a set of intricate PQC pathways comprising of molecular chaperones and protein degradation systems that operate constantly to decrease the levels of misfolded proteins that otherwise would easily form aggregates in crowded cellular environments. Protein aggregates typically show poor solubility in aqueous cellular environments, have no physiological function *per se* and could instead elicit cytotoxicity.¹ By untangling and unfolding such aberrant protein species, the ATP fueled chaperone machineries are able to “repair” and rescue proteins, which leads to a considerable reduction in the risk of proteotoxicities in cells. Protein degradation pathways also represent an important line of defense by clearing misfolded proteins and preventing their accumulation.¹ However, in aging and/or stressed cells, such defense mechanisms could become overwhelmed leading to the buildup of potentially toxic protein aggregate species. Many disease-linked mutant proteins also form such aggregates that are refractory to PQC systems, including degradation pathways.¹⁵

Due to various protein biosynthetic errors and considerable attenuation of basic PQC pathways, erythroid maturation is highly exposed to protein misfolding/aggregation. The first PQC challenge during erythropoiesis involves the folding and assembly of the α -globin chains that show a high degree of instability. In the absence of the partnering β -globin, the free α -chains with heme/iron could readily misfold to form protein aggregate deposits called Heinz bodies (for a review, see Voon *et al.*¹⁶). These highly toxic protein aggregates, when accumulated, could trigger the generation of reactive oxygen species (ROS)¹⁷ that damage cellular proteins, nucleic acids and lipids and induce oxidative stress in erythroblasts leading to premature cell death (Figure 1B).¹⁸ This is circumvented to a certain degree with the assistance of a dedicated chaperone named alpha hemoglobin stabilizing protein (AHSP). AHSP mimics the α -helix-loop- α -helix motif of β -globin and assists in the folding of α -chains in a “template” directed manner^{19,20} (for a review, see Weiss *et al.*)²¹. Apart from the α -chain instability, the generally high synthesis rates of globin proteins (300 mg of Hb per hour in healthy adult humans²²) during this atypical state could also proportionally increase the level of intrinsic errors in folding and assembly²³ of Hb. In particular, heme/iron imbalances could result in globin misfolding, which could induce severe oxidative stress in erythroblasts. A tightly regulated supply of iron to support the production of heme is

required for efficient Hb biogenesis. Heme synthesis is mediated by conjugating iron and protoporphyrin in a series of enzymatic reactions occurring in mitochondria and cytosol.²⁴ The hydroxyl radicals produced by elevated levels of free heme/iron undergoing the Fenton reaction in erythroblast cytosol could damage and induce the aggregation of both Hb and other critical biomolecules.²⁵

The next PQC challenge in red blood cell maturation occurs from the reduction/disruption of crucial PQC pathways that typically protect cells against protein aggregation. In order to make space for the increasing levels of Hb, the proteome of the terminally differentiating erythroblasts is rapidly reduced to 2-5% via bulk degradation of many cellular proteins and organelles³ by the

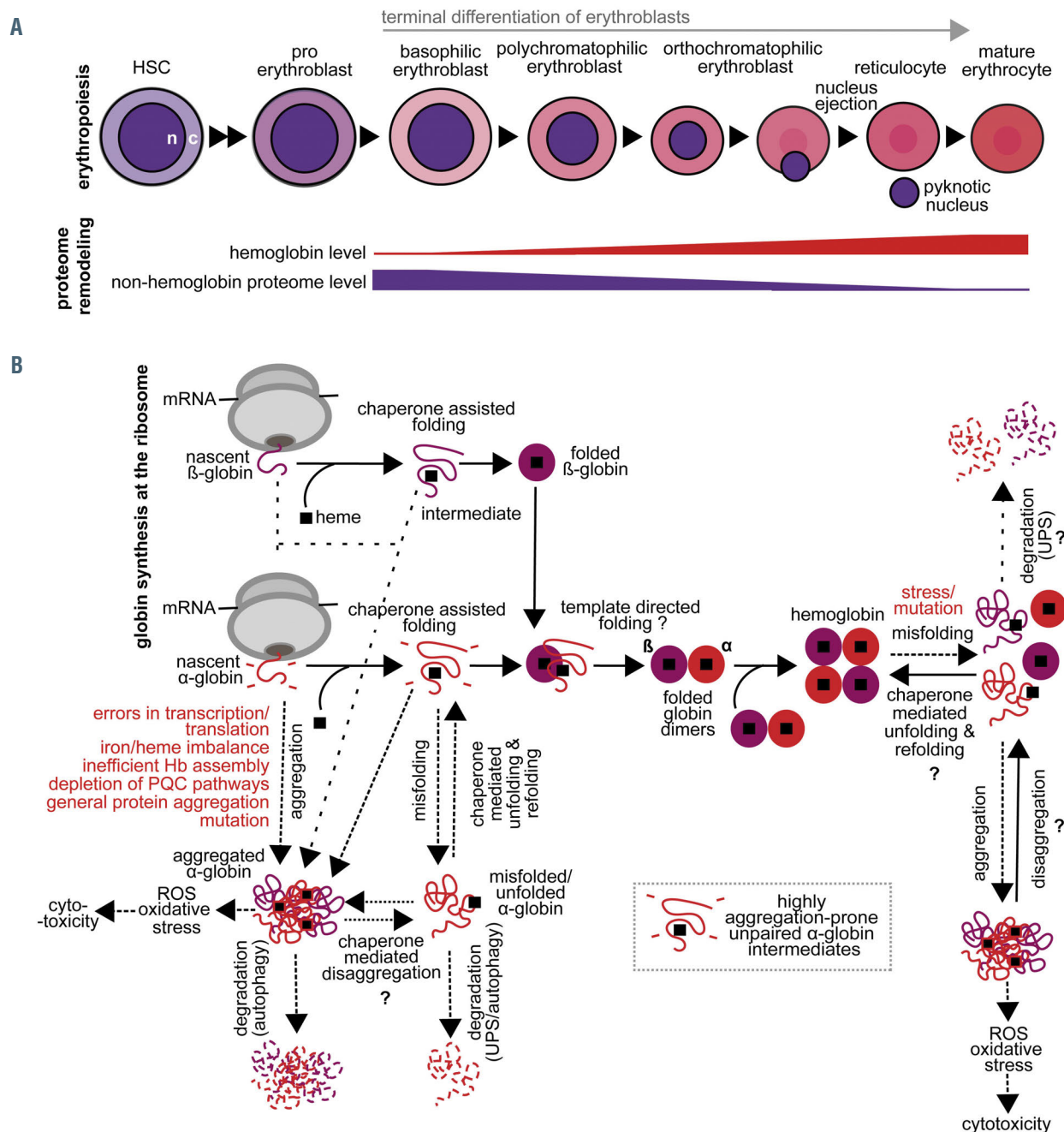


Figure 1. Biogenesis of hemoglobin during erythropoiesis. (A) A simplified schematic diagram showing the key cell stages of erythropoiesis. Hematopoietic stem cells (HSC) differentiate into a common myeloid progenitor, which further transition into a committed erythroid lineage. The proerythroblast is the earliest morphologically identifiable erythroid precursor cell in the bone marrow. Erythropoietin (EPO) signaling initiates terminal differentiation of erythroblasts to generate mature erythrocytes. During terminal differentiation, cells reduce in size and undergo major changes including chromatin condensation, proteome remodeling and ultimately the elimination of cellular organelles to provide room for hemoglobin (Hb). Hb expression levels in differentiating cells are indicated by intensity of the red color. (B) Chaperone assisted folding and assembly of Hb. The folding of nascent globin chains is assisted by chaperones such as the α -Hb-stabilizing protein (AHSP), heat shock protein 70 (Hsp70) and heat shock protein 90 (Hsp90). Errors in Hb subunit synthesis and assembly, iron/heme imbalances, deficiencies in protein quality control activities and exposure to reactive oxygen species (ROS), however, could trigger the misfolding and aggregation of globin proteins. In particular, misfolded and unassembled α -globin chains are highly prone to form cytotoxic aggregates leading to ineffective erythropoiesis. c: cytosol; n: nucleus; UPS: ubiquitin proteasome system.

ubiquitin proteasome system (UPS) and the autophagy pathway.^{26,27} This drastic proteome remodeling expectedly depletes components of chaperone and proteolytic machineries and decreases the ability of these cells to induce global PQC pathways that help buffer against proteotoxic stresses.²⁸ For example, unlike other cell types, reticulocytes show inability to fully recover critical cellular functions such as protein synthesis after heat shock.^{4,29} On the whole, terminally differentiating erythroblasts seem particularly vulnerable to stresses associated with protein misfolding and aggregation.

The Hsp70 chaperone system

Hsp70 forms one of the most abundant and highly conserved molecular chaperone systems critical for maintaining cellular proteostasis. This highly versatile chaperone system supports a plethora of housekeeping and stress-related cellular repair processes that protect cells against proteotoxic stresses (for a review, see Rosenzweig *et al.*³⁰). The key housekeeping activities include facilitating folding of newly synthesized proteins, transport of polypeptides across cellular membranes, assembly/disassembly of protein complexes and regulation of protein activity. In stressed cells, the Hsp70 chaperone system functions to prevent aggregation of aberrant proteins, refold misfolded proteins, solubilize aggregated proteins, and cooperate with cellular degradation machineries to clear terminally damaged proteins (for a review, see Rosenzweig *et al.*³⁰).

The chaperoning functions of Hsp70 are tightly regulated via the cooperation of dedicated cochaperones from the J-domain protein (JDP) family and nucleotide exchange factors (NEF) that fine-tune Hsp70's ATP-dependent allosteric control of substrate binding and release (Figure 2A). JDP form the largest and the most diverse family of cochaperones in humans (over 42 members) and provide specificity to the Hsp70 family (13 homologs in humans) by selecting substrates.^{30,31} Concomitant interaction of Hsp70 with a JDP and substrate boosts ATP hydrolysis in Hsp70. This dual trigger allows Hsp70 to efficiently trap and unfold substrates (Figure 2A).³² The timely release of substrates is mediated by nucleotide exchange factors that release ADP and allow subsequent rebinding of ATP, thus resetting the Hsp70 chaperone to its open, low substrate affinity state to receive a new client.^{30,33}

Hsp70 generally shows a high affinity towards misfolded and aggregated substrates, and a low affinity for native proteins, which may, thus be considered as the products of such polypeptide unfolding enzymes.³⁴ As earlier stated, the energy from ATP hydrolysis drives the iterative protein unfolding cycles of Hsp70 that allow the refolding of misfolded proteins (Figure 2A). Hsp70 and other protein folding chaperone systems (*e.g.*, Hsp60 and Hsp90) promote the buildup and maintenance of relatively high levels of native protein conformers under non-equilibrium stress conditions where without chaperones or ATP, the denatured protein conformers would readily seek equilibrium and turn into stable inactive misfolded species.³⁵ Conceptually, this aligns with Erwin Schrödinger's view, which states that living matter evades the decay to equilibrium.³⁶ The term "evades" implies that living cells must constantly consume energy in order to avoid spontaneous entropy-driven decomposition of

their macromolecules (*e.g.*, proteins), leading to cell death. This is possible because the biosphere is not a closed system: the energy from the sun is harnessed by photosynthesis to produce ATP for all organisms to fuel their repair (and replace) mechanisms. The chaperone-based protein repair mechanisms constantly counteract the natural entropic tendency of proteins to misfold and further decay by hydrolysis and oxidation into simpler molecules. In other words, when acting as ATP-fueled iterative unfolding nanomachines, chaperones such as Hsp70 can correct or "repair" structurally damaged proteins as they are formed under stressful non-equilibrium conditions.³⁷ Erythropoiesis is a prime example of how Hsp70's protein repair and regulatory functions are fully deployed to support cell differentiation and viability.

Multifaceted roles of the Hsp70 chaperone system in erythropoiesis

During red blood cell generation, the Hsp70 chaperone system functions in a number of regulatory and PQC activities. By changing its cochaperones, the Hsp70 chaperone could target different clientele and switch between functions, which allows this highly versatile chaperone system to rapidly respond to different cell growth and differentiation conditions.^{38,39} The main roles of Hsp70 during erythropoiesis include: (i) aiding in maintaining erythroid progenitors (ii) assessing fitness of progenitors prior to initiating lineage specific terminal cell differentiation (iii) supporting Hb biogenesis (iv) counteracting proteotoxicities and preventing premature apoptosis of differentiating erythroblasts and (v) conceivably promoting viability of differentiated (mature) erythrocytes via protein repair.

Hsp70 regulates dormancy and cell cycle quiescence of erythroid precursor cells

Continuous proliferation and differentiation of hematopoietic stem cells into committed erythroid progenitor cells⁶ is required for maintaining healthy levels of mature erythrocytes in the peripheral vasculature. The cyclin dependent cell cycle entry from G1 to S phase during proliferation of hematopoietic stem cells is modulated largely by the opposing actions of cyclin dependent kinases (CDK) and cyclin-dependent kinase inhibitors (CDKi).⁴⁰ In order to terminate the dormancy of hematopoietic stem cells and initiate cell cycle entry, cyclin D1, the regulatory subunit of CDK4 and CDK6, has to translocate from the cytosol to the nucleus.^{41,42} This key step in HSC proliferation is mediated by the constitutively expressed heat shock cognate protein 70 (Hsc70/HSPA8), which binds to cyclin D1 and shuttles it across the nuclear membrane (Figure 3).⁴¹ Here, HSPA8 appears to recognize a peptide segment in an unstructured (likely a looped or terminal) region exposed on the surface of folded cyclin D1. Similar types of interactions between Hsp70 and native proteins leading to regulatory activities have been demonstrated with clathrin triskelions, immunoglobulin heavy chain, *Escherichia coli* heat shock transcription factor σ 32 and plasmid replication protein RepE.⁴³⁻⁴⁵ The cyclin D1-HSPA8 complex is retained in the cytosol by forming additional interaction(s) with p57^{KIP2} and p27^{KIP1}, two critical CDKs that are known to prevent the cell cycle progression of

hematopoietic stem cells (Figure 3).⁴¹ It is tempting to speculate that through complexing, the CDKs mask the nuclear localization related signal of HSPA8^{41,42} until the CDKs are degraded via stem cell factor signaling coupled to the initiation of erythropoiesis. ERK signaling, which plays a modulatory role in erythropoiesis⁴⁶ also plays a role in the nuclear shuttling of Hsp70,⁴⁷ but little is known about how these signals are integrated, if at all. The rodent mammalian relative of Dnaj (MRJ), an ortholog of human JDP DNAJB6, was identified from recent stem cell

work⁴⁸ to play a role in promoting cell quiescence by binding to a cyclin D1 inhibitor.⁴⁹ The same JDP was implicated in playing a role in stem cell self-renewal.⁵⁰ Whether MRJ/DNAJB6 or another JDP directs the selection of clients in the CDK-HSPA8-cyclin D1-mediated HSC proliferation pathway remains to be determined. The terminal differentiation of erythroblasts also requires cell cycle regulating cyclins. Cyclins A2 and D3 are required to control cytokinesis, erythrocyte size and number.^{51,52} Here too, the Hsp70 system facilitates the

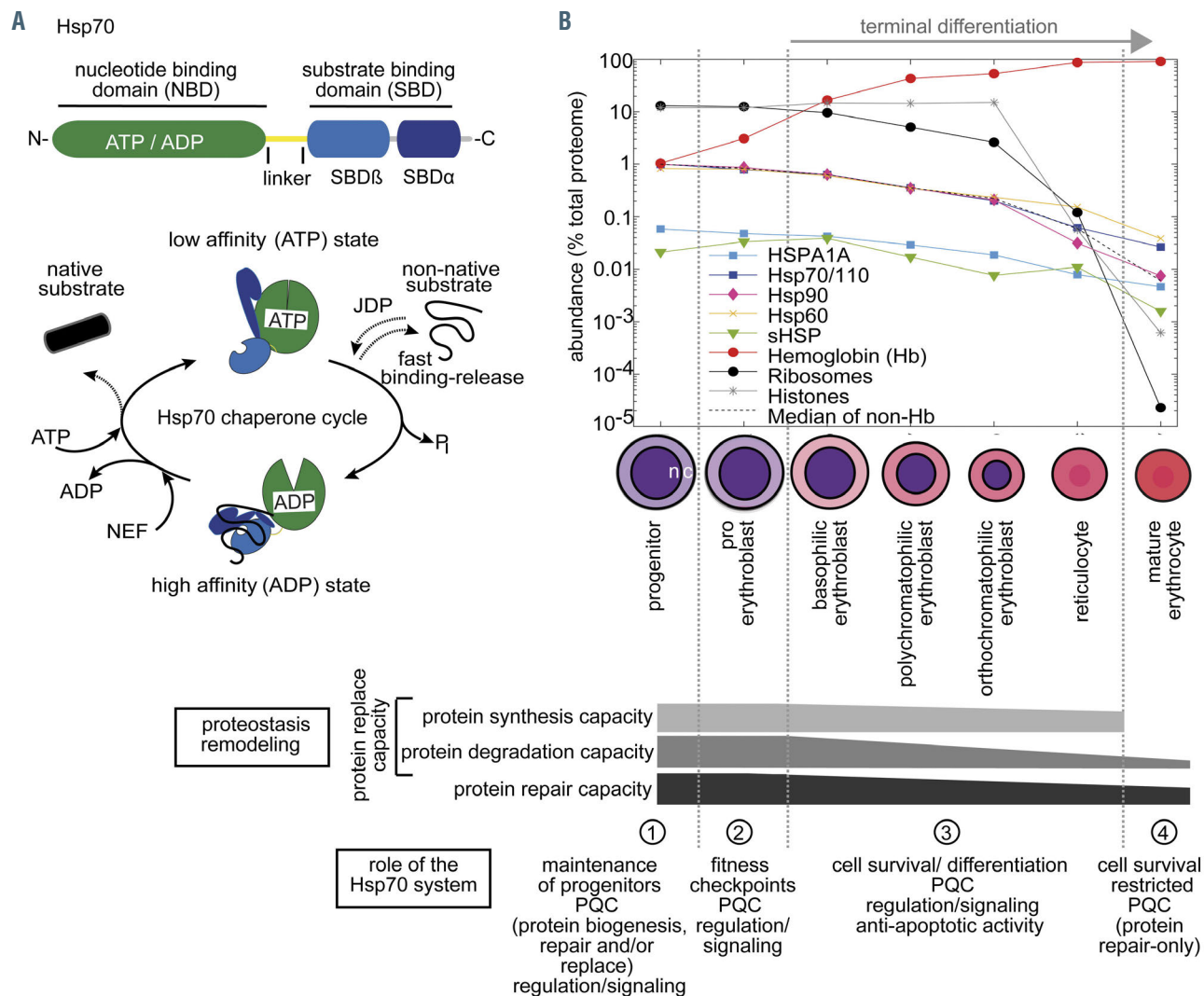


Figure 2. Roles of the Hsp70 chaperone system in differentiating erythroblasts and mature erythrocytes. (A) Domain organization of the heat shock protein 70 (Hsp70) chaperone (top); the Hsp70 chaperoning cycle (bottom). Substrate binding is dictated in Hsp70 by the allosteric coupling of ATP binding and hydrolysis at the N-terminal nucleotide binding domain (NBD), which results in conformational changes at the substrate binding domain (SBD).⁴⁴ The conformational cycle linked to substrate capture is defined by ATP hydrolysis driven large scale movements in the α -helical-lid domain (SBD α) that closes over the β -sandwich substrate binding subdomain (SBD β) in the ADP state, resulting in low substrate off-rates (i.e., high affinity towards bound substrates).³⁰ J-domain proteins (JDP) select substrates for Hsp70. Concomitant interactions of the Hsp70 (in ATP state) with JDP and substrate result in increased stimulation of ATP hydrolysis trapping the substrate in Hsp70. Subsequently, nucleotide exchange factors (NEF) induce ADP dissociation from Hsp70 allowing ATP rebinding, which triggers substrate release to complete Hsp70 cycle. Substrate unfolding and refolding is facilitated by multiple cycles of substrate binding and release. Hsp70 recognizes a highly degenerative and frequently occurring peptide motif enriched with five hydrophobic amino acids, flanked by preferentially positively charged amino acids (statistically occurring in every 30-40 residues in polypeptide chains).¹⁴⁸ Such hydrophobic motifs are typically buried inside a natively folded protein, but become exposed in unfolded or misfolded conformers, which allow the Hsp70 machinery to discriminate between natively folded and unfolded/misfolded/aggregated substrates.³⁰ (B) Expression profiles of selected chaperone systems in different stages of erythropoiesis from quantitative proteomics data.³⁵ The black dotted line represents the median relative abundance of non-hemoglobin (Hb) proteins in each cell type. The cytosolic Hsp70/110, Hsp60, and Hsp90 initially represent about 1% of the total proteome in erythroid progenitor stages. Their abundance, however, gradually decreases as the proportion of Hb increases during erythropoiesis, but much less so than ribosomes and histones. Below, multifaceted functions of the Hsp70 chaperone system at major steps of red blood cell generation. Ability to synthesize proteins is lost in mature erythrocytes. Protein degradation capacity is largely reduced in mature erythrocytes. A selective Hsp70 system seems to drive protein repair in terminally differentiated erythrocytes. PQC: protein quality control.

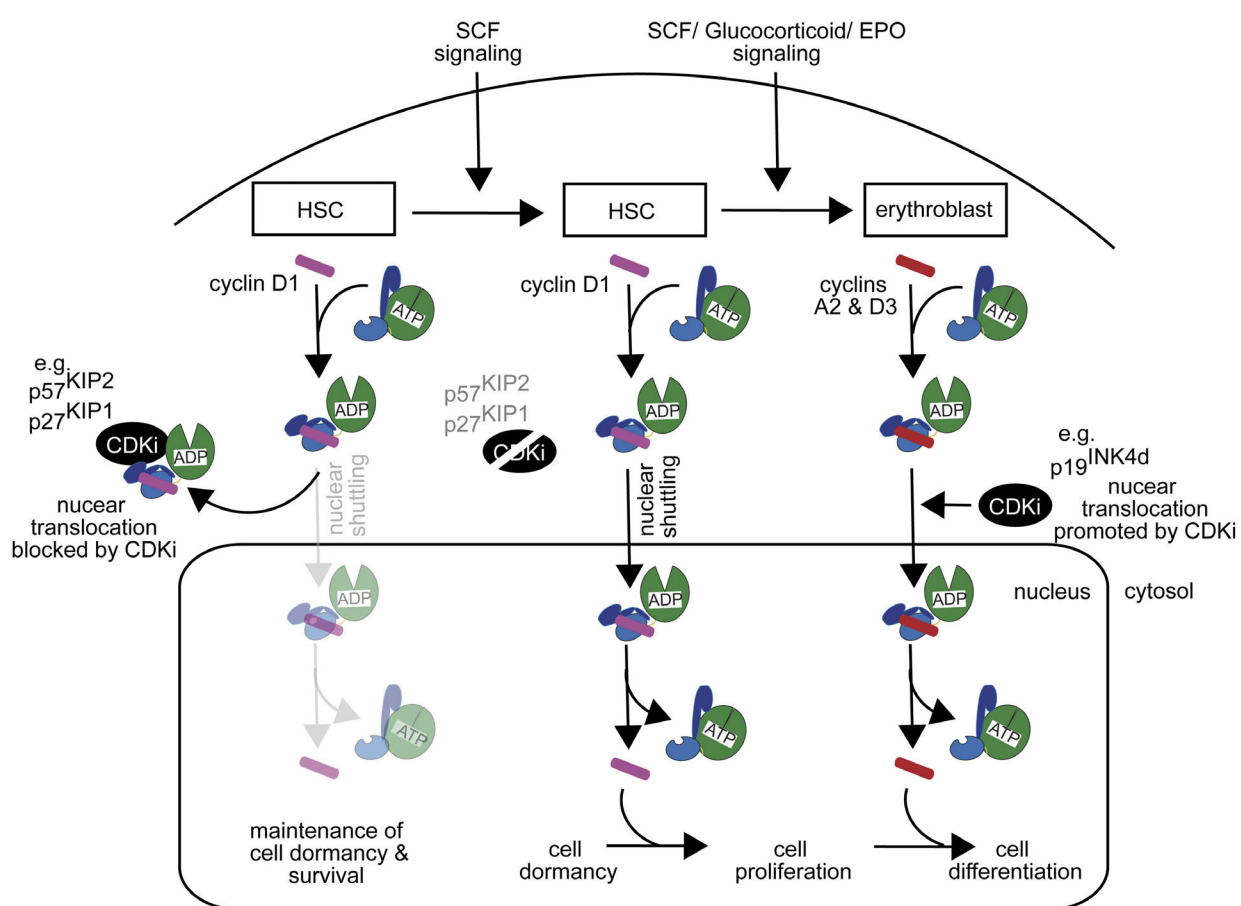


Figure 3. Hsp70 chaperone system modulates the maintenance of dormancy and cell cycle quiescence of stem cell progenitors of erythrocytes. Heat shock protein 70 (Hsp70) binds and shuttles key cyclins that control proliferation and differentiation of erythroid precursor cells. Growth factor regulated cyclin-dependent kinase inhibitors (CDKi) appear to modulate these activities by interacting (directly or indirectly) with Hsp70-cyclin complexes. EPO: erythropoietin; HSC: hematopoietic stem cell; SCF: stem cell factor.

shuttling of cyclins A2 and D3 and co-operate with CDKi to regulate terminal differentiation of erythroblasts. An analysis of erythroblasts obtained from differentiating human cord blood CD34⁺ cells shows that only three out of the seven CDKi (p18^{INK4c}, p19^{INK4d} and p27^{KIP1}) are expressed to significant levels during early and late terminal differentiation steps of red blood cells. In contrast to the functions of p57^{KIP2} and p27^{KIP1} in HSC, p19^{INK4d} appears to be promoting erythroblast differentiation by facilitating nuclear localization of the stress inducible Hsp70 (HSPA1A) through the activation of the ERK, but not AKT, signal transduction pathway (Figure 3).⁴⁷ p19^{INK4d} may even play a role in the proteostasis-based fitness checkpoints in human erythroblasts (see below). How EPO stimulation leads to the induction and ERK-mediated nuclear translocation of Hsp70 and the role of CDKi in modulating this process during erythropoiesis remains to be dissected.^{53,54}

The mammalian mitochondrial Hsp70 (mortalin/HSPA9) is also implicated in the proliferation/maintenance of early progenitors of erythrocytes.⁵⁵ HSPA9 cooperates with the inner mitochondrial translocase (TIM) complex to facilitate the translocation of mitochondrial matrix proteins that are essential for mitochondrial function and cell viability.⁵⁶ Therefore, it is conceivable that any depletion of HSPA9 levels leads to increased mitochondrial dysfunction and activation of pro-apoptotic

factors that induce hematopoietic progenitor cell death.⁵⁷ Intriguingly, however, compared to progenitors of other lineages of hematopoiesis, a greater reduction of BFU-E progenitors was observed when *HSPA9* was knocked down in rodents, suggesting that this Hsp70 paralog possibly plays an additional role(s) in maintaining the erythroid progenitor cell niche.⁵⁸

Hsp70 checks the fitness of erythroblasts at the initiation of erythropoiesis

The continuous generation of large amounts of red blood cells to traffic O₂/CO₂ in vertebrates comes with a heavy energy cost (ATP-wise). By allowing only healthy erythroid progenitors to undergo cell differentiation in part increases the fidelity of this process. In order to select healthy progenitors, two fitness checkpoints seem to have evolved around the Hsp70 chaperone system. In both checkpoints, the Hsp70 chaperone appears to monitor proteostasis deficiencies in EPO stimulated erythroid progenitors that are primed to undergo differentiation. By acting as a sensor of global folding status, Hsp70 is able to gauge the levels of misfolded/aggregated proteins in these cells. The first fitness checkpoint seems to be initiated by momentarily triggering a pro-apoptotic insult during EPO stimulation, which induces mitochondria to undergo transient depolarization.⁵⁹ This prompts the activation of several pro-apoptotic signals including the release of the

mitochondria localized apoptosis-inducing factor (AIF, AIFM1).⁵⁹⁻⁶² The AIF released into the cytosol enters the nucleus via a nuclear localization signal⁶³ and initiates caspase-independent chromatin condensation, DNA fragmentation and nuclear shrinkage to fully commit cells to apoptosis.⁶² In healthy erythroblasts, however, Hsp70 chaperone appears to play an important role in neutralizing this pro-apoptotic signaling pathway (Figure 4A). Cytosol-localized Hsp70 (primarily the stress induced HSPA1A) directly interacts with AIF and prevents its translocation into the nucleus.^{59,63,64} On the contrary, in “unhealthy” erythroblasts (e.g., cells experiencing acute oxidative stress), Hsp70 is largely sequestered away by the accumulating misfolded/aggregated proteins. This sequestration prevents the neutralization of AIF signaling, thus leading to fitness checkpoint failure and rapid elimination of unhealthy cells (Figure 4B).

The second checkpoint appears to monitor the capacity of Hsp70 to protect GATA-1 from caspase-3 mediated proteolytic cleavage. EPO stimulation triggers the translocation of HSPA1A from the cytosol to the nucleus.⁶⁵ In healthy erythroblasts, the nuclear translocated HSPA1A binds directly to GATA-1 and prevents the transcription factor from being cleaved, which allows the initiation of erythropoiesis (Figure 4A).⁶⁵ However, if there is a deficiency in Hsp70 levels, activity and/or the chaperone is insufficiently translocated to the nucleus due to the sequestration away by cytosolic protein aggregates,⁶⁶ the unprotected GATA-1 becomes targeted by caspase-3 (Figure 4B). Reduction in the level of GATA-1 inhibits both the terminal differentiation program and anti-cell death signaling via Bcl-xL⁶⁷ that ultimately trigger clearance of unhealthy cells via apoptosis. This fitness checkpoint seems to function throughout the early stages of erythropoiesis. During the latter stage of erythropoiesis, a small heat shock protein (sHSP) named Hsp27 (also known as HSPB1) translocates to the nucleus (triggered by post-translational modifications) and appears to outcompete Hsp70 from binding to GATA-1, which results in the degradation of the transcription factor.⁶⁸ In a nutshell, i) adequate nuclear and cytosolic levels of “free” Hsp70 chaperones and ii) favorable inputs from both of the proteostasis fitness checkpoints seem to be required to selectively initiate the terminal differentiation of healthy erythroblasts.

Hsp70's role in hemoglobin folding and assembly

Despite decades of research, the mechanistic understanding of the folding and assembly of Hb (Figure 1B) remains incomplete. In particular, little is known about how heme moieties are inserted into nascent globin chains during *de novo* folding. Several chaperones including Hsp70, Hsp90, and AHSP have been recognized to assist in globin folding and assembly in erythrocytes.^{66,69,70} Whether Hsp70 directly assists in Hb biogenesis is still an open question. Early studies have identified a role for Hsp70 in stabilizing α -globin and preventing its aggregation during erythropoiesis.⁶⁶ However, this could also result indirectly through the regulation of heme regulated inhibitor of translation (HRI) by Hsp70, which affects Hb assembly. HRI is the main kinase, which fine-tunes the cellular levels of heme and globin proteins to facilitate efficient Hb assembly during erythropoiesis.⁷¹⁻⁷³ In healthy erythroblasts with sufficient levels of heme, HRI is kept inactive by an autoregulatory mechanism involv-

ing complex formation with heme and HSPA8.^{74,75} When cellular heme levels decrease, the inhibition is released and the activated kinase rapidly phosphorylates the eukaryotic translation initiation factor 2 α (eIF2 α). This halts protein synthesis and prevents the overproduction of aggregate-prone globin chains.^{72,73,76} Under proteotoxic stress conditions, HRI is similarly activated to block Hb production, but now as a result of HSPA8 being sequestered away by misfolded/aggregated proteins.⁷⁷ This activation appears to be independent of heme levels in erythroblasts.^{75,77} Apart from inhibiting protein translation, HRI initiates an integrated stress response in erythroid precursors by selectively switching-on the transcriptional factor ATF-4 signaling pathway to induce multiple antioxidants that help mitigate oxidative stress.⁷⁸ The triggering of this mechanism can be clearly observed in heat shocked erythroblasts.^{73,77} The activity of HRI is critical for the viability of stressed erythroid progenitors since induction of Hsp70 and other chaperones alone is insufficient to mitigate proteotoxicity in these cells.^{72,79} Additionally, Hsp70 may in part help fold HRI adding another level of complexity to this regulation.⁷⁵ In essence, Hsp70 directly and/or indirectly facilitates the efficient biogenesis of Hb during erythropoiesis.

Clearance of aberrant proteins by the Hsp70 system during erythropoiesis

Triggering of ineffective erythropoiesis as a result of increased levels of protein aggregation has been observed in disease conditions such as β -thalassemia (see section on Hsp70 associated blood disorders).⁶⁶ Interestingly, the induction of Hsp70, but not other major stress chaperones, has been detected in heat shocked erythroblasts.^{4,80} This demonstrates the existence of a somewhat specialized stress response in erythroblasts to perhaps selectively induce Hsp70-based PQC activities. Previous work has shown that rabbit reticulocyte lysates have the capacity to resolve *in vitro* generated protein aggregates⁸¹ suggesting that differentiating erythroblasts possess strong protein disaggregation/refolding activity. This activity is most likely generated via the recently discovered Hsp70-based protein disaggregases in human cells.⁸²⁻⁸⁷ These disaggregases could potentially co-operate with cellular protein degradation systems⁸² to rapidly clear aggregated proteins and reduce associated toxicities to facilitate erythropoiesis

Suppression of apoptosis in differentiating erythroblasts by Hsp70

HSPA1A, which is upregulated in response to proteostasis insults has been demonstrated to block pro-apoptotic pathways that lead to caspase activation in cells.⁸⁸ Erythroblasts appear to rely on the same Hsp70 homolog to prevent premature apoptosis during terminal differentiation.⁸⁹⁻⁹¹ This necessity may partially explain why there is an unusually high level of HSPA1A present even in early erythroid progenitors primed to undergo erythropoiesis (Figure 2B). Additionally, the EPO signaling induced mitochondrial HSPA9 could also inhibit apoptosis in part by suppressing the production of ROS.⁵⁹ These Hsp70 mediated anti-apoptotic signals together with the induction of anti-apoptotic protein Bcl-xL by GATA-1⁶⁷ appears to help prevent erythroblasts from undergoing premature death despite the considerable proteostasis challenges associated with normal erythropoiesis.

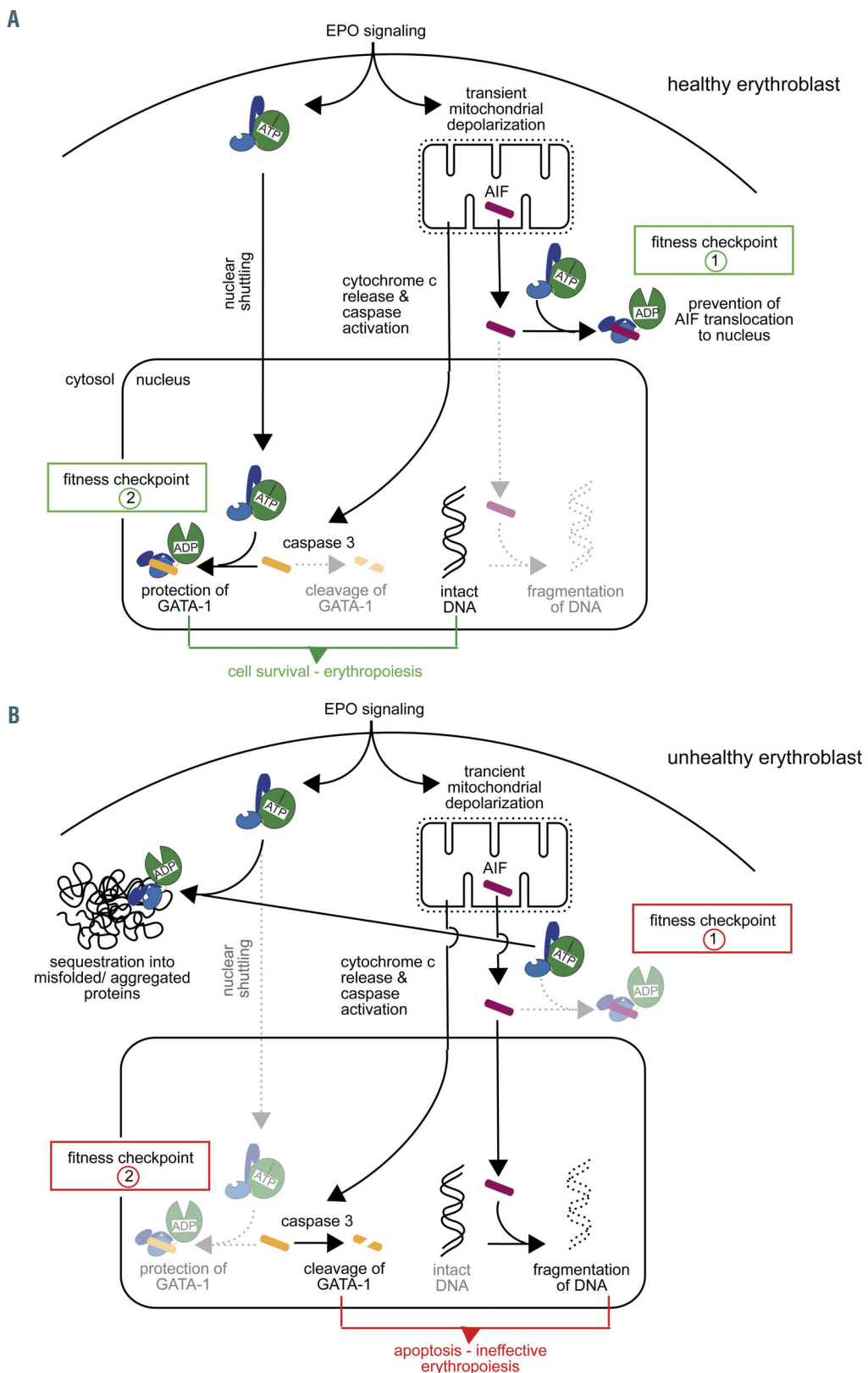


Figure 4. Hsp70 facilitates proper initiation of erythropoiesis. Heat shock protein 70 (Hsp70) is utilized as a stress sensor molecule in two fitness checkpoints to assess proteostasis deficiencies in erythroid progenitors. (A) Checkpoint 1, in essence, "gauges" and tests whether erythroblasts contain sufficient Hsp70 levels in the cytosol to block the nuclear translocation of apoptosis-inducing factor (AIF), a pro-apoptotic factor released from transiently depolarized mitochondria as a result of erythropoietin (EPO) signaling. In unhealthy cells, Hsp70 is sequestered away by protein aggregates and consequently AIF translocates into the nucleus to initiate cell death. Conversely, checkpoint 2 evaluates the ability of Hsp70 to protect GATA-1, the master regulator of erythropoiesis, from caspase 3 cleavage. This too indirectly evaluates the Hsp70 chaperoning capacity in early erythroblasts. Satisfaction from both tests (green) appears to be required to initiate a robust terminal differentiation process. (B) Both fitness checkpoints fail (red) in "unhealthy" cells (e.g., due to increased oxidative stress) containing high levels of misfolded and aggregated proteins that sequester Hsp70.

Quantitative proteomics highlight vital protein quality control functions related to mature erythrocyte survival

Mature erythrocytes show a remarkable ability to survive up to 120 days in the circulation⁶ while supporting a plethora of enzymatic reactions required for preserving the cytoskeletal ultrastructure, biomolecule trafficking across membranes and signal transduction (e.g., for maintaining lipid homeostasis⁹²). Apart from the mechanical stress insults that induce shape changes while navigating through the vasculature, these cells could be subjected to a range of environmental (e.g., chronic hypoxia at high altitudes, hyperosmotic shock, and energy depletion) or chemical (e.g., oxidative stress and high intracellular Ca^{2+} levels) stresses⁹³ that could trigger protein misfolding, damage and/or aggregation. Such conditions could potentially cause eryptosis, a process by which mature erythrocytes undergo apoptosis-like cell death. Unlike other cell types that contain stress-sensing and signaling pathways (e.g., HSF-1 transcription factor-mediated heat shock response) to produce large quantities of new chaperones to help buffer against such proteostasis insults,¹ mature erythrocytes that lack ribosomes have to utilize already existing PQC elements present in their vestigial proteome to counteract protein misfolding/aggregation.

Advancements in mass spectrometry-based quantitative analytical methods have identified over 2,600 proteins in the vestigial proteome of mature human red blood cells (2-5% of the progenitor proteome).⁹⁴ We performed an enrichment analysis on these proteins or protein classes focusing on function to uncover probable biological processes important for erythrocyte survival. We compared published label-free quantitative proteomics data obtained from complete cytosolic extracts of mature erythrocytes (originating from age-matched, healthy donors),⁹⁴ to human cells (unstressed Jurkat cells) that have not massively accumulated Hb and carbonic anhydrase, and neither eliminated their transcription and translation machineries, nor lost their endoplasmic reticulum (ER), nuclei and mitochondrial compartments (Figure 5; *Online Supplementary Tables S1-4*).⁹⁵ As expected, our analysis showed that mature erythrocytes (likely containing ~1% reticulocytes with ribosomes and ER),⁹⁴ are markedly enriched with Hb, carbonic anhydrase and antioxidant enzymes, such as catalases (Figure 5A). Our analysis also confirmed that mature erythrocytes are severely depleted in DNA polymerases, transcription factors, RNA polymerases, ribosomes, as well as nuclear, ER and mitochondrial proteins compared to Jurkat cells (Figure 5A). On average, the replacement of the proteome with high levels of Hb and carbonic anhydrases in mature erythrocytes should theoretically reduce the levels of any other given protein by ~280-fold in abundance compared to Jurkat cells.^{94,95} Thus, it is reasonable to assume that proteins or protein classes that are significantly less depleted than ~280-fold have been purposefully retained to sustain functions associated with the maintenance and survival of mature erythrocytes. For example, compared to Jurkat cells, the cytoskeletal proteins are 44-fold more abundant than the average non-Hb protein in erythrocytes thus supporting this view (Figure 5A). We also detected a high level of Hsp60 chaperones that facilitate in the folding and assembly of cytoskeletal proteins. The above observations highlight the critical role of these pro-

teins in maintaining cell shape and cytoskeletal integrity of red blood cells.

The role of Hsp70 in terminally differentiated erythrocytes

Molecular chaperones make up approximately 5% of the total protein mass of naïve mammalian cells, and up to 10% in stress-resistant cancer cells, attesting to their central role in maintaining cell viability. The Hsp70-JDP-NEF machinery alone contributes to ~1% of the total protein mass of most mammalian cells.⁹⁶ Comparatively, the chaperome of mature erythrocytes is 0.28% of the total protein mass (including Hb) (*Online Supplementary Tables S1-2*). The erythrocyte Hsp70-JDP-NEF machinery, however, accounts for about a third of the mature erythrocyte chaperome (0.1% of the total protein mass; Figure 5; *Online Supplementary Table S2*). From a proteostasis angle, it is somewhat puzzling as to why this particular chaperone system, which is conventionally thought to function in *de novo* folding of newly synthesized proteins,⁹⁷ is maintained at relatively high levels in terminally differentiated erythrocytes that lack protein-synthesizing capability.

Up to a certain point, protein repair is less costly than protein replacement

At the cellular level, life may evade protein decay by maintaining a subtle balance between ATP-fueled protein repair by unfolding chaperones and ATP-fueled protein replacement mediated by controlled degradation of irreversibly damaged proteins followed by transcription, translation, folding and assembly of new functional proteins. Noticeably, in terms of ATP cost, it is energetically cheaper to repair structurally damaged proteins with unfolding chaperones than to degrade them by the proteasome and synthesize replacements at the cost of at least two ATP molecules per peptide bond.³⁷

Mature erythrocytes are an extreme case of living cells that completely lack protein replacement mechanisms. This leaves protein repair as the sole mechanism to counteract the time-dependent entropic decay of labile proteins into aggregates and support erythrocyte survival in circulation. Intriguingly, we detected all the components of the Hsp70 chaperone system necessary for protein repair in the vestigial proteome of mature red blood cells. These include the constitutively expressed HSPA8, a selective set of JDP cochaperones (DNAJA and DNAJB) that recognize misfolded/aggregated proteins, and Hsp110-type nucleotide exchange factors that support protein disaggregation/refolding in human cells (Figure 5C; *Online Supplementary Tables S1-2*).^{82-84,86,98,99} When combined, the identified Hsp70 chaperone system components were 14-fold more enriched in mature erythrocytes with respect to Jurkat cells (Figure 5A, red bars). Interestingly, the DNAJA and DNAJB cochaperones showed significant qualitative rearrangements in mature erythrocytes, compared to Jurkat cells (Figures 5B and C). The JDP composition shifted from a DNAJA:DNAJB ratio of ~2:1 in Jurkat cells (Figure 5B) to a DNAJB class-dominated ratio (approximately DNAJA:DNAJB = 1:9) in erythrocytes (Figure 5C). Hsp110 cochaperones were also re-arranged in erythrocytes; HYOU1 (the ER-resident HSP110) and HSPH3 (APG-1, cytosolic) were considerably depleted, while the proportion of HSPH2 (APG-2, cytosolic) was only slightly decreased from ~9% (of the Hsp70/110 chaperome) in Jurkat cells to ~7% in total erythrocyte cytosol (Figures 5B and C). In

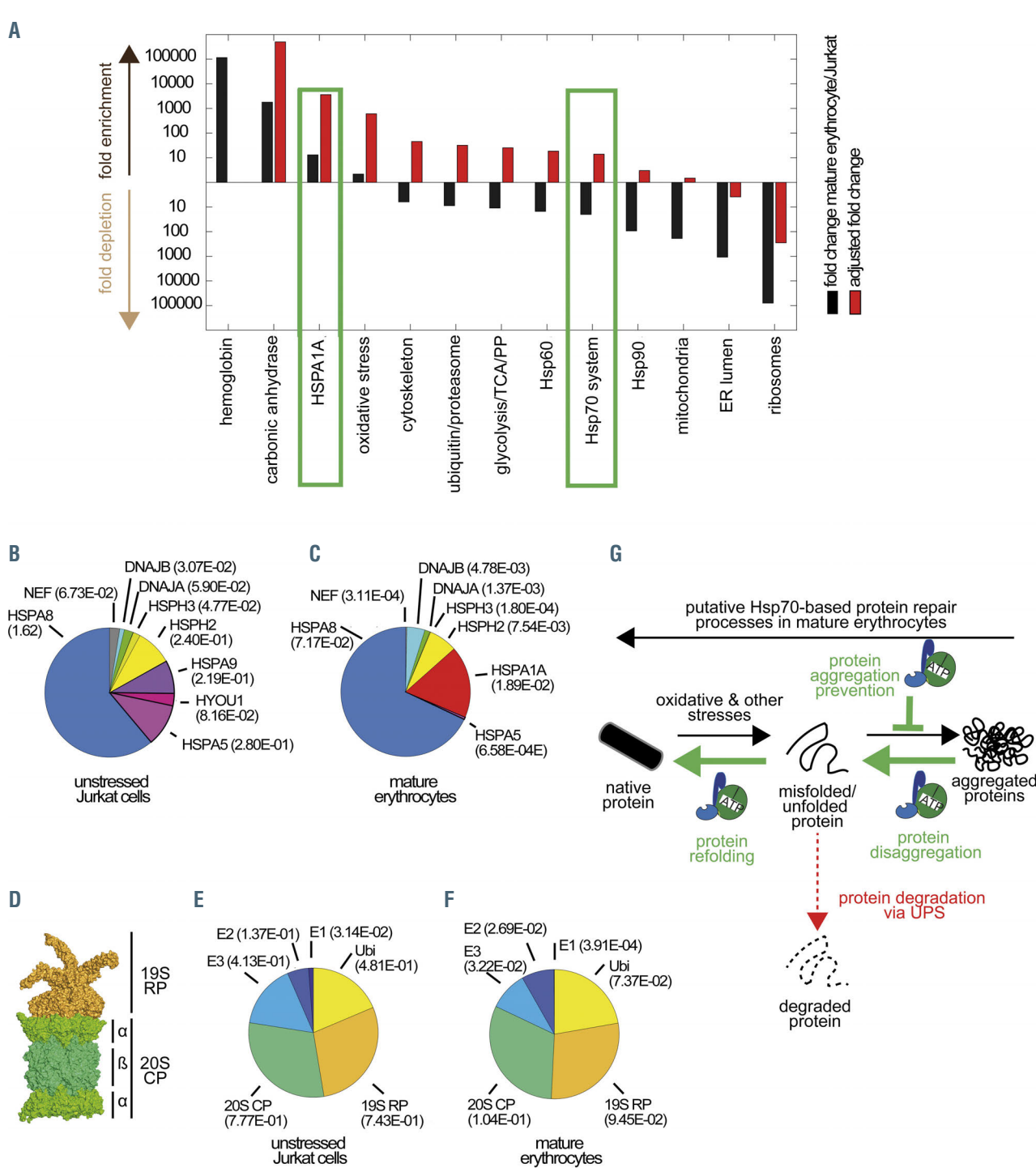


Figure 5. Hsp70 mediates protein repair function in mature erythrocytes. (A) Mass-fraction abundance of proteins in mature erythrocytes. Black bars indicate mass-wise enrichment or depletion of selected proteins and protein categories in total erythrocytes in comparison to unstressed Jurkat cells (control). Red bars indicate adjusted fold changes in the enrichment or depletion of selected proteins and protein categories normalized to the average abundance of all non-hemoglobin (Hb) proteins in total mature erythrocytes over Jurkat cells. Proteins linked to oxidative stress, cytoskeleton, ubiquitin/proteasome, glycolysis/tricarboxylic acid (TCA) cycle/pentose phosphate (PP), mitochondria, endoplasmic reticulum (ER) lumen and ribosomes were defined according to gene ontology annotations; the remaining categories (Hb, carbonic anhydrase, HSPA1A, Hsp70 system, Hsp60, Hsp90) were custom-defined. (B-C) Mass fractions of members of the Hsp70 system comprising of Hsp70, J-domain proteins (JDP) and nucleotide exchange factors (NEF) in unstressed Jurkat cells (B) and in mature erythrocytes (C). Values within brackets indicate mass fraction of Hsp70 chaperones and cochaperones as percent of the total proteome. NEF types include HSPBP1 and BAG-family proteins. Hsp110-type NEF vital for protein disaggregation (HSPH1-3) are indicated separately. A complete list of mass fractions of individual chaperones and cochaperones are provided in the *Online Supplementary Tables* S1-2. (D) Surface representation of the human 26S proteasome (PDB entry 5L4G). Core particle (CP) in green; regulatory particle (RP) in orange. (E-F) Mass fractions of members of the ubiquitin proteasome system (UPS) in unstressed Jurkat cells (E), and in mature erythrocytes (F). E1, E2 and E3 ubiquitin ligase enzymes indicated in different shades of blue. Ubiquitin (Ubi), CP, RP proteins are shown in yellow, green and orange, respectively. Values within brackets indicate mass fraction of the protein/protein groups as percent of the total proteome. Complete list of mass fractions of individual chaperones and cochaperones are provided in the *Online Supplementary Tables* S3-4. The analyzed proteomics datasets were obtained from Label-Free Quantification (LFQ) experiments.^{5,94,95,149} For each quantified protein/protein group, LFQ values were obtained from the MaxQuant software¹⁵⁰ and were proportional to the mass-wise abundance of the corresponding polypeptides. LFQ values were normalized by the sum of all LFQ values from a given sample and indicated as the relative mass-wise abundance of a protein/protein group and termed as mass fractions. (G) Putative Hsp70-based protein repair-only functions in mature erythrocytes.

essence, quantitative proteomic analysis revealed a strong bias towards maintaining a set of fully operational Hsp70 machineries conceivably functioning in specific protein repair activities important for the survival of mature erythrocytes (Figure 5G). We also noticed a clear enrichment of the stress-induced form of Hsp70, HSPA1A (13-fold more enriched than in Jurkat cells, and >3,500 times more abundant than the average non-Hb protein) in mature erythrocytes (Figures 5A and C). Analysis of the levels of this chaperone during red blood cell formation indicated that the HSPA1A is present 83-fold higher even in erythroblast progenitors compared to unstressed Jurkat cells, and then only decreases approximately 10-fold during terminal differentiation (Figure 2B; *Online Supplementary Figure S1*). The high levels of HSPA1A perhaps largely facilitate the blocking of erythroblasts from undergoing premature apoptosis during differentiation.^{89,91} However, in mature erythrocytes, HSPA1A may serve a different purpose where it could also form chaperone machines that primarily solubilize and repair misfolded/aggregated proteins. Functional studies are now required to deconvolute from the alternative, whereby some of the more abundant chaperones such as the Hsp70 linger in mature erythrocytes simply because of an incomplete proteome reduction.

We also noticed the retention of a fully functional UPS, perhaps more fine-tuned to the needs of mature erythrocyte maintenance (Figures 5A, D to F; *Online Supplementary Tables S3-4*). Although UPS proteins are 10-fold less abundant in erythrocytes than in Jurkat cells, they are 32-times less depleted than the average non-Hb protein (Figure 5A). A basal protein degradation system is likely needed to prevent the cytotoxic accumulation of terminally-damaged proteins in these cells (Figure 5G). As expected, the E2-E3 hybrid enzyme UBE2O was present in mature erythrocytes perhaps to more selectively target unpaired/damaged α -globin chains.²⁷ We also, however, observed a considerable enrichment of Cullin-RING E3 ubiquitin ligase family members. It is somewhat puzzling as to why such E3 ubiquitin ligases are retained in post-mitotic terminally differentiated erythrocytes, given that their functions are mainly associated with gene transcription, cell cycle and development.¹⁰⁰ In contrast, we observed the absence of E3 ubiquitin ligases that target misfolded proteins for degradation, such as members of the UBR family¹⁰¹⁻¹⁰³ and STUB1/CHIP, which directly binds and ubiquitinate Hsp70 substrates¹⁰⁴ (*Online Supplementary Tables S3-4*). This implies that protein degradation is considerably regulated and clearance of misfolded proteins might be kept to a minimal to further promote protein repair over proteolysis in mature erythrocytes. Importantly, we also detected an enrichment of metabolic enzymes required to support glycolysis and the pentose phosphate cycle. These catabolic and metabolic pathways are vital for importing and breaking down glucose to produce ATP. The ATP generated from an active glycolysis reaction could supply the energy needed to support (i) chaperone-based protein repair (ii) UPS-mediated protein degradation and (iii) active ion pumps required for maintaining the steep ion gradients across plasma membrane in erythrocytes. Taking everything into account, it is intriguing to speculate that the retained Hsp70 chaperone system together with the UPS is cogged towards primarily repairing proteins in mature red blood cells. This is of particular interest given the wide array of hematological diseases associated with Hb aggregation.

Hsp70 associated blood disorders

The Hsp70 chaperone has been implicated in the pathophysiology of several prominent blood disorders in humans. Below we describe how this chaperone system may act as an important modifier which influences both the severity and progression of hematological disorders such as β -thalassemia, sickle cell disease, myelodysplastic syndromes, polycythemia vera and Diamond Blackfan anemia. Importantly, the ineffective erythropoiesis observed in these disorders is intimately linked to several key functions of the Hsp70 chaperone system in red blood cell differentiation.

Mislocalization of Hsp70 drives ineffective erythropoiesis in β -thalassemia

β -thalassemia is an autosomal recessive disease with three clinical phenotypes: β -thalassemia major (severe anemia), intermedia (mild to moderate anemia) and minor (clinically asymptomatic, patients act as "carriers" of the disease). One hallmark of this disease is the premature apoptosis of differentiating erythroblasts in the bone marrow and the rapid destruction of circulating erythrocytes by the reticuloendothelial system. β -thalassemia arises from a series of point mutations and deletions that reduce or prevent the production of functional β -globin. The decrease in β -globin levels correlates with the severity of the condition.¹⁰⁵ Apart from the mutation driven β -globin dosage effect, it was also found that the co-inheritance of the genetic variants of the globin genes has a modifying effect on the severity of the disease,^{105,106} which could be partly attributed to protein misfolding and aggregation. At a mechanistic level, the decrease in β -globin levels leads to increased aggregation of unpaired α -globin chains,¹⁰⁷ which triggers acute oxidative stress in erythroblasts leading to premature apoptosis.¹⁰⁸

The Hsp70 chaperone system plays a pivotal role in the pathogenesis of β -thalassemia. During erythropoiesis, the stress-induced form of Hsp70 (HSPA1A) translocates in to the nucleus to protect GATA-1 from caspase-3 cleavage and initiate terminal differentiation (Figure 4).⁶⁵ However, in β -thalassemia, this translocation step is largely impeded as a result of Hsp70 being sequestered into cytosolic aggregates formed by excess unpaired α -globin chains.⁶⁶ This ultimately results in GATA-1 cleavage, which triggers ineffective erythropoiesis leading to anemia. In parallel, sequestration of cytosolic Hsp70 by protein aggregates could also i) compromise the overall chaperoning capacity of early erythroblasts and ii) affect protein synthesis due to HRI activation.⁷⁶ Although, a reduction in protein synthesis may temporally help prevent further accumulation of aggregate-prone proteins, such as α -globin chains,⁷⁶ it may also considerably affect the overall Hb biogenesis in these already compromised red blood cells.⁷⁷ This mechanism may partly contribute to microcytosis that causes mild anemia in β -thalassemia minor.

A recent breakthrough study showed an unexpected suppression of the disease phenotype in a mouse model of β -thalassemia intermedia when UBE2O, which helps clear unpaired α -globin chains, was knocked out ($Hbb^{hs3/4} Ube2o^{-/-}$).²⁷ The mitigation of anemia in these animals resulted from an increase in erythrocyte levels. Intriguingly, the erythrocytes generated in $Hbb^{hs3/4} Ube2o^{-/-}$ animals were relatively healthier to those that were produced in $Hbb^{hs3/4}$ genetic background. The $Hbb^{hs3/4} Ube2o^{-/-}$

erythrocytes also showed a dramatic decrease in the levels of aggregated Hb. The authors speculated that the observed decrease in α -globin aggregation resulted from an increase in eIF2 α phosphorylation, which reduced the production of globin chains (approximately 20% and 40% reduction in α - and β -globin, respectively, compared to control animals).²⁷ However, the steady-state α -globin: β -globin ratio in the soluble protein fraction, in which the aggregate prone α -globin was still largely in excess, did not change between *Hbb*^{h/s}/⁺ and *Hbb*^{h/s}/⁺ *Ube2o*^{-/-} cells. A closer look at the chaperone levels in the *Hbb*^{h/s}/⁺ *Ube2o*^{-/-} erythrocytes suggests an alternative explanation. The study shows that the deletion of UBE2O resulted in elevated levels of AHSP. Similarly, the Hsp70 and Hsp90 chaperone systems were also induced in these cells.²⁷ Such chaperone inductions could boost the protein repair capacity consequently leading to the observed decrease in α -globin precipitation in *Hbb*^{h/s}/⁺ *Ube2o*^{-/-} erythroblasts despite defects in degrading excess α -globin. The moderate decrease in α -globin synthesis may also help reduce the burden on PQC machineries contributing to the remarkable rescue of erythroblasts in the *Hbb*^{h/s}/⁺ *Ube2o*^{-/-} animals. Based on the findings from our proteomics data analysis (Figure 5), we speculate that the degradation of a certain amount of damaged proteins, despite the inability to replace them, might be tolerated and perhaps advantageous for the long-term survival of mature erythrocytes under healthy conditions. However, in unhealthy erythroblasts (e.g., early β -thalassemic erythroblasts¹⁰⁸), a strong induction of the UPS due to stress could generate an aberrant PQC condition where even foldable conformers of proteins might be partitioned towards rapid degradation.¹⁰¹ Such a condition could disrupt the fine balance between protein repair and clearance in these cells (Figure 5G). A careful study of the potential misregulation of PQC pathways in erythroblasts is required to fully comprehend the underlining mechanism of pathology in β -thalassemia. It is tempting to speculate that even slight increases in the levels of certain Hsp70 machineries at pre- or very early stages of erythropoiesis may favorably tilt the folding equilibrium of globin chains and minimize the formation of cytotoxic Hb aggregates. Such chaperone manipulations at clinical level could result in reducing the symptoms of β -thalassemia.

Hsp70, a key modulator of inflammation in sickle cell disease?

Sickle cell disease (SCD) is another autosomal recessive genetic disorder associated with chronic anemia. SCD results from massive cyclic-polymerization of a structurally aberrant variant of adult Hb S (HbS) under hypoxic conditions. The resulting HbS fibers deform mature erythrocytes into rigid "sickle" shaped cells that aggregate and readily undergo premature destruction in the vasculature. Whether these conditionally formed reversible protein fibers (distinct from amyloid-type fibers formed e.g., in neurodegenerative disorders) trigger any proteostasis insult involving the Hsp70 system is unknown. The Hsp70 chaperone, however, may play an important role in activating the inflammatory response in SCD.^{109,110} Stressed cells have been observed to secrete Hsp70 into the extracellular matrix.¹⁰⁹ Immune cells generate specific peptides from secreted Hsp70 that act as key mediators of stress-induced inflammation.¹¹¹⁻¹¹³ A considerable buildup of circulating Hsp70 levels have been detected in patients with SCD¹⁰⁹

suggesting that there is an active secretion of Hsp70 by blood cells. Under hypoxic conditions, sickled erythrocytes show differential recruitment of the stress-inducible HSPA1A to the cell membrane,¹¹⁴ possibly representing an early step in this secretion process. Interestingly, a similar observation was recently noted in β -thalassemia intermedia.¹¹⁵ Together, the observations suggest that the high levels of extracellularly circulating Hsp70 may serve as an important immune modulator that trigger inflammation in these hemoglobinopathies, leading to increased red blood cell destruction by macrophages.

Haploinsufficiency of Hsp70 associated with myelodysplastic syndromes

Myelodysplastic syndromes (MDS) are a heterogeneous, but closely related group of hematopoietic malignancies characterized by ineffective erythropoiesis leading to peripheral blood cytopenias.¹¹⁶ The mitochondria localized HSPA9 is strongly implicated as a protein that contributes to MDS. The HSPA9 locus (5q31.2) is frequently deleted in patients with MDS, leading to a haploinsufficiency of this chaperone.¹¹⁷ Recent work showed that mutating HSPA9 causes an MDS-like phenotype in zebrafish¹¹⁸ and a knockdown in rodents results in considerable delay in erythroid progenitor maturation.⁵⁸ HSPA9 is implicated in the pathogenesis of MDS at two levels. First, the haploinsufficiency of the chaperone may contribute to the phenotype as a result of altered mitochondrial import and refolding of heme-synthesis enzymes required for heme biogenesis during erythropoiesis.⁵⁵ Second, a decrease in HSPA9 could activate p53, a nuclear transcription factor, resulting in cell cycle arrest and premature apoptosis of hematopoietic progenitor cells.⁵⁷

Further, a recent study demonstrated that defects in EPO induced nuclear translocation of Hsp70 in erythroblasts could also be an important driver of these disorders.¹¹⁹ The ineffective erythropoiesis observed in MDS could largely be reversed by protecting GATA-1 from caspase 3 cleavage using an Hsp70 variant (lacking the nuclear export signal) that accumulates in the nucleus.¹¹⁹ Protein aggregates containing aberrant p53 (as in cancer cells)^{120,121} have been detected in erythroblasts in some forms of MDS.¹²² These aggregates could conceivably sequester Hsp70, thus triggering ineffective erythropoiesis in a similar mechanism to that in β -thalassemia. Alternatively, defective EPO signaling or/and other mechanisms affecting nuclear transportation of proteins, could lead to the Hsp70 trafficking defect observed in MDS.¹¹⁹

Hsp70 is a modifier of polycythemia vera

Polycythemia vera is a hyperproliferative disorder characterized by increased synthesis of red blood cells resulting in hyperviscosity of whole-blood. Recent proteomic studies on polycythemia vera have shown that increased levels of Hsp70 along with Hsp90 stabilize JAK2 kinase. This triggers a prolonged aberrant activation of the kinase, which results in massive proliferation of erythroid progenitors and abnormal stimulation of erythropoiesis.¹²³⁻¹²⁶ Inhibition of either Hsp70 or Hsp90 has been demonstrated to promote the apoptosis of the abnormally proliferating erythroid progenitors and is currently being investigated as a potential therapeutic approach to delay the progression of this disease in humans.^{123,126}

Haploinsufficiency of Hsp70 modulates Diamond Blackfan anemia

Diamond Blackfan anemia (DBA) is a rare congenital bone marrow failure syndrome resulting from ineffective erythropoiesis.¹²⁷ In this disease, erythroid differentiation arrests between BFU-E and CFU-E stages.¹²⁸ More than 70% of the cases of DBA occur due to haploinsufficiency of genes that encode for the small and large ribosomal subunit proteins.¹²⁹⁻¹³¹ The defective ribosome biogenesis triggers ineffective erythropoiesis in part due to the decreased production of GATA-1.¹³² This is further promoted by imbalances in globin chain and heme synthesis leading to α -globin aggregation and induction of oxidative stress in erythroblasts¹³³ similar to β -thalassemia. Additionally, in DBA associated with RPL11, but not RPL19 haploinsufficiency, the Hsp70 chaperone is considerably degraded in the erythroblasts via the UPS.^{133,134} The reason for the rapid degradation of Hsp70 in some permutations of this disorder remains unclear. Recent work shows that aberrations in chromatin organization resulting from low levels of the global chromatin organizer SATB1 prevents the induction of Hsp70 in early erythroblasts in DBA.¹³⁵ Together, these observations suggest that the differential Hsp70 expression and degradation rates may have considerable effect on red blood cell viability, differentiation and Hb biogenesis, thus partly explaining the variability in the observed phenotypes of DBA. Remarkably, the restoration of Hsp70 levels in affected erythroblasts inhibits premature apoptosis and substantially restores erythropoiesis in DBA,^{133,134} thus providing an important therapeutic avenue for the treatment of this blood disorder.

A predicted pathological role for Hsp70 in congenital sideroblastic anemias

Congenital sideroblastic anemias (CSA) are inherited rare blood disorders characterized by erythroblasts displaying ring sideroblasts formed by the pathological depositions of iron in mitochondria. Patients with CSA show a significant reduction in the regeneration of erythrocytes leading to anemic conditions. The ineffective erythropoiesis in CSA is caused by defects in iron-sulfur cluster biogenesis essential for a broad range of cellular functions. Patients with CSA show mutations in genes directly (e.g., *GLRX5*, *ABCB7*)^{136,137} and indirectly (e.g., *HSPA9*)^{138,139} associated with this biosynthetic pathway. It is important to note that the ring sideroblasts are uncommon in MDS cases that are also associated with *HSPA9* deletion mutations (see above), but whether this is due to

an epistatic suppression by another modifier remains to be investigated.¹³⁸ As in CSA, HSPA9 may also play an indirect role in some forms of dyserythropoietic anemias that are also characterized by pathological iron-loading defects and ineffective erythropoiesis¹⁴⁰ and warrants further investigation.

Age-associated anemia

Aging is attributed to a decline in hematopoiesis with high incidents of anemia.¹⁴¹ The viability and self-renewal of HSC/early erythroid progenitors depend on maintaining robust PQC activity and high levels of Hsp70.^{142,143,144} These abilities decline in stem cells during aging.^{145,146} As a consequence, Hsp70-mediated functions such as maintenance of erythroid dormancy, cell cycle quiescence and cell cycle entry may breakdown leading to an age-related exhaustion of HSC.

Concluding remarks

Recent findings have considerably broadened our understanding of the multifaceted roles of Hsp70 in erythrocyte differentiation and how deficiencies in its activity modify several blood disorders in humans. The tuning of the Hsp70 chaperone system to cater to different PQC needs during erythropoiesis sheds extremely valuable insight on cell repair and viability and provides a conceptual framework for investigating chaperone-based therapeutic avenues for a wide spectrum of blood disorders.

Disclosures

No conflicts of interest to disclose.

Contributions

NBN conceptualized the work. BF, PG and NBN analyzed published proteomics data. YM, BF, SJ, PG and NBN wrote and edited the manuscript.

Acknowledgements

We thank Andrew Perkins (Australian Center for Blood Diseases) David Ron (Cambridge Institute for Medical Research) for critically reading the manuscript.

Funding

This work was supported by a special Recruitment Grant from the Monash University Faculty of Medicine Nursing and Health Sciences with funding from the State Government of Victoria and the Australian Government to NBN.

References

1. Labbadia J, Morimoto RI. The biology of proteostasis in aging and disease. *Annu Rev Biochem*. 2015;84:435-464.
2. Vonk WI, Rainbolt TK, Dolan PT, Webb AE, Brunet A, Frydman J. Differentiation drives widespread rewiring of the neural stem cell chaperone network. *Mol Cell*. 2020;78:329-345.
3. Gautier E-F, Ducamp S, Leduc M, et al. Comprehensive proteomic analysis of human erythropoiesis. *Cell Rep*. 2016;16(5):1470-1484.
4. Banerji SS, Theodorakis N, Morimoto RI. Heat shock-induced translational control of HSP70 and globin synthesis in chicken reticulocytes. *Mol Cell Biol*. 1984;4(11):2437-2448.
5. Gautier EF, Leduc M, Cochet S, et al. Absolute proteome quantification of highly purified populations of circulating reticulocytes and mature erythrocytes. *Blood Adv*. 2018;2(20): 2646-2657.
6. Hall JE. Red blood cells, anemia and polycythemia. Guyton and Hall Textbook of Medical Physiology 13 ed. Philadelphia: Elsevier Health Sciences; 2015. Chapter 33:445-454.
7. Higgins JM. Red blood cell population dynamics. *Clin Lab Med*. 2015;35(1):43-57.
8. Li H, Natarajan A, Ezike J, et al. Single cell resolution of glucocorticoid effects on erythroid progenitor cells. *Blood*. 2018;132 (Suppl 1):S751.
9. Peslak SA, Wenger J, Bernis JC, et al. EPO-mediated expansion of late-stage erythroid progenitors in the bone marrow initiates recovery from sublethal radiation stress. *Blood*. 2012;120(12):2501-2511.
10. Wierenga AT, Vellenga E, Schuringa JJ. Down-regulation of GATA1 uncouples STAT5-induced erythroid differentiation from stem/progenitor cell proliferation. *Blood*. 2010;115(22):4367-4376.
11. Chiba T, Ikawa Y, Todokoro K. GATA-1 transactivates erythropoietin receptor gene, and erythropoietin receptor-mediated signals enhance GATA-1 gene expression. *Nucleic Acids Res*. 1991;19(14):3843-3848.
12. Bain BJ, Bates I, Laffan MA. Reference

ranges and normal values. In: Lewis SM, editor. Dacie and Lewis Practical Haematology. 12 ed. China: Elsevier 2017:2-17.

13. Roux-Dalval F, Gonzalez de Peredo A, Simo C, et al. Extensive analysis of the cytoplasmic proteome of human erythrocytes using the peptide ligand library technology and advanced mass spectrometry. *Mol Cell Proteomics*. 2008;7(11):2254-2269.
14. Goloubinoff P, Sassi AS, Fauvet B, Barducci A, De Los Rios P. Chaperones convert the energy from ATP into the nonequilibrium stabilization of native proteins. *Nat Chem Biol*. 2018;14(4):388-395.
15. Stefani M. Protein misfolding and aggregation: new examples in medicine and biology of the dark side of the protein world. *Biochim Biophys Acta*. 2004;1739(1):5-25.
16. Voon HPJ, Vadolas J. Controlling α -globin: a review of α -globin expression and its impact on β -thalassemia. *Haematologica*. 2008;93(12):1868-1876.
17. Bank A. Hemoglobin synthesis in β -thalassemia: the properties of the free α -chains. *J Clin Invest*. 1968;47(4):860-866.
18. Fibach E, Dana M. Oxidative stress in beta-thalassemia. *Mol Diagn Ther*. 2019;23(2):245-261.
19. Feng L, Gell DA, Zhou S, et al. Molecular mechanism of AHSP-mediated stabilization of α -hemoglobin. *Cell*. 2004;119(5):629-640.
20. Mollan TL, Khandros E, Weiss MJ, Olson JS. Kinetics of α -globin binding to α -hemoglobin stabilizing protein (AHSP) indicate preferential stabilization of hemicrome folding intermediate. *J Biol Chem*. 2012;287(14):11338-11350.
21. Weiss MJ, Zhou S, Feng L, et al. Role of alpha hemoglobin stabilizing protein in normal erythropoiesis and β -thalassemia. *Ann NY Acad Sci*. 2005;1054(1):103-117.
22. Barrett KE, Barman SM, Brooks H, Yuan J. Ganong's review of medical physiology. 26 ed. New York: McGraw-Hill Medical; 2019:543-551.
23. Drummond DA, Wilke CO. The evolutionary consequences of erroneous protein synthesis. *Nat Rev Genet*. 2009;10(10):715.
24. Camaschella C, Hoffbrand AV, Hershko C. Iron metabolism, iron deficiency and disorders of haem synthesis. *Postgrad Haematol*. 2015;21-39.
25. Kruszewski M. Labile iron pool: the main determinant of cellular response to oxidative stress. *Mutat Res*. 2003;551(1-2):81-92.
26. Yanagitani K, Juszkiewicz S, Hegde RS. UBE2O is a quality control factor for orphans of multiprotein complexes. *Science*. 2017;357(6350):472-475.
27. Nguyen AT, Prado MA, Schmidt PJ, et al. UBE2O remodels the proteome during terminal erythroid differentiation. *Science*. 2017;357(6350):471.
28. Pilla E, Schneider K, Bertolotti A. Coping with protein quality control failure. *Annu Rev Cell Dev Biol*. 2017;33:439-465.
29. Mizuno S. Temperature sensitivity of protein synthesis initiation: inactivation of a ribosomal factor by an inhibitor formed at elevated temperatures. *Arch Biochem Biophys*. 1977;179(1):289-301.
30. Rosenzweig R, Nillegoda NB, Mayer MP, Bukau B. The Hsp70 chaperone network. *Nat Rev Mol Cell Biol*. 2019;11:665-680.
31. Kampinga HH, Craig EA. The HSP70 chaperone machinery: J-proteins as drivers of functional specificity. *Nat Rev Mol Cell Biol*. 2010;11(8):579-592.
32. Kityk R, Kopp J, Mayer MP. Molecular mechanism of J-domain-triggered ATP hydrolysis by Hsp70 chaperones. *Mol Cell*. 2018;69(2):227-237.
33. Cyr DM. Swapping nucleotides, tuning Hsp70. *Cell*. 2008;133(6):945-947.
34. Finka A, Mattoo RU, Goloubinoff P. Experimental milestones in the discovery of molecular chaperones as polypeptide unfolding enzymes. *Annu Rev Biochem*. 2016;85:715-742.
35. De Los Rios P, Barducci A. Hsp70 chaperones are non-equilibrium machines that achieve ultra-affinity by energy consumption. *Elife*. 2014;3:e02218.
36. Schrödinger E. What is life? The physical aspect of the living cell. Cambridge University Press; 1944.
37. Sharma SK, De los Rios P, Christen P, Lustig A, Goloubinoff P. The kinetic parameters and energy cost of the Hsp70 chaperone as a polypeptide unfoldase. *Nat Chem Biol*. 2010;6(12):914-920.
38. Trinklein ND, Chen WC, Kingston RE, Myers RM. Transcriptional regulation and binding of heat shock factor 1 and heat shock factor 2 to 32 human heat shock genes during thermal stress and differentiation. *Cell Stress Chaperon*. 2004;9(1):21.
39. Saretzki G, Armstrong L, Leake A, Lako M, von Zglinicki T. Stress defense in murine embryonic stem cells is superior to that of various differentiated murine cells. *Stem Cells*. 2004;22(6):962-971.
40. Matsumoto A, Takeishi S, Kanie T, et al. p57 is required for quiescence and maintenance of adult hematopoietic stem cells. *Cell Stem Cell*. 2011;9(3):262-271.
41. Zou P, Yoshihara H, Hosokawa K, et al. p57kip2 and p27kip1 cooperate to maintain hematopoietic stem cell quiescence through interactions with Hsc70. *Cell Stem Cell*. 2011;9(3):247-261.
42. Tesio M, Trumpp A. Breaking the cell cycle of HSCs by p57 and friends. *Cell Stem Cell*. 2011;9(3):187-192.
43. Böcking T, Aguet F, Harrison SC, Kirchhausen T. Single-molecule analysis of a molecular disassembler reveals the mechanism of Hsc70-driven clathrin uncoating. *Nat Struct Mol*. 2011;18(3):295.
44. Chakraborty A, Mukherjee S, Chattopadhyay R, Roy S, Chakrabarti S. Conformational adaptation in the *E. coli* sigma 32 protein in response to heat shock. *J Phys Chem*. 2014;118(18):4798-4802.
45. Marcinowski M, Höller M, Feige MJ, Baerend D, Lamb DC, Buchner J. Substrate discrimination of the chaperone BiP by autonomous and cochaperone-regulated conformational transitions. *Nat Struct Cell Biol*. 2011;18(2): 150.
46. Zhang J, Socolovsky M, Gross AW, Lodish HF. Role of Ras signaling in erythroid differentiation of mouse fetal liver cells: functional analysis by a flow cytometry-based novel culture system. *Blood*. 2003;102(12):3938-3946.
47. Han X, Zhang J, Peng Y, et al. Unexpected role for p19INK4d in posttranscriptional regulation of GATA1 and modulation of human terminal erythropoiesis. *Blood*. 2017;129(2):226-237.
48. Sterrenberg JN, Blatch GL, Edkins AL. Human DNAJ in cancer and stem cells. *Cancer Lett*. 2011;312(2):129-142.
49. Zhang Y, Yang Z, Cao Y, et al. The Hsp40 family chaperone protein DnaJ β 6 enhances Schlafin1 nuclear localization which is critical for promotion of cell-cycle arrest in T-cells. *Biochem J*. 2008;413(2):239-250.
50. Watson ED, Mattar P, Schuurmans C, Cross JC. Neural stem cell self-renewal requires the Mrj co-chaperone. *Dev Dynam*. 2009;238(10):2564-2574.
51. Ludwig LS, Cho H, Wakabayashi A, et al. Genome-wide association study follow-up identifies cyclin A2 as a regulator of the transition through cytokinesis during terminal erythropoiesis. *Am J Hematol*. 2015;90(5):386-391.
52. Sankaran VG, Ludwig LS, Sicinska E, et al. Cyclin D3 coordinates the cell cycle during differentiation to regulate erythrocyte size and number. *Genes Dev*. 2012;26(18):2075-2087.
53. Arai A, Kanda E, Miura O. Rac is activated by erythropoietin or interleukin-3 and is involved in activation of the Erk signaling pathway. *Oncogene*. 2002;21(17):2641.
54. Song H, Kim W, Kim S-H, Kim K-T. VRK3-mediated nuclear localization of HSP70 prevents glutamate excitotoxicity-induced apoptosis and A β accumulation via enhancement of ERK phosphatase VHR activity. *Sci Rep*. 2016;6:38452.
55. Shan Y, Cortopassi G. Mitochondrial Hsp90/Mortalin regulates erythroid differentiation via iron-sulfur cluster assembly. *Mitochondrion*. 2016;26:94-103.
56. Yamamoto H, Momose T, Yatsukawa Y-i, et al. Identification of a novel member of yeast mitochondrial Hsp70-associated motor and chaperone proteins that facilitates protein translocation across the inner membrane. *FEBS Lett*. 2005;579(2):507-511.
57. Liu T, Krysiak K, Shirai CL, et al. Knockdown of HSPA9 induces TP53-dependent apoptosis in human hematopoietic progenitor cells. *PLoS One*. 2017;12(2):e0170470.
58. Chen TH-P, Kambal A, Krysiak K, et al. Knockdown of Hsp90, a del (5q31.2) gene, results in a decrease in hematopoietic progenitors in mice. *Blood*. 2011;117(5):1530-1539.
59. Weiss MJ, dos Santos CO. Chaperoning erythropoiesis. *Blood*. 2009;113(10):2136-2144.
60. Zermati Y, Garrido C, Amsellem S, et al. Caspase activation is required for terminal erythroid differentiation. *J Exp Med*. 2001;193(2):247-254.
61. Kolbus A, Pilat S, Husak Z, et al. Raf-1 antagonizes erythroid differentiation by restraining caspase activation. *J Exp Med*. 2002;196(10):1347-1353.
62. Cande C, Vahsen N, Garrido C, Kroemer G. Apoptosis-inducing factor (AIF): caspase-independent after all. *Cell Death Differ*. 2004;11(6):591.
63. Gurbuxani S, Schmitt E, Cande C, et al. Heat shock protein 70 binding inhibits the nuclear import of apoptosis-inducing factor. *Oncogene*. 2003;22(43):6669.
64. Lui JC-K, Kong S-K. Heat shock protein 70 inhibits the nuclear import of apoptosis-inducing factor to avoid DNA fragmentation in TF-1 cells during erythropoiesis. *FEBS Lett*. 2007;581(1):109-117.
65. Ribeil JA, Zermati Y, Vandekerckhove J, et al. Hsp70 regulates erythropoiesis by preventing caspase-3-mediated cleavage of GATA-1. *Nature*. 2007;445(7123):102-105.
66. Arlet JB, Ribeil JA, Guillemin F, et al. HSP70 sequestration by free alpha-globin promotes ineffective erythropoiesis in beta-thalassemia. *Nature*. 2014;514(7521):242-246.
67. Gregory T, Yu C, Ma A, Orkin SH, Blobel GA, Weiss MJ. GATA-1 and erythropoietin cooperate to promote erythroid cell survival by regulating bcl-xL expression. *Blood*. 1999;94(1):87-96.
68. de Thonel A, Vandekerckhove J, Lanneau D, et al. HSP27 controls GATA-1 protein level during erythroid cell differentiation. *Blood*. 2010;116(1):85-96.
69. Ghosh A, Garee G, Sweeny EA, Nakamura Y, Stuehr DJ. Hsp90 chaperones hemoglobin

maturation in erythroid and nonerythroid cells. *Proc Natl Acad Sci U S A.* 2018;115(6):E1117-E1126.

70. Kihm AJ, Kong Y, Hong W, et al. An abundant erythroid protein that stabilizes free α -haemoglobin. *Nature.* 2002;417(6890):758.

71. Liu S, Bhattacharya S, Han A, et al. Heme-regulated eIF2 α kinase is necessary for adaptive gene expression in erythroid precursors under the stress of iron deficiency. *Br J Haematol.* 2008;143(1):129-137.

72. Zhang S, Macias-Garcia A, Ulirsch JC, et al. HRI coordinates translation necessary for protein homeostasis and mitochondrial function in erythropoiesis. *eLife.* 2019;8:e46976.

73. Han AP, Yu C, Lu L, et al. Heme-regulated eIF2 α kinase (HRI) is required for translational regulation and survival of erythroid precursors in iron deficiency. *EMBO J.* 2001;20(23):6909-6918.

74. Thulasiraman V, Xu Z, Uma S, Gu Y, Chen JJ, Matts RL. Evidence that Hsc70 negatively modulates the activation of the heme-regulated eIF2 α kinase in rabbit reticulocyte lysate. *Eur J Biochem.* 1998;255(3):552-562.

75. Uma S, Thulasiraman V, Matts RL. Dual role for Hsc70 in the biogenesis and regulation of the heme-regulated kinase of the alpha subunit of eukaryotic translation initiation factor 2. *Mol Cell Biol.* 1999;9:5861-5871.

76. Han A-P, Fleming MD, Chen J-J. Heme-regulated eIF2 α kinase modifies the phenotypic severity of murine models of erythropoietic protoporphyrin and β -thalassemia. *J Clin Invest.* 2005;115(6):1562-1570.

77. Lu L, Han A-P, Chen J-J. Translation initiation control by heme-regulated eukaryotic initiation factor 2 α kinase in erythroid cells under cytoplasmic stresses. *Mol Cell Biol.* 2001;21(23):7971-7980.

78. Suragani RN, Zachariah RS, Velazquez JG, et al. Heme-regulated eIF2 α kinase activated Atf4 signaling pathway in oxidative stress and erythropoiesis. *Blood.* 2012;119(22):5276-5284.

79. Zhang S, Macias-Garcia A, Velazquez J, Paltrinieri E, Kaufman RJ, Chen J-J. HRI coordinates translation by eIF2 α P and mTORC1 to mitigate ineffective erythropoiesis in mice during iron deficiency. *Blood.* 2018;131(4):450-461.

80. Morimoto R, Fodor E. Cell-specific expression of heat shock proteins in chicken reticulocytes and lymphocytes. *J Cell Biol.* 1984;99(4):1316-1323.

81. Lee GJ, Roseman AM, Saibil HR, Vierling E. A small heat shock protein stably binds heat-denatured model substrates and can maintain a substrate in a folding-competent state. *EMBO J.* 1997;16(3):659-671.

82. Nillegoda NB, Wentink AS, Bukau B. Protein disaggregation in multicellular organisms. *Trends Biochem Sci.* 2018;43(4):285-300.

83. Rampelt H, Kirstein-Miles J, Nillegoda NB, et al. Metazoan Hsp70 machines use Hsp110 to power protein disaggregation. *EMBO J.* 2012;31(21):4221-4235.

84. Mattoo RU, Sharma SK, Priya S, Finka A, Goloubinoff P. Hsp110 is a bona fide chaperone using ATP to unfold stable misfolded polypeptides and reciprocally collaborate with Hsp70 to solubilize protein aggregates. *J Biol Chem.* 2013;288(29):21399-21411.

85. Nillegoda NB, Kirstein J, Szlachcic A, et al. Crucial HSP70 co-chaperone complex unlocks metazoan protein disaggregation. *Nature.* 2015;524(7564):247.

86. Nillegoda NB, Stank A, Malinvernini D, et al. Evolution of an intricate J-protein network driving protein disaggregation in eukaryotes. *Elife.* 2017;6:e24560.

87. Kirstein J, Arnsburg K, Scior A, et al. In vivo properties of the disaggregase function of J-proteins and Hsc70 in *Caenorhabditis elegans* stress and aging. *Aging Cell.* 2017;16(6):1414-1424.

88. Beere HM, Green DR. Stress management—heat shock protein-70 and the regulation of apoptosis. *Trends Cell Biol.* 2001;11(1):6-10.

89. Li C-Y, Lee J-S, Ko Y-G, Kim J-I, Seo J-S. Heat shock protein 70 inhibits apoptosis downstream of cytochrome c release and upstream of caspase-3 activation. *J Biol Chem.* 2000;275(33):25665-25671.

90. Bivik C, Rosdahl I, Öllinger K. Hsp70 protects against UVB induced apoptosis by preventing release of cathepsins and cytochrome c in human melanocytes. *Carcinogenesis.* 2007;28(3):537-544.

91. Gao T, Newton AC. The turn motif is a phosphorylation switch that regulates the binding of Hsp70 to protein kinase C. *J Biol Chem.* 2002;277(35):31585-31592.

92. Mohandas N, Gallagher PG. Red cell membrane: past, present, and future. *Blood.* 2008;112(10):3939-3948.

93. Pretorius E, du Plooy JN, Bester J. A comprehensive review on eryptosis. *Cell Physiol Biochem.* 2016;39(5):1977-2000.

94. Bryk AH, Wiśniewski JR. Quantitative analysis of human red blood cell proteome. *J Proteome Res.* 2017;16(8):2752-2761.

95. Finka A, Sood V, Quadroni M, De Los Rios P, Goloubinoff P. Quantitative proteomics of heat-treated human cells show an across-the-board mild depletion of housekeeping proteins to massively accumulate few HSPs. *Cell Stress Chaperon.* 2015;20(4):605-620.

96. Finka A, Goloubinoff P. Proteomic data from human cell cultures refine mechanisms of chaperone-mediated protein homeostasis. *Cell Stress Chaperon.* 2013;18(5):591-605.

97. Balchin D, Hayter-Hartl M, Hartl FU. In vivo aspects of protein folding and quality control. *Science.* 2016;353(6294):aac4354.

98. Nillegoda NB, Bukau B. Metazoan Hsp70-based protein disaggregases: emergence and mechanisms. *Front Mol Biosci.* 2015;2(57):eCollection.

99. Shorter J. The mammalian disaggregase machinery: Hsp110 synergizes with Hsp70 and Hsp40 to catalyze protein disaggregation and reactivation in a cell-free system. *PLoS One.* 2011;6(10):e26319.

100. Sarikas A, Hartmann T, Pan Z-Q. The cullin protein family. *Genome Biol.* 2011;12(4):220.

101. Nillegoda NB, Theodoraki MA, Mandal AK, et al. Ubr1 and Ubr2 function in a quality control pathway for degradation of unfolded cytosolic proteins. *Mol Biol Cell.* 2010;21(13):2102-2116.

102. Theodoraki MA, Nillegoda NB, Saini J, Caplan AJ. A network of ubiquitin ligases is important for the dynamics of misfolded protein aggregates in yeast. *J Biol Chem.* 2012;287(28):23911-23922.

103. Sultana R, Theodoraki MA, Caplan AJ. UBR1 promotes protein kinase quality control and sensitizes cells to Hsp90 inhibition. *Exp Cell Res.* 2012;318(1):53-60.

104. McDonough H, Patterson C. CHIP: a link between the chaperone and proteasome systems. *Cell Stress Chaperon.* 2008;8(4):303.

105. Taher AT, Weatherall DJ, Cappellini MD. Thalassaemia. *Lancet.* 2018;391(10116):155-167.

106. Gringras P, Wonke B, Old J, et al. Effect of alpha thalassaemia trait and enhanced gamma chain production on disease severity in beta thalassaemia major and intermedia. *Arch Dis Child.* 1994;70(1):30-34.

107. dos Santos CO, Costa FF. AHSP and beta-thalassemia: a possible genetic modifier. *Hematology.* 2005;10(2):157-161.

108. Khandros E, Thom CS, D'Souza J, Weiss MJ. Integrated protein quality-control pathways regulate free α -globin in murine β -thalassemia. *Blood.* 2012;119(22):5265-5275.

109. Adewoye AH, Klings ES, Farber HW, et al. Sickle cell vaso-occlusive crisis induces the release of circulating serum heat shock protein-70. *Am J Hematol.* 2005;78(3):240-242.

110. Sundd P, Gladwin MT, Novelli EM. Pathophysiology of sickle cell disease. *Annu Rev Pathol Mech.* 2019;14:263-292.

111. Elsner L, Flugge PF, Lozano J, et al. The endogenous danger signals HSP70 and MICA cooperate in the activation of cytotoxic effector functions of NK cells. *J Cell Mol Med.* 2010;14(4):992-1002.

112. De Maio A, Vazquez D. Extracellular heat shock proteins: a new location, a new function. *Shock.* 2013;40(4):239-246.

113. Multhoff G, Pfister K, Gehrmann M, et al. A 14-mer Hsp70 peptide stimulates natural killer (NK) cell activity. *Cell Stress Chaperon.* 2001;6(4):337-344.

114. Biondani A, Turrini F, Carta F, et al. Heat-shock protein-27, -70 and peroxiredoxin-II show molecular chaperone function in sickle red cells: Evidence from transgenic sickle cell mouse model. *Proteomics Clin Appl.* 2008;2(5):706-719.

115. Levin C, Koren A, Rebibo-Sabbah A, Koifman N, Brenner B, Aharon A. Extracellular vesicle characteristics in beta-thalassemia as potential biomarkers for spleen functional status and ineffective erythropoiesis. *Front Physiol.* 2018;9:1214.

116. Ogawa S. Genetics of MDS. *Blood.* 2019;133(10):1049-1059.

117. Horrigan SK, Arbivea ZH, Xie HY, et al. Delineation of a minimal interval and identification of 9 candidates for a tumor suppressor gene in malignant myeloid disorders on 5q31. *Blood.* 2000;95(7):2372-2377.

118. Craven SE, French D, Ye W, de Sauvage F, Rosenthal A. Loss of Hsp90 β in zebrafish recapitulates the ineffective hematopoiesis of the myelodysplastic syndrome. *Blood.* 2005;105(9):3528-3534.

119. Frisan E, Vandekerckhove J, de Thonel A, et al. Defective nuclear localization of Hsp70 is associated with dyserythropoiesis and GATA-1 cleavage in myelodysplastic syndromes. *Blood.* 2012;119(6):1532-1542.

120. Xu J, Reumers J, Couceiro JR, et al. Gain of function of mutant p53 by coaggregation with multiple tumor suppressors. *Nat Chem Biol.* 2011;7(5):285-295.

121. de Oliveira GA, Rangel LP, Costa DC, Silva JL. Misfolding, aggregation, and disordered segments in c-Abl and p53 in human cancer. *Front Oncol.* 2015;5:97.

122. Malcovati L, Karimi M, Papaemmanuil E, et al. SF3B1 mutation identifies a distinct subset of myelodysplastic syndrome with ring sideroblasts. *Blood.* 2015;126(2):233-241.

123. Gallardo M, Barrio S, Fernandez M, et al. Proteomic analysis reveals heat shock protein 70 has a key role in polycythemia Vera. *Mol Cancer.* 2013;12(1):142.

124. Sevin M, Girodon F, Garrido C, de Thonel A. HSP90 and HSP70: implication in inflammation processes and therapeutic approaches for myeloproliferative neoplasms. *Mediators Inflamm.* 2015;2015:970242.

125. Vainchenker W, Kralovics R. Genetic basis and molecular pathophysiology of classical myeloproliferative neoplasms. *Blood.* 2017;129(6):667-679.

126. Marubayashi S, Koppikar P, Taldone T, et al. HSP90 is a therapeutic target in JAK2-dependent

dent myeloproliferative neoplasms in mice and humans. *J Clin Invest.* 2010;120(10):3578-3593.

127. Nathan DG, Clarke BJ, Hillman DG, Alter BP, Housman DE. Erythroid precursors in congenital hypoplastic (Diamond-Blackfan) anemia. *J Clin Invest.* 1978;61(2):489-498.

128. Ohene-Abuakwa Y, Orfali KA, Marius C, Ball SE. Two-phase culture in Diamond Blackfan anemia: localization of erythroid defect. *Blood.* 2005;105(2):838-846.

129. Choesmel V, Fribourg S, Aguissa-Touré A-H, et al. Mutation of ribosomal protein RPS24 in Diamond-Blackfan anemia results in a ribosome biogenesis disorder. *Hum Mol Genet.* 2008;17(9):1253-1263.

130. Farrar JE, Nater M, Caywood E, et al. Abnormalities of the large ribosomal subunit protein, Rpl35a, in Diamond-Blackfan anemia. *Blood.* 2008;112(5):1582-1592.

131. Quarello P, Garelli E, Brusco A, et al. High frequency of ribosomal protein gene deletions in Italian Diamond-Blackfan anemia patients detected by multiplex ligation-dependent probe amplification assay. *Haematologica.* 2012;97(12):1818-1817.

132. Ludwig LS, Gazda HT, Eng JC, et al. Altered translation of GATA1 in Diamond-Blackfan anemia. *Nat Med.* 2014;20(7):748-753.

133. Rio S, Gastou M, Karboul N, et al. Regulation of globin-heme balance in Diamond-Blackfan anemia by HSP70/GATA1. *Blood.* 2019;133(12):1358-1370.

134. Gastou M, Rio S, Dussiot M, et al. The severe phenotype of Diamond-Blackfan anemia is modulated by heat shock protein 70. *Blood Adv.* 2017;1(22):1959-1976.

135. Wilkes MC, Takasaki K, Youn M, Chae H-D, Narla A, Sakamoto KM. Chromatin Organization By SATB1 Regulates HSP70 Induction in Early Erythropoiesis and Lost in Diamond Blackfan Anemia. *Blood.* 2018;132(Suppl 1):S2591.

136. Allikmets R, Raskind WH, Hutchinson A, Schueck ND, Dean M, Koeller DM. Mutation of a putative mitochondrial iron transporter gene (ABC7) in X-linked sideroblastic anemia and ataxia (XLSA/A). *Hum Mol Genet.* 1999;8(5):743-749.

137. Liu G, Guo S, Anderson GJ, Camaschella C, Han B, Nie G. Heterozygous missense mutations in the GLRX5 gene cause sideroblastic anemia in a Chinese patient. *Blood.* 2014;124(17):2750-2751.

138. Schmitz-Abe K, Ciesielski SJ, Schmidt PJ, et al. Congenital sideroblastic anemia due to mutations in the mitochondrial HSP70 homologue HSPA9. *Blood.* 2015;126(25):2734-2738.

139. Furuyama K, Kaneko K. Iron metabolism in erythroid cells and patients with congenital sideroblastic anemia. *Int J Hematol.* 2018;107(1):44-54.

140. Lefèvre C, Bondu S, Le Goff S, Kosmider O, Fontenay M. Dyserythropoiesis of myelodysplastic syndromes. *Curr Opin Hematol.* 2017;24(3):191-197.

141. Gazit R, Weissman IL, Rossi DJ. Hematopoietic stem cells and the aging hematopoietic system. *Semin Hematol.* 2008;45(4):218-224.

142. Pang Q, Keeble W, Christianson TA, Faulkner GR, Bagby GC. FANCC interacts with Hsp70 to protect hematopoietic cells from IFN- γ /TNF- α -mediated cytotoxicity. *EMBO J.* 2001;20(16):4478-4489.

143. Mortensen M, Soilleux EJ, Djordjevic G, et al. The autophagy protein Atg7 is essential for hematopoietic stem cell maintenance. *J Exp Med.* 2011;208(3):455-467.

144. De Franceschi L, Bertoldi M, De Falco L, et al. Oxidative stress modulates heme synthesis and induces peroxiredoxin-2 as a novel cytoprotective response in β -thalassemic erythropoiesis. *Haematologica.* 2011;96(11):1595-1604.

145. Higuchi-Sanabria R, Frankino PA, Paul III JW, Tronnes SU, Dillin A. A futile battle? Protein quality control and the stress of aging. *Dev Cell.* 2018;44(2):139-163.

146. Vilchez D, Saez I, Dillin A. The role of protein clearance mechanisms in organismal ageing and age-related diseases. *Nat Commun.* 2014;5:5659.

147. Zhuravleva A, Clerico EM, Giersch LM. An interdomain energetic tug-of-war creates the allosterically active state in Hsp70 molecular chaperones. *Cell.* 2012;151(6):1296-1307.

148. Rudiger S, Germeroth L, Schneider-Mergener J, Bukau B. Substrate specificity of the DnaK chaperone determined by screening cellulose-bound peptide libraries. *EMBO J.* 1997;16(7):1501-1507.

149. Pesciotta EN, Lam H-S, Koskenkov A, et al. In-depth, label-free analysis of the erythrocyte cytoplasmic proteome in diamond blackfan anemia identifies a unique inflammatory signature. *PLoS One.* 2015;10(10):e0140036.

150. Cox J, Mann M. MaxQuant enables high peptide identification rates, individualized ppb-range mass accuracies and proteome-wide protein quantification. *Nat Biotechnol.* 2008;26(12):1367.

Chronic organ injuries in children with sickle cell disease



Ferrata Storti Foundation

Slimane Allali,^{1,2,3} Melissa Taylor,^{1,3,4} Joséphine Brice^{1,3,5} and Mariane de Montalembert^{1,3,5}

¹Department of General Pediatrics and Pediatric Infectious Diseases, Reference Center for Sickle Cell Disease, Necker Hospital for Sick Children, Assistance Publique – Hôpitaux de Paris (AP-HP), Université de Paris, Paris; ²Laboratory of Cellular and Molecular Mechanisms of Hematological Disorders and Therapeutical Implications, Université de Paris, Imagine Institute, Inserm U1163, Paris; ³Laboratory of Excellence GR-Ex, Paris; ⁴Paris-Cardiovascular Research Centre (PARCC), Université de Paris, Inserm U970, Paris and ⁵Institut National de la Transfusion Sanguine (INTS), Université de Paris, Inserm U1134, Paris, France

Haematologica 2021
Volume 106(6):1535-1544

ABSTRACT

Median life expectancy of patients with sickle cell disease has increased to up to 55 years but there are still frequent cases of premature death, mostly in patients with pre-existing organ failure such as pulmonary hypertension, kidney injury, and cerebral vasculopathy. Most organ injuries remain asymptomatic for a long time and can only be detected through early systematic screening. Protocols combining assessment of velocities on transcranial Doppler and regular transfusions in patients with abnormal velocities have been demonstrated to dramatically reduce the risk of stroke. In contrast, no consensus has been reached on systematic screening or therapy for silent cerebral infarcts. The prognostic significance of increased tricuspid regurgitant jet velocity on echocardiography has not yet been identified in children, whereas increased albuminuria is a good predictor of kidney injury. Finally, screening for hip and eye disorder is recommended; however, different countries adopt different screening strategies. Hydroxyurea is probably of potential benefit in preventing chronic organ damage but this requires further study in order to be fully demonstrated. Efficacy and safety of the other new drugs available are also under investigation.

Introduction

In high-income countries, >98% of children affected by sickle cell disease (SCD) reach adulthood, and the disease has shifted from being a fatal illness in children to a chronic disease with multiple organ dysfunction in adults.¹⁻⁴ Median life expectancy has increased to up to approximately 55 years,⁴⁻⁸ which remains far below the life expectancy of ethnicity-matched non-SCD controls.⁴ Fatalities mostly occur in patients with pre-existing organ failure, such as kidney injury, cerebral vasculopathy, and pulmonary hypertension.^{7,8} Most organ injuries remain asymptomatic for several decades and can only be detected through early systematic screening. Identification of early predictors of organ damage could help guide the initiation of specific treatments for the injured organ, prevent secondary worsening, and optimize SCD management. To date, increased velocities on transcranial Doppler in children and elevated tricuspid regurgitant jet velocity in adults are the only validated predictors of risk of stroke and death, respectively.^{9,10} Biological predictors of severity are mostly limited to hemolysis markers, and have weak individual predictive values.^{5,11-15} There is still no genetic signature of severity robust enough to predict individual outcome.¹⁶ Thus, regular screening for early signs of organ dysfunction appears to be the best strategy for the prevention of secondary organ failure and early mortality. In this review, we describe the main chronic organ dysfunctions reported in children with SCD and propose a checklist of screening tests.

Pathophysiology of chronic organ injury

SCD originates from the sickle mutation on the *HBB* gene (Glu6Val, βS), the most common and severe form being homozygous HbSS. Other forms of SCD

Correspondence:

MARIANE DE MONTALEMBERT
mariane.demontal@nck.aphp.fr

Received: September 25, 2020.

Accepted: November 6, 2020.

Pre-published: February 25, 2021.

<https://doi.org/10.3324/haematol.2020.271353>

©2021 Ferrata Storti Foundation

Material published in *Haematologica* is covered by copyright. All rights are reserved to the Ferrata Storti Foundation. Use of published material is allowed under the following terms and conditions: <https://creativecommons.org/licenses/by-nc/4.0/legalcode>. Copies of published material are allowed for personal or internal use. Sharing published material for non-commercial purposes is subject to the following conditions: <https://creativecommons.org/licenses/by-nc/4.0/legalcode>, sect. 3. Reproducing and sharing published material for commercial purposes is not allowed without permission in writing from the publisher.



include compound heterozygous conditions, such as hemoglobin C (HbC) with HbS (HbSC), HbS with β -thalassemia (HbS/ β^0 -thalassemia or HbS/ β^+ -thalassemia), and HbS with other β -globin variants resulting in sufficient HbS expression to cause sickling. Under deoxygenation, sickle hemoglobin (HbS) polymerizes and erythrocytes undergo a rapid but reversible change in shape, resulting in both chronic hemolysis and small-vessel obstruction, which have long been recognized as the main contributors to SCD pathophysiology.¹⁷ Paradoxically, tissue injury is exacerbated by reperfusion-enabled re-entry of oxygen during the ischemia/reperfusion process (I/R). I/R is responsible for systemic inflammation, hypercoagulability, and endothelial dysfunction via various mechanisms.¹⁸ Endothelial vasoregulatory dysfunction is observed from childhood,^{19,20} and chronic anemia is responsible for concomitant increased blood flow. The association of macrovascular hyperemia and microvascular hypoperfusion, that Hebbel *et al.* referred to as the sickle cell "perfusion paradox", is extremely challenging for major organs such as the brain, kidney, and heart, which may fail to respond and adapt to the need for increased oxygen.¹⁸ Moreover, systemic inflammation is amplified by the release of free heme and hemoglobin during hemolysis, inducing oxidative stress, cell death, and vascular integrity damage.²¹ Heme was notably shown to be a potent activator of endothelial cells, leading to an increased expression of major adhesion molecules such as P-selectin.²¹ Finally, each organ (and, indeed, each patient) represents a unique combination of hypoxia, inflammatory and oxidative stress, activation of innate immunity, hyperviscosity and hypercoagulability in response to genetic and environmental age-dependent drivers. Organ defense may be adapted for a certain length of time, or 'over-adapted', for example, when neoangiogenesis induces the generation of a network of collateral vessels which are prone to ruptures, provoking ocular or cerebral hemorrhages. Sickling-related acute events may be regressive with unsickling but endothelial damage is most often irreversible.

Chronic organ injuries will be presented here according to their impact on mortality in adult patients.

Cardiovascular abnormalities

Main cardiovascular disorders in SCD are pulmonary hypertension (PHT) and left ventricular dysfunction. These are the main contributors to SCD-related mortality in adults, accounting for >30% of all deaths among SCD patients in the US.²² They are more frequent and severe in patients with HbSS or HbS/ β^0 -thalassemia.^{23,24}

Pulmonary hypertension

In addition to the pathophysiology common to all organ injuries described above, increased cardiac output resulting from chronic anemia is a risk factor for PHT in SCD. Hypoxia induces smooth muscle cell and intimal proliferation, and *in situ* thrombosis can increase pulmonary vascular resistance. These factors contribute to the development of PHT and right heart enlargement, which ultimately leads to right heart failure. In addition, post-capillary PHT is promoted by diastolic dysfunction, which may be related to myocardial fibrosis. In children, however, PHT seems to be mostly related to increased

cardiac output while pulmonary vascular resistance remains normal.²⁵

Historically, PHT in adults and children was defined as a mean pulmonary artery pressure (mPAP) ≥ 25 mmHg but the current threshold proposed by the 6th World Symposium on Pulmonary Hypertension is > 20 mmHg.²⁶ Prevalence in adults with SCD ranges from 10% to 33% when measured by right heart catheterization (RHC) or echocardiography, respectively.²⁴ Pulmonary artery systolic pressure (PASP) is assessed on echocardiography by the quantification of the tricuspid regurgitant jet velocity (TRV) using the modified Bernoulli equation. Raised TRV was shown to be a risk factor for death in adults.^{10,27,28} However, the positive predictive value of TRV for diagnosing PHT in adults remains controversial. No study has assessed the correlation between TRV and RHC in SCD children. Given the risk of RHC procedure in this patient population, it is only recommended when TRV is > 3 m/s and is only to be carried out in experienced pediatric centers.²⁶ In a meta-analysis using a threshold of TRV ≥ 2.5 m/s, 21% (95%CI: 17-26%) of children and adolescents were considered to have elevated PASP, which was positively associated with age.²⁹ Nevertheless, TRV ≥ 2.5 m/s may be observed as early as three years of age in SCD children.³⁰ Several studies have shown the influence of hemolysis on the occurrence of PHT in children.³¹⁻³⁴ Hemoglobin oxygen desaturation is frequently reported in SCD children, especially at night and after exercise, but its association with elevated TRV is more controversial.^{31,34}

In contrast with adults, increased TRV in SCD children has not so far been associated with increased mortality in adulthood. In a cross-sectional study of 483 adolescents and adults with SCD, raised TRV was associated with poor exercise capacity.³⁵ Furthermore, one study of 160 HbSS patients aged 3-20 years showed that baseline elevation in TRV was associated with a 4.4-fold increase in the odds of a 10% or more decline in age-standardized 6-minute-walk distance over a median of 22 months.³² Importantly, evaluation of PHT should not be based on a single assessment of TRV, as demonstrated in a follow-up cohort of 120 children with SCD, in which an improvement in TRV values was observed over a period of 15 \pm 9 months in half of the patients, although there was no clear explanation for this.³⁶

Screening and prevention

US recommendations suggest performing an echocardiography when symptoms are suggestive of PHT, whereas many European experts recommend measuring TRV once a year in children, usually after five years of age.^{37,38} In cases of elevated TRV, the cardiopulmonary risk should be evaluated by a full workup including electrocardiography (ECG), chest radiography, functional respiratory tests with 6-minute-walk distance measurement, cardiopulmonary exercise test, overnight oxygen saturation monitoring, polysomnography for obstructive sleep apnea, and measurement of brain natriuretic peptide (BNP) and N-terminal pro-BNP levels. TRV ≥ 2.5 m/s should suggest the need to optimize SCD treatment, although prospective controlled studies have not demonstrated the benefits of hydroxyurea and chronic transfusion on PHT. Retrospective data suggest either improvement of PHT with hydroxyurea³⁹ or no effect of the drug.^{31,33}

Left ventricular diastolic dysfunction

SCD patients usually exhibit left ventricular (LV) dilation, closely correlated to the severity of anemia. Over time, progressive dilation leads to increased wall stress, increased LV mass, and impaired LV filling, which is associated with increased mortality in SCD adults.^{23,40} Diastolic dysfunction is linked to microscopic myocardial fibrosis in transgenic SCD mice, and to diffuse myocardial fibrosis on cardiac magnetic resonance imaging (MRI) in patients.^{40,41}

Myocardial ischemia

Myocardial ischemia in SCD patients appears to be related to microvascular perfusion defect rather than to coronary artery occlusion.⁴² A few cases of acute myocardial ischemia or subclinical myocardial injuries have been reported in children with SCD.^{42,45} In a series of 22 SCD children with chest pain, or ECG or echocardiographic signs (LV dilation or hypokinesis) who underwent single photon emission computed tomography, myocardial hypoperfusion was found in eight of them. Perfusion defects were more frequent in older children. In this study, myocardial perfusion was reassessed in three patients after 6 months of hydroxyurea and was found to be improved.⁴³

Cardiac iron overload

The heart does not appear to be an early target for iron deposition in chronically transfused SCD patients, and this is particularly the case in young patients.^{44,45} In a multicentric study of regularly transfused SCD patients either on manual exchange transfusion (n=30) or erythrocytapheresis (n=11), none had cardiovascular MRI values of T2*<20 ms, in spite of high median ferritin levels (2,700 and 2,400 ng/mL for manual exchange and erythrocytapheresis procedures, respectively) and liver iron content (10 and 14 mg/g dry weight for manual exchange and erythrocytapheresis procedures, respectively).⁴⁴ The rarity of cardiac iron overload may partly be explained by the fact that, in SCD, iron is efficiently recycled by erythropoiesis or trapped within macrophages because of chronic inflammation.⁴⁴

Lung disease

Respiratory complications were found to be the second cause of death (at 28%) in adults with SCD in the US between 1999 and 2009.²² Chronic complications in SCD include chronic dyspnea, reduced exercise capacity, and loss of lung function. Abnormalities in lung function have frequently been reported in children with SCD, although results remain a subject of debate, both regarding the frequency of these abnormalities and the predominant restrictive or obstructive pattern.⁴⁶⁻⁴⁸ A review of 149 children aged 6-19 years, of whom 139 were followed prospectively for a median of 4.3 years, found normal, obstructive, restrictive, non-specific, and mixed baseline lung function patterns in 70%, 16%, 7%, 6%, and 1% of patients, respectively.⁴⁹ Baseline lung function patterns were not associated with pain or acute chest syndrome rate either before the pulmonary function tests or during follow-up. In contrast, another study found that occurrence of acute chest syndrome was associated with a greater decline in lung function.⁵⁰ In a prospective study of

146 patients with HbSS or HbS/β⁰ thalassemia, normal, obstructive, restrictive, and non-specific lung function patterns were observed in 61%, 19%, 9%, and 11% of patients, respectively.⁵¹ Older age, patient or family history of asthma or wheezing, and higher lactate dehydrogenase levels were independent predictors of obstruction. One study reported that 96.5% of patients had normal lung function at eight years of age, but the authors observed a longitudinal decline in lung volumes through adolescence, with a restrictive pattern in 19% of patients by the age of 17.⁵² Discrepancies between studies may be due to the different thresholds used for defining patterns and to the small numbers of patients, most often analyzed retrospectively in cross-sectional studies. Lung function may also vary depending on geographical area, with a higher reported prevalence of restrictive patterns in patients from sub-Saharan Africa compared to those from high-income countries.⁴⁸ Overall, obstruction seems to predominate in children whereas restriction is more common in adults.⁵³ Asthma has been found to be associated with acute chest syndrome occurrence and pain⁵⁴ but its effect on lung function growth is not clear.⁵⁵ Unresolved issues include the question as to whether there is a link between abnormal lung function and relevant outcomes such as progressive dyspnea, pulmonary hypertension, and early mortality.⁴⁹

Screening and prevention

The question of systematically screening all SCD children with pulmonary function tests remains a subject of debate.^{37,58,55} Proponents argue that identifying an undiagnosed obstructive pattern may help to prevent acute asthma crises and therefore reduce the risk of acute chest syndrome.

Kidney disease

Renal complications in SCD include hyposthenuria, glomerular hyperfiltration, glomerulosclerosis, albuminuria, and end-stage renal disease. These are responsible for approximately 14-16% of mortality in adults with SCD in the US and are more frequent in patients with HbSS and HbS/β⁰-thalassemia.⁵⁶ In addition to the pathophysiological processes previously described in SCD organ injuries, kidney injury is enhanced by the particularly hypoxic, acidic, and hypertonic environment of the renal medulla which induces red blood cell sickling in the vasa recta, with ischemia and infarction of the tubular cells. The kidney is a very good example of the "perfusion paradox" in SCD, with the association of macrovascular whole-kidney hyperemia, and microvascular medullary blood flow hypoperfusion. In young patients, elevated cardiac output leads to increased renal blood flow, glomerular hypertrophy, and increased glomerular filtration rate (GFR), the latter being observed as early as childhood.⁵⁷ GFR then decreases with age, especially in patients developing kidney disease. In addition to hyperperfusion, there is a decrease in vascular resistance, which might be related to heme-driven heme oxygenase-1 induction and the release of vasorelaxants such as prostaglandins.⁵⁶ I/R injuries and heme release seem to play a major role in the development of acute kidney injury (AKI) and chronic kidney disease (CKD) via oxidative stress, apoptosis induction, and activation of the complement system.^{58,59}

Renal manifestations vary greatly depending on the patient and his or her age. Hyposthenuria is observed from infancy in the majority of children. Enuresis is very frequent and may have a severe psychological impact. Hyperfiltration occurs very early, as evidenced by 99-technetium diethylenetriaminepentaacetate (DTPA) plasma clearance measurements in infants with SCD aged 9-19 months enrolled in the BABY HUG trial.⁵⁷ Baseline DTPA glomerular filtration rate (GFR) was $125 \pm 34 \text{ mL/min/1.73 m}^2$ (range: 40-300 mL/min/1.73 m²) compared with the published normal value of $91 \pm 18 \text{ mL/min/1.73 m}^2$ (10-90% range: 60-120 mL/min/1.73 m²) for this age group.⁵⁷ On average, baseline DTPA GFR increased by 3 mL/min/1.73 m² for every one month increase in age.⁵⁷ Hyperfiltration, defined as estimated GFR (eGFR) $> 180 \text{ mL/min/1.73 m}^2$, was also evidenced using cystatin C measurement in a cohort of 91 children with HbSS and HbS/β⁰-thalassemia aged 5-21 years.⁶⁰ Thirty-nine patients (43%) had hyperfiltration and nine of them (23%) progressed to microalbuminuria, defined as albumin to creatinine ratio 30-300 mg/g, compared with three of the 52 patients (6%) without hyperfiltration. Several studies have demonstrated that hyperfiltration increases during early childhood, remains stable before adolescence, then decreases as progressive CKD continues.⁶⁰⁻⁶² eGFR $< 90 \text{ mL/min/1.73 m}^2$ is seen in 8-21% of adolescents.⁶¹⁻⁶³ Albuminuria may develop in some children. In a series of 410 SCD patients aged 2-21 years, microalbuminuria was found in 21% (70% of them were HbSS and HbS/β⁰-thalassemics); macroalbuminuria (defined as albumin to creatinine ratio $\geq 300 \text{ mg/g creatinine}$) was presented in three HbSS patients. In HbSS and HbS/β⁰-thalassemics, abnormal albuminuria was associated with older age and lower baseline hemoglobin level.⁶¹

SCD patients with CKD may have a stable renal function but are at risk of AKI during vaso-occlusive crisis or other concomitant illness.⁶⁴ In a retrospective study, AKI was found in 17% of 197 admissions for vaso-occlusive pain.⁶⁴ At admission, every 'one unit' drop in hemoglobin levels compared to patients' baseline values increased the risk of AKI by 49%. Ketorolac administration (in terms of total days and doses) was also associated with AKI but the role of non-steroidal anti-inflammatory drugs (NSAID) could not be formally confirmed because of the retrospective nature of the study. The impact of the decrease in hemoglobin levels on the occurrence of AKI compared to baseline values has also been observed in children during acute chest syndrome,⁶⁵ and may reflect a direct toxic effect of free heme or hemoglobin released during hemolysis on the kidney.

Renal dysfunction is more severe and frequent in patients with HbSS and HbS/β⁰-thalassemia, and is associated with anemia.⁶⁶ As in other diseases, nocturnal hypertension and hyperuricemia have been associated with lower eGFR.⁶⁷ The predictive value of an APOL1 genetic profile has recently been suggested for onset of renal disease in children with SCD.⁶⁸

Screening and prevention

Screening for kidney disease should not be based on serum creatinine level in children with SCD because of increased eGFR, often lower muscle mass, and increased tubular secretion of creatinine.⁶¹ Albuminuria is a good predictor of risk for CKD and can be used for routine screening. The National Heart Lung and Blood Institute

recommends screening for albuminuria starting at ten years of age for all SCD patients.⁶⁸ The gold standard for measuring GFR is inulin clearance but this is costly. Therefore, cystatin C and creatinine-based estimations of GFR (Schwartz equation using patient height and creatinine value) may be more relevant for annual screening.⁶⁹ In children, it must be remembered that a normal GFR is an alarm signal as it should, in fact, be elevated in the context of initial hyperfiltration.

Hydroxyurea may be considered in patients with elevated microalbuminuria but the results of existing studies are controversial. Hydroxyurea was not superior to placebo in the prevention of hyperfiltration in the BABY-HUG trial, although it was associated with a better concentrating ability and less renal enlargement.^{69,70} In pediatric series, hydroxyurea was associated with a trend for a decrease in the frequency of microalbuminuria⁷¹⁻⁷³ and with a significant decrease in DTPA GFR in 23 children with a median age of 7.5 years.⁷⁴

Very few studies have reported the use of angiotensin converting enzyme inhibitors (ACE I), combined or not with hydroxyurea, in SCD children with albuminuria.^{71,75} Albuminuria decreased in some children treated with ACE I but some patients experienced hyperkalemia, prompting interruption of ACE I therapy.

Cerebrovascular disease

Patients affected with SCD may suffer from ischemic and hemorrhagic stroke, silent cerebral infarction, and neurological decline. Cerebrovascular events account for approximately 12% of SCD-related mortality in the US.²² In children, these represent the third cause of death after infections and hematologic complications (acute splenic sequestration and other causes of acute anemia).⁷⁶ Furthermore, cerebrovascular events are responsible for a high rate of motor and cognitive disabilities.⁷⁷ The brain provides a good illustration of the "perfusion paradox" of SCD, combining hyperperfusion within the arteries of the circle of Willis and microvascular hypoperfusion. Hemolysis and I/R injuries generate inflammation, endothelial dysfunction, and intimal hyperplasia. The roles of hemodynamic changes and procoagulant status are still under investigation.^{18,77}

Cerebral vasculopathy mostly affects HbSS and HbS/β⁰-thalassemia patients. Events may be overt or so-called 'silent', which is an inappropriate term since silent cerebral infarcts (SCI) were found to be associated with cognitive defects.⁷⁸ Overt events are mostly ischemic, occurring with two peaks of frequency either before the age of ten or after 40 years of age, but may also be hemorrhagic with an increasing incidence associated with age. Risk factors include a lower steady-state Hb level, prior transient ischemic attack, recent or frequent acute chest syndromes, high systolic blood pressure,¹¹ nocturnal hypoxemia,⁷⁹ a past history of bacterial meningitis,¹¹ and the presence of silent infarcts on MRI.⁸⁰ The role of co-existent G6PD deficiency is controversial, as it was found to increase the risk of stroke in one,⁸¹ but not all, studies.⁸² Increased HbF level and presence of α-thalassemia may have a protective effect.⁸¹ Hemorrhagic strokes may complicate moyo-moya syndromes or may be related to ruptured aneurysm, the prevalence of which is increased in SCD patients, most likely due to the effect of flow disturbances on the vascular wall.⁷⁷

SCI are the most common neurological events in SCD children, occurring in approximately one-third of patients before the age of 14 years; there is no plateau with increasing age.⁸³ Reported risk factors for SCI include male gender, lower baseline hemoglobin concentrations, higher baseline systolic blood pressure, and previous seizures.⁷⁸

Screening and prevention

The brain is probably the only organ for which preventive strategies have shown efficacy in SCD patients. Transcranial Doppler (TCD) measures the flow velocity in the large intracranial arteries of the circle of Willis where stenosis or flow turbulences may induce a local acceleration. Children may be stratified as being at low, intermediate, or high risk of stroke according to normal, conditional, or abnormal velocities, respectively.⁹ Adams *et al.* showed that children with time-averaged mean velocity (TAMV) measured in the distal internal carotid artery or middle cerebral artery ≥ 200 cm/s had a 6-fold higher risk of stroke than children with normal TCD velocities (TAMV < 170 cm/s).⁹ For these high-risk patients, initiation of monthly blood transfusion reduced the risk of stroke by 90%.⁸⁴ Alternatively, hydroxyurea has been used for primary and secondary stroke prevention in low-resource settings.⁸⁵ Cerebral vasculopathy revealed by abnormal TCD is an indication for hematopoietic stem cell transplant in children with HLA-identical sibling. When velocities are normal, the current recommendation in children with HbSS and HbS/ β^0 -thalassemia is annual TCD screening from 2 to ≥ 16 years.⁸⁷ Conditional TCD is an intermediate category that warrants performing MRI/magnetic resonance angiography (MRA) and controlling TCD, as conversion to abnormal TCD may occur.⁸⁶ Many teams consider conditional velocities as an indication for hydroxyurea treatment.⁸⁸ Very low blood-flow velocities (< 70 cm/s) suggest post-stenotic demodulation or near-occlusive arterial disease.⁸⁷ Finally, elevated velocities (> 160 cm/s) in the extracranial part of the internal carotid artery are also associated with increased risk of stroke, notably in patients who are free of intracranial arterial vasculopathy;^{88,89} however, there is still no clear recommendation on which treatment strategy to use. Our personal recommendation is to use the same strategy for both intra- and extra-cranial abnormalities. TCD may detect blood flow alterations before occurrence of MRI/MRA abnormalities allowing for early management at a stage when it might be possible to prevent the situation worsening.⁹⁰ MRI/MRA is recommended in children with conditional TCD findings and in children with incomplete TCD assessment, usually due to a lack of a bone window or to an underlying arterial occlusion. In 2014, a panel of experts did not recommend systematic MRI in asymptomatic children with HbSS and HbS/ β^0 -thalassemia.⁸⁷ However, brain MRI can reveal aneurysms or SCI, which are associated with decreased cognitive ability, and these might benefit from hydroxyurea treatment. Therefore, some centers recommend performing brain MRI in SCD children at least once.⁹¹ Our personal experience is to recommend systematic MRI at around six years of age (an age at which it is expected that most children would have already started school) since early diagnosis of SCI usually leads to a more thorough evaluation of academic ability and performance with implementation of educational and psychological

support when required. Management of SCI is still non-consensual. Hydroxyurea has been suggested to reduce their extension or recurrence.⁹² Use of chronic transfusion is a subject of debate as this therapy has only moderate efficacy on the progression of SCI.⁹¹

Liver disease

The main acute manifestations of liver disease in SCD include sickle cell hepatic crisis, sickle cell intrahepatic cholestasis, and hepatic sequestration, while chronic manifestations include cholelithiasis, sickle cell cholangiopathy, auto-immune hepatitis, viral hepatitis, and iron overload.⁹³ The prevalence of liver disease in adults with SCD is estimated to be approximately 10%.⁹³ In a cohort of 3,500 adult patients, liver failure was considered to be the cause of death in 7% of cases.⁸ Hepatobiliary complications are more rarely reported in children with SCD, most probably because they are not routinely screened for and are thus under-diagnosed.⁹⁴

The pathophysiology of these complications is mostly related to the sickling of red blood cells, resulting in sinusoidal obstruction and ischemia of hepatocytes, as well as ischemia of bile ducts leading to cholangiopathy. Hemolysis-related hyperbilirubinemia promotes biliary lithiasis. Liver damage in SCD may also be due to iron overload, viral infection, or autoimmune disorders, the frequency of which is increased in SCD patients compared to the general population.⁹⁵

A retrospective review of 616 SCD children followed-up in a reference center for both SCD and hepatology found that 37% had presented at least one hepatobiliary complication.⁹⁴ Among chronic complications, gallstones were diagnosed in 25% of children, cholangiopathy in 0.8%, autoimmune hepatitis in 0.5%, transfusion iron overload in 3%, and iron chelator toxicity was suspected in 0.8%. Over half of the gallstones were discovered incidentally, although complications occurred in 42% of cases, mostly occurring as pain, as well as cholecystitis, cholangitis, and pancreatitis. Among acute complications, the combined prevalence of acute sickle cell crisis, sickle cell intrahepatic cholestasis, and acute hepatic sequestration was approximately 6%.⁹⁴ Post-transfusion iron overload is usually asymptomatic in children but may have severe consequences in adults.⁹³

Screening and prevention

In order to prevent gallstone-related complications, we recommend abdominal ultrasonography once a year after the age of five years, and elective cholecystectomy in case of gallstone even in asymptomatic patients, although there is currently no consensus for this preventive strategy.^{87,96} Liver injury can be screened by performing twice-yearly liver tests (mainly alanine aminotransferase [ALT] and conjugated bilirubin).⁹⁴ In patients with dilated bile ducts, MR-cholangiography should be performed and hypergammaglobulinemia should also be screened for as autoantibodies for autoimmune liver disease. Liver MRI should be performed every year in children aged > 5 years undergoing a monthly transfusion program in order to assess liver iron content. Iron chelation is recommended in case of iron overload but adhesion to chelator therapy is often low.⁴⁴ Lastly, anti-hepatitis B immunization is mandatory.

Ophthalmic disease

Patients affected with SCD are at risk of retinopathy, which may result in sight-threatening complications, such as vitreous hemorrhage and retinal detachment. Ocular manifestations of SCD differ from previously described complications as peripheral retinopathy is more frequent in patients with HbSC than in patients with HbSS.^{97,98} The reasons for this finding are not fully understood although the blood hyperviscosity commonly observed in HbSC patients (who display higher hemoglobin levels than HbSS patients) could contribute to retinal ischemia. On the other hand, it has been hypothesized that increased vascular endothelial growth factor (VEGF) and angiopoietin production in response to chronic anemia could play a role by promoting angiogenesis.⁹⁹

The prevalence of retinopathy has been estimated at 24% in HbSS and HbS/β⁰ adult patients *versus* 61% in HbSC and HbS/β⁺ patients.⁹⁷ Non-proliferative retinopathy includes salmon-patch hemorrhages, iridescent spots, black sunbursts, and arteriovenous anastomoses. Patients are usually asymptomatic as long as the retinopathy is non-proliferative but secondary development of neovascularization, presenting as sea fans, bears the risk of vision loss due to vitreous hemorrhage or retinal detachment. A retrospective review of 263 children with SCD found proliferative retinopathy in seven cases (2.7%), including six with HbSC (occurring at a median age of 13.7 years; range: 9-18), one with HbSS (occurring at 16 years of age), and none with HbS/β-thalassemia.⁹⁸ More recently, a high prevalence of temporal macular retinal atrophy diagnosed by optical coherence tomography (OCT) has been reported in SCD patients, including children, which may have direct consequences on visual function with impaired color vision ability and contrast sensitivity, even when visual acuity is preserved.¹⁰⁰ In a retrospective series of 81 children (mean age 12 years; standard deviation [SD]: 3.5 years) with SCD (64 HbSS, 7 HbS/β⁰-thalassemia, 10 HbSC), temporal macular retinal atrophy was observed in 64% of cases with no significant difference in prevalence between HbSS and HbSC genotype.¹⁰¹ In this series, peripheral retinopathy was observed in 11% of patients and was more severe in children with HbSC.

Recent multimodal MRI evaluation of the visual cortex in 25 SCD children (mean age: 12.3 years; SD: 1.9 years) compared to 31 controls, found increased posterior pericalcarine cortical thickness, with different trajectory of cortical maturation and decreased connectivity within visual neural networks.¹⁰² Whether these changes may represent useful predictors of visual impairment in adulthood needs to be assessed by further studies.

Screening and prevention

There is universal consensus on the recommendation that children with SCD should be screened regularly for retinopathy with a dilated fundoscopic examination, starting earlier in children with HbSC than in children with HbSS genotypes.^{37,38,98} Nine and 13 years of age have been proposed as appropriate time points to start systematic controls in HbSC and HbSS children, respectively.⁹⁷ However, since temporal macular retinal atrophy seems to occur early in the course of SCD, especially for patients with HbSS,¹⁰⁰ we personally recommend annual controls, including OCT, starting at six years of age. A simple annual survey is recommended for children with non-proliferative retinopathy and laser photocoagulation

is generally proposed to children with severe proliferative retinopathy.

Hip abnormalities

Osteonecrosis of the femoral head (ONFH) is the main osteoarticular complication of SCD with an estimated prevalence ranging from 10% to 30% in adults.¹⁰³ This relatively high frequency may be explained by several factors. Firstly, vascularization of superior femoral epiphysis depends on the retinacular vessels, which originate from branches of the medial circumflex arteries in a terminal vascularization model, with limited possibilities of reperfusion when these vessels are occluded by sickling red blood cells. In addition, the balance between osteoblastogenesis and osteoclastogenesis is most likely modified in patients with SCD during hypoxia-reperfusion cycles.¹⁰⁴ Lastly, vitamin D deficiency is frequent in patients with SCD and may contribute to bone fragility.¹⁰⁵

In a study of 2,590 SCD children and adults followed-up in the 1980s for an average of 6 years, 10% of patients had ONFH at study inclusion.¹⁰⁶ The prevalence of ONFH for patients aged 5-9 years, 10-14 years, and 15-24 years was 1.3%, 4.6%, and 8.2%, respectively. At follow-up, children with HbSS and α-thalassemia were at the greatest risk for osteonecrosis. The frequency of painful crises, age, and hematocrit were positively associated with osteonecrosis.¹⁰⁶ The influence of hydroxyurea on the incidence of OFNH is much debated, although the interpretation of most studies is limited by the fact that they are cross-sectional and retrospective, including only a limited number of patients.¹⁰³

Screening and prevention

It has been shown that early treatment of ONFH, either conservative or operative, can lead to good functional outcomes with 75% of congruent hips at skeletal maturity.¹⁰⁷ Early diagnosis is therefore mandatory. There is agreement on the need to investigate all children with SCD presenting intermittent or chronic hip pain for avascular necrosis by means of a full history and physical examination, X-ray, and MRI, as needed. Advice from an orthopedic department should be requested.³⁷ At a pre-collapse stage, ONFH is, however, asymptomatic, and this observation has led a French panel of experts to recommend systematic hip X-ray after the age of 6 years with a checkup every 1-3 years.³⁸

Conclusion

The median life expectancy of patients with SCD has increased to up to 55 years, which can be considered a significant achievement with regard to the natural history of the disease.³ However, detection and management of chronic organ failure still need to be improved in order to reach the life expectancy of the general population without major disabilities. Detecting and preventing early organ injury would not only reduce early mortality but may also improve quality of life. There is still no consensus on the best strategies for detecting and preventing chronic organ dysfunction in SCD patients. For these reasons, we propose a summary of the main recommendations from both a US and a European panel of experts on SCD in Table 1.^{37,108}

Apart from stroke prevention, the quality of evidence regarding the efficacy of actual screening strategies is still not high enough. Moreover, the ability of chronic transfusion, hydroxyurea and other drugs to prevent chronic organ failure has not been demonstrated by controlled studies. However, several encouraging studies do suggest a potential benefit of hydroxyurea to prevent degradation of renal function. The impact of new drugs such as crizanluzimab and voxelotor on organ function is still under investigation. While there are still no individual predictive

factors, current strategy options may be to propose hydroxyurea to all HbSS and HbS/β⁰ children; this option has been considered by US and British experts.³⁷ Another option may be to take the view that the potential severity of SCD in adults justifies proposing hematopoietic stem cell transplantation (and, in the future, gene therapy) even in asymptomatic patients. This debate is still ongoing, but it will be essential that patients help define their own health priorities and play a role in the design of clinical research.

Table 1. Screening tools in children and adolescents for the detection of chronic organ complications of sickle cell disease.

Organ	Screening tool (apart from history and physical examination)	US recommendations for screening	Recommendations from a European panel of experts for screening	Evidence-based treatment (EBT)
Heart				
Pulmonary hypertension	TRV on echocardiography	In case of symptoms or suggestive signs	Yearly Systematic in all children >5 years	No EBT HU suggested
Myocardial ischemia	ECG	In case of symptoms or suggestive signs	In case of symptoms or suggestive signs Consider cardiac MRI	No EBT HU suggested
Lung and airways				
Pulmonary disease	Pulmonary function tests	In case of symptoms	Yearly Systematic in all children >5 years	Anti-asthmatic treatments if necessary
Upper airway obstruction	ENT control (+ polysomnography when necessary)	Yearly	Yearly	Adeno-/tonsillectomy if upper airway obstruction
Kidney				
Renal failure	Blood pressure Creatinine, albuminuria	Systematic screening	Yearly systematic screening	No EBT HU suggested if microalbuminuria ACE inhibitor suggested if proteinuria
Brain				
Cerebral vasculopathy	Transcranial doppler	Yearly screening from age 2 to at least 16 years in SCA patients	Yearly screening from age 2 to at least 16 years in SCA patients	Monthly transfusion in patients with velocities >200 cm/s
Silent infarct	Academic performance Neurocognitive screening Cerebral MRI	No systematic MRI in asymptomatic children	No consensus Systematic MRI starting at 6 years old for some experts	No EBT HU suggested if silent infarct
Liver				
Cholangiopathy	Liver tests Abdominal ultrasonography	No systematic screening	Abdominal ultrasonography once a year from age 5	No consensus Elective cholecystectomy even in asymptomatic patients for some experts
Transfusion iron overload	Ferritin Liver iron content on hepatic MRI	Systematic screening in chronically transfused patients	Systematic screening in chronically transfused patients	Iron chelation
Eye				
Retinopathy	Dilated fundoscopic examination OCT	No consensus	Yearly examination after 10 years old (6 years old for some experts)	Laser photocoagulation if severe proliferative retinopathy
Hip				
Osteonecrosis of the femoral head	Radiography MRI	In case of symptoms (hip pain)	Systematic radiography after the age of 6 years, and then every 1-3 years according to the clinical findings	Conservative or operative treatment

ACE: angiotensin-converting enzyme; ENT: ear, nose and throat; HU: hydroxyurea; MRI: magnetic resonance imaging; OCT: optical coherence tomography; SCA: sickle cell anemia (patients with HbSS and HbS/β⁰-thalassemia genotypes); TRV: tricuspid regurgitant jet velocity.

Disclosures

No conflicts of interest to disclose.

Contributions

MM wrote the first draft of the manuscript; SA, MT and JB assisted in writing the manuscript.

References

1. Quinn CT, Rogers ZR, McCavit TL, Buchanan GR. Improved survival of children and adolescents with sickle cell disease. *Blood*. 2010;115(17):3447-3452.
2. Couque N, Girard D, Ducrocq R, et al. Improvement of medical care in a cohort of newborns with sickle-cell disease in North Paris: impact of national guidelines. *Br J Haematol*. 2016;173(6):927-937.
3. DeBaun MR. Perspective: thinking beyond survival. *Nature*. 2014;515(7526):S16.
4. Lubeck D, Agodoa I, Bhakta N, et al. Estimated life expectancy and income of patients with sickle cell disease compared with those without sickle cell disease. *JAMA Netw Open*. 2019;2(11):e1915374.
5. Elmariah H, Garrett ME, De Castro LM, et al. Factors associated with survival in a contemporary adult sickle cell disease cohort. *Am J Hematol*. 2014;89(5):530-535.
6. Lanzkron S, Carroll CP, Haywood C Jr. Mortality rates and age at death from sickle cell disease: U.S., 1979-2005. *Public Health Rep*. 2013;128(2):110-116.
7. Chaturvedi S, Ghafuri DL, Jordan N, Kassim A, Rodeghier M, DeBaun MR. Clustering of end-organ disease and earlier mortality in adults with sickle cell disease: a retrospective-prospective cohort study. *Am J Hematol*. 2018;93(9):1153-1160.
8. Habibi A, Ngo S, Audureau E, et al. Causes of death in 198 sickle cell adult patients: old and new trends. *Blood*. 2019;134(Suppl 1):1031.
9. Adams R, McKie V, Nichols F, et al. The use of transcranial ultrasonography to predict stroke in sickle cell disease. *N Engl J Med*. 1992;326(9):605-610.
10. Gladwin MT, Sachdev V, Jison ML, et al. Pulmonary hypertension as a risk factor for death in patients with sickle cell disease. *N Engl J Med*. 2004;350(9):886-895.
11. Ohene-Frempong K, Weiner SJ, Sleeper LA, et al. Cerebrovascular accidents in sickle cell disease: rates and risk factors. *Blood*. 1998;91(1):288-294.
12. Platt OS, Brambilla DJ, Rosse WF, et al. Mortality in sickle cell disease. Life expectancy and risk factors for early death. *N Engl J Med*. 1994;330(23):1639-1644.
13. Kato GJ, McGowan V, Machado RF, et al. Lactate dehydrogenase as a biomarker of hemolysis-associated nitric oxide resistance, priapism, leg ulceration, pulmonary hypertension, and death in patients with sickle cell disease. *Blood*. 2006;107(6):2279-2285.
14. Nouraie M, Lee JS, Zhang Y, et al. The relationship between the severity of hemolysis, clinical manifestations and risk of death in 415 patients with sickle cell anemia in the US and Europe. *Haematologica*. 2013;98(3):464-472.
15. Meier ER, Wright EC, Miller JL. Reticulocytosis and anemia are associated with an increased risk of death and stroke in the newborn cohort of the Cooperative Study of Sickle Cell Disease. *Am J Hematol*. 2014;89(9):904-906.
16. Habara A, Steinberg MH. Minireview: genetic basis of heterogeneity and severity in sickle cell disease. *Exp Biol Med (Maywood)*. 2016;241(7):689-696.
17. Ware RE, de Montalembert M, Tshilolo L, Abboud MR. Sickle cell disease. *Lancet*. 2017;390(10091):311-323.
18. Hebbel RP, Belcher JD, Vercellotti GM. The multifaceted role of ischemia/reperfusion in sickle cell anemia. *J Clin Invest*. 2020;130(3):1062-1072.
19. Gladwin MT, Schechter AN, Ognibene FF, et al. Divergent nitric oxide bioavailability in men and women with sickle cell disease. *Circulation*. 2003;107(2):271-278.
20. de Montalembert M, Aggoun Y, Niakate A, Szezepanski I, Bonnet D. Endothelial-dependent vasodilation is impaired in children with sickle cell disease. *Haematologica*. 2007;92(12):1709-1710.
21. Belcher JD, Chen C, Nguyen J, et al. Heme triggers TLR4 signaling leading to endothelial cell activation and vaso-occlusion in murine sickle cell disease. *Blood*. 2014;123(3):377-390.
22. Hamideh D, Alvarez O. Sickle cell disease related mortality in the United States (1999-2009). *Pediatr Blood Cancer*. 2013;60(9):1482-1486.
23. Gladwin MT, Sachdev V. Cardiovascular abnormalities in sickle cell disease. *J Am Coll Cardiol*. 2012;59(13):1123-1133.
24. Wood KC, Gladwin MT, Straub AC. Sickle cell disease: at the crossroads of pulmonary hypertension and diastolic heart failure. *Heart*. 2020;106(8):562-568.
25. Chaudry RA, Cikes M, Karu T, et al. Paediatric sickle cell disease: pulmonary hypertension but normal vascular resistance. *Arch Dis Child*. 2011;96(2):131-136.
26. Rosenzweig EB, Abman SH, Adatia I, et al. Paediatric pulmonary arterial hypertension: updates on definition, classification, diagnostics and management. *Eur Respir J*. 2019;53(1):1801916.
27. Cabrita IZ, Mohammed A, Layton M, et al. The association between tricuspid regurgitation velocity and 5-year survival in a North West London population of patients with sickle cell disease in the United Kingdom. *Br J Haematol*. 2013;162(3):400-408.
28. Gladwin MT, Barst RJ, Gibbs JS, et al. Risk factors for death in 632 patients with sickle cell disease in the United States and United Kingdom. *PLoS One*. 2014;9(7):e99489.
29. Caughey MC, Poole C, Ataga KI, Hinderliter AL. Estimated pulmonary artery systolic pressure and sickle cell disease: a meta-analysis and systematic review. *Br J Haematol*. 2015;170(3):416-424.
30. Colombatti R, Maschietto N, Varotto E, et al. Pulmonary hypertension in sickle cell disease children under 10 years of age. *Br J Haematol*. 2010;150(5):601-609.
31. Minniti CP, Sable C, Campbell A, et al. Elevated tricuspid regurgitant jet velocity in children and adolescents with sickle cell disease: association with hemolysis and hemoglobin oxygen desaturation. *Haematologica*. 2009;94(3):340-347.
32. Gordeuk VR, Minniti CP, Nouraie M, et al. Elevated tricuspid regurgitation velocity and decline in exercise capacity over 22 months of follow up in children and adolescents with sickle cell anemia. *Haematologica*. 2011;96(1):33-40.
33. Ambrusko SJ, Gunawardena S, Sakara A, et al. Elevation of tricuspid regurgitant jet velocity, a marker for pulmonary hypertension in children with sickle cell disease. *Pediatr Blood Cancer*. 2006;47(7):907-913.
34. Campbell A, Minniti CP, Nouraie M, et al. Prospective evaluation of haemoglobin oxygen saturation at rest and after exercise in paediatric sickle cell disease patients. *Br J Haematol*. 2009;147(3):352-359.
35. Sachdev V, Kato GJ, Gibbs JS, et al. Echocardiographic markers of elevated pulmonary pressure and left ventricular diastolic dysfunction are associated with exercise intolerance in adults and adolescents with homozygous sickle cell anemia in the United States and United Kingdom. *Circulation*. 2011;124(13):1452-1460.
36. Hebson C, New T, Record E, et al. Elevated tricuspid regurgitant velocity as a marker for pulmonary hypertension in children with sickle cell disease: less prevalent and predictive than previously thought? *J Pediatr Hematol Oncol*. 2015;37(2):134-139.
37. Yawn BP, Buchanan GR, Afenyi-Annan AN, et al. Management of sickle cell disease: summary of the 2014 evidence-based report by expert panel members. *JAMA*. 2014;312(10):1033-1048.
38. de Montalembert M, Tshilolo L, Allali S. Sickle cell disease: a comprehensive program of care from birth. *Hematology Am Soc Hematol Educ Program*. 2019;2019(1):490-495.
39. Pashankar FD, Carbonella J, Bazzi-Asaad A, Friedman A. Longitudinal follow up of elevated pulmonary artery pressures in children with sickle cell disease. *Br J Haematol*. 2009;144(5):736-741.
40. Alsaeed T, Niss O, Powell AW, et al. Diastolic dysfunction is associated with exercise impairment in patients with sickle cell anemia. *Pediatr Blood Cancer*. 2018;65(8):e27113.
41. Niss O, Fleck R, Makue F, et al. Association between diffuse myocardial fibrosis and diastolic dysfunction in sickle cell anemia. *Blood*. 2017;130(2):205-213.
42. Pavlu J, Ahmed RE, O'Regan DP, Partridge J, Lefroy DC, Layton DM. Myocardial infarction in sickle-cell disease. *Lancet*. 2007;369(9557):246.
43. de Montalembert M, Maounoury C, Acar P, Brousse V, Sidi D, Lenoir G. Myocardial ischaemia in children with sickle cell disease. *Arch Dis Child*. 2004;89(4):359-362.
44. de Montalembert M, Ribeil JA, Brousse V, et al. Cardiac iron overload in chronically transfused patients with thalassemia, sickle cell anemia, or myelodysplastic syndrome. *PLoS One*. 2017;12(3):e0172147.
45. Badawy SM, Liem RI, Rigsby CK, Labotka RJ, Defreitas RA, Thompson AA. Assessing cardiac and liver iron overload in chronically transfused patients with sickle cell disease. *Br J Haematol*. 2016;175(4):705-713.
46. Sylvester KP, Patey RA, Milligan P, et al. Pulmonary function abnormalities in children with sickle cell disease. *Thorax*. 2004;59(1):67-70.
47. Tassel C, Arnaud C, Kulpa M, et al. Leukocytosis is a risk factor for lung function

deterioration in children with sickle cell disease. *Respir Med.* 2011;105(5):788-795.

48. Arigiani M, Kitenge R, Castriotta L, et al. Lung function in children with sickle cell disease from Central Africa. *Thorax.* 2019;74(6):604-606.

49. Cohen RT, Strunk RC, Rodeghier M, et al. Pattern of lung function is not associated with prior or future morbidity in children with sickle cell anemia. *Ann Am Thorac Soc.* 2016;13(8):1314-1323.

50. Lunt A, McGhee E, Sylvester K, et al. Longitudinal assessment of lung function in children with sickle cell disease. *Pediatr Pulmonol.* 2016;51(7):717-723.

51. Aretta M, Campbell A, Nouraie M, et al. Abnormal pulmonary function and associated risk factors in children and adolescents with sickle cell anemia. *J Pediatr Hematol Oncol.* 2014;36(3):185-189.

52. MacLean JE, Atenafu E, Kirby-Allen M, et al. Longitudinal decline in lung volume in a population of children with sickle cell disease. *Am J Respir Crit Care Med.* 2008;178(10):1055-1059.

53. Koubourlis AC. Lung function in sickle cell disease: an elusive relationship. *Pediatr Pulmonol.* 2016;51(7):665-667.

54. Boyd JH, Macklin EA, Strunk RC, DeBaun MR. Asthma is associated with acute chest syndrome and pain in children with sickle cell anemia. *Blood.* 2006;108(9):2923-2927.

55. Field JJ, DeBaun MR, Yan Y, Strunk RC. Growth of lung function in children with sickle cell anemia. *Pediatr Pulmonol.* 2008;43(11):1061-1066.

56. Nath KA, Hebbel RP. Sickle cell disease: renal manifestations and mechanisms. *Nat Rev Nephrol.* 2015;11(3):161-171.

57. Ware RE, Rees RC, Sarnaik SA, et al. Renal function in infants with sickle cell anemia: baseline data from the BABY HUG trial. *J Pediatr.* 2010;156(1):66-70.

58. Merle NS, Grunenwald A, Rajaratnam H, et al. Intravascular hemolysis activates complement via cell-free heme and heme-loaded microvesicles. *JCI Insight.* 2018;3(12):e96910.

59. Van Avondt K, Nur E, Zeerleder S. Mechanisms of haemolysis-induced kidney injury. *Nat Rev Nephrol.* 2019;15(11):671-692.

60. Lebensburger JD, Aban I, Pernell B, et al. Hyperfiltration during early childhood precedes albuminuria in pediatric sickle cell nephropathy. *Am J Hematol.* 2019;94(4):417-423.

61. McPherson Yee M, Jabbar SF, Osunkwo I, et al. Chronic kidney disease and albuminuria in children with sickle cell disease. *Clin J Am Soc Nephrol.* 2011;6(11):2628-2633.

62. Aygun B, Mortier NA, Smeltzer MP, Hankins JS, Ware RE. Glomerular hyperfiltration and albuminuria in children with sickle cell anemia. *Pediatr Nephrol.* 2011;26(8):1285-1290.

63. Bodas P, Huang A, O'Riordan MA, Sedor JR, Dell KM. The prevalence of hypertension and abnormal kidney function in children with sickle cell disease - a cross sectional review. *BMC Nephrol.* 2013;14:237.

64. Baddam S, Aban I, Hilliard L, Howard T, Askenazi D, Lebensburger JD. Acute kidney injury during a pediatric sickle cell vaso-occlusive pain crisis. *Pediatr Nephrol.* 2017;32(8):1451-1456.

65. Lebensburger JD, Palabindela P, Howard TH, Feig DI, Aban I, Askenazi DJ. Prevalence of acute kidney injury during pediatric admissions for acute chest syndrome. *Pediatr Nephrol.* 2016;31(8):1363-1368.

66. Aban I, Baddam S, Hilliard LM, Howard TH, Feig DI, Lebensburger JD. Severe anemia early in life as a risk factor for sickle-cell kidney disease. *Blood.* 2017;129(3):385-387.

67. Lebensburger JD, Cutter GR, Howard TH, Muntner P, Feig DI. Evaluating risk factors for chronic kidney disease in pediatric patients with sickle cell anemia. *Pediatr Nephrol.* 2017;32(9):1565-1573.

68. Zahr RS, Rampersaud E, Kang G, et al. Children with sickle cell anemia and APOL1 genetic variants develop albuminuria early in life. *Haematologica.* 2019;104(9):e385-e387.

69. Wang WC, Ware RE, Miller ST, et al. Hydroxycarbamide in very young children with sickle-cell anaemia: a multicentre, randomised, controlled trial (BABY HUG). *Lancet.* 2011;377(9778):1663-1672.

70. Alvarez O, Miller ST, Wang WC, et al. Effect of hydroxyurea treatment on renal function parameters: results from the multi-center placebo-controlled BABY HUG clinical trial for infants with sickle cell anemia. *Pediatr Blood Cancer.* 2012;59(4):668-674.

71. McKie KT, Hanevold CD, Hernandez C, Waller JL, Ortiz L, McKie KM. Prevalence, prevention, and treatment of microalbuminuria and proteinuria in children with sickle cell disease. *J Pediatr Hematol Oncol.* 2007;29(3):140-144.

72. Lebensburger J, Johnson SM, Askenazi DJ, Rozario NL, Howard TH, Hilliard LM. Protective role of hemoglobin and fetal hemoglobin in early kidney disease for children with sickle cell anemia. *Am J Hematol.* 2011;86(5):430-432.

73. Zahr RS, Hankins JS, Kang G, et al. Hydroxyurea prevents onset and progression of albuminuria in children with sickle cell anemia. *Am J Hematol.* 2019;94(1):E27-E29.

74. Aygun B, Mortier NA, Smeltzer MP, Shulkin BL, Hankins JS, Ware RE. Hydroxyurea treatment decreases glomerular hyperfiltration in children with sickle cell anemia. *Am J Hematol.* 2013;88(2):116-119.

75. Fitzhugh CD, Wigfall DR, Ware RE. Enalapril and hydroxyurea therapy for children with sickle nephropathy. *Pediatr Blood Cancer.* 2005;45(7):982-985.

76. Desselas E, Thuret I, Kagueldou F, et al. Mortality in children with sickle cell disease in mainland France from 2000 to 2015. *Haematologica.* 2020;105(9):e440-443.

77. DeBaun MR, Kirkham FJ. Central nervous system complications and management in sickle cell disease. *Blood.* 2016;127(7):829-838.

78. DeBaun MR, Armstrong FD, McKinstry RC, Ware RE, Vichinsky E, Kirkham FJ. Silent cerebral infarcts: a review on a prevalent and progressive cause of neurologic injury in sickle cell anemia. *Blood.* 2012;119(20):4587-4596.

79. Kirkham FJ, Hewes DK, Prengler M, Wade A, Lane R, Evans JP. Nocturnal hypoxaemia and central-nervous-system events in sickle-cell disease. *Lancet.* 2001;357(9269):1656-1659.

80. Miller ST, Macklin EA, Pegelow CH, et al. Silent infarction as a risk factor for overt stroke in children with sickle cell anemia: a report from the Cooperative Study of Sickle Cell Disease. *J Pediatr.* 2001;139(3):385-390.

81. Bernaudin F, Verlhac S, Chevret S, et al. G6PD deficiency, absence of alpha-thalassemia, and hemolytic rate at baseline are significant independent risk factors for abnormally high cerebral velocities in patients with sickle cell anemia. *Blood.* 2008;112(10):4314-4317.

82. Miller ST, Milton J, Steinberg MH. G6PD deficiency and stroke in the CSSCD. *Am J Hematol.* 2011;86(3):331.

83. Bernaudin F, Verlhac S, Arnaud C, et al. Impact of early transcranial Doppler screening and intensive therapy on cerebral vasculopathy outcome in a newborn sickle cell anemia cohort. *Blood.* 2011;117(4):1130-1140; quiz 1436.

84. Adams RJ, McKie VC, Hsu L, et al. Prevention of a first stroke by transfusions in children with sickle cell anemia and abnormal results on transcranial Doppler ultrasound. *N Engl J Med.* 1998;339(1):5-11.

85. Abdullahi SU, DeBaun MR, Jordan LC, Rodeghier M, Galadanci NA. Stroke recurrence in Nigerian children with sickle cell disease: evidence for a secondary stroke prevention trial. *Pediatr Neurol.* 2019;95:73-78.

86. Hankins JS, Fortner GL, McCarville MB, et al. The natural history of conditional transcranial Doppler flow velocities in children with sickle cell anaemia. *Br J Haematol.* 2008;142(1):94-99.

87. Lee YS, Jung KH, Roh JK. Diagnosis of moyamoya disease with transcranial Doppler sonography: correlation study with magnetic resonance angiography. *J Neuroimaging.* 2004;14(4):319-323.

88. Deane CR, Goss D, Bartram J, et al. Extracranial internal carotid arterial disease in children with sickle cell anemia. *Haematologica.* 2010;95(8):1287-1292.

89. Bernaudin F, Verlhac S, Arnaud C, et al. Chronic and acute anemia and extracranial internal carotid stenosis are risk factors for silent cerebral infarcts in sickle cell anemia. *Blood.* 2015;125(10):1653-1661.

90. Mirre E, Brousse V, Berteloot L, et al. Feasibility and efficacy of chronic transfusion for stroke prevention in children with sickle cell disease. *Eur J Haematol.* 2010;84(3):259-265.

91. DeBaun MR, Gordon M, McKinstry RC, et al. Controlled trial of transfusions for silent cerebral infarcts in sickle cell anemia. *N Engl J Med.* 2014;371(8):699-710.

92. Hankins JS, Helton KJ, McCarville MB, Li CS, Wang WC, Ware RE. Preservation of spleen and brain function in children with sickle cell anemia treated with hydroxyurea. *Pediatr Blood Cancer.* 2008;50(2):293-297.

93. Gardner K, Suddle A, Kane P, et al. How we treat sickle hepatopathy and liver transplantation in adults. *Blood.* 2014;123(15):2302-2307.

94. Allali S, de Montalembert M, Brousse V, et al. Hepatobiliary complications in children with sickle cell disease: a retrospective review of medical records from 616 patients. *J Clin Med.* 2019;8(9):1481.

95. Jitnaruch S, Fitzpatrick E, Deheragoda M, et al. Autoimmune liver disease in children with sickle cell disease. *J Pediatr.* 2017;189:79-85.

96. Goodwin EF, Partain PI, Lebensburger JD, Fineberg NS, Howard TH. Elective cholecystectomy reduces morbidity of cholelithiasis in pediatric sickle cell disease. *Pediatr Blood Cancer.* 2017;64(1):113-120.

97. van Beers EJ, van Tuijn CF, Mac Gillavry MR, van der Giessen A, Schnog JJ, Biemond BJ. Sickle cell disease-related organ damage occurs irrespective of pain rate: implications for clinical practice. *Haematologica.* 2008;93(5):757-760.

98. Gill HS, Lam WC. A screening strategy for the detection of sickle cell retinopathy in pediatric patients. *Can J Ophthalmol.* 2008;43(2):188-191.

99. Mohan JS, Lip PL, Blann AD, Bareford D, Lip

GY. The angiopoietin/Tie-2 system in proliferative sickle retinopathy: relation to vascular endothelial growth factor, its soluble receptor Flt-1 and von Willebrand factor, and to the effects of laser treatment. *Br J Ophthalmol.* 2005;89(7):815-819.

100. Martin GC, Denier C, Zambrowski O, et al. Visual function in asymptomatic patients with homozygous sickle cell disease and temporal macular atrophy. *JAMA Ophthalmol.* 2017;135(10):1100-1105.

101. Martin GC, Albuison E, Brousse V, de Montalembert M, Bremond-Gignac D, Robert MP. Paramacular temporal atrophy in sickle cell disease occurs early in childhood. *Br J Ophthalmol.* 2019;103(7):906-910.

102. Manara R, Dalla Torre A, Lucchetta M, et al. Visual cortex changes in children with sickle cell disease and normal visual acuity: a multimodal magnetic resonance imaging study. *Br J Haematol.* 2021;192(1):151-157.

103. Adesina OO, Neumayr LD. Osteonecrosis in sickle cell disease: an update on risk factors, diagnosis, and management. *Hematology Am Soc Hematol Educ Program.* 2019;2019(1):351-358.

104. Dalle Carbonare L, Matte A, Valenti MT, et al. Hypoxia-reperfusion affects osteogenic lineage and promotes sickle cell bone disease. *Blood.* 2015;126(20):2320-2328.

105. Chapelon E, Garabedian M, Brousse V, Souberbielle JC, Bresson JL, de Montalembert M. Osteopenia and vitamin D deficiency in children with sickle cell disease. *Eur J Haematol.* 2009;83(6):572-578.

106. Milner PF, Kraus AP, Sebes JI, et al. Sickle cell disease as a cause of osteonecrosis of the femoral head. *N Engl J Med.* 1991;325(21):1476-1481.

107. Mallet C, Abitan A, Vidal C, et al. Management of osteonecrosis of the femoral head in children with sickle cell disease: results of conservative and operative treatments at skeletal maturity. *J Child Orthop.* 2018;12(1):47-54.

108. de Montalembert M, Ferster A, Colombatti R, Rees DC, Gulbis B. ENERCA clinical recommendations for disease management and prevention of complications of sickle cell disease in children. *Am J Hematol.* 2011;86(1):72-75.

Oncorequisite role of an aldehyde dehydrogenase in the pathogenesis of T-cell acute lymphoblastic leukemia



Ferrata Storti Foundation

Chujing Zhang,¹ Stella Amanda,¹ Cheng Wang,² Tze King Tan,¹ Muhammad Zulfaqar Ali,¹ Wei Zhong Leong,¹ Ley Moy Ng,¹ Shojiro Kitajima,³ Zhenhua Li,⁴ Allen Eng Juh Yeh,^{1,4} Shi Hao Tan¹ and Takaomi Sanda^{1,5}

¹Cancer Science Institute of Singapore, National University of Singapore, Singapore;

²Department of Anatomy, National University of Singapore, Singapore; ³Institute for Advanced Biosciences, Keio University, Tsuruoka, Japan; ⁴VIVA-NUS CenTRAL, Department of Pediatrics, National University of Singapore, Singapore and

⁵Department of Medicine, Yong Loo Lin School of Medicine, National University of Singapore, Singapore.

Haematologica 2021
Volume 106(6):1545-1558

ABSTRACT

Aldehyde dehydrogenases (ALDH) are overexpressed in various types of cancers. One of the ALDH family genes, *ALDH1A2*, is aberrantly expressed in more than 50% of cases of T-cell acute lymphoblastic leukemia (T-ALL). However, its molecular function and role in the pathogenesis of T-ALL are largely unknown. Chromatin immunoprecipitation-sequencing and RNA-sequencing analyses showed that the oncogenic transcription factor *TAL1* and its regulatory partners bind to the intronic regulatory element of the *ALDH1A2* gene, directly inducing a T-ALL-specific isoform with enzymatic activity. *ALDH1A2* was preferentially expressed in the *TAL1*-positive T-ALL subgroup. In T-ALL cell lines, depletion of *ALDH1A2* inhibited cell viability and induced apoptosis. Interestingly, gene expression and metabolomic profiling revealed that *ALDH1A2* supported glycolysis and the tricarboxylic acid cycle, accompanied by NADH production, by affecting multiple metabolic enzymes to promote ATP production. Depletion of *ALDH1A2* increased the levels of reactive oxygen species, while the levels were reduced by *ALDH1A2* overexpression both *in vitro* and *in vivo*. Overexpression of *ALDH1A2* accelerated tumor onset and increased tumor penetrance in a zebrafish model of T-ALL. Taken together, our results indicate that *ALDH1A2* protects against intracellular stress and promotes T-ALL cell metabolism and survival. *ALDH1A2* overexpression enables leukemic clones to sustain a hyper-proliferative state driven by oncogenes.

Introduction

T-cell acute lymphoblastic leukemia (T-ALL) is a hematologic malignancy that arises from immature T-cell precursors.^{1,2} This type of leukemia occurs mostly in children but is also found in adults. A number of chromosomal and genetic abnormalities have been identified in T-ALL, many of which affect genes encoding transcription factors.³ Gene expression and mutational profiles have demonstrated that T-ALL cases can be classified into mutually exclusive subgroups based on the expression of several transcription factors (*TAL1*, *TAL2*, *LYL1*, *LMO1*, *LMO2*, *TLX1/HOX11*, *TLX3/HOX11L2*, *HOXA* and *NKX3-1*).⁴⁻⁶ This suggests that each transcription factor drives a distinct cellular program that may work in concert with other molecular pathways in T-ALL cells.

TAL1-positive T-ALL constitutes the largest subgroup, accounting for 40-60% of all primary cases.^{4,7-11} One of the known downstream targets of *TAL1* in T-ALL cells is *ALDH1A2*,^{12,13} a member of the aldehyde dehydrogenase (ALDH) family of genes that encode oxidoreductases. ALDH proteins convert a variety of aldehydes into carboxylic acids.^{14,15} They detoxify endogenous aldehydes, generated during the

Correspondence:

TAKAOMI SANDA
takaomi_sanda@nus.edu.sg

Received: December 18, 2019.

Accepted: May 14, 2020.

Pre-published: May 15, 2020.

<https://doi.org/10.3324/haematol.2019.245639>

© 2021 Ferrata Storti Foundation

Material published in *Haematologica* is covered by copyright. All rights are reserved to the Ferrata Storti Foundation. Use of published material is allowed under the following terms and conditions: <https://creativecommons.org/licenses/by-nc/4.0/legalcode>. Copies of published material are allowed for personal or internal use. Sharing published material for non-commercial purposes is subject to the following conditions: <https://creativecommons.org/licenses/by-nc/4.0/legalcode>, sect. 3. Reproducing and sharing published material for commercial purposes is not allowed without permission in writing from the publisher.



metabolism of membrane lipids, amino acids, carbohydrates and steroids.¹⁶ The reaction is NAD(P)⁺-dependent and generates an important component of the cellular antioxidant system, NAD(P)H, which also acts as an essential coenzyme in several metabolic pathways, such as glycolysis and the tricarboxylic acid (TCA) cycle.¹⁴ Retinaldehyde dehydrogenases, a subfamily of *ALDH* genes, including *ALDH1A2*, are also capable of converting retinaldehyde into retinoic acid. ALDH activity has also been implicated as a cancer stem cell marker in various solid tumors.^{17,18} The Aldefluor assay is commonly used to isolate an ALDH-positive population to refine the cancer stem cell population.^{17,19} Overexpression of *ALDH* genes confers drug resistance to cancer cells.²⁰ These findings suggest that high levels of ALDH activity may be advantageous and, even required, for cancer cell maintenance.

In this study, we elucidated the molecular function and role of *ALDH1A2* in the pathogenesis of T-ALL. We demonstrated that *ALDH1A2* is directly activated by TAL1 and protects against intracellular stress, supporting leukemia cell metabolism and promoting leukemia cell survival.

Methods

Cell samples

Human leukemia cell lines were cultured in RPMI-1640 medium (BioWest) supplemented with 10% fetal bovine serum (BioWest). A T-ALL patient-derived xenograft sample was provided by Alejandro Gutierrez (Boston Children's Hospital) and expanded in NSG mice. Mouse protocols were approved by the Institutional Animal Care and Use Committee.

Knockdown and overexpression experiments

For knockdown experiments, short-hairpin RNA (shRNA) was inserted into a pLKO.1-puro lentivirus vector. For overexpression experiments, *ALDH1A2* cDNA cloned from Jurkat cells was inserted into a MSCV-IRES-GFP retrovirus vector. For inhibition of the regulatory element, single-guide RNA (sgRNA) was inserted into a FgH1tUTG lentivirus vector (Addgene plasmid #70183). Virus was produced by co-transfected the construct with the packaging and envelope plasmids into 293T cells using FuGENE6 (Roche).

Quantitative reverse transcription polymerase chain reaction

Total RNA was extracted from cells using a NucleoSpin RNA kit (Macherey-Nagel) and reverse-transcribed using a QuantiTect kit (Qiagen). Quantitative reverse transcription polymerase chain reaction (qRT-PCR) was performed on a QuantStudio3 real-time PCR system (Thermo Fisher Scientific) using Power SYBR Green PCR Master Mix (Roche). The primer sequences are described in the *Online Supplementary Information*.

Western blot analysis

Equivalent amounts of protein were resolved on a sodium dodecylsulfate polyacrylamide gel electrophoresis gel, transferred onto polyvinylidene difluoride membranes (Bio-Rad), and subjected to immunoblot analysis with specific antibodies against *ALDH1A2* (Abcam), TAL1 (Millipore), PARP, caspase-3, α -tubulin, and β -actin (Cell Signaling Technology). The proteins were detected using an enhanced chemiluminescence reagent (Thermo).

Confocal microscopic imaging

Images of EGFP-fused *ALDH1A2* protein localization in live cells were captured using an Olympus FV1000 TIRF confocal

microscope (C4). Colocalization of signals was analyzed using IMARIS 9.5 software after staining with Mito Tracker Red CMXRos (Thermo) and Hoechst.

Intracellular reactive oxygen species assay

The cells were treated with freshly prepared CellROX Deep Red reagent (Thermo Fisher Scientific). Fluorescence signals were analyzed with a BD SR II flow cytometer using BD FACSDiva™ software and FlowJo software.

Metabolomic profiling

The extracted metabolites were used for a capillary electrophoresis time-of-flight mass spectrometry basic scan, conducted by Human Metabolome Technologies (see details in the *Online Supplementary Information*). The number of metabolites was normalized to cell volume detected by a Scepter 2.0 cell counter (Millipore).

Extracellular flux analysis

The cells were resuspended in Seahorse assay medium (Agilent) and seeded into XF24 plates. Extracellular acidification rate and the oxygen consumption rate were measured by Seahorse XF24 (Agilent). The details are provided in the *Online Supplementary Information*.

Chromatin immunoprecipitation sequencing and RNA-sequencing

Chromatin immunoprecipitation (ChIP)-sequencing analysis was done in our previous study.²¹ For RNA-sequencing, RNA was extracted using an miRNeasy kit (Qiagen) followed by DNase treatment (Ambion). Construction of the strand-specific library and sequencing of the single-end 100-bp-long reads by a BGISEQ sequencer were conducted at BGI Biotech (Hong Kong). The details are described in the *Online Supplementary Information*.

Zebrafish transgenesis

Zebrafish protocols were approved by the Institutional Animal Care and Use Committee. The human *ALDH1A2* or *mCherry* gene was cloned under the zebrafish *rag2* promoter and injected into zebrafish embryos to create *Tg(rag2: ALDH1A2)* or a control *Tg(rag2: mCherry)* line. The *rag2-myr-mAKT2* construct was kindly provided by Alejandro Gutierrez.²²

Results

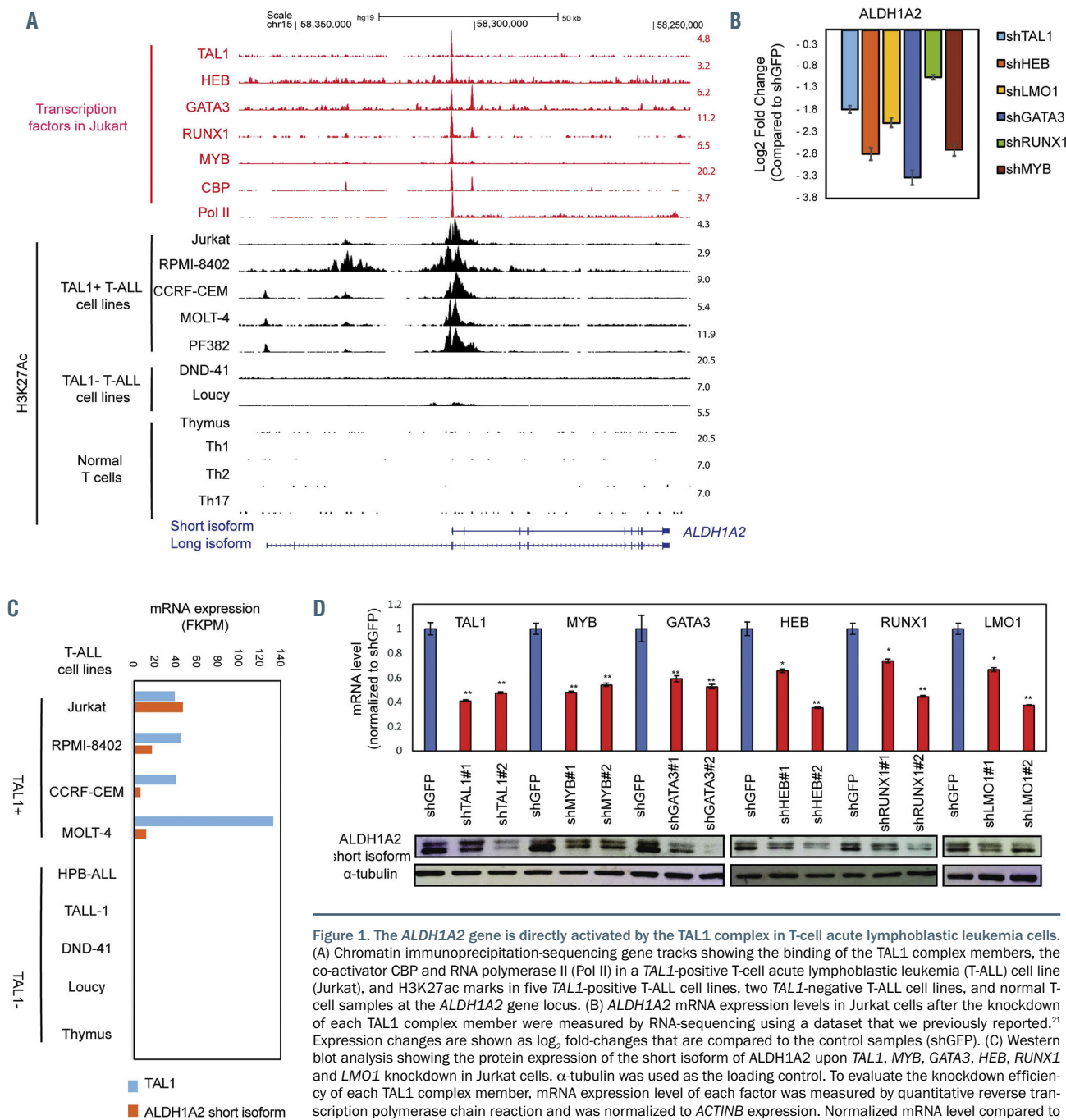
The *ALDH1A2* gene is directly activated by the TAL1 complex in T-cell acute lymphoblastic leukemia

To identify the targets directly regulated by TAL1 in T-ALL cells, we referred to a previously performed ChIP-sequencing dataset for TAL1 and other members of the transcriptional complex in a T-ALL cell line (Jurkat).¹³ We integrated this result with the RNA-sequencing dataset after knocking down each factor in the same cell line, which was generated in our recent study,²¹ to select genes that were positively regulated by the TAL1 complex. We further filtered genes that were associated with a high level of an active histone mark (H3K27ac) in T-ALL cells but not in normal thymus cells (*Online Supplementary Figures S1A and B*), representing high-confidence TAL1 targets that were aberrantly activated in T-ALL cells.

ALDH1A2 was among the top hits. An early study showed that the TAL1/GATA3/LMO complex binds at the intronic region of the *ALDH1A2* gene and induces its expression in T-ALL cells.¹² Consistently, our ChIP-

sequencing analysis demonstrated that TAL1 and its binding partners (HEB, GATA3, RUNX1 and MYB) bind within the intron with the co-activator CBP and RNA polymerase II in Jurkat cells (Figure 1A). Knocking down each of these factors resulted in downregulation of *ALDH1A2* mRNA expression in the same cell line, as determined by RNA-sequencing (Figure 1B, *Online Supplementary Figure S1B*). The result was validated at the protein level (Figure 1C). Importantly, the TAL1-bound region was associated with a high level of H3K27ac signals in multiple *TAL1*-positive

T-ALL cell lines but not in *TAL1*-negative cell lines (Figure 1A). This status corresponded to an *ALDH1A2* mRNA expression pattern that was detected only in *TAL1*-positive T-ALL cell lines (Figure 1D). Similarly, in the primary T-ALL cells from three independent cohorts,^{4,23,24} *ALDH1A2* expression was significantly higher in the *TAL1*/2- and *LMO1*/2-subgroups than in the *TLX*, *LYL/LMO* and *HOXA*-positive subgroups (Figure 1E, *Online Supplementary Figure S1C*, *Online Supplementary Table S1*). Furthermore, the results from the analysis of the



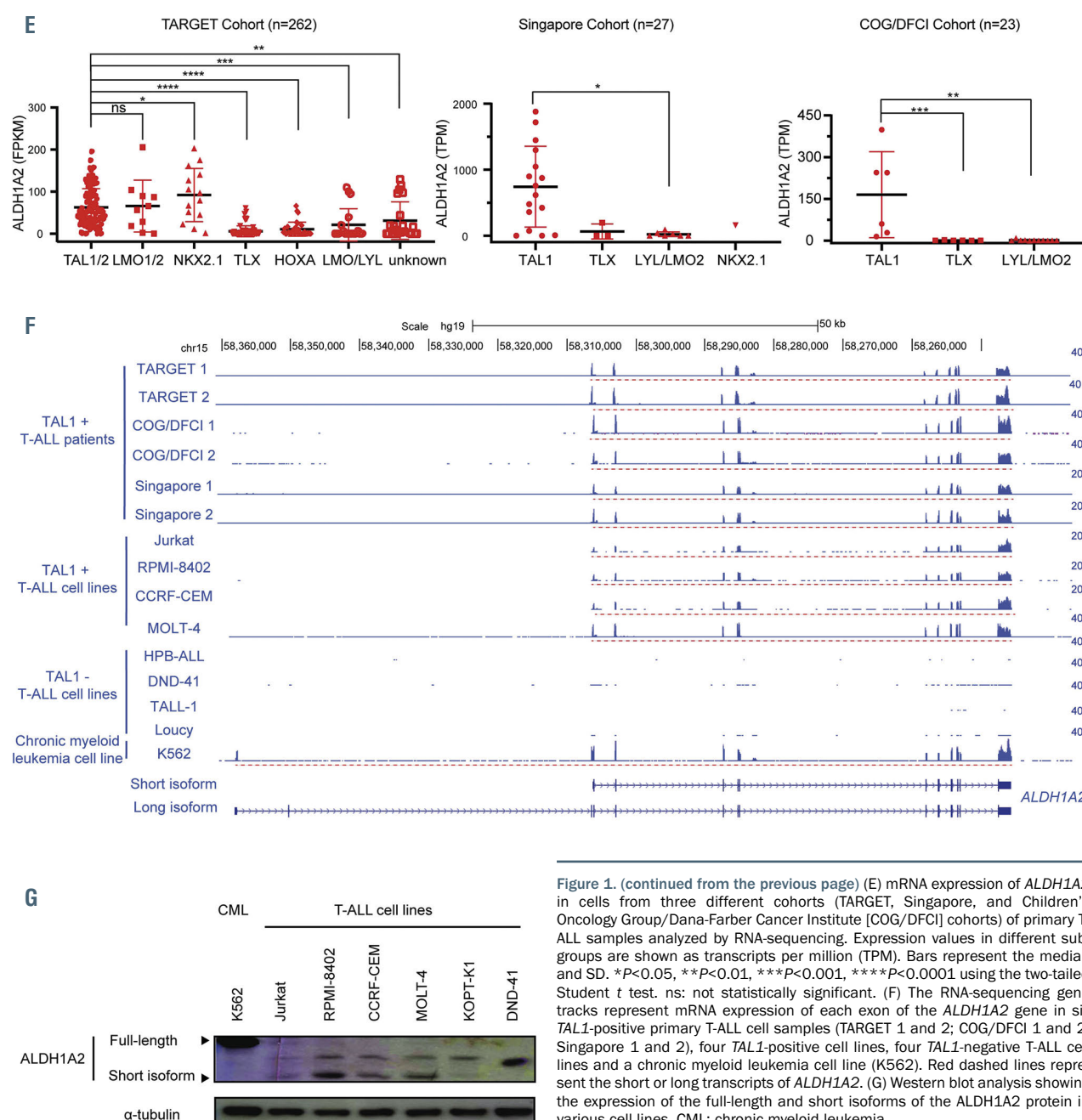


Figure 1. (continued from the previous page) (E) mRNA expression of *ALDH1A2* in cells from three different cohorts (TARGET, Singapore, and Children's Oncology Group/Dana-Farber Cancer Institute [COG/DFCI] cohorts) of primary T-ALL samples analyzed by RNA-sequencing. Expression values in different subgroups are shown as transcripts per million (TPM). Bars represent the median and SD. * $P<0.05$, ** $P<0.01$, *** $P<0.001$, **** $P<0.0001$ using the two-tailed Student *t* test. ns: not statistically significant. (F) The RNA-seq gene tracks represent mRNA expression of each exon of the *ALDH1A2* gene in six *TAL1*-positive primary T-ALL cell samples (TARGET 1 and 2; COG/DFCI 1 and 2; Singapore 1 and 2), four *TAL1*-positive cell lines, four *TAL1*-negative T-ALL cell lines and a chronic myeloid leukemia cell line (K562). Red dashed lines represent the short or long transcripts of *ALDH1A2*. (G) Western blot analysis showing the expression of the full-length and short isoforms of the *ALDH1A2* protein in various cell lines. CML: chronic myeloid leukemia.

Cancer Cell Line Encyclopedia dataset showed the highest expression of *ALDH1A2* mRNA in T-ALL samples among 40 cancer types²⁵ (Online Supplementary Figure S1D).

Notably, RNA-seq analysis demonstrated that only the short isoform, which lacks the first three exons, but not the full-length (long) isoform of *ALDH1A2*, was expressed in the *TAL1*-positive T-ALL cells, including primary samples and cell lines (Figure 1F). This result was consistent with that from an earlier study.¹² In contrast, K562 cells, a chronic myeloid leukemia cell line, expressed the long isoform of *ALDH1A2* but not the short isoform (Figure 1F, bottom). The difference in protein size was confirmed by western blot (Figure 1G).

It is noteworthy that the H3K27ac marks were not observed in normal T cells (Figure 1A). Consistent with this finding, in an analysis of a public dataset of normal human

hematopoietic cells,²⁶ *ALDH1A2* expression was not detected in T cells (Online Supplementary Figure S1E). Similarly, the mouse *Aldh1a2* gene was not expressed in hematopoietic cells, while it was detected in bone marrow stroma cells (Online Supplementary Figure S1F). Furthermore, recent single-cell RNA-seq studies confirmed that *ALDH1A2* is expressed in thymic stroma cells but not in any T-cell subpopulations both in mice and human cells.^{27,28} These results further indicated that *ALDH1A2* is aberrantly activated in cases of *TAL1*-positive T-ALL.

The short isoform of *ALDH1A2* possesses enzymatic activity and is localized in the cytoplasm

We next investigated the function of the short isoform of the *ALDH1A2* protein. The analysis of the amino acid sequence indicated that the short isoform retains function-

ally critical residues, such as the NAD binding site and the enzymatic catalytic residues, but lacks 96 amino acids in the N-terminus (Figure 2A) that are a part of the homotetrameric interface (Figure 2B). Hence, we postulated that the short isoform might have attenuated enzymatic activity or a different subcellular localization compared to the long isoform.

To investigate this, we first produced each isoform of ALDH1A2 as a purified recombinant His-tagged protein (*Online Supplementary Figure S2A*) and performed an *in vitro* enzymatic assay. We incubated each isoform with a substrate (retinaldehyde) and a coenzyme (NAD⁺) and measured the amount of NADH produced over 20 min (Figure 2C). This analysis revealed that the short isoform had enzymatic ability, although slightly lower than that of the long isoform (Figure 2C, *Online Supplementary Figure S2B*). Next, we analyzed the effect of ALDH1A2 on the production of retinoic acid using a reporter system. We cloned a trimerized retinoic acid responsive element, which can be activated by the retinoic acid receptor complex, into the luciferase plasmid and then established Jurkat cells that stably express this construct²⁹ (*Online Supplementary Figure S2C*). In this setting, the luciferase activity is dependent on the amount of retinoic acid produced internally in the Jurkat cells. We then knocked down the endogenous ALDH1A2 by lentiviral shRNA transduction. The luciferase activity was significantly downregulated after ALDH1A2 had been depleted (*Online Supplementary Figure S2C*), indicating that the short isoform of ALDH1A2 can mediate the production of retinoic acid in T-ALL cells.

We next analyzed the subcellular localization of the short isoform of the endogenous ALDH1A2 protein. We used the CRISPR/Cas9-mediated method to introduce an EGFP gene fused to the 3' end of the endogenous ALDH1A2 gene into both Jurkat and K562 cells (*Online Supplementary Figures S2D* and *E*). We then analyzed the localization of the EGFP signal in the nucleus (with Hoechst staining), mitochondria (with Mitotracker staining) or cytoplasm (without staining). The results demonstrated that the short isoform of ALDH1A2 in Jurkat cells was localized in the cytoplasm with no co-localization in mitochondria or the nucleus (Figure 2D, *Online Supplementary Figure S2F*), which was similar to the pattern observed for the K562 cells that expressed the long isoform. These results indicate that the short isoform of ALDH1A2 possesses intact enzymatic functions and the same localization pattern as observed for the long isoform.

ALDH1A2 supports T-cell acute lymphoblastic leukemia cell survival and viability

We next analyzed whether ALDH1A2 expression confers any functional advantage to T-ALL cells. We first evaluated the phenotype after depletion of ALDH1A2 by blocking the regulatory element. We designed two independent sgRNA (#1 and #2), which targeted the TAL1-bound region (Figure 3A). We transduced each of them under a doxycycline-inducible system together with a catalytically inactive Cas9 (dCas9) protein fused with the KRAB repressor, thereby epigenetically silencing the transcriptional activity at the TAL1-bound region. We observed successful downregulation of ALDH1A2 protein after the induction of each sgRNA (Figure 3B). Importantly, apoptotic cell death was induced after 72 h of induction, as evidenced by the cleavage of caspase-3 and PARP (markers of apoptosis) (Figure 3B).

To independently validate this result, we utilized a lentiviral shRNA system to knock down ALDH1A2 and analyzed the number of annexin-V-positive cells, which is another means to detect apoptosis. The result confirmed that depletion of ALDH1A2 induced apoptosis in multiple TAL1/ALDH1A2-positive T-ALL cell lines but not in the negative cell lines (Figure 3C). Consistently, cell viability was reduced after the shRNA knockdown of ALDH1A2 in an ALDH1A2-positive cell line (Jurkat) (Figure 3D). Conversely, forced expression of ALDH1A2 in an ALDH1A2-negative T-ALL cell line (DND-41) increased cell viability (Figure 3E).

WIN 18,446 is reported to be a pan-ALDH1A inhibitor.³⁰ It has been shown to strongly inhibit the enzymatic activity of ALDH1A2 both *in vitro* and *in vivo*.^{31,32} Since ALDH1A2 is the only member of the ALDH1A family of genes expressed in T-ALL (*Online Supplementary Figure S3A*), we tested the effect of WIN 18,446 on cell viability of several T-ALL cell lines. Strikingly, two TAL1/ALDH1A2-positive cell lines (Jurkat and RPMI-8402) were more sensitive to this small-molecule inhibitor than two TAL1/ALDH1A2-negative cell lines (KOPT-K1 and DND-41) (Figure 3F, *Online Supplementary Figure S3B*). These results indicate that the expression of ALDH1A2 is associated with the viability and survival of T-ALL cells. This phenotype was not rescued by the addition of all-trans retinoic acid (*Online Supplementary Figure S3C*), thus suggesting that this mechanism is likely independent of the amount of retinoic acid produced.

ALDH1A2 affects metabolic pathways in T-cell acute lymphoblastic leukemia cells

We next investigated the molecular mechanisms by which ALDH1A2 supports cell viability and prevents apoptosis. We performed global gene expression profiling by RNA-sequencing after sgRNA-mediated ALDH1A2 depletion. We selected genes that were significantly downregulated (n=96) or upregulated (n=19) in the ALDH1A2-depleted samples compared to the control samples (Figure 4A, *Online Supplementary Figure S4A*, *Online Supplementary Table S2*). Interestingly, the downregulated genes included a number of metabolic enzymes and transporters involved in the glycolysis pathway (yellow, Figure 4A and B, *Online Supplementary Figure 4B* and *C*). In contrast, several enzymes involved in amino acid metabolism, such as ASS1 and ASNS, were upregulated after ALDH1A2 depletion (Figure 4A, *Online Supplementary Figure S4A*). The result was validated for each enzyme individually by qRT-PCR (*Online Supplementary Figure S4D*).

This finding prompted us to analyze the metabolic state of the T-ALL cells. We performed a capillary electrophoresis time-of-flight mass spectrometry analysis to measure the relative levels of 200 metabolites involved in the major metabolomics pathways after depletion of ALDH1A2 in Jurkat cells (Figure 4C). Strikingly, ALDH1A2 depletion resulted in a reduction in the intermediate metabolites involved in the glycolysis pathway (pink). Suppressed glucose metabolism was accompanied by a reduction in acetyl-CoA (yellow), which is one of the key carbon sources that drive the TCA cycle. We also observed a reduction in citric acid, *cis*-aconitic acid and isocitric acid (yellow), likely due to the decreased integration of glycolysis-derived acetyl-CoA into the TCA cycle.

It is noteworthy that the levels of metabolites derived

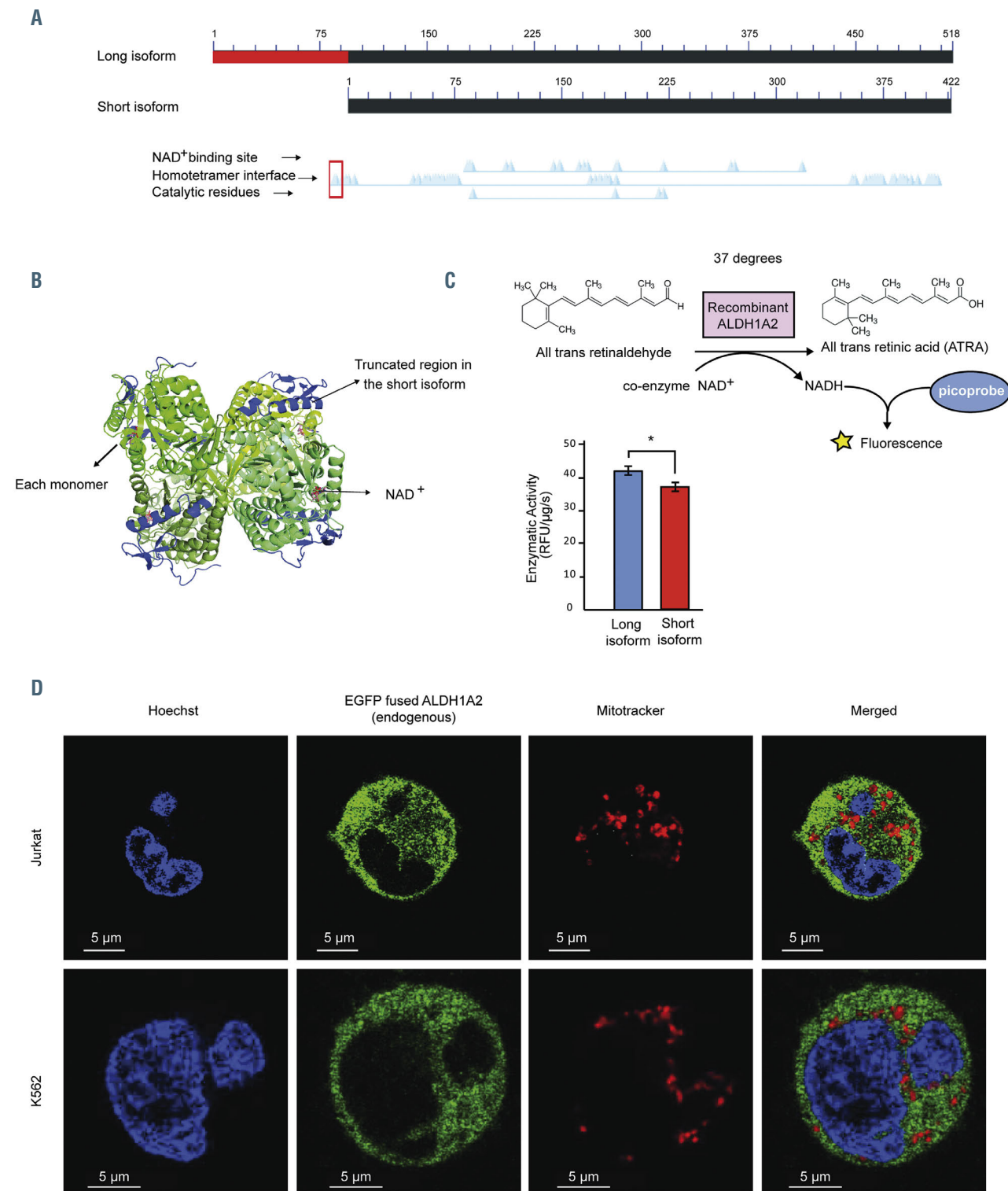


Figure 2. The short isoform of ALDH1A2 has enzymatic activity and is localized in the cytoplasm. (A) Protein domains of the ALDH1A2. NAD⁺ binding site, homotetramer interface and catalytic residues are indicated individually by blue triangles. The truncated short isoform lacks 96 amino acids at the N-terminus. The deleted tetramer interface of the short isoform is marked with a red block. (B) The crystal structure of the homotetrameric ALDH1A2 long isoform (PDB: 4X2Q) is presented as a cartoon model generated by PyMOL. Each monomer is colored in a different shade of green. Within a monomer, the region absent in the short isoform is colored blue. (C) A scheme showing the *in vitro* enzymatic assay. The enzymatic activity of each isoform was evaluated by the velocity of the kinetics curve (see *Online Supplementary Figure S3B*). Error bars represent the standard deviation for technical replicates. * $P<0.05$ using the two-tailed Student *t* test. (D) Confocal images showing the cellular localization of the endogenous EGFP-fused ALDH1A2 proteins in Jurkat and K562 cells. Hoechst and Mitotracker staining evidence the nucleus and mitochondria, respectively.

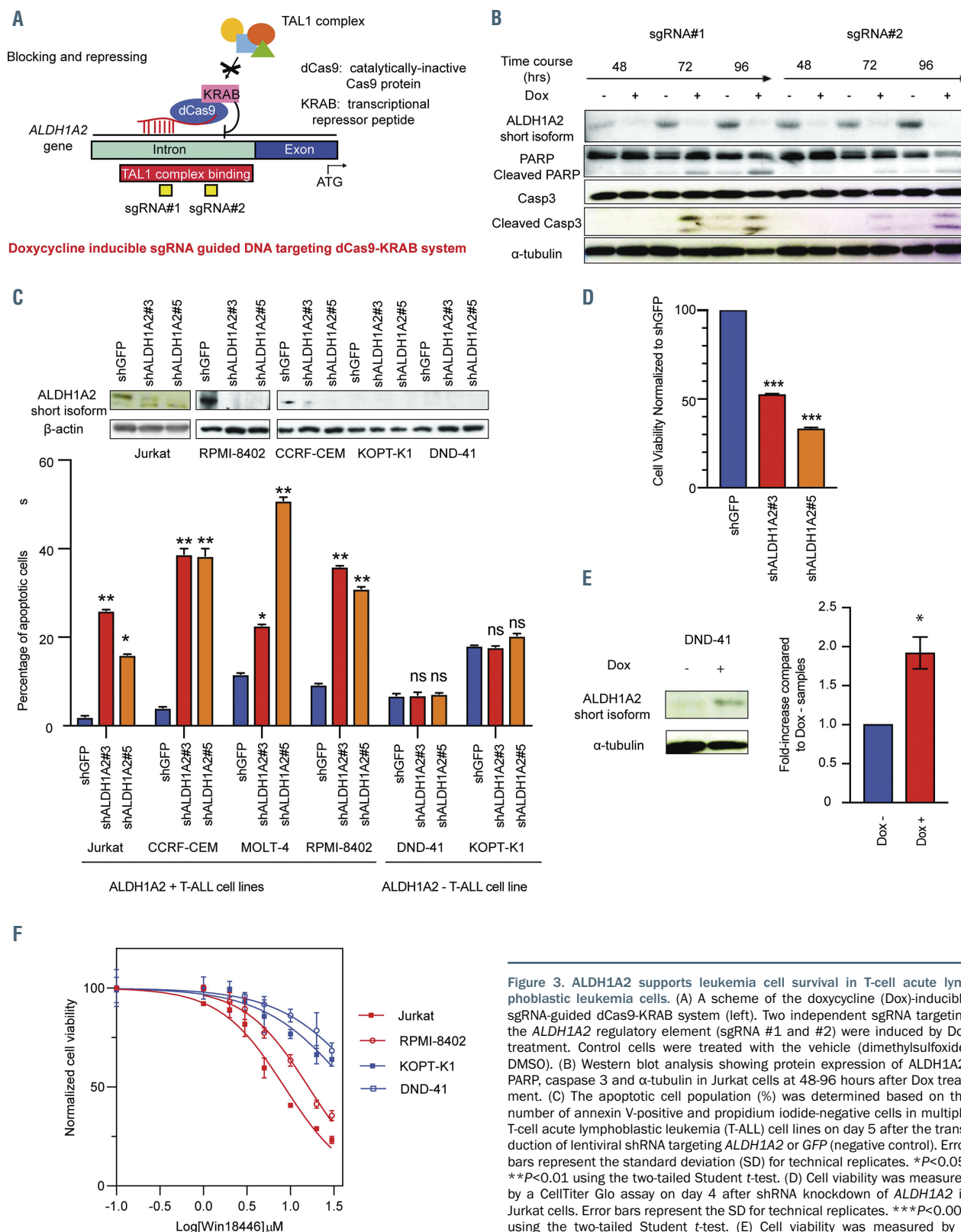


Figure 3. ALDH1A2 supports leukemia cell survival in T-cell acute lymphoblastic leukemia cells. (A) A scheme of the doxycycline (Dox)-inducible sgRNA-guided dCas9-KRAB system (left). Two independent sgRNA targeting the ALDH1A2 regulatory element (sgRNA #1 and #2) were induced by Dox treatment. Control cells were treated with the vehicle (dimethylsulfoxide, DMSO). (B) Western blot analysis showing protein expression of ALDH1A2, PARP, caspase 3 and α -tubulin in Jurkat cells at 48-96 hours after Dox treatment. (C) The apoptotic cell population (%) was determined based on the number of annexin V-positive and propidium iodide-negative cells in multiple T-cell acute lymphoblastic leukemia (T-ALL) cell lines on day 5 after the transduction of lentiviral shRNA targeting ALDH1A2 or GFP (negative control). Error bars represent the standard deviation (SD) for technical replicates. * $P<0.05$, ** $P<0.01$ using the two-tailed Student *t*-test. (D) Cell viability was measured by a CellTiter Glo assay on day 4 after shRNA knockdown of ALDH1A2 in Jurkat cells. Error bars represent the SD for technical replicates. *** $P<0.001$ using the two-tailed Student *t*-test. (E) Cell viability was measured by a CellTiter Glo assay on day 4 after the induction of ALDH1A2 expression by Dox treatment in DND-41 cells. Error bars represent the SD for technical replicates. * $P<0.05$ using the two-tailed Student *t*-test. (F) Cell viability was measured by CellTiter Glo assays on day 7 after treatment with WIN 18,446 at different doses in two TAL1/ALDH1A2-positive (Jurkat and RPMI-8402) and two TAL1/ALDH1A2-negative (KOPT-K1 and DND-41) T-ALL cell lines. Nonlinear regression fit curves are shown. Error bars represent the standard error of the mean for technical replicates.

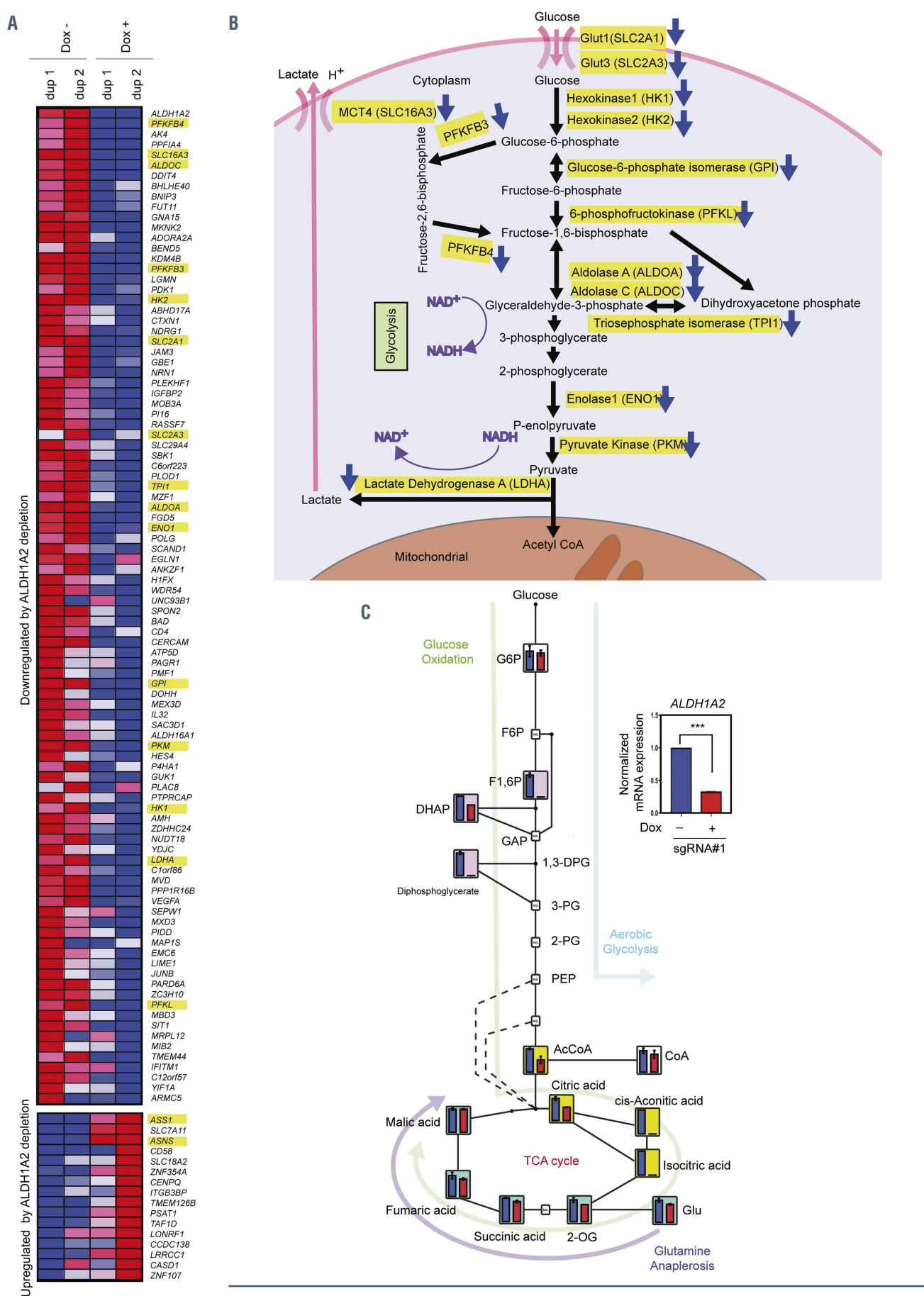


Figure 4. Legend on following page.

Figure 4. ALDH1A2 affects metabolic pathways in T-cell acute lymphoblastic leukemia cells. (A) sgRNA #1 was introduced into Jurkat cells by doxycycline (Dox) treatment for 72 h in duplicate (dup 1 and dup 2). Differentially expressed genes were selected based on the following criteria: $P < 0.05$, \log_2 fold change < -0.4 or > 0.4 , and mean transcript per million (TPM) value of the control > 250 . Heatmap image showing relative mRNA expression levels of the differentially expressed genes in the control (Dox-) and ALDH1A2-depleted cells (Dox+). The genes involved in the glycolysis pathway are highlighted. (B) A scheme showing the metabolic enzymes involved in the glycolysis pathway. The genes significantly downregulated by ALDH1A2 depletion are highlighted. (C) ALDH1A2 expression was depleted in Jurkat cells by Dox-inducible sgRNA-mediated transcriptional repression in biological duplicates. Downregulation of ALDH1A2 mRNA expression was confirmed by quantitative reverse transcription polymerase chain reaction. *** $P < 0.001$ using the two-tailed Student *t* test. Relative amounts of the metabolites in the glycolysis pathway and the tricarboxylic acid cycle were measured by capillary electrophoresis time-of-flight mass spectrometry in the control cells (blue) and the ALDH1A2-depleted cell samples (red). Error bars represent the standard deviation for biological replicates.

from 2-oxoglutarate in the TCA cycle were not affected (blue). This finding suggests that the TCA cycle, suppressed by the loss of ALDH1A2, might be supplemented by glutaminolysis through which external glutamine is converted into 2-oxoglutarate. Glutamine has been reported to be the major carbon source for T-ALL cells with activated NOTCH1.^{33,34} Indeed, depletion of glutamine in culture media induced apoptosis, which was further increased by ALDH1A2 depletion after 24 h of doxycycline treatment (*Online Supplementary Figure S4E* and *F*). In the presence of glutamine, ALDH1A2 depletion alone did not induce apoptosis before 48 h of induction (Figure 3B, *Online Supplementary Figure S4E* and *F*). Thus, these results suggest that external glutamine might be used to replenish downstream metabolites to maintain the TCA cycle in the absence of ALDH1A2, and that ALDH1A2 and glutaminolysis pathways may compensate each other.

ALDH1A2 supports cellular aerobic glycolysis and energy production in T-cell acute lymphoblastic leukemia cells

Our results suggest that ALDH1A2 directly or indirectly affects major metabolic pathways. In particular, aerobic glycolysis is a hallmark of cancer metabolism and has also been reported to be activated in T-ALL cells.³⁵ Because metabolic profiling can represent only the static state, we then analyzed the dynamic state of these pathways after ALDH1A2 depletion using the Seahorse XF24 platform.

We first measured the extracellular acidification rate (ECAR), which is an indicator of lactic acid fermentation and thus reflects the activity of glycolysis. We incubated the cells under conditions of glucose starvation, added glucose, and then measured the ECAR in both the control and ALDH1A2-depleted cells. Strikingly, ALDH1A2 depletion inhibited aerobic glycolysis, as shown by the reduction of the baseline ECAR ("glycolysis" in Figure 5A). This trend was more significant upon the addition of oligomycin, which is an inhibitor of complex V in the electron transport chain and thus maximizes cellular aerobic glycolysis by disturbing mitochondrial respiration ("glycolytic capacity"). Treatment with 2-deoxy-D-glucose, which competitively inhibits the production of glucose-6-phosphate from glucose, completely abolished these activities in both control and ALDH1A2-depleted cells ("glycolytic reserve"), indicating that the effect of ALDH1A2 is glucose-dependent. These results demonstrated that the expression of ALDH1A2 promotes cellular glycolysis and contributes to the maintenance of metabolome plasticity by increasing cellular glycolytic capacity in T-ALL cells.

Because ALDH1A2 affects glycolysis and the TCA cycle, which are the major sources of energy production, we also analyzed the effect of ALDH1A2 depletion on oxidative phosphorylation in mitochondria. We measured the oxygen consumption rate to determine changes in the level of oxidative phosphorylation-dependent ATP generation. As expected, the basal respiration level was

decreased after ALDH1A2 depletion (Figure 5B). To further support this finding, we analyzed the ratio of NAD⁺/NADH and the amount of ATP in the same setting. Consistently, depletion of ALDH1A2 increased the ratio of NAD⁺/NADH, thus preventing NADH production (Figure 5C). ATP production normalized by the number of cells was also decreased by ALDH1A2 depletion (Figure 5D). Furthermore, in the cells cultured in glucose-free medium, ALDH1A2 depletion inhibited ATP production more strongly than it did in the control cells (*Online Supplementary Figure S5A*). These results indicate that ALDH1A2 supports energy production, which explains the cell phenotype after ALDH1A2 depletion.

ALDH1A2 reduces the level of reactive oxygen species in T-cell acute lymphoblastic leukemia cells

A high level of oxidative phosphorylation in mitochondria has been known to produce oxidative stress such as reactive oxygen species (ROS). On the other hand, previous studies provided evidence that ALDH family proteins help to alleviate intracellular ROS.³⁶⁻³⁸ The underlying mechanism is attributable to the ability of these proteins to clear cellular aldehydes, which are known ROS inducers.³⁹⁻⁴¹ Thus, we next measured the total level of intracellular ROS after depletion of ALDH1A2 in Jurkat cells using three different settings (sgRNA, shRNA and a small-molecule inhibitor).

Strikingly, genetic inhibition with shRNA (Figure 6A) or sgRNA (Figure 6B) resulted in significant increases in ROS levels. Similarly, treatment with WIN 18,446 increased the level of ROS in Jurkat cells (Figure 6C) as well as in primary leukemia cells that were harvested from a patient-derived xenograft mouse model (Figure 6D), both of which expressed only the short isoform of ALDH1A2 (*Online Supplementary Figure S6A*). Conversely, overexpression of the short isoform of ALDH1A2 reduced the level of ROS (Figure 6E). Furthermore, treatment with N-acetyl cysteine, an antioxidant, was able to reduce the ROS level after ALDH1A2 depletion in Jurkat cells (*Online Supplementary Figure S6B*). Importantly, in the setting of sgRNA knockout, ROS was increased at 48 h after doxycycline treatment (Figure 6B) before the induction of apoptosis was observed (Figure 3B). This suggests that accumulation of ROS could be a cause of apoptosis but not a consequence of cell death. These results indicate that although ALDH1A2 supports energy production, which potentially increases oxidative stress, it more predominantly plays a role protecting against the production of ROS and thus supports cell survival, which also explains the phenotype after ALDH1A2 depletion. Of note, N-acetyl cysteine treatment did not restore cell viability after ALDH1A2 depletion (*data not shown*), suggesting that the cell viability phenotype was mainly attributable to the maintenance of glycolysis and energy production.

ALDH1A2 overexpression accelerates tumorigenesis in a zebrafish model of T-cell acute lymphoblastic leukemia

Finally, we investigated the effect of *ALDH1A2* overexpression on tumorigenesis *in vivo* using a zebrafish model. We overexpressed the short isoform of the human *ALDH1A2* gene with a fluorescent marker (mCherry) under the *rag2* promoter in lymphocytes (*Online Supplementary Figure S7A*). We confirmed that transgenes were successfully integrated into the genome (*Online Supplementary Figure S7B*) and mCherry was expressed in the thymus (*Online Supplementary Figure S7C*). We then sorted mCherry-positive cells from the *ALDH1A2*-transgenic and control fish and measured the ROS levels. Strikingly, the ROS level was significantly lower in the

ALDH1A2-transgenic fish than in the control fish (Figure 7A), supporting our results in cell lines.

We next monitored tumor development using offsprings from one of the established founder lines. However, we did not observe any spontaneous tumor development in the *ALDH1A2* single transgenic fish (*Online Supplementary Figure S7C*). Hence, we then cross-bred this line with a transgenic line overexpressing a myristoylated, constitutively active mouse *Akt2* gene (*myr-mAkt2*) which can cause T-ALL²² (*Online Supplementary Figure S7B*). Interestingly, overall penetrance was significantly increased up to 60% and tumor onset was slightly accelerated in the double transgenic animals as compared to the *myr-mAkt2* single transgenic animals (Figure 7B,

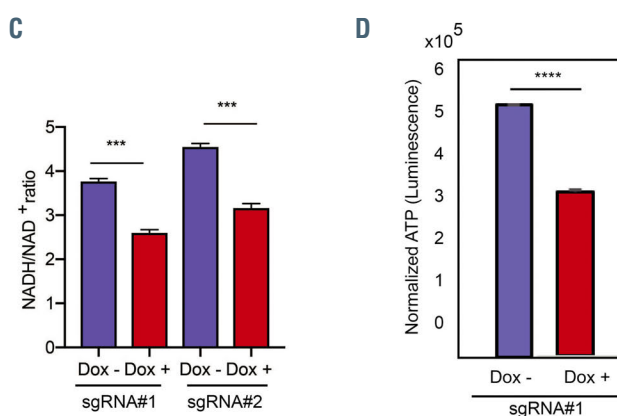
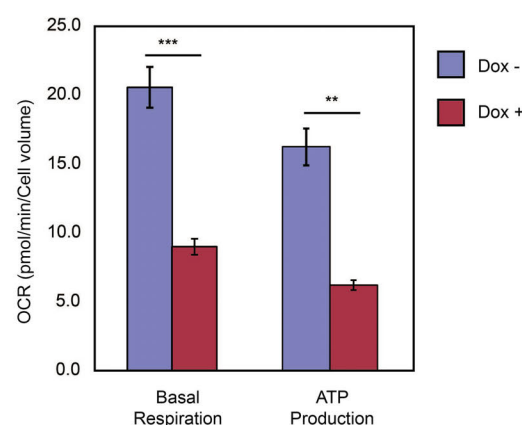
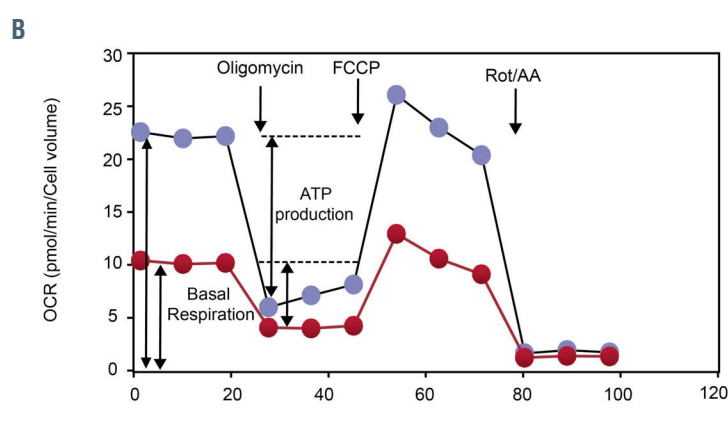
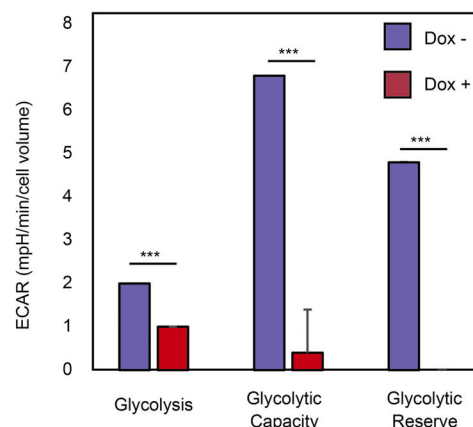
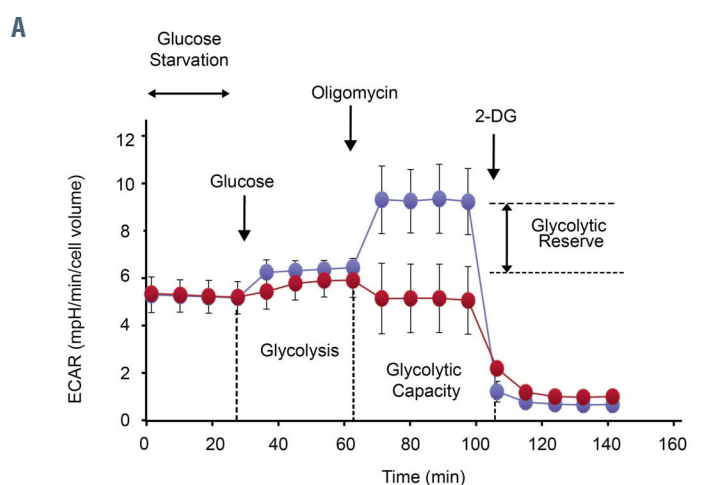


Figure 5. ALDH1A2 supports cellular aerobic glycolysis and energy production in T-cell acute lymphoblastic leukemia cells. (A) Real-time curves showing the normalized extracellular acidification rate (ECAR) readings for the control (blue) and ALDH1A2-depleted (red) cell samples. Bar graphs with normalized ECAR showing the changes in glycolysis, glycolytic capacity and glycolytic reserve after ALDH1A2 depletion. (B) Real-time curves showing the normalized oxygen consumption rate (OCR) readings for the control (blue) and ALDH1A2-depleted (red) cell samples. Bar graphs with normalized OCR showing the changes in basal respiration and ATP production after ALDH1A2 depletion. (C) Quantification of the NADH to NAD⁺ ratio after ALDH1A2 depletion. (D) Quantification of the ATP levels after ALDH1A2 depletion. All error bars represent the standard deviation for technical replicates. **P<0.01, ***P<0.001, ****P<0.0001 using the two-tailed Student *t* test.

Online Supplementary Figure S7D). These results indicate that although overexpression of *ALDH1A2* alone does not have oncogenic capability, it can promote T-cell leukemogenesis induced by a driver oncogene.

Discussion

ALDH1A2 is one of the first reported downstream targets of *TAL1* in T-ALL cells. Using the subtractive PCR method,

Ono *et al.* isolated *ALDH1A2* in T-ALL cell lines that co-expressed *TAL1*, *LMO* and *GATA3*.¹² Our ChIP-sequencing and RNA-sequencing experiments also demonstrated that *ALDH1A2* is directly activated by the *TAL1* complex via an intronic regulatory element in T-ALL cells. The short isoform of *ALDH1A2* is specifically expressed in T-ALL cells. Importantly, *ALDH1A2* expression is highly specific to T-ALL cells, mostly to the *TAL1*-positive subgroup. Thus, using a novel approach, our studies reconfirmed that *ALDH1A2* is a signature gene of *TAL1*-positive T-ALL.

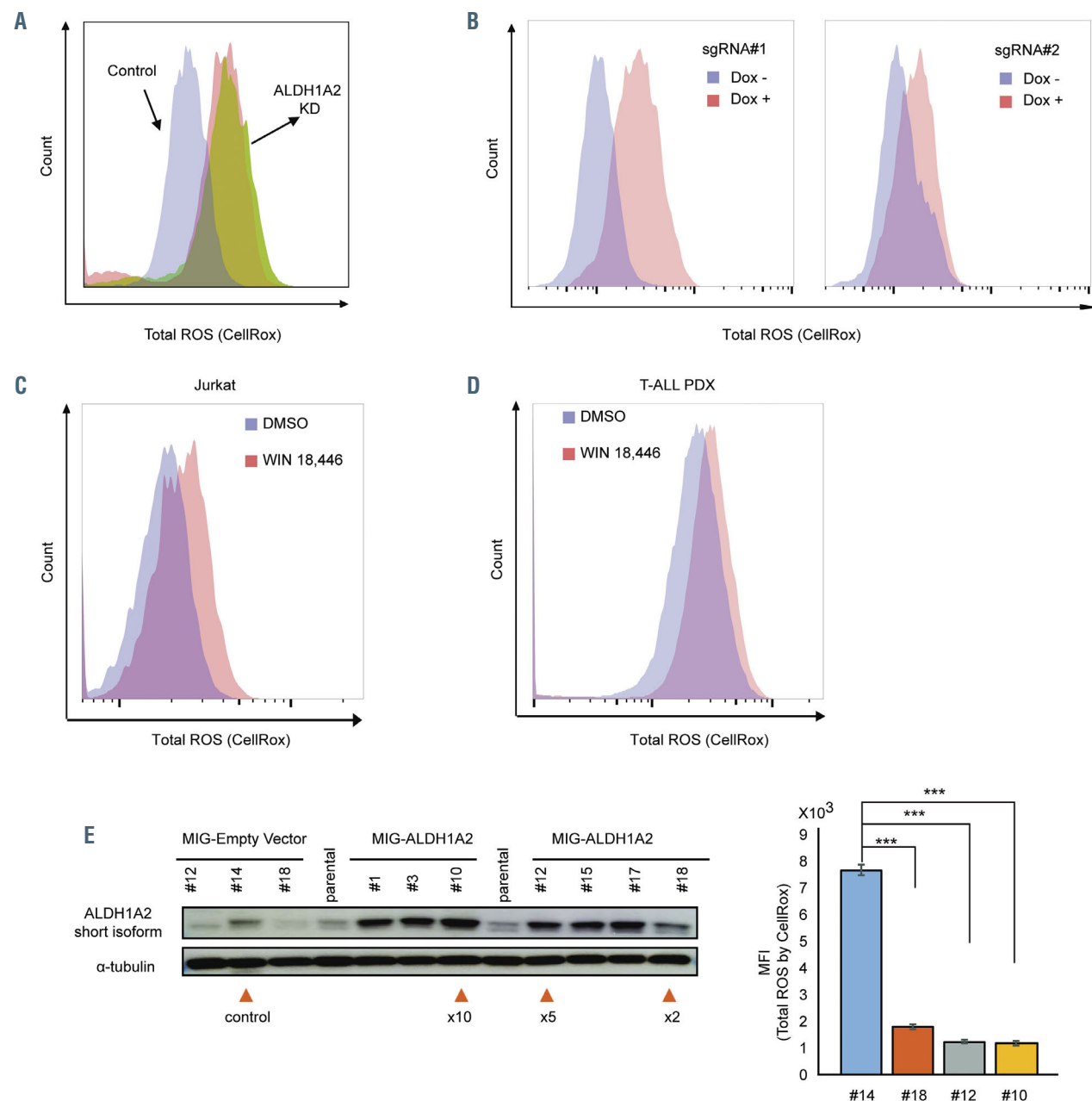


Figure 6. *ALDH1A2* reduces the levels of reactive oxygen species (ROS) in T-cell acute lymphoblastic leukemia cells. (A, B) Total reactive oxygen species (ROS) levels were measured by flow cytometry analysis using CellROX staining at 72 h after shRNA-mediated *ALDH1A2* depletion (A) or at 48 h after sgRNA-mediated *ALDH1A2* depletion (B) in Jurkat cells. (C, D) Total ROS levels were measured by flow cytometry analysis using CellROX staining at 72 h after treatment with WIN 18,446 of Jurkat cells (C) or primary T-cell acute lymphoblastic leukemia cells harvested from a patient-derived xenograft model (D). (E) Jurkat cells were transduced with *ALDH1A2* cDNA or an empty vector by MSCV retrovirus infection. The level of expression of the short isoform of *ALDH1A2* in established Jurkat single clones was measured by western blot. MIG-ALDH1A2 #10, #12 and #18 were selected as the overexpressing clones, and they expressed different levels of *ALDH1A2*. MIG-EV #14 was selected as the control. Total ROS levels were measured by flow cytometry analysis using CellROX staining and are reported as mean fluorescence intensity (MFI). Error bars represent the standard deviation for biological replicates. ***P<0.001 using the two-tailed Student t test.

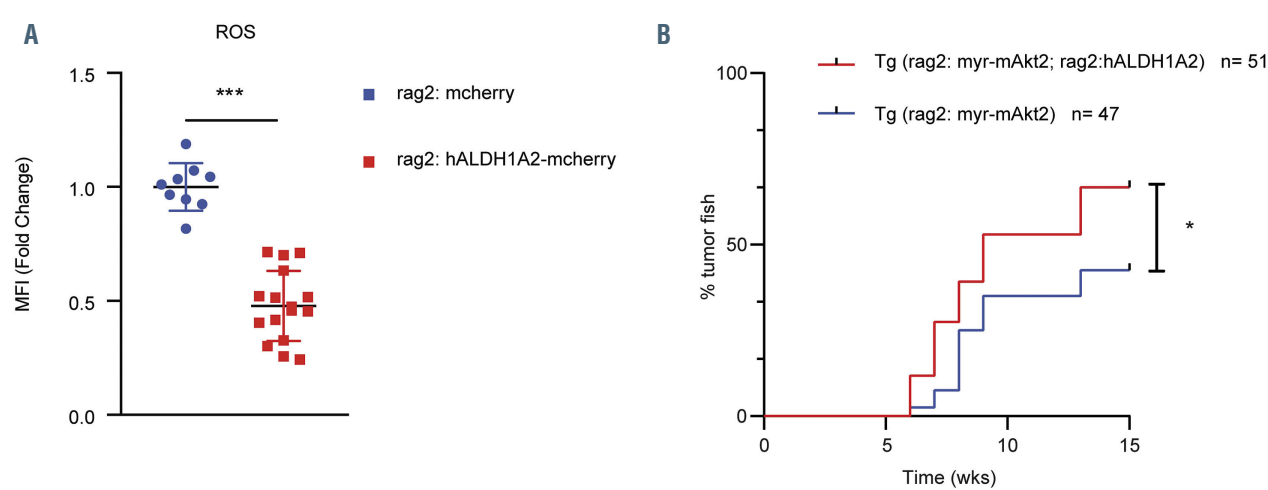


Figure 7. *ALDH1A2* overexpression accelerates tumorigenesis in a zebrafish model. (A) Total reactive oxygen species levels in the mCherry-positive cells from the control and *ALDH1A2*-transgenic zebrafish were measured by flow cytometry and shown by mean fluorescent intensity as the fold-change compared to control cell samples. (B) Tumor development (lymphoma-like and leukemia-like phenotypes) in the single and double transgenic zebrafish was recorded according to the criteria defined by Langenau et al.⁵⁰ Tumor onset and penetrance were evaluated by Kaplan-Meier curve analysis. * $P<0.05$ using the Gehan-Breslow-Wilcoxon test.

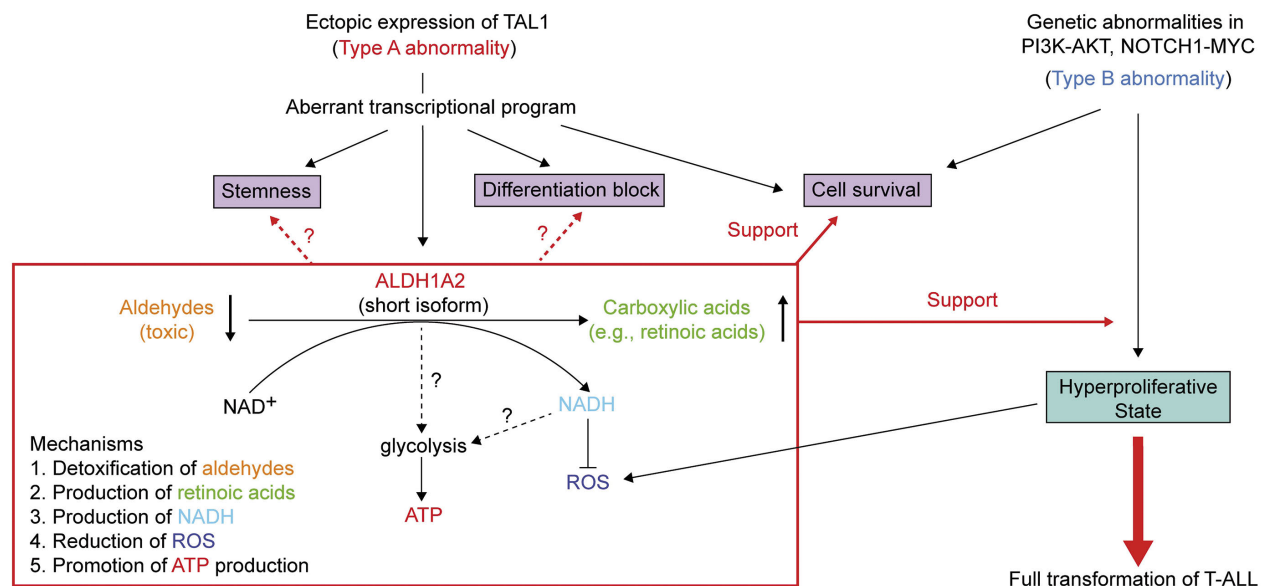


Figure 8. Scheme showing the oncorequisite role of *ALDH1A2* for full transformation of T-cell acute lymphoblastic leukemia.

However, the molecular functions and roles of *ALDH1A2* in the pathogenesis of T-ALL had not been elucidated previously. Here, we first experimentally proved that the T-ALL-specific isoform possesses an enzymatic activity that catalyzes retinaldehyde to retinoic acid with the production of NADH. Thus, the main mechanism involving this protein is characterized by ectopic expression through the activation of an alternative promoter bound by TAL1 rather than the expression of a dominant-negative protein or a loss of function. Additionally, we showed that this protein can reduce ROS levels and support energy production in T-ALL cells. Although the direct mechanism by which *ALDH1A2* promotes the glycolysis pathway remains unelucidated, one possibility is that the high levels of NADH caused by *ALDH1A2* overexpression might lead to pseudo-hypoxic

conditions that upregulate the expression of metabolic enzymes. Alternatively, the reduction in ROS level might lead to upregulation of metabolic enzymes. Further investigation is needed.

In malignant cells, regulation of ROS and metabolic state is crucial to maintain cell proliferation and survival. Although it has been reported that ROS can promote the proliferation and survival of T-ALL cells,⁴² it is maintained at low levels in the T-ALL leukemia-initiating cells in a mouse model.⁴³ It is also noteworthy that, in more than 50% of the *TAL1*-positive T-ALL cases, genetic abnormalities in the PI3K-AKT pathway and the NOTCH1-MYC pathway have been observed,^{4,8-11,44} and these pathways can promote several metabolic processes.⁴⁵ In particular, MYC has been known to promote glutaminolysis. Metabolic dependence on the TCA cycle

has also been reported in the *Myc*-induced zebrafish T-ALL model.⁴⁶ However, hypermetabolic and hyperproliferative states often induce ROS production through the upregulation of mitochondrial bioenergetics. Hence, malignant cells may need to balance the ROS level depending on their state of proliferation. Thus, ALDH1A2 expression may be ideal for leukemic or pre-leukemic clones to protect cells from ROS production and further promote metabolism (Figure 8).

Genetic abnormalities in T-ALL can be classified into “type A” and “type B” abnormalities. The former refer to abnormal expression of transcription factor genes, such as *TAL1*, that delineate distinct molecular pathways, which are more prevalent in one subgroup than others.^{4,47-49} The latter refer to oncogenic pathways that are commonly observed across different subgroups of T-ALL, for example, PI3K-AKT and NOTCH1-MYC.^{2,48,49} Considering the high occurrence of *ALDH1A2* expression with PI3K-AKT and NOTCH1-MYC abnormalities in the *TAL1*-positive subgroup, these pathways may compensate for each other and synergize, which would lead to further increases in cell proliferation and metabolism. *ALDH1A2* expression may be advantageous as a preceding event that serves as a “requisite” before the cells activate other oncogenic pathways, making it an “oncorequisite”.

Disclosures

No conflicts of interest to disclose.

Contributions

CZ, SA, CW, MZA, WZL and SHT performed the experiments; ZL and AEJY provided primary samples; TKT and LMN performed the computational analysis; SK advised on the metabolome analysis; CZ and TS designed the research and wrote the paper.

Acknowledgments

We thank Nature Publishing Group Language Editing for editing the manuscript. We thank members of the Sanda laboratory for discussions, and Motomi Osato, Michelle Mok, Akiko Nambu and Lee Shuying for technical advice. The results published here are in whole or part based upon data generated by the Therapeutically Applicable Research to Generate Effective Treatments (<https://ocg.cancer.gov/programs/target>) initiative, phs000218. The data used for this analysis are available at <https://portal.gdc.cancer.gov/projects>.

Funding

The research was supported by the National Research Foundation (NRF) Singapore and the Singapore Ministry of Education (MOE) under its Research Centers of Excellence initiative. The research was also supported by the NRF under its Competitive Research Programme (NRF-NRFF2013-02) and the RNA Biology Center at CSI Singapore, NUS, from funding by the Singapore MOE's Tier 3 grants (MOE2014-T3-1-006). AEJY is supported by the National Medical Research Council, Singapore (NMRC/CSA/0053/2013 and MOH-CSASI18may-0004).

References

1. Pui CH, Robison LL, Look AT. Acute lymphoblastic leukaemia. *Lancet*. 2008;371(9617):1030-1043.
2. Aifantis I, Raetz E, Buonamici S. Molecular pathogenesis of T-cell leukaemia and lymphoma. *Nat Rev Immunol*. 2008;8(5):380-390.
3. Armstrong SA, Look AT. Molecular genetics of acute lymphoblastic leukemia. *J Clin Oncol*. 2005;23(26):6306-6315.
4. Liu Y, Easton J, Shao Y, et al. The genomic landscape of pediatric and young adult T-lineage acute lymphoblastic leukemia. *Nat Genet*. 2017;49(8):1211-1218.
5. Ferrando AA, Neuberg DS, Staunton J, et al. Gene expression signatures define novel oncogenic pathways in T cell acute lymphoblastic leukemia. *Cancer Cell*. 2002;1(1):75-87.
6. Soulier J, Clappier E, Cayuela JM, et al. HOXA genes are included in genetic and biologic networks defining human acute T-cell leukemia (T-ALL). *Blood*. 2005;106(1):274-286.
7. O'Neil J, Shank J, Cusson N, Murre C, Kelliher M. TAL1/SCL induces leukemia by inhibiting the transcriptional activity of E47/HEB. *Cancer Cell*. 2004;5(6):587-596.
8. O'Neil J, Calvo J, McKenna K, et al. Activating Notch1 mutations in mouse models of T-ALL. *Blood*. 2006;107(2):781-785.
9. Tremblay M, Tremblay CS, Herblot S, et al. Modeling T-cell acute lymphoblastic leukemia induced by the SCL and LMO1 oncogenes. *Genes Dev*. 2010;24(11):1093-1105.
10. Gutierrez A, Sanda T, Greblunaite R, et al. High frequency of PTEN, PI3K, and AKT abnormalities in T-cell acute lymphoblastic leukemia. *Blood*. 2009;114(3):647-650.
11. Bornschein S, Demeyer S, Stirparo R, et al. Defining the molecular basis of oncogenic cooperation between TAL1 expression and Pten deletion in T-ALL using a novel pro-T-cell model system. *Leukemia*. 2018;32(4):941-951.
12. Ono Y, Fukuhara N, Yoshie O. TAL1 and LIM-only proteins synergistically induce retinaldehyde dehydrogenase 2 expression in T-cell acute lymphoblastic leukemia by acting as cofactors for GATA3. *Mol Cell Biol*. 1998;18(12):6959-6950.
13. Sanda T, Lawton LN, Barrasa MI, et al. Core transcriptional regulatory circuit controlled by the TAL1 complex in human T cell acute lymphoblastic leukemia. *Cancer Cell*. 2012;22(2):209-221.
14. Marchitt SA, Brocker C, Stagos D, Vasilious V. Non-P450 aldehyde oxidizing enzymes: the aldehyde dehydrogenase superfamily. *Expert Opin Drug Metab Toxicol*. 2008;4(6):697-720.
15. Black W, Vasilious V. The aldehyde dehydrogenase gene superfamily resource center. *Hum Genomics*. 2009;4(2):136-142.
16. Vasilious V, Pappa A, Estey T. Role of human aldehyde dehydrogenases in endobiotic and xenobiotic metabolism. *Drug Metab Rev*. 2004;36(2):279-299.
17. Marcato P, Dean CA, Pan D, et al. Aldehyde dehydrogenase activity of breast cancer stem cells is primarily due to isoform ALDH1A3 and its expression is predictive of metastasis. *Stem Cells*. 2011;29(1):32-45.
18. Moreb JS. Aldehyde dehydrogenase as a marker for stem cells. *Curr Stem Cell Res Ther*. 2008;3(4):237-246.
19. Marcato P, Dean CA, Giacomantonio CA, Lee PW. Aldehyde dehydrogenase: its role as a cancer stem cell marker comes down to the specific isoform. *Cell Cycle*. 2011;10(9):1378-1384.
20. Moreb JS, Ucar D, Han S, et al. The enzymatic activity of human aldehyde dehydrogenases 1A2 and 2 (ALDH1A2 and ALDH2) is detected by Aldefluor, inhibited by diethylaminobenzaldehyde and has significant effects on cell proliferation and drug resistance. *Chem Biol Interact*. 2012;195(1):52-60.
21. Leong WZ, Tan SH, Ngoc PCT, et al. ARID5B as a critical downstream target of the TAL1 complex that activates the oncogenic transcriptional program and promotes T-cell leukemogenesis. *Genes Dev*. 2017;31(23-24):2343-2360.
22. Gutierrez A, Greblunaite R, Feng H, et al. Pten mediates Myc oncogene dependence in a conditional zebrafish model of T cell acute lymphoblastic leukemia. *J Exp Med*. 2011;208(8):1595-1603.
23. Qian M, Zhang H, Kham SK, et al. Whole-transcriptome sequencing identifies a distinct subtype of acute lymphoblastic leukemia with predominant genomic abnormalities of EP300 and CREBBP. *Genome Res*. 2017;27(2):185-195.
24. Aries IM, Bodaar K, Karim SA, et al. PRC2 loss induces chemoresistance by repressing apoptosis in T cell acute lymphoblastic leukemia. *J Exp Med*. 2018;215(12):3094-3114.
25. Ghandi M, Huang FW, Jane-Valbuena J, et al. Next-generation characterization of the Cancer Cell Line Encyclopedia. *Nature*. 2019;569(7757):503-508.
26. Casero D, Sandoval S, Seet CS, et al. Long non-coding RNA profiling of human lymphoid progenitor cells reveals transcriptional divergence of B cell and T cell lineages. *Nat Immunol*. 2015;16(12):1282-1291.

27. Park JE, Botting RA, Dominguez Conde C, et al. A cell atlas of human thymic development defines T cell repertoire formation. *Science*. 2020;367(6480):eaya3224.

28. Kernfeld EM, Genga RMJ, Neherin K, et al. A single-cell transcriptomic atlas of thymus organogenesis resolves cell types and developmental maturation. *Immunity*. 2018;48(6):1258-1270.e6.

29. Balkan W, Colbert M, Bock C, Linney E. Transgenic indicator mice for studying activated retinoic acid receptors during development. *Proc Natl Acad Sci U S A*. 1992;89(8):3347-3351.

30. Arnold SL, Kent T, Hogarth CA, et al. Pharmacological inhibition of ALDH1A in mice decreases all-trans retinoic acid concentrations in a tissue specific manner. *Biochem Pharmacol*. 2015;95(3):177-192.

31. Paik J, Haenisch M, Muller CH, et al. Inhibition of retinoic acid biosynthesis by the bisdichloroacetyl diamine WIN 18,446 markedly suppresses spermatogenesis and alters retinoid metabolism in mice. *J Biol Chem*. 2014;289(21):15104-15117.

32. Amory JK, Muller CH, Shimshoni JA, et al. Suppression of spermatogenesis by bisdichloroacetyl diamines is mediated by inhibition of testicular retinoic acid biosynthesis. *J Androl*. 2011;32(1):111-119.

33. O'Neil J, Grim J, Strack P, et al. FBW7 mutations in leukemic cells mediate NOTCH pathway activation and resistance to gamma-secretase inhibitors. *J Exp Med*. 2007;204(8):1813-1824.

34. Herranz D, Ambesi-Impiombato A, Sudderth J, et al. Metabolic reprogramming induces resistance to anti-NOTCH1 therapies in T cell acute lymphoblastic leukemia. *Nat Med*. 2015;21(10):1182-1189.

35. Kishton RJ, Barnes CE, Nichols AG, et al. AMPK is essential to balance glycolysis and mitochondrial metabolism to control T-ALL cell stress and survival. *Cell Metab*. 2016;23(4):649-662.

36. Singh S, Brocker C, Koppaka V, et al. Aldehyde dehydrogenases in cellular responses to oxidative/electrophilic stress. *Free Radic Biol Med*. 2013;56:89-101.

37. Sun X, Zhu H, Dong Z, et al. Mitochondrial aldehyde dehydrogenase-2 deficiency compromises therapeutic effect of ALDH bright cell on peripheral ischemia. *Redox Biol*. 2017;13:196-206.

38. Kim J, Chen CH, Yang J, Mochly-Rosen D. Aldehyde dehydrogenase 2*2 knock-in mice show increased reactive oxygen species production in response to cisplatin treatment. *J Biomed Sci*. 2017;24(1):33.

39. Yang G, Ibuki Y, α, β -unsaturated aldehyde-induced delays in nucleotide excision repair and the contribution of reactive oxygen species. *Chem Res Toxicol*. 2018;31(2):145-155.

40. Novitskiy G, Traore K, Wang L, Trush MA, Mezey E. Effects of ethanol and acetaldehyde on reactive oxygen species production in rat hepatic stellate cells. *Alcohol Clin Exp Res*. 2006;30(8):1429-1435.

41. Tamura M, Ito H, Matsui H, Hyodo I. Acetaldehyde is an oxidative stressor for gastric epithelial cells. *J Clin Biochem Nutr*. 2014;55(1):26-31.

42. Silva A, Girio A, Cebola I, et al. Intracellular reactive oxygen species are essential for PI3K/Akt/mTOR-dependent IL-7-mediated viability of T-cell acute lymphoblastic leukemia cells. *Leukemia*. 2011;25(6):960-967.

43. Giambra V, Jenkins CR, Wang H, et al. NOTCH1 promotes T cell leukemia-initiating activity by RUNX-mediated regulation of PKC- θ and reactive oxygen species. *Nat Med*. 2012;18(11):1693-1698.

44. Hsieh AL, Walton ZE, Altman BJ, Stine ZE, Dang CV. MYC and metabolism on the path to cancer. *Semin Cell Dev Biol*. 2015;43:11-21.

45. Lien EC, Lyssiotis CA, Cantley LC. Metabolic reprogramming by the PI3K-Akt-mTOR pathway in cancer. *Recent Results Cancer Res*. 2016;207:39-72.

46. Anderson NM, Li D, Peng HL, et al. The TCA cycle transferase DLST is important for MYC-mediated leukemogenesis. *Leukemia*. 2016;30(6):1365-1374.

47. Seki M, Kimura S, Isobe T, et al. Recurrent SPI1 (PU.1) fusions in high-risk pediatric T cell acute lymphoblastic leukemia. *Nat Genet*. 2017;49(8):1274-1281.

48. Belver L, Ferrando A. The genetics and mechanisms of T cell acute lymphoblastic leukaemia. *Nat Rev Cancer*. 2016;16(8):494-507.

49. Iacobucci I, Mullighan CG. Genetic basis of acute lymphoblastic leukemia. *J Clin Oncol*. 2017;35(9):975-983.

50. Langenau DM, Traver D, Ferrando AA, et al. Myc-induced T cell leukemia in transgenic zebrafish. *Science*. 2003;299(5608):887-890.

Philadelphia-like acute lymphoblastic leukemia is associated with minimal residual disease persistence and poor outcome. First report of the minimal residual disease-oriented GIMEMA LAL1913

Sabina Chiaretti,^{1*} Monica Messina,^{1,2*} Irene Della Starza,^{1,2} Alfonso Piciocchi,² Luciana Cafforio,¹ Marzia Cavalli,¹ Akram Taherinasab,¹ Michela Ansuinelli,¹ Loredana Elia,¹ Guglielmo Albertini Petroni,¹ Roberta La Starza,³ Martina Canichella,¹ Alessia Lauretti,¹ Maria Cristina Puzzolo,¹ Valentina Pierini,³ Alessandra Santoro,⁴ Orietta Spinelli,⁵ Valerio Apicella,¹ Saveria Capria,¹ Francesco Di Raimondo,⁶ Paolo De Fabritiis,⁷ Cristina Papayannidis,⁸ Anna Candoni,⁹ Roberto Cairoli,¹⁰ Marco Cerrano,¹¹ Nicola Fracchiolla,¹² Daniele Mattei,¹³ Chiara Cattaneo,¹⁴ Antonella Vitale,¹ Enrico Crea,² Paola Fazi,² Cristina Mecucci,³ Alessandro Rambaldi,⁵ Anna Guarini,¹⁵ Renato Bassan¹⁶ and Robin Foà¹

¹Hematology Unit, Department of Translational and Precision Medicine, Sapienza University, Rome; ²GIMEMA Data Center, Fondazione GIMEMA Franco Mandelli Onlus, Rome; ³Hematology and Bone Marrow Transplantation Unit, Department of Medicine, University of Perugia, Perugia; ⁴Hematology and Bone Marrow Transplant Unit, Ospedali Riuniti Villa Sofia-Cervello, Palermo; ⁵Hematology and Bone Marrow Transplant Unit, Ospedale Papa Giovanni XXIII, Bergamo; ⁶Haematology Unit, Department of General Surgery and Medical-Surgical Specialties, University of Catania, Catania; ⁷Hematology Unit, S. Eugenio Hospital, Rome; ⁸Seragnoli Institute of Hematology, Bologna University School of Medicine, Bologna; ⁹Clinica di Ematologia e Unità di terapie Cellulari 'Carlo Melzi'-Azienda Sanitaria-Universitaria Integrata, Udine; ¹⁰Hematology Unit, Niguarda Hospital, Milan; ¹¹Hematology Unit, Department of Oncology, Presidio Molinette, AOU Città della Salute e della Scienza di Torino, Torino; ¹²UOC Oncoematologia, Fondazione IRCCS Ca' Granda Ospedale Maggiore Policlinico di Milano, Università degli Studi di Milano, Milan; ¹³Department of Hematology, Ospedale S. Croce, Cuneo; ¹⁴Department of Hematology, ASST Spedali Civili, Brescia; ¹⁵Department of Molecular Medicine, Sapienza University, Rome and ¹⁶Hematology Unit, Ospedale dell'Angelo and Ospedale Ss Giovanni e Paolo, Mestre, Venezia, Italy

*SC and MM contributed equally as co-first authors.

ABSTRACT

Early recognition of Philadelphia-like (Ph-like) acute lymphoblastic leukemia (ALL) cases could impact on the management and outcome of this subset of B-lineage ALL. In order to assess the prognostic value of the Ph-like status in a pediatric-inspired, minimal residual disease (MRD)-driven trial, we screened 88 B-lineage ALL cases negative for major fusion genes (*BCR-ABL1*, *ETV6-RUNX1*, *TCF3-PBX1* and *KMT2A*) enrolled in the GIMEMA LAL1913 front-line protocol for adult *BCR/ABL1*-negative ALL. The screening - performed using the "BCR/ABL1-like predictor" - identified 28 Ph-like cases (31.8%), characterized by *CRLF2* overexpression (35.7%), JAK/STAT pathway mutations (33.3%), *IKZF1* (63.6%), *BTG1* (50%) and *EBF1* (27.3%) deletions, and rearrangements targeting tyrosine kinases or *CRLF2* (40%). The correlation with outcome highlighted that: i) the complete remission rate was significantly lower in Ph-like compared to non-Ph-like cases (74.1% vs. 91.5%, $P=0.044$); ii) at time point 2, decisional for transplant allocation, 52.9% of Ph-like cases versus 20% of non-Ph-like were MRD-positive ($P=0.025$); iii) the Ph-like profile was the only parameter associated with a higher risk of being MRD-positive at time point 2 ($P=0.014$); iv) at 24 months, Ph-like patients had a significantly inferior event-free and disease-free survival compared to non-Ph-like patients (33.5% vs. 66.2%, $P=0.005$ and 45.5% vs. 72.3%, $P=0.062$, respectively). This study documents



Ferrata Storti Foundation

Haematologica 2021
Volume 106(6):1559-1568

Correspondence:

SABINA CHIARETTI
chiaretti@bce.uniroma1.it

Received: January 24, 2020.

Accepted: May 20, 2020.

Pre-published: May 28, 2020.

<https://doi.org/10.3324/haematol.2020.247973>

© 2021 Ferrata Storti Foundation

Material published in *Haematologica* is covered by copyright. All rights are reserved to the Ferrata Storti Foundation. Use of published material is allowed under the following terms and conditions: <https://creativecommons.org/licenses/by-nc/4.0/legalcode>. Copies of published material are allowed for personal or internal use. Sharing published material for non-commercial purposes is subject to the following conditions: <https://creativecommons.org/licenses/by-nc/4.0/legalcode>, sect. 3. Reproducing and sharing published material for commercial purposes is not allowed without permission in writing from the publisher.



that Ph-like patients have a lower complete remission rate, event-free survival and disease-free survival, as well as a greater MRD persistence also in a pediatric-oriented and MRD-driven adult ALL protocol, thus reinforcing that the early recognition of Ph-like ALL patients at diagnosis is crucial to refine risk-stratification and to optimize therapeutic strategies. Clinicaltrials.gov. Identifier: 02067143.

Introduction

Philadelphia-like (Ph-like) acute lymphoblastic leukemia (ALL) accounts for 15-30% of B-lineage ALL, with an increasing incidence starting from adolescence. The growing interest in this subgroup of ALL arises from the distinctive gene expression profile - that resembles that of the true Ph-positive cases - and by the unfavorable clinical outcome.^{1,2} In-depth and large-scale genetic characterization has shown that the majority of Ph-like ALL cases carry fusion genes involving tyrosine kinases (*i.e.*, ABL-class and *JAK2* rearrangements), or cytokine receptor rearrangements (*i.e.*, *P2RY8/CRLF2* and *IGH/CRLF2*), frequently associated with mutations of the JAK/STAT pathway genes.³⁻⁵ Among the other co-operating events, a relevant role is played by *IKZF1* deletions present in about 70% of cases.^{4,7} The possibility of recognizing these cases at diagnosis has important prognostic implications and would also pave the way to testing tyrosine kinase inhibitors (TKI) and other targeted therapeutic approaches that have proven successful in pre-clinical models and *in vivo* in a few relapsed patients.^{3,8-12} So far, several strategies¹³⁻¹⁵ have been reported in an attempt to identify Ph-like cases, but none of them is deemed as the gold standard for the diagnostic work-up of these patients. To this end, our group recently reported a predictive tool called “*BCR/ABL1*-like predictor” based on the levels of expression of nine genes together with *CRLF2* transcript quantification.⁷ From a clinical standpoint, Ph-like patients are characterized by a worse outcome which is due to an inferior response to induction therapy, a higher incidence of relapses and lower survival.^{1,2,4} Since minimal residual disease (MRD) is considered today the most important prognostic factor in ALL, the role of the Ph-like status has been investigated in the context of MRD-driven protocols, with contradicting results. Roberts and colleagues reported in a pediatric cohort that Ph-like patients, though displaying higher MRD levels at the end of induction, had a survival probability similar to that of non-Ph-like childhood ALL when treated with intensive therapies.¹⁶ Opposite results were obtained by Heatley *et al.*¹⁴ who demonstrated that, despite a risk-adjusted treatment approach, a high rate of relapse was recorded among children who were retrospectively identified as Ph-like. In adolescents and young adults, the results of the CALGB10403 trial, based on a pediatric inspired regimen, have shown that parameters associated with inferior survival rates were indeed represented by the Ph-like signature and obesity.¹⁷ In adult cohorts, all reported studies so far agree on a shorter survival likelihood for Ph-like ALL compared to non-Ph-like patients.^{5-7,18,19} However, the data are still insufficient to elucidate whether intensive treatments are capable of abolishing the negative impact of the Ph-like status on prognosis: conflicting results have been reported in the studies by Jain *et al.*²⁰ and Herold *et al.*⁶ Likewise, the role of the Ph-like status in the context of MRD-driven clinical trials is still unclear, since the data produced by the

German study group were derived from a small cohort of patients.⁶

In order to clarify these aspects, we hereby evaluated the incidence and clinical-biological features of Ph-like cases - identified using the *BCR/ABL1*-like predictor⁷ - and the prognostic role of the Ph-like profile in terms of complete remission (CR) achievement, MRD persistence and survival in a cohort of adult ALL patients homogeneously and intensively treated in the pediatric-oriented, MRD-driven LAL1913 GIMEMA front-line protocol for adult Ph-negative ALL.

Methods

Study population and experimental strategy

This study included B-lineage ALL patients negative for major molecular aberrations (*BCR/ABL1*, *KT2MA* and *TCF3/PBX1*, B-NEG) enrolled in the GIMEMA LAL1913 front-line clinical trial (clinicaltrials.gov. Identifier: 02067143; *Online Supplementary Figure S1*) - designed for Ph-negative ALL patients aged 18-65 years - based on a pediatric-oriented backbone, in which Peg-asparaginase was administered instead of asparaginase, and on a MRD-driven transplant allocation;²⁰ MRD time-points and MRD analysis are detailed in the *Online Supplementary Materials and Methods*. The EC study number approval is 5629.

Diagnostic bone marrow samples were available from 105 patients (median age 38.7 years, range, 18.2-64.7). Baseline patients' characteristics are summarized in the *Online Supplementary Table S1*; there were no differences in clinical-biological features between our cohort and the remaining population enrolled in the protocol (*Online Supplementary Table S2*). All cases underwent centralized molecular screening: i) the “*BCR/ABL1*-like predictor” assay, ii) sequencing of the JAK/STAT and RAS cascades by next-generation sequencing (NGS), iii) Multiplex Ligation-dependent Probe Amplification (MLPA), iv) targeted RNA sequencing. In 17 cases, the *BCR/ABL1*-like predictor was not feasible due to lack of RNA (*Online Supplementary Table S3*; *Online Supplementary Figure S2*).

BCR/ABL1-like predictor

In order to detect the Ph-like cases, we applied the “*BCR/ABL1*-like predictor”⁷ to 88 patients (*Online Supplementary Materials and Methods*).

Screening of recurrent mutations and deletions

The members of the JAK/STAT (*JAK1*, *JAK2*, *JAK3*, *IL7R* and *CRLF2*) and RAS (*FLT3*, *NRAS*, *KRAS* and *PTPN11*) pathways (181 amplicons) were sequenced by NGS (*Online Supplementary Materials and Methods*).

NGS experiments were performed in 91 cases (74 in common with the *BCR/ABL1*-like predictor analysis - 24 Ph-like and 50 non-Ph-like ALL cases -, *Online Supplementary Materials and Methods* and Table 3). Variants recognized as single nucleotide polymorphisms (SNP) were excluded, unless of prognostic value or previously reported in Ph-like ALL.²¹

Recurrent deletions (*IKZF1*, *CDKN2A/2B*, *PAX5*, *EBF1*, *BTG1*,

Table 1. Comparison between Philadelphia-like (Ph-like) and non-Ph-like clinical features.

	Ph-like	non-Ph-like	P
N	28	60	
Age, median (range)	42.24 (18.18-64.53)	34.52 (18.23-64.59)	ns
Wbc x10 ⁹ /L, median (range)	3.34 (0.23-347)	5.74 (1-75.5)	ns
Hb g/dL, median (range)	8.70 (3.70-13.00)	9.75 (5.00-15.70)	0.034
Plt x10 ⁹ /L, median (range)	40 (1.23-399)	66.5 (7.5- 630)	ns
Sex, N (%)			
M	19 (67.9%)	34 (56.7%)	ns
F	9 (32.1%)	26 (43.3%)	
Risk category, N (%)			
Standard risk	14 (56%)	34 (63%)	ns
No Standard risk	11 (44%)	20 (37%)	

Ph-like: Philadelphia-like; N: number; WBC: white blood cell; Plt: platelet; M: male; F: female; ns: not significant.

RB1, *ETV6* and *CRLF2*) were screened in 87 samples (70 in common with the *BCR/ABL1*-like predictor analysis - 22 Ph-like and 48 non-Ph-like ALL cases -, *Online Supplementary Table S3*), by the Salsa MLPA P335 ALL-IKZF1 kit (MRC-Holland, Amsterdam, the Netherlands) and analyzed according to the Coffalyser manual.²² *P2RY8/CRLF2* was inferred when a deletion within the PAR1 region was documented. Samples were defined *IKZF1*+/ *CDKN2A/2B* and/or *PAX5* when *IKZF1* deletion co-occurred with *CDKN2A/2B* and/or *PAX5* deletions.²³

Targeted RNA-sequencing and FISH analysis

In order to detect fusion genes, libraries were prepared using the TruSight RNA Pan-Cancer Panel (Illumina, San Diego, CA) kit, targeting 1385 cancer- genes (*Online Supplementary Materials and Methods*).

Double-color fluorescence *in situ* hybridization (FISH) studies were performed in 20 B-ALL, 13 Ph-like and seven non-Ph-like with high levels of *CRLF2* expression (*Online Supplementary Materials and Methods*).

Overall, 85 cases were screened (25 Ph-like and 60 non-Ph-like ALL cases, *Online Supplementary Table S3*).

Statistical analyses

Patients' characteristics were compared by chi-squared or Fisher's exact test for categorical variables and Wilcoxon test for continuous data. Overall survival (OS), disease-free survival (DFS) and event-free survival (EFS) were estimated by the Kaplan-Meier product-limit and compared by log-rank test. OS was defined as the time between the date of diagnosis and death for any cause; patients still alive were censored at the time of the last follow-up. DFS was defined as the time between the evaluation of CR - after the induction phase - and relapse or death in CR; patients still alive in first CR, were censored at the time of the last follow-up. Finally, EFS was defined as the time between diagnosis and non-achievement of CR in the induction phase, relapse or death in CR, whichever occurred first; patients still alive, in first CR, were censored at the time of the last follow-up.

Multivariate analysis was performed with the Cox proportional hazards regression model to adjust the effect of *BCR/ABL1*-like predictor for clinically relevant parameters (age, white blood cell [WBC] count, hemoglobin [Hb] level, platelet count, sex and allogeneic transplant [HSCT] and for genetic aberrations impacting on prognosis [*IKZF1*+/ *CDKN2A/2B* and/or *PAX5*, *K/NRAS* clonal mutations, *JAK/STAT* clonal mutations].^{21,22} All tests were 2-sided, accepting $P<0.05$ as statistically

significant. All analyses relied on the SAS v9.4 software. Study data were collected and managed using REDCap²⁴ electronic data capture tools hosted at the GIMEMA Foundation.

Results

Incidence and clinical features of Ph-like acute lymphoblastic leukemia

We identified 28 (31.8%) Ph-like cases with a median score of 0.85 (range, -0.18 to 6.37); the remaining 60 cases had a median score equal to -1.24 (range, -1.7 to -0.33). Overall, the clinical features (age, sex, WBC and platelet counts) at diagnosis of Ph-like and of non-Ph-like cases were similar. Ph-like patients had lower Hb levels ($P=0.016$), as detailed in Table 1. The incidence of Ph-like ALL cases was slightly higher in adults (≥ 36 years) than in young adults (18-35 years), being 36.2% (17 of 47) and 26.8% (11 of 41), respectively. As per clinical protocol guidelines, only 45% of Ph-like cases were assigned to the high-risk category.

Genetic features of Ph-like acute lymphoblastic leukemia cases

The identified Ph-like cases were evaluated for the following genetic features: *CRLF2* expression levels (n=28), *JAK/STAT* and *RAS* pathways mutations (n=24), CNA aberrations (n=22) and fusion genes (n=23), the latter either by RNA-sequencing and/or FISH. A *CRLF2* overexpression, defined as $\Delta Ct < 8$,²⁵ was found in 10 of 28 Ph-like cases (35.7%). Among the *CRLF2*-high cases with a ΔCt value < 4.5 , we observed that three harbored a *CRLF2* rearrangement, with one displaying a concomitant F232C *CRLF2* mutation. Of the remaining seven *CRLF2*-high cases, three had a concomitant rearrangement (two *ABL*-class and one *DDX3X/USP9X*), one displayed a *JAK1* and *RAS* mutation, and in two cases the mutational screening could not be performed due to lack of genomic material; finally, in one case no additional lesions were detected. Among the 24 Ph-like cases analyzed for the mutational status, we detected a total of 13 *JAK/STAT* pathway mutations - nine clonal and four subclonal - in eight cases (33.3%). Despite a high heterogeneity among samples, the most frequently mutated genes were *JAK1* - affected by five mutations mainly targeting the hotspot V658 - and *JAK2* - affected by three mutations focused in the

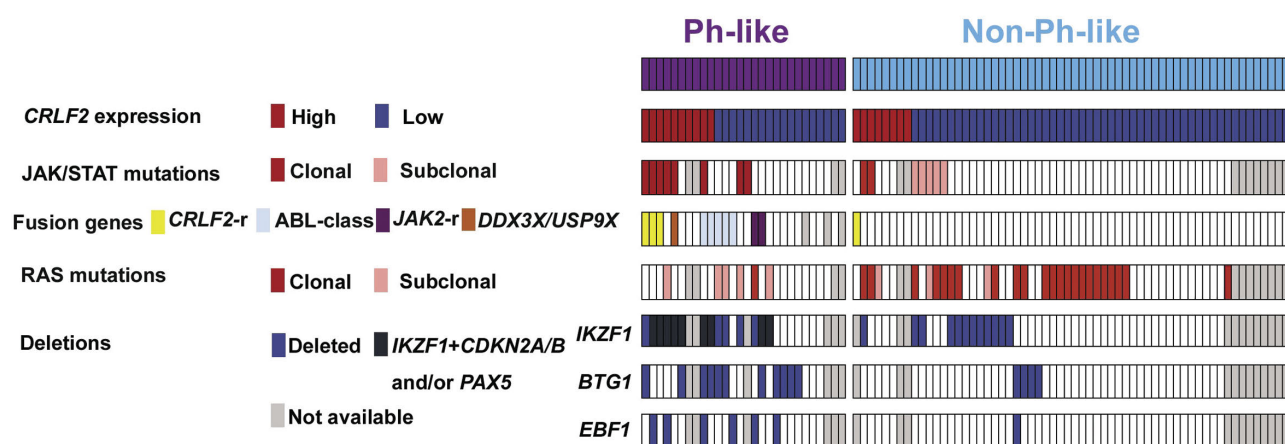


Figure 1. Distribution of the genetic lesions in the Philadelphia-like (Ph-like) and non-Ph-like cases study. Only the samples evaluated for the BCR/ABL1-like predictor and mutational status are depicted.

hotspot R683. *IL7R* and *CRLF2* were mutated in two samples, while *JAK3* only in one. Furthermore, six of the eight mutated samples (75%) displayed a concomitant *CRLF2* overexpression. Nine RAS pathway mutations - only one being clonal - were found in six patients (25%). The most frequent mutations (n=5) involved the hotspot G12-13 of *KRAS* and *NRAS*. CNA analysis in Ph-like cases revealed *IKZF1*, *BTG1*, *CDKN2A/2B*, *PAX5* and *EBF1* deletions in 14 (63.6%), 11 (50%), seven (31.8%), seven (31.8%) and six (27.3%) cases, respectively. Furthermore, *IKZF1* + *CDKN2A/2B* and *PAX5* deletions, known to confer a very poor outcome, were identified in 10 cases (45.5%). Finally, RNA-sequencing and/or FISH experiments of the Ph-like ALL cases revealed 11 TK activating lesions (47.8%): five ABL-class fusion genes (three *NUP214/ABL1*, one *ZC3HAV1/ABL2* and one *EBF1/PDGFRB*), two *BCR/JAK2*, three *CRLF2-r* and 1 *DDX3X/USP9X*, the latter known to be associated with *CRLF2* deregulation.²⁶

Overall, Ph-like associated lesions were identified in 70.8% (17 of 24) of cases and are summarized in Table 2.

When the genetic landscape of Ph-like ALL was compared to that of the non-Ph-like cases, significant differences emerged. As shown in Table 3, *CRLF2*-high was significantly more frequent in Ph-like ALL (35.7% vs. 13.3%, $P=0.018$). Similarly, clonal JAK/STAT mutations were specific of the Ph-like subset (33.3% vs. 4%, $P=0.001$), while RAS pathway clonal mutations were more frequent in non-Ph-like than in Ph-like ALL cases (46% vs. 4.2%, $P=0.001$). Coincidence analysis (CNA) documented that *IKZF1*, *EBF1* and *BTG1* deletions were significantly more common of the Ph-like than in the non-Ph-like subset (63.6%, 50% and 27.3% vs. 25%, 7.8% and 2.1%, respectively; $P=0.002$, $P<0.001$ and $P=0.007$); *CDKN2A/2B* and *PAX5* deletions were equally distributed among Ph-like and non-Ph-like cases (31.8% vs. 47.9% and 31.8% vs. 22.9%, respectively).

The analysis of fusion genes, performed on a total of 85 patients, showed that rearrangements involving TK or cytokine receptors were significantly higher in the Ph-like cases with ten fusion genes involving either *CRLF2* or a TK compared to only one *CRLF2-r* case in the non-BCR/ABL1-like cases (43.5% vs. 1.6%, $P<0.001$).

The genetic lesions documented in both the Ph-like and

non-Ph-like subgroups are detailed in the *Online Supplementary Table S3* and their distribution is provided in Figure 1; further details on non-Ph-like ALL cases, as well as on NGS coverage, are provided in the *Online Supplementary Results* and *Online Supplementary Table S5*, respectively.

Response to treatment, minimal residual disease evaluation and transplant allocation

The Ph-like status was significantly associated with response to treatment: in fact, Ph-like patients had a significantly inferior CR rate at time point 1 (TP1) compared to non-Ph-like cases (74.1% vs. 91.5%, $P=0.044$, Table 4) and this translated into a lower probability of CR achievement ($P=0.038$, $OR=0.265$, 95% Confidence Interval [CI]: 0.071-0.921, *Online Supplementary Table S6*). The latter data retained statistical significance also in a multivariate model adjusted for clinically relevant parameters, as well as for genetic lesions with a prognostic relevance.

MRD evaluation - feasible in 64 patients at TP1, 62 at TP2 and 49 at TP3 - showed that at TP1, 77.8% of Ph-like cases and 41.3% of non-Ph-like were MRD-positive ($P=0.012$); at TP2, 52.9% of Ph-like cases and 20% of non-Ph-like were MRD-positive ($P=0.025$); similarly, at TP3, 41.7% of Ph-like cases and 13.5% of non-Ph-like cases were MRD-positive ($P=0.05$). These data, summarized in Table 4, indicate that in the Ph-like patients there is a significantly higher MRD persistence at all TP evaluated compared to non-Ph-like cases. Consistently, the univariate analyses for MRD results showed that - when considering both clinically relevant parameters and genetic prognostic markers - only the Ph-like status was a risk factor for being MRD-positive at TP2 ($P=0.014$, $OR=4.5$, 95% CI: 1.373-15.508) (Table 5).

As a consequence, HSCT rate in first CR was significantly higher ($P=0.015$) in Ph-like vs. non-Ph-like cases (eight of 20 vs. 6 of 54, 40% vs. 11%, respectively), in line with the guidelines of the trial, in which MRD persistence was a criterion for HSCT allocation. Importantly, among five MRD+ Ph-like patients who did not undergo a transplant, four relapsed at a median period a 7.8 months from CR, whereas no relapses occurred in the three MRD+ Ph-like patients undergoing HSCT.

Table 2A. Genetic features of *BCR/ABL1*-like cases. *BCR/ABL1*-like *BCR/ABL1* -like prediction, scoring, *CRLF2* expression and mutational screening.

Record ID	<i>BCR/ABL1</i> -like prediction	Score	<i>CRLF2</i> expression	RAS pathway status	RAS pathway mutations (VAF)	JAK/STAT pathway status	JAK/STAT pathway mutations (VAF)
B-ALL_1	<i>BCR/ABL1</i> -like	3.073	Low	WT		WT	
B-ALL_3	<i>BCR/ABL1</i> -like	0.928	Low	M	FLT3_ITD (5.4%)	WT	
B-ALL_4	<i>BCR/ABL1</i> -like	0.347	Low	WT		WT	
B-ALL_7	<i>BCR/ABL1</i> -like	1.216	High	WT		M clonal	<i>JAK1</i> DI630-631V (44.5%); <i>JAK1</i> V658I (35.5%)
B-ALL_16	<i>BCR/ABL1</i> -like	0.788	Low	WT		WT	
B-ALL_22	<i>BCR/ABL1</i> -like	0.157	Low	M	FLT3_V491L (11.2%)	WT	
B-ALL_26	<i>BCR/ABL1</i> -like	3.128	High	M	NRAS_G13D (4.1%)	M clonal	<i>JAK1</i> V658I (35.5%)
B-ALL_31	<i>BCR/ABL1</i> -like	2.382	High	WT		M clonal	<i>CRLF2</i> _F232C (46.8%)
B-ALL_32	<i>BCR/ABL1</i> -like	5.720	Low	WT		WT	
B-ALL_34	<i>BCR/ABL1</i> -like	0.725	Low	M	PTPN11_Y279 S (1.9%); NRAS_G12D (2.6%); KRAS_G12GG (5.2%)	WT	
B-ALL_36	<i>BCR/ABL1</i> -like	0.205	High	WT		M clonal	<i>JAK2</i> _R683G (43.9%)
B-ALL_37	<i>BCR/ABL1</i> -like	0.386	Low	WT		WT	
B-ALL_41	<i>BCR/ABL1</i> -like	0.726	Low	M	KRAS_G12A (4.4%); PTPN11_V194L (4.5%)	M clonal	<i>IL7R</i> _INDEL (38.4%); <i>JAK2</i> _C618F (3.3%)
B-ALL_44	<i>BCR/ABL1</i> -like	1.587	High	WT		WT	
B-ALL_45	<i>BCR/ABL1</i> -like	0.262	Low	WT		M clonal	<i>JAK3</i> _T21M (19.1%); <i>JAK1</i> _T688I (5.7%)
B-ALL_46	<i>BCR/ABL1</i> -like	2.449	Low	WT		WT	
B-ALL_52	<i>BCR/ABL1</i> -like	1.013	Low	WT		WT	
B-ALL_55	<i>BCR/ABL1</i> -like	0.544	Low	WT		WT	
B-ALL_61	<i>BCR/ABL1</i> -like	2.722	Low	NA		NA	
B-ALL_62	<i>BCR/ABL1</i> -like	0.335	High	NA		NA	
B-ALL_64	<i>BCR/ABL1</i> -like	-0.043	Low	WT		WT	
B-ALL_73	<i>BCR/ABL1</i> -like	0.048	Low	M clonal	KRAS_G12D (35.9%)	WT	
B-ALL_76	<i>BCR/ABL1</i> -like	1.971	Low	NA		NA	
B-ALL_81	<i>BCR/ABL1</i> -like	1.150	High	WT		WT	
B-ALL_92	<i>BCR/ABL1</i> -like	-0.112	High	NA		NA	
B-ALL_96	<i>BCR/ABL1</i> -like	6.371	High	WT		M clonal	<i>CRLF2</i> _V136M (60%)
B-ALL_97	<i>BCR/ABL1</i> -like	3.432	High	WT		M clonal	<i>JAK2</i> _R683G (10.2%); <i>IL7R</i> _S185C (18.1%); <i>JAK1</i> _V658F (13.8%)
B-ALL_100	<i>BCR/ABL1</i> -like	-0.180	Low	WT		WT	

ALL: acute lymphoblastic leukemia; VAF: variant allele frequency; FISH: fluorescence *in situ* hybridization; RNA seq: RNA sequencing; WT: wild-type; NA: not analyzed.

Survival analyses

Survival analyses at 24 months showed that Ph-like ALL patients had a significantly inferior EFS than non-Ph-like patients (33.5% vs. 66.2%, $P=0.005$); this difference was also evident with regard to DFS (45.5% vs. 72.3%, $P=0.062$), though to a lesser extent, as illustrated in Figure 2; OS was also investigated, and although not significant, it was inferior in Ph-like ALL cases than in non-Ph-like patients (48.5% vs. 72.9%, $P=0.16$, *Online Supplementary Figure S3*). The lack of significance is most likely due to the fact that a higher number of Ph-like patients, because of persistent MRD positivity, underwent, as per protocol guidelines, HSCT (40% vs. 11% in Ph-like vs. non-Ph-like cases, respectively, $P=0.015$).

In a multivariate model for EFS, adjusting for relevant clinical parameters - including HSCT, evaluated as a time

dependent covariate - and genetic prognostic markers, the Ph-like profile, age and Hb levels were the only risk factors that retained statistical significance (Table 6). Notably, however, Ph-like patients undergoing an allogeneic transplant showed a trend towards better EFS ($P=0.078$).

Discussion

The possibility of an early recognition of Ph-like ALL patients offers the unprecedented opportunity to refine the prognostic categories of Ph-negative ALL, and to better understand the reasons for the poor outcome. In the present study, we investigated a cohort of adult B-NEG ALL patients enrolled in the front-line GIMEMA LAL1913 protocol,²⁰ based on a pediatric-inspired backbone and in

Table 2B. Copy number aberration (CNA) analysis, and RNA-sequencing/FISH analyses.

Record ID	<i>IKZF1</i>	<i>CDKN2A/2B</i>	<i>PAX5</i>	<i>IKZF1 + CDKN2A</i> and/or <i>PAX5</i>	<i>BTG1</i>	<i>EBF1</i>	<i>CDKN2A/2B</i> and/or <i>RB1</i>	Gene rearrangements (RNAseq and or FISH analysis)
B-ALL_1	no-Δ	no-Δ	no-Δ		no-Δ	Δ	no-Δ	<i>EBF1/PDGFRB</i>
B-ALL_3	Δ	Δ	Δ	Yes	no-Δ	no-Δ	Δ	No
B-ALL_4	no-Δ	no-Δ	no-Δ		Δ	no-Δ	Δ	No
B-ALL_7	Δ		no-Δ	Yes	no-Δ	no-Δ	Δ	<i>DDX3X/USP9X</i>
B-ALL_16	Δ		Δ	Yes	Δ	no-Δ	Δ	<i>BCR/JAK2</i>
B-ALL_22	Δ	no-Δ	no-Δ		Δ	no-Δ	Δ	<i>NUP214/ABL1</i>
B-ALL_26	Δ	no-Δ	Δ	Yes	no-Δ		no-Δ	No
B-ALL_31	Δ	no-Δ	Δ	Yes	no-Δ		no-Δ	<i>IGH/CRLF2</i>
B-ALL_32	no-Δ	no-Δ	no-Δ		no-Δ	no-Δ	no-Δ	NA
B-ALL_34	Δ	no-Δ	no-Δ		Δ	no-Δ	no-Δ	<i>NUP214/ABL1</i>
B-ALL_36	Δ		no-Δ	Yes	no-Δ	no-Δ	Δ	<i>P2RY8/CRLF2</i>
B-ALL_37	no-Δ	no-Δ	no-Δ		Δ		no-Δ	No
B-ALL_41	Δ		no-Δ	Yes	no-Δ	no-Δ	Δ	No
B-ALL_44Δ	Δ	no-Δ	Δ	Yes	Δ	no-Δ	Δ	<i>ZC3HAV1/ABL2</i>
B-ALL_45	NA	NA	NA		NA	NA	NA	No
B-ALL_46	no-Δ	no-Δ	no-Δ		no-Δ	no-Δ	no-Δ	No
B-ALL_52	no-Δ	Δ	Δ		Δ	no-Δ	Δ	No
B-ALL_55	no-Δ	no-Δ	no-Δ		Δ	no-Δ	no-Δ	No
B-ALL_61	NA	NA	NA		NA	NA	NA	No
B-ALL_62	NA	NA	NA		NA	NA	NA	No
B-ALL_64	NA	NA	NA		NA	NA	NA	NA
B-ALL_73	Δ	no-Δ	no-Δ		no-Δ	Δ	no-Δ	<i>BCR/JAK2</i>
B-ALL_76	NA	NA	NA		NA	NA	NA	NA
B-ALL_81	Δ	Δ	no-Δ	Yes	Δ	no-	Δ	No
B-ALL_92	NA	NA	NA		NA	NA	NA	No
B-ALL_96	Δ	no-Δ	Δ	Yes	Δ	Δ	no-Δ	<i>NUP214/ABL1</i>
B-ALL_97	Δ	no-Δ	no-Δ		Δ	no-Δ	no-Δ	<i>IGH/CRLF2</i>
B-ALL_100	no-Δ	no-Δ	no-Δ		no-Δ	no-Δ	no-Δ	No

which MRD quantification at week 10 is pivotal for transplant allocation, in order to assess the prognostic impact of the Ph-like status. In particular, we aimed at understanding the interplay between the Ph-like status and MRD response. Furthermore, we sought to analyze the clinical and genetic features, the hematologic responses to treatment and the outcome of the identified Ph-like ALL patients.

The screening carried out using the *BCR/ABL1*-like predictor⁷ led to the identification of 28 Ph-like cases - representing 31.8% of the B-NEG cohort - with a slightly higher incidence in adults than in young adults. This finding is in agreement with the recently reported data in other adult cohorts and resembles the epidemiologic behavior of "true Ph-positive" ALL.^{5,6,19} The comparison of the clinical-biological features of Ph-like and non-Ph-like cases revealed a substantial homogeneity in terms of WBC count and sex distribution, as in the GMALL and the MDACC clinical trials,^{6,19} and at variance from Roberts and colleagues⁵ who reported that adult *BCR/ABL1*-like patients have a higher WBC and are prevalently of male sex. In children, an association with hyperleukocytosis has been described by Den Boer *et al.*¹ and Reshmi *et al.*,²⁷ the latter based on the COG AALL1131 high-risk cohort.

The association with male sex was documented in the Total Therapy XV cohort.¹⁶ On the contrary, Roberts and colleagues²⁸ did not find significant differences in the WBC count and sex in the standard-risk subset of childhood B-ALL patients enrolled in the COG AALL0331. In addition to the WBC count and sex, it is worth underlying that in our study the population of Ph-like patients was allocated to both the standard- (56%) and high-risk (44%) categories: this finding has important clinical implications since the prompt identification of these cases might lead to a better therapeutic stratification that ultimately would avoid undertreating these high-risk patients. In adults, a similar distribution was reported also by Herold *et al.*,⁶ while in the pediatric setting this issue is still controversial. Indeed, most Ph-like cases were associated to a high risk in both the COALL and DCOG cohorts,¹ while in the Total Therapy XV trial¹⁶ Ph-like cases were equally distributed in the standard and high National Cancer Institute (NCI) risk groups. Of note, in the report on 139 children classified as standard-risk, Roberts and colleagues²⁸ showed that the Ph-like status did not affect outcome, suggesting that in children risk stratification is clinically more significant than the genomic features.

From a genetic standpoint, the present study further cor-

Table 3. Comparison between Philadelphia-like (Ph-like) and non-Ph-like genetic features.

	<i>BCR/ABL1</i> -like	non- <i>BCR/ABL1</i> -like	P
<i>CRLF2</i> expression level			
<i>CRLF2</i> overexpressing samples	10/28 (35.7%)	8/60 (13.3%)	0.018
Mutational status			
RAS pathway mutated samples	6/24 (25%)	26/50 (52%)	0.025
Clonal RAS mutated	1/24 (4.16%)	23/50 (46%)	0.001
JAK/STAT pathway mutated samples	8/24 (33.3%)	7/50 (14%)	0.04
Clonal JAK/STAT mutated	8/24 (33.3%)	2/50 (4%)	0.001
Copy number aberrations			
<i>IKZF1</i> deleted	14/22 (63.6%)	12/48 (25%)	0.002
<i>IKZF1+ CDKN2A/2B</i> and/or <i>PAX5</i>	10/22 (45.5%)	7/48 (14.6%)	0.007
<i>BTG1</i> deleted	11/22 (50%)	4/48 (8.3%)	<0.001
<i>EBF1</i> deleted	6/22 (27.3%)	1/48 (2.1%)	0.003
<i>CDKN2A/2B</i> deleted	7/22 (31.8%)	23/48 (47.9%)	ns
<i>PAX5</i> deleted	7/22 (31.8%)	11/48 (22.9%)	ns
TK or cytokine receptor fusion genes	10/23 (43.5%)	1/37 (2.7%)	<0.001

TK: tyrosine kinase; ns: not significant.

Table 4. Complete remission achievement and minimal residual disease evaluation in Philadelphia-like (Ph-like) and non-Ph-like cases.

	Ph-like	non-Ph-like	P
CR achievement	20 (74.1%)	54 (91.5%)	0.044
TP1 (week 4)			
MRD-positive patients	14/18 (77.8%)	19/46 (41.3%)	0.012
TP2 (week 10)			
MRD-positive patients	9/17 (52.9%)	9/45 (20%)	0.025
TP3 (week 16)			
MRD-positive patients	5/12 (41.7%)	5/37 (13.5%)	0.05

Ph-like: Philadelphia-like; CR: complete remission; TP: time point; MRD: minimal residual disease.

Table 5. Univariate analyses for minimal residual disease at time point 2, considering clinically relevant variables and molecular prognostic markers.

	Univariate analysis for MRD_TP2	P
	OR (95%CI)	
Ph-like vs. non-Ph-like	4.5 (1.373-15.508)	0.014
Age	1.012 (0.98-1.045)	0.475
WBC	1.013 (1-1.033)	0.133
Plts	0.987 (0.974-0.998)	0.0365
Hb	0.832 (0.638-1.06)	0.152
F vs. M	0.459 (0.145-1.315)	0.1602
No SR vs. SR	0.304 (0.065-1.048)	0.083
<i>IKZF1+ CDKN2A/2B</i> and/or <i>PAX5</i> vs <i>IKZF1</i> -only/WT	1.869 (0.49-6.674)	0.339
Cell cycle genes deletion vs WT	0.88 (0.279-2.773)	0.8253
RAS clonal vs WT/M subclonal	0.8 (0.239-2.51)	0.706
JAK/STAT clonal vs WT/M subclonal	2.596 (0.463-13.293)	0.2482

MRD: minimal residual disease; Ph-like: Philadelphia-like; WBC: white blood cell; Plt: platelet; Hb: hemoglobin; F: female; M: male; SR: standard risk; WT: wild-type; WT/M: wild-type/ mutated; OR: odds ratio; CI: Confidence Interval.

roborates the notion that *CRLF2* overexpression, JAK/STAT mutations and deletions of *IKZF1*, *BTG1* and *EBF1* are significantly more frequent in Ph-like ALL cases. In addition, we observed that clonal JAK/STAT mutations were almost exclusively found in Ph-like ALL, while clonal RAS mutations were specific of non-Ph-like cases, thus suggesting that they play a different role in the two molecular subtypes. Moreover, when focusing on *CRLF2* overexpression, it emerges that it is not sufficient to induce a Ph-like profile: indeed, of the eight Ph-like cases that were fully characterized, seven had at least another lesion.

Furthermore, the results on the incidence of rearrangements targeting TK and cytokine receptors indicate that they prevail in the Ph-like subgroup, with ABL-class gene rearrangements outnumbering the other lesions. Thus, we could identify at least one underlying genetic lesion in 70.8% of Ph-like patients. Not for all cases was it possible to perform an extensive biological screening due to the lack of genomic material (four cases) and RNA-sequencing was carried out using targeted approaches and not genome-wide tools. This may help to explain why no further genetic lesions could be found in the remaining cases (29.2%)

Table 6. Summary of univariate and multivariate analyses for event-free survival, considering clinically relevant variables and molecular prognostic markers.

	Univariate analysis for EFS HR (95%CI)	P	Multivariate analysis for EFS HR (95%CI)	P
Ph-like vs. non-Ph-like	2.6 (1.3-5.19)	0.007	2.3 (1.124-4.92)	0.023
Age	1.03 (1.01-1.05)	0.004	1.04 (1.015-1.067)	0.002
WBC	1.005 (0.999-1.010)	0.074		
Plt	0.993 (0.986-0.999)	0.023		
Hb	0.81 (0.69-0.94)	0.006	0.782 (0.649-0.943)	0.01
F vs. M	0.78 (0.41-1.5)	0.455		
No SR vs. SR	1.89 (0.97-3.67)	0.062		
HSCT vs. No HSCT as a time dependent covariate	1.04 (0.35-3.10)	0.939		
<i>IKZF1+CDKN2A/2B</i> and/or <i>PAX5</i> vs. <i>IKZF1</i> -only/WT	1.73 (0.76-3.98)	0.193		
Cell cycle genes deletion vs. WT	0.967 (0.451-2.069)	0.93		
RAS clonal vs. WT/M subclonal	0.604 (0.269-1.358)	0.222		
JAK/STAT clonal vs. WT/M subclonal	0.85 (0.26-2.82)	0.796		

EFS: event-free survival; Ph-like: Philadelphia-like; WBC: white blood cell; Plt: platelet; Hb: hemoglobin; F: female; M: male; SR: standard risk; WT: wild-type; HSCT: allogeneic stem cell transplant; WT/M: wild-type/mutated; OR: odds ratio; CI: Confidence Interval.

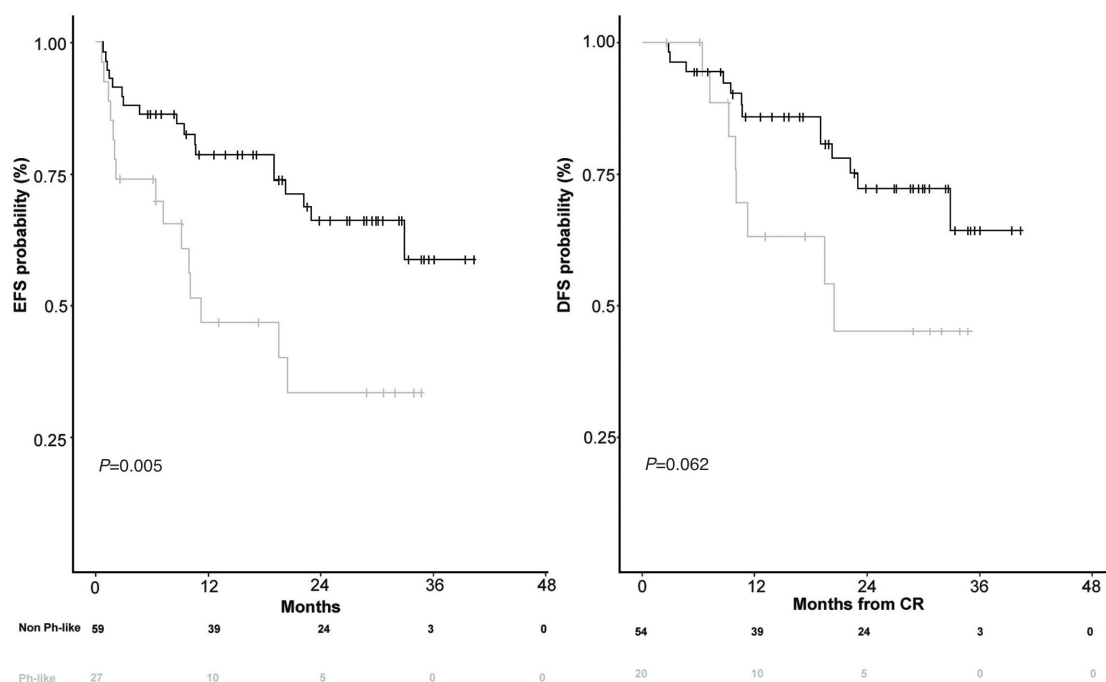


Figure 2. Survival curves of Philadelphia-like (Ph-like) and non-Ph-like patients. event-free survival and disease-free survival.

that proved positive with the BCR/ABL1 predictor. The validity and reproducibility of the *BCR-ABL1*-like predictor has been externally validated by other institutions and from external samples in Europe, showing an overall concordance with other tools (FISH and NGS) of 88%.²⁹

With regards to the relationship between the Ph-like status, MRD response and outcome, we showed that Ph-like ALL patients have a higher risk of CR failure: in fact, 74.1% of Ph-like ALL and 91.4% non-Ph-like achieved a CR. This difference was neither detected in the intensive GMALL trials 06/99 and 07/03 – in which all patients achieved a CR, albeit with a short duration –, nor in the

hyper-CVAD-based protocols or the augmented BFM regimen administered at MDACC.¹⁹

More importantly, our study allowed to correlate the Ph-like status with MRD, that is presently regarded as the most important prognostic marker in ALL management. In fact, this analysis showed that in the GIMEMA LAL1913 protocol, at all TP analyzed, the percentage of MRD-positive patients was significantly higher in the Ph-like ALL subset than in non-Ph-like cases. This difference was particularly evident at TP2 (HSCT decisional point), when 52.9% of Ph-like and only 20% of non-Ph-like cases were MRD-positive. Indeed, when both clinically relevant

parameters and genetic prognostic markers were taken into account the Ph-like profile proved the only risk factor for MRD positivity at TP2. Thus, considering both response to induction treatment and MRD monitoring, the Ph-like status, if identified early, permits not only to recognize patients who are likely to be refractory to induction treatment, but also to identify - within cases who achieve a CR - those who are likely to remain MRD-positive. This strong association may allow to anticipate therapeutic changes.

To our knowledge, this is the first study that analyzes the interaction between the Ph-like status and MRD - assessed by quantitative PCR of the IG and TR gene rearrangements - in a broad cohort of uniformly and prospectively treated adult ALL patients within a clinical trial. Similar results were provided by Herold and colleagues⁶ who found that Ph-like patients were less likely to achieve a MRD-negative status in a small cohort of 31 patients with overlapping MRD and Ph-like status information. In the pediatric setting, contradicting results have been reported.^{14,16}

Furthermore, the comparison of survival curves highlighted that Ph-like patients experienced a significantly worse EFS at 24 months compared to that of non-Ph-like cases (33.5% and 66.2%, respectively). Along the same line, also in cases achieving a CR, the Ph-like profile had a negative prognostic impact, as shown by the worse DFS of Ph-like patients. Although limited by the small sample size, our study demonstrates that transplant is beneficial in these cases and should be pursued at the earliest opportunity, as shown by the high rate of relapses within non-transplanted Ph-like patients (4 of 5 MRD positive patients relapsed).

Lastly, in all outcome parameters evaluated - CR achievement, MRD at TP2 and EFS - the Ph-like status emerged as an independent prognostic marker.

In addition to confirming the inferior outcome of Ph-like ALL patients, these data indicate that the differences between Ph-like and non-Ph-like cases are not abolished by pediatric-like intensive therapeutic schemes, in agreement with the results of the MDACC group.¹⁸ Based on the MRD findings hereby reported, this is primarily contributed to the significantly lower rates of complete molecular responses observed in Ph-like patients.

In light of the poor outcome of Ph-like ALL and of the possibility of using targeted approaches,³⁰ different clinical trials specifically designed for Ph⁺ ALL and Ph-like ALL cases are testing the efficacy of dasatinib (clinicaltrials.gov. Identifier: 02420717, 02883049, 03564470 and 02143414) or of dasatinib in combination with blinatumomab (clinicaltrials.gov. Identifier: SWOG-S1318 and NCT02143414). Other studies are investigating the impact of blinatumomab in combination with chemotherapy in Ph-negative B-lineage ALL (GIMEMA LAL2317, clinicaltrials.gov. Identifier: 03367299 and 02003222). In these latter studies, it is investigated if the addition of blinatumomab can

increase the rates of CR and MRD-negativity in Ph-like patients, as already observed in Ph⁺ ALL.³² In support of the fact that Ph-like patients may benefit from targeted treatment, a recent study from Tanasi and colleagues has reported that the introduction of TKI front-line was associated with a 3-years OS of 77%.³¹ Other compounds, such as ruxolitinib (clinicaltrials.gov. Identifier: 02420717, 03571321 and 02723994) and the histone deacetylase inhibitor chidamide (clinicaltrials.gov. Identifier: 03564470) are under investigation.

Taken together, the results of this study carried out on adult B-NEG ALL cases enrolled in the front-line GIMEMA LAL1913 clinical protocol confirm that the BCR/ABL1-like predictor⁷ is a valid tool to rapidly recognize Ph-like cases that account for about 30% of adult B-NEG ALL. In addition, we could show that also in a pediatric-oriented and MRD-driven clinical trial Ph-like patients have a lower probability of achieving a CR, are more likely to remain MRD-positive and have a significantly shorter EFS. The Ph-like profile is an independent risk factor for CR failure and MRD-persistence, thus further underlying the need that Ph-like cases - a primary unmet clinical need in ALL - are rapidly recognized at diagnosis in order to refine the risk stratification of Ph-negative ALL and optimize patients' management. Further investigations are currently ongoing to unravel if within Ph-like ALL there are subgroups of patients with a different outcome likelihood.

Disclosures

No conflicts of interest to disclose.

Contributions

SC designed research, analyzed data, provided clinical samples and clinical data, and wrote the manuscript; MM performed experiments, analyzed data and wrote the manuscript; AP performed statistical analyses; IDS, LC, AT, MC, LE, GAP, RLS, MCAL, MCP, VP, AS, OS, VA performed experiments; SC, FDR, PDF, CP, AC, RC, MC, NF, DM, CC, AV, provided samples and clinical data; EC and PF contributed to protocol management; AG and CM critically revised the manuscript; AR and RB designed the trial and critically revised the manuscript; RF designed the research and the trial, and critically revised the manuscript.

Acknowledgments

The authors wish to thank Grazia Fazio and Chiara Palmi for support in TruSight Pancancer and MLPA experiments, Associazione Italiana per la Ricerca sul Cancro (AIRC) 5x1000, Special Program Metastases (21198), Milan (Italy) to RF; Finanziamento Medi Progetti Universitari 2015 to SC (Sapienza University of Rome); Bandi di Ateneo per la Ricerca (Sapienza University of Rome, RM11816436B712AF) to SC and PRIN 2017 (2017PPS2X4_002) to SC, CM, and RLS; Fondazione Cassa di Risparmio di Perugia (grant number 2018.0418.021) to RLS.

References

1. Den Boer ML, van Slegtenhorst M, De Menezes RX, et al. A subtype of childhood acute lymphoblastic leukaemia with poor treatment outcome: a genome-wide classification study. Lancet Oncol. 2009;10(2):125-134.
2. Mullighan CG, Su X, Zhang J, et al. Deletion of IKZF1 and prognosis in acute lymphoblastic leukemia. N Engl J Med. 2009;360(5):470-480.
3. Roberts KG, Morin RD, Zhang J, et al. Genetic alterations activating kinase and cytokine receptor signaling in high-risk acute lymphoblastic leukemia. Cancer Cell. 2012;22(2):153-166.
4. Roberts KG, Li Y, Payne-Turner D, et al. Targetable kinase-activating lesions in Ph-like acute lymphoblastic leukemia. N

Engl J Med. 2014;371(11):1005-1015.

5. Roberts KG, Gu Z, Payne-Turner D, et al. High frequency and poor outcome of Philadelphia chromosome-like acute lymphoblastic leukemia in adults. *J Clin Oncol.* 2017;35(4):394-401.

6. Herold T, Schneider S, Metzeler KH, et al. Adults with philadelphia chromosome-like acute lymphoblastic leukemia frequently have igh-CRLF2 and JAK2 mutations, persistence of minimal residual disease and poor prognosis. *Haematologica.* 2017; 102(1):130-138.

7. Chiaretti S, Messina M, Grammatico S, et al. Rapid identification of BCR/ABL1-like acute lymphoblastic leukaemia patients using a predictive statistical model based on quantitative real time-polymerase chain reaction: clinical, prognostic and therapeutic implications. *Br J Haematol.* 2018;181(5):642-652.

8. Maude SL, Tasian SK, Vincent T, et al. Targeting JAK1/2 and mTOR in murine xenograft models of Ph-like acute lymphoblastic leukemia. *Blood.* 2012; 120(17):3510-3518.

9. Lengline E, Beldjord K, Dombret H, et al. Successful tyrosine kinase inhibitor therapy in a refractory B-cell precursor acute lymphoblastic leukemia with EBF1-PDGFRB fusion. *Haematologica.* 2013;98(11):146-148.

10. Weston BW, Hayden MA, Roberts KG, et al. Tyrosine kinase inhibitor therapy induces remission in a patient with refractory EBF1-PDGFRB-positive acute lymphoblastic leukemia. *J Clin Oncol.* 2013;31(25):e413-416.

11. Fazio F, Barberi W, Cazzaniga G, et al. Efficacy of imatinib and chemotherapy in a pediatric patient with Philadelphia-like acute lymphoblastic leukemia with EBF1-PDGFRB fusion transcript. *Leuk Lymphoma.* 2020;61(2):469-472.

12. Tasian SK, Teachey DT, Li Y, et al. Potent efficacy of combined PI3K/mTOR and JAK or ABL inhibition in murine xenograft models of Ph-like acute lymphoblastic leukemia. *Blood.* 2017;129(2):177-187.

13. Harvey RC, Kang H, Roberts KG, et al. Development and validation of a highly sensitive and specific gene expression classifier to prospectively screen and identify B-precursor acute lymphoblastic leukemia (ALL) patients with a Philadelphia chromosome-like ("Ph-like" or "BCR-ABL1-Like") signature for therapeutic targeting and clinical intervention. *Blood.* 2013;122(21):826.

14. Heatley SL, Sadras T, Kok CH, et al. High prevalence of relapse in children with Philadelphia-like acute lymphoblastic leukemia despite risk-adapted treatment. *Haematologica.* 2017;102(12):e490-e493.

15. Roberts KG. The biology of Philadelphia chromosome-like ALL. *Best Pract Res Clin Haematol.* 2017;30(3):212-221.

16. Roberts KG, Pei D, Campana D, et al. Outcomes of children with BCR-ABL1-like acute lymphoblastic leukemia treated with risk-directed therapy based on the levels of minimal residual disease. *J Clin Oncol.* 2014;32(27):3012-3020.

17. Stock W, Luger SM, Advani AS, et al. A pediatric regimen for older adolescents and young adults with acute lymphoblastic leukemia: results of CALGB 10403. *Blood.* 2019;133(14):1548-1559.

18. Tasian SK, Hurtz C, Wertheim GB, et al. High incidence of Philadelphia chromosome-like acute lymphoblastic leukemia in older adults with B-ALL. *Leukemia.* 2017; 31(4):981-984.

19. Jain N, Roberts KG, Jabbour E, et al. Ph-like acute lymphoblastic leukemia: a high-risk subtype in adults. *Blood.* 2017;129(5):572-581.

20. Bassan R, Chiaretti S, Paoloni F, et al. First results of the GIMEMA LAL1913 protocol for adult patients with Philadelphia-negative acute lymphoblastic leukemia (Ph- ALL). On behalf of the GIMEMA Acute Leukemia Working Group. *PS919. HemaSphere.* 2018;2(S1):408.

21. Messina M, Chiaretti S, Wang J, et al. Prognostic and therapeutic role of targetable lesions in B-lineage acute lymphoblastic leukemia without recurrent fusion genes. *Oncotarget.* 2016;7(12):13886-13901.

21. Messina M, Chiaretti S, Fedullo AL, et al. Clinical significance of recurrent copy number aberrations in B-lineage acute lymphoblastic leukaemia without recurrent fusion genes across age cohorts. *Br J Haematol.* 2017;178(4):583-587.

23. Fedullo AL, Messina M, Elia L, et al. Prognostic implications of additional genomic lesions in adult Ph+ acute lymphoblastic leukemia. *Haematologica.* 2019; 104(2):312-318.

24. Harris PA, Taylor R, Thielke R, Payne J, Gonzalez N, Conde JG. Research electronic data capture (REDCap). A metadata-driven methodology and workflow process for providing translational research informatics support. *J Biomed Inform.* 2009;42(2):377-381.

25. Chiaretti S, Brugnoletti F, Messina M, et al. CRLF2 overexpression identifies an unfavourable subgroup of adult B-cell precursor acute lymphoblastic leukemia lacking recurrent genetic abnormalities. *Leuk Res.* 2016;41:36-42.

26. Russell LJ, Jones L, Enshaei A, et al. Characterisation of the genomic landscape of CRLF2-rearranged acute lymphoblastic leukemia. *Genes Chromosomes Cancer.* 2017;56(5):363-372.

27. Reshmi SC, Harvey RC, Roberts KG, et al. Targetable kinase gene fusions in high-risk B-ALL: A study from the Children's Oncology Group. *Blood.* 2017;129(25):3352-3361.

28. Roberts KG, Reshmi SC, Harvey RC, et al. Genomic and outcome analyses of Ph-like ALL in NCI standard-risk patients: a report from the children's oncology group. *Blood.* 2018;132(8):815-824.

29. Chiaretti S, Taherinasab A, Canichella M, et al. The Validation of the BCR/ABL1-like predictor across laboratories shows reproducibility of results. *Blood.* 2019; 134 (Suppl 1):S5211.

30. Chiaretti S, Messina M, Foà R. BCR/ABL1-like acute lymphoblastic leukemia: how to diagnose and treat? *Cancer.* 2019;125(2): 194-204.

31. Tanasi I, Ba I, Sirvent N, et al. Efficacy of tyrosine kinase inhibitors in Ph-like acute lymphoblastic leukemia harboring ABL-class rearrangements. *Blood.* 2019;134(16): 1351-1355.

32. Foà R, Bassan R, Vitale A, et al. GIMEMA Investigators. Dasatinib-olinatatumomab for Ph-positive acute lymphoblastic leukemia in adults. *N Engl J Med.* 2020;383(17):1613-1623.

RUNX1-EVI1 disrupts lineage determination and the cell cycle by interfering with RUNX1 and EVI1 driven gene regulatory networks

Sophie G. Kellaway, Peter Keane, Ella Kennett and Constanze Bonifer

Institute of Cancer and Genomic Sciences, University of Birmingham, Birmingham, UK



Ferrata Storti Foundation

Haematologica 2021
Volume 106(6):1569-1580

ABSTRACT

Hematological malignancies are characterized by a block in differentiation, which in many cases is caused by recurrent mutations affecting the activity of hematopoietic transcription factors. RUNX1-EVI1 is a fusion protein encoded by the t(3;21) translocation linking two transcription factors required for normal hematopoiesis. RUNX1-EVI1 expression is found in myelodysplastic syndrome, secondary acute myeloid leukemia, and blast crisis of chronic myeloid leukemia; with clinical outcomes being worse than in patients with RUNX1-ETO, RUNX1 or EVI1 mutations alone. RUNX1-EVI1 is usually found as a secondary mutation, therefore the molecular mechanisms underlying how RUNX1-EVI1 alone contributes to poor prognosis are unknown. In order to address this question, we induced expression of RUNX1-EVI1 in hematopoietic cells derived from an embryonic stem cell differentiation model. Induction resulted in disruption of the RUNX1-dependent endothelial-hematopoietic transition, blocked the cell cycle and undermined cell fate decisions in multipotent hematopoietic progenitor cells. Integrative analyses of gene expression with chromatin and transcription factor binding data demonstrated that RUNX1-EVI1 binding caused a re-distribution of endogenous RUNX1 within the genome and interfered with both RUNX1 and EVI1 regulated gene expression programs. In summary, RUNX1-EVI1 expression alone leads to extensive epigenetic reprogramming which is incompatible with healthy blood production.

Introduction

The development of acute myeloid leukemia (AML) is a step-wise process wherein cells acquire multiple additional genetic changes following the occurrence of the initial driver mutation which eventually leads to the development of overt disease. A number of driver mutations, such as the t(8;21) translocation which gives rise to the fusion protein RUNX1-ETO are compatible with a pre-leukemic state.¹ However, another fusion protein, RUNX1-EVI1 is found most commonly as a secondary mutation²⁻⁴ and is associated with a particularly poor prognosis. The RUNX1-EVI1 onco-fusion protein is a product of the t(3;21)(q26;q22) translocation which links sequences from *RUNX1* to the entire length of the *MDS-EVI1* or *EVI1* (also known as *MECOM*) locus. Elucidating the molecular basis of the phenotypic changes induced by RUNX1-EVI1 alone is complicated by the fact that it is expressed on a background of other mutations and thus unique transcriptional rewiring is seen in each patient.⁵

Both RUNX1 and EVI1 play important roles in normal hematopoiesis and in various hematological malignancies. RUNX1 (also known as AML1) is a transcription factor essential for initial specification of hematopoietic cells,⁶ and is frequently found to be mutated in leukemia.^{7,8} RUNX1 contains a DNA-binding domain – the runt homology domain (RUNT) at the N-terminus, which is preserved in RUNX1-EVI1 and a transactivation domain which is lost.⁷ MDS-EVI1 and EVI1 arise from alternative transcripts from the *MECOM* gene which have both overlapping and opposing functions – EVI1 can be a repressor of gene transcription, whereas MDS-EVI1 has activating functions.⁹ MDS-EVI1 is essential for long-term survival of

Correspondence:

CONSTANZE BONIFER
c.bonifer@bham.ac.uk

Received: November 5, 2019.

Accepted: April 9, 2020.

Pre-published: April 16, 2020.

<https://doi.org/10.3324/haematol.2019.241885>

©2021 Ferrata Storti Foundation

Material published in *Haematologica* is covered by copyright. All rights are reserved to the Ferrata Storti Foundation. Use of published material is allowed under the following terms and conditions: <https://creativecommons.org/licenses/by-nc/4.0/legalcode>. Copies of published material are allowed for personal or internal use. Sharing published material for non-commercial purposes is subject to the following conditions: <https://creativecommons.org/licenses/by-nc/4.0/legalcode>, sect. 3. Reproducing and sharing published material for commercial purposes is not allowed without permission in writing from the publisher.



hematopoietic stem cells¹⁰ and is also expressed throughout embryonic hematopoiesis.¹¹ EVI1 is able to bind DNA via ten zinc-fingers, but MDS1-EVI1 additionally contains a proline-rich domain with homology to SET domains.¹² RUNX1, EVI1 and MDS-EVI1 have all been associated with cell cycle regulation alongside the control of differentiation.¹³⁻¹⁵

Mice carrying a *RUNX1-EVI1* transgene present with disrupted hematopoiesis and with varying degrees of leukemic transformation that is ultimately embryonic lethal.¹⁶⁻¹⁸ In a cell line model of t(3;21) it was shown that RUNX1-EVI1 blocks differentiation by binding to chromatin at both normal RUNX1 binding sites and elsewhere, co-ordinating a transcriptional network that is dependent on GATA2 rather than RUNX1.¹⁹ These studies suggest that RUNX1-EVI1 acts in a dominant negative fashion to RUNX1,²⁰ but has additional effects, likely due to interference with EVI1 binding and interactions.

In order to understand the molecular effects of RUNX1-EVI1 expression in the absence of other mutations, we integrated gene expression and chromatin immunoprecipitation followed by sequencing (ChIP-seq) data from blood precursor cells derived from a mouse embryonic stem cell line (mESC) in which we induced RUNX1-EVI1 at the onset of hematopoiesis. We show that RUNX1-EVI1 induction leads to a block in the cell cycle and interferes with both the EVI1 and the RUNX1 driven developmental programs, with cells adopting a multi-lineage gene expression pattern. Moreover, RUNX1-EVI1 orchestrates redistribution and increased binding of endogenous RUNX1, and increases chromatin accessibility at sites enriched in PU.1 motifs. Taken together we show that RUNX1-EVI1 expression is incompatible with normal hematopoietic stem cell function.

Methods

Mouse *RUNX1-EVI1* embryonic stem cell line generation

RUNX1-EVI1 from the pME18s-RUNX1-EVI1 plasmid (a gift from Kinuko Mitani, Dokkyo Medical University, Japan) was cloned into the p2lox-targeting vector (a gift from Michael Kyba, University of Minnesota). A2lox mESC (a gift from Michael Kyba) were transduced with 20 µg of p2lox-RUNX-EVI1 using the 4D-Nucleofector (Lonza) with the mouse ES program, with the P3 primary cell kit.

Embryonic stem cell line differentiation

ESC were differentiated as previously described. Briefly, cells were plated into bacterial-grade dishes, after 3.25 days the resulting embryoid bodies were dispersed using TrypLE express (Gibco) to single cells and FLK1+ cells were purified by magnetic cell sorting. These FLK1+ cells were then cultured in gelatin-coated flasks with mouse vascular endothelial growth factor and mouse interleukin 6. After 1 day 0.5 µg/ml doxycycline was added where appropriate and cells cultured for a further 18 hours.

Fluorescence associated cell sorting

Cell populations were identified and sorted on day 2 of blast culture based on surface markers. For experiments including hemogenic endothelium (HE) the floating and adherent cells were pooled. These cells were stained with KIT-APC (BD pharmingen), Tie2-PE (eBioscience) and CD41-PE-Cy7 (eBioscience) and analyzed on a Cyan ADP flow cytometer

(Beckman Coulter) with data analysis using FlowJo, or sorted on a fluorescence associated cell sorting (FACS) Aria cell sorter (BD Biosciences). Progenitors matured in liquid culture were stained with CD11b-PE (eBioscience) and F4/80-APC (eBioscience).

Gene expression analysis

RNA was isolated from sorted cells using the NucleoSpin RNA kit (Macherey-Nagel). RNA sequencing (RNA-seq) libraries were prepared from two biological replicates using the True-Seq strand-ed total RNA kit (Illumina).

DNaseI-sequencing

DNase I hypersensitive sites sequencing (DNaseI-seq) was performed as previously described.²¹ 3x10⁵ sorted cells were added directly to DNaseI (Worthington Biochemical Corporation) used between 6 and 13 U/mL for 3 minutes at 22°C. The reaction was terminated by addition of sodium dodecyl sulfate to 0.5% and cell lysates treated with 0.5 mg/mL proteinase K. DNA was isolated by phenol/chloroform extraction and used to generate a library using the KAPA hyper prep kit, according to the manufacturer's instructions.

Chromatin immunoprecipitation sequencing

ChIP-seq was performed essentially as described.²² KIT+ floating progenitor cells were double crosslinked, nuclei prepared²² then sonicated for eight cycles of 30 seconds (s) off using a Picoruptor (Diagenode). Immunoprecipitation was carried out overnight at 4°C, washed and eluted. Extracted DNA was then used to generate a library using the KAPA hyper prep kit.

Data availability

All sequencing data have been deposited at National Center for Biotechnology Information under the number GSE143460. Further methods, including bioinformatic analysis are detailed in the *Online Supplementary Appendix*.

Results

RUNX1-EVI1 disrupts hematopoietic growth and differentiation

In order to understand the direct effects of RUNX1-EVI1 fusion protein induction on hematopoietic specification we needed to express RUNX1-EVI1 in primary cells in the absence of other mutations. Initial attempts to express the protein in purified human CD34+ cells by retroviral transduction were unsuccessful indicating that expressing uncontrolled levels of this protein may be toxic for the cells (unpublished data). In order to circumvent these problems, we generated a mESC line expressing a human *RUNX1-EVI1* cDNA under the control of a doxycycline (dox)-inducible promoter (Figure 1A). The *RUNX1-EVI1* transgene was derived from the t(3;21) SKH1 cell line²³ and comprised amino acids from the N-terminus of RUNX1 translocated to the MDS1-EVI1 isoform (*Online Supplementary Figure S1A*). We used a well characterized *in vitro* differentiation system that recapitulates the different steps of embryonic hematopoietic specification *in vitro*,^{11,24} namely mesoderm specification into endothelial cells, followed by endothelial-hematopoietic transition (EHT) which gives rise to multipotent hematopoietic progenitor (HP) cells (Figure 1A, lower panel) during blast culture. The EHT is crucially dependent on the expression of *Runx1*,^{6,25} and is also the stage at which *Evi1* expression is maximal before being downregulated.¹¹ We therefore

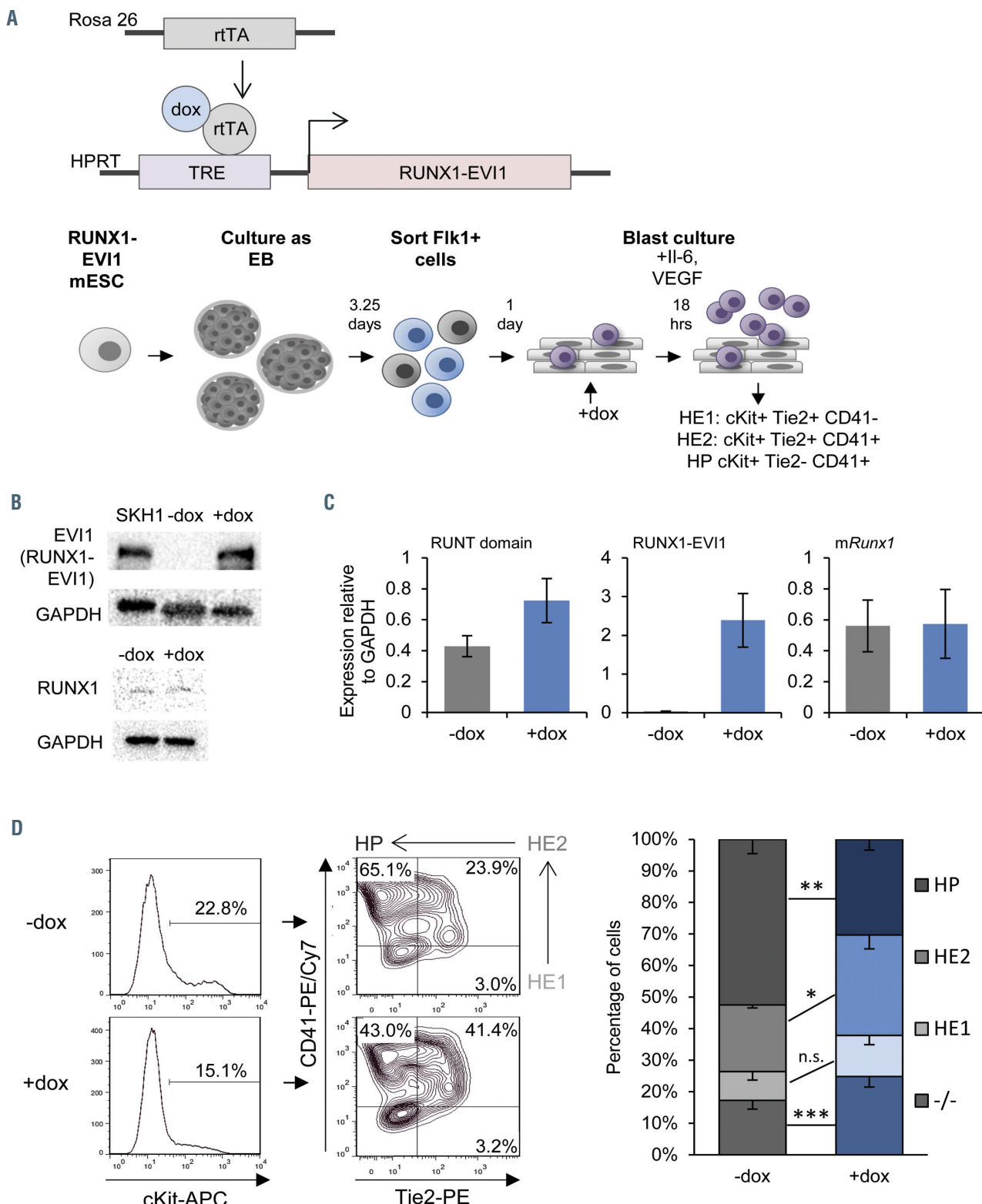


Figure 1. Induction of RUNX1-EVI1 perturbs *Runx1* dependent endothelial to hematopoietic transition. (A) Overview of the generation of dox-inducible RUNX1-EVI1 embryonic stem cells (ESC), *in vitro* differentiation of ESC to hematopoietic progenitors and timing induction of RUNX1-EVI1. (B) RUNX1-EVI1 was expressed at a comparable level to that in the human t(3;21) cell line SKH-1 shown by western blot. Note that the antibody against EVI-1 does not recognize the endogenous mouse protein. RUNX1 protein levels were unaffected by induction of RUNX1-EVI1. (C) Expression of RUNX1-EVI1 was at a physiological level, equal to that of the endogenous *Runx1*, shown by quantitative reverse transcriptase polymerase chain reaction, normalized to glyceraldehyde 3-phosphate dehydrogenase (GAPDH). Runt domain primers bind the 5' end of the gene and so both endogenous *Runx1* and RUNX1-EVI1 are detected, *mRunx1* primers bind the 3' end and so only endogenous *Runx1* is detected. (D) The composition of the day 2 blast culture, 18 hours following doxycycline (dox) induction, was analyzed by flow cytometry using antibodies against cKit, Tie2 and CD41; representative plots for -dox and +dox samples are shown (left, with the Tie2/CD41 plots pre-gated by cKit+) with the average percentage of each population (right), error bars represent standard error of the mean, n=5, *P<0.05, **P<0.01, ***P<0.005.

induced *RUNX1-EVI1* expression in newly forming HP (*Online Supplementary Figure S1B*), when *Runx1* becomes upregulated as shown in the schematic in Figure 1A. These time points were used for all subsequent experiments, with the cells sorted from the day 2 blast culture being used for genome-wide analysis. Since differentiation in this system is transient, we also used cell sorting to obtain cells from earlier differentiation stages which enabled us to study the effect of *RUNX1-EVI1* expression at these stages as well. We titrated induction of *RUNX1-EVI1* such that the protein expression was at a level similar to that seen in the SKH1 cells, and gene expression was at a similar level to endogenous *RUNX1*, which itself was

stably expressed (Figures 1B and C).

Induction of *RUNX1-EVI1* led to a partial disruption of the EHT following 18 hours of dox induction (Figure 1D), with a reduction in cKit+ Tie2- CD41+ HP and a reciprocal increase in hematopoietic committed HE cells (HE2, cKit+ Tie2+ CD41+). This result is concordant with the notion that *RUNX1-EVI1* acts as a dominant negative to *RUNX1*, since the earlier uncommitted endothelial cells which had not yet upregulated *Runx1* (HE1, cKit+ Tie2+ CD41-) were unaffected. Inducing *RUNX1-EVI1* prior to the EHT hampers hematopoietic differentiation leading to a considerably greater proportion of Tie2- CD41- negative cells (*Online Supplementary Figure S1C*).

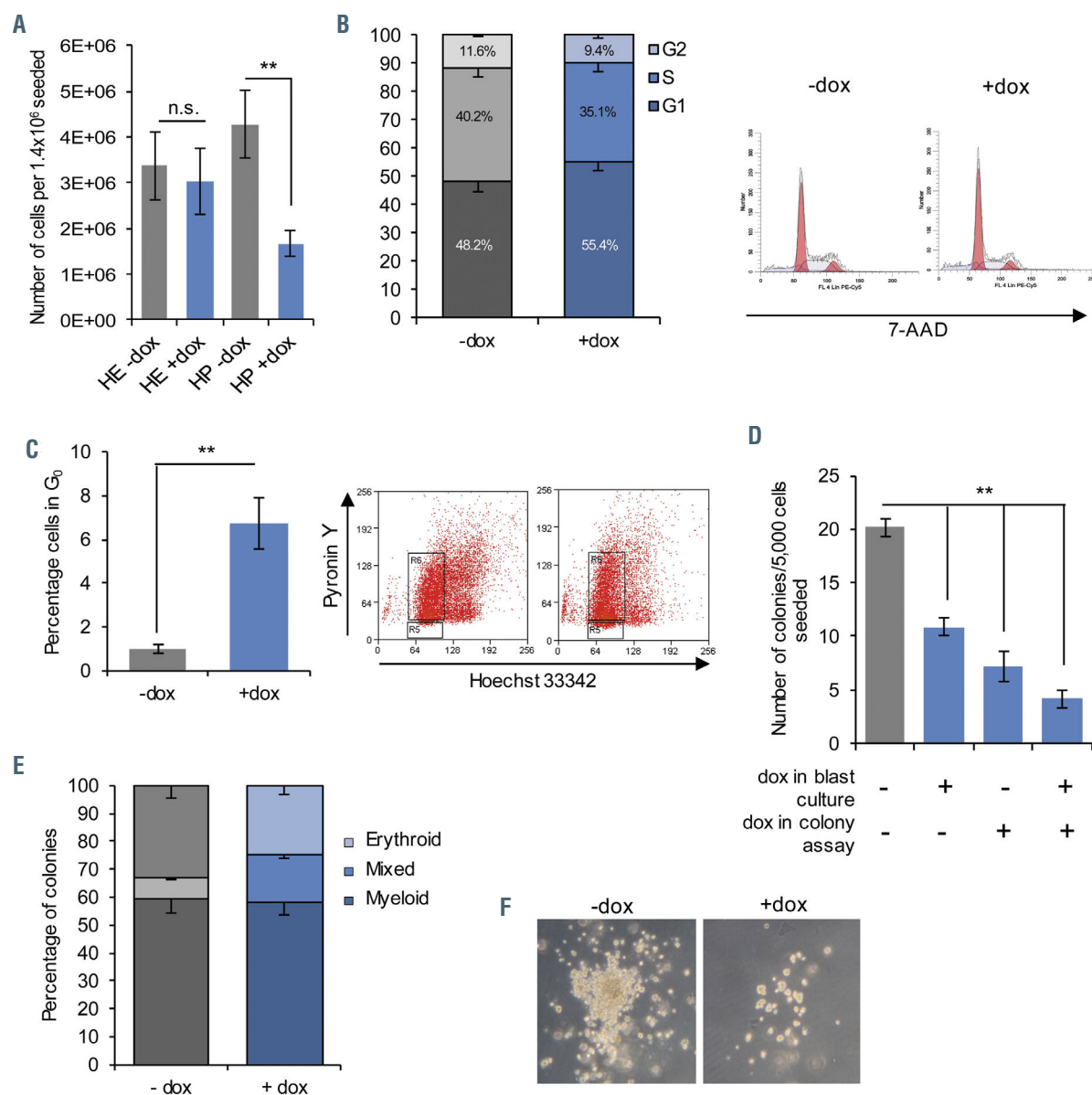


Figure 2. *RUNX1-EVI1* expression causes reduced cell cycling and colony forming capacity in hematopoietic progenitors. (A) Fewer floating hematopoietic progenitor (HC) cells were present in day 2 blast culture, following induction of *RUNX1-EVI1*, n=5, **P<0.01. Cell cycle stages, n=3. (B) and quiescence, n=5 (C) were assessed in the whole blast culture at the same time-point, showing an increased proportion of cells in G_0 and G_1 . Example flow cytometry plots are shown to the right, *P<0.05, **P<0.01. (D) Floating progenitor cells with *RUNX1-EVI1* induced formed fewer colonies, n=3, **P<0.01 (E) Colonies following doxycycline (dox) induction in blast culture only were comprised of approximately equivalent proportions of granulocyte/macrophage (GM), erythroid (Ery) or mixed colonies, with a slight increase in the mixed-type at the expense of singular lineage, n=3. All error bars (A to E) represent standard error of the mean. (F) Representative brightfield images of colonies with and without dox induction in blast culture only.

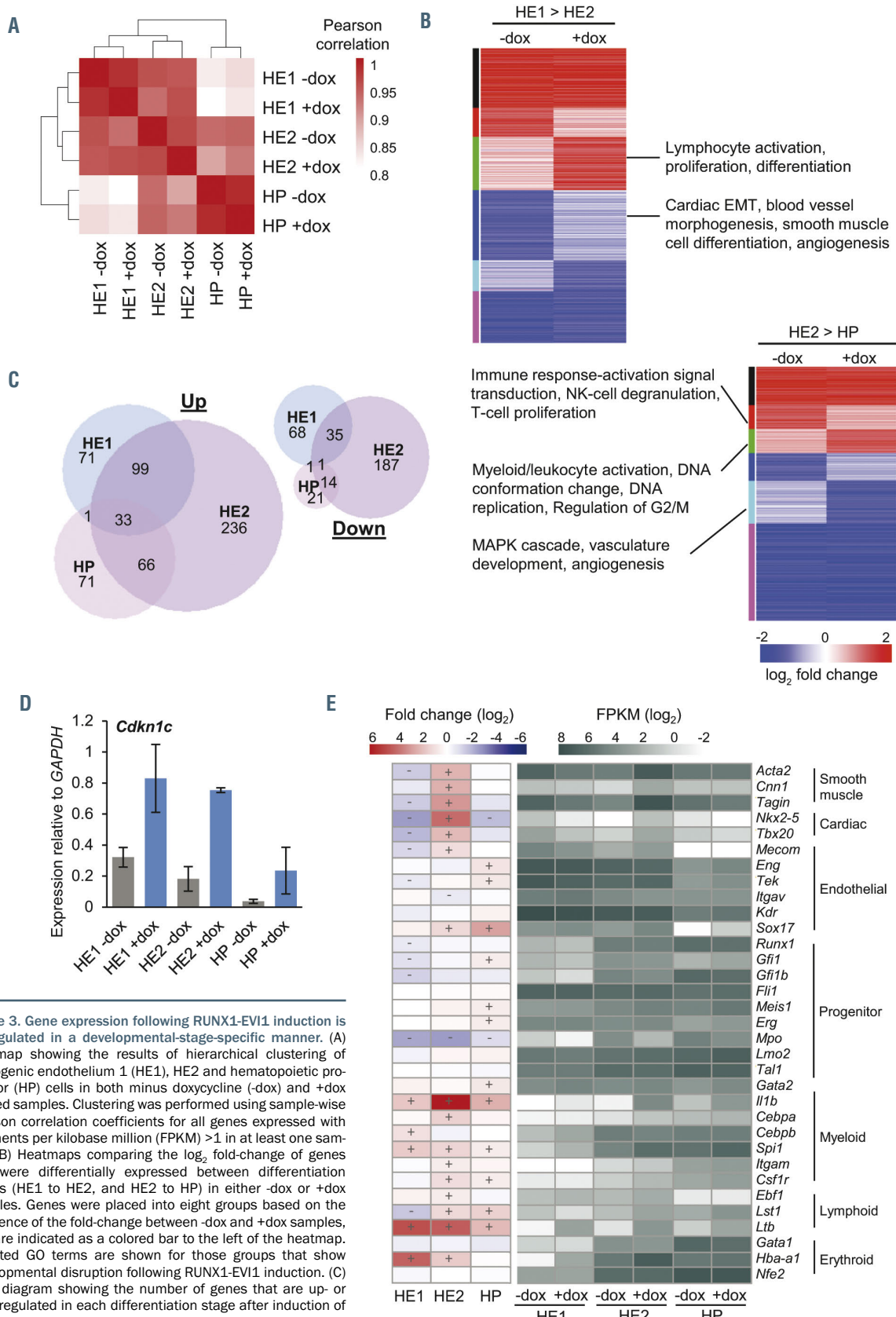


Figure 3. Gene expression following RUNX1-EVI1 induction is de-regulated in a developmental-stage-specific manner. (A) Heatmap showing the results of hierarchical clustering of hemogenic endothelium 1 (HE1), HE2 and hematopoietic progenitor (HP) cells in both minus doxycycline (-dox) and +dox treated samples. Clustering was performed using sample-wise Pearson correlation coefficients for all genes expressed with fragments per kilobase million (FPKM) >1 in at least one sample. (B) Heatmaps comparing the \log_2 fold-change of genes that were differentially expressed between differentiation stages (HE1 to HE2, and HE2 to HP) in either -dox or +dox samples. Genes were placed into eight groups based on the difference of the fold-change between -dox and +dox samples, and are indicated as a colored bar to the left of the heatmap. Selected GO terms are shown for those groups that show developmental disruption following RUNX1-EVI1 induction. (C) Venn diagram showing the number of genes that are up- or downregulated in each differentiation stage after induction of RUNX1-EVI1. (D) Quantitative reverse transcriptase polymerase chain reaction expression of *Cdkn1c*, relative to glyceraldehyde 3-phosphate dehydrogenase (*Gapdh*), $n=3$, error bars represent standard error of the mean. (E) Heatmaps showing \log_2 fold change (left) and \log_2 FPKM for selected genes involved in various mesodermal lineages, +/- on the heatmap indicates those which show a fold change in expression of at least 1.5. EMT: epithelial-to-mesenchymal transition.

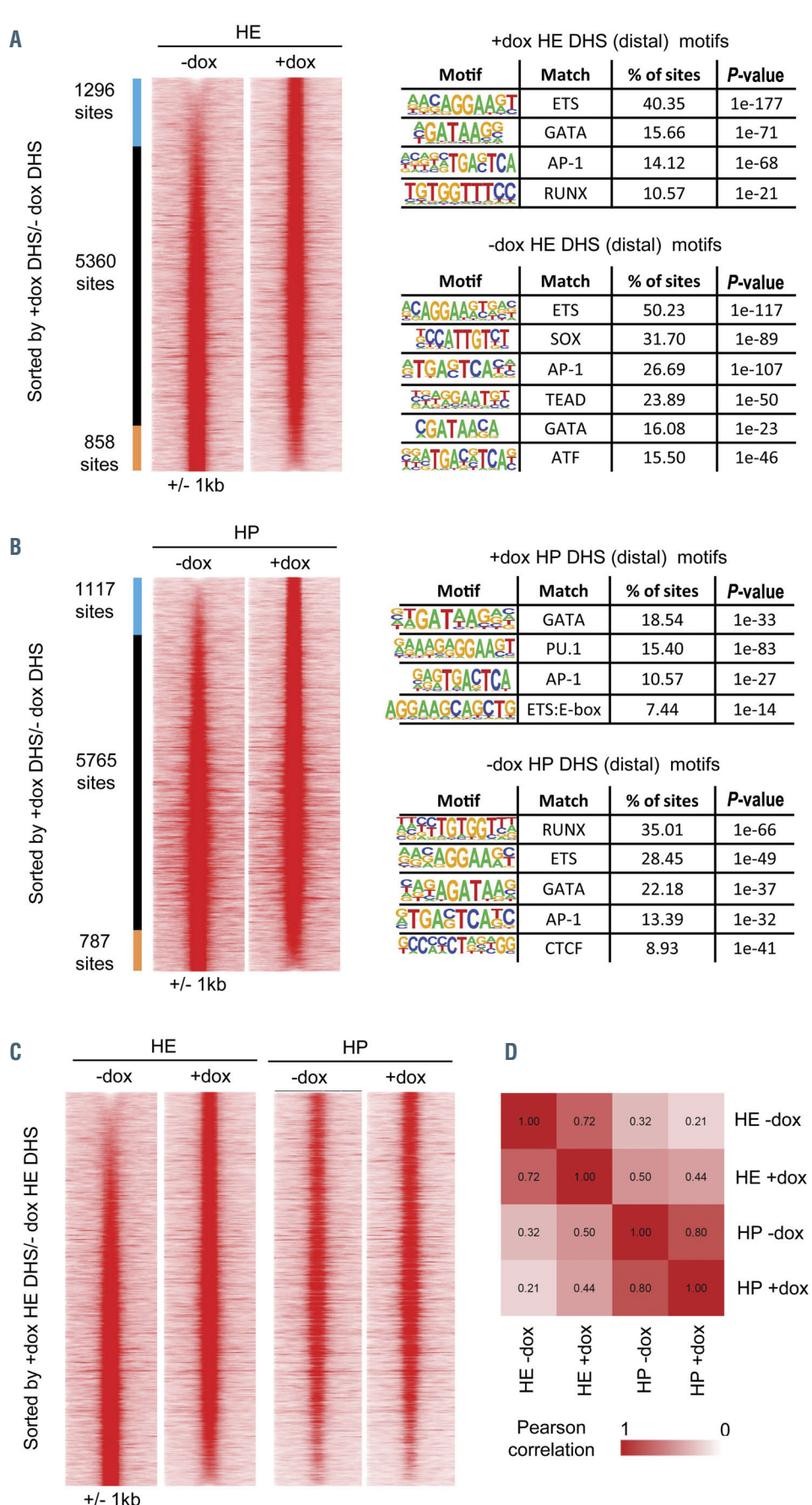


Figure 4. RUNX1-EVI1 induction causes specific changes to chromatin accessibility. Comparison of distal DNasel hypersensitive sites sequencing (DNasel-seq) peaks in (A) hemogenic endothelium (HE) cells (cKit⁺, Tie2⁺, CD41⁺) and (B) hematopoietic progenitor (HP) cells (cKit⁺, Tie2⁺, CD41⁺). Peaks are ordered according to the fold-difference of the normalized tag-count between -dox and plus doxycycline (+dox) treated cells and are presented as a heatmap of the tag-density for each sample. Peaks that are specific to a sample (fold-difference >2) are indicated as colored bars to the left of the density plots, with the number of peaks in each group shown. The results of a *de-novo* motif search conducted within the specific sets of peaks are also shown (C) Comparison of the tag-density profiles of the peaks found in HE cells to the same sites measured in HP cells (D) Heatmap showing the results of hierarchical clustering of the Pearson correlation values of the distal DNasel hypersensitive sites (DHS). The actual Pearson correlation values are shown on the heatmap.

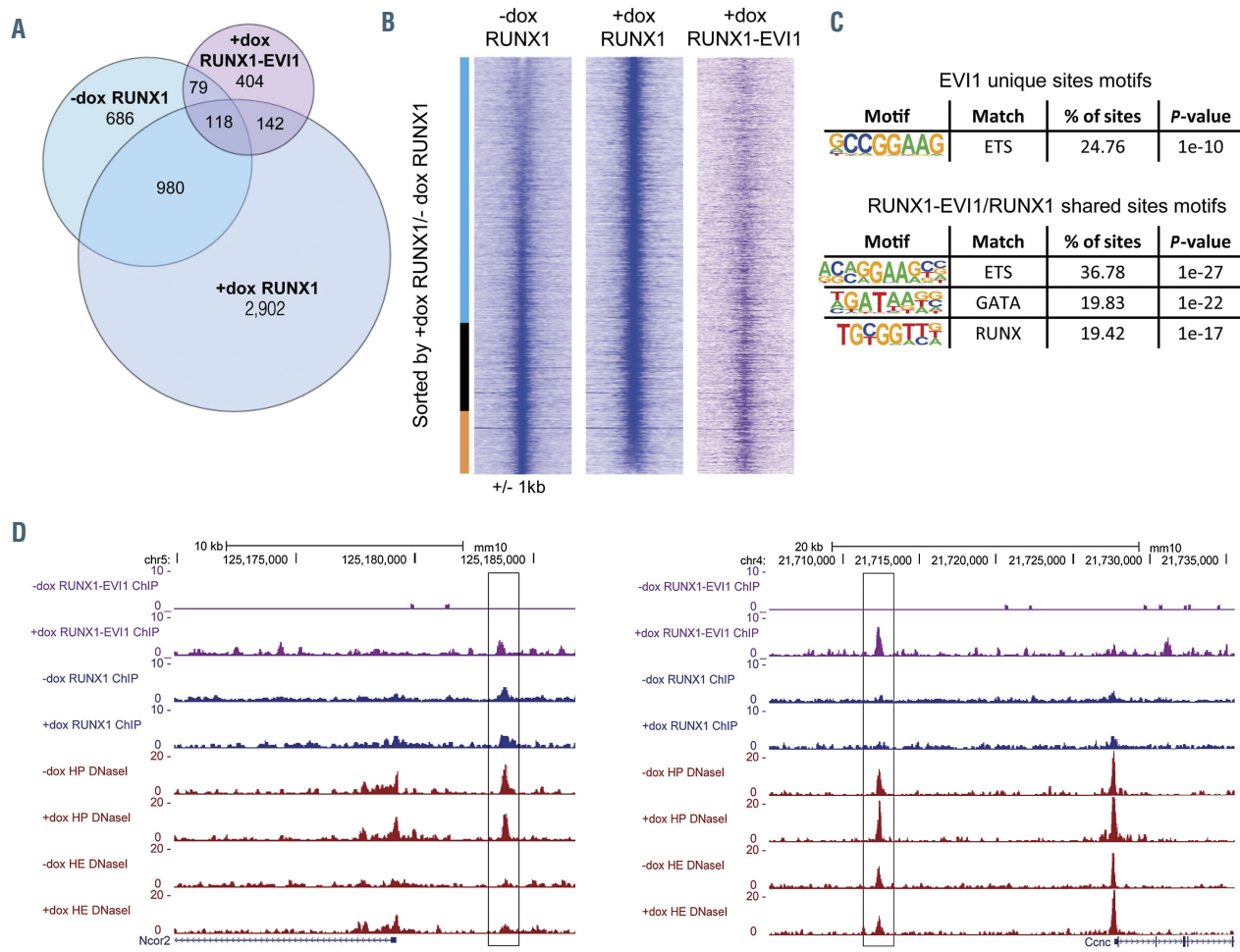


Figure 5. RUNX1-EVI1 disrupts RUNX1 binding but also binds to unique binding sites. (A) Venn diagram showing the number of uniquely called and overlapping RUNX1 and RUNX1-EVI1 chromatin immunoprecipitation sequencing (ChIP-seq) peaks. (B) Comparison of RUNX1 binding in -dox and +dox treated cells, RUNX1 ChIP-seq peaks were ranked according to the fold difference of the normalized plus doxycycline (+dox) / -dox tag count across a 2 kilobase (kb) window. The tag-density of the RUNX1-EVI1 ChIP-seq peaks is plotted alongside. The bar alongside indicates the +dox specific sites (blue), shared sites (black) and -dox specific sites (orange). (C) *De novo* motif enrichment was conducted within the RUNX1-EVI1 ChIP-seq peaks, at both the unique sites and those which were also bound by RUNX1 in either -dox, +dox or both. (D) Genome browser screenshots showing an example site where both RUNX1 and RUNX1-EVI1 bind (left, Ncor2 locus) and where RUNX1-EVI1 binds in the absence of RUNX1 (right, Ccnc locus).

The EHT process is a true cellular transition that is cell cycle independent.²⁶ Whilst we observed a reduction in the proportion of HP related to perturbation of the EHT, we also noted a considerably lower total number of HP than in the control (Figure 2A). This result could be explained by an increase in cells not actively cycling in G0/G1 (48.2% vs. 55.4% without and with RUNX1-EVI1, Figure 2B), specifically by increased numbers of cells in G0 (5.4% with RUNX1-EVI1 compared to <1% without, Figure 2C). We also found a modest increase in apoptotic cells (Online Supplementary Figure S2A).

In order to investigate whether RUNX1-EVI1 expression not only disrupted the EHT, but also affected the ability of progenitor cells to terminally differentiate, we induced RUNX1-EVI1 in newly forming progenitors and placed the progenitors into methylcellulose colony forming unit assays. We first carried out colony-forming unit assays in the absence of dox in the methylcellulose medium. RUNX1-EVI1 protein was quickly lost following the withdrawal of dox (Online Supplementary Figure S2B). Despite RUNX1-EVI1 being absent, we saw an overall reduction in

the number of colonies formed (Figure 2D; *Online Supplementary Figure S2C*) primarily accounted for by a reduction the number of myeloid (-dox 58±13, +dox 42±11 per 5,000 HP seeded) and erythroid colonies (-dox 26±7, +dox 20±4), with a concomitant increase in the proportion of mixed lineage colonies, or those of unclear lineage (-dox 29±9, +dox 26±6, Figure 2E). The colonies which did form were generally smaller with fewer healthy cells (Figure 2F), which may relate to the previously observed increase in apoptosis (Online Supplementary Figure S2A). When RUNX1-EVI1 expression was either induced or maintained in the HP when they were plated into methylcellulose, colony-forming capacity was further reduced (Figure 2D). Importantly, we did not see enhanced myeloid differentiation after RUNX1-EVI1 induction when HP were cultured in liquid or semi-solid medium (Figure 2E; *Online Supplementary Figure S2D*). These data suggest that whilst RUNX1-EVI1 expression affects the differentiation capacity of HP, there was some reversibility of this phenotype and the continued expression of RUNX1-EVI1 caused ongoing changes.

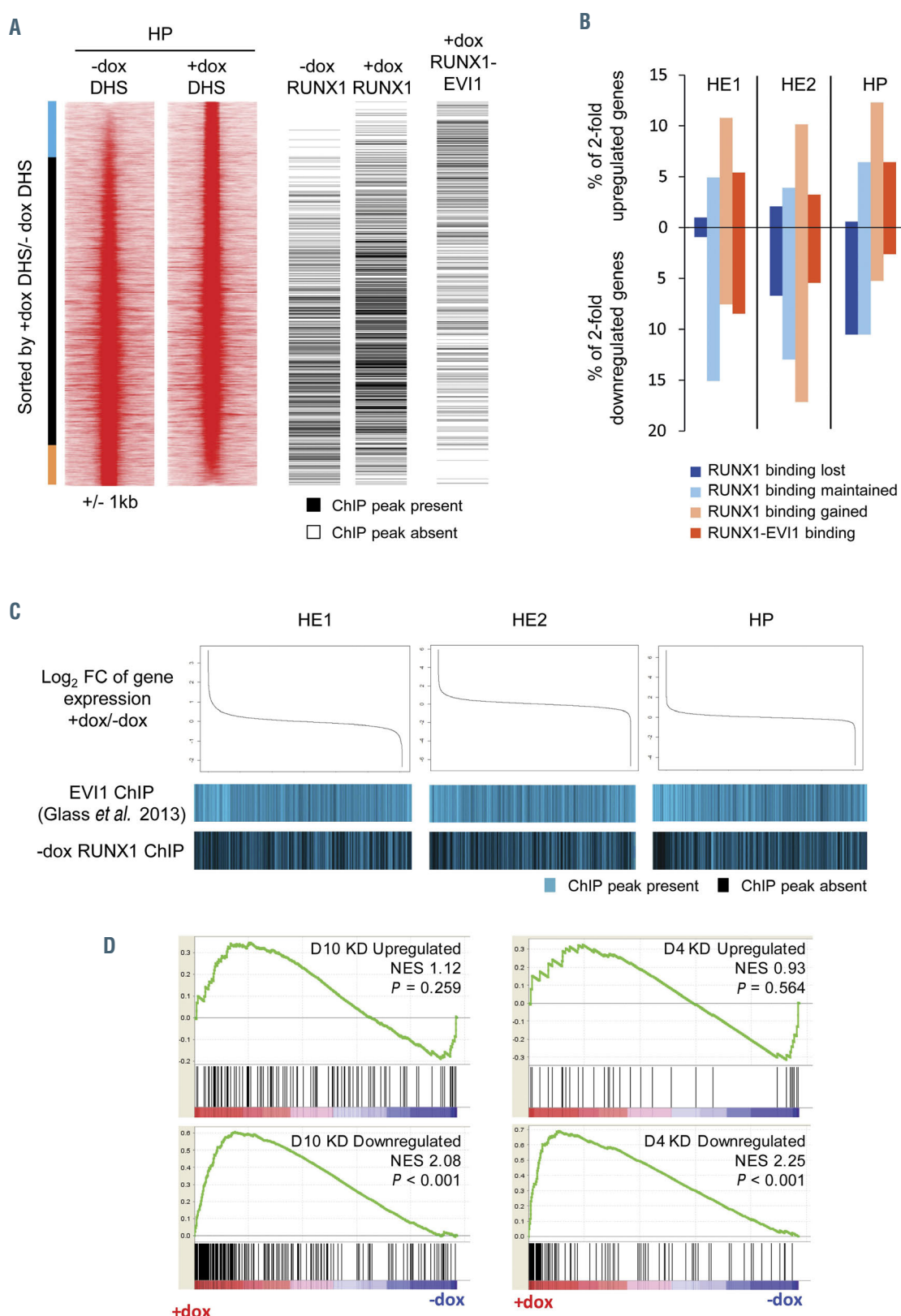


Figure 6. Changes to chromatin organisation and gene expression are modulated by RUNX1 and RUNX1-EVI1 binding. (A) Comparison of RUNX1 and RUNX1-EVI1 binding sites to DNase I hypersensitive sites sequencing (DNaseI-seq) data from hematopoietic progenitor (HE) cells. DNaseI-seq peaks are ranked according to the fold-difference of the plus doxycycline (+dox)/-dox normalized tag-count, with the presence (black) or absence (white) of a chromatin immunoprecipitation sequencing (ChIP-seq) peak indicated alongside. The bar alongside indicates the +dox specific DNaseI sites (blue), shared sites (black) and -dox specific sites (orange). (B) The percentage of 2-fold de-regulated genes at each stage which have an associated RUNX1 or RUNX1-EVI1 binding site. (C) Comparison of changes in gene expression to the binding patterns of wild-type EVI1 and RUNX1. Gene expression was ranked by fold change (top), with the presence or absence of wild-type EVI1²⁷ or RUNX1 binding associated with each gene is indicated below in blue. (D) Gene set enrichment analysis comparing changes in gene expression after RUNX1-EVI1 induction in HP to genes that are up- and downregulated following 4 and 10 days of RUNX1-EVI1 knockdown in the SKH1 cell line.¹⁹ Genes that are upregulated following RUNX1-EVI1 induction correspond closely to genes that are downregulated after RUNX1-EVI1 knock-down in the SKH1 cell line.

Taken together, our data show that RUNX1-EVI1 expression is incompatible with multipotent precursor development, and when induced in precursors, leads to cell cycle arrest and an increase in apoptosis.

RUNX1-EVI1 induction alters gene expression in a differentiation-stage dependent and independent fashion

We next wanted to understand the molecular basis of the observed phenotypes. To this end, we sorted HE1, HE2 and HP cells on the basis of their surface marker phenotypes, as described in Figure 1A and D and performed RNA-seq on the resulting matched cell populations. Biological duplicates were well correlated (*Online Supplementary Figure S3A*) and the average was used for further analysis. Hierarchical clustering of these datasets (Figure 3A) showed that the overall gene expression patterns in the different cell types were preserved in the presence of RUNX1-EVI1, but with genes being de-regulated at every stage, particularly in HE2 cells (*Online Supplementary Figure S3B*, *Supplementary Tables S1 to S3*). A subset of these genes were validated by quantitative reverse transcriptase polymerase chain reaction (qRT-PCR) (*Online Supplementary Figure S3C*) and the HP gene expression changes, being the target cell for the leukemic transformation, were compared to two previously published t(3;21) patient RNA-seq datasets (*Online Supplementary Figure S3D*). This analysis showed that those genes which are specific to t(3;21) patients as compared to healthy CD34+ cells were upregulated following induction of RUNX1-EVI1 in HP, with genes such as *Cdh5*, *Hes1*, *Maff* and *Arhgef12* being overexpressed in both patients and HP expressing RUNX1-EVI1.

The differentiation of blood cells in the *in vitro* differentiation system is not entirely synchronous, therefore RUNX1-EVI1 induction occurs in different cell types representing a differentiation trajectory. Many changes normally seen within the differentiation process were maintained after induction. For example, genes which were up- or downregulated during the transition from HE1 to HE2 or HE2 to HP continued to be up- or downregulated (Figure 3B; *Online Supplementary Tables S4 and S5*), including those essential for these transitions such as *Tek* and *Gfi1b*. However, a subset of genes failed to be up- or downregulated to the extent it normally should. For example, some regulators of the MAPK pathway including *Mapk3* and *Dusp6* were downregulated during the transition from HE2 to HP more than they should be following RUNX1-EVI1 induction. Alongside these developmental changes, a core set of genes were upregulated at least 2-fold in two, or all three cell types (Figures 3C and D), including *Dusp5*, *Cdkn1c* and *Pdgfa*. *Cdkn1c* is a negative regulator of the cell cycle and its universal upregulation may underpin the cell cycle arrest (Figures 2B and C) and the de-regulation of multiple cell cycle associated genes (*Online Supplementary Figure S3E*).

We also examined how stage-specific gene expression changes related to the differentiation program using known marker genes. In HE cells, the expression of the vascular/smooth muscle program was deregulated (Figure 3E). The smooth muscle genes *Acta2*, *Tagln*, *Cnn1* and the genes encoding the cardiac regulator TBX20 and homeobox protein Nkx-2.5 were further downregulated in HE1, but were then upregulated when RUNX1-EVI1 was induced in HE2. When specifically examining hematopoietic

lineage gene signatures, we did not see a downregulation of myeloid or erythroid genes as expected from the colony forming assays. Indeed, we found a widespread, albeit modest (>1.5-fold), increase in expression of genes related to a multipotent progenitor identity with the concomitant expression of a multi-lineage gene expression program consisting of myeloid, lymphoid and megakaryocyte/erythroid genes (Figure 3E; *Online Supplementary Figure S3C*). Taken together, these results suggest that RUNX1-EVI1 induction causes a cell cycle and differentiation arrest that is associated with a disturbance of the balance between the hematopoietic and vascular/smooth muscle fate.

Disturbed lineage specification is caused by chromatin changes associated with altered RUNX1 binding

In order to understand how RUNX1-EVI1 induction reprograms the chromatin landscape, we performed and integrated ChIP-seq analysis for both RUNX1 and RUNX1-EVI1 in HP, with data from DNaseI-seq experiments performed on sorted cKit+ HP, and HE (cKit+, Tie2+, CD41-/+). Induction of RUNX1-EVI1 led to changes to chromatin accessibility in the HE and HP cells and an increased proportion of distal DNaseI hypersensitive sites (DHS) (*Online Supplementary Figure S4A*). Few DHS changed at promoter sites (*Online Supplementary Figure S4B*). We therefore focussed on the analysis of distal DHS and ranked them by the fold change in tag count at each site. 1,296 DHS were gained and 858 lost in the HE when RUNX1-EVI1 was expressed (Figure 4A). The gained sites showed a specific enrichment of RUNX motifs, whilst the sites lost contained SOX, TEAD and AP-1 motifs. In HP cells, RUNX1-EVI1 induction had a completely different effect as here we observed a loss rather than a gain of RUNX motif enrichment (Figure 4B). Taken together, this result suggested a shift in chromatin patterns in HE from those of the vascular/endothelial lineages^{11,22} towards a HP-like pattern. We confirmed this result by plotting the HP DNaseI-seq peaks alongside those of the HE (Figure 4C) and by performing a correlation analysis (Figure 4D). These analyses demonstrated that the HE chromatin pattern was more similar to that of HP cells following induction of RUNX1-EVI1, despite the cells still displaying surface markers and an overall gene expression signature of the HE (Figures 1C and 3A). Furthermore, in HP we also saw a shift from the ETS motif to a PU.1 specific motif, which was consistent with the upregulation of *Spi1* (encoding PU.1) expression, indicating that the chromatin accessibility pattern was being rewired towards myelopoiesis.

In order to test how these results related to the interplay of RUNX1-EVI1 with RUNX1, we compared ChIP-seq for RUNX1 with and without induction of RUNX1-EVI1, to the binding of RUNX1-EVI1 itself in cKit+ HP. The antibody we used against human EVI1 did not recognize the endogenous murine EVI1 and thus exclusively measured binding of the exogenous protein. We analyzed only high-confidence ChIP-seq peaks, which had been filtered for the presence of a DHS at the same site, to minimize noise associated with the technical difficulty of these ChIP experiments.

Around half of RUNX1-EVI1 binding sites overlapped with those of RUNX1 (Figure 5A), including those RUNX1 sites that were either maintained or gained following RUNX1-EVI1 induction. This result suggests that the pre-

dominant mechanism of action of RUNX1-EVI1 is not the displacement of RUNX1. This finding was confirmed by examining the proximity of RUNX1 and RUNX1-EVI1 ChIP peaks (*Online Supplementary Figure S5A*). The RUNX1 and RUNX1-EVI1 peak summits were distributed similarly prior to and following induction of RUNX1-EVI1, both overlapping the same sites and next to each other. More strikingly, induction caused a large movement of RUNX1 within the genome with the loss of over a third of pre-existing RUNX1 sites and considerably more gained RUNX1 sites. Most gained sites were not associated with RUNX1-EVI1 binding (Figure 5B) nor did they have any specific motif enrichment not present in the shared sites (*Online Supplementary Figure S5B*) but were instead found in promoters (*Online Supplementary Figure S5C*). This movement was a real re-distribution as the overall level of RUNX1 protein was unchanged (Figure 1B).

When RUNX1-EVI1 bound in concert with RUNX1, or displaced RUNX1, its binding sites were enriched for RUNX and GATA motifs (Figure 5C and D; *Online Supplementary Figure S5D*), suggesting that RUNX1-EVI1 can also bind via the RUNT homology domain. Unique RUNX1-EVI1 ChIP peaks, however, were enriched for ETS-like motifs (Figure 5C), which may be indicative of binding via the EVI1 portion of the protein²⁷ in the absence of RUNX1, an example of which is shown in Figure 5D and the *Online Supplementary Figure S5D*.

RUNX1-EVI1 disrupts RUNX1 and EVI1 driven gene regulatory networks

We next integrated the RUNX1 and RUNX1-EVI1 ChIP-seq data with the DNaseI-seq and RNA-seq data to investigate how the binding of RUNX1-EVI1 and the movement of RUNX1 influenced changes in gene expression. We observed that the DHS that were lost following induction of RUNX1-EVI1 were associated with lost RUNX1 binding as well. However, RUNX1 moved to chromatin which was already accessible and DHS which were gained were associated with RUNX1-EVI1 binding (Figure 6A; *Online Supplementary Figure S6A*). When considering genes which were at least 2-fold deregulated, those which were downregulated - particularly in HP - were associated with reduced RUNX1 binding (Figure 6B), indicating that RUNX1-EVI1 induction interfered with gene activation by RUNX1. The proportion of changed genes associated with lost RUNX1 binding increased throughout differentiation, as the reliance on RUNX1 increased. Both up- and downregulated genes at all stages were associated with new RUNX1 binding sites, again matching the trend in chromatin accessibility. RUNX1-EVI1 bound de-regulated genes were predominantly upregulated in HP cells, but more were downregulated in HE cells. We therefore compared how the gene expression changes related to endogenous EVI1 and RUNX1 binding sites, by plotting which genes were associated with EVI1 binding from a public EVI1 ChIP dataset,²⁷ and the genes associated with our RUNX1 ChIP in uninduced HP against gene expression changes following RUNX1-EVI1 (Figure 6C; *Online Supplementary Figure S6B*). Genes which changed expression, were either upregulated or downregulated, were enriched for EVI1 binding and depleted for RUNX1 binding, particularly in the HP. Therefore, neither RUNX1 nor EVI1 is solely associated with up- or downregulation of their target genes but instead we see a complex and stage-specific pattern of interference.

Finally, to examine which changes were a direct response to binding and which were a result of the cells' changing identity, we employed gene set enrichment analysis comparing the genes upregulated in HP following induction of RUNX1-EVI1 to those downregulated following small interfering RNA knockdown of RUNX1-EVI1 in a human cell line¹⁹ (Figure 6D) and observed a good correlation. These genes include hematopoietic genes (*Online Supplementary Table S6*) such as *Gata2* (a RUNX1 target) and *Meis1* (a target of both RUNX1 and RUNX1-EVI1). By contrast, the genes downregulated following RUNX1-EVI1 induction in HP did not correlate well with those upregulated following RUNX1-EVI1 knockdown with the exception of a small subset of genes such as *Mpo* and *Rab44* which are neither RUNX1 nor RUNX1-EVI1 targets.

These results suggest that RUNX1-EVI1 is likely to interfere with the repressive activities of both RUNX1 and EVI1 with the balance of lineage decisions depending on the differentiation stage at the time point of induction.

Discussion

RUNX1-EVI1 expression is only found as a secondary event in myeloid malignancies. Our study shows that its expression as sole oncogene in untransformed myeloid progenitor cells is incompatible with blood cell differentiation. We also found that RUNX1-EVI1 induction disrupts the RUNX1 driven endothelial-hematopoietic transition, in a similar fashion to RUNX1-ETO.²⁸ Expression of RUNX1-EVI1 HP cells disrupted their colony forming capacity and led to extensive de-regulation of gene expression. However, the underlying molecular cause was different. As with RUNX1-ETO, genes of the stem cell program were upregulated, but the arrest in differentiation after RUNX1-EVI1 induction was associated with the rapid activation of a multi-lineage gene expression program and a profound disturbance of hematopoietic lineage specification.

Induction of RUNX1-EVI1 in cells committed to the hematopoietic fate is associated with the activation of a pan-lineage hematopoietic gene expression program and a failure in fully downregulating factors associated with a vascular gene expression program. This behavior is reminiscent of mutations in lineage commitment factors, such as PAX5. Knock-out of PAX5 leads to a block in B-cell differentiation which is associated with an inability to activate the B-cell gene expression program, but also an inability to repress the myeloid program,^{29,30} generating progenitors with a multi-lineage gene expression pattern and the inability to commit to a specific lineage. Alongside the differentiation associated phenotype, we found that RUNX1-EVI1 caused a partial cell cycle arrest and increase in apoptosis which is likely to be associated with increased expression of *Cdkn1c*, leading to the stage-specific deregulation of cell cycle genes. *Cdkn1c* encodes the cell cycle inhibitor p57^{Kip2} which is important in maintenance of the adult hematopoietic stem cell compartment,³¹ and has been shown to be deregulated by both EVI1 and MDS-EVI1 thus causing cell cycle mis-regulation.^{13,32}

Our results indicate that the phenotype caused by RUNX1-EVI1 induction is a result of interference with both RUNX1 and EVI1 driven gene regulatory networks. Similar to PAX5, both RUNX1 and EVI1 interact with co-

activators and co-repressors to affect gene expression, depending on the genomic context.^{9,33-35} In accordance with this notion, we did not find RUNX1-EVI1 behaving solely as a repressor or activator of gene expression, with further variation based on the differentiation stage. In early HE, when *Mecom* expression reaches its peak, we observed a bias towards repression of RUNX1-EVI1 target genes and an activation of the hematopoietic program, indicating that the fusion protein interfered with both the repressive and activating function of EVI1. Conversely, we found a bias towards gene activation in HP for multiple programs where *Runx1* expression was upregulated. This result suggests that RUNX1-EVI1 interfered with the repressive activity of RUNX1 which is known to co-operate with other factors to shut down the endothelial gene expression program.^{36,37} This idea is further supported by our finding that downregulated gene expression in HP can largely be accounted for by lost RUNX1 binding. In contrast, upregulated gene expression is independent of new RUNX1 binding and is therefore likely caused by other transcription factors. These may include PU.1, which is a known mediator of EVI1 function in myeloid malignancy^{38,39} and which was precociously upregulated following induction of RUNX1-EVI1. PU.1 is a master myeloid regulator which co-operates with RUNX1 in normal hematopoiesis,^{40,41} and also has roles in cell cycle regulation in stem cells.⁴² Alongside gene expression being upregulated, open chromatin sites gained in HP were enriched for PU.1 motifs and PU.1 target genes such as *Csf1r*⁴³ were upregulated.

In conclusion, we found that RUNX1-EVI1 disrupts the

function of the endogenous RUNX1 and EVI1 in a developmental program specific fashion leading to loss of cell cycle control and an inability of hematopoietic precursor cells to execute and maintain regulated cell fate commitment decisions. Our results explain why RUNX1-EVI1 is associated with particularly poor prognosis. It adds to a growing number of oncogenes that as sole drivers are incompatible with hematopoietic stem cell function.⁴⁴ Our results also highlight the fact that whilst targeting transcription factors such as RUNX1 is a therapy currently being developed,⁴⁵ cross-talk between multiple transcription networks in the presence of several mutated or mis-expressed transcription factors must also be considered.

Disclosures

No conflicts of interest to disclose.

Contributions

SK performed experiments and data analysis and wrote the paper; PK performed data analysis; EK performed experiments and CB conceived the study and wrote the paper.

Acknowledgments

The authors would like to thank the Genomics Birmingham Sequencing Facility for their expert sequencing service, and the University of Birmingham Flow Cytometry service and Dr Mary Clarke for expert cell sorting.

Funding

SGK received funding from Kay Kendall Leukemia Fund and PK received funding from Bloodwise, awarded to CB.

References

1. Wiemels JL, Xiao Z, Buffler PA, et al. In utero origin of t(8;21) AML1-ETO translocations in childhood acute myeloid leukemia. *Blood*. 2002;99(10):3801-3805.
2. Rubin CM, Larson RA, Anastasi J, et al. t(3;21)(q26;q22): A recurring chromosomal abnormality in therapy-related myelodysplastic syndrome and acute myeloid leukemia. *Blood*. 1990;76(12):2594-2598.
3. Lugthart S, Gröschel S, Beverloo HB, et al. Clinical, molecular, and prognostic significance of WHO type inv(3)(q21q26.2)/t(3;3) (q21;q26.2) and various other 3q abnormalities in acute myeloid leukemia. *J Clin Oncol*. 2010;28(24):3890-3898.
4. Nukina A, Kagoya Y, Watanabe-Okochi N, et al. Single-cell gene expression analysis reveals clonal architecture of blast-phase chronic myeloid leukaemia. *Br J Haematol*. 2014;165(3):414-416.
5. Assi SA, Imperato MR, Coleman DJL, et al. Subtype-specific regulatory network rewiring in acute myeloid leukemia. *Nat Genet*. 2019;51(1):151-162.
6. Lancrin C, Sroczynska P, Stephenson C, Allen T, Kouskoff V, Lacaud G. The haemangioblast generates haematopoietic cells through a haemogenic endothelium stage. *Nature*. 2009;457(7231):892-895.
7. Sood R, Kamikubo Y, Liu P. Role of RUNX1 in hematological malignancies. *Blood*. 2017;129(15):2070-2082.
8. Papaemmanuil E, Gerstung M, Bullinger L, et al. Genomic classification and prognosis in acute myeloid leukemia. *N Engl J Med*. 2016;374(23):2209-2221.
9. Soderholm J, Kobayashi H, Mathieu C, Rowley JD, Nucifora G. The leukemia-associated gene MDS1/EVI1 is a new type of GATA-binding transactivator. *Leukemia*. 1997;11(3):352-358.
10. Kataoka K, Sato T, Yoshimi A, et al. *Evi1* is essential for hematopoietic stem cell self-renewal, and its expression marks hematopoietic cells with long-term multilineage repopulating activity. *J Exp Med*. 2011;208(12):2403-2416.
11. Goode Debbie K, Obier N, Vijayabaskar MS, et al. Dynamic gene regulatory networks drive hematopoietic specification and differentiation. *Dev Cell*. 2016;36(5):572-587.
12. Glass C, Wilson M, Gonzalez R, Zhang Y, Perkins AS. The role of EVI1 in myeloid malignancies. *Blood Cells Mol Dis*. 2014;53(1):67-76.
13. Kustikova OS, Schwarzer A, Stahlhut M, et al. Activation of *Evi1* inhibits cell cycle progression and differentiation of hematopoietic progenitor cells. *Leukemia*. 2012;27(5):1127-1138.
14. Kilbey A, Stephens V, Bartholomew C. Loss of cell cycle control by deregulation of cyclin-dependent kinase 2 kinase activity in *Evi-1* transformed fibroblasts. *Cell Growth Differ*. 1999;10(9):601-610.
15. Friedman AD. Cell cycle and developmental control of hematopoiesis by *Runx1*. *J Cell Physiol*. 2009;219(3):520-524.
16. Maki K, Yamagata T, Yamazaki I, Oda H, Mitani K. Development of megakaryoblastic leukaemia in *Runx1-Evi1* knock-in chimaeric mouse. *Leukemia*. 2006;20(8):1458-1460.
17. Cuenco GM, Nucifora G, Ren R. Human AML1/MDS1/EVI1 fusion protein induces an acute myelogenous leukemia (AML) in mice: A model for human AML. *Proc Natl Acad Sci U S A*. 2000;97(4):1760-1765.
18. Maki K, Yamagata T, Asai T, et al. Dysplastic definitive hematopoiesis in *AML1/EVI1* knock-in embryos. *Blood*. 2005;106(6):2147-2155.
19. Loke J, Assi SA, Imperato MR, et al. RUNX1-ETO and RUNX1-EVI1 differentially reprogram the chromatin landscape in t(8;21) and t(3;21) AML. *Cell Rep*. 2017;19(8):1654-1668.
20. Tanaka T, Mitani K, Kurokawa M, et al. Dual functions of the *AML1/Evi-1* chimeric protein in the mechanism of leukemogenesis in t(3;21) leukemias. *Mol Cell Biol*. 1995;15(5):2383-2392.
21. Bert AG, Johnson BV, Baxter EW, Cockerill PN. A modular enhancer is differentially regulated by GATA and NFAT elements that direct different tissue-specific patterns of nucleosome positioning and inducible chromatin remodeling. *Mol Cell Biol*. 2007;27(8):2870-2885.
22. Obier N, Cauchy P, Assi SA, et al. Cooperative binding of AP-1 and TEAD4 modulates the balance between vascular smooth muscle and hemogenic cell fate. *Development*. 2016;143(23):4324-4340.
23. Mitani K, Ogawa S, Tanaka T, et al. Generation of the *AML1-EVI-1* fusion gene in the t(3;21)(q26;q22) causes blastic crisis in chronic myelocytic leukemia. *EMBO J*. 1994;13(3):504-510.
24. Sroczynska P, Lancrin C, Pearson S, Kouskoff V, Lacaud G. In vitro differentiation of embryonic stem cells as a model of early hematopoietic development. In: C.W. ES, ed. *Leukemia. Methods in Molecular Biology™ (Methods and Protocols)*. Humana Press. 2009.
25. Chen MJ, Yokomizo T, Zeigler BM,

Dzierzak E, Speck NA. Runx1 is required for the endothelial to haematopoietic cell transition but not thereafter. *Nature*. 2009;457(7231):887-891.

26. Eilken HM, Nishikawa S-I, Schroeder T. Continuous single-cell imaging of blood generation from haemogenic endothelium. *Nature*. 2009;457(7231):896-900.

27. Glass C, Wuertzer C, Cui X, *et al*. Global identification of EVI1 target genes in acute myeloid leukemia. *PLoS One*. 2013;8(6):e67134.

28. Regha K, Assi SA, Tsoulaki O, Gilmour J, Lacaud G, Bonifer C. Developmental-stage-dependent transcriptional response to leukaemic oncogene expression. *Nat Commun*. 2015;6(1):7203.

29. Nutt SL, Heavey B, Rolink AG, Busslinger M. Commitment to the B-lymphoid lineage depends on the transcription factor Pax5. *Nature*. 1999;401(6753):556-562.

30. Delogu A, Schebesta A, Sun Q, Aschenbrenner K, Perlot T, Busslinger M. Gene repression by Pax5 in B cells is essential for blood cell homeostasis and is reversed in plasma cells. *Immunity*. 2006;24(3):269-281.

31. Matsumoto A, Takeishi S, Kanie T, *et al*. p57 is required for quiescence and maintenance of adult hematopoietic stem cells. *Cell Stem Cell*. 2011;9(3):262-271.

32. Zhang Y, Stehling-Sun S, Lezon-Geyda K, *et al*. PR-domain-containing Mds1-Evi1 is critical for long-term hematopoietic stem cell function. *Blood*. 2011;118(14):3853-3861.

33. Durst KL, Hiebert SW. Role of RUNX family members in transcriptional repression and gene silencing. *Oncogene*. 2004;23(24):4220-4224.

34. Petrovick MS, Hiebert SW, Friedman AD, Hetherington CJ, Tenen DG, Zhang DE. Multiple functional domains of AML1: PU.1 and C/EBP alpha synergize with different regions of AML1. *Mol Cell Biol*. 1998;18(7):3915-3925.

35. Palmer S, Brouillet J-P, Kilbey A, *et al*. Evi-1 Transforming and repressor activities are mediated by CtBP co-repressor proteins. *J Biol Chem*. 2001;276(28):25834-25840.

36. Thambyrajah R, Mazan M, Patel R, *et al*. GFI1 proteins orchestrate the emergence of haematopoietic stem cells through recruitment of LSD1. *Nat Cell Biol*. 2016;18(1):21-32.

37. Lanclin C, Mazan M, Stefanska M, *et al*. GFI1 and GFI1B control the loss of endothelial identity of hemogenic endothelium during hematopoietic commitment. *Blood*. 2012;120(2):314-322.

38. Ayoub E, Wilson MP, McGrath KE, *et al*. EVI1 overexpression reprograms hematopoiesis via upregulation of Spi1 transcription. *Nat Commun*. 2018;9(1): 4239.

39. Laricchia-Robbio L, Premanand K, Rinaldi CR, Nucifora G. EVI1 impairs myelopoiesis by deregulation of PU.1 function. *Cancer Res*. 2009;69(4):1633-1642.

40. Huang G, Zhang P, Hirai H, *et al*. PU.1 is a major downstream target of AML1 (RUNX1) in adult mouse hematopoiesis. *Nat Genet*. 2008;40(1):51-60.

41. Hu Z, Gu X, Baroidan K, *et al*. RUNX1 regulates corepressor interactions of PU.1. *Blood*. 2011;117(24):6498-6508.

42. Staber Philipp B, Zhang P, Ye M, *et al*. Sustained PU.1 levels balance cell-cycle regulators to prevent exhaustion of adult hematopoietic stem cells. *Mol Cell*. 2013;49(5):934-946.

43. Aikawa Y, Katsumoto T, Zhang P, *et al*. PU.1-mediated upregulation of CSF1R is crucial for leukemia stem cell potential induced by MOZ-TIF2. *Nat Med*. 2010;16(5):580-585.

44. Di Genua C, Norfo R, Rodriguez-Meira A, *et al*. Cell-intrinsic depletion of Aml1-ETO-expressing pre-leukemic hematopoietic stem cells by K-Ras activating mutation. *Haematologica*. 2019;104(11):2215-2224.

45. Bushweller JH. Targeting transcription factors in cancer — from undruggable to reality. *Nat Rev Cancer*. 2019;19(11):611-624.

A frequent nonsense mutation in exon 1 across certain HLA-A and HLA-B alleles in leukocytes of patients with acquired aplastic anemia



Ferrata Storti Foundation

Hiroki Mizumaki,¹ Kazuyoshi Hosomichi,² Kohei Hosokawa,¹ Takeshi Yoroidaka,¹ Tatsuya Imai,¹ Yoshitaka Zaimoku,¹ Takamasa Katagiri,³ Mai Anh Thi Nguyen,¹ Dung Cao Tran,¹ Mahmoud Ibrahim Yousef Elbadry,^{1,4} Kazuhisa Chonabayashi,⁵ Yoshinori Yoshida,⁵ Hiroyuki Takamatsu,¹ Tatsuhiko Ozawa,⁶ Fumihiro Azuma,⁷ Hiroyuki Kishi,⁶ Yoichi Fujii,⁸ Seishi Ogawa,^{8,9} Atsushi Tajima² and Shinji Nakao¹

¹Department of Hematology, Kanazawa University, Kanazawa, Japan; ²Department of Bioinformatics and Genomics, Graduate School of Advanced Preventive Medical Sciences, Kanazawa University, Kanazawa, Japan; ³Clinical Laboratory Sciences, Kanazawa University Graduate School, Kanazawa, Japan; ⁴Department of Internal Medicine, Division of Hematology, Faculty of Medicine, Sohag University, Sohag, Egypt; ⁵Center for iPS Cell Research and Application, Kyoto University, Kyoto, Japan; ⁶Department of Immunology, University of Toyama, Toyama, Japan; ⁷HLA Laboratory, Japanese Red Cross Kanto-Koshinetsu Block Blood Center, Kotoku, Japan; ⁸Department of Pathology and Tumor Biology, Graduate School of Medicine, Kyoto University, Kyoto, Japan and ⁹Department of Medicine, Center for Hematology and Regenerative Medicine (HERM), Karolinska Institute, Stockholm, Sweden

Haematologica 2021
Volume 106(6):1581-1590

ABSTRACT

Leukocytes that lack expression of HLA alleles are frequently detected in patients with acquired aplastic anemia (AA) who respond to immunosuppressive therapy, although the exact mechanisms underlying the HLA loss and HLA allele repertoire likely to acquire loss-of-function mutations are unknown. We identified a common nonsense mutation at codon 19 (c.19C>T, p.R7X) in exon 1 (*Exon1^{mut}*) of different HLA-A and -B alleles in HLA-lacking granulocytes from AA patients. A droplet digital polymerase chain reaction assay capable of detecting as few as 0.07% *Exon1^{mut}* HLA alleles in total DNA revealed that the mutation was present in 29% (101/353) of AA patients, with a median allele frequency of 0.42% (range, 0.071% to 21.3%). *Exon1^{mut}* occurred in only 12 different HLA-A (n=4) and HLA-B (n=8) alleles, including *B*40:02* (n=31) and *A*02:06* (n=15), which correspond to four HLA class I supertypes (A02, A03, B07, and B44). The percentages of patients who possessed at least one of these 12 HLA alleles were significantly higher in the 353 AA patients (92%, *P*<0.001) and in 83 AA patients with copy number neutral loss of heterozygosity in chromosome 6p (100%, *P*<0.001) than the percentage (81%) in 18,604 Japanese healthy individuals. Eighty-two percent (37/45) of AA patients with *Exon1^{mut}* responded to immunosuppressive therapy. Small populations of leukocytes that lack particular HLA-A or B alleles due to *Exon1^{mut}* are common in AA patients. The detection of *Exon1^{mut}* using a droplet digital polymerase chain reaction assay without the need for HLA typing may serve as a powerful tool for diagnosing the immune pathophysiology of patients with bone marrow failure.

Correspondence:

SHINJI NAKAO
snakao8205@staff.kanazawa-u.ac.jp

Received: February 16, 2020.

Accepted: May 14, 2020.

Pre-published: May 21, 2020.

<https://doi.org/10.3324/haematol.2020.247809>

©2021 Ferrata Storti Foundation

Material published in *Haematologica* is covered by copyright. All rights are reserved to the Ferrata Storti Foundation. Use of published material is allowed under the following terms and conditions:

<https://creativecommons.org/licenses/by-nc/4.0/legalcode>. Copies of published material are allowed for personal or internal use. Sharing published material for non-commercial purposes is subject to the following conditions: <https://creativecommons.org/licenses/by-nc/4.0/legalcode>, sect. 3. Reproducing and sharing published material for commercial purposes is not allowed without permission in writing from the publisher.



Introduction

Acquired aplastic anemia (AA) is a rare condition characterized by pancytopenia and bone marrow hypoplasia resulting from immune-mediated suppression of hematopoietic stem progenitor cells (HSPC).¹ Among several different immune mechanisms, cytotoxic T lymphocytes that recognize auto-antigens presented by HSPC are thought to play a critical role in the development of AA,²⁻⁷ based on the finding that leukocytes that lack particular HLA-A or HLA-B alleles (HLA-allele

lacking leukocytes: HLA-LL) are often detected in the peripheral blood of AA patients.^{8,9} The presence of HLA-LL represents compelling evidence to support the involvement of cytotoxic T lymphocytes specific to HSPC in the development of bone marrow failure, and the detection of these leukocytes would be useful for diagnosing immune pathophysiology in patients with AA and other types of bone marrow failure, including low-risk myelodysplastic syndrome. However, assays for detecting HLA-LL, such as flow cytometry using monoclonal antibodies specific to HLA-A or HLA-B alleles and single nucleotide polymorphism (SNP) arrays, have not been popularized because of the need for HLA typing and low frequencies of copy number neutral loss of heterozygosity of the short arm of chromosome 6 (6pLOH).^{10,11}

6pLOH was considered the most common way for HSPC to lose HLA alleles.¹⁰⁻¹⁵ We recently reported that, using targeted deep sequencing with a next-generation sequencer, somatic loss-of-function mutations of *HLA-B*40:02* were frequently detected in granulocytes of AA patients possessing *HLA-B*40:02*. These results strongly suggested that antigen presentation by HSPC via HLA-B4002 plays a critical role in the pathogenesis of AA.⁹ Loss-of-function mutations in HLA class I alleles other than *HLA-B*40:02* were also detected in patients with AA. Babushok *et al.* identified mutations in several HLA class I alleles in leukocytes of AA patients, including *HLA-A*33:03*, *A*68:01* and *HLA-B*14:02*.¹⁴ We recently analyzed leukocytes of AA patients with 6pLOH and detected somatic loss-of-function mutations in *HLA-A*02:06* and *B*54:01*.^{16,17} However, HLA class I alleles responsible for autoantigen presentation in AA patients without *HLA-B*40:02*, who account for approximately 80% of all AA patients, are largely unknown due to the limited number of AA patients who have been studied for loss-of-function mutations in HLA class I alleles.

To identify HLA class I alleles other than *HLA-B*40:02* that are involved in the autoantigen presentation of AA, we performed targeted next-generation sequencing in AA patients with HLA-LL who had HLA class I alleles other than *HLA-B*40:02*. During the course of the mutation analysis, we identified a nonsense mutation at codon 19 (c.19C>T, p.R7X) in exon 1 (*Exon1^{mut}*) of some HLA-A or HLA-B alleles. Surprisingly, *Exon1^{mut}* was shared by different HLA-A or HLA-B alleles and was prevalent in AA patients although their variant allelic frequencies (VAF) were very low. A sensitive assay that can detect *Exon1^{mut}* could help to identify HLA-A or HLA-B alleles that are responsible for autoantigen presentation and provide insight into the immune pathophysiology of bone marrow failure.

Against this backdrop, we developed a highly sensitive droplet digital PCR (ddPCR) assay for detecting *Exon1^{mut}*, and determined the prevalence of *Exon1^{mut}* and HLA alleles likely to acquire this mutation in AA patients.

Methods

Detailed information on the materials and methods are provided in the *Online Supplementary Data*.

Patients

Twenty Japanese AA patients with HLA-LL who did not have an *HLA-B*40:02* allele were analyzed for the presence of loss-of-function mutations in HLA alleles. We studied a total of 353

Table 1. Baseline characteristics of the patients with aplastic anemia.

Characteristics	N. of patients
Total	353
Age in years, median (range)	63 (11-93)
Sex, male/female	167/186
Severity	
Non-severe AA	202
Severe/very severe AA	151
Patients with increased GPI ⁻ granulocytes, n (%)	245 (69.4)
None (<0.003%)	108
0.003-1.0%	177
>1.0%	68
IST prior to sampling, n (%)	61 (17.2)
CsA±TPO-RA	31
rATG+CsA±TPO-RA	30

GPI: glycosylphosphatidylinositol-anchored proteins deficient; AA: aplastic anemia; IST: immunosuppressive therapy; CsA: cyclosporine; TPO-RA: thrombopoietin receptor agonist; ATG: antithymocyte globulin.

Japanese AA patients, including the 20 patients who were further analyzed for the prevalence and clinical significance of *Exon1^{mut}* in AA between 2010 and 2018 (Table 1). A schematic of the experiments is provided in *Online Supplementary Figure S1*. All patients were genotyped for HLA-A, HLA-B, HLA-C, and HLA-DRB1 alleles using the PCR sequence-specific oligonucleotide method. All patients provided consent to participation in this study, which was conducted in accordance with the Declaration of Helsinki and approved by the ethics committee of the Kanazawa University Institute of Medical, Pharmaceutical, and Health Sciences.

Detection of glycosylphosphatidylinositol-deficient cells and cells with 6p loss of heterozygosity

Glycosylphosphatidylinositol-anchored protein-deficient (GPI) cells were detected using high sensitivity flow cytometry, as previously described.¹⁸ 6pLOH was assessed using a SNP array-based method with GeneChip 500K arrays (Affymetrix, Japan) or a ddPCR assay with a QX200 AutoDG Droplet Digital PCR System (Bio-Rad, CA, USA), as previously described.^{9,10}

Deep sequencing of HLA class I genes

From peripheral blood samples of the 20 patients with HLA-LL, which were stained with anti-HLA-allele-specific and lineage-specific monoclonal antibodies, paired fractions of granulocytes and CD3⁺ T cells were sorted and were subjected to DNA extraction (*Online Supplementary Figure S2*). The monoclonal antibodies used in this study are summarized in *Online Supplementary Table S1*. Nucleotide sequences of HLA-A and HLA-B genes in sorted granulocytes of patients with HLA-LL were determined using a next-generation sequencer (Miseq; Illumina, CA, USA).

Digital droplet polymerase chain reaction assay for detecting *Exon1^{mut}*

We developed a sensitive ddPCR assay for precise detection of *Exon1^{mut}* in the peripheral blood of AA patients using the QX200 ddPCR system. Briefly, we designed two different sets of primer pairs complementary to the consensus sequences of HLA-A and HLA-B alleles, and locked nucleic acid-based probes complementary to wild-type and mutant-specific sequences (*Online Supplementary Table S2*). Detailed protocols for ddPCR are provided in the *Online Supplementary Methods*.

Determination of HLA alleles that acquired *Exon1^{mut}*

HLA alleles that acquired *Exon1^{mut}* were determined by deep sequencing with the next-generation sequencer, or deduced from

alleles contained in the lost haplotype due to 6pLOH that was accompanied by *Exon1^{mut}* (Online Supplementary Figure S3). The low VAF of *Exon1^{mut}* (VAF <1%) was confirmed by deep sequencing with unique molecular identifiers (xGen® Dual Index UMI Adapters: Integrated DNA Technologies, IA, USA).¹⁹ The correlation between *Exon1^{mut}* VAF determined by deep sequencing with unique molecular identifiers and those determined by the ddPCR assay was examined using 24 different samples (Online Supplementary Figure S4). HLA class I alleles acquiring *Exon1^{mut}* were determined using the nearest allele-specific SNP. Details on deep

sequencing with unique molecular identifiers are provided in the Online Supplementary Methods.

Statistical analysis

Comparisons were performed using the Fisher exact test for categorical variables and Mann-Whitney U test for continuous variables with a two-tailed significance level of 0.05. Statistical analyses were performed using the EZR software program.²⁰ Graphs were generated using GraphPad PRISM7.0 (GraphPad Software Inc, CA, USA).

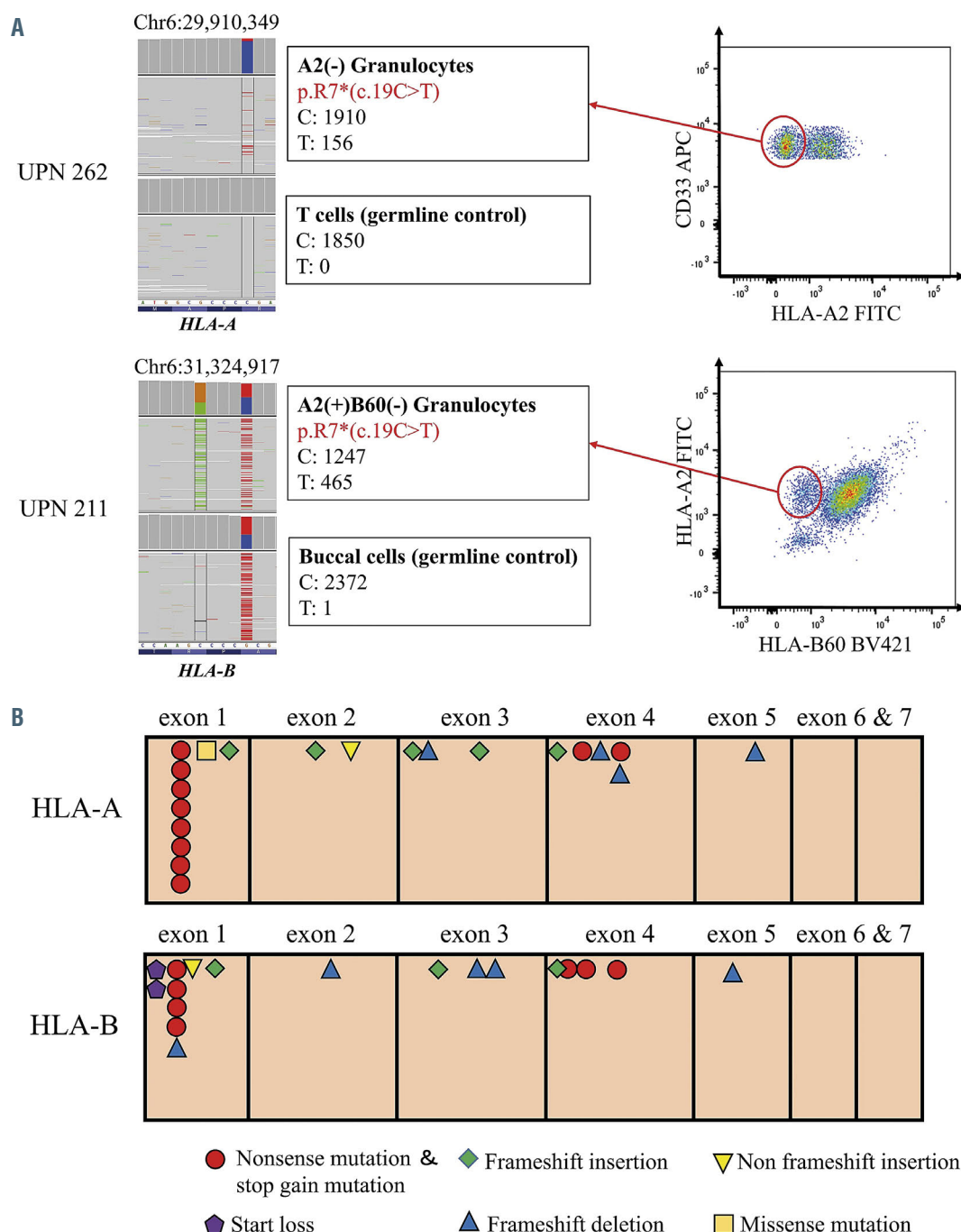


Figure 1. Identification of *Exon1^{mut}* in patients with aplastic anemia. (A) *Exon1^{mut}* [p.R7*(c.19C>T)] was detected by targeted deep sequencing of sorted HLA-A2- granulocytes (UPN 262) and HLA-A2+B60- granulocytes (UPN 211) in two patients with aplastic anemia. Sequencing results of sorted HLA-allele lacking leukocytes from these two patients and germline controls and flow cytometry results of granulocytes are shown. (B) Loss-of-function mutations detected in 14 patients by targeted deep sequencing. *Exon1^{mut}* was detected in HLA-A alleles of eight patients and HLA-B alleles of four patients. UPN: unique patient number.

Results

Identification of *Exon1^{mut}* in different HLA-A and HLA-B alleles in HLA-lacking leukocytes from patients with aplastic anemia

To identify HLA class I alleles other than *HLA-B*40:02* that are critically involved in autoantigen presentation in AA, we sequenced HLA-A and HLA-B alleles of sorted granulocytes from 20 patients with HLA-LL not possessing *HLA-B*40:02*. The clinical characteristics of these 20 patients are shown in *Online Supplementary Table S3*. HLA-A⁻ granulocytes or HLA-A⁺B⁻ granulocytes, accounting for 2.4–99.8% of all granulocytes, were detected in these patients (*Online Supplementary Figure S5*, *Online Supplementary Table S3*). Median read depths of the HLA-A and HLA-B alleles were 925 and 1,012 for targeted deep sequencing and 43,013 and 35,267 for amplicon sequencing, respectively. Of the 20 AA patients assessed, six had 6pLOH alone, ten had various loss-of-function mutations in addition to 6pLOH, and four had only somatic loss-of-function mutations in HLA-A. Three (UPN 210, 335, and 348) of the 14 patients with loss-of-function mutations had the mutations in HLA-B of sorted HLA-A⁺ granulo-

cytes. Of note, 12 of 14 patients with loss-of-function mutations had *Exon1^{mut}* in HLA-A (*A*02:06*, $n=7$; *A*31:01*, $n=1$) and HLA-B (*B*13:01*, $n=1$; *B*40:01*, $n=2$; and *B*54:01*, $n=1$). The other two patients (UPN 335 and UPN 210) had different loss-of-function mutations from *Exon1^{mut}* in *HLA-B*40:03* and *HLA-B*54:01*, respectively. Interestingly, a frameshift mutation of *HLA-B*54:01* also occurred at codon 19 (c.19delC, p.R7Efs) in exon 1 (Figure 1A and B, *Online Supplementary Table S4*).

Exon1^{mut} detection using a sensitive droplet digital polymerase chain reaction assay

To detect *Exon1^{mut}* with high sensitivity and specificity, we established a ddPCR assay that allows for precise measurement of mutant allele frequency without the need for HLA typing. Tested samples containing a fixed amount of wild-type DNA and serial dilutions of *Exon1^{mut}* template DNA revealed a detection limit of 0.07% for both HLA-A and HLA-B (*Online Supplementary Figure S6*). The ddPCR assay yielded 0% to 0.042% (median, 0.009%) positive dots in peripheral blood of 24 healthy individuals, validating the cut-off value of 0.07%. The ddPCR assay was able to detect *Exon1^{mut}*, which had an allelic frequency of <1.0%

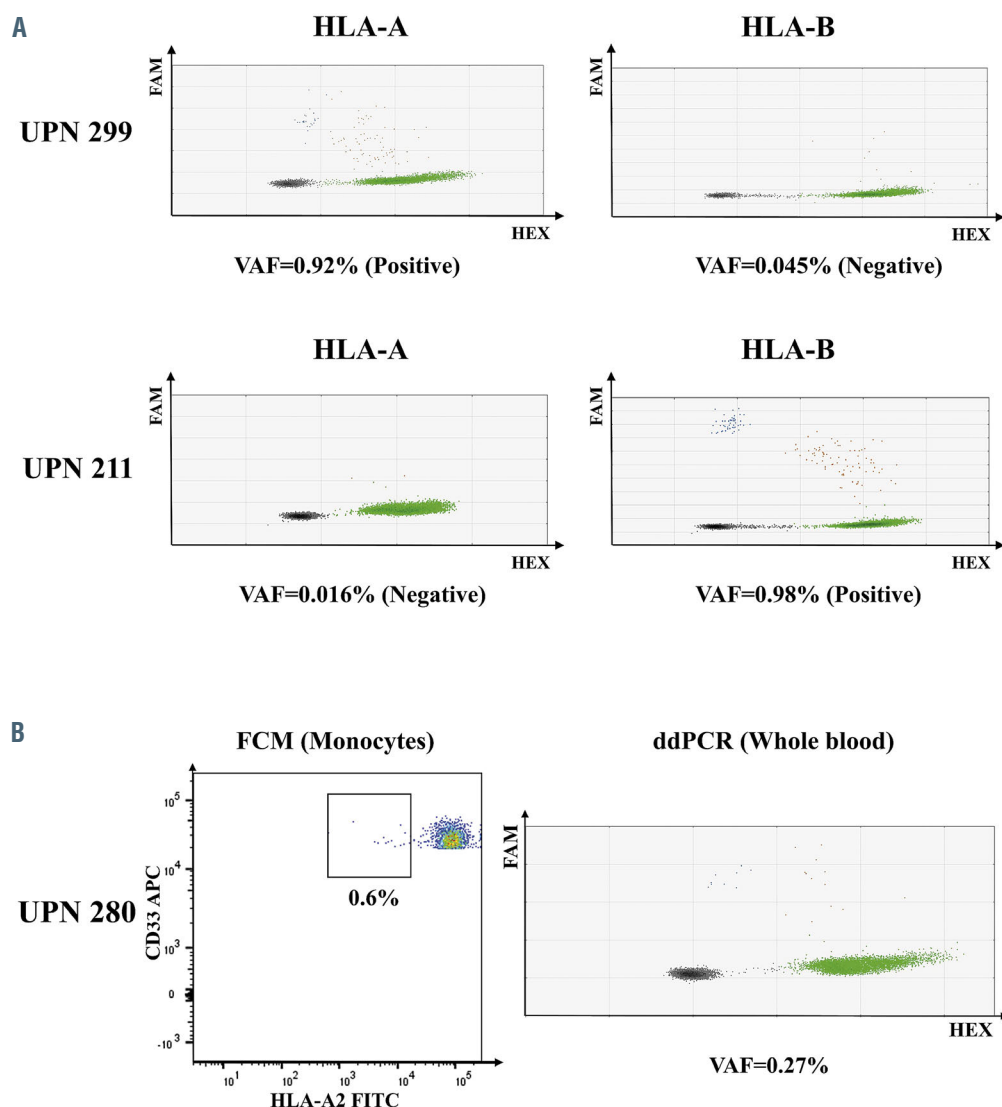


Figure 2. Detection of *Exon1^{mut}* using the droplet digital polymerase chain reaction assay. (A) Representative droplet digital polymerase chain reaction (ddPCR) plots of *Exon1^{mut}* in two patients with aplastic anemia. The ddPCR assay detected 0.92% *Exon1^{mut}* DNA in *HLA-A*02:06* of UPN 299 and 0.98% *Exon1^{mut}* DNA in *HLA-B*40:01* of UPN 211. (B) A minor population of HLA-allele-lacking leukocytes in UPN 280 detected by flow cytometry and the ddPCR assay. The ddPCR assay detected 0.27% *Exon1^{mut}* in whole blood where granulocytes and monocyte with *Exon1^{mut}* were diluted with lymphocytes without *Exon1^{mut}*. The percentage of *Exon1^{mut}*-positive cells was consistent with the percentage of HLA-A2⁻ monocytes (0.6%) detected by flow cytometry. UPN: unique patient number; VAF: variant allele frequency; FCM: flow cytometry.

(Figure 2A), clearly showing the presence of HLA-LL in patients for whom flow cytometry analysis of monocytes using anti-HLA-A2 antibodies produced unequivocal results regarding the presence of HLA-A2-lacking monocytes (Figure 2B).

Prevalence of *Exon1^{mut}* in patients with aplastic anemia

Using two different ddPCR mixtures for HLA-A and HLA-B, the presence of *Exon1^{mut}* was evaluated in all of the 353 patients. *Exon1^{mut}* was detected in 101 (28.6%) of the 353 patients, with the median frequency of 0.42% (range, 0.071% to 21.3%). The prevalence of *Exon1^{mut}* was similar in HLA-A and HLA-B alleles in both treatment-naïve patients (n=291) and treated patients (n=62). Among the AA patients with *Exon1^{mut}*, those who had been treated had a higher median frequency of *Exon1^{mut}* than those who were untreated (0.96% vs. 0.33%, $P=0.0079$) (Figure 3A). Figure 3B shows the relationships between the presence of cells with *Exon1^{mut}*, 6pLOH and a paroxysmal nocturnal hemoglobinuria (PNH) phenotype in the patients. Fifty-six (55.4%) and 67 (66.3%) of the 101 patients with *Exon1^{mut}* had 6pLOH and PNH phenotype cells, respectively. Ten (2.8%) of the 353 patients had *Exon1^{mut}* alone. The frequency of *Exon1^{mut}* was much lower than that of 6pLOH in 36 patients possessing both clones ($P<0.001$) (Figure 3C).

Long-term persistence of *Exon1^{mut}*-positive cells

Serial blood samples were available for longitudinal analyses of *Exon1^{mut}* in 13 patients who responded to immunosuppressive therapy (cyclosporine [CsA] alone in 6 and rabbit antithymocyte globulin [rATG] + CsA in 5) or anabolic steroids (n=2). *Exon1^{mut}* was persistently detected for 14-86 months in nine patients, including one patient (UPN 299) who had been off treatment for 7 years, suggesting that *Exon1^{mut}*-positive leukocytes are derived from long-lasting HSPC (Figure 4A). The VAF of *Exon1^{mut}* increased in two (15%, UPN 333 and UPN 339), remained stable in four (31%), and decreased in three (23%) patients. *Exon1^{mut}* became undetectable at 7-33 months after the first detection of *Exon1^{mut}* in the other four patients, all of whom were being treated with CsA. Figure 4B shows a gradual decline of the *Exon1^{mut}* frequency over 3 years in one patient (UPN 213).

HLA-A and HLA-B alleles that acquire *Exon1^{mut}*

Among the 101 patients with *Exon1^{mut}*, HLA alleles that acquired *Exon1^{mut}* could be determined by targeted deep sequencing with (n=21) or without (n=37) unique molecular identifiers, or deduced from alleles contained in the lost haplotype due to 6pLOH that was accompanied by *Exon1^{mut}* (n=10) (Online Supplementary Figure S2). In the

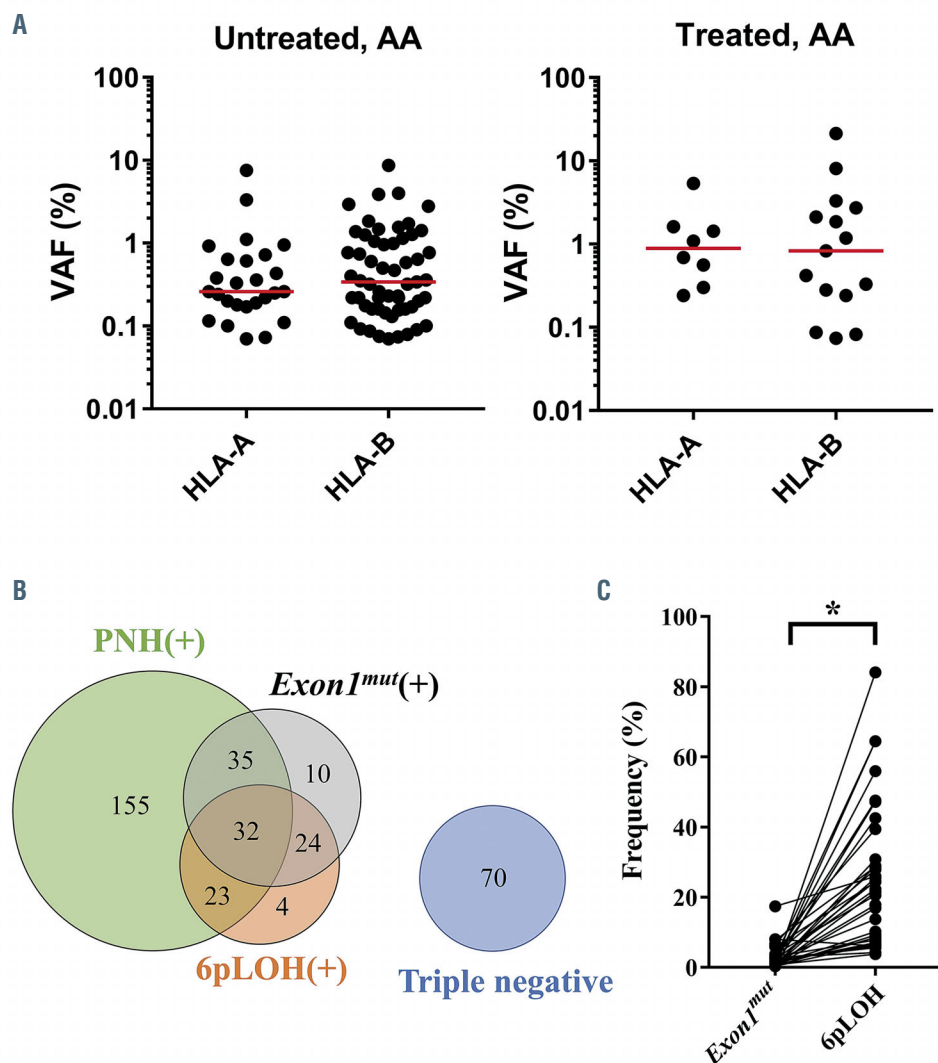


Figure 3. Prevalence and clone size of *Exon1^{mut}* in patients with aplastic anemia. (A) Mutant allele frequency of *Exon1^{mut}* in 291 and 62 *Exon1^{mut}* positive untreated and treated patients with aplastic anemia, respectively. Red bars indicate median mutant allele frequencies of *Exon1^{mut}*. **(B)** The prevalence of *Exon1^{mut}* and its relationship with paroxysmal nocturnal hemoglobinuria phenotype (PNH) and copy number neutral loss of heterozygosity of the short arm of chromosome 6 (6pLOH). *Exon1^{mut}*-positive patients accounted for 58% of 6pLOH⁺ PNH⁺ patients and for 67% of 6pLOH⁺ patients. **(C)** Frequency of *Exon1^{mut}* and 6pLOH in individual patients who were positive for both mutant clones. The frequencies of both clones were determined by droplet digital polymerase chain reaction analysis. * $P<0.001$. VAF: variant allele frequency; AA: aplastic anemia; UPN: unique patient number.

other 33 patients with *Exon1^{mut}*, HLA-A or HLA-B alleles that acquired *Exon1^{mut}* could not be determined or deduced due to very low VAF (<0.2%), the absence of allele-specific SNP near *Exon1^{mut}* in HLA-A or HLA-B alleles that are useful for identify missing HLA alleles, or the absence of coexisting 6pLOH. For the 68 patients in whom HLA alleles that acquired *Exon1^{mut}* could be determined, the following 12 alleles were identified: *A*02:01* (n=2), *A*02:06* (n=15), *A*02:07* (n=1), *A*31:01* (n=3), *B*13:01* (n=2), *B*40:01* (n=3), *B*40:02* (n=31), *B*40:03* (n=1), *B*44:03* (n=1), *B*54:01* (n=6), *B*55:02* (n=2), and *B*56:01* (n=1)

(Figure 5A). HLA class I supertypes of these alleles, which are defined by similarities in the antigen-presenting amino-acid motif of HLA alleles, were confined to only four supertypes: A02, A03, B07, and B44, except for *HLA-B*13:01* that does not belong to any of the 14 supertypes.²¹

When comparing the frequency of these 12 alleles between a healthy control population and our study cohort, 81% of 18,604 healthy Japanese individuals possessed at least one of the 12 alleles, while the prevalence was 92% in the 353 patients with AA ($P<0.001$) and 100% in the 83 patients with 6pLOH ($P<0.001$) (Figure 5B), sug-

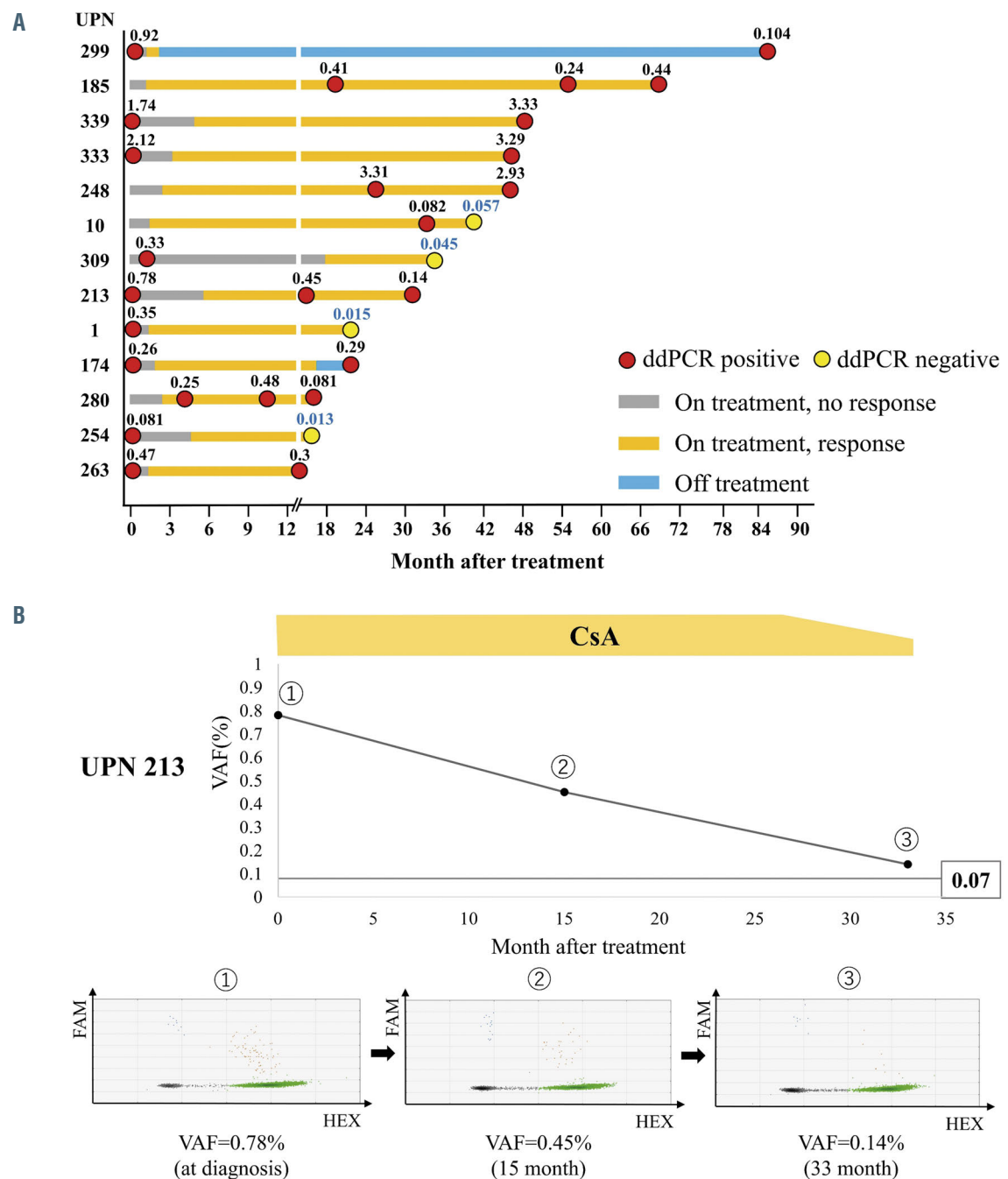


Figure 4. Temporal changes in allelic frequency of *Exon1^{mut}*. (A) Allelic frequencies of *Exon1^{mut}* determined at different time points in 13 patients and their disease status. (B) Representative scattergrams from UPN 213 showing a gradual decline in *Exon1^{mut}* frequency over the course of 3 years. UPN: unique patient number; ddPCR: droplet digital polymerase chain reaction; CsA: cyclosporine A; VAF: variant allele frequency.

gesting the involvement of these alleles in the development of AA.

Loss of HLA-B expression from *Exon1^{mut}*-positive leukocytes

Although *Exon1^{mut}* in leukocytes is expected to result in lack of the corresponding HLA allele, the phenotype of these leukocytes is difficult to examine since the VAF of *Exon1^{mut}* is very low. We previously established six induced pluripotent stem (iPS) cell clones from peripheral blood monocytes of an AA patient (UPN 333) whose monocytes included approximately 60% HLA-A24⁺Bw6⁻ cells (Figure 6A).¹⁷ Deep sequencing revealed the presence of *Exon1^{mut}* in sorted HLA-A24⁺Bw6⁻ cells and also in one (clone C1) of the six iPS cell clones. When a wild-type iPS clone (clone E1) and clone C1 were induced to differentiate into CD34⁺ cells, all clone E1-derived CD34⁺ cells expressed HLA-Bw6 (B5401), while all clone C1-derived CD34⁺ cells lacked HLA-Bw6 (Figure 6B). The ddPCR assay using DNA from wild-type and *Exon1^{mut}*-positive iPS cell-derived CD34⁺ cells revealed that the VAF of *Exon1^{mut}* were 0.041% and 49%, respectively, as expected (Figure 6C).

Clinical characteristics of aplastic anemia patients with *Exon1^{mut}*

Of the 291 patients whose peripheral blood samples were examined for *Exon1^{mut}* and GPI⁻ cells before treatment, 151 were evaluable for response to immunosuppressive therapy (CsA alone, n=68; CsA+rATG, n=83). The other 140 patients were excluded from the analysis of the relationship between the response to immunosuppressive therapy and the presence of *Exon1^{mut}* or GPI⁻ cells because no data on the response to immunosuppressive therapy were available in 84, and the remaining 56 received no treatment (n=25) or treatments other than immunosuppressive therapy (n=31), such as anabolic steroids and thrombopoietin receptor agonists, and allogeneic stem cell transplantation. An increase in GPI⁻ cells was noted in 76% (34/45) of patients with *Exon1^{mut}* and in 76% (81/106) without *Exon1^{mut}* ($P=1.0$). In terms of response to immunosuppressive therapy, 82% (37/45) of patients with *Exon1^{mut}* responded to CsA (n=14) or CsA+rATG (n=23), while 75% (79/106) of those without *Exon1^{mut}* responded to CsA (n=35) or CsA+rATG (n=44) ($P=0.40$). The response rate to immunosuppressive ther-

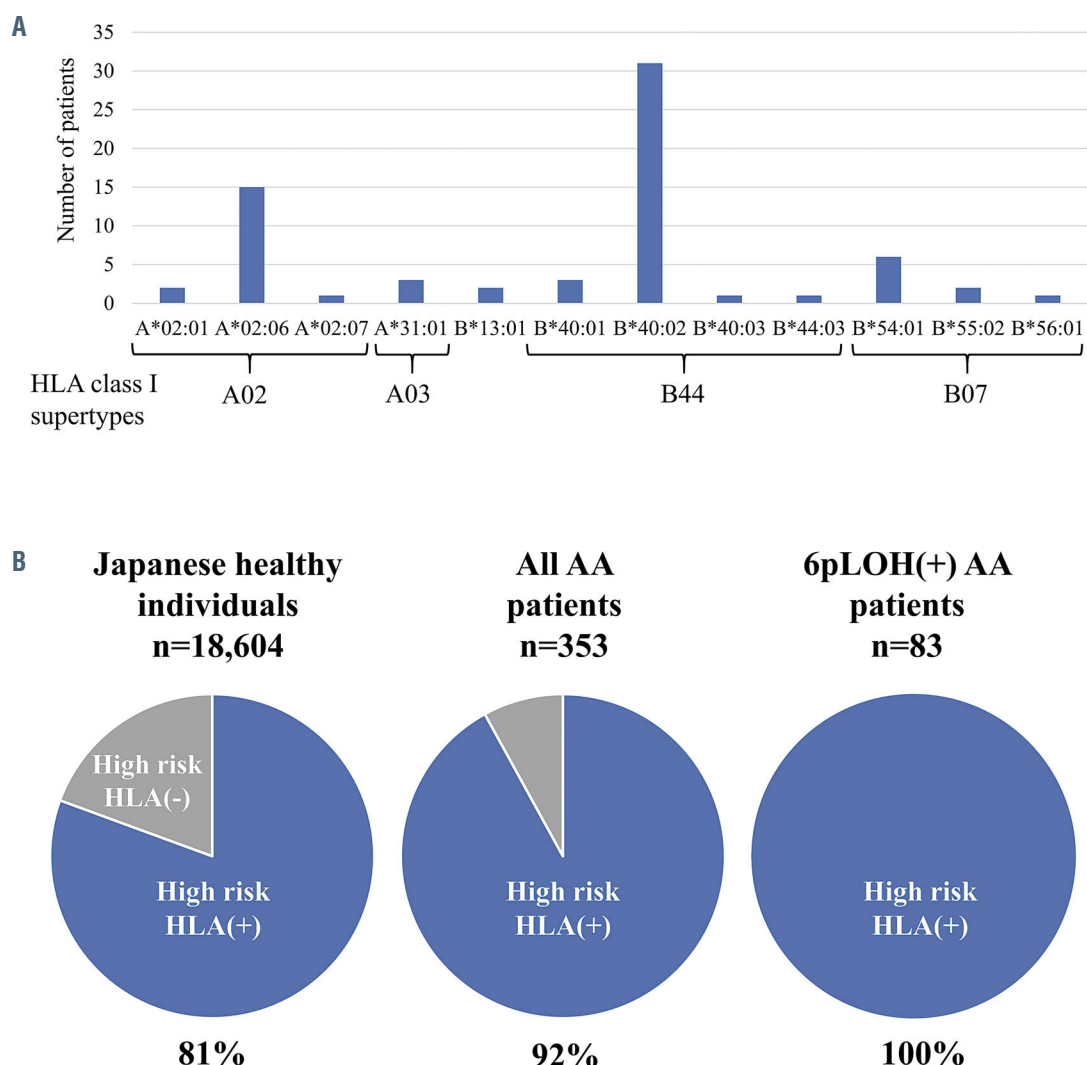


Figure 5. HLA alleles that acquired *Exon1^{mut}*. (A) The number of cases that acquired *Exon1^{mut}* in the corresponding HLA alleles are shown. HLA numbers shown below the bar graph denote the HLA class I supertypes to which each allele belongs. (B) Proportions that the 12 HLA alleles account for in the different populations. AA: aplastic anemia; 6pLOH: copy number neutral loss of heterozygosity of the short arm of chromosome 6.

py in patients with *Exon1^{mut}* was significantly higher than that (54%, 13/24) in patients who were negative for all of *Exon1^{mut}*, GPI cells, and 6pLOH ($P=0.023$).

Discussion

Targeted deep sequencing of HLA genes of leukocytes obtained from AA patients with HLA-LL revealed a unique nonsense mutation at codon 19 (c.19C>T, p.R7X) in exon 1 (*Exon1^{mut}*) of different HLA-A and HLA-B alleles. This mutation has been previously reported in Japanese and American AA patients, but did not draw attention because the mutation was detectable in only a limited number of patients.^{9,14} Our highly sensitive ddPCR assay enabled the detection of minor *Exon1^{mut}* clones and detected the mutant DNA in nearly one third of Japanese AA patients regardless of the presence of 6pLOH. *Exon1^{mut}* was also detected in two of eight Finnish AA patients we stud-

ied (*unpublished observation*). Interestingly, a frameshift mutation (c.19delC, p.R7Efs) was also identified at codon 19 of *HLA-B*54:01* in a patient (UPN 210) without *Exon1^{mut}*, suggesting that the codon 19 in exon 1 of *HLA-A* and *HLA-B* may be a specific position at which somatic mutations are likely to occur.

The loss of HLA from CD34⁺ cells due to *Exon1^{mut}* was verified by phenotypic analysis of *Exon1^{mut}*-positive iPS cell-HSPC that were derived from monocytes of an AA patient who had approximately 14% *Exon1^{mut}*-positive cells among the granulocyte population.¹⁷ *Exon1^{mut}* has also been detected in several squamous cell carcinomas, such as head and neck tumors, oral cancers, and anal cancers, in previous studies.²²⁻²⁵ The solid tumors that lost HLA class I expression due to *Exon1^{mut}* were thought to have escaped T-cell attack and acquired a proliferative advantage. Taken together, these findings suggest that *Exon1^{mut}* is a common mechanism by which HSPC lose HLA, allowing them to escape from the effects of cytotoxic T lymphocytes in AA patients.

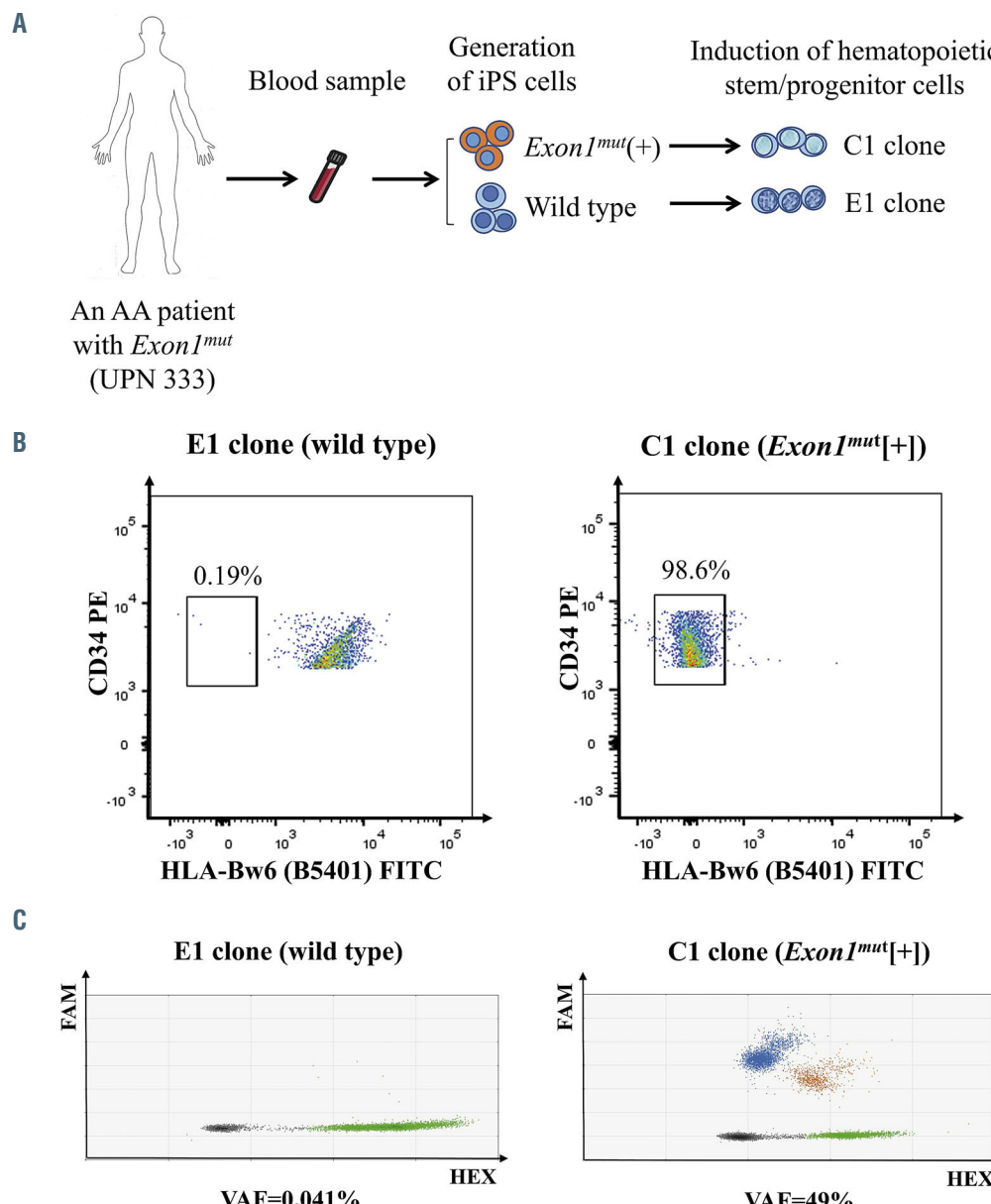


Figure 6. HLA allele expression by *Exon1^{mut}*-positive hematopoietic stem and progenitor cells. (A) Establishment of induced pluripotent stem cell (iPSC)-derived hematopoietic stem cells from monocytes of an aplastic anemia patient with *Exon1^{mut}* (UPN 333). (B) HLA-Bw6 (B5401) expression by CD34⁺ cells derived from a wild-type iPSC clone (left) and an *Exon1^{mut}*-positive iPSC clone (right). (C) *Exon1^{mut}* detection in DNA from wild-type (left) and *Exon1^{mut}*-positive (right) iPSC-derived CD34⁺ cells. Numbers below the scattergram denote the variant allele frequency of *Exon1^{mut}*. AA: aplastic anemia; UPN: unique patient number; iPSCs: induced pluripotent stem cells; VAF: variant allele frequency.

We previously used targeted deep sequencing to identify frequent loss-of-function mutations in three HLA class I alleles, *B*40:02*, *A*02:06*, and *B*54:01*.^{9,16,17} The highly sensitive ddPCR assay described herein that was capable of detecting *Exon1^{mut}* newly identified three HLA-A (*A*02:01*, *A*02:07*, *A*31:01*) and six HLA-B alleles (*B*13:01*, *B*40:01*, *B*40:03*, *B*44:03*, *B*55:02*, *B*56:01*) as HLA alleles that are susceptible to allelic loss. Compared with their frequency in the general Japanese population, these HLA alleles were found to be highly enriched in AA patients. Among the 14 HLA class I supertypes that are defined based on similarities in the antigen-presenting peptide motif, the 12 alleles mentioned above belong to only four of the supertypes.²¹ These findings suggest that autoantigens of AA may be presented to T cells by these specific HLA alleles on HSPC.

Like HSPC positive for 6pLOH, those positive for *Exon1^{mut}* are thought to escape the attack of cytotoxic T lymphocytes specific to autoantigens presented by the missing HLA-A or HLA-B allele and contribute to hematopoiesis over the long-term. However, it is unclear why *Exon1^{mut}* occurs more frequently in HSPC than loss-of-function mutations in other positions of HLA class I alleles. Shukla *et al.* reported different hotspots of mutations in class I HLA genes according to cancer type, and identified *Exon1^{mut}* only in head and neck squamous cell cancers.²⁴ HSPC may thus share a common property in that *Exon1^{mut}* is likely to occur in class I HLA genes in head and neck squamous cell cancers.

The median VAF of *Exon1^{mut}* in patients with *Exon1^{mut}* patients was only 0.42%, a level that cannot be detected by targeted deep sequencing. This low VAF was in sharp contrast to the high proportion of concomitant 6pLOH in individual patients (Figure 3C). We previously reported that 6pLOH⁺ leukocytes were often polyclonal, consisting of leukocytes having different breakpoints of uniparental disomy in the short arm of chromosome 6.¹⁰ This polyclonality may account for the high proportion of 6pLOH. Although the leukocytes with *Exon1^{mut}* represent a minor leukocyte population, the long-term (1–7 years) persistence of these mutated leukocytes indicates that they are derived from HSPC with self-renewal capacity. Arends *et al.* showed that clone size of cells with somatic mutations of epigenetic regulation genes expanded from most immature hematopoietic stem cells to mature peripheral blood cells in patients with clonal hematopoiesis of indeterminate potential.²⁶ Leukocyte positive for *Exon1^{mut}* may also be derived from most immature hematopoietic stem cells. The persistence of similarly minor clones in peripheral blood has been reported for GPI[−] granulocytes in AA, the median frequency of which was 0.25%.^{18,27} In contrast to *PIGA*-mutated or 6pLOH⁺ leukocytes, which can be oligoclonal and dysfunctional due to the lack of all GPI-anchored proteins or a large segment of 6p, *Exon1^{mut}*-positive leukocytes are derived from a single HSPC that is phenotypically normal except for the lack of one HLA allele. According to Dingli's hypothesis, approximately 400 HSPC are actively involved in human hematopoiesis.²⁸ Thus, the small proportion of *Exon1^{mut}*-positive leukocytes among the entire leukocyte population may reflect an average clone size of individual HSPC in the bone marrow.

HLA-LL are useful markers that indicate the presence of an immune pathophysiology in patients with bone mar-

row failure. Here we showed a high response rate to immunosuppressive therapy in patients with *Exon1^{mut}*, although patients without *Exon1^{mut}* also had a high response rate likely due to the high prevalence of GPI-cells.^{29–31} Several methods can be used to detect HLA-LL, including flow cytometry assays with monoclonal antibodies specific to HLA-A or HLA-B alleles, ddPCR or SNP arrays for detecting 6pLOH, and targeted deep sequencing.^{6–10,12} However, these methods require HLA typing of patients, take a long time to produce results, and are unable to detect HLA-LL that account for less than 1% of total leukocytes. The ddPCR assay used in the present study to detect *Exon1^{mut}* enables the detection of HLA-LL accounting for as few as 0.07% of the total leukocyte population within 6 h of blood collection, highlighting the powerful nature of this assay for diagnosing immune pathophysiology in patients with bone marrow failure.

Disclosures

No conflicts of interest to disclose.

Contributions

HM, TI, KT, YZ and SN collected clinical data and blood samples. FA performed HLA genotyping. YF and SO conducted the SNP array analyses. YZ, HT, TO, HK and AM generated an original monoclonal antibody specific to HLA-B13, B60 and B61. HM and TY performed cell sorting. HM, KHosomichi, TI, YZ and AT performed deep sequencing. HM, YZ, NMA and TCD performed the droplet digital polymerase chain reaction. KC and YY generated the induced pluripotent stem cells. MIE performed the *in vitro* experiments. HM, KHosokawa and SN designed the research and wrote the manuscript. All authors critically reviewed the manuscript and checked the final version.

Acknowledgements

The authors thank the patients and donors and their physicians, including M. Yamaguchi of Ishikawa Prefectural Central Hospital of Kanazawa, Ishikawa, T. Takaku of Juntendo University Hospital of Bunkyo-ku, Tokyo, H. Yano of Kainan Hospital of Yatomi, Aichi, K. Watamoto of Komaki City Hospital of Komaki, Aichi, M. Mizutani of Matsusaka Central General Hospital of Matsusaka, Mie, S. Morishima of University of Ryukyu Hospital of Nishihara, Okinawa, and Mikko Keränen, Sofie Lun-d-gren and Satu Mustjoki of the University of Helsinki, Helsinki, Finland for sending their patients' samples for screening for *Exon1^{mut}*, and the Advanced Preventive Medical Sciences Research Center, Kanazawa University for the use of facilities. HM is a PhD candidate at Kanazawa University and this work is submitted in partial fulfillment of the requirements for the PhD.

Funding

This work was supported by MEXT KAKENHI (Grant-in-Aid for Scientific Research [B], grant number: 16H05335 and 19H03686) to SN, MEXT KAKENHI (Grant-in-Aid for Young Scientists [B], grant number: 17K16184) to K. Hosokawa, MEXT KAKENHI (Grant-in-Aid for Scientific Research [C], grant number: 17K09007) to TK, MEXT KAKENHI (Grant-in-Aid for Scientific Research on Innovative Areas, grant number: 16H06502 and 19H05344) to K. Hosomichi, Hokuriku Bank Research Grant for Young Scientists to TK and Hokkoku Foundation for Cancer Research to TK and KHosokawa.

References

- Young NS. Aplastic anemia. *N Engl J Med.* 2018;379(17):1643-1656.
- Zeng W, Nakao S, Takamatsu H, et al. Characterization of T-cell repertoire of the bone marrow in immune-mediated aplastic anemia: evidence for the involvement of antigen-driven T-cell response in cyclosporine-dependent aplastic anemia. *Blood.* 1999;93(9):3008-3016.
- Nakao S, Takami A, Takamatsu H, et al. Isolation of a T-cell clone showing HLA-DRB1*0405-restricted cytotoxicity for hematopoietic cells in a patient with aplastic anemia. *Blood.* 1997;89(10):3691-3699.
- Risitano AM, Maciejewski JP, Green S, et al. In-vivo dominant immune responses in aplastic anaemia: molecular tracking of putatively pathogenetic T-cell clones by TCR beta-CDR3 sequencing. *Lancet.* 2004;364(9431):355-364.
- Włodarski MW, Gondek LP, Nearman ZP, et al. Molecular strategies for detection and quantitation of clonal cytotoxic T-cell responses in aplastic anemia and myelodysplastic syndrome. *Blood.* 2006;108(8):2632-2641.
- Inaguma Y, Akatsuka Y, Hosokawa K, et al. Induction of HLA-B*40:02-restricted T cells possessing cytotoxic and suppressive functions against haematopoietic progenitor cells from a patient with severe aplastic anaemia. *Br J Haematol.* 2016;172(1):131-134.
- Espinosa JL, Elbadry MI, Chonabayashi K, et al. Hematopoiesis by iPSC-derived hematopoietic stem cells of aplastic anemia that escape cytotoxic T-cell attack. *Blood Adv.* 2018;2(4):390-400.
- Maruyama H, Katagiri T, Kashiwase K, et al. Clinical significance and origin of leukocytes that lack HLA-A allele expression in patients with acquired aplastic anemia. *Exp Hematol.* 2016;44(10):931-939.e3.
- Zaimoku Y, Takamatsu H, Hosomichi K, et al. Identification of an HLA class I allele closely involved in the autoantigen presentation in acquired aplastic anemia. *Blood.* 2017;129(21):2908-2916.
- Katagiri T, Sato-Otsubo A, Kashiwase K, et al. Frequent loss of HLA alleles associated with copy number-neutral 6pLOH in acquired aplastic anemia. *Blood.* 2011;118(25):6601-6609.
- Yoshizato T, Dumitriu B, Hosokawa K, et al. Somatic mutations and clonal hematopoiesis in aplastic anemia. *N Engl J Med.* 2015;373(1):35-47.
- Afable MG 2nd, Włodarski M, Makishima H, et al. SNP array-based karyotyping: differences and similarities between aplastic anemia and hypocellular myelodysplastic syndromes. *Blood.* 2011;117(25):6876-6884.
- Betensky M, Babushok D, Roth JJ, et al. Clonal evolution and clinical significance of copy number neutral loss of heterozygosity of chromosome arm 6p in acquired aplastic anemia. *Cancer Genet.* 2016;209(1-2):1-10.
- Babushok DV, Duke JL, Xie HM, et al. Somatic HLA mutations expose the role of class I-mediated autoimmunity in aplastic anemia and its clonal complications. *Blood Adv.* 2017;1(22):1900-1910.
- Montes P, Kerick M, Bernal M, et al. Genomic loss of HLA alleles may affect the clinical outcome in low-risk myelodysplastic syndrome patients. *Oncotarget.* 2018;9(97):36929-36944.
- Imi T, Katagiri T, Hosomichi K, et al. Sustained clonal hematopoiesis by HLA-lacking hematopoietic stem cells without driver mutations in aplastic anemia. *Blood Adv.* 2018;2(9):1000-1012.
- Elbadry MI, Mizumaki H, Hosokawa K, et al. Escape hematopoiesis by HLA-B5401-lacking hematopoietic stem progenitor cells in men with acquired aplastic anemia. *Haematologica.* 2019;104(10):e447-e450.
- Hosokawa K, Sugimori C, Ishiyama K, et al. Establishment of a flow cytometry assay for detecting paroxysmal nocturnal hemoglobinuria-type cells specific to patients with bone marrow failure. *Ann Hematol.* 2018;97(12):2289-2297.
- MacConaill LE, Burns RT, Nag A, et al. Unique, dual-indexed sequencing adapters with UMIs effectively eliminate index cross-talk and significantly improve sensitivity of massively parallel sequencing. *BMC Genomics.* 2018;19(1):30.
- Kanda Y. Investigation of the freely available easy-to-use software 'EZR' for medical statistics. *Bone Marrow Transplant.* 2013;48(3):452-458.
- Sidney J, Peters B, Frahm N, et al. HLA class I supertypes: a revised and updated classification. *BMC Immunol.* 2008;9:1.
- Pickering CR, Zhang J, Yoo SY, et al. Integrative genomic characterization of oral squamous cell carcinoma identifies frequent somatic drivers. *Cancer Discov.* 2013;3(7):770-781.
- Mouw KW, Cleary JM, Reardon B, et al. Genomic evolution after chemoradiotherapy in anal squamous cell carcinoma. *Clin Cancer Res.* 2017;23(12):3214-3222.
- Shukla SA, Rooney MS, Rajasagi M, et al. Comprehensive analysis of cancer-associated somatic mutations in class I HLA genes. *Nat Biotechnol.* 2015;33(11):1152-1158.
- Li YY, Chung GT, Lui VW, et al. Exome and genome sequencing of nasopharynx cancer identifies NF-κappaB pathway activating mutations. *Nat Commun.* 2017;8:14121.
- Arends CM, Galan-Sousa J, Hoyer K, et al. Hematopoietic lineage distribution and evolutionary dynamics of clonal hematopoiesis. *Leukemia.* 2018;32(9):1908-1919.
- Sugimori C, Mochizuki K, Qi Z, et al. Origin and fate of blood cells deficient in glycosylphosphatidylinositol-anchored protein among patients with bone marrow failure. *Br J Haematol.* 2009;147(1):102-112.
- Dingli D, Traulsen A, Pacheco JM. Compartmental architecture and dynamics of hematopoiesis. *PLoS One.* 2007;2(4):e345.
- Sugimori C, Chuhjo T, Feng X, et al. Minor population of CD55-CD59- blood cells predicts response to immunosuppressive therapy and prognosis in patients with aplastic anemia. *Blood.* 2006;107(4):1308-1314.
- Kulagin A, Lisukov I, Ivanova M, et al. Prognostic value of paroxysmal nocturnal haemoglobinuria clone presence in aplastic anaemia patients treated with combined immunosuppression: results of two-centre prospective study. *Br J Haematol.* 2014;164(4):546-554.
- Narita A, Muramatsu H, Sekiya Y, et al. Paroxysmal nocturnal hemoglobinuria and telomere length predicts response to immunosuppressive therapy in pediatric aplastic anemia. *Haematologica.* 2015;100(12):1546-1552.

Post-transplant cyclophosphamide versus anti-thymocyte globulin for graft-versus-host disease prevention in haploidentical transplantation for adult acute lymphoblastic leukemia



Ferrata Storti Foundation

Arnon Nagler,^{1*} Abraham S. Kanate,^{2*} Myriam Labopin,^{3*} Fabio Ciceri,⁴ Emanuele Angelucci,⁵ Yener Koc,⁶ Zafer Gülbas,⁷ William Arcese,⁸ Johanna Tischer,⁹ Pietro Piotelli,¹⁰ Hakan Ozdogu,¹¹ Boris Afanasyev,¹² Depei Wu,¹³ Mutlu Arat,¹⁴ Zinaida Peric,¹⁵ Sebastian Giebel,¹⁶ Bipin Savani¹⁷ and Mohamad Mohty¹⁸

Haematologica 2021
Volume 106(6):1591-1598

¹Chaim Sheba Medical Center, Tel Aviv University, Tel-Hashomer, Israel; ²West Virginia University, Morgantown, WV, USA; ³Department of Hematology and EBMT Paris study office / CEREST-TC, Saint Antoine Hospital, Paris, France; ⁴Ospedale San Raffaele s.r.l., Milano, Italy; ⁵Ospedale San Martino, Department of Hematology II, Genova, Italy; ⁶Medical Park Hospitals, Stem Cell Transplant Unit, Antalya, Turkey; ⁷Anadolu Medical Center Hospital, Bone Marrow Transplantation Department, Kocaeli, Turkey; ⁸“Tor Vergata” University of Rome, Stem Cell Transplant Unit, Policlinico Universitario Tor Vergata, Rome, Italy; ⁹Klinikum Grosshadern, Med. Klinik III, Munich, Germany; ¹⁰Ospedale San Gerardo, Clinica Ematologica dell'Università Milano-Biocca, Monza, Italy; ¹¹Baskent University Hospital, Hematology Division, Bone Marrow Transplantation Unit, Adana, Turkey; ¹²First State Pavlov Medical University of St. Petersburg, Raisa Gorbacheva Memorial Research Institute for Pediatric Oncology, Hematology, and Transplantation, St. Petersburg, Russia; ¹³First Affiliated Hospital of Soochow University, Department of Hematology, Suzhou, China; ¹⁴Florence Nightingale Sisli Hospital, Hematopoietic Stem Cell Transplantation Unit, Istanbul, Turkey; ¹⁵University Hospital Center Zagreb, School of Medicine, University of Zagreb, Zagreb, Croatia; ¹⁶Department of Bone Marrow Transplantation and Oncohematology, Maria Skłodowska-Curie Memorial Cancer Center and Institute of Oncology, Gliwice, Poland; ¹⁷Department of Hematology-Oncology, Vanderbilt University Medical Center, Nashville, TN, USA and ¹⁸Department of Hematology and EBMT Paris study office / CEREST-TC, Saint Antoine Hospital, INSERM UMR 938 and Université Pierre et Marie Curie, Paris, France

*AN, ASK and ML contributed equally as co-first authors.

ABSTRACT

Graft-versus-host disease (GvHD) prophylaxis for unmanipulated haploidentical hematopoietic cell transplantation includes post-transplant cyclophosphamide (PTCy) and anti-thymocyte globulin (ATG). Utilizing data in the European Society for Blood and Marrow Transplantation registry, we compared ATG- versus PTCy-based GvHD prophylaxis in 434 adults with acute lymphoblastic leukemia undergoing haploidentical hematopoietic cell transplantation. Of the 434 patients included in this study, ATG was used in 98 and PTCy in 336. The median follow-up was approximately 2 years. The baseline characteristics of the patients were similar between the groups except that the ATG group was more likely to have had relapsed/refractory acute lymphoblastic leukemia ($P=0.008$), had conditioning not including total body irradiation ($P<0.001$), have had peripheral blood as the source of their grafts ($P\leq 0.001$) and to have been transplanted in an earlier time-period (median year of transplantation: 2011 vs. 2015). The 100-day rates of grade II-IV and III-IV acute GvHD were similar in the ATG and PTCy groups, as were 2-year chronic GvHD rates. On multivariate analysis, leukemia-free survival and overall survival were better with PTCy than with ATG prophylaxis. Relapse incidence was lower in the PTCy group ($P=0.03$), while non-relapse mortality was not different. Advanced disease and lower performance score were associated with poorer leukemia-free survival and overall survival and advanced disease

Correspondence:

ABRAHAM S. KANATE
askanate@hsc.wvu.edu

Received: January 12, 2020.

Accepted: April 28, 2020.

Pre-published: April 30, 2020.

<https://doi.org/10.3324/haematol.2020.247296>

©2021 Ferrata Storti Foundation

Material published in *Haematologica* is covered by copyright. All rights are reserved to the Ferrata Storti Foundation. Use of published material is allowed under the following terms and conditions: <https://creativecommons.org/licenses/by-nc/4.0/legalcode>. Copies of published material are allowed for personal or internal use. Sharing published material for non-commercial purposes is subject to the following conditions: <https://creativecommons.org/licenses/by-nc/4.0/legalcode>, sect. 3. Reproducing and sharing published material for commercial purposes is not allowed without permission in writing from the publisher.



was associated with inferior GvHD-free/relapse-free survival. Compared to bone marrow grafts, peripheral grafts were associated with higher rates of GvHD. In patients with acute lymphoblastic leukemia undergoing unmanipulated haploidentical hematopoietic cell transplantation, PTCy for GvHD prevention resulted in a lower incidence of relapse and improved leukemia-free survival and overall survival, compared to ATG.

Introduction

Despite significant advances in the management of adult acute lymphoblastic leukemia (ALL), disease relapse remains a significant impediment to long-term leukemia-free survival,¹ especially in adult patients aged >20 years and in those with advanced (relapsed/refractory) disease.² Although fraught with challenges of disease relapse and non-relapse mortality, allogeneic hematopoietic cell transplantation (HCT) is a potentially curative option for these patients, and is often considered in high-risk and advanced ALL.²⁻⁴ In the absence of a suitable HLA-matched donor, allogeneic transplantation from a related haploidentical donor can be considered and such donors are a readily available source of grafts for most patients irrespective of racial/ethnic background. Indeed, the use of haploidentical HCT has increased steadily over the years in various hematologic malignancies including acute leukemia.^{4,5} To mitigate the risk of greater HLA-disparity and resultant graft rejection and graft-*versus*-host disease (GvHD) which were seen with haploidentical HCT, T-cell depletion was used historically, but this strategy was associated with higher risks of non-relapse mortality, disease relapse and delayed immune reconstitution.⁶⁻⁹

The use of unmanipulated, T-cell-replete grafts has revived haploidentical transplantation. Immunosuppression using anti-thymocyte globulin (ATG) in this setting has shown favorable results.^{10,11} Wang *et al.* conducted a biologically randomized trial, specifically in ALL patients in first complete remission, comparing matched sibling donor *versus* haploidentical donor transplantation using ATG-based GvHD prophylaxis and reported a similar 3-year leukemia-free survival (60% *vs.* 61% by the intention-to-treat analysis). The administration of post-transplant cyclophosphamide (PTCy) after an unmanipulated haploidentical allograft has shown favorable results and has become widely utilized in the past decade.^{12,13} Registry data also support unmanipulated haploidentical HCT as a viable treatment option for ALL patients.^{14,15}

Although both strategies are effective as GvHD prophylaxis, there is a paucity of comparative data on ATG *versus* PTCy in haploidentical transplantation. Ruggeri *et al.* conducted a retrospective study using data from the European Society for Blood and Marrow Transplantation (EBMT) registry on 308 patients with acute myeloid leukemia, and compared outcomes between those given ATG (n=115) or PTCy (n=193) as a GvHD prevention strategy. On multivariate analysis, compared to ATG, PTCy use was associated with significantly better leukemia-free survival ($P=0.03$) and GvHD-free/relapse-free survival (GRFS) ($P=0.03$). To our knowledge, no studies have reported comparative data between ATG and PTCy platforms in ALL patients undergoing haploidentical transplantation.¹⁶ We used the EBMT database to conduct a comparative analysis between ATG and PTCy strategies in ALL patients undergoing haploidentical HCT

using bone marrow or peripheral blood as the source of hematopoietic cells for the graft.

Methods

Data source and patients

This is a retrospective multicenter analysis using the dataset of the Acute Leukemia Working Party of the EBMT group registry. The EBMT is a voluntary working group of more than 600 transplant centers that are required to report, annually, all consecutive hematopoietic cell transplants and follow-ups. Audits are performed routinely to determine the accuracy of the data. The study was planned and approved by the Acute Leukemia Working Party of the EBMT. In addition, the study protocol was approved by the institutional review board at each site and complied with country-specific regulatory requirements. The study was conducted in accordance with the Declaration of Helsinki and Good Clinical Practice guidelines.

The subjects included in this analysis were adults (≥ 18 years) with ALL who underwent their first haploidentical HCT between 2007 and 2017, were reported to the "Promise" database of the EBMT and received either ATG or PTCy as a GvHD prevention strategy. Recipients of haploidentical transplantation (mismatched by at least two or more HLA-loci to donors) received unmanipulated, bone marrow or peripheral blood grafts with additional GvHD prophylaxis, which consisted predominantly of a calcineurin inhibitor plus mycophenolate mofetil or a calcineurin inhibitor plus methotrexate. Patients who received grafts that had been manipulated *ex vivo* (T-cell-depleted or CD34-selected grafts) or who received both ATG and PTCy (n=37) were excluded.

Study endpoints and definitions

The primary endpoint for this study was leukemia-free survival. Secondary endpoints were acute GvHD, chronic GvHD, relapse incidence, non-relapse mortality, GRFS and overall survival. Refined GRFS was defined as survival without the following events: grade III or IV acute GvHD, severe chronic GvHD, disease relapse, or death from any cause after haploidentical HCT.^{17,18} Leukemia-free survival was calculated until the date of first relapse, death from any cause or the last follow-up for patients alive in complete remission. Relapse was defined as disease recurrence and appearance of blasts in the peripheral blood or bone marrow ($>5\%$) after having achieved complete remission. Non-relapse mortality was defined as death from any cause other than relapse. Acute GvHD was graded according to the modified Seattle Glucksberg criteria¹⁹ and chronic GvHD according to the revised Seattle criteria.²⁰ The conditioning regimen was defined as myeloablative when it contained total body irradiation (TBI) at a dose >6 Gray or a total dose of busulfan >8 mg/kg (orally) or >6.4 mg/kg (intravenously). All other conditioning regimens were defined as reduced intensity.²¹ Neutrophil engraftment was defined as the first of 3 successive days with an absolute neutrophil count $\geq 500/\mu\text{L}$.

Statistical analysis

Patient-, disease-, and transplant-related characteristics for the

two cohorts (reducing intensity/myeloablative conditioning) were compared using χ^2 statistics for categorical variables and the Mann-Whitney test for continuous variables. Survival statistics (leukemia-free survival, overall survival and GRFS) were estimated by the Kaplan-Meier method. Cumulative incidence functions were used to estimate neutrophil engraftment, acute GvHD, chronic GvHD, relapse incidence and non-relapse mortality. Competing risks were death for engraftment and relapse incidence, relapse for non-relapse mortality, and relapse or death for acute and chronic GvHD. Univariate analysis (*Online Supplementary Table S1*) was carried out using the log-rank test for GRFS, overall survival and leukemia-free survival, and the Gray test for cumulative incidence functions. A Cox proportional hazards model was used for multivariate regression. All variables differing significantly between the two groups or factors associated with one outcome in univariate analysis were included in the Cox model. To test for a center effect, we introduced a random effect or frailty for each center into the model.^{22,23} Results are expressed as a hazard ratio (HR) with a 95% confidence interval (95% CI). All tests were two-sided. The type I error rate was fixed at 0.05 for the determination of factors associated with time-to-event outcomes. Statistical analyses were performed with SPSS 24.0 (SPSS Inc, Chicago, IL, USA) and R 3.4.0 (R Core Team [2017]. R: A language and environment for statistical computing. R Foundation for Statistical Computing, Vienna, Austria. URL <https://www.R-project.org/>).

Results

Baseline characteristics

In all, 434 patients undergoing haploidentical HCT for ALL were included in the study, which comprised two groups divided according to which GvHD prophylaxis the patients received: ATG (n=98) or PTCy (n=336). Baseline patient-, disease- and transplantation-related characteristics are shown in Table 1. There were no significant differences between the groups in terms of patients' age, gender, ALL subtype, Karnofsky Performance Score <90, HCT-Comorbidity Index ≥ 3 , donors' age and donor-recipient combinations of sex and cytomegalovirus serological status. ATG recipients were more likely to have relapsed/refractory ALL compared to PTCy recipients (30.6% vs. 16.4%, respectively; $P=0.008$). Although the difference was not statistically significant, myeloablative conditioning regimens were given to a greater proportion of PTCy-treated patients than ATG-treated patients (78.3% vs. 69.4%, respectively; $P=0.07$). The PTCy group was more likely to have received TBI (45.2% vs. 26.5%; $P\leq 0.001$). A TBI dose of ≥ 10 Gy was administered to 25.8% of the patients in the PTCy group and 14.3% of those in the ATG group. Bone marrow was the graft source in 52.1% and 31.6% of patients in the PTCy and ATG groups, respectively ($P\leq 0.001$). ATG-based haploidentical transplants were carried out during an earlier period (median year of transplant, 2011) compared to PTCy-based transplants (median year of transplant, 2015) ($P\leq 0.0001$). The median follow-up for survivors in the ATG and PTCy groups was 55 months (range, 14-79) and 22 months (range, 12-37), respectively.

Engraftment

The cumulative incidence of engraftment at day 60 was 91.7% (95% CI: 83.7-95.8) and 92.5% (95% CI: 89-95) in the ATG and PTCy groups, respectively ($P=0.11$).

Table 1. Baseline patient-, donor- and transplant-related characteristics in the entire cohort of haploidentical donor transplant recipients and groups stratified by graft-versus-host disease prevention strategy.

Baseline variable	All patients N = 434	By GvHD prophylaxis		
		ATG, N=98	PTCy, N=336	P-value
Recipients' age in years, median (range)	35.6 (18-76)	35.5 (18-76)	36 (18-73)	0.93
Male recipient*, n (%)	274 (63)	61 (62.2)	213 (63.8)	0.78
ALL subtype, n (%)				
Ph-negative B-ALL	154 (35.4)	34 (34.7)	120 (35.7)	0.51
Ph-positive B-ALL	140 (32.3)	36 (36.7)	104 (31.0)	
T-ALL	140 (32.3)	28 (28.6)	112 (33.3)	
Remission status, n (%)				
CR1	208 (47.9)	41 (41.8)	167 (49.7)	0.008
CR2 or beyond	141 (32.5)	27 (27.6)	114 (33.9)	
Advanced (r/r)	85 (19.6)	30 (30.6)	55 (16.4)	
KPS, n (%)				
≥ 90	293 (72)	64 (65.3)	229 (68.2)	0.71
<90	114 (28)	23 (23.5)	91 (27.0)	
Missing	27	11	16	
Comorbidity Index, n (%)				
≤ 2	188 (79)	27 (71.1)	161 (80.5)	0.19
≥ 3	50 (21)	11 (28.9)	39 (19.5)	
Missing	196	60	136	
Prior autologous transplantation, n (%)	21 (4.8)	5 (5)	16 (4.8)	0.8
Conditioning intensity, n (%)				
Myeloablative	331 (76.3)	68 (69.4)	263 (78.3)	0.07
Reduced intensity	103 (23.7)	30 (30.6)	73 (21.7)	
Total body irradiation, n (%)	178 (41)	26 (26.5)	152 (45.2)	<0.001
Additional GvHD prophylaxis, n (%)				
Cyclosporine/MTX	23 (5.4)	14 (14.9)	9 (2.7)	NA
Cyclosporine/MMF	205 (47.3)	4 (4.3)	201 (59.8)	
Tacrolimus/MMF	88 (20.6)	3 (3.2)	85 (25.5)	
Sirolimus/MMF	29 (6.8)	21 (22.3)	8 (2.4)	
Cyclosporine/MMF/MTX	45 (10.5)	40 (42.5)	5 (1.5)	
MTX				
Cyclosporine	16 (3.8)	6 (6.4)	10 (3)	
Tacrolimus	10 (2.3)	1 (1.1)	9 (2.7)	
Tacrolimus/sirolimus	4 (0.9)	1 (1.1)	3 (0.9)	
MMF	3 (0.7)	0	3 (0.9)	
Sirolimus	1 (0.2)	1 (1.1)	0	
Tacrolimus/MMF/MTX	3 (0.7)	3 (3.2)	0	
Missing	7	4	3	
Graft source, n (%)				
Bone marrow	206 (47.5)	31 (31.6)	175 (52.1)	<0.001
Peripheral blood	228 (52.5)	67 (68.4)	161 (47.9)	
Donors' age in years, median (range)	40.2 (8-74)	43.4 (18-74)	39.7 (8-74)	0.38
Female D → male R*, n (%)	122 (28.2)	30 (30.6)	92 (27.5)	0.55
D7R CMV status, n (%)				
Negative/negative	57 (13.5)	19 (20.2)	38 (11.6)	0.19
Positive/negative	39 (9.3)	9 (9.6)	30 (9.2)	
Negative/positive	59 (14)	12 (12.8)	47 (14.4)	
Positive/positive	266 (63.2)	54 (57.5)	212 (64.8)	
Missing	13	4	9	
Year of transplant, median (range)	2015 (2007-2017)	2011 (2007-2017)	2015 (2008-2017)	<0.0001
Follow-up in months, median (range)	24.4 (12-40)	55 (14-79)	22 (12-37)	

*Data on sex missing for two patients. GvHD: graft-versus-host disease; ATG: anti-thymocyte globulin; PTCy: post-transplant cyclophosphamide; ALL: acute lymphoblastic leukemia; Ph: Philadelphia chromosome; CR1: first complete remission; CR2: second complete remission; r/r: relapsed/refractory; KPS: Karnofsky Performance Score; MTX: methotrexate; MMF: mycophenolate mofetil; NA: not available; D: donor; R: recipient; CMV: cytomegalovirus.

Acute and chronic graft-versus-host disease

The cumulative incidence of grade II-IV acute GvHD at day 100 (Table 2) in the ATG group was 32.7% (95% CI: 23.4-42.3) compared to 30.5% (95% CI: 25.5-35.6) in the PTCy group ($P=0.37$). The corresponding rates of severe (grades III-IV) acute GvHD were 11.6% (95% CI: 6.1-18.9) and 14.1% (95% CI: 10.6-18.2) in the ATG and PTCy groups respectively ($P=0.56$). On multivariate analy-

sis (Table 3) there was no difference in the risk of grade II-IV acute GvHD in the ATG group relative to the PTCy group ($HR=0.92$, 95% CI: 0.55-1.51; $P=0.73$). Independently of the GvHD prevention strategy, on multivariate analysis, the use of peripheral blood allografts was associated with higher rates of grade II-IV acute GvHD ($HR=1.64$, 95% CI: 1.06-2.53; $P=0.03$), whereas a diagnosis of T-ALL ($HR=0.52$, 95% CI: 0.32-0.85; $P=0.008$) and reduced intensity conditioning ($HR=0.57$, 95% CI: 0.34-0.97) were associated with a lower risk (Table 3).

The cumulative incidence of chronic GvHD at 2 years after haploidentical transplantation was 27.7% (95% CI: 17.8-38.5) and 31.7% (95% CI: 26.1-37.4) in the ATG and PTCy groups, respectively (Table 2). The corresponding incidences of extensive chronic GvHD were 7.8% (95% CI: 3.1-15.2) and 12.1% (95% CI: 8.4-16.5), respectively ($P=0.37$). Multivariate analysis (Table 3) showed no difference in chronic GvHD outcomes between the two groups ($HR=0.79$, 95% CI: 0.38-1.64; $P=0.52$). The use of peripheral blood as the graft source was associated with a higher risk of chronic GvHD ($HR=1.82$, 95% CI: 1.03-3.23; $P=0.04$), independently of the GvHD prevention used. Recipient cytomegalovirus seropositive status was associated with a lower risk of chronic GvHD ($HR=0.52$, 95% CI: 0.3-0.9; $P=0.02$).

Non-relapse mortality and relapse

Among the ALL patients who underwent haploidentical transplantation, the 2-year non-relapse mortality was

Table 2. Post-transplant outcomes (unadjusted) by graft-versus-host disease prevention strategy.

Post-transplant outcomes*	ATG (95% CI)	PTCy (95% CI)	P-value
Engraftment	91.7% (83.7-95.8)	92.5% (89-95)	0.11
Acute GvHD II-IV	32.7% (23.4-42.3)	30.5% (25.5-35.6)	0.37
Acute GvHD III-IV	11.6% (6.1-18.9)	14.1% (10.6-18.2)	0.56
Chronic GvHD	27.7% (17.8-38.5)	31.7% (26.1-37.4)	0.58
Extensive chronic GvHD	7.8% (3.1-15.2)	12.1% (8.4-16.5)	0.37
Relapse incidence	43% (32-53.5)	33.8% (28.1-39.5)	0.11
Non-relapse mortality	32.9% (23.1-43.1)	26.7% (21.8-31.8)	0.23
Leukemia free survival	24.1% (14.5-33.8)	39.6% (33.6-45.5)	0.007
Overall survival	27.4% (17.4-37.3)	48.4% (42.3-54.6)	0.001
GvHD/relapse-free survival	20% (10.9-29.1)	31.8% (26.2-37.5)	0.04

*All outcomes are at 2 years except for acute graft-versus-host disease which is at 100 days after transplantation. ATG: anti-thymocyte globulin; PTCy: post-transplant cyclophosphamide; 95% CI: 95% confidence interval; GvHD: graft-versus-host disease.

Table 3. Multivariate analysis of post-transplant outcomes and baseline variables.

Post-transplant outcomes	PTCy vs. ATG	Ph ⁺ B-ALL	T-ALL	Age (per 10 years)	≥CR2	Advanced	KPS ≥ 90	RIC vs. MAC	PB vs. BM	Female (D) → male (R)	CMV (R) +	CMV (D) -	TBI vs. Center chemo
Relapse													
HR (95% CI)	0.61 (0.39-0.94)	0.66 (0.39-1.12)	1.05 (0.69-1.6)	0.97 (0.83-1.14)	2.06 (1.32-3.21)	4.99 (3.13-7.93)	0.98 (0.65-1.48)	1.08 (0.67-1.74)	0.971 (0.66-1.44)	0.84 (0.56-1.27)	1.14 (0.70-1.87)	0.92 (0.59-1.43)	0.97 (0.67-1.42)
P-value	0.03	0.12	0.81	0.72	0.001	<10-5	0.93	0.74	0.88	0.42	0.59	0.7	0.88 0.39
NRM													
HR (95% CI)	0.68 (0.42-1.11)	1.26 (0.76-2.1)	1.04 (0.62-1.74)	1.1 (0.94-1.3)	1.71 (1.07-2.72)	1.82 (1.02-3.24)	0.46 (0.30-0.7)	0.97 (0.59-1.6)	1.48 (0.97-2.26)	0.76 (0.47-1.22)	0.90 (0.53-1.55)	1.33 (0.82-2.23)	0.59 (0.38-0.92)
P-value	0.12	0.37	0.88	0.24	0.02	0.04	0.0003	0.91	0.07	0.25	0.71	0.27	0.02 0.43
LFS													
HR (95% CI)	0.67 (0.46-0.97)	0.94 (0.63-1.35)	1.06 (0.76-1.5)	1.04 (0.93-1.17)	1.91 (1.37-2.66)	3.35 (2.3-4.88)	0.68 (0.5-0.93)	1.06 (0.74-1.52)	1.06 (0.76-1.46)	0.8 (0.58-1.1)	0.95 (0.65-1.39)	1.11 (0.78-1.57)	0.79 (0.58-1.07)
P-value	0.03	0.69	0.72	0.48	0.0001	<10-5	0.01	0.75	0.75	0.16	0.81	0.56	0.13 0.16
OS													
HR (95% CI)	0.6 (0.42-0.84)	0.92 (0.63-1.35)	1.06 (0.75-1.49)	1.07 (0.95-1.2)	1.88 (1.33-2.64)	3.13 (2.15-4.55)	0.61 (0.45-0.827)	0.96 (0.68-1.38)	1.29 (0.96-1.75)	0.75 (0.54-1.04)	1.07 (0.73-1.58)	1.17 (0.82-1.66)	0.78 (0.58-1.06)
P-value	0.003	0.67	0.75	0.26	0.0003	<10-5	0.001	0.84	0.09	0.08	0.73	0.4	0.12 0.91
GRFS													
HR (95% CI)	0.79 (0.57-1.11)	0.88 (0.62-1.24)	1 (0.72-1.35)	1 (0.90-1.11)	1.42 (1.05-1.92)	2.45 (1.73-3.47)	0.77 (0.58-1.02)	0.94 (0.68-1.31)	1.18 (0.89-1.57)	0.97 (0.73-1.31)	1.05 (0.75-1.49)	1.08 (0.79-1.49)	0.87 (0.66-1.15)
P-value	0.17	0.47	0.94	0.96	0.02	<10-5	0.07	0.71	0.26	0.85	0.77	0.63	0.34 0.24
Acute GvHD II-IV													
HR (95% CI)	0.92 (0.55-1.51)	1.09 (0.68-1.77)	0.52 (0.32-0.85)	0.86 (0.73-1.01)	0.98 (0.63-1.54)	1.71 (0.98-2.99)	1.15 (0.73-1.81)	0.57 (0.34-0.97)	1.64 (1.06-2.53)	1.36 (0.9-2.06)	1.11 (0.64-1.94)	1.29 (0.78-2.15)	1.26 (0.83-1.92)
P-value	0.73	0.72	0.008	0.06	0.94	0.06	0.55	0.04	0.03	0.14	0.72	0.32	0.28 0.12
chronic GvHD													
HR (95% CI)	0.79 (0.38-1.64)	0.83 (0.45-1.53)	0.63 (0.35-1.16)	0.89 (0.74-1.07)	0.95 (0.56-1.6)	0.77 (0.35-1.68)	0.69 (0.41-1.17)	0.65 (0.33-1.26)	1.82 (1.03-3.23)	1.26 (0.77-2.07)	0.52 (0.3-0.9)	1.11 (0.63-1.97)	0.93 (0.54-1.58)
P-value	0.52	0.55	0.14	0.22	0.83	0.51	0.17	0.20	0.04	0.35	0.02	0.71	0.77 0.02

PTCy: post-transplant cyclophosphamide; ATG: anti-thymocyte globulin; Ph: Philadelphia chromosome; ALL: acute lymphoblastic leukemia; ≥CR2: second complete remission or beyond; KPS: Karnofsky Performance Score; RIC: reduced intensity conditioning; MAC: myeloablative conditioning; PB: peripheral blood graft; BM: bone marrow graft; D: donor; R: recipient; CMV: cytomegalovirus; TBI: total body irradiation; NRM: non-relapse mortality; LFS: leukemia-free survival; OS: overall survival; GRFS: GvHD-free/relapse-free survival; GvHD: graft-versus-host disease.

32.9% (95% CI: 23.1-43.1) and 26.7% (95% CI: 21.8-31.8) in the ATG and PTCy groups, respectively ($P=0.23$) (Table 2). On multivariate analysis, there was no significant difference in non-relapse mortality between the groups ($HR=0.68$, 95% CI: 0.42-1.11; $P=0.12$). Independently of whether patients received ATG or PTCy as GvHD prophylaxis, pre-transplant status of being in second or further complete remission or having advanced disease was associated with higher rates of non-relapse mortality (Table 3). A Karnofsky Performance Score ≥ 90 was associated with a lower non-relapse mortality rate ($HR=0.46$, 95% CI: 0.30-0.7; $P=0.0003$). Use of TBI in conditioning was associated with lower non-relapse mortality ($HR=0.59$, 95% CI: 0.38-0.92; $P=0.02$) compared to regimens containing only chemotherapy.

The cumulative incidence of ALL relapse at 2 years was similar between the ATG and PTCy groups, being 43% (95% CI: 32-53.5) and 33.8% (95% CI: 28.1-39.5), respectively ($P=0.11$) (Table 2). On multivariate analysis, PTCy as GvHD prophylaxis was associated with a lower risk of

relapse ($HR=0.61$, 95% CI: 0.39-0.94; $P=0.03$). Disease status, i.e. being in second complete remission or beyond ($HR=2.06$, 95% CI: 1.32-3.21; $P=0.001$) or having advanced ALL ($HR=4.99$, 95% CI: 3.13-7.93; $P<10^{-5}$) were noted to be independent risk factors for post-transplant relapse (Table 3). Figure 1A and B show the adjusted non-relapse mortality and relapse incidence in the ATG and PTCy groups, respectively.

Survival

With a median follow-up of 24 months, the 2-year leukemia-free survival rates in the ATG and PTCy groups were 24.1% (95% CI: 14.5-33.8) and 39.6% (95% CI: 33.6-45.5), respectively ($P=0.007$) (Table 2). On multivariate analysis (Table 3), relative to the ATG group, patients in the PTCy group had a lower risk of therapy failure (the inverse of leukemia-free survival) ($HR=0.67$, 95% CI: 0.46-0.97; $P=0.03$). Independently of the GvHD prevention strategy, a disease status of second complete remission or beyond ($HR=1.91$, 95% CI: 1.37-2.66; $P=0.0001$) and

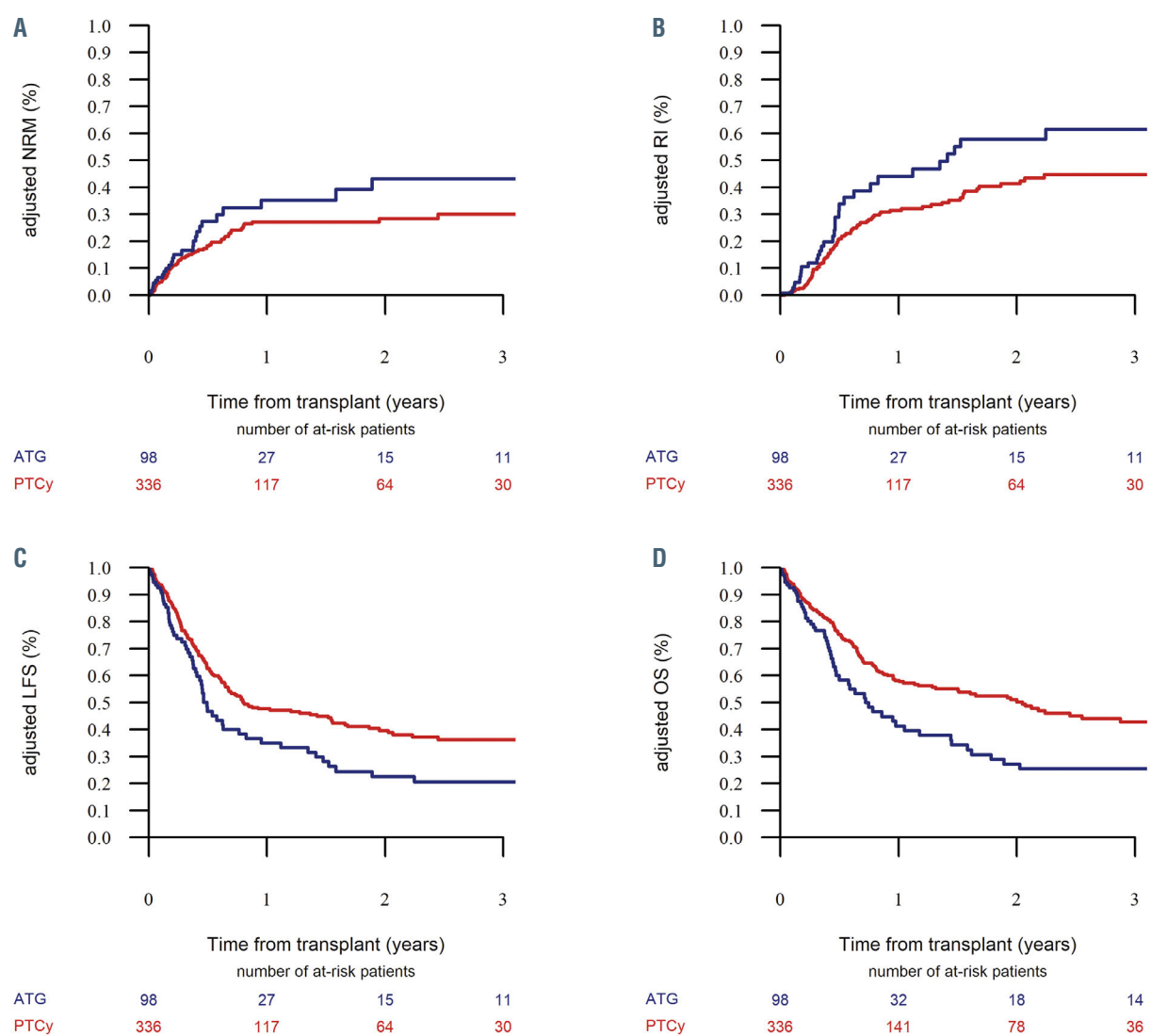


Figure 1. Adjusted outcomes of patients with acute lymphoblastic leukemia undergoing haploidentical transplantation stratified by type of graft-versus-host disease prophylaxis. Data for recipients of anti-thymocyte globulin are shown in blue, those for recipients of post-transplant cyclophosphamide are shown in red. (A) Adjusted incidence of non-relapse mortality (NRM). (B) Adjusted relapse incidence (RI). (C) Adjusted estimates of leukemia-free survival (LFS), (D) Adjusted estimates of overall survival (OS).

advanced ALL (HR=3.35, 95% CI: 2.3-4.88; $P<10^{-5}$) were associated with an increased risk of therapy failure, whereas a Karnofsky Performance Score ≥ 90 was associated with better leukemia-free survival (HR=0.68, 95% CI: 0.5-0.93; $P=0.01$). Figure 1C shows the adjusted leukemia-free survival in the ATG and PTCy groups.

The 2-year overall survival rates were 27.4% (95% CI: 17.4-37.3) in the ATG group and 48.4% (95% CI: 42.3-54.6) in the PTCy group ($P=0.001$) (Table 2, Figure 1D). On multivariate analysis (Table 3), PTCy prophylaxis was associated with better survival compared to ATG prophylaxis (HR=0.6, 95% CI: 0.42-0.82; $P=0.003$). Independently of the GvHD prevention strategy, disease status of second complete remission or beyond (HR=1.88, 95% CI: 1.33-2.64; $P=0.0003$) and advanced ALL (HR=3.13, 95% CI: 2.15-4.55; $P<10^{-5}$) were associated with lower survival, whereas a Karnofsky Performance Score ≥ 90 was associated with improved overall survival (HR=0.96, 95% CI: 0.68-1.38; $P=0.001$). Figure 1D shows adjusted overall survival in the ATG and PTCy groups.

The 2-year GRFS rates in the ATG and PTCy groups were 20% (95% CI: 10.9-29.1) and 31.8% (95% CI: 26.2-37.5), respectively ($P=0.04$) (Table 2). On multivariate analysis there was no significant difference in GRFS between the ATG and PTCy groups ($P=0.17$) (Table 3). However, disease status of second complete remission or beyond (HR=1.42, 95% CI: 1.05-1.92; $P=0.02$) and advanced ALL (HR=2.45, 95% CI: 1.73-3.47; $P<10^{-5}$) were associated with a worse GRFS, whereas a Karnofsky Performance Score ≥ 90 was associated with a better GRFS (HR=0.77, 95% CI: 0.58-1.02; $P=0.07$).

Causes of death

At last follow-up, a total of 225 patients had died, including 66 patients in the ATG group (67.3%) and 159 patients (47.3%) in the PTCy group (Table 4). The three most common causes of death in the ATG and PTCy groups were ALL relapse (36.5% vs. 38.1%), GvHD (19.1% vs. 14.2%) and infections (31.8% vs. 30.3%). In the PTCy group, veno-occlusive disease and graft failure was the cause of death in six (3.9%) and three (1.9%) patients, respectively, while in the ATG group no death was attributed to these. Secondary malignancy as a cause of death was limited to one patient in the entire cohort (in the PTCy group).

Discussion

GvHD prevention strategies such as ATG, and more recently PTCy, accompanying unmanipulated haploidentical allografts have reinvigorated and ushered in a new era of haploidentical HCT for hematologic malignancies. While ATG is directed against a wide range of epitopes, thus allowing extensive T-cell depletion,^{24,25} PTCy selectively targets alloreactive T cells rapidly proliferating early after an HLA-mismatched transplant, without affecting the non-dividing hematopoietic progenitor cells.^{12,26} In this study we compared post-transplant outcomes in adult patients with ALL undergoing haploidentical HCT using ATG or PTCy platforms as GvHD prophylaxis and made some important observations. First, no differences in outcome related to acute GvHD, chronic GvHD and non-relapse mortality were seen between the ATG and PTCy groups. Second, relapse risk was signifi-

Table 4. Causes of death in patients with acute lymphoblastic leukemia undergoing haploidentical transplantation with anti-thymocyte globulin or post-transplant cyclophosphamide as graft-versus-host disease prophylaxis.

Cause of Death	ATG N=66 (%)	PTCy N=159 (%)
ALL relapse	23 (37.1)	59 (38.6)
Graft-versus-host disease	12 (19.4)	22 (14.4)
Infection	21 (33.9)	49 (32.0)
Veno-occlusive disease	0	6 (3.9)
Failure/rejection	0	3 (2.0)
Cardiac toxicity	1 (1.6)	0
Secondary malignancy	0	2 (1.3)
Hemorrhage	1 (1.6)	4 (2.6)
Interstitial pneumonitis	2 (3.2)	5 (3.3)
Multi-organ failure	2 (3.2)	3 (2.0)
Missing	4	6

ATG: anti-thymocyte globulin; PTCy: post-transplant cyclophosphamide; ALL: acute lymphoblastic leukemia.

cantly higher among patients who received ATG than in those who received PTCy. Third, leukemia-free survival and overall survival were both significantly better in patients treated with PTCy than in those treated with ATG, but there was no difference in GRFS between the groups.

The cumulative incidences of GvHD, including grade II-IV acute GVHD, grade III-IV (severe) acute GvHD and chronic GvHD were similar in the ATG and PTCy groups. The incidence of severe acute GvHD in the ATG group (11.6%) is comparable to the incidences in previous observational studies.^{11,25} Interestingly, in the ALL-specific prospective study by Wang *et al.*, the incidence of severe acute GvHD was only 6% in the group that underwent haploidentical HCT with ATG prophylaxis.²⁷ The incidence of severe acute GvHD in the PTCy group in this study (14.6%) is higher than the previously reported 4-5%.^{12,15} The higher incidence of acute GvHD may be related to the substantial proportions of patients in this study who were given myeloablative conditioning (76%), TBI (41%), and peripheral blood products (52%) and had advanced disease (20%) at the time of HCT, compared to the proportions in other studies. However, the incidences of chronic GvHD in the ATG (28%) and PTCy (32%) groups are comparable to those in prior reports.^{11,25,27} It is noteworthy that additional immunosuppression in the ATG group consisted predominantly of cyclosporine/methotrexate/mycophenolate (42.5%) or sirolimus/mycophenolate (22.3%), whereas in the PTCy group 85% of the patients received a calcineurin inhibitor (cyclosporine or tacrolimus) with mycophenolate (Table 1).

The incidences of non-relapse mortality in the ATG and PTCy groups were similar (33% vs. 27%, respectively), likely reflecting the similarity in GvHD incidences as noted above. The major causes of non-relapse mortality in both groups were GvHD and infection. Interestingly, in the PTCy group, six patients died of veno-occlusive disease presumably related to myeloablative conditioning with TBI, and three patients from graft failure likely due to more bone marrow grafts being used in this group. However, on multivariate analysis, only advanced disease state (relapsed beyond second complete remission and refractory ALL) was an independent predictor of poor

non-relapse mortality. Although most patients received ablative doses of TBI, a lower non-relapse mortality was associated with TBI-based conditioning compared to chemotherapy alone (HR=0.59; $P=0.02$). An explanation for this intriguing observation is unknown, but it is possible that younger patients with better performance scores and co-morbidity indices were more likely to receive ablative TBI. It should be noted that previous EBMT reports have indeed suggested better leukemia-free survival related to TBI use in ALL patients, but this was due to a lower relapse incidence and not to a decrease in non-relapse mortality.²⁸⁻³⁰

With respect to post-transplant relapse, a statistically significant, 10% absolute improvement was noted in favor of PTCy compared to the ATG group. It is likely that the higher risk of relapse in the ATG group was driven by the higher proportion of patients with advanced ALL (30%). Indeed, advanced disease status was a strong independent predictor of ALL relapse. Given the unique biology of ALL it is also possible that, as fewer patients given ATG received TBI as part of their conditioning, this may have increased the relapse incidence in this group, although not to a statistically significant extent.^{28,29,31} Disease relapse was the most common cause of death in both groups, highlighting the need for further studies on mitigating post-transplant ALL relapse.

In univariate analysis, improved leukemia-free survival, overall survival and GRFS rates were noted in the PTCy group compared to ATG group ($P<0.05$), however, in multivariate analysis, only leukemia-free survival and overall survival remained significantly improved. This could perhaps be due to a higher proportion of patients with advanced disease together with the higher relapse incidence in the ATG group. Indeed, the leukemia-free survival in the ATG group in this study was inferior to that in the prospective study by Wang *et al.*, possibly due to the greater proportion of patients in this study with advanced age and disease status.²⁷ Nevertheless, 15% and 20% improvements in leukemia-free survival and overall survival, respectively, were noted in the PTCy group. For both these outcome measures, disease status at the time of haploidentical HCT and Karnofsky Performance Score were strong independent predictors of survival. Albeit limited by the small sample size, a subset analysis evaluating outcomes stratified by graft source (peripheral blood *vs.* bone marrow) showed interesting results (*Online Supplementary Table S2*). In peripheral blood haploidentical HCT recipients, the 2-year leukemia-free survival, overall survival and GRFS rates were significantly better in the PTCy group, in which there was also a trend toward lower non-relapse mortality. It is worth noting that the relapse risk was similar in the ATG and PTCy groups in peripheral blood haploidentical graft recipients. In contrast, for bone marrow haploidentical HCT, no differences were noted in leukemia-free survival, overall survival, GRFS or non-relapse mortality between the ATG and PTCy groups. However, the 2-year relapse incidence among bone marrow graft recipients receiving ATG prophylaxis was 55% compared to 33.7% with PTCy prophylaxis ($P=0.06$). Although not statistically significant, it

is plausible that the inferior relapse and survival outcomes in the ATG group are at least partly due to the high relapse risk in the bone marrow graft recipients.³²

The inherent limitations of this study are reflected by the nature of the data captured by a registry. Detailed information regarding remission status, such as minimal residual disease, and conditioning regimen, including TBI dose and the timing and dose of PTCy and ATG administration, were not uniformly available. For instance, details pertaining to the type of ATG product (thymoglobulin *vs.* ATG-Fresenius) were unavailable in the registry. The dose of ATG was documented for only 81 subjects, with the median dose being 20 mg/kg. By univariate analysis, the only impact of ATG dose (< or ≥ 20 g/kg) on transplant outcomes, was a lower incidence of grade II-IV acute GvHD associated with a higher ATG dose (23% *vs.* 53%; $P=0.007$) (*Online Supplementary Table S3*). The registry data precluded evaluation of the reason for choosing a specific graft source, GvHD prophylaxis platform or conditioning regimen for an individual patient. Haploidentical HCT with ATG was more likely during an earlier time period compared to PTCy (median, 2011 *vs.* 2015). It is, therefore, possible that improvements in transplant technology and supportive care may have had an impact on these outcomes. To address this potential bias, we performed a univariate analysis restricted to the years 2007-2014, and found that the use of PTCy as GvHD prophylaxis was still associated with improved leukemia-free and overall survival (*data not shown*), congruent with results for the entire study duration. As expected, institutional practices and preferences may skew the data. However, no “center effect” was noted except for chronic GvHD by regression analysis. The sample size limited the power to detect small differences and interactions between variables and transplant outcomes in our population. With a median follow-up of approximately 2 years, it is not known whether these results will remain unchanged with longer-term follow-up. Notwithstanding these limitations, this analysis is the largest and only comparative study evaluating outcomes of haploidentical allogeneic HCT in adult ALL patients given PTCy or ATG as the backbone of their GvHD prophylaxis. It is noteworthy that, compared to ATG, PTCy as GvHD prophylaxis was associated with improved leukemia-free survival and overall survival and lower relapse risk.

In conclusion, in the absence of prospective, randomized data, our results suggest that PTCy as GvHD prophylaxis may be considered over ATG in patients with ALL undergoing haploidentical HCT. Our data warrant confirmation in prospective randomized studies.

Disclosures

No conflicts of interest to disclose.

Contributions

AN and MM conceived and designed the study; ML collected, assembled and analyzed data; ASK, AN and ML prepared the first draft of the manuscript; and all authors contributed to data interpretation, helped revise the manuscript, and gave final approval of the manuscript.

References

1. Juliusson G, Karlsson K, Lazarevic VL, et al. Hematopoietic stem cell transplantation rates and long-term survival in acute myeloid and lymphoblastic leukemia. *Cancer*. 2011;117(18):4238-4246.
2. Fielding AK, Richards SM, Chopra R, et al. Outcome of 609 adults after relapse of acute lymphoblastic leukemia (ALL); an MRC UKALL12/ECOG 2993 study. *Blood*. 2007; 109(3):944.
3. Gupta V, Richards S, Rowe J. Allogeneic, but not autologous, hematopoietic cell transplantation improves survival only among younger adults with acute lymphoblastic leukemia in first remission: an individual patient data meta-analysis. *Blood*. 2013; 121(2):339.
4. D'Souza A, Lee S, Zhu X, Pasquini M. Current use and trends in hematopoietic cell transplantation in the United States. *Biol Blood Marrow Transplant*. 2017;23(9):1417-1421.
5. Mancusi A, Ruggeri L, Velardi A. Haploidentical hematopoietic transplantation for the cure of leukemia: from its biology to clinical translation. *Blood*. 2016;128 (23):2616.
6. Henslee-Downey P, Parrish R, MacDonald J, et al. Combined in vitro and in vivo T lymphocyte depletion for the control of graft-versus-host disease following haploidentical marrow transplant. *Transplantation*. 1996; 61(5):738-745.
7. Dodero A, Carniti C, Raganato A, et al. Haploidentical stem cell transplantation after a reduced-intensity conditioning regimen for the treatment of advanced hematologic malignancies: posttransplantation CD8-depleted donor lymphocyte infusions contribute to improve T-cell recovery. *Blood*. 2009;113(19):4771-4779.
8. Kanda Y, Oshima K, Asano-Mori Y, et al. In-vivo alemtuzumab enables haploidentical human leukocyte antigen-mismatched hematopoietic stem-cell transplantation without ex vivo graft manipulation. *Transplantation*. 2005;79(10):1351-1357.
9. Aversa F, Terenzi A, Tabilio A, et al. Full haplotype-mismatched hematopoietic stem-cell transplantation: a phase II study in patients with acute leukemia at high risk of relapse. *J Clin Oncol*. 2005;23(15):3447-3454.
10. Lu D-P, Dong L, Wu T, et al. Conditioning including antithymocyte globulin followed by unmanipulated HLA-mismatched/haploidentical blood and marrow transplantation can achieve comparable outcomes with HLA-identical sibling transplantation. *Blood*. 2006;107(8):3065.
11. Wang Y, Liu D-H, Liu K-Y, et al. Long-term follow-up of haploidentical hematopoietic stem cell transplantation without in vitro T cell depletion for the treatment of leukemia. *Cancer*. 2013;119(5):978-985.
12. Luznik L, Jalla S, Engstrom L, Iannone R, Fuchs E. Durable engraftment of major histocompatibility complex-incompatible cells after nonmyeloablative conditioning with fludarabine, low-dose total body irradiation, and posttransplantation cyclophosphamide. *Blood*. 2001;98(12):3456-3464.
13. O'Donnell P, Luznik L, Jones R, et al. Nonmyeloablative bone marrow transplantation from partially HLA-mismatched related donors using posttransplantation cyclophosphamide. *Biol Blood Marrow Transplant*. 2002;8(7):377-386.
14. Santoro N, Ruggeri A, Labopin M, et al. Unmanipulated haploidentical stem cell transplantation in adults with acute lymphoblastic leukemia: a study on behalf of the Acute Leukemia Working Party of the EBMT. *J Hematol Oncol*. 2017;10(1):113.
15. Srour SA, Milton DR, Bashey A, et al. Haploidentical transplantation with posttransplantation cyclophosphamide for high-risk acute lymphoblastic leukemia. *Biol Blood Marrow Transplant*. 2017;23(2):318-324.
16. Iskra Pusic, Steven Z. Pavletic. Challenges in conducting studies in chronic graft-versus-host disease. *Clin Hematol Int*. 2019;1(1):36-44.
17. Holtan SG, DeFor TE, Lazaryan A, et al. Composite end point of graft-versus-host disease-free, relapse-free survival after allogeneic hematopoietic cell transplantation. *Blood*. 2015;125(8):1333-1338.
18. Ruggeri A, Labopin M, Ciceri F, Mohty M, Nagler A. Definition of GvHD-free, relapse-free survival for registry-based studies: an ALWP-EBMT analysis on patients with AML in remission. *Bone Marrow Transplantation*. 2015;51(4):610.
19. Przepiorka D, Weisdorf D, Martin P, et al. 1994 Consensus Conference on Acute GVHD Grading. *Bone Marrow Transplant*. 1995;15(6):825-828.
20. Lee SJ, Vogelsang G, Flowers MED. Chronic graft-versus-host disease. *Biol Blood Marrow Transplant*. 2003;9(4):215-233.
21. Bacigalupo A, Ballen K, Rizzo D, et al. Defining the intensity of conditioning regimens: working definitions. *Biol Blood Marrow Transplant*. 2009;15(12):1628-1633.
22. Hougaard P. Frailty models for survival data. *Lifetime Data Anal*. 1995;1(3):255-273.
23. Andersen PK, Klein JP, Zhang M-J. Testing for centre effects in multi-centre survival studies: a Monte Carlo comparison of fixed and random effects tests. *Stat Med*. 1999;18(12):1489-1500.
24. Mohty M, Bacigalupo A, Saliba F, et al. New directions for rabbit antithymocyte globulin (Thymoglobulin®) in solid organ transplants, stem cell transplants and autoimmunity. *Drugs*. 2014;74(14):1605-1634.
25. Ruggeri A, Sun Y, Labopin M, et al. Post-transplant cyclophosphamide versus anti-thymocyte globulin as graft-versus-host disease prophylaxis in haploidentical transplant. *Haematologica*. 2017;102(2):401.
26. Kanakry C, Ganguly S, Zahurak M, et al. Aldehyde dehydrogenase expression drives human regulatory T cell resistance to post-transplantation cyclophosphamide. *Sci Transl Med*. 2013;5(21):211ra157.
27. Wang Y, Liu Q-F, Xu L-P, et al. Haploidentical versus matched-sibling transplant in adults with Philadelphia-negative high-risk acute lymphoblastic leukemia: a biologically phase III randomized study. *Clin Cancer Res*. 2016;22(14):3467.
28. Giebel S, Labopin M, Socié G, et al. Improving results of allogeneic hematopoietic cell transplantation for adults with acute lymphoblastic leukemia in first complete remission: an analysis from the Acute Leukemia Working Party of the European Society for Blood and Marrow Transplantation. *Haematologica*. 2017;102 (1):139-149.
29. Pavlù J, Labopin M, Zoellner AK, et al. Allogeneic hematopoietic cell transplantation for primary refractory acute lymphoblastic leukemia: a report from the Acute Leukemia Working Party of the EBMT. *Cancer*. 2017;123(11):1965-1970.
30. Rashmi R, Poddar, Sorab Gupta, Sebastian Giebel, et al. Current status and perspectives of irradiation-based conditioning regimens for patients with acute leukemia undergoing hematopoietic stem cell transplantation. *Clin Hematol Int*. 2019;1(1):19-27.
31. Eder S, Canaani J, Beohou E, et al. Thiopeta-based conditioning versus total body irradiation as myeloblastic conditioning prior to allogeneic stem cell transplantation for acute lymphoblastic leukemia: a matched-pair analysis from the Acute Leukemia Working Party of the European Society for Blood and Marrow Transplantation. *Am J Hematol*. 2017;92(10):997-1003.
32. Nagler A, Labopin M, Shimoni A, et al. Mobilized peripheral blood stem cells compared with bone marrow as the stem cell source for unrelated donor allogeneic transplantation with reduced-intensity conditioning in patients with acute myeloid leukemia in complete remission: an analysis from the Acute Leukemia Working Party of the European Group for Blood and Marrow Transplantation. *Biol Blood Marrow Transplant*. 2012;18(9):1422-1429.

Allogeneic hematopoietic cell transplantation with non-myeloablative conditioning for patients with hematologic malignancies: improved outcomes over two decades



Ferrata Storti Foundation

Jason P. Cooper,^{1,2} Barry E. Storer,^{1,2} Noa Granot,¹ Boglarka Gyurkocza,^{1,2*} Mohamed L. Sorror,^{1,2} Thomas R. Chauncey,^{1,2,3} Judith Shizuru,⁴ Georg-Nikolaus Franke,⁵ Michael B. Maris,⁶ Michael Boyer,⁷ Benedetto Bruno,⁸ Firoozeh Sahebi,⁹ Amelia A. Langston,¹⁰ Parameswaran Hari,¹¹ Edward D. Agura,¹² Søren Lykke Petersen,¹³ Richard T. Maziarz,¹⁴ Wolfgang Bethge,¹⁵ Julie Asch,¹⁶ Jonathan A. Gutman,¹⁷ Gitte Olesen,¹⁸ Andrew M. Yeager,¹⁹ Kai Hübel,²⁰ William J. Hogan,²¹ David G. Maloney,^{1,2} Marco Mielcarek,^{1,2} Paul J. Martin,^{1,2} Mary E. D. Flowers,^{1,2} George E. Georges,^{1,2} Ann E. Woolfrey,^{1,2} H. Joachim Deeg,^{1,2} Bart L. Scott,^{1,2} George B. McDonald,^{1,2} Rainer Storb^{1,2} and Brenda M. Sandmaier^{1,2}

Haematologica 2021

Volume 106(6):1599-1607

¹Fred Hutchinson Cancer Research Center, Seattle, WA, USA; ²University of Washington, Seattle, WA, USA; ³Veterans Affairs Puget Sound Health Care System, Seattle, WA, USA; ⁴Stanford University, Palo Alto, CA, USA; ⁵University of Leipzig, Leipzig, Germany; ⁶Colorado Blood Cancer Institute at HealthONE Presbyterian/St. Luke Medical Center, Denver, CO, USA; ⁷University of Utah, Salt Lake City, UT, USA; ⁸University of Turin, Turin, Italy; ⁹City of Hope/Kaiser Permanente Medical Group, Duarte, CA, USA; ¹⁰Winship Cancer Institute at Emory University, Atlanta, GA, USA; ¹¹Medical College of Wisconsin, Milwaukee, WI, USA; ¹²Baylor University, Dallas, TX, USA; ¹³University of Copenhagen Rigshospitalet, Copenhagen, Denmark; ¹⁴Oregon Health and Science University, Portland, OR, USA; ¹⁵University of Tübingen, Tübingen, Germany; ¹⁶LDS Hospital, Salt Lake City, UT, USA; ¹⁷University of Colorado, Denver, CO, USA; ¹⁸Aarhus University, Aarhus, Denmark; ¹⁹University of Arizona Cancer Center, Tucson, AZ, USA; ²⁰University Hospital of Cologne, Cologne, Germany and ²¹Mayo Clinic, Rochester, MN, USA

*Current address: Memorial Sloan Kettering Cancer Center and Weill Cornell Medical College, New York, NY, USA.

ABSTRACT

We have used a non-myeloablative conditioning regimen for allogeneic hematopoietic cell transplantation for the past 20 years. During that period, changes in clinical practice have been aimed at reducing morbidity and mortality from infections, organ toxicity, and graft-versus-host disease. We hypothesized that improvements in clinical practice led to better transplantation outcomes over time. From 1997–2017, 1,720 patients with hematologic malignancies received low-dose total body irradiation ± fludarabine or clofarabine before transplantation from HLA-matched sibling or unrelated donors, followed by mycophenolate mofetil and a calcineurin inhibitor ± sirolimus. We compared outcomes in three cohorts by year of transplantation: 1997–2003 (n=562), 2004–2009 (n=594), and 2010–2017 (n=564). The proportion of patients ≥60 years old increased from 27% in 1997–2003 to 56% in 2010–2017, and with scores from the Hematopoietic Cell Transplantation Comorbidity Index of ≥3 increased from 25% in 1997–2003 to 45% in 2010–2017. Use of unrelated donors increased from 34% in 1997–2003 to 65% in 2010–2017. When outcomes from 2004–2009 and 2010–2017 were compared to 1997–2003, improvements were noted in overall survival ($P=0.0001$ for 2004–2009 and $P\leq0.0001$ for 2010–2017), progression-free survival ($P=0.002$ for 2004–2009 and $P<0.0001$ for 2010–2017), non-relapse mortality ($P<0.0001$ for 2004–2009 and $P<0.0001$ for 2010–2017), and in rates of grades 2–4 acute and chronic graft-versus-host disease. For patients with hematologic malignancies who underwent transplantation with non-myeloablative conditioning, outcomes have improved during the past two decades. Trials reported are registered under clinicaltrials.gov. Identifiers: NCT00003145,

Correspondence:

JASON P. COOPER
jpc cooper@fredhutch.org

Received: January 27, 2020.

Accepted: May 27, 2020.

Pre-published: June 4, 2020.

<https://doi.org/10.3324/haematol.2020.248187>

©2021 Ferrata Storti Foundation

Material published in *Haematologica* is covered by copyright. All rights are reserved to the Ferrata Storti Foundation. Use of published material is allowed under the following terms and conditions: <https://creativecommons.org/licenses/by-nc/4.0/legalcode>. Copies of published material are allowed for personal or internal use. Sharing published material for non-commercial purposes is subject to the following conditions: <https://creativecommons.org/licenses/by-nc/4.0/legalcode>, sect. 3. Reproducing and sharing published material for commercial purposes is not allowed without permission in writing from the publisher.



NCT00003196, NCT00003954, NCT00005799, NCT00014235, NCT00027820, NCT00031655, NCT00060424, NCT00075478, NCT00078858, NCT00110058, NCT00397813, NCT00793572, NCT01231412, NCT01252667, NCT01527045.

Introduction

In 1997 we introduced a minimally intensive conditioning regimen for allogeneic hematopoietic cell transplantation (HCT) that enabled treating elderly and medically infirm younger patients with advanced hematologic malignancies in the outpatient setting. We previously reported outcomes for patients who underwent HCT from 1997–2009 using this regimen, which included low-dose total body irradiation (TBI) with or without fludarabine.¹ Five-year overall survival ranged from 25% to 60% (depending on disease type, comorbidities, and graft-versus-host disease [GvHD]), non-relapse mortality (NRM) was 24%, and relapse-related mortality was 35%. The most significant contributor to NRM was GvHD.

Between 1997 and 2017 a number of changes in clinical practice were introduced that were aimed at improving HCT outcomes including reductions in the use of systemic glucocorticoids as treatment for acute GvHD,^{2,3} use of ursodiol to reduce hepatic complications,^{4,5} addition of sirolimus for control of GvHD,⁶⁻⁸ use of fluoroquinolones for antibacterial prophylaxis during periods of neutropenia,⁹⁻¹¹ use of more mold-active azoles for antifungal prophylaxis,^{12,13} and initiation of pre-emptive antiviral therapy based on more sensitive polymerase chain reaction (PCR)-based cytomegalovirus (CMV) diagnostic testing.¹⁴⁻¹⁶

During the same time period, patient and donor characteristics as well as indications for HCT also changed. The proportion of patients older than 60 years increased from 27% to 56%, proportion of patients with hematopoietic cell transplantation-comorbidity index (HCT-CI)¹⁷ scores ≥ 3 increased from 25% to 45%, use of unrelated donors increased from 35% to 65%, and increasing numbers of patients underwent HCT for acute myeloid leukemia (AML) while decreasing numbers of patients underwent HCT for multiple myeloma and chronic myelogenous leukemia (CML). The current study analyzed whether benefits associated with the changes in clinical care for patients undergoing HCT outweighed the adverse outcomes expected from older patient age, increased comorbidities, and greater use of unrelated donors. To that end, we compared outcomes in three cohorts of patients by year of HCT: 1997–2003, 2004–2009, and 2010–2017.

Methods

Patients

Between December 16, 1997 and June 30, 2017, 1,720 consecutive patients with hematologic malignancies underwent HCT at the Fred Hutchinson Cancer Research Center (FHCRC) or collaborating centers. We included patients who were entered onto prospective clinical trials registered with clinicaltrials.gov at both FHCRC and collaborating centers (Online Supplementary Table S1), and patients transplanted outside of prospective trials at FHCRC. This study was approved by the Institutional Review Board (IRB) at FHCRC and all patients signed IRB-approved consents.

Graft source, conditioning, and post-engraftment immunosuppression

All patients received unmodified grafts consisting of granulocyte colony-stimulating factor (GCSF)-mobilized peripheral blood stem cells (PBSC). Donors and recipients were matched at HLA-A, -B, -C, -DRB1, and -DQB1 by high-resolution typing except for 104 unrelated donor-recipient pairs who were mismatched at the level of one HLA class I allele. Conditioning regimens and immunosuppression to aid engraftment and control GvHD are summarized in the *Online Supplementary Table S1*.

Clinical endpoints

Patients had bone marrow aspirations to assess disease status on days 28, 84, and 365 after HCT, and otherwise as clinically indicated. Acute and chronic GvHD were diagnosed and graded as previously described.^{18,19} Relapse was defined as recurrence of malignancy based on imaging, marrow morphology, flow cytometry, cytogenetics, and/or disease-specific molecular markers. Progression was defined as $\geq 50\%$ increase in disease burden.²⁰ Relapse-related mortality included deaths after relapse or progression of disease present before HCT, regardless of other events. NRM included deaths in the absence of relapse or progression.

Clinical assessment of organ complications and infections through day 100

Liver injury was assessed according to peak bilirubin concentration.¹⁹ Acute kidney injury was defined as a serum creatinine concentration that was at least 2-fold higher than the baseline value.²¹ CMV infection was defined as the presence of pp65 antigen or DNA in plasma,²² and CMV disease was defined as dysfunction of an organ infected by CMV.²³ One or more positive blood cultures for gram-negative bacteria were defined as gram-negative bacteremia; gram-negative organisms tend to cause the most serious infections in patients who are neutropenic after HCT.²⁴ Invasive fungal infections were defined according to consensus criteria and included cases deemed proven or probable.²⁵

Statistical analysis

Overall survival (OS) and progression-free survival (PFS) were estimated using the Kaplan-Meier method. Rates of acute and chronic GvHD, relapse or progression, and NRM were estimated according to standard methods.²⁶ Death was treated as a competing risk factor for all other time-to-event endpoints. Relapse was treated as a competing risk for NRM. Relapse-related mortality refers to survival after relapse among patients that relapsed. Multivariate Cox regression analysis of cause-specific hazards, stratified by center, was used for adjusted comparisons between groups defined by year of HCT. Adjusted estimates of survival and cumulative incidence were based on methods previously described.²⁷ Briefly, the adjusted curves represent the hypothetical outcomes for the three transplant eras if each era had the patient characteristics of the first era, based on results from the adjusted Cox regression models. Multivariate logistic regression was used for adjusted comparisons of rates of elevated bilirubin and creatinine. The adjusted models included the following variables that varied over era of HCT and were potentially related to one or more endpoints: treatment type (on-protocol, off-protocol); age (≤ 49 , 50–59, or ≥ 60 years); disease relapse risk (low, standard,

high); multiple myeloma diagnosis; AML diagnosis; CMV serostatus (recipient and donor negative, recipient and/or donor positive); donor relation (related, unrelated); sex mismatch (female to male, others); prior HCT (no, yes); HLA-allele mismatch (no, yes); HCT-CI (0, 1–2, 3, ≥4, or missing). All *P*-values were two-sided and are unadjusted for multiple comparisons.

Results

Study population

Our study population of 1,720 total patients in three tertiles is summarized in Table 1 and consisted of 562 patients who underwent HCT during the period from

Table 1. Transplant and patient characteristics by transplant era.

	1997–2003 (n = 562)		2004–2009 (n = 594)		2010–2017 (n = 564)		P
	n	%	n	%	n	%	
Transplant characteristics							
Conditioning regimen ^a							
TBI 2 Gy	127	33	99	17	53	9	
TBI 2 Gy + fludarabine	435	77	454	76	283	50	
TBI 3 Gy + fludarabine			37	6	173	31	
TBI 4–4.5 Gy + fludarabine			4	1	16	3	
TBI 2 Gy + clofarabine					40	7	
GVHD prophylaxis ^b							
CI + MMF	562	100	529	89	451	80	
CI + MMF + sirolimus			65	11	113	20	
Patient characteristics							
Center / treatment ^c							
Non-FH on-protocol	287	51	208	35	130	23	< 0.0001
FH on-protocol	264	47	327	55	333	59	
FH off-protocol	11	2	59	10	101	18	
Diagnosis							
ALL	17	3	30	5	45	8	< 0.0001
AML	90	16	184	31	167	30	
CLL	62	11	65	11	73	13	
CML	39	7	12	2	6	1	
HL	34	6	30	5	17	3	
MDS / MPN	84	15	71	12	90	16	
MM	129	22	95	16	56	10	
NHL	101	18	101	17	107	19	
WM	6	1	6	1	2	< 1	
Donor ^d							
Related	371	66	249	42	197	35	< 0.0001
Unrelated	191	34	345	58	367	65	
Disease risk group ^e							
Low	129	23	131	22	169	30	0.002
Standard	270	48	297	50	276	49	
High	163	29	166	28	118	21	
Age, years							
≤ 49	174	31	131	22	102	18	< 0.0001
50–59	236	42	208	35	147	26	
≥ 60	152	27	255	43	316	56	
Sex match							
Female to male	169	30	137	23	141	25	0.04
Others	393	70	457	77	423	75	
CMV serostatus							
R–/D–	129	23	172	29	169	30	0.02
R+/D–	141	25	172	29	158	28	
R+/D+	84	15	73	12	68	12	
R–/D+	208	37	177	30	169	30	
HCT-CI ^f							
0	118	21	89	15	56	10	< 0.0001
1,2	129	23	137	23	152	27	
3	73	13	131	22	113	20	
≥ 4	67	12	125	21	141	25	
Missing	174	31	113	19	102	18	
HLA-allele mismatch ^g							
No	534	95	552	93	530	94	0.72
Yes	28	5	42	7	34	6	
Prior HCT ^h							
No	427	76	416	70	433	77	0.008
Yes	135	24	179	30	131	23	

continued on next page

continued from previous page

TBI: total body irradiation; Gy: Gray; GvHD: graft-versus-host disease; CI: calcineurin inhibitor; MMF: mycophenolate mofetil; FH: Fred Hutchinson Cancer Research Center; ALL: acute lymphoblastic leukemia; AML: acute myeloid leukemia; CLL: chronic lymphocytic leukemia; CML: chronic myelogenous leukemia; HL: Hodgkin lymphoma; MDS: myelodysplastic syndromes; MPN: myeloproliferative neoplasms; MM: multiple myeloma; NHL: non-Hodgkin lymphoma; WM: Waldenström macroglobulinemia; CMV: cytomegalovirus; R: recipient; D: donor; HCTCI: hematopoietic cell transplantation comorbidity index; GCSF: granulocyte colony-stimulating factor; PBSC: peripheral blood stem cells. ^aFludarabine was given at a dose of 30 mg/m²/day IV on days 4, 3, and 2 before HCT. Clofarabine was given at a dose of 30-50 mg/m²/day on days 6, 5, 4, 3, and 2 before HCT. TBI was given on the day before donor hematopoietic cell infusion. ^bAll related (n=815) and most unrelated recipients (n=727) received MMF for at least 28 days after related HCT and 56 days after unrelated HCT, with either cyclosporine or tacrolimus, for at least 80 days, with the majority of patients receiving a calcineurin inhibitor for 150-180 days after HCT. The remaining unrelated recipients (n=178 total - zero during 1997-2003, 65 during 2004-2009, and 113 during 2010-2017) received sirolimus from day -3 to either day 80 or 180, in addition to MMF (days zero to 40 or 96) and cyclosporine (days -3 to 150-180). ^cOn-protocol patients were those transplanted on active clinical trials. Off-protocol patients were those transplanted outside of an active clinical study. All patients signed consent giving permission for their clinical data to be used for research studies such as this one. ^dGCSF-mobilized PBSC grafts contained a median of 8.0x10⁶ CD34⁺ cells/kg (range, 0.2-42.6x10⁶ CD34⁺ cells/kg) and 3.1x10⁸ CD3⁺ cells/kg (range, 0.1-296.0x10⁸ CD3⁺ cells/kg). ^eKahl disease risk groups assigned as described.²⁰ ^fHematopoietic cell transplantation comorbidity index (HCTCI) assigned as described.¹⁷ ^gDonors and recipients were matched at HLA-A, -B, -C, -DRB1, and -DQB1 by high-resolution typing except for the specified number of unrelated donor-recipient pairs who were mismatched at the level of one HLA class I allele. ^hIncludes planned autologous, failed autologous, and failed allogeneic transplantation. The number of patients who had a prior planned autologous HCT decreased from 107 (19%) during 1997-2003 to one during 2010-2017; 23 patients (4%) had an unsuccessful prior autologous HCT during 1997-2003, increasing to 120 patients (21%) during 2010-2017; 3 patients (<1%) had an unsuccessful prior allogeneic HCT during 1997-2003, increasing to 22 patients (4%) during 2010-2017. ⁱP-values reflect any pattern of variation over the three time periods, including trends over time.

1997-2003, 594 from 2004-2009, and 564 from 2010-2017. An increasing number and proportion of patients underwent HCT at FHCRC over time ($P<0.0001$) on protocols considered standard-of-care. The proportion of patients age ≥ 60 years at the time of HCT increased, as did the proportion of patients with an HCT-CI score ≥ 3 . Unrelated donors were utilized more frequently over time. The distribution of diagnoses changed over time ($P<0.0001$), most notably with an increase in the proportion of patients with AML (16% during 1997-2003 and 30% during 2010-2017) and decreases in CML and multiple myeloma.

The distribution of disease relapse risk groups changed over time ($P<0.0001$), with a decreasing proportion of patients with high-risk disease and an increasing proportion with low-risk disease.

A minority of patients had a prior HCT, but the types of prior HCT changed over time. The number of patients who had a prior planned autologous HCT decreased from 107 (19%) during 1997-2003 to one during 2010-2017, while the number of patients who had unsuccessful prior autologous or allogeneic HCT increased (Table 1). Planned autologous HCT were typically performed in conjunction with a tandem allogeneic HCT for patients with multiple myeloma.

Major endpoints by era of transplant

Associations of major endpoints with the time period of HCT are summarized in Table 2 and Figures 1 and 2. As described in the Methods section, results were adjusted for risk factors that varied over the three time periods and were potentially related to one or more endpoints of interest. OS, PFS, and NRM all had a significant association with the era of HCT. When compared to 1997-2003, significant improvements were noted during 2004-2009 and 2010-2017 for OS (hazard ratio [HR] 0.72, $P=0.0001$ and HR 0.60, $P<0.0001$), PFS (HR 0.78, $P=0.002$ and HR 0.63, $P<0.0001$), and NRM (HR 0.58, $P<0.0001$ and HR 0.52, $P<0.0001$). The risk of relapse or progression was lower during 2010-2017 when compared to 1997-2003 (HR 0.71, $P=0.006$). The incidence of relapse-related mortality trended toward improvement in later time periods, but the differences from 1997-2003 were not statistically significant.

Rates of grades 2-4 acute GvHD, grades 3-4 acute GvHD, and chronic GvHD were all significantly associated with time period of HCT and, when compared to 1997-2003, all improved significantly during 2004-2009 and 2010-2017. Given we increasingly used 'triple

immunosuppression' consisting of MMF, a calcineurin inhibitor, and sirolimus for patients undergoing HCT from unrelated donors,^{6,8} we evaluated its impact on acute GvHD separately. Adding sirolimus reduced the rates of grades 2-4 and 3-4 acute GvHD when compared to patients who received MMF and a calcineurin inhibitor without sirolimus (HR 0.52, 95% CI: 0.40-0.67, $P<0.0001$ and HR 0.54, 95% CI: 0.29-1.01, $P=0.05$, respectively).

Association of relapse or progression with era of transplant in patients with acute myeloid leukemia in remission

Since the overall rate of relapse or progression was significantly decreased in the most recent time period, we evaluated whether this was also true for the 351 patients with AML in first or second complete remission (CR1/CR2): 64 during 1997-2003, 147 during 2004-2009, and 140 during 2010-2017. Among these patients, measurable (minimal) residual disease (MRD) at the time of HCT as determined by flow cytometry, cytogenetics, or molecular analysis was detected in 16 patients (11%) during 2004-2009 and 32 patients (23%) during 2010-2017. Data were unavailable prior to 2004. We found no statistically significant change in the rate of relapse for patients with AML in CR1/CR2 over time. When compared to 1997-2003, the adjusted HR for relapse during 2004-2009 was 0.84 (95% CI: 0.4-1.6, $P=0.61$) and during 2010-2017 was 0.89 (95% CI: 0.4-1.8, $P=0.75$).

Associations of organ complications and infections with era of transplant

Associations of liver and kidney injuries, gram-negative bacteremia, invasive fungal infections, and CMV infection with era of HCT are shown in Table 3. Compared to 1997-2003, the incidences of patients having liver or kidney complications, gram-negative bacteremia, or an invasive fungal infection through day 100 were significantly lower in the two most recent time periods of HCT.

Serologic CMV infection was evaluated in recipients who were seropositive at the time of HCT as these patients were at the highest risk for development of CMV disease and CMV-associated mortality.²⁸ CMV diagnostic testing evolved during the three time periods, and we included measurement via both the pp65 antigen detection assay and PCR-based detection of CMV DNA in plasma in our analysis. While the incidence of CMV reactivation did not significantly change over time, the incidence of CMV disease was significantly decreased in the most recent era ($P=0.001$).

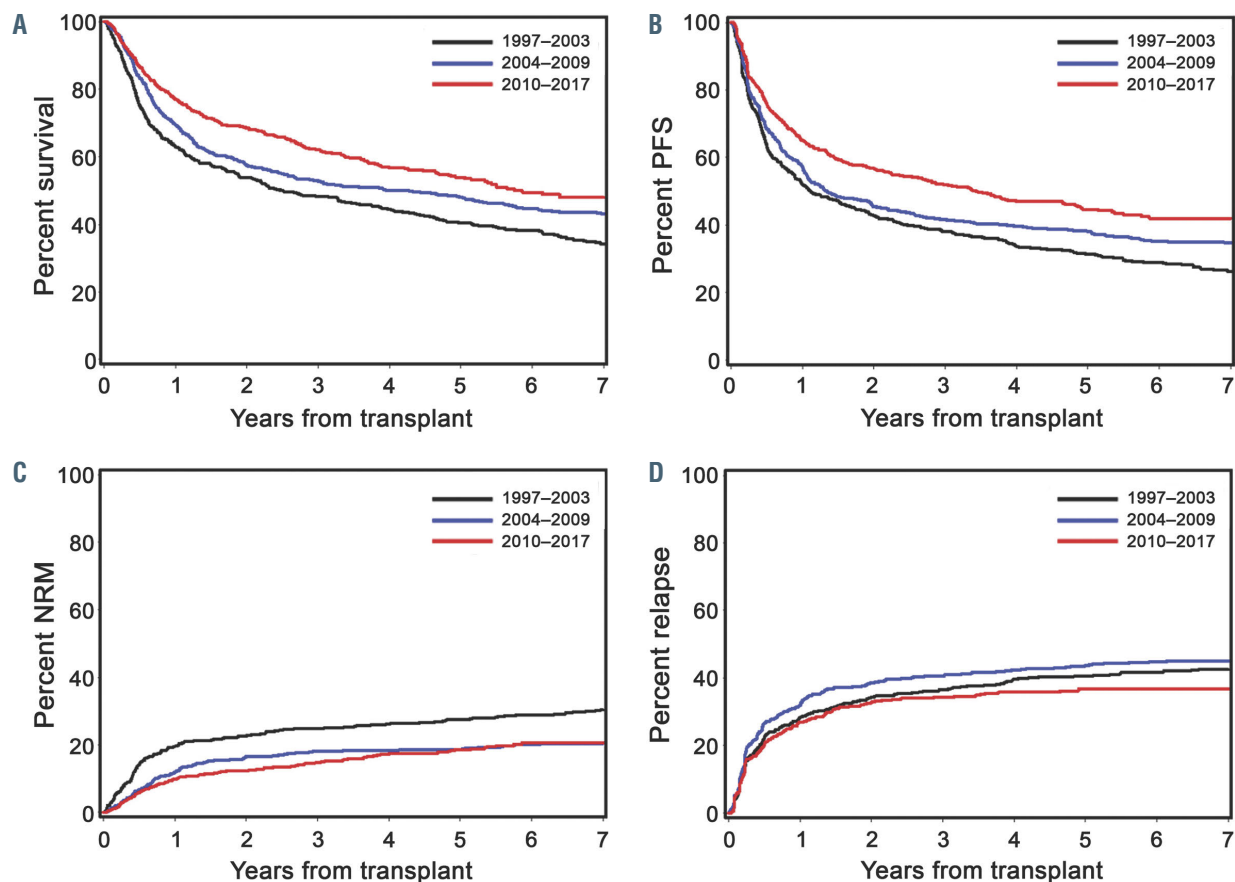


Figure 1. Adjusted cumulative incidence rates of major clinical endpoints by era of transplant. (A) Overall survival, (B) progression-free survival (PFS), (C) non-relapse mortality (NRM), and (D) relapse. Era of transplant: 1997–2003 (black line), 2004–2009 (blue line), and 2010–2017 (red line).

Comparison of endpoints in two most recent transplant eras

Comparisons of clinical endpoints and in the incidences of organ complications and infections in the most recent transplant era (2010–2017) to those in 2004–2009 are shown in the *Online Supplementary Tables S2 and S3*. OS, PFS, relapse rate, and the rate of grades 2–4 acute GvHD significantly improved in the most recent era as compared to 2004–2009. Over this same time period, significant improvements were also noted in the incidences of gram-negative bacteremias, invasive fungal infections, and in CMV antigenemia and disease.

Discussion

Over the period from 1997–2017, we found marked improvements in OS, PFS, NRM, and in the rates of acute and chronic GvHD after HCT with non-myeloablative conditioning. We also noted a trend toward reduced relapse-related mortality. During this same time period, patient age and burden of comorbidity at the time of HCT increased, higher proportions received grafts from unrelated donors, and AML became the leading indication for HCT, while the numbers of patients with multiple myeloma and CML declined. Consistent with these shifts in diagnoses, there was a decrease in patients who underwent HCT after a prior planned autologous transplan-

tion, which is likely related to the decrease in multiple myeloma as an indication (decreased use of planned tandem autologous-allogeneic transplantation),²⁹ and increases in prior unsuccessful autologous HCT for non-Hodgkin lymphoma and prior unsuccessful allogeneic HCT for AML. These data underscore the fact that non-myeloablative conditioning has been increasingly recognized as an option for patients with recurrent hematologic malignancies after prior HCT with high-intensity conditioning regimens.³⁰ Interestingly we did not see an increase in the number of patients with MDS who underwent HCT, despite the increasing recognition of MDS-associated mortality risk and life expectancy benefit of HCT for patients with high-risk MDS.^{31,32} We suspect that this lack of increase in MDS patients may be due to referral patterns from providers who are unaware that HCT is a therapeutic option for their MDS patients who are older or medically infirm.

The substantial reduction in NRM, lower risk of relapse seen primarily in the most recent cohort, and modest improvement in relapse-related mortality all contributed to increased overall survival. Contributors to the improvement in NRM over time are summarized in Table 4 and include the reductions seen in liver and kidney complications; decreases in incidences of gram-negative bacteremia, invasive fungal infections, and CMV disease; and reduced rates of acute and chronic GvHD. We speculate that several changes in clinical practice contributed to the

Table 2. Association of transplant era with major endpoints.

	Adjusted ^a (n=1,668)	HR (95% CI)	P
Overall survival			
1997 – 2003	1.0		
2004 – 2009	0.72 (0.6 – 0.9)	0.0001	
2010 – 2017	0.60 (0.5 – 0.7)	<0.0001	
Progression-free survival			
1997 – 2003	1.0		
2004 – 2009	0.78 (0.7 – 0.9)	0.002	
2010 – 2017	0.63 (0.5 – 0.8)	<0.0001	
Relapse/progression			
1997 – 2003	1.0		
2004 – 2009	0.93 (0.8 – 1.1)	0.52	
2010 – 2017	0.71 (0.6 – 0.9)	0.006	
Non-relapse mortality			
1997 – 2003	1.0		
2004 – 2009	0.58 (0.5 – 0.7)	<0.0001	
2010 – 2017	0.52 (0.4 – 0.7)	<0.0001	
Relapse-related mortality ^b			
1997 – 2003	1.0		
2004 – 2009	0.85 (0.7 – 1.1)	0.15	
2010 – 2017	0.80 (0.6 – 1.0)	0.10	
Acute GvHD grade 2–4			
1997 – 2003	1.0		
2004 – 2009	0.81 (0.7 – 1.0)	0.03	
2010 – 2017	0.64 (0.5 – 0.8)	<0.0001	
Acute GvHD grade 3–4			
1997 – 2003	1.0		
2004 – 2009	0.67 (0.5 – 1.0)	0.03	
2010 – 2017	0.54 (0.4 – 0.8)	0.004	
Chronic GvHD			
1997 – 2003	1.0		
2004 – 2009	0.59 (0.5 – 0.7)	<0.0001	
2010 – 2017	0.57 (0.5 – 0.7)	<0.0001	

HR: hazard ratio; CI: confidence interval; GvHD: graft-versus-host disease; MM: multiple myeloma; AML: acute myeloid leukemia; CMV: cytomegalovirus; R: recipient; D: donor; HCT: hematopoietic cell transplantation; HCTCI: hematopoietic cell transplantation comorbidity index. ^aAdjusted for transplant center (stratification); treatment type (on-protocol, off-protocol), age (<49, 50–59, ≥60 years); disease risk group (low, standard, high); MM diagnosis; AML diagnosis; CMV (R– and D–, R+ or D+); donor relation (related, unrelated); sex mismatch (female to male, others); prior HCT (no, yes); allele mismatch (no, yes); and HCTCI (0, 1–2, 3, ≥4, missing). Kahl disease risk groups and HCTCI assigned as described.^{17,20} ^bRelapse-related mortality refers to survival after relapse among patients that relapsed.

reduction in NRM. Topically-active glucocorticoids such as beclomethasone dipropionate were introduced which, when given with prednisone to patients with gastrointestinal GvHD in a randomized, placebo-controlled trial, allowed for a rapid taper of prednisone dosing starting 10 days after initiation, significantly reduced the risk of GvHD-treatment failure, and reduced the risk of mortality by 37% after a median follow-up of 3.6 years.³ Decreases in the use of systemic glucocorticoids for treatment of acute GvHD, along with the addition of sirolimus to MMF with a calcineurin inhibitor as GvHD prophylaxis have also resulted in lower rates of fungal infections² and CMV reactivation.^{6,8} Changes in infection prophylaxis also likely contributed to reductions in NRM. This included a shift in antibacterial prophylaxis from cephalosporins to fluoroquinolones during periods of neutropenia,^{9–11} a shift in antifungal prophylaxis from fluconazole to extended-spectrum triazoles (itraconazole, voriconazole, posaconazole) with greater activity against mold,^{12,13} empirical anti-

Table 3. Association of transplant era with incidences of organ complications and infections.

	Adjusted ^a OR (95% CI)	P
Organ Toxicity (n=1,548)		
Bilirubin > 4 mg/dL		
1997 – 2003	1.0	
2004 – 2009	0.28 (0.18 – 0.42)	< 0.0001
2010 – 2017	0.22 (0.14 – 0.35)	< 0.0001
Bilirubin > 10 mg/dL		
1997 – 2003	1.0	
2004 – 2009	0.18 (0.08 – 0.43)	0.0001
2010 – 2017	0.21 (0.09 – 0.50)	0.0005
Creatinine > 2x baseline		
1997 – 2003	1.0	
2004 – 2009	0.63 (0.47 – 0.84)	0.002
2010 – 2017	0.71 (0.52 – 0.97)	0.03
Infections (n=1,502)	HR (95% CI)	P
Gram-negative bacteremia		
1997 – 2003	1.0	
2004 – 2009	0.82 (0.70 – 0.97)	0.02
2010 – 2017	0.68 (0.56 – 0.82)	< 0.0001
Invasive fungal infection		
1997 – 2003	1.0	
2004 – 2009	0.75 (0.63 – 0.89)	0.0008
2010 – 2017	0.63 (0.52 – 0.76)	< 0.0001
CMV antigenemia ^b		
1997 – 2003	1.0	
2004 – 2009	1.15 (0.94 – 1.40)	0.18
2010 – 2017	0.86 (0.69 – 1.08)	0.19
CMV disease ^b		
1997 – 2003	1.0	
2004 – 2009	0.86 (0.70 – 1.06)	0.16
2010 – 2017	0.66 (0.52 – 0.85)	0.001

OR: odds ratio; HR: hazard ratio; CI: confidence interval; MM: multiple myeloma; AML: acute myeloid leukemia; R: recipient; D: donor; CMV: cytomegalovirus; HCT: hematopoietic cell transplantation; HCTCI: hematopoietic cell transplantation comorbidity index. ^aAdjusted for transplant center; treatment type (protocol, treatment plan); age (<49, 50–59, ≥60 years); disease risk group (low, standard, high); MM diagnosis; AML diagnosis; CMV (R– and D–, R+ or D+); donor relation (related, unrelated); sex mismatch (female to male, others); prior HCT (no, yes); allele mismatch (no, yes); and HCTCI (0, 1–2, 3, ≥4, missing). ^bCMV endpoints evaluated only among seropositive recipients at HCT (n = 911 for multivariate analysis).

fungal therapy for patients with pulmonary nodules,³³ and the adoption of pre-emptive antiviral therapy driven by highly sensitive PCR-based CMV DNA diagnostic testing of blood samples.^{14–16}

Reduction in the incidences of acute GvHD in our later patient cohorts were due, in part, to the increasing use of sirolimus as a component of GvHD prophylaxis for unrelated recipients^{6,8} and the adoption of ursodiol to prevent cholestasis and hyperbilirubinemia.⁴ In addition to our data here documenting the beneficial effect of sirolimus, we recently reported the results of a randomized phase III trial showing that the addition of sirolimus to the standard prophylactic regimen of MMF and cyclosporine in unrelated recipients reduced the day 100 cumulative incidence of grades 2–4 acute GvHD (26% vs. 52%), resulting in significantly reduced use of steroids and markedly improved 1-year NRM, PFS, and OS.⁸ While there was no difference in chronic GvHD between the two groups, patients affected by chronic GvHD in the triple-drug group had a trend towards lower NRM after 1 year compared with those in the standard group (4% in triple-drug group vs. 15% in the standard group). Ursodiol use, at a dose of 12 mg/kg/day

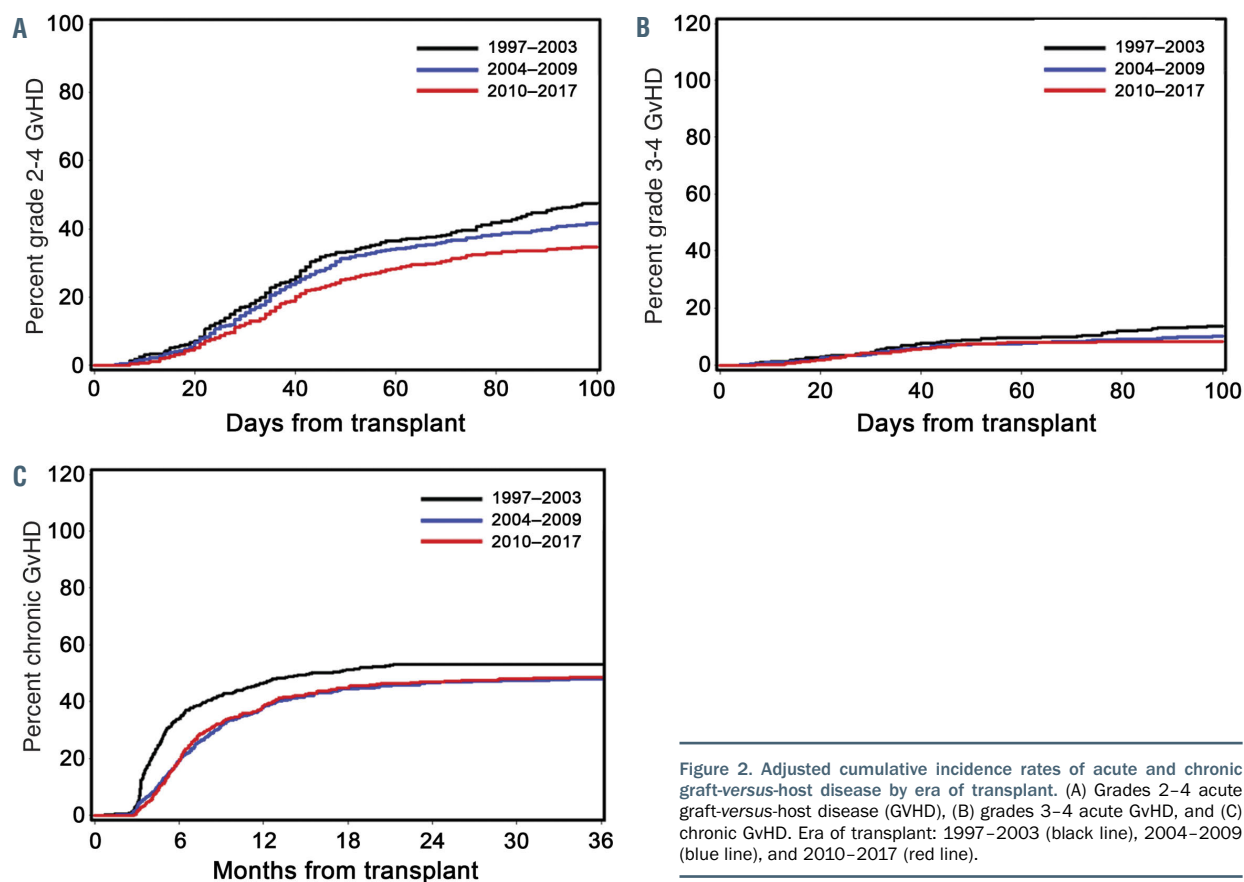


Figure 2. Adjusted cumulative incidence rates of acute and chronic graft-versus-host disease by era of transplant. (A) Grades 2–4 acute graft-versus-host disease (GvHD), (B) grades 3–4 acute GvHD, and (C) chronic GvHD. Era of transplant: 1997–2003 (black line), 2004–2009 (blue line), and 2010–2017 (red line).

starting on the day before HCT, significantly reduced the incidences of stages 2–4 liver and intestinal acute GvHD and grades 3–4 acute GvHD, and improved both 1-year OS and NRM.⁴

The overall incidence of relapse was significantly lower during 2010–2017 compared to earlier time periods. This corresponded both with an increasing use of higher TBI doses (3–4.5 Gy) for patients who did not receive preceding myelosuppressive chemotherapy, and with an increasing proportion of patients who underwent HCT with diseases at a lower risk of relapse. The majority of our patients who received increased TBI dosing carried a diagnosis of AML, MDS, or a myeloproliferative neoplasm based on a prospective TBI dose escalation study showing a reduction in relapse with higher TBI dosing in MDS/MPN patients who had not had previous myelosuppressive (induction-type) chemotherapy.³⁴ The lower grade MDS/MPN patients benefitted by increasing the TBI dose to 3 Gy whereas the patients with excess blasts or a history of CMML benefitted by increasing the TBI dose to 4.5 Gy. Based on the findings in the low grade MDS patients, the TBI dose was increased to 3 Gy in AML patients who had not received induction chemotherapy in the preceding 3–6 months or had a previous allogeneic transplant from a different donor. In a sub-analysis, we found no significant change in the rate of relapse in the subset of AML patients who underwent HCT in CR1/CR2, a finding that has also been noted in AML patients who predominantly received high-intensity conditioning prior to HCT.³⁵ While we also noted an increase in the number of AML patients in CR1/CR2 with MRD at the time of non-myeloablative HCT, we recognize that

the detection of MRD and its association with disease risk-stratification relative to HCT evolved over our time period of analysis and may have affected the selection of patients in our cohort who underwent HCT after non-myeloablative conditioning *versus* receiving other therapies.

The overall incidence of relapse-related mortality trended toward improvement for our 2004–2009 and 2010–2017 patient cohorts. Hypomethylating agents, in particular, gained increasing use for the treatment of relapsed myeloid malignancies during our later time periods,^{36,37} and are likely a contributor to the observed modest attenuation of relapse-related mortality. More recently, there has been an expansion in the treatment armamentarium for relapsed disease including ibrutinib, venetoclax, and enasidinib,^{38–40} checkpoint inhibitors,^{41,42} tyrosine kinase inhibitors,⁴³ and monoclonal antibodies.^{44,45} Many of these agents were used too infrequently to have influenced the outcomes reported here, but we anticipate that their use will increase and may lead to further reduction in mortality after relapse.

Interestingly, we found that the significant improvements in OS, PFS, rate of grades 2–4 acute GvHD, and in the incidence of infectious complications continued to occur over our total period of analysis. However, the statistically significant improvements in other clinical outcomes were limited to particular eras. For example, NRM, relapse-related mortality, rate of grades 3–4 acute GvHD, rate of chronic GvHD, and the incidences of liver and kidney injury improved significantly only when 2004–2009 was compared to 1997–2003; the rate of relapse or progression improved significantly only in the most recent

Table 4. Summary of changes in clinical practice that affected non-relapse mortality over time.

Increased use of topically-active GI glucocorticoids for patient with GI acute GvHD
Decreased use of systemic glucocorticoids for patients with acute GvHD
Addition of sirolimus to CI and MMF for GvHD prophylaxis
Increased use of ursodiol to prevent cholestasis and hyperbilirubinemia
Increased use of fluoroquinolones as antibacterial prophylaxis in neutropenic patients
Increased use of mold-active triazoles as antifungal prophylaxis
Increased use of empiric antifungal therapy for patients with pulmonary nodules
Increasing use of pre-emptive antiviral therapy for CMV viremia

NRM: non-relapse mortality; GI: gastrointestinal; GvHD: graft-versus-host disease; CI: calcineurin inhibitor; MMF: mycophenolate mofetil; CMV: cytomegalovirus.

era. While those outcomes which did not show statistical improvements in the most recent era had hazard ratios that trended toward improvement, it is likely that the continual improvement in OS and PFS had different predominant components at different times: improvements in NRM, relapse-related mortality, and organ toxicity contributing earlier (between 1997–2003 and 2004–2009) and improvement in the rate of relapse contributing later (between 2004–2009 and 2010–2017).

The present findings are similar to those of prior analyses which predominantly included patients who received high-intensity conditioning.^{35,46,47} It is notable, however, that in these prior studies the increased use of lower-intensity conditioning regimens and granulocyte colony-stimulating factor-mobilized peripheral blood stem cell (PBSC) grafts were cited as prominent reasons for the improved outcomes – particularly reductions in NRM. The homogeneous nature of the current patient population, with all patients receiving lower-intensity conditioning regimens and HLA-matched PBSC grafts, allowed us to more independently appraise the influence of changes in supportive care that are critical for successful outcomes after HCT.

In conclusion, we show that improvements in supportive care after HCT with non-myeloablative conditioning for patients with advanced hematologic malignancies during the past two decades have yielded higher rates of overall survival and PFS and lower risks of NRM, grades 2–4 acute GvHD, and chronic GvHD. During this period, the age of patients and burden of comorbidity at the time of HCT has increased, and use of unrelated donors has also increased, thereby making allogeneic HCT more widely available for patients with otherwise incurable hematologic malignancies. These results should encourage the referral of elderly and medically infirm younger patients with hematologic malignancies for evaluation at a transplant center.

Disclosures

No conflicts of interest to disclose.

Contributions

JPC, BES, NG, GMcD, RS and BMS contributed to the conception and design; RS and BMS secured financial support; RS and BMS provided administrative support; BG, MLS, TRC, JS, G-NF, MBM, MB, BB, FS, AAL, PH, EDA, SLP, RTM, WB, JA, JAG, GO, AMY, KH, WJH, DGM, MM, PJM, MEDF, GEG, AEW, HJD, BLS, GBMcD, RS and BMS provided study materials or patients; JPC, BG, MLS, TRC, JS, G-NF, MBM, MB, BB, FS, AAL, PH, EDA, SLP, RTM, WB, JA, JAG, GO, AMY, KH, WJH, DGM, MM, PJM, MEDF, GEG, AEW, HJD, BLS, GBMcD, RS and BMS collected and assembled data; JPC, BES, NG, GMcD, RS and BMS analyzed and interpreted data; all authors contributed to the writing and final approval of the manuscript.

Acknowledgments

The authors are grateful to the research nurses and data coordinators who implemented the study protocols; to the many physicians, nurses, physician assistants, nurse practitioners, pharmacists, and support staff who cared for our patients; and to the patients who allowed us to care for them and participated in our research. We are deeply indebted to Helen S. Crawford for assistance in preparing the manuscript, tables, and figures. The content is solely the responsibility of the authors and does not represent the official views of the institutions who provided funding support.

Funding

Research reported in this publication was supported by P01 HL36444, P01 HL122173, and T32 HL007093 from the NHLBI; P01 CA078902 and P30 CA015704 from the NCI and NIH; and grants from the Laura Landro Solomon Endowment Fund and Gabrielle's Angels Foundation.

References

1. Storb R, Gyurkocza B, Storer BE, et al. Graft-versus-host disease and graft-versus-tumor effects after allogeneic hematopoietic cell transplantation. *J Clin Oncol.* 2013; 31(12):1530-1538.
2. Mielcarek M, Storer BE, Boeckh M, et al. Initial therapy of acute graft-versus-host disease with low-dose prednisone does not compromise patient outcomes. *Blood.* 2009;113(13):2888-2894.
3. Hockenberry DM, Cruickshank S, Rodell TC, et al. A randomized, placebo-controlled trial of oral beclomethasone dipropionate as a prednisone-sparing therapy for gastrointestinal graft-versus-host disease. *Blood.* 2007;109(10):4557-4563.
4. Ruutu T, Eriksson B, Remes K, et al. Ursodeoxycholic acid for the prevention of hepatic complications in allogeneic stem cell transplantation. *Blood.* 2002; 100(6):1977-1983.
5. Fried RH, Murakami CS, Fisher LD, Willson RA, Sullivan KM, McDonald GB. Ursodeoxycholic acid treatment of refractory chronic graft-versus-host disease of the liver. *Ann Intern Med.* 1992;116(8):624-629.
6. Kornblit B, Maloney DG, Storer BE, et al. A randomized phase II trial of tacrolimus, mycophenolate mofetil and sirolimus after non-myeloablative unrelated donor transplan-
7. Armand P, Kim HT, Sainvil MM, et al. The addition of sirolimus to the graft-versus-host disease prophylaxis regimen in reduced intensity allogeneic stem cell transplantation for lymphoma: a multicentre randomized trial. *Br J Haematol.* 2016; 173(1):96-104.
8. Sandmaier BM, Kornblit B, Storer BE, et al. Addition of sirolimus to standard cyclosporine plus mycophenolate mofetil-based graft-versus-host disease prophylaxis for patients after unrelated non-myeloablative haemopoietic stem cell transplantation: a multicentre, randomised, phase 3

trial. *Lancet Haematol.* 2019;6(8):e409-e418.

9. Gafter-Gvili A, Fraser A, Paul M, van de Wetering M, Kremer L, Leibovici L. Antibiotic prophylaxis for bacterial infections in afebrile neutropenic patients following chemotherapy. *Cochrane Database Syst Rev.* 2005(4):CD004386.

10. Gafter-Gvili A, Fraser A, Paul M, et al. Antibiotic prophylaxis for bacterial infections in afebrile neutropenic patients following chemotherapy. *Cochrane Database Syst Rev.* 2012;1:CD004386.

11. Reuter S, Kern WV, Sigge A, et al. Impact of fluoroquinolone prophylaxis on reduced infection-related mortality among patients with neutropenia and hematologic malignancies. *Clin Infect Dis.* 2005;40(8):1087-1093.

12. Robenshtok E, Gafter-Gvili A, Goldberg E, et al. Antifungal prophylaxis in cancer patients after chemotherapy or hematopoietic stem-cell transplantation: systematic review and meta-analysis. *J Clin Oncol.* 2007;25(34):5471-5489.

13. Ethier MC, Science M, Beyene J, Briel M, Lehrnbecher T, Sung L. Mould-active compared with fluconazole prophylaxis to prevent invasive fungal diseases in cancer patients receiving chemotherapy or haematopoietic stem-cell transplantation: a systematic review and meta-analysis of randomised controlled trials. *Br J Cancer.* 2012;106(10):1626-1637.

14. Peggs KS, Preiser W, Kottaridis PD, et al. Extended routine polymerase chain reaction surveillance and pre-emptive antiviral therapy for cytomegalovirus after allogeneic transplantation. *Br J Haematol.* 2000;111(3):782-790.

15. Mori T, Okamoto S, Watanabe R, et al. Dose-adjusted preemptive therapy for cytomegalovirus disease based on real-time polymerase chain reaction after allogeneic hematopoietic stem cell transplantation. *Bone Marrow Transplant.* 2002;29(9):777-782.

16. Reusser P, Einsele H, Lee J, et al. Randomized multicenter trial of foscarnet versus ganciclovir for preemptive therapy of cytomegalovirus infection after allogeneic stem cell transplantation. *Blood.* 2002;99(4):1159-1164.

17. Sorror ML, Maris MB, Storb R, et al. Hematopoietic cell transplantation (HCT)-specific comorbidity index: a new tool for risk assessment before allogeneic HCT. *Blood.* 2005;106(8):2912-2919.

18. Filipovich AH, Weisdorf D, Pavletic S, et al. National Institutes of Health consensus development project on criteria for clinical trials in chronic graft-versus-host disease: I. Diagnosis and staging working group report. *Biol Blood Marrow Transplant.* 2005;11(12):945-956.

19. Przepiorka D, Weisdorf D, Martin P, et al. 1994 Consensus Conference on Acute GVHD Grading. *Bone Marrow Transplant.* 1995;15(6):825-828.

20. Kahl C, Storer BE, Sandmaier BM, et al. Relapse risk in patients with malignant diseases given allogeneic hematopoietic cell transplantation after nonmyeloablative conditioning. *Blood.* 2007;110(7):2744-2748.

21. Hingorani SR, Guthrie K, Batchelder A, et al. Acute renal failure after myeloablative hematopoietic cell transplant: incidence and risk factors. *Kidney Int.* 2005;67(1):272-277.

22. Boeckh M, Huang M, Ferrenberg J, et al. Optimization of quantitative detection of cytomegalovirus DNA in plasma by real-time PCR. *J Clin Microbiol.* 2004;42(3):1142-1148.

23. Ljungman P, Griffiths P, Paya C. Definitions of cytomegalovirus infection and disease in transplant recipients. *Clin Infect Dis.* 2002;34(8):1094-1097.

24. Chien JW, Boeckh MJ, Hansen JA, Clark JG. Lipopolysaccharide binding protein promoter variants influence the risk for gram-negative bacteremia and mortality after allogeneic hematopoietic cell transplantation. *Blood.* 2008;111(4):2462-2469.

25. De Pauw B, Walsh TJ, Donnelly JP, et al. Revised definitions of invasive fungal disease from the European Organization for Research and Treatment of Cancer/Invasive Fungal Infections Cooperative Group and the National Institute of Allergy and Infectious Diseases Mycoses Study Group (EORTC/MSG) Consensus Group. *Clin Infect Dis.* 2008;46(12):1813-1821.

26. Gooley TA, Leisenring W, Crowley J, Storer BE. Estimation of failure probabilities in the presence of competing risks: new representations of old estimators. *Stat Med.* 1999;18(6):695-706.

27. Storer BE, Gooley TA, Jones MP. Adjusted estimates for time-to-event endpoints. *Lifetime Data Anal.* 2008;14(4):484-495.

28. Ljungman P, Aschan J, Lewensohn-Fuchs I, et al. Results of different strategies for reducing cytomegalovirus-associated mortality in allogeneic stem cell transplant recipients. *Transplantation.* 1998;66(10):1330-1334.

29. Krishnan A, Pasquini MC, Logan B, et al. Autologous haemopoietic stem-cell transplantation followed by allogeneic or autologous haemopoietic stem-cell transplantation in patients with multiple myeloma (BMT CTN 0102): a phase 3 biological assignment trial. *Lancet Oncol.* 2011;12(13):1195-1203.

30. Gyurkocza B, Storb R, Chauncey TR, Maloney DG, Storer BE, Sandmaier BM. Second allogeneic hematopoietic cell transplantation for relapse after first allografts. *Leuk Lymphoma.* 2019;60(7):1758-1766.

31. Greenberg PL, Tuechier H, Schanz J, et al. Revised international prognostic scoring system for myelodysplastic syndromes. *Blood.* 2012;120(12):2454-2465.

32. Koreth J, Pidaia J, Perez WS, et al. Role of reduced-intensity conditioning allogeneic hematopoietic stem-cell transplantation in older patients with de novo myelodysplastic syndrome: an international collaborative decision analysis. *J Clin Oncol.* 2013;31(21):2662-2670.

33. Dignan FL, Evans SO, Ethell ME, et al. An early CT-diagnosis-based treatment strategy for invasive fungal infection in allogeneic transplant recipients using caspofungin first line: an effective strategy with low mortality. *Bone Marrow Transplant.* 2009;44(1):51-56.

34. Monaco F, Scott BL, Chauncey TR, et al. Total body irradiation dose escalation decreases risk of progression and graft rejection after hematopoietic cell transplantation for myelodysplastic syndromes or myeloproliferative neoplasms. *Haematologica.* 2019;104(6):1221-1229.

35. Canaani J, Beohou E, Labopin M, et al. Trends in patient outcome over the past two decades following allogeneic stem cell transplantation for acute myeloid leukaemia: an ALWP/EBMT analysis. *J Intern Med.* 2019;285(4):407-418.

36. Graef T, Kuendgen A, Fenk R, Zohren F, Haas R, Kobbe G. Successful treatment of relapsed AML after allogeneic stem cell transplantation with azacitidine. *Leuk Res.* 2007;31(2):257-259.

37. Platzbecker U, Wermke M, Radke J, et al. Azacitidine for treatment of imminent relapse in MDS or AML patients after allogeneic HSCT: results of the RELAZA trial. *Leukemia.* 2012;26(3):381-389.

38. Ryan CE, Sahaf B, Logan AC, et al. Ibrutinib efficacy and tolerability in patients with relapsed chronic lymphocytic leukemia following allogeneic HCT. *Blood.* 2016;128(25):2899-2908.

39. Stein EM, DiNardo CD, Pollyea DA, et al. Enasidenib in mutant IDH2 relapsed or refractory acute myeloid leukemia. *Blood.* 2017;130(6):722-731.

40. Konopleva M, Pollyea DA, Potluri J, et al. Efficacy and biological correlates of response in a phase II study of venetoclax monotherapy in patients with acute myelogenous leukemia. *Cancer Discov.* 2016;6(10):1106-1117.

41. Davids MS, Kim HT, Bachireddy P, et al. Ipilimumab for patients with relapse after allogeneic transplantation. *N Engl J Med.* 2016;375(2):143-153.

42. Haverkos BM, Abbott D, Hamadani M, et al. PD-1 blockade for relapsed lymphoma post-allogeneic hematopoietic cell transplant: high response rate but frequent GVHD. *Blood.* 2017;130(2):221-228.

43. Metzelder SK, Schroeder T, Finck A, et al. High activity of sorafenib in FLT3-ITD-positive acute myeloid leukemia synergizes with allo-immune effects to induce sustained responses. *Leukemia.* 2012;26(11):2353-2359.

44. Ueda M, de Lima M, Caimi P, et al. Concurrent blinatumomab and donor lymphocyte infusions for treatment of relapsed pre-B-cell ALL after allogeneic hematopoietic cell transplant. *Bone Marrow Transplant.* 2016;51(9):1253-1255.

45. Kantarjian HM, DeAngelo DJ, Stelljes M, et al. Inotuzumab ozogamicin versus standard therapy for acute lymphoblastic leukemia. *N Engl J Med.* 2016;375(8):740-753.

46. Hahn T, McCarthy PL, Jr, Hassebroek A, et al. Significant improvement in survival after allogeneic hematopoietic cell transplantation during a period of significantly increased use, older recipient age, and use of unrelated donors. *J Clin Oncol.* 2013;31(19):2437-2449.

47. Gooley TA, Chien JW, Pergam SA, et al. Reduced mortality after allogeneic hematopoietic-cell transplantation. *N Engl J Med.* 2010;363(22):2091-2101.



Prognostic significance of translocations in the presence of mutated IGHV and of cytogenetic complexity at diagnosis of chronic lymphocytic leukemia

Nyla A. Heerema,¹ Natarajan Muthusamy,² QiuHong Zhao,² Amy S. Ruppert,² Heather Breidenbach,¹ Leslie A. Andritsos,² Michael R. Grever,² Kami J. Maddocks,² Jennifer Woyach,² Farrukh Awan,² Meixiao Long,² Amber Gordon,² Caitlin Coombes² and John C. Byrd²

¹Department of Pathology, The Ohio State University Wexner Medical Center and

²Department of Hematology, The Ohio State University Wexner Medical Center, Columbus, OH, USA

ABSTRACT

Mutations of the IGH variable region in patients with chronic lymphocytic leukemia are associated with a favorable prognosis, whereas cytogenetic complexity (≥ 3 unrelated aberrations) and translocations have been associated with an unfavorable prognosis. While mutational status of IGHV is stable, cytogenetic aberrations frequently evolve. However, the relationships of these features as prognosticators at diagnosis are unknown. We examined the CpG-stimulated metaphase cytogenetic features detected within 1 year of diagnosis of chronic lymphocytic leukemia and correlated these features with outcome and other clinical features including IGHV mutational status. Of 329 untreated patients, 53 (16.1%) had a complex karyotype, and 85 (25.8%) had a translocation. The median time to first treatment (TFT) was 47 months. In univariable analyses, significant risk factors for shorter TFT ($P < 0.05$) were Rai stage 3-4, β -microglobulin > 3.5 mg/L, log-transformed white blood cell count, unmutated IGHV, a complex karyotype, a translocation, and trisomy 8, del(11q) or del(17p) detected by fluorescence *in situ* hybridization. In multivariable analysis, there was a significant effect modification of IGHV status on the relationship between translocation and TFT ($P = 0.002$). In IGHV-mutated patients, those with a translocation had an over 3.5 times higher risk of starting treatment than those without a translocation ($P < 0.001$); however, among IGHV-unmutated patients, a translocation did not significantly increase the risk of starting treatment (hazard ratio 1.00, $P = 0.99$). The effect of Rai stage 3-4, log-transformed white blood cell count and complex karyotype remained statistically significant, whereas that of del(17p) did not ($P = 0.51$). In summary, the presence of a translocation in IGHV-mutated patients appeared to negate the improved prognosis of mutated IGHV, but the presence of a translocation did not have an effect on TFT in high-risk IGHV-unmutated patients.

Correspondence:

NYLA A. HEEREMA

Nyla.heerema@osumc.edu

Received: November 20, 2018.

Accepted: May 8, 2020.

Pre-published: May 15, 2020.

<https://doi.org/10.3324/haematol.2018.212571>

©2021 Ferrata Storti Foundation

Material published in *Haematologica* is covered by copyright.

All rights are reserved to the Ferrata Storti Foundation. Use of published material is allowed under the following terms and conditions:

<https://creativecommons.org/licenses/by-nc/4.0/legalcode>.

Copies of published material are allowed for personal or internal use. Sharing published material for non-commercial purposes is subject to the following conditions:

<https://creativecommons.org/licenses/by-nc/4.0/legalcode>, sect. 3. Reproducing and sharing published material for commercial purposes is not allowed without permission in writing from the publisher.



Introduction

Chronic lymphocytic leukemia (CLL) has a varied clinical course. Some patients have an indolent disease with a lifespan similar to that of their peers without the disease. Other patients have rapid disease progression, require treatment early in the course of the disease, are less responsive to therapy, or exhibit short remission after therapy and have a relatively short overall survival. Factors that have prognostic significance include clinical variables such as gender, age and Rai/Binet stage, and biological factors such as IGHV mutational status, ZAP70 status and genetic abnormalities as detected by fluorescence *in situ* hybridization (FISH). IGHV mutational status is a significant and independent prognostic factor that does not change over the course of the disease. Patients with unmutated IGHV have a worse prognosis than those with mutated IGHV.¹⁻³

The karyotype of the patient is another genetic factor that influences disease course and response to therapy. The complexity of the karyotype is prognostic with three or more unrelated abnormalities predictive of a more adverse prognosis.⁴⁻¹² Furthermore, a complex karyotype has been associated with unmutated IGHV, CD38 expression and deletion of 17p or mutated *TP53*.^{5,9,11,13-16} Additional studies showed that in addition to complex karyotypes, translocations, particularly unbalanced translocations, were associated with a poor prognosis, reflected as both an increased risk of requirement for treatment and a shortened overall survival.^{5,9,17-19} Translocations have also been associated with a complex karyotype and with deletions of 17p, and in some cases with del(11q),⁹ but not in others.²⁰ While these studies are informative, the relationship of translocations to mutated *versus* unmutated IGHV detected early in the course of the disease is unclear.

Traditionally metaphase cytogenetic studies of CLL have been minimally informative, as CLL cells do not readily divide spontaneously in culture, nor do they respond to traditional B-cell mitogens. The advent of CpG oligodeoxynucleotide stimulation of CLL cells has facilitated detection of cytogenetic abnormalities in up to 80% of CLL patients.^{17,21-26} As a result of this increased detection of karyotypic abnormalities, the significance of translocations and of a complex karyotype at disease diagnosis and during disease progression can be assessed more accurately. As CLL progresses, the karyotype frequently evolves.^{27,28} Therefore, the significance of karyotypic complexity and/or translocations at disease presentation is not clear. We examined CpG-stimulated karyotypes completed within 1 year of diagnosis of CLL and correlated the presence of a translocation and of complexity with disease prognosticators such as IGHV mutational status, sex, age, Rai stage, FISH abnormalities and with time to first treatment (TFT).

Methods

Patients and samples

All patients had immunophenotypically defined B-cell CLL as outlined by the International Workshop on CLL Revised CLL Guidelines.²⁹ Peripheral blood or bone marrow was collected from patients after having obtained written informed consent in accordance with the Declaration of Helsinki and under a protocol approved by the institutional review board of The Ohio State University (Columbus, OH, USA).

Cytogenetic analyses

Cells were stimulated with CpG oligodeoxynucleotides and analyzed according to standard laboratory procedures (described in detail in the *Online Supplementary Methods*). FISH using probes for *D13S319*, *D12Z3*, *ATM*, *TP53*, *BCL6*, *MYC*, *MYB* (Abbott Molecular, Des Plaines, IL, USA) and *SEC63* (Empire Genomics, Buffalo, NY, USA) were done according to the manufacturers' recommendations.

Patients' inclusion criteria

Patients with CLL who had cytogenetic analyses between December 2006 and December 2013 and were within 1 year of diagnosis were identified from The Ohio State University Wexner Medical Center databases. Balanced and unbalanced translocations and insertions were identified. Inversions were

considered as balanced translocations, and "adds" as unbalanced translocations. A complex karyotype was defined as ≥ 3 independent aberrations on metaphase cytogenetics. The association of complex karyotype defined as ≥ 5 independent aberrations with outcome was also examined. Baseline characteristics were obtained from the patients' charts. White blood cell (WBC) count and β_2 -microglobulin concentration, determined within 90 days of diagnosis were used.

Statistical analyses

The patients' demographic and genetic characteristics were described using mean and standard deviation or median and range for continuous variables, and frequency and percentage for categorical variables. Associations between translocations or cytogenetic complexity with FISH abnormalities were tested using Fisher exact tests. Cases with both balanced and unbalanced translocations were classified together for statistical analyses.

TFT was calculated from the date of diagnosis until the date of first treatment or last follow-up, censoring patients who had not started treatment at the date last seen; patients who died prior to starting treatment were censored at the date last seen. Kaplan-Meier curves were used to estimate TFT probability, and Cox proportional hazard models were used to examine the association between potential risk factors and TFT. Table 1 shows variables considered for modeling. WBC counts were log-transformed.

Significant risk factors from univariable Cox models were included in the multivariable Cox model. Due to missing values in IGHV mutation status (n=37, 11%), WBC count (n=83, 25%), and β_2 -microglobulin (n=146, 44%), a multiple imputation procedure was applied to obtain combined results from 15 multiply imputed datasets. Using stepwise backward selection, variables that reached statistical significance after adjusting for all other covariates remained in the final model. To evaluate for potential effect modification, pairwise interactions among all variables in the final model were further tested, and TFT curves were generated.

Among patients who started chemoimmunotherapy, overall survival from the start of therapy was determined. Univariable analyses were performed testing for risk factors associated with overall survival, but multivariable analyses were precluded because of the limited number of deaths. The analyses were conducted using Stata 14, SAS 9.4 and the statistical significance was set as $P < 0.05$.

Results

Patients' characteristics

Diagnostic samples meeting the above criteria were identified for 329 patients. The patients' clinical data are presented in Table 1. The median age of the patients was 60 years (range, 34-88), 36.8% were female, and 90.2% had Rai stage 0-2.

Unbalanced translocations are more frequent in complex karyotypes, but balanced translocations are more frequent in non-complex karyotypes

Translocations occurred in 85 (25.8%) patients: 29 with balanced, 48 with unbalanced and eight with both a balanced and an unbalanced translocation. Defining complexity as ≥ 3 unrelated aberrations, 16.1% of patients had complex karyotypes, while 7.6% had ≥ 5 aberrations. The distributions of karyotype complexity,

defined as ≥ 3 aberrations, and the presence of a translocation are shown in Table 2. Of the 85 cases with a translocation, 46 also had a complex karyotype and 39 did not. Unbalanced translocations were more frequent in cases with a complex karyotype (41/46), while balanced translocations were more frequent in non-complex cases (24/39). No translocation was identified in 244 cases; 237 of these had non-complex karyotypes.

Translocations and complex karyotypes occur more frequently in unmutated IGHV chronic lymphocytic leukemia

IGHV data were available for 292 patients; data were not available for 37 patients (Table 3). Unmutated IGHV was found in 148 patients; 51 (34.5%) had a translocation, and 97 (65.5%) did not have a translocation; 31 (20.9%) had complex karyotypes (≥ 3 aberrations), while

Table 1. The patients' baseline characteristics and associations with time to first treatment.

Patients' characteristics (n=329)	N.	%	HR	95% CI	P-value
Age at diagnosis, years					
Mean (SD)	60 (11)				
Median (range)	60 (34-88)		1.00	0.99-1.02	0.64
Sex					
Male	208	63.2			
Female	121	36.8	0.90	0.64-1.27	0.55
Complexity					
Median (range)	1 (0-17)		1.16	1.11-1.22	<0.001
< 3 Abnormalities	276	83.9			
≥ 3 Abnormalities	53	16.1	2.92	1.98-4.31	<0.001
Translocation					
Neither	244	74.2			
Balanced	29	9.1	2.64*	1.87-3.71	<0.001
Unbalanced	56	16.7			
Rai stage at diagnosis					
0-2	296	90.2			
3-4	32	9.8	3.73	2.32-5.99	<0.001
IGHV unmutated					
No	144	49.3			
Yes	148	50.7	3.48	2.38-5.08	<0.001
Trisomy 3					
No	312	94.8			
Yes	17	5.2	1.06	0.49-2.27	0.88
Trisomy 8					
No	314	95.4			
Yes	15	4.6	2.53	1.36-4.71	0.003
Trisomy 12					
No	251	76.3			
Yes	78	23.7	1.23	0.84-1.81	0.29
Del(13q)					
No	155	47.1			
Yes	174	52.9	0.78	0.56-1.09	0.15
Del(17p)					
No	298	90.6			
Yes	31	9.4	2.10	1.31-3.37	0.002
Del(6q)					
No	315	95.7			
Yes	14	4.3	1.73	0.85-3.55	0.13
Del(11q)					
No	285	86.6			
Yes	44	13.4	2.92	1.98-4.31	<0.001
β -microglobulin >3.5 mg/L					
No	165	90.2			
Yes	18	9.8	2.33	1.11-4.88	0.025
WBC, $\times 10^9/L$					
Median (range)	17.5 (2.9-392.6)		1.72**	1.35-2.20	<0.001

HR: hazard ratio; 95% CI: 95% confidence interval; SD: standard deviation; WBC: white blood cell count. The results for trisomy 3, trisomy 8, trisomy 12, del(13q), del(17p), del(6q) and del(11q) were determined from fluorescence *in situ* hybridization data. Trisomy 3 was determined using the *BCL6* probe, trisomy 8 using the *MYC* probe, trisomy 12 using the D12Z3 (centromere 12) probe, del(13q) using the D13S319 probe, del(17p) using the *TP53* probe, del(6q) using the *MYB* and/or *SEC63* probes and del(11q) using the *ATM* probe.*HR for balanced and unbalanced translocations combined compared to no translocations, **HR for log-transformed WBC.

117 (79.1%) had non-complex karyotypes. Of the 144 patients with mutated IGHV, 20 (13.9%) had a translocation, 124 (86.1%) did not have a translocation, 12 (8.3%) had complex karyotypes, and 132 (91.7%) had non-complex karyotypes.

Outcome

The median follow-up for censored patients was 30 months (range, 0.03-102 months). The median TFT for the entire cohort was 47 months (95% confidence interval [95% CI]: 39-61 months). Higher karyotype complexity was significantly associated with TFT (hazard ratio [HR]=1.16, 95% CI: 1.11-1.22; $P<0.001$), as was complex karyotype defined using ≥ 3 aberrations (HR=2.92, 95% CI: 1.98-4.31; $P<0.001$) and ≥ 5 aberrations (HR=2.93, 95% CI: 1.79-4.79; $P<0.001$). Since there was no difference in the ability to discriminate TFT when defining complexity as ≥ 3 or ≥ 5 aberrations (*Online Supplementary Table S1*, *Online Supplementary Figure S1*), all further analyses used the definition of ≥ 3 abnormalities.

In univariable models, the following variables were significant for a shorter TFT: presence of a translocation (HR=2.64, 95% CI: 1.87-3.71; $P<0.001$), Rai stage 3-4 (HR=3.73, 95% CI: 2.32-5.99; $P<0.001$), karyotype complexity (HR=2.92, 95% CI: 1.98-4.31, $P<0.001$), unmutated IGHV (HR=3.48, 95% CI: 2.38-5.08; $P<0.001$), three copies of *MYC* (HR=2.53, 95% CI: 1.36-4.71; $P=0.003$), del(17p) (HR=2.10, 95% CI: 1.31-3.37; $P=0.002$), del(11q) (HR=2.92, 95% CI: 1.98-4.31; $P<0.001$), β_2 -microglobulin >3.5 mg/L (HR=2.33, 95% CI: 1.11-4.88; $P=0.025$), and log-transformed WBC count (HR=1.72, 95% CI: 1.35-2.20; $P<0.001$) (Table 1).

In the multivariable regression model, there was signifi-

cant effect modification of IGHV status on the relationship between translocations and TFT ($P=0.002$) (Table 4). In IGHV-mutated patients, those with a translocation had over 3.5 times the risk of starting treatment relative to those without a translocation (HR=3.53, 95% CI: 1.76-7.06; $P<0.001$); however, in IGHV-unmutated patients, a translocation did not significantly increase the risk of starting treatment (HR=1.00, 95% CI: 0.61-1.64; $P=0.99$) (Figure 1). This effect modification appears consistent across groups defined by complex karyotype (*Online Supplementary Figure S2*). We did not detect a significant interaction between IGHV and karyotype complexity (Figure 2A), nor between translocations and complexity (Figure 2B). Examination of both the presence of a translocation and karyotype complexity in the analysis of TFT showed that among the 85 patients with a translocation, karyotype complexity added prognostic information (HR=2.31, 95% CI: 1.25-4.26; $P=0.007$). Independently of IGHV status and translocations, Rai stage 3-4 (HR=1.78, 95% CI: 1.06-2.98; $P=0.029$), log-transformed WBC count (HR=1.44, 95% CI: 1.13-1.85; $P=0.004$) and karyotype complexity (HR=1.78, 95% CI: 1.08-2.93; $P=0.025$) remained statistically significant in the multivariable model (Table 4). Notably, once these variables were accounted for in the model, del(17p) did not add significant information ($P=0.51$). Using a higher frequency of del(17p) with a 20% cut off, del(17p) still was not significant in the multivariable analysis ($P=0.51$). Similarly, del(11q) was no longer significant in the multivariable model.

Among 139 patients who started CLL treatment, 54 received chemotherapeutic. With a median follow-up of 43.9 (range, 3.4-94.0) months from the start of CLL

Table 2. Association between karyotype complexity (≥ 3 aberrations) and translocations. Unbalanced translocations are more frequent in patients with complex karyotypes, but balanced translocations are more frequent in those with non-complex karyotypes.

	Total	Translocation		No Translocation	Total
		Balanced	Unbalanced		
Complex karyotype	46	5	41	7	53
Non-complex karyotype	39	24	15	237	276
Total	85	29	56	244	329

Table 3. Associations of IGHV with karyotype complexity (≥ 3 aberrations) and translocations. Translocations and complex karyotypes occur more frequently in unmutated IGHV chronic lymphocytic leukemia.

	Translocation	No Translocation	Complex karyotype	Non-complex karyotype	Total
Mutated IGHV	20	124	12	132	144
Unmutated IGHV	51	97	31	117	148
Total	71	221	43	249	292

mlGHV, mutated IGHV; umlGHV, unmutated IGHV

Table 4. Multivariable model of factors significantly associated with time to first treatment.

Characteristics	HR	95% CI	P-value
IGHV mutated: translocation present vs. absent	3.53	1.76-7.06	0.002
IGHV unmutated: translocation present vs. absent	1.00	0.61-1.64	
Karyotype complexity, ≥ 3 abnormalities: present vs. absent	1.78	1.08-2.93	0.025
WBC (log-transformed)	1.44	1.13-1.85	0.004
Rai stage: 3-4 vs. 0-2	1.78	1.06-2.98	0.029

HR: hazard ratio; 95% CI: 95% confidence interval; WBC: white blood cell count.

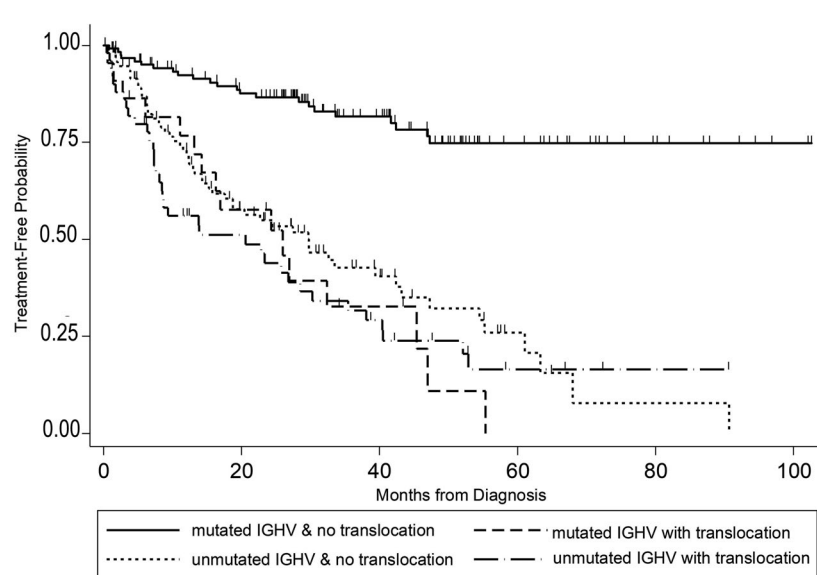


Figure 1. Time to first treatment of patients with chronic lymphocytic leukemia. Data are plotted for patients according to whether they had mutated or unmutated IGHV and whether they did or did not have a translocation.

treatment, 13 deaths occurred. The overall survival estimates are 91% (95% CI: 79%-96%) at 1 year, 84% (95% CI: 70%-92%) at 3 years, and 77% (95% CI 61%-87%) at 5 years after starting CLL treatment. In these treated patients, Rai stage 3-4 and del(17p) were associated with shorter survival in univariable analyses with a hazard ratio of 5.36 (95% CI: 1.62-17.76), and 6.88 (95% CI: 2.20-21.50), respectively.

Table 5 shows correlations of interphase FISH abnormalities with both the presence of a translocation and with karyotype complexity. Del(11q), del(17p), three copies of *MYC*, and three copies of *BCL6* were all highly associated both with the presence of a translocation and with karyotypic complexity. An opposite trend was seen for cases with del(13q); del(13q) was more frequent both in cases without a translocation and in non-complex cases. Trisomy 12 was frequent in complex cases, but was not associated with the presence of a translocation. Deletion of 6q was not associated with either karyotypic complexity or the presence of a translocation. Deletion of 13q as the sole FISH-identified abnormality, typically indicative of a good prognosis, occurred in 119 cases. Twelve of these cases had a translocation, and three had a complex karyotype. In addition, ten cases with a translocation had no abnormalities detected by FISH, emphasizing the need for metaphase cytogenetics.

Discussion

Previous studies have found a significant impact of translocations on the outcome of patients with CLL.^{5,9,17-19} We show that when detected within 1 year of diagnosis, the presence of a translocation in cases with mutated IGHV appears to negate the positive impact of mutated IGHV. However, in cases of unmutated IGHV, the presence of a translocation did not appear to influence prognosis. In this study, patients with mutated IGHV who did not have a translocation had a significantly longer TFT than those with mutated IGHV and a translocation or those with unmutated IGHV regardless of the presence of a translocation (Figure 1).

Baliakas *et al.*⁹ found that translocations were strongly associated with CD38⁺ expression, karyotypic complexity, abnormal 17p and abnormal 11q. However, the presence of a translocation did not influence TFT, although those cases with an unbalanced translocation and those with a complex karyotype had a significantly shorter TFT. Translocations were also associated with complexity, del(17p), and del(11q) in our series. However, when considering their impact on outcome, those cases with a mutated IGHV and a translocation had a poor TFT compared with cases with mutated IGHV and no translocation. Rigolin *et al.*¹⁹ showed that unbalanced translocations were associated with shorter TFT and overall survival. In our studies, both balanced and unbalanced translocations were considered together and overall had an impact on TFT.

These results add to the factors that may influence the outcome of CLL patients with mutated IGHV. IGHV-mutated patients with high expression of CD49d and those with high expression of CXCR4 have an inferior outcome compared to patients with low expression of these variables.³⁰⁻³² As neither CD49d nor CXCR4 was evaluated in our patients, we are unable to compare their effects with those of the presence of a translocation. Whether these factors influence chromosome instability, a possible factor in generation of a translocation, was not investigated.

Complex karyotypes have also been associated with an adverse prognosis in CLL.^{4-16,19} While some studies^{15,16} found that the association of karyotypic complexity was more significant when complexity was defined as ≥ 5 aberrations than when defined as ≥ 3 aberrations, we found that complexity defined as ≥ 3 abnormalities was as significant as complexity defined as ≥ 5 abnormalities. Although karyotypic complexity detected within 1 year of diagnosis of CLL remained significant in a multivariable analysis, the hazard ratio for the presence of a translocation in patients with mutated IGHV was much higher than that for karyotypic complexity (HR for complexity=1.78, HR for presence of a translocation=3.53). Among patients with a translocation, karyotypic complexity added prognostic information.

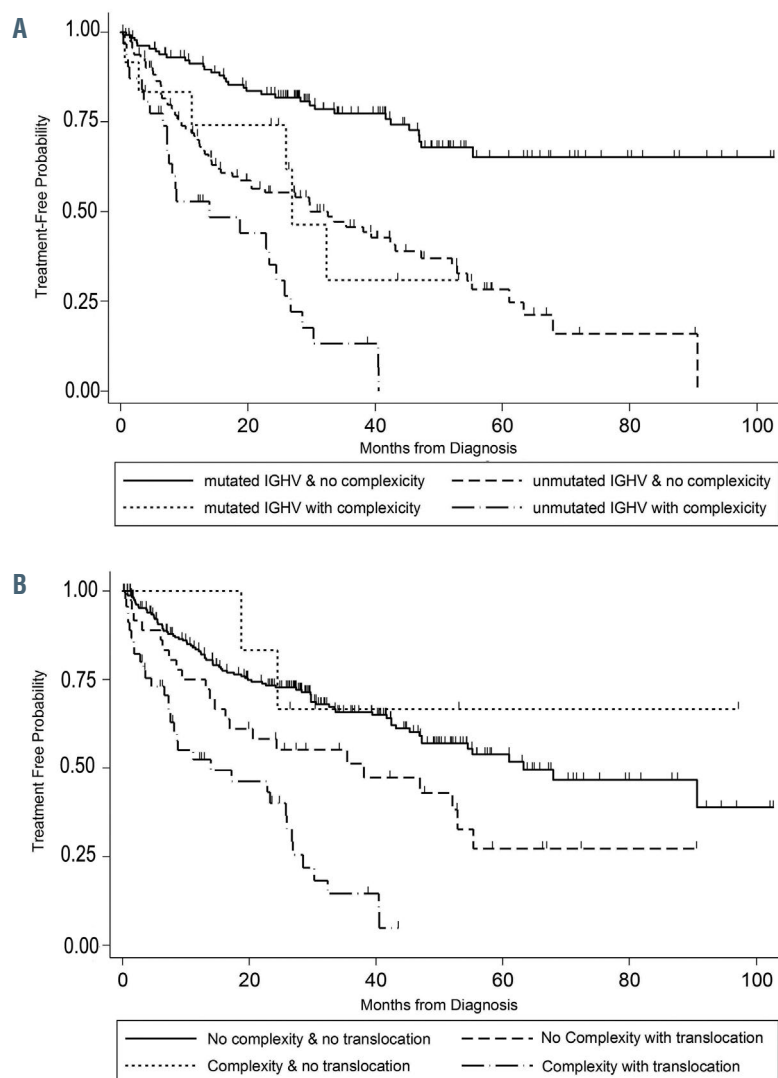


Figure 2. Time to first treatment of patients with chronic lymphocytic leukemia. (A) Data are plotted for patients according to whether they had mutated or unmutated IGHV and a complex (≥ 3 aberrations) or non-complex karyotype. (B) Data are plotted for patients according to whether they did or did not have a translocation and whether they had a complex (≥ 3 aberrations) or non-complex karyotype.

This study also showed that CLL patients with a higher WBC count were likely to require treatment earlier than those with a lower WBC count. This is consistent with the findings of the study by Del Giudice *et al.*,³³ who showed that in patients with Binet stage A CLL, a higher WBC count independently predicted a shorter time to treatment. Since a higher WBC count is consistent with a greater disease burden, this is compatible with the hypothesis that patients with a greater disease burden, regardless of other factors, have a shorter TFT.

A del(17p) has also been associated with a poor outcome.^{1,5,34-38} However, when detected within 1 year of diagnosis, it was no longer significant in a multivariable analysis, independently of other variables. It is known that del(17p) frequently occurs with disease progression and that a higher frequency of del(17p) may be significant.^{39,40} We, therefore examined whether a higher frequency of this abnormality was significant. Using a 20% cutoff, higher frequency of del(17p) was also not significant in the multivariable analysis ($P=0.51$). Furthermore, our patients were within 1 year of diagnosis, which is consistent with the findings of Tam *et al.*,³⁹ who showed that a del(17p) in asymptomatic CLL patients does not necessarily convey a poor prognosis. It also has been shown that del(17p) in association with a complex karyotype predicts a particu-

larly poor outcome.^{15,20,41} Although our patients with del(17p) were statistically associated with a complex karyotype, 11/30 of our del(17p) cases did not have a complex karyotype. The loss of significance of del(17p) in a multivariable analysis may in part reflect this.

In these studies, FISH abnormalities typically associated with a poor outcome (three copies of *MYC*, del(17p), del(11q) and three copies of *BCL6*) were more frequent in cases with a translocation and in those with a complex karyotype. Trisomy 12 showed no association with the presence of a translocation, but was more frequent in complex cases than in non-complex cases (35.9% and 21.4%, respectively; $P=0.033$). Deletions of 13q, typically associated with a good outcome, were more frequent in cases without a translocation and in non-complex cases, consistent with its association with a good outcome. However, del(13q) as a sole FISH abnormality was present in 12 cases with a translocation and in three cases with a complex karyotype, thus 15 of 119 cases (12.6%) with del(13q) as the only FISH-detected abnormality had poor metaphase cytogenetics, identifying these patients as possibly not having the good prognosis typically associated with sole del(13q). Fifty-seven cases had no FISH abnormality (Table 5); ten of these had a translocation, and one had a complex karyotype. These results indicate the

Table 5. Associations between translocations or karyotype complexity with abnormalities detected by interphase fluorescence *in situ* hybridization.

	Total	MYC		Del(17p)		Del(11q)		Trisomy 12		Del(13q)		Trisomy BCL6		Del(6q)		Normal FISH
		normal	x3	No	Yes	No	Yes	No	Yes	No	Yes	No	Yes	No	Yes	
Translocation	85	75	10	62	23	64	21	62	23	51	34	75	10	79	6	10
No translocation	244	239	5	237	7	221	23	189	55	104	140	237	7	237	7	47
P-value		0.001		<0.001		0.001		0.459		0.008		0.003		0.207		
Complex ≥3	53	45	8	34	19	38	15	34	19	32	21	43	10	48	5	1
Not complex	276	269	7	265	11	247	29	217	59	123	153	269	7	268	8	56
P-value		0.001		<0.001		0.001		0.033		0.037		<0.001		0.057		

importance of metaphase cytogenetics in order to risk-stratify patients accurately.

The reason a translocation may negate the good prognosis associated with mutated IGHV is not known. Both the presence of a translocation and a complex karyotype may reflect an underlying genetic instability in CLL. The strong correlation of translocations and complex karyotypes with del(17p), and therefore loss of TP53, which is known to be associated with genetic instability,⁴² supports this. However, the majority of patients with translocations or complex karyotypes did not have del(17p); thus, other factors must contribute to genetic instability in CLL. Other factors that have been associated with genetic instability include telomere shortening, abnormal ATM, lack of correct kinetochore-microtubule attachment, activation-induced cytidine deaminase, defective mitosis and replication stress. Further investigations are needed to identify whether these or other factors contribute to genetic instability in CLL.

These studies have some significant limitations. These include the relatively low number of patients with translocations (85/329), the retrospective nature of the study, and the younger age of patients (median, 60 years). Because of the retrospective nature of this study, some factors, significantly TP53 mutational status and CD49d expression, could not be included as they were not determined routinely. Additionally, both WBC count and β_2 -microglobulin level had a 90-day window, as they were not collected routinely at diagnosis. Also, although all cytogenetic studies were performed within 1 year of diagnosis, they were done at different time-points within this 1-year time-frame.

These results support performing metaphase cytogenetic analysis on cultures stimulated with a CpG

oligodeoxynucleotide prospectively at diagnosis on all patients with CLL to verify these findings and to determine whether these findings apply with current targeted therapies. The use of CpG oligodeoxynucleotide stimulation is required to adequately define abnormal clones in CLL,^{5,17,21-26} thus enabling the detection of translocations that are prognostic early in the course of the disease. This additional prognostic factor may help to provide a more precise prognosis for CLL patients, and may more accurately define specific treatment options that will be beneficial to these patients. While the presence of a translocation has previously been shown to correlate with a poor prognosis, this study indicates that in patients with unmutated IGHV, translocations may not affect prognosis. However, detection of a translocation in patients with mutated IGHV may affect prognosis as early as the time of diagnosis.

Disclosures

No conflicts of interest to disclose.

Contributions

NAH did the research. NAH and NM designed the research and wrote the paper. ASR and QZ performed the statistical analysis. LAA, MRG, KJM, JW, FA, ML, AG, CC and JCB contributed samples and data. All authors contributed to writing and finalizing the manuscript and approved its submission.

Funding

This work was supported by Leukemia and Lymphoma Society SCOR grant #7004-11, NCI-7 P50 CA140158-02, and NCI-P30 CA016058, which supports the OSU Comprehensive Cancer Center's Shared Resources, and the D Warren Brown Foundation.

References

- Byrd JC, Gribben JG, Peterson BL, et al. Select high-risk genetic features predict earlier progression following chemoimmunotherapy with fludarabine and rituximab in chronic lymphocytic leukemia: justification for risk-adapted therapy. *J Clin Oncol.* 2006;24(3):437-443.
- Oscier DG, Gardiner AC, Mould SJ, et al. Multivariate analysis of prognostic factors in CLL: clinical stage, IGHV gene mutational status, and loss or mutation of the p53 gene are independent prognostic factors. *Blood.* 2002;100(4):1177-1184.
- Hamblin TJ, Davis Z, Gardiner A, Oscier DG, Stevenson FK. Unmutated Ig V(H) genes are associated with a more aggressive form of chronic lymphocytic leukemia. *Blood.* 1999;94(6):1848-1854.
- Haferlach C, Dicker F, Weiss T, et al. Toward a comprehensive prognostic scoring system in chronic lymphocytic leukemia based on a combination of genetic parameters. *Genes Chromosomes Cancer.* 2010;49(9):851-859.
- Haferlach C, Dicker F, Schnittger S, Kern W, Haferlach T. Comprehensive genetic characterization of CLL: a study on 506 cases analysed with chromosome banding analysis, interphase FISH, IgV(H) status and immunophenotyping. *Leukemia.* 2007;21(12):2442-2451.
- Woyach JA, Ruppert AS, Guinn D, et al. BTK(C481S)-mediated resistance to ibrutinib in chronic lymphocytic leukemia. *J Clin Oncol.* 2017;35(18):1487-1443.
- Woyach JA, Lozanski G, Ruppert AS, et al. Outcome of patients with relapsed or refractory chronic lymphocytic leukemia treated with flavopiridol: impact of genetic features. *Leukemia.* 2012;26(6):1442-1444.
- Jaglowski SM, Ruppert AS, Heerema NA, et al. Complex karyotype predicts for inferior outcomes following reduced-intensity conditioning allogeneic transplant for chronic lymphocytic leukaemia. *Br J Haematol.* 2012;159(1):82-87.
- Baliakas P, Iskas M, Gardiner A, et al. Chromosomal translocations and karyotype complexity in chronic lymphocytic leukemia: a systematic reappraisal of classic cytogenetic data. *Am J Hematol.* 2014;89(3):249-255.
- Rogers KA, Huang Y, Ruppert AS, et al. A single-institution retrospective cohort study of first-line R-EPOCH chemoimmunotherapy for Richter syndrome demonstrating complex chronic lymphocytic leukaemia karyotype as an adverse prognostic factor. *Br J Haematol.* 2018;180(2):259-266.
- Rigolin GM, Formigaro L, Cavallari M, et al. An extensive molecular cytogenetic characterization in high-risk chronic lymphocytic leukaemia. *Br J Haematol.* 2012;159(1):82-87.

phocytic leukemia identifies karyotype aberrations and TP53 disruption as predictors of outcome and chemorefractoriness. *Oncotarget*. 2017;8(17):28008-28020.

12. Rigolin GM, Cavallari M, Quaglia FM, et al. In CLL, comorbidities and the complex karyotype are associated with an inferior outcome independently of CLL-IPI. *Blood*. 2017;129(26):3495-3498.
13. Le Bris Y, Struski S, Guièze R, et al. Major prognostic value of complex karyotype in addition to TP53 and IGHV mutational status in first-line chronic lymphocytic leukemia. *Hematol Oncol*. 2017;35(4):664-670.
14. Cavallari M, Cavazzini F, Bardi A, et al. Biological significance and prognostic/predictive impact of complex karyotype in chronic lymphocytic leukemia. *Oncotarget*. 2018;9(76):34398-34412.
15. Baliakas P, Jeromin S, Iskas M, et al. Cytogenetic complexity in chronic lymphocytic leukemia: definitions, associations, and clinical impact. *Blood*. 2019;133(11):1205-1216.
16. Rigolin GM, del Giudice I, Formigaro L, et al. Chromosome aberrations detected by conventional karyotyping using novel mitogens in chronic lymphocytic leukemia: clinical and biologic correlations. *Genes Chromosomes Cancer*. 2015;54(12):818-826.
17. Mayr C, Speicher MR, Kofler DM, et al. Chromosomal translocations are associated with poor prognosis in chronic lymphocytic leukemia. *Blood*. 2006;107(2):742-751.
18. Van Den Neste E, Robin V, Francart J, et al. Chromosomal translocations independently predict treatment failure, treatment-free survival and overall survival in B-cell chronic lymphocytic leukemia patients treated with cladribine. *Leukemia*. 2007;21(8):1715-1722.
19. Rigolin GM, Saccetti E, Guardalben E, et al. In chronic lymphocytic leukaemia with complex karyotype, major structural abnormalities identify a subset of patients with inferior outcome and distinct biological characteristics. *Br J Haematol*. 2018;181(2):229-233.
20. Herling CD, Klaumünzer M, Rocha CK, et al. Complex karyotypes and KRAS and POT1 mutations impact outcome in CLL after chlorambucil-based chemotherapy or chemoimmunotherapy. *Blood*. 2016;128(3):395-404.
21. Decker T, Schneller F, Kronschnabl M, et al. Immunostimulatory CpG-oligonucleotides induce functional high affinity IL-2 receptors on B-CLL cells: costimulation with IL-2 results in a highly immunogenic pheno-
- type. *Exp Hematol*. 2000;28(5):558-568.
22. Decker T, Schneller F, Sparwasser T, et al. Immunostimulatory CpG-oligonucleotides cause proliferation, cytokine production, and an immunogenic phenotype in chronic lymphocytic leukemia B cells. *Blood*. 2000;95(3):999-1006.
23. Dicker F, Schnittger S, Haferlach T, Kern W, Schoch C. Immunostimulatory oligonucleotide-induced metaphase cytogenetics detect chromosomal aberrations in 80% of CLL patients: a study of 132 CLL cases with correlation to FISH, IgVH status, and CD38 expression. *Blood*. 2006;108(9):3152-3160.
24. Muthusamy N, Breidenbach H, Andritsos L, et al. Enhanced detection of chromosomal abnormalities in chronic lymphocytic leukemia by conventional cytogenetics using CpG oligonucleotide in combination with pokeweed mitogen and phorbol myristate acetate. *Cancer Genet*. 2011;204(2):77-83.
25. Put N, Konings P, Rack K, et al. Improved detection of chromosomal abnormalities in chronic lymphocytic leukemia by conventional cytogenetics using CpG oligonucleotide and interleukin-2 stimulation: a Belgian multicentric study. *Genes Chromosomes Cancer*. 2009;48(10):843-853.
26. Struski S, Gervais C, Helias C, et al. Stimulation of B-cell lymphoproliferations with CpG-oligonucleotide DSP30 plus IL-2 is more effective than with TPA to detect clonal abnormalities. *Leukemia*. 2009;23(3):617-619.
27. Haferlach C, Jeromin S, Nadarajah N, et al. Cytogenetic and molecular genetic clonal evolution in CLL is associated with an unmutated IGHV status and frequently leads to a combination of loss of 17p and TP53 mutation. *Blood*. 2016;128(22):3213-3213.
28. Stilgenbauer S, Sander S, Bullinger L, et al. Clonal evolution in chronic lymphocytic leukemia: acquisition of high-risk genomic aberrations associated with unmutated VH, resistance to therapy, and short survival. *Haematologica*. 2007;92(9):1242-1245.
29. Hallek M, Cheson BD, Catovsky D, et al. iwCLL guidelines for diagnosis, indications for treatment, response assessment, and supportive management of CLL. *Blood*. 2018;131(25):2745-2760.
30. Pepper C, Buggins AG, Jones CH, et al. Phenotypic heterogeneity in IGHV-mutated CLL patients has prognostic impact and identifies a subset with increased sensitivity to BTK and PI3Kδ inhibition. *Leukemia*. 2015;29(3):744-747.
31. Baumann T, Delgado J, Santacruz R, et al. CD49d (ITGA4) expression is a predictor of time to first treatment in patients with chronic lymphocytic leukaemia and mutated IGHV status. *Br J Haematol*. 2016;172(1):48-55.
32. Gattei V, Bulian P, Del Principe MI, et al. Relevance of CD49d protein expression as overall survival and progressive disease prognosticator in chronic lymphocytic leukemia. *Blood*. 2008;111(2):865-873.
33. Del Giudice I, Mauro FR, De Propriis MS, et al. White blood cell count at diagnosis and immunoglobulin variable region gene mutations are independent predictors of treatment-free survival in young patients with stage A chronic lymphocytic leukemia. *Haematologica*. 2011;96(4):626-630.
34. Dohner H, Stilgenbauer S, Benner A, et al. Genomic aberrations and survival in chronic lymphocytic leukemia. *N Engl J Med*. 2000;343(26):1910-1916.
35. Foa R, Del Giudice I, Guarini A, Rossi D, Gaidano G. Clinical implications of the molecular genetics of chronic lymphocytic leukemia. *Haematologica*. 2013;98(5):675-685.
36. Lin TS, Ruppert AS, Johnson AJ, et al. Phase II study of flavopiridol in relapsed chronic lymphocytic leukemia demonstrating high response rates in genetically high-risk disease. *J Clin Oncol*. 2009;27(35):6012-6018.
37. Zenz T, Eichhorst B, Busch R, et al. TP53 mutation and survival in chronic lymphocytic leukemia. *J Clin Oncol*. 2010;28(29):4473-4479.
38. Stephens DM, Ruppert AS, Weirda WG, et al. Externally validated predictive clinical model for untreated del(17p13.1) chronic lymphocytic leukemia patients. *Am J Hematol*. 2015;90(11):967-969.
39. Tam CS, Shanafelt TD, Wierda WG, et al. De novo deletion 17p13.1 chronic lymphocytic leukemia shows significant clinical heterogeneity: the M. D. Anderson and Mayo Clinic experience. *Blood*. 2009;114(5):957-964.
40. Van Dyke DL, Werner L, Rassenti LZ, et al. The Dohner fluorescence in situ hybridization prognostic classification of chronic lymphocytic leukaemia (CLL): the CLL Research Consortium experience. *Br J Haematol*. 2016;173(1):105-113.
41. Yu L, Kim HT, Kasar S, et al. Survival of del17p CLL depends on genomic complexity and somatic mutation. *Clin Cancer Res*. 2017;23(3):735-745.
42. Liu G, Parant JM, Lang G, et al. Chromosome stability, in the absence of apoptosis, is critical for suppression of tumorigenesis in Trp53 mutant mice. *Nat Genet*. 2004;36(1):63-68.



Fibrinogen interaction with complement C3: a potential therapeutic target to reduce thrombosis risk

Rhodri J. King,^{1*} Katharina Schuett,^{2*} Christian Tiede,³ Vera Jankowski,⁴ Vicky John,¹ Abhi Trehan,¹ Katie Simmons,⁵ Sreenivasan Ponnambalam,⁶ Robert F. Storey,⁷ Colin W.G. Fishwick,⁵ Michael J. McPherson,³ Darren C. Tomlinson³ and Ramzi A. Ajjan¹

¹Leeds Institute for Cardiovascular and Metabolic Medicine, Leeds University, Leeds, UK; ²Department of Internal Medicine I, University Hospital Aachen, Aachen, Germany, ³Bioscreening Technology Group in the School of Molecular and Cellular Biology, University of Leeds, Leeds, UK, ⁴Institute for Molecular and Cardiovascular Research, Aachen University, Aachen, Germany, ⁵School of Chemistry, University of Leeds, Leeds, UK, ⁶School of Molecular & Cellular Biology, University of Leeds, Leeds, UK and ⁷School of Medicine, University of Sheffield, Sheffield, UK

*RJK and KS contributed equally as co-first authors.

ABSTRACT

Complement C3 binds fibrinogen and compromises fibrin clot lysis, thereby enhancing the risk of thrombosis. We investigated the role of the fibrinogen-C3 interaction as a novel therapeutic target to reduce thrombosis risk by analyzing: (i) consistency in the fibrinolytic properties of C3; (ii) binding sites between fibrinogen and C3; and (iii) modulation of fibrin clot lysis by manipulating fibrinogen-C3 interactions. Purified fibrinogen and C3 from the same individuals (n=24) were used to assess inter-individual variability in the anti-fibrinolytic effects of C3. Microarray screening and molecular modeling evaluated C3 and fibrinogen interaction sites. Novel synthetic conformational proteins, termed affimers, were used to modulate the C3-fibrinogen interaction and fibrinolysis. C3 purified from patients with type 1 diabetes showed enhanced prolongation of fibrinolysis compared with healthy control protein (195±105 and 522±166 s, respectively; $P=0.04$), with consistent effects but a wider range (5-51% and 5-18% lysis prolongation, respectively). Peptide microarray screening identified two potential C3-fibrinogen interaction sites within the fibrinogen β chain (residues 424-433 and 435-445). One fibrinogen-binding affimer that was isolated displayed sequence identity with C3 in an exposed area of the protein. This affimer abolished C3-induced prolongation of fibrinolysis (728±25.1 s to 632±23.7 s; $P=0.005$) and showed binding to fibrinogen in the same region that is involved in C3-fibrinogen interactions. Moreover, it shortened plasma clot lysis of patients with diabetes, cardiovascular disease or controls by 7-11%. C3 binds fibrinogen β -chain and disruption of the fibrinogen-C3 interaction using affimer proteins enhances fibrinolysis, which represents a potential novel tool to reduce thrombosis in high-risk individuals.

Correspondence:

RA AJJAN
r.ajjan@leeds.ac.uk

Received: October 1, 2019.

Accepted: April 29, 2020.

Pre-published: April 30, 2020.

<https://doi.org/10.3324/haematol.2019.239558>

©2021 Ferrata Storti Foundation

Material published in *Haematologica* is covered by copyright. All rights are reserved to the Ferrata Storti Foundation. Use of published material is allowed under the following terms and conditions: <https://creativecommons.org/licenses/by-nc/4.0/legalcode>. Copies of published material are allowed for personal or internal use. Sharing published material for non-commercial purposes is subject to the following conditions: <https://creativecommons.org/licenses/by-nc/4.0/legalcode>, sect. 3. Reproducing and sharing published material for commercial purposes is not allowed without permission in writing from the publisher.



Introduction

Hypofibrinolysis is associated with increased risk of atherothrombotic events.¹⁻³ Although most studies have only shown an association between hypofibrinolysis and cardiovascular disease, a more recent longitudinal study in a large population of patients with acute coronary syndrome demonstrated that prolonged fibrin clot lysis is an independent predictor of cardiovascular mortality.⁴ Therefore, it was proposed that reducing residual thrombosis risk in patients with coronary artery disease requires targeting the fibrinolytic system in addition to administering antiplatelet therapies. Indeed the combination of anticoagulant and antiplatelet therapies reduces vascular thrombotic events but at the expense of increased risk of bleeding.⁵ Therefore, a more targeted approach is required which improves hypofibrinolysis

and reduces the risk of vascular thrombosis without increasing bleeding events.

Complement C3, which is incorporated into fibrin clots, has been shown to modulate fibrin clot lysis,⁶ an effect that may be exaggerated in patients with higher vascular risk.⁷ C3 plasma levels have shown correlations with *ex-vivo* plasma clot lysis in individuals with diabetes as well as in healthy controls.^{7,8} Moreover, plasma levels of this protein were independent predictors of resistance to fibrinolysis in 875 high-vascular-risk patients with type 2 diabetes.⁹ These data suggest that C3 represents a credible therapeutic target to shorten fibrin clot lysis and ultimately reduce thrombosis risk. However, these functional studies were conducted using pooled C3 and studies assessing consistency of the response in different individuals, crucial to establish the therapeutic potential of C3, are lacking.

We have recently demonstrated that fibrin clot lysis can be modulated, leading to stabilization of the clot, by using small conformational proteins, termed affimers.^{10,11} Affimer technology was able to correct abnormal lysis of clots made from plasma samples of individuals with hemophilia, indicating a potential therapeutic role for these proteins. However, it remains unknown whether affimers can be used to enhance clot lysis, particularly in individuals at high vascular risk.

The aim of this work was to establish the role of C3 as a therapeutic target for enhancing fibrinolysis and reducing thrombosis risk. Therefore, we studied: (i) consistency in the fibrinolytic properties of C3 in healthy controls and patients with high vascular risk; (ii) potential binding sites between fibrinogen and C3; and (iii) modulation of fibrin clot lysis by targeted interference of fibrinogen-C3 interactions.

Methods

Only a brief description is provided here; full details can be found in the *Online Supplement*.

Recruitment of patients

We recruited 12 patients with type 1 diabetes (T1DM) and 12 age- and sex-matched controls to purify fibrinogen and C3. We additionally tested 24 stored plasma samples from individuals with high vascular risk. Ethical approval for the study was provided by the Leeds East, National Research Ethics Service committee and informed consent was obtained from participants in accordance with the Declaration of Helsinki.

Protein purification and turbidimetric analysis

Fibrinogen and complement C3 were purified as described elsewhere⁷ and clots were formed from purified fibrinogen in the presence or absence of corresponding C3 from the same individual. Time from full clot formation to 50% lysis was calculated and is presented as clot lysis time throughout this work.

Peptide microarray

A peptide microarray chip containing overlapping 15 amino acid peptides of the fibrinogen molecule (PEPperPRINT, Germany) was synthesized to screen against pooled C3 (0.8 to 8 µg/mL) purified from six healthy individuals.

Non-antibody synthetic proteins (affimers)

Affimers are small proteins composed of a scaffold protein that constrains two variable conformational nine amino acid loops.^{11,12}

Panning and protein production

A phage display library of affimer proteins, comprising 1.3×10^{10} random variable clones, was screened against human fibrinogen. In order to select specific affimers capable of targeting fibrinogen-C3 interactions, competitive elution with C3 for 20 min was applied in the fourth panning.

Affimers and fibrinolysis

Fibrinogen was incubated with affimer A6 at room temperature for 30 min after which C3 and factor XIII were added and clot formation/lysis was triggered as described previously.¹³

Plasma samples were mixed with increasing concentrations of affimer A6 or control scaffold and then turbidimetric experiments were performed, as described elsewhere.¹³

Molecular modeling

In order to identify potential sites of ligand binding on C3, the molecular modeling software Autoligand was employed to scan the whole protein.¹⁴ Molecular modeling was used to predict binding sites of any peptide sequences identified from the microarray screening and affimer work using the webserver Pepsite2[®] (<http://pepsite2.russelllab.org>). Images were viewed and produced using Pymol (The PyMOL Molecular Graphics System, Version 2.0 Schrödinger, LLC).¹⁵

Mass spectrometry

Purified C3 from six subjects with type 1 diabetes mellitus and six healthy controls was digested by trypsin and analyzed by matrix-assisted laser desorption/ionization -time-of-flight mass spectrometry (MALDI-TOF/MS) as described elsewhere.¹⁶ To compare potential differences between *in vivo* and *in vitro* C3 glycation, we undertook *in vitro* glycation of the protein as previously described¹⁷ and post-translational modifications were assessed as above.

Statistical analysis

Between-group comparisons of normally and non-normally distributed variables were carried out by independent Student *t* and Mann-Whitney U tests, respectively. Pearson and Spearman coefficients were applied to assess correlations between normally and non-normally distributed variables, respectively. Based on previous data⁷ and assuming a common standard deviation of the variable studied of 225 seconds (s) we calculated that the number of samples analyzed (n=24 in total) would be enough to detect a difference of 270 s in C3-induced prolongation of clot lysis time (power 80% at $P<0.05$).

Results

Patients' characteristics

Twelve patients with type 1 diabetes and 12 healthy controls were recruited. Their characteristics are shown in Table 1. The patients with diabetes were on no medications other than subcutaneous insulin injections and had no clinically significant microvascular or macrovascular complications of diabetes. The healthy controls were also not taking any prescribed medication.

Effect of C3 on lysis time

One control sample did not lyse within the allotted time and was, therefore, excluded from further analysis. The mean lysis time of all clots made from fibrinogen in the absence and presence of corresponding C3 was 2691 ± 105 and 3057 ± 172 s ($P<0.01$). The mean lysis time of clots

made from purified fibrinogen of healthy controls and patients with type 1 diabetes was 2510 ± 132 s and 2857 ± 151 s, respectively ($P=0.07$). Following the addition of C3, there was an increase in lysis time in both groups to 2705 ± 180 s and 3379 ± 259 s, respectively, with individual data provided in Figure 1A. The degree of C3-induced prolongation in lysis time was greater in the diabetes samples (179 ± 101 and 522 ± 166 s; $P=0.04$) (Figure 1B and C), and showed a broader range of 144–1476 s (5–51%) among the patients with diabetes, compared with the 108–480 s (5–18%) in controls. These data show that C3 consistently prolongs clot lysis time in both healthy controls and patients with diabetes, although there was wider inter-individual variability in the degree of prolongation in the group with diabetes.

C3-fibrinogen interaction sites

Our data have so far shown that C3 represents a credible target to modulate fibrinolysis and we therefore investigated fibrinogen-C3 binding sites. Using peptide microarray screening of the whole fibrinogen molecule, we identified complex spot patterns, based on peptides with the consensus motifs $A^{136}VSQTSSSSFQYMYL^{150}$ (peptide A), $A^{428}QCSKEDGGGWWY^{434}$ (peptide B) and $A^{434}YNRCHAANPNGRYY^{447}$ (peptide C), which are all located within the β chain of fibrinogen (Uniprot ID

Table 1. Clinical variables of controls and patients with type 1 diabetes. Data are presented as mean \pm standard error of mean.

Variable	Type 1 diabetes (n=12)	Controls (n=12)	P value
Age (years)	25.1 ± 1.7	27.9 ± 1.3	0.2
Sex (M/F, n)	7/5	9/3	
Duration of diabetes (months)	108 ± 68	-	
Current smokers (n)	2	0	
Systolic BP (mmHg)	119 ± 4.6	121 ± 3.8	0.73
Diastolic BP (mmHg)	76 ± 4	76 ± 2.5	0.85
BMI (kg/m^2)	25.4 ± 0.96	23.5 ± 0.6	0.12
C3 (mg/mL)	1.34 ± 0.06	1.39 ± 0.07	0.54
Fibrinogen (mg/mL)	$2.0 (\pm 0.32)$	$2.2 (\pm 0.27)$	0.2
Plasma glucose (mmol/L)	12.8 ± 1	4.4 ± 0.2	<0.0001
Total cholesterol (mmol/L)	4.8 ± 0.35	4.8 ± 0.32	0.97
Triglycerides (mmol/L)	1.3 ± 0.15	1.1 ± 0.11	0.16
TSH (mU/L)	2.5 ± 0.32	2.1 ± 0.18	0.33
Free T4 (pmol/L)	14.3 ± 0.39	15 ± 0.45	0.24
Creatinine ($\mu\text{mol}/\text{L}$)	76.8 ± 4.6	81 ± 4.2	0.52
Plasma clot lysis (seconds)	427.5 ± 14.6	425 ± 7.9	0.88

M: male, F: female; BP: blood pressure; BMI: body mass index; C3: complement C3; TSH: thyroid-stimulating hormone; T4: thyroxine.

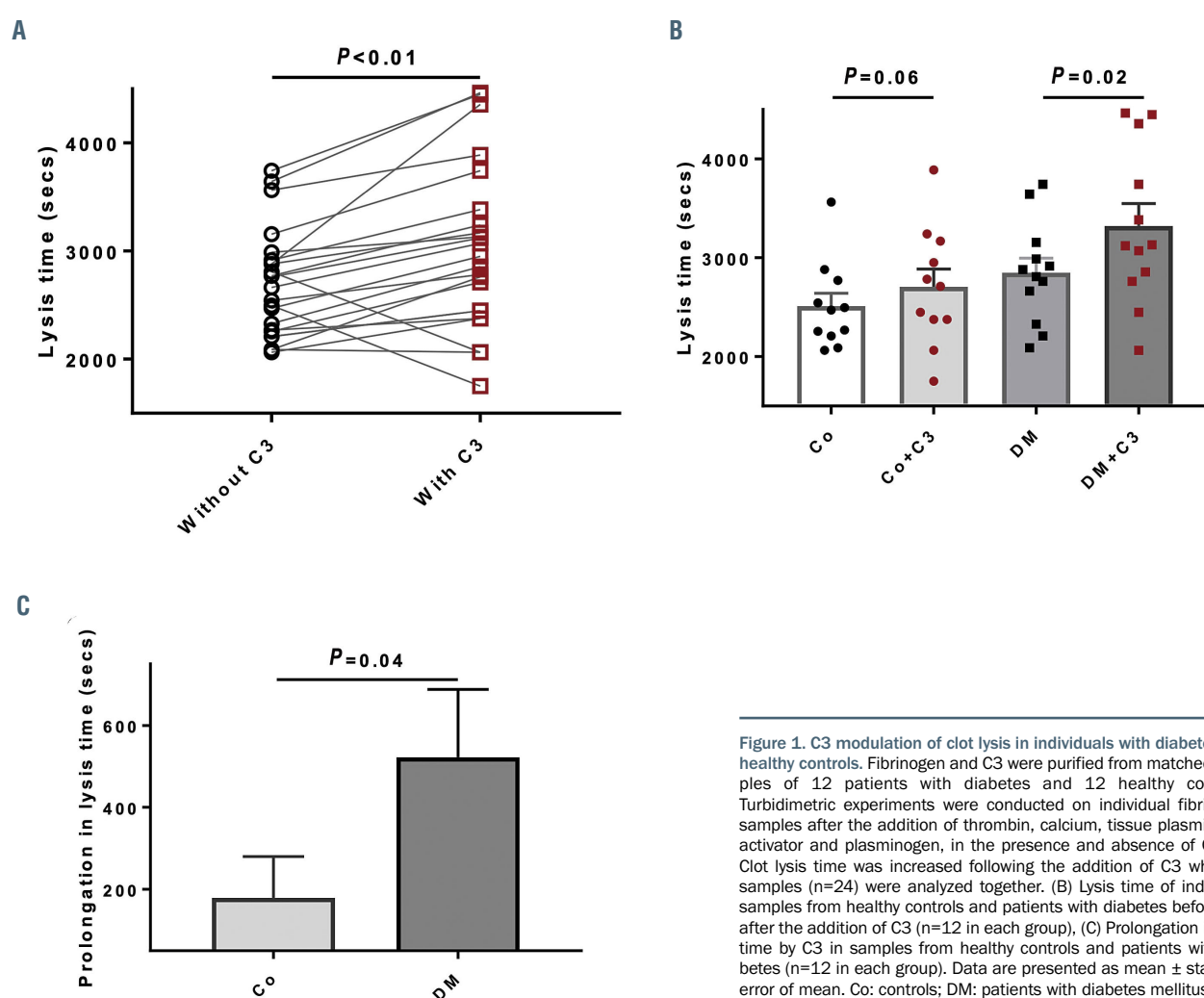


Figure 1. C3 modulation of clot lysis in individuals with diabetes and healthy controls. Fibrinogen and C3 were purified from matched samples of 12 patients with diabetes and 12 healthy controls. Turbidimetric experiments were conducted on individual fibrinogen samples after the addition of thrombin, calcium, tissue plasminogen activator and plasminogen, in the presence and absence of C3. (A) Clot lysis time was increased following the addition of C3 when all samples (n=24) were analyzed together. (B) Lysis time of individual samples from healthy controls and patients with diabetes before and after the addition of C3 (n=12 in each group). (C) Prolongation in lysis time by C3 in samples from healthy controls and patients with diabetes (n=12 in each group). Data are presented as mean \pm standard error of mean. Co: controls; DM: patients with diabetes mellitus.

P02675). Two of these peptides (B and C) were in close proximity in the N terminus of the β -chain and shared one amino acid. One peptide was closer to the C-terminal region of the β chain of fibrinogen, as shown in Figure 2. These data indicate that the β chain of fibrinogen contains key binding sites for C3.

Use of affimers for modulation of C3-induced prolongation of fibrinolysis

Isolation of affimer A6

Sixteen fibrinogen-binding affimers, which competed with C3 for fibrinogen binding, were sequenced and revealed eight distinct sequences. Each affimer is composed of a scaffold protein and two nine amino acid loops. We identified one affimer (A6) which showed sequence identity in one of its loops with residues Ser 38-His 47 of C3 (Uniprot ID P01024) (Figure 3A). This site resides in an exposed area of C3 with the potential to interact with other plasma proteins, as predicted by molecular modeling (Figure 3B).

Effects of affimer A6 on fibrinolysis

Using pooled fibrinogen from healthy controls, we investigated changes in lysis time after the addition of A6, C3 or a combination of the two. A6 did not have a significant effect on clot lysis whereas C3 prolonged clot lysis,

an effect that was completely abolished by the addition of A6 (Figure 4A). Affimer A6 had no effect on lysis time when C3 was substituted by plasmin inhibitor, indicating a C3-specific effect (Figure 4A).

Given the results of the purified protein experiments, we next analyzed plasma samples. A dose-response curve, using pooled healthy control plasma samples, verified that a 1:1 molar concentration of fibrinogen:affimer A6 is optimal for modulation of clot lysis (Figure 4B). Using this molar ratio, affimer A6 reduced the lysis time of clots made from pooled healthy control plasma from 593 ± 17 s to 542 ± 10 s (7%, $P < 0.05$) with a decrease from 618 ± 13 s to 548 ± 15 s for clots made from plasma from patients with diabetes (11%, $P < 0.05$) (Figure 4C). We also tested the effect of affimer A6 in individual samples and not only pooled plasma. Affimer A6 reduced plasma clot lysis in 24 patients with high vascular risk (11 with coronary artery disease and 13 with type 2 diabetes) from 1237 ± 150 s to 1120 ± 129 s (10%, $P < 0.05$) (Figure 4D).

Binding sites of affimer A6 on fibrinogen

Following the results of the microarray screening of C3 and fibrinogen, the sequences for the two random loops of A6 were individually entered into the Pepsite2 webserver to predict where A6 might be binding to the β -chain of fibrinogen (PDB code 3GHG; ¹⁸). The strongest binding

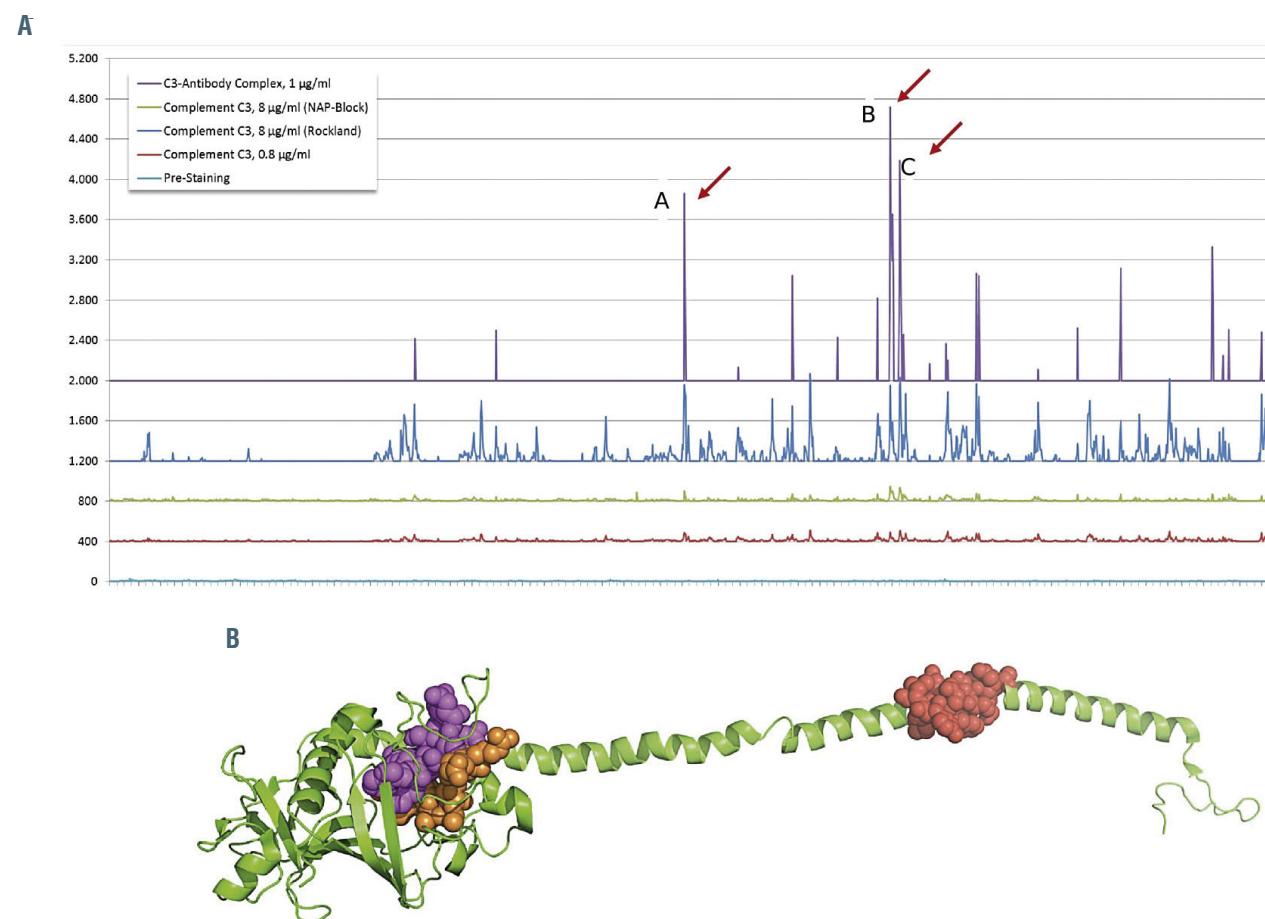


Figure 2. Fibrinogen peptide binding to C3 and location within the fibrinogen molecule. (A) Intensity plot of fibrinogen peptide binding to C3 showing mainly three binding sites (visualized as 3 distinct intensity peaks, red arrows), all located on the fibrinogen β chain (A, B and C). (B) The peptide sequences identified by the microarray screening are illustrated within the crystal structure of the β chain of fibrinogen. The red spheres indicate peptide A (436 AVSQTSSSFQYMYL 150), pink spheres indicate peptide B (423 QCSKEDGGGWY 154) and orange spheres indicate peptide C (434 YNRCHAANPNGR 145).

prediction for the two loops on the β chain was adjacent to the peptide sequences (peptides B and C) identified by the microarray screening (Figure 4E).

Mechanistic insight into potential enhancement of fibrinolysis prolongation by C3 from patients with diabetes

We have previously shown that pooled C3 purified from patients with diabetes may have enhanced anti-fibrinolytic effects compared with the protein from healthy controls.⁷ The current work, using C3 purified from individual plasma samples, demonstrates that C3 from patients with diabetes has enhanced anti-fibrinolytic activity compared with control protein, at least in some samples. We therefore investigated whether increased protein glycation may be one of the mechanisms involved in the enhanced anti-fibrinolytic effects of C3. Mass spectrometry identified similar glycation of amino acids serine, threonine, arginine, and asparagine in C3 samples from controls and patients with diabetes. However, additional lysine residues were noted to be glycated in all six diabetes samples but not in the control group, affecting six separate residues, with a mean of 3 ± 0.9 modifications in each sample. Details of the glycated lysine residues and positions within C3 are illustrated in Figure 5A and B. A

characteristic mass-spectrum of a fragment of C3 analyzed by tandem mass spectrometry, with the molecular weight of 1,206 Daltons after tryptic digestion, is shown in Figure 5C together with the protein glycation score. We verified the molecular mass of 1,206 as a characteristic post-translational glycation modification of the fragment with the molecular weight of 882 of C3. This molecular mass 1,206 m/z shows glycation of lysine, highlighted by an asterisk in the amino acid sequence $\beta K^*GPLLNLK^{*1206}$. Although the additional glycation of C3 in patients with diabetes was associated with longer clot lysis time, the Spearman coefficient did not demonstrate a significant correlation between number of glycated lysine residues within C3 and *ex vivo* plasma clot lysis time (Spearman $r=0.19$, $P=0.73$).

Discussion

There are a number of novel findings in this work that can be summarized as follows: (i) C3 purified from individual patients consistently prolongs clot lysis; (ii) the β chain of fibrinogen in the area of Cys424-Arg445 represents one region of interaction with complement C3; and (iii) affimer proteins provide a tool for targeted modula-

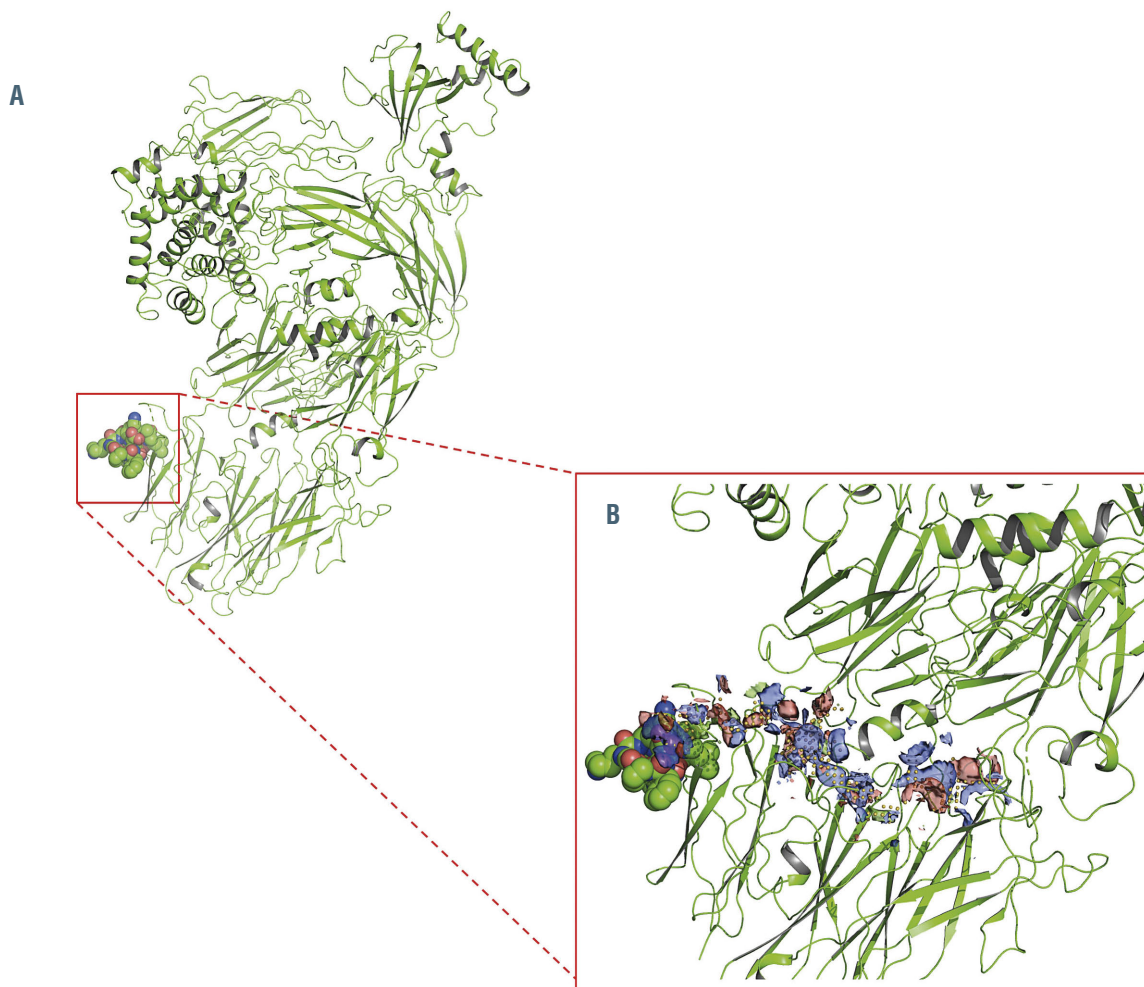


Figure 3. Affimer A6 sequence identity with C3 and potential protein-protein interaction sites on C3. (A) Loop 2 of affimer A6 showing sequence identity with the area represented by red spheres on the C3 molecule. (B) Enlargement of the area of potential protein-protein interaction sites on complement C3 (labeled in different colors) identified as the best scoring site using the SiteMap module of Glide (Schrodinger Inc).

tion of fibrin clot lysis by interfering with fibrinogen-C3 interactions.

While C3 protein purified from individual plasma samples consistently prolonged clot lysis, an inter-individual variability in the response was noted, which may be related to the degree of incorporation of C3 into the clot.¹⁹ This was particularly pronounced in C3 purified from patients with diabetes, which may be related to alternative post-translational modifications in the protein. We identified

six lysine residues that were glycated in samples from patients with type 1 diabetes, but not in samples from controls. The variability in glycation sites comparing individuals with type 1 diabetes suggests that the ability of lysine residues on C3 to undergo glycation has a large inter-individual variability, which may modulate the antifibrinolytic effects of the protein. Interestingly, *in vitro* glycation of C3 showed largely similar patterns, favoring glycation of certain lysine residues, suggesting this consis-

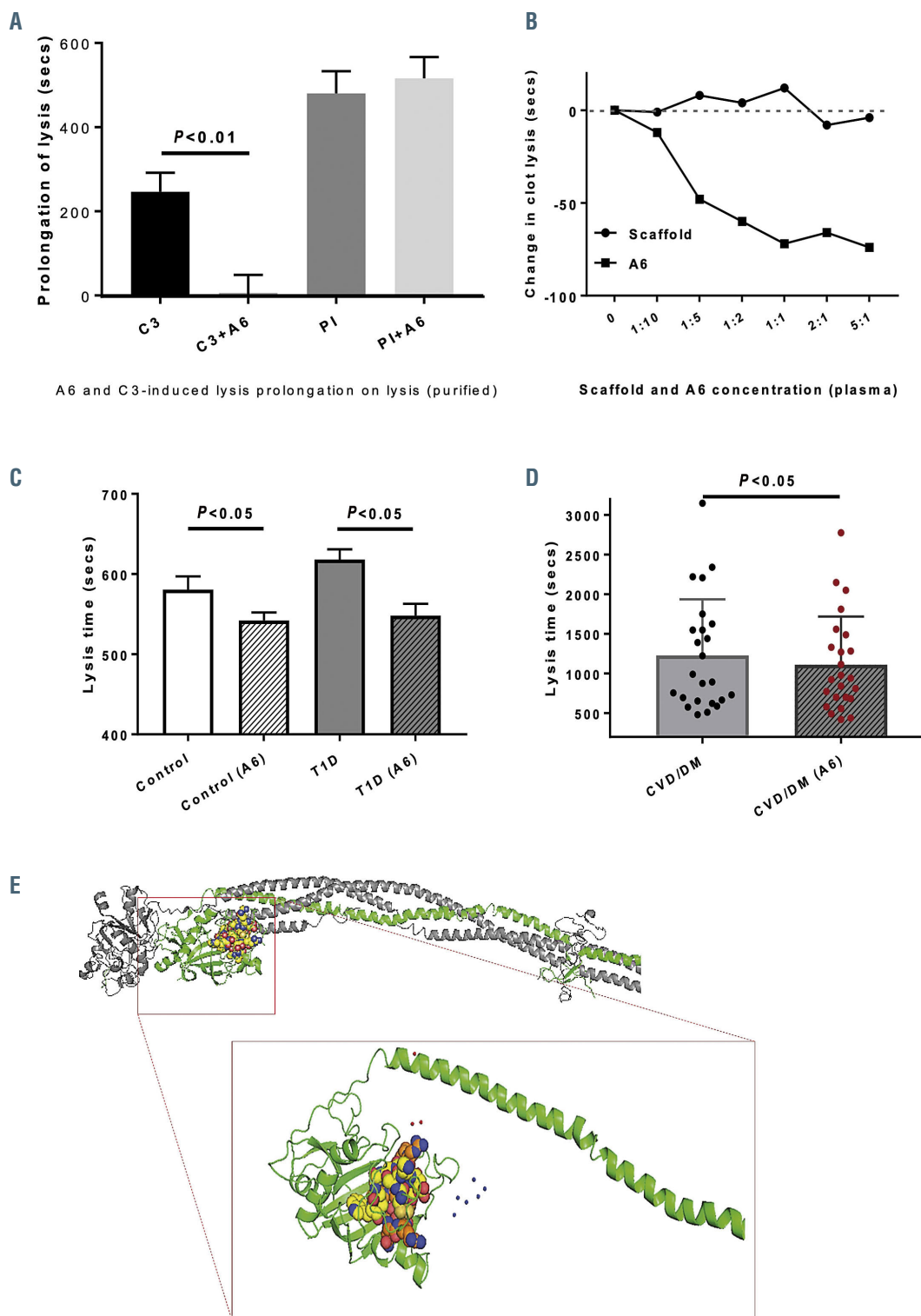


Figure 4. Modulation of C3-induced prolongation of fibrinolysis by affimer A6 and potential interaction sites on fibrinogen. (A) Pre-incubation of fibrinogen with affimer A6 completely abolished complement C3-mediated prolongation of lysis with no effect observed on prolongation of lysis by plasmin inhibitor indicating a C3-specific effect. (B) Dose-response curve using different molar ratios of affimer A6:fibrinogen (or scaffold-only control protein), conducted on pooled plasma samples from 12 individuals. (C) Effects of affimer A6 on plasma clot lysis using pooled healthy control plasma (control, $n=12$) or plasma from patients with type 1 diabetes (patients, $n=12$). Results represent the mean \pm standard error of mean of three independent experiments each performed in duplicate, unpaired *t*-test. (D) The effect of affimer A6 on plasma clot lysis in 24 patients with high vascular risk (11 with coronary artery disease and 13 with type 2 diabetes). (E) The crystal structure of fibrinogen with predicted binding sites of loop 1 (red) and loop 2 (blue) of affimer A6 within the β chain (shown in green), lying in close proximity to peptide motifs B and C identified from microarray screening (colored spheres). C3: complement C3; A6: affimer A6; PI: plasmin inhibitor; T1D: type 1 diabetes; CVD: cardiovascular disease; DM: diabetes mellitus.

tency is related to a steric effect. Previous work has shown that glycation of proteins involved in coagulation and lysis alters clot structure and/or the efficiency of fibrinolysis. For example, fibrinogen glycation alters fibrin network characteristics and the degree of protein glycation correlates with glycemic control measured as HbA1c.^{20,21} Proteins in the fibrinolytic system are also affected, as plasminogen glycation in diabetes compromises conversion to plasmin and modulates enzyme activity.²² There was no clear correlation between the number of lysine residues glycated and the antifibrinolytic effects of C3 but this may be due to the small number of samples analyzed or it may simply indicate that some lysine residues are more important than others and extensive glycation of multiple residues is not required to observe an effect. Overall, however, our data suggest that glycation of C3 increases its antifibrinolytic effect, although it remains unclear which lysine residues are important for the observed effect.

Our binding studies indicate that three areas on the β chain of fibrinogen play a role in C3-fibrinogen interactions. In particular, two of these areas, located in the N-terminus, were in close proximity and separated by a single amino acid. We should acknowledge that the microarray technique only identifies linear interactions and it is possible that additional conformational interactions take place between the two proteins. However, we should not underestimate the importance of linear binding between

proteins with previous work demonstrating the importance of such interactions between fibrinogen and factor XIII.²³

A key finding of our work is a proof of concept for a novel methodology to modulate fibrin clot lysis, and hence thrombosis risk, in individuals with diabetes. We describe a new technique that identified a small binding protein with two variable loops (affimer A6), with one of the loops sharing sequence identity with an exposed portion of C3, likely to be involved in protein-protein interactions. Interestingly, affimer A6 was able to abolish C3-induced prolongation of lysis with high specificity, regardless of whether C3 was purified from samples from controls or patients with type 1 diabetes. Moreover, affimer A6 was capable of reducing plasma clot lysis in samples from both healthy controls and patients with diabetes. We and others have shown that changes in clot lysis by 6–18% are clinically significant^{24–26} and therefore the observed 7–11% reduction in clot lysis by affimer A6 is likely to be clinically meaningful. Although speculative, this targeted effect on clot lysis is unlikely to increase bleeding risk significantly, making this approach clinically promising.

The predicted binding sites of both loops of affimer A6 were in close proximity within the β chain of fibrinogen and close to the region of fibrinogen that interacts with C3 as determined by microarray screening. Considering the data together, it appears that the N terminus of the β chain of fibrinogen is a binding site for complement C3,

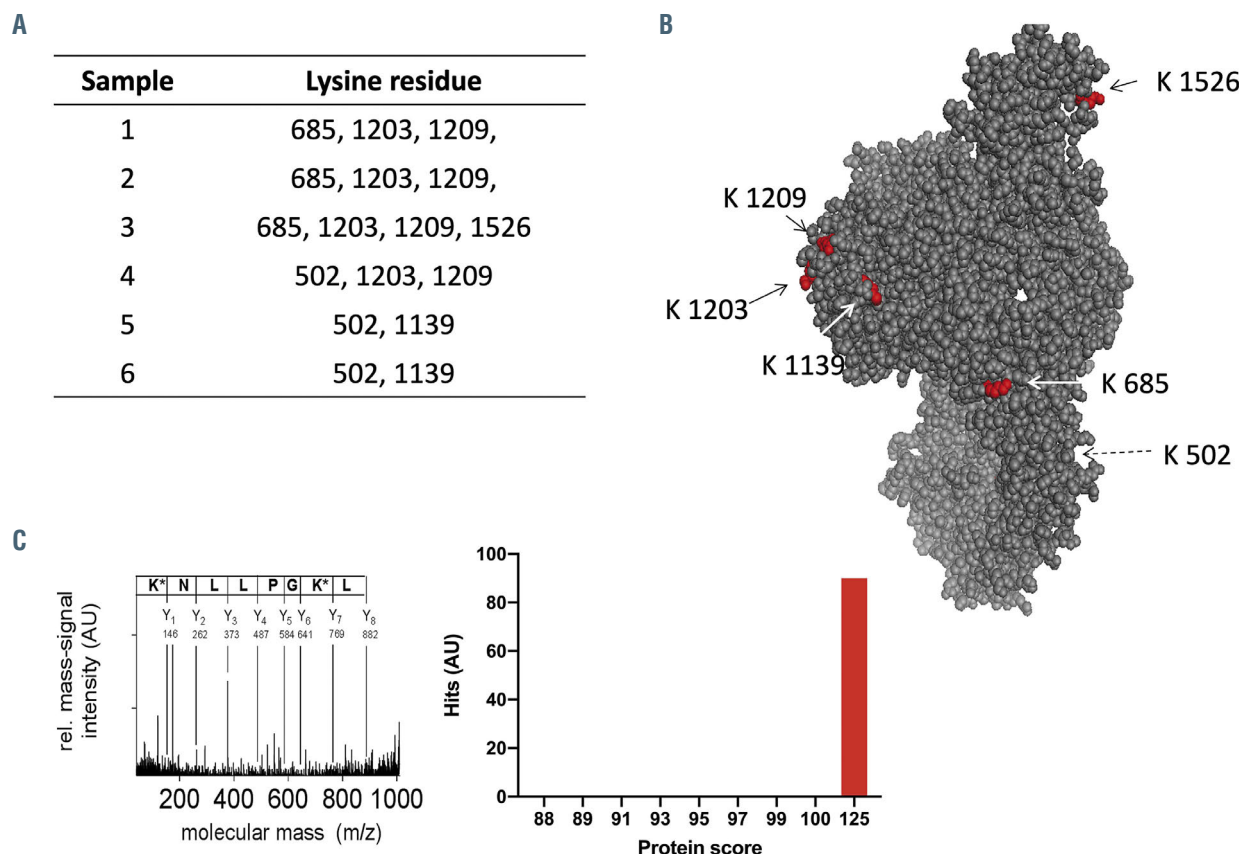


Figure 5. In-vivo glycation of C3 and lysine residues involved. Six individual C3 samples from patients with type 1 diabetes and healthy controls were analyzed by matrix-assisted laser desorption/ionization mass-spectrometry (MALDI-MS) for post-translational glycation. (A) Six lysine residues showed additional glycation in samples from the patients with diabetes. (B) The spatial position of glycated residues within C3 are shown. (C) Detailed analysis of the tandem mass spectrometry fragment from C3 with the molecular mass of 1,206 Daltons and the interpretation by the Mascot search engine is shown together with a protein score of 125 for post-translational glycation modification. AU: arbitrary units.

which may be important for the development of agents that improve the efficiency of fibrinolysis, particularly in patients with high vascular risk. These findings open a new avenue for the identification of therapeutic targets to modulate the hypofibrinolytic environment in high-risk patients, which may have future clinical implications.

In conclusion, our work shows that C3 represents a credible therapeutic target to reduce thrombosis risk. The β chain of fibrinogen represents an interaction site with C3, and modulation of this interaction can abolish C3-induced prolongation of clot lysis in a specific manner. This targeted approach has the potential for use in the development of novel therapeutic agents for the reduction of thrombotic vascular occlusion.

Future work should concentrate on investigating the *in vivo* role of affimer A6 in limiting vascular occlusion, using animal models of thrombosis. Additionally, our data suggest that a specific site of the β chain of fibrinogen, which may be amenable to small molecule intervention, represents a possible new therapeutic target to improve fibrinolysis and reduce thrombosis in high-risk conditions.

Disclosures

No conflicts of interest to disclose.

References

1. Lisman T. Decreased plasma fibrinolytic potential as a risk for venous and arterial thrombosis. *Semin Thromb Hemost*. 2017;43(2):178-184.
2. Kearney K, Tomlinson D, Smith K, Aijan R. Hypofibrinolysis in diabetes: a therapeutic target for the reduction of cardiovascular risk. *Cardiovasc Diabetol*. 2017;16(1):34.
3. Undas A. Fibrin clot properties and their modulation in thrombotic disorders. *Thromb Haemost*. 2014;112(1):32-42.
4. Sumaya W, Wallentin L, James SK, et al. Fibrin clot properties independently predict adverse clinical outcome following acute coronary syndrome: a PLATO substudy. *Eur Heart J*. 2018;39(13):1078-1085.
5. Eikelboom JW, Connolly SJ, Bosch J, et al. Rivaroxaban with or without aspirin in stable cardiovascular disease. *N Engl J Med*. 2017;377(14):1319-1330.
6. Hertel E, Stehouwer CD, van Greevenbroek MM. The complement system in human cardiometabolic disease. *Mol Immunol*. 2014;61(2):135-148.
7. Hess K, Alzahrani SH, Mathai M, et al. A novel mechanism for hypofibrinolysis in diabetes: the role of complement C3. *Diabetologia*. 2012;55(4):1103-1113.
8. Howes JM, Richardson VR, Smith KA, et al. Complement C3 is a novel plasma clot component with anti-fibrinolytic properties. *Diab Vasc Dis Res*. 2012;9(3):216-225.
9. Hess K, Alzahrani SH, Price JF, et al. Hypofibrinolysis in type 2 diabetes: the role of the inflammatory pathway and comple-
10. Kearney KJ, Pechlivanis N, King R, et al. Affimer proteins as a tool to modulate fibrinolysis, stabilize the blood clot, and reduce bleeding complications. *Blood*. 2019;133(11):1233-1244.
11. Tiede C, Bedford R, Heseltine SJ, et al. Affimer proteins are versatile and renewable affinity reagents. *Elife*. 2017;6:e24903.
12. Tiede C, Tang AA, Deacon SE, et al. Adhiron: a stable and versatile peptide display scaffold for molecular recognition applications. *Protein Eng Des Sel*. 2014;27(5):145-155.
13. Carter AM, Cymbalista CM, Spector TD, Grant PJ. Heritability of clot formation, morphology, and lysis: the EuroCLOT study. *Arterioscler Thromb Vasc Biol*. 2007;27(12):2783-2789.
14. Harris R, Olson AJ, Goodsell DS. Automated prediction of ligand-binding sites in proteins. *Proteins*. 2008;70(4):1506-1517.
15. Trabuco LG, Lise S, Petsalaki E, Russell RB. PepSite: prediction of peptide-binding sites from protein surfaces. *Nucleic Acids Res*. 2012;40(Web Server issue):W423-W427.
16. Rueth M, Lemke HD, Preisinger C, et al. Guanidinylation of albumin decreased binding capacity of hydrophobic metabolites. *Acta Physiol (Oxf)*. 2015;215(1):13-23.
17. Kimmel J. Guanidination of proteins. *Meth Enzymol*. 1967;11:584-589.
18. Kollman JM, Pandi L, Sawaya MR, Riley M, Doolittle RF. Crystal structure of human fibrinogen. *Biochemistry*. 2009;48(18):3877-3886.
19. Balakumar P, Maung U, Jagadeesh G. Prevalence and prevention of cardiovascular disease and diabetes mellitus. *Pharmacol Res*. 2016;113(Pt A):600-609.
20. Pieters M, van Zyl DG, Rheeder P, et al. Glycation of fibrinogen in uncontrolled diabetic patients and the effects of glycaemic control on fibrinogen glycation. *Thromb Res*. 2007;120(3):439-446.
21. Pieters M, Covic N, Loots DT, et al. The effect of glycaemic control on fibrin network structure of type 2 diabetic subjects. *Thromb Haemost*. 2006;96(5):623-629.
22. Aijan RA, Gamelin T, Standeven KF, et al. Diabetes is associated with post-translational modifications in plasminogen resulting in reduced plasmin generation and enzyme specific activity. *Blood*. 2013;122(1):134-142.
23. Smith KA, Pease RJ, Avery CA, et al. The activation peptide cleft exposed by thrombin cleavage of FXIII-A(2) contains a recognition site for the fibrinogen alpha chain. *Blood*. 2013;121(11):2117-2126.
24. Neergaard-Petersen S, Hvas AM, Kristensen SD, et al. The influence of type 2 diabetes on fibrin clot properties in patients with coronary artery disease. *Thromb Haemost*. 2014;112(6):1142-1150.
25. Undas A, Wiek I, Stepien E, Zmudka K, Tracz W. Hyperglycemia is associated with enhanced thrombin formation, platelet activation, and fibrin clot resistance to lysis in patients with acute coronary syndrome. *Diabetes Care*. 2008;31(8):1590-1595.
26. Alzahrani SH, Hess K, Price JF, et al. Gender-specific alterations in fibrin structure function in type 2 diabetes: associations with cardiometabolic and vascular markers. *J Clin Endocrinol Metab*. 2012;197(12):E2282-E2287.

Contributions

RJK and KS performed the research, analyzed data and wrote the manuscript. CT, VJ and KS performed the research, analyzed data and revised the manuscript. VJ and AT researched data and revised the manuscript. SP, MJM and RFS revised the manuscript. CWGF and DT designed experiments and revised the manuscript. RAA conceived the study, designed experiments, analyzed data and wrote the manuscript.

Funding

RJK was funded by a PhD Fellowship from the Sir Jules Thorn Charitable Trust. KS is supported by the German Research Foundation (DFG)(SFB/TRR219 C-07; HE 5666/1-2 to KS (née Hess)) and by a grant from the Interdisciplinary Center for Clinical Research within the faculty of Medicine at the RWTH Aachen University (K7-2). VJ was supported by the German Research Foundation (DFG)(SFB/TRR219 S-03, C-04, M-05, IHST 948/4S-1 FU6.6). We also wish to thank Diabetes UK for funding part of this work, the National Institute of Health Research and British Heart Foundation for constant support, along with help from the Biomedical Health Research Centre for the BioScreening Technology Group and the Stratified Medicine Hub at the University of Leeds who funded the initial NABP screens. We would also like to thank AVACTA Life Sciences for their support.



Deciphering the Ets-1/2-mediated transcriptional regulation of *F8* gene identifies a minimal *F8* promoter for hemophilia A gene therapy

Rosella Famà,^{1*} Ester Borroni,^{1*} Simone Merlin,¹ Chiara Airolidi,² Silvia Pignani,¹ Alessia Cucci,¹ Davide Corà,^{2,3} Valentina Bruscaggin,¹ Sharon Scardellato,¹ Stefania Faletti,⁴ Giuliana Pelicci,^{2,4} Mirko Pinotti,⁵ Gillian E. Walker¹ and Antonia Follenzi¹

¹Department of Health Sciences, Università del Piemonte Orientale, Novara;

²Department of Translational Medicine, Università del Piemonte Orientale, Novara;

³Center for Translational Research on Autoimmune and Allergic Disease (CAAD),

University of Piemonte Orientale, Novara; ⁴Department of Experimental Oncology, IEO,

European Institute of Oncology IRCCS, Milan and ⁵Department of Life Sciences and

Biotechnology, Università di Ferrara, Ferrara, Italy

*RF and EB contributed equally as co-first authors

ABSTRACT

A major challenge in the development of a gene therapy for hemophilia A is the selection of cell type- or tissue-specific promoters to ensure factor VIII (FVIII) expression without eliciting an immune response. As liver sinusoidal endothelial cells are the major FVIII source, understanding the transcriptional F8 regulation in these cells would help to optimize the minimal F8 promoter (pF8) to efficiently drive FVIII expression. *In silico* analyses predicted several binding sites (BS) for the E26 transformation-specific (Ets) transcription factors Ets-1 and Ets-2 in the pF8. Reporter assays demonstrated a significant up-regulation of pF8 activity by Ets-1 or Ets-1/Ets-2 combination, while Ets-2 alone was ineffective. Moreover, Ets-1/Ets-2-DNA binding domain mutants (DBD) abolished promoter activation only when the Ets-1 DBD was removed, suggesting that pF8 up-regulation may occur through Ets-1/Ets-2 interaction with Ets-1 bound to DNA. pF8 carrying Ets-BS deletions unveiled two Ets-BS essential for pF8 activity and response to Ets overexpression. Lentivirus-mediated delivery of green fluorescent protein (GFP) or FVIII cassettes driven by the shortened promoters, led to GFP expression mainly in endothelial cells in the liver and to long-term FVIII activity without inhibitor formation in HA mice. These data strongly support the potential application of these promoters in hemophilia A gene therapy.

Correspondence:

ANTONIA FOLLENZI
antonia.follenzi@med.uniupo.it

Received: October 3, 2019.

Accepted: May 20, 2020.

Pre-published: May 28, 2020.

<https://doi.org/10.3324/haematol.2019.239202>

©2021 Ferrata Storti Foundation

Material published in *Haematologica* is covered by copyright. All rights are reserved to the Ferrata Storti Foundation. Use of published material is allowed under the following terms and conditions:

<https://creativecommons.org/licenses/by-nc/4.0/legalcode>.

Copies of published material are allowed for personal or internal use. Sharing published material for non-commercial purposes is subject to the following conditions:

<https://creativecommons.org/licenses/by-nc/4.0/legalcode>, sect. 3. Reproducing and sharing published material for commercial purposes is not allowed without permission in writing from the publisher.



Introduction

Hemophilia A (HA) is a recessive X-linked bleeding disorder caused by a number of *F8* gene mutations which associate with deficiencies of the coagulation factor VIII (FVIII).^{1,2} As HA is a monogenic disease with a lifelong elevated bleeding risk with no conclusive therapeutic options, it is an ideal candidate for gene therapy.³ In the last years many forward steps in the development of new therapeutic strategies have been made, thus rapidly changing the therapeutic landscape of HA. The introduction of the extended half-life FVIII concentrates, of the bi-specific monoclonal antibody Emicizumab and the start of gene therapy clinical trials have remarkably contributed to the improvement of patient care.⁴

The development of effective gene therapeutic approaches for HA, has seen little progression when compared to hemophilia B5. This is due to the complexity of FVIII synthesis, the size of the FVIII protein (2,351 amino acids) and its high immunogenic properties, with the development of neutralizing antibodies in 25% of patients when FVIII is exogenously administered.^{6,7} As it stands, the goal is to provide a single dose therapy that is effective and offers a lasting cure with sustained FVIII activity to HA patients.

When considering gene therapy approaches aimed at restoring and sustaining FVIII activity, the liver is considered the primary target organ, as it is the principal site of FVIII synthesis and possesses the necessary tolerogenic properties.⁸ The identity of liver cells capable of synthesizing and releasing FVIII has generated an extensive debate over the years.⁹ This has significantly influenced the understanding of the regulatory elements involved in promoting the preferential expression of FVIII in liver cells. The *F8* promoter (pF8), reported to be a 1.2 kb region upstream of the *F8* translation start site, was first described in 1984.¹⁰ With hepatocytes originally considered the major source of FVIII,^{11,12} the first *in vitro* studies aimed at elucidating the transcription factors (TF) responsible for pF8 activation, were performed using hepatocyte-derived cell lines. In hepatocytes, Figueiredo and McGlynn described the region from -279 and -64 to be responsible for maximal promoter activity.^{13,14} They identified and confirmed the binding of several hepatic TF, such as CCAAT/enhancer-binding proteins (C/EBP α and C/EBP β), and hepatocyte nuclear factor 1 (HNF-1) and 4 (HNF-4). Other TF binding sites (TFBS) on pF8 were also identified in this study, however, to date their involvement has never been thoroughly investigated.

While heavily debated, it has recently been demonstrated that liver *FVIII* production predominantly occurs in the liver sinusoidal endothelial cells (LSEC),¹⁵⁻¹⁸ which represent a principal but not exclusive source.¹⁹⁻²² In fact, detection of FVIII mRNA in many tissues, suggests that a highly complex and likely tissue-specific transcriptional regulation exists. Recently, our group described pF8's ability to direct a specific and long-term FVIII expression in LSEC after a lentiviral vector (LV)-delivery in HA mice.²³ Importantly, this targeted restoration of FVIII did not trigger an immune response, one of the major obstacles for the successful treatment of HA patients. In the present study, we used data from an *in silico* analysis of the pF8 region,²³ to extrapolate and assess the role of the most represented endothelial-specific TFBS on *F8* transcriptional regulation. Understanding the stimuli and the TF required for maximal promoter activity in endothelial cells (EC), offers an important forward step in the development of gene therapeutic approaches for HA. To date, several clinical trials using the adeno-associated viral vectors (AAV) to deliver FVIII in HA patients have started. Despite the promising results, some concerns have been raised, like the vector dose, the variability of FVIII activity among the different subjects and the decline of FVIII expression over time.²⁴ Our optimization of the minimal pF8 size opens up the possibility to explore new perspectives in the field of HA gene therapy by introducing for the first time a pF8 suitable for vectors with a limited expression cassette, like the AAV which, to date, are the only ones successfully used in clinical trials for HA.

Methods

Animal studies

Experiments, described in the *Online Supplementary Appendix*, were performed according to an approved protocol by the Animal Care and Use Committee of the University of Eastern Piedmont and the Italian Health Ministry, Italy (Project n. DB064.5, date of approval n°492/2016-PR 17/05/2016).

Identification of putative endothelial transcription factors binding sites on the *F8* promoter

In silico prediction of TFBS distribution on pF8 was retrieved from a previous analysis performed by Merlin *et al.*²³ using PROMO 3.0.²⁵ In order to identify potential endothelial TFBS, two parameters were considered: the number of consensus sites identified on pF8 using a stringent dissimilarity rate (<3) and the expression and functional role of TF in EC.

Generation of the constructs

The full-length human pF8 (1,175 basepairs [bp]) was excised from a plasmid already available in our laboratory and cloned with Xhol-HindIII into a promoterless pNL1.1 vector at the 5' of NanoLuc® luciferase reporter gene. Serial deletions of pF8 were generated via polymerase chain reaction using diverse primer sets carrying restriction sites, while E26 transformation-specific (Ets)-core sequence (GGAA) deletions were performed using site-directed mutagenesis, according to the manufacturer's instructions (Stratagene, San Diego, CA, USA).

Human Ets-1 cDNA was obtained from Origene (#RC227466) while Ets-2 cDNA expressing vector (CMV-Ets-2 in pCDNA 3.1) was available in our laboratory. Ets-1 and Ets-2 DNA binding domains were removed by mutagenesis according to the protocol described by Follo *et al.*²⁶ All mutagenesis primers are listed in the *Online Supplementary Tables S2 to S4*.

The single guide RNA (sgRNAF8.1, sgRNAF8.2 and the control sgRNAF7.5) were designed using ZiFit web tool, as described by Pignani *et al.*²⁷, scanning for the *S. Pyogenes* PAM sequence (NGG) both in the sense and antisense strands. dCas9-VPR was a gift from Dr George Church (Addgene plasmid # 63798).

Transient transfection and luciferase assays

For the luciferase reporter assay, ECV-304 and HEK293T cells were seeded in a 24-well plate at a density of 5×10^4 cells/well 24 hours (h) prior to transfection. Luciferase pF8 reporter plasmids along with Ets-1 and/or Ets-2 expressing constructs, or dCas9-VPR and gRNA, were transfected (1 μ g) into cells using the Lipofectamine 2000 transfection reagent (Thermo Fisher Scientific), according to the manufacturer's instructions. Firefly luciferase vector pGL4.54 (TK-Firefly; #E5061, Promega) was used as an internal control. In order to maintain the amount of total DNA, the pUC19 vector was used to transfect cells. After 24 h, the cells were lysed, and luciferase activity assayed performed using the Dual-Luciferase Reporter Assay System (Promega). Both firefly and NanoLuc signals were measured at 562 nm using a Victor X microplate reader (PerkinElmer). Results are expressed as mean \pm standard deviation (SD) of the fold change, calculated as the average of the ratio of stimulated to non-stimulated promoter.

Statistical analysis

All data were continuous and expressed as an average \pm SD. Parametric analysis was used because the groups were balanced with the same number of observations. One-way analysis of variance (ANOVA) was performed to compare changes in promoter activity among promoter variants and to separately evaluate the difference in Ets-response of each promoter tested. Two-way ANOVA was carried out to compare changing in FVIII activity over time and among the mice groups. *P*-values less than 0.05 were considered statistically significant for the overall test while Bonferroni's adjustment was used for multiple comparisons. The statistical analyses were performed with GraphPad Prism 5.0 (GraphPad Software).

Results

In silico prediction of endothelial transcription factors involved in F8 promotor regulation

By taking advantage of the *in silico* analysis on pF8 previously performed in our laboratory,²³ we mapped all the TFBS on pF8 recognized by TF expressed by endothelial cells (Figure 1A). In total, we identified 16 TFBS which interestingly all belonged to the Ets family. Further, each was distributed in the first -600 bp of pF8 (Figure 1A). In order to improve the accuracy of the analysis, we reduced the dissimilarity rate parameter from 5 to 3, opting to

assess the role of these TF in pF8 regulation (Figure 1A, black asterisk). Using this approach, we identified seven endothelial BS, four recognized by Ets-1, two by Ets-2 and one by Elk-1, with two of the Ets-1 sites overlapping those of Ets-2 and Elk-1 (Figure 1B).

Both Ets-1 and Ets-2 are well-known TF, being downstream effectors of the RAS/ERK signaling pathways and regulating several genes involved in endothelial functions including angiogenesis.²⁸⁻³¹ Based on their redundant contribution in crucial endothelial cell processes,²⁸ we focused our studies on the potential co-operative role of Ets-1 and Ets-2 in regulating FVIII expression.

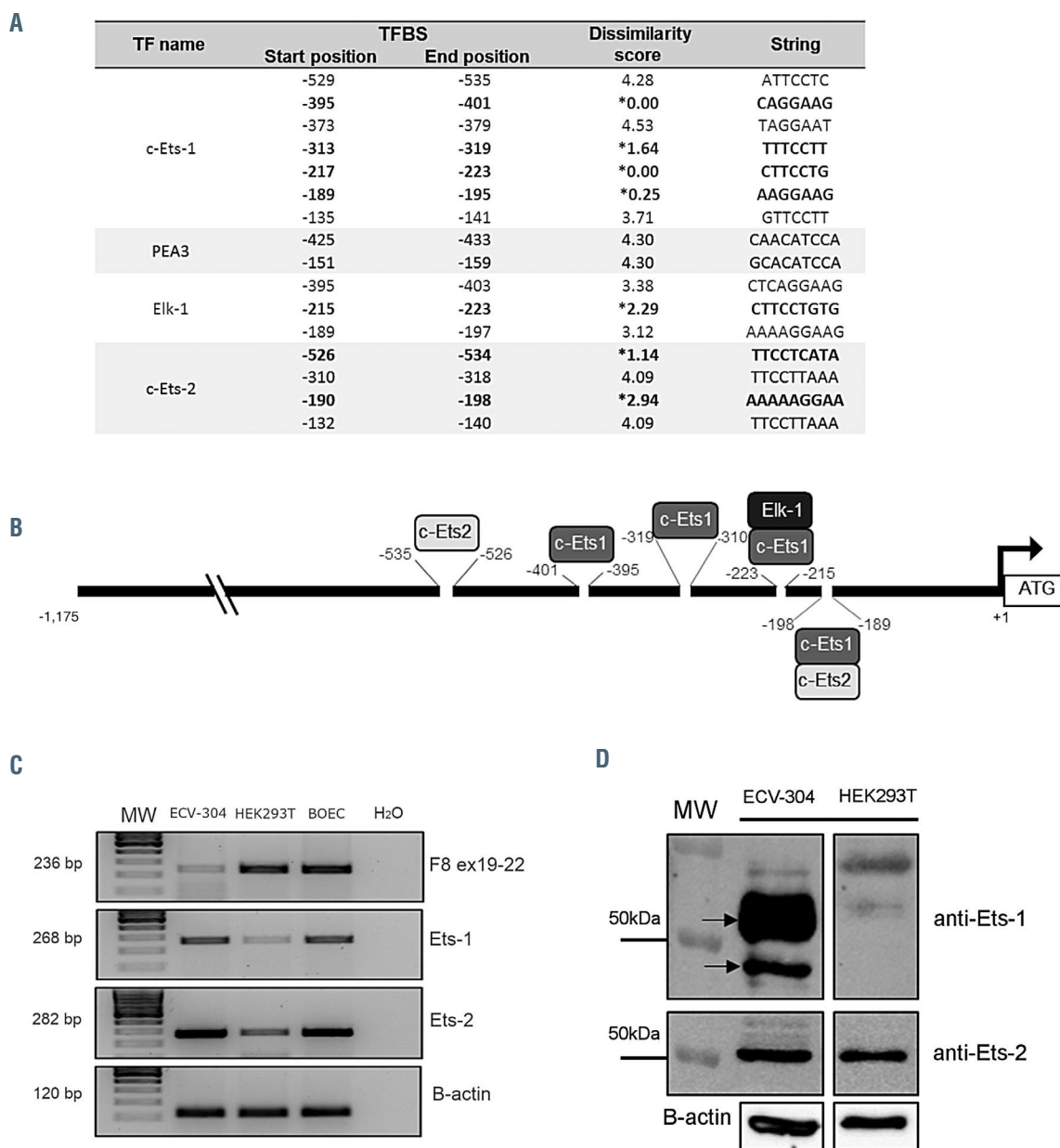


Figure 1. F8 promoter showing several putative E26 transformation-specific (Ets) binding motifs for Ets-1 and Ets-2 transcription factors. (A) Table showing the endothelial binding sites (BS) on F8 promoter (pF8) identified by *in silico* analysis. Black asterisks indicate BS with a dissimilarity score <3 selected to evaluate their role in promoter regulation. (B) Schematic representation of the distribution of the selected Ets-BS on the proximal pF8 (-1,175 basepairs). (C) Reverse transcriptase polymerase chain reaction (RT-PCR) analysis of factor VIII (FVIII), Ets-1 and Ets-2 expression in ECV-304 and HEK293T cell lines. Blood outgrowth endothelial cells (BOEC), were used as positive control. Base pairs on the left indicate the expected PCR products size. (D) Western immunoblot analysis on ECV-304 and HEK293T whole cell lysates using the anti-Ets-1 and anti-Ets-2 antibodies. Black arrows indicate the major Ets-1 isoforms p51 (51 kDa) and p42 (42 kDa). Black lines indicated the expected weight of protein detected (for antibodies and reagents see the *Online Supplementary Appendix*).

Ets-1 and Ets-2 *in vitro* co-operation in *F8* promoter regulation

In order to explore the role of Ets-1 and Ets-2 in pF8 regulation, the -1,175 bp region of pF8 was cloned into the Nanoluc vector, and pF8 activity assessed in the presence of Ets-1, Ets-2 or in combination. Two human cell lines were transfected: ECV-304 and HEK293T. The ECV-304, previously considered as spontaneously transformed human umbilical endothelial cells,³² were selected as a model expressing FVIII, Ets-1 and Ets-2 at the mRNA and protein level, while HEK293T as cells expressing low levels of Ets-1 and Ets-2 (Figure 1C and D). The luciferase assays showed different but consistent results between the two cell types tested. A 3- and 5-fold upregulation was observed in ECV-304 upon co-transfection of pF8 with Ets-1 and Ets-1/Ets-2, respectively (Figure 2A). No significant effect was observed with Ets-2 alone. This data highlights that Ets-1 appears to play a major role on pF8 transactivation. In HEK293T cells where Ets-1 is expressed at

negligible levels, we observed a 7-fold up-regulation of pF8 only in response to Ets-1 overexpression, with no further increase observed in presence of Ets-2 (Figure 2B). These results reinforce the central role of Ets-1 in regulating pF8 and highlight the presence of cell-specific regulatory mechanisms.

In order to elucidate whether the pF8 up-regulation observed in ECV-304 in response to Ets-1 and Ets-2 is mediated by a direct DNA binding of Ets, we generated Ets mutants carrying an in-frame deletion of their DNA binding domain (DBD) (Figure 2C). We evaluated their co-operation with the wild-type (WT) counterparts in the regulation of pF8 activity. Ets-1 without DBD failed to upregulate the pF8, while Ets-1 co-expressed with the Ets2-DBD mutant, preserved the 5-fold increase in pF8 activity, as observed with the WT proteins (Figure 2D). These results suggest that in the regulation of pF8, Ets-1 may directly bind the DNA, while Ets-2 modulates pF8 through its interaction with Ets-1.³³

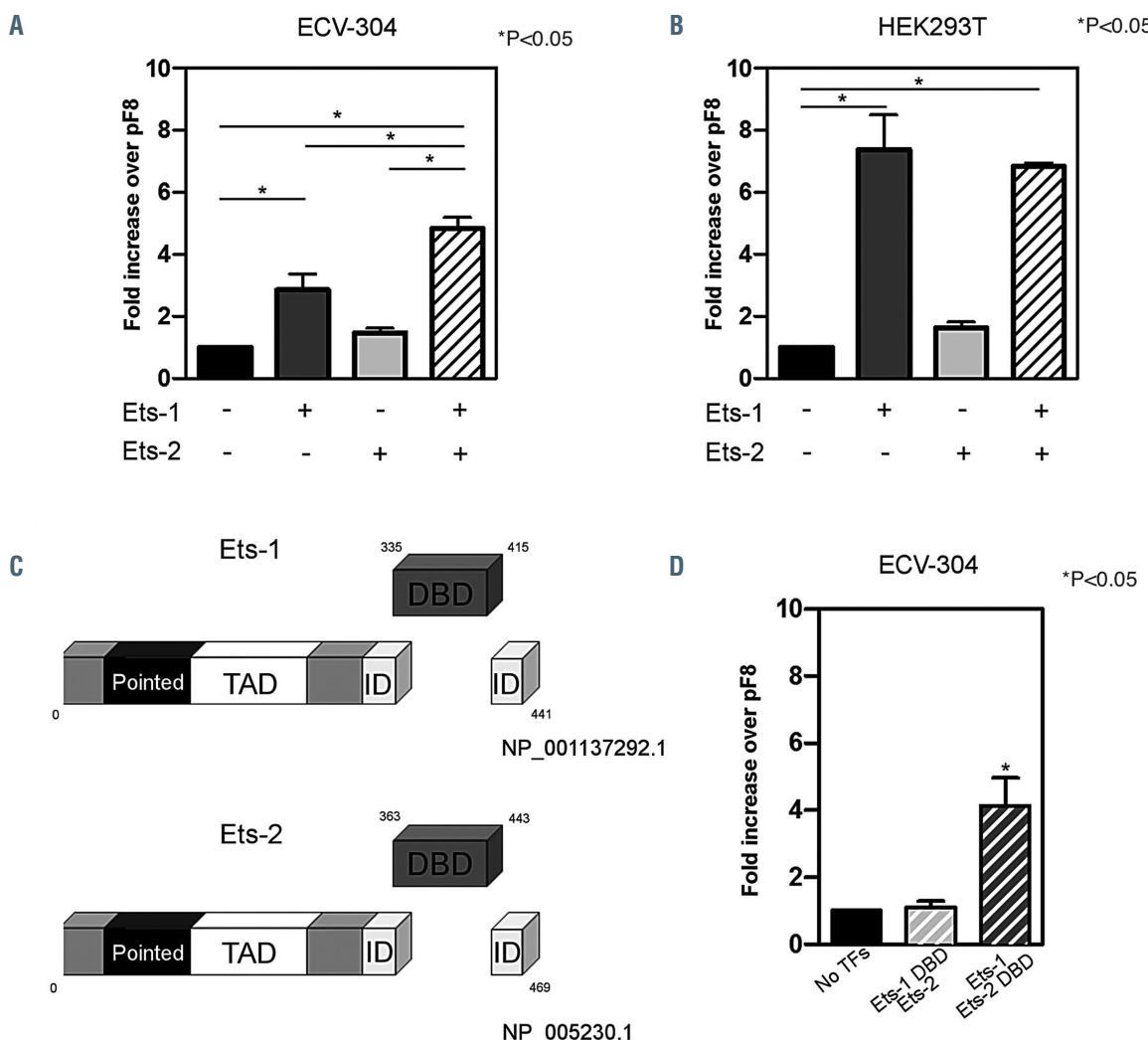


Figure 2. *In vitro* Ets-1 and Ets-2 co-operation in *F8* promoter transactivation. (A and B) Histograms report the fold increase of luciferase activity after transfection of *F8* promotor (pF8) alone (set as 1) or in combination with Ets-1, Ets-2 or both in (A) ECV-304 or (B) HEK293T cell lines. (C) Schematic representation of Ets-1 and Ets-2 protein structure, with highlighted amino acid position of the DNA binding domain (DBD). For both proteins, TAD indicates the transactivation domain while ID indicates the inhibitory domain. (D) Histograms report the fold increase of luciferase activity after transfection of pF8-1175 alone (set as 1) or with the combination of Ets-DBD with the non-mutated counterparts. Results are expressed as mean \pm standard deviation from three independent experiments performed in triplicate. * $P<0.05$.

Identification of key Ets-responsive elements in the *F8* proximal promoter region

In order to decipher the importance of each Ets BS in pF8 activity, we generated several pF8 mutants and tested their impact. We adopted two different strategies. The

first aimed at eliminating progressively the Ets BS by performing deletions of pF8 (Figure 3A and B). Using this approach in ECV-304 cells, we observed that the basal activity of the full-length promoter (pF8-1,175) was maintained in pF8-600 and pF8-446, where one Ets-2 BS was

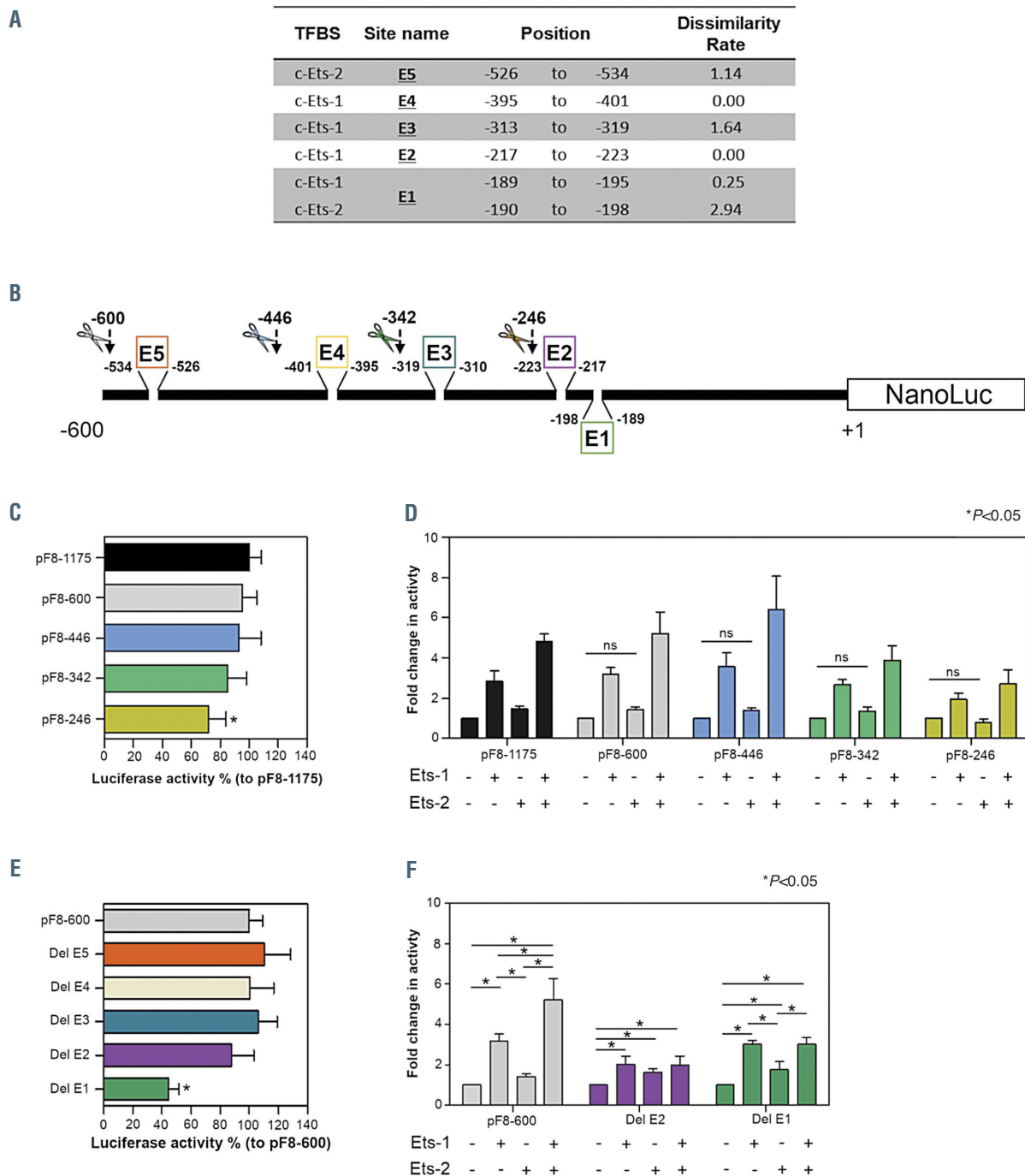


Figure 3. Crucial E26 transformation-specific-responsive elements are localized in the first 342 bases of *F8* promoter region. (A) Table summarizing the Ets-1 and Ets-2 binding sites distributed across the *F8* promoter (pF8) and scheme of mutagenesis strategies used to investigate the role of each E26 transformation-specific binding site (Ets-BS). Ets-BS destroyed by mutagenesis are highlighted in black and are indicated with E followed by a number. Only Ets-BS with a dissimilarity score <3 were disrupted by mutagenesis. (B) Schematic representation of mutagenesis strategies used to perform single or multiple deletions of Ets-BS on pF8. Colored boxes highlight the Ets-BS which underwent to a single deletion. Colored scissors indicate the points on pF8 where it was cut to generate the shortened forms with multiple ETS-BS deletions. (C and D) Histograms representing fold change in luciferase activity of shortened promoters at (C) basal level or after overexpression of (D) Ets-1, Ets-2 or both. (E and F) Histograms showing changing in luciferase activity of Ets-BS single deleted promoters at (E) basal level or after overexpression of (F) Ets-1, Ets-2 or both. All experiments were performed in ECV-304 cells. Results are expressed as mean \pm standard deviation from three independent experiments performed in triplicate. * $P<0.05$.

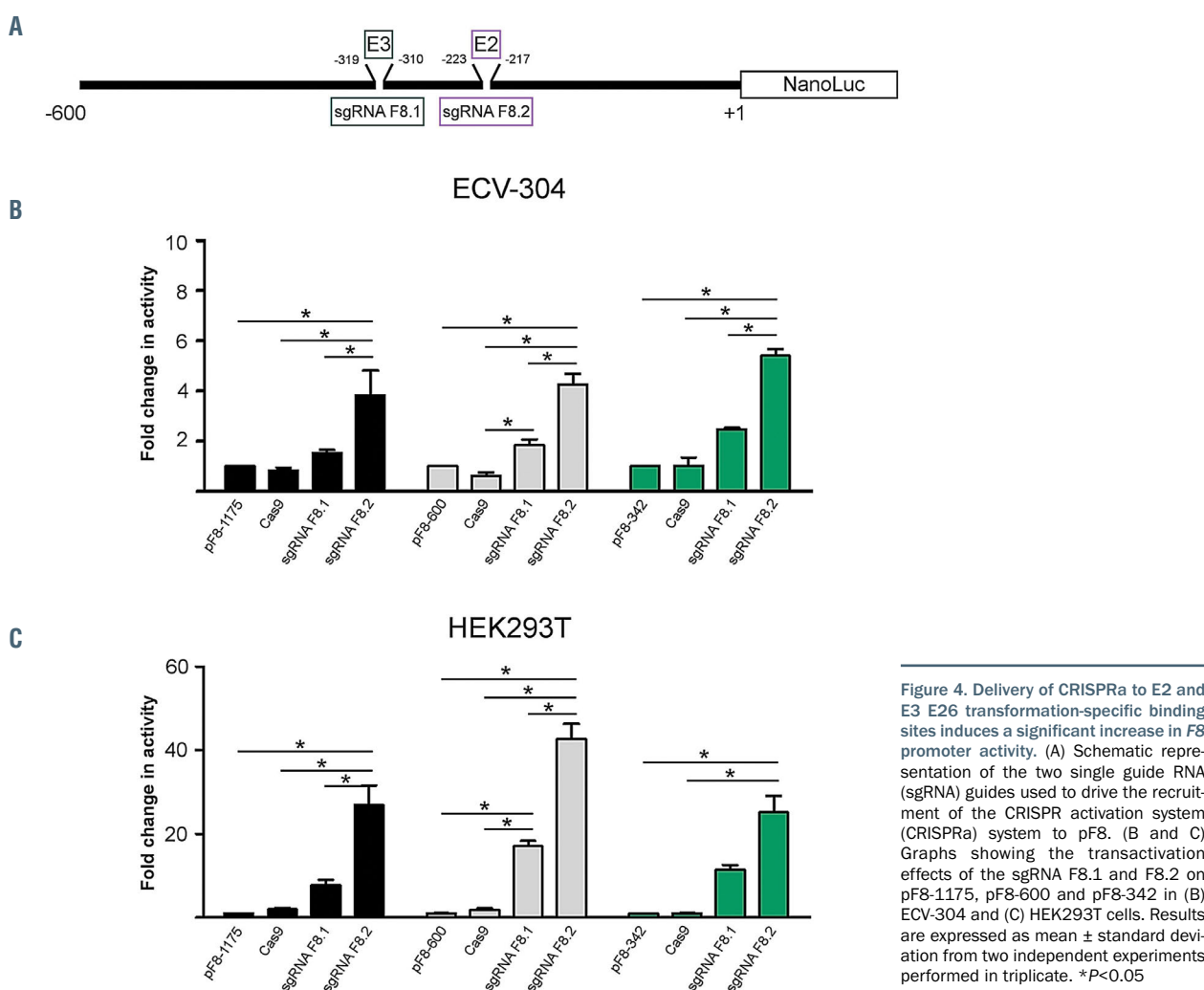
eliminated. Further shortening of the promoter (pF8-342) caused a minimal reduction of its activity with respect to pF8-1175, while a significant reduction (<20-40% pF8-1,175) was observed with the pF8-246 (Figure 3C). Analysis of the shortened pF8 promoters in response to Ets overexpression, confirmed that pF8-600 and pF8-446 maintain the same response as pF8-1175, demonstrating a 3- and 5-fold upregulation with Ets-1 and Ets-1/Ets-2 combined (Figure 3D). Despite a clear reduction in its promoter activity, pF8-342 interestingly maintained a ~3- to 5-fold activation with Ets-1 or Ets-1/Ets-2 combined, indicating that a specific response is maintained despite the elimination of one Ets-1 and one Ets-2 BS. When the pF8 was shortened further to 246 bp, a dramatic reduction in promoter activity was observed and was sustained despite Ets overexpression (Figure 3D). This was also validated in HEK293T cells (*Online Supplementary Figure S1A and B*). Overall, these results suggest that pF8 regulation may depend on the number of available Ets BS.

The second mutagenesis approach focused on the importance of each Ets site identified using a dissimilarity score <3. This approach selectively deleted the GGAA core from E1, E2, E3, E4, E5 Ets-1 and Ets-2 BSs (Figure 3B). As the Ets BSs are in the first 600 bp of pF8, we used pF8-600 to normalize the results as it preserves all the identified endothelial TFBS. Using this approach, we iden-

tified two important BS: -189 to -198 (E1) and -217 to -223 (E2). The disruption of E1 drastically reduced pF8 basal activity by approximately 60%, while the others failed to alter its activation (Figure 3E; *Online Supplementary Figures S1C and S2A*). Of note, the disruption of E1 site even preserving a response to Ets-1 overexpression abrogated the co-operative up-regulation mediated by Ets-1/2, thus agreeing with the elimination of the only Ets-2 site overlapping that of Ets-1. On the other hand, disruption of the E2 site decreased exclusively the pF8 up-regulation in response to Ets overexpression (Figure 3F; *Online Supplementary Figures S1D and S2B*). Overall, the E1 and E2 sites appear to be central to pF8 regulation with E2 maintaining the basal pF8 activity in the absence of an Ets-induced upregulation.

Enhancement of *F8* promoter activity by delivery of CRISPR/VPR activation system to E2 and E3 E26 transformation-specific binding sites

CRISPR activation system (CRISPRa) is an emerging tool that exploits deactivated Cas9, single guide RNA (sgRNA) and transcription activators for gene activation. We have recently described the potential of the CRISPR activation system in transactivating and upregulating pF8 activity by using two specific sgRNA targeting the first 300 bp of the promoter region.²⁷ Based on our *in silico*



sanalysis, these sgRNA guides, F8.1 and F8.2, mediate the recruitment of deactivated Cas9 fused to a tripartite transcriptional activator (VPR)³⁴ to the two promoter regions encompassing E3 (-313 to -319) and E2 (-219 to -223) Ets-1 BS, respectively (Figure 4A). In order to further demonstrate the central role of E2 in the modulation of pF8 activity, we transfected both ECV-304 and HEK293T cells with CRISPRa system using sgRNA F8.1 and F8.2 as reference

guides covering the essential E2 and the E3 Ets-1 BS. As a negative control guide we performed the same experiment using a sgRNA targeting coagulation Factor VII promoter (pF7) (Online Supplementary Figure S3). By applying this approach to pF8-1175, pF8-600 and pF8-446, we confirmed the ability of CRISPRa to upregulate the promoter activity. Importantly, the efficiency of the system was dependent on the cell type, the sgRNA used and the pro-

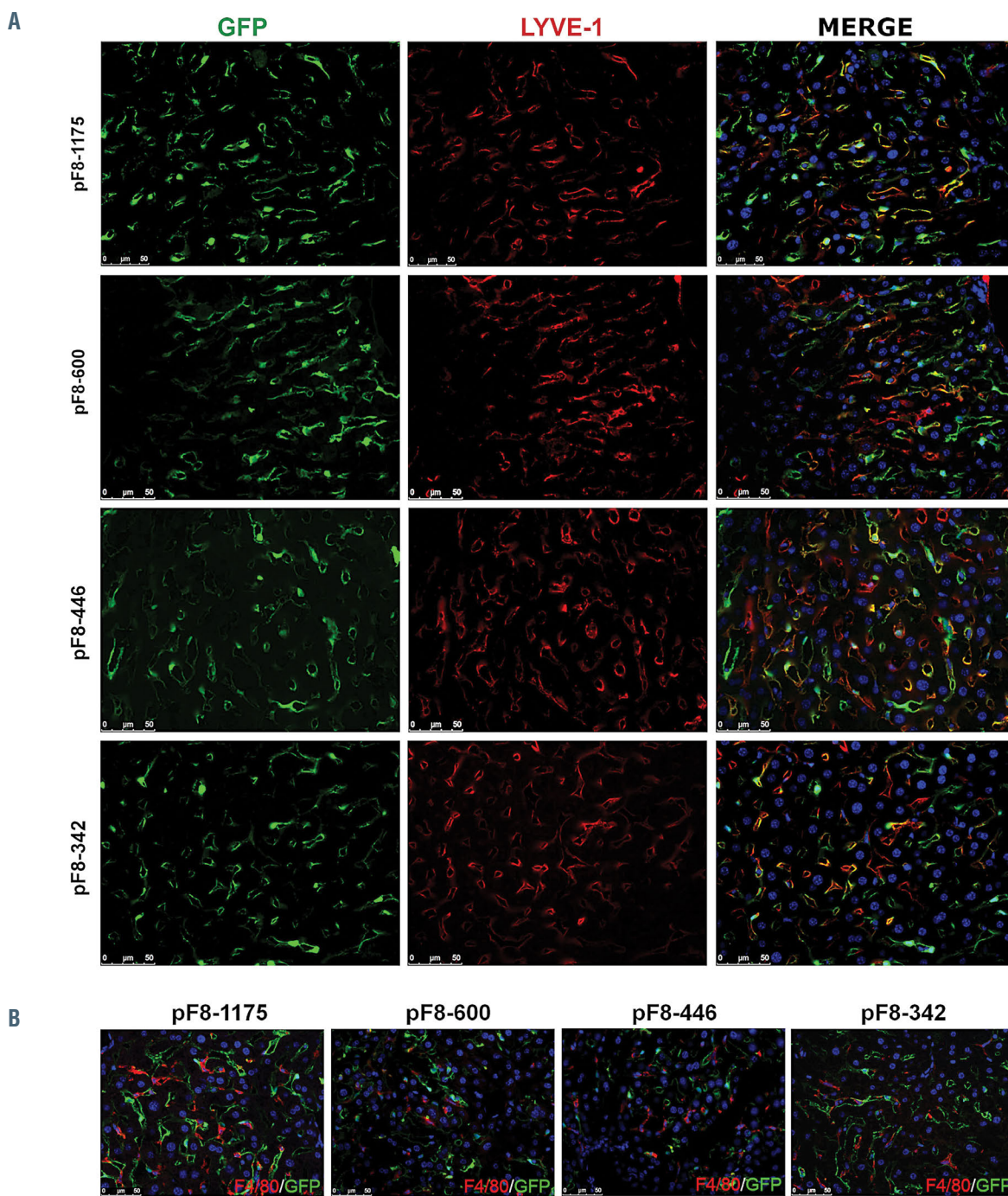


Figure 5. F8 shortened promoters drive green fluorescent protein expression in hepatic endothelial cells. Immunofluorescence analyses of C57BL/6 livers 2 weeks after lentiviral vector (LV) LV.pF8-600.GFP, LV.pF8-446.GFP or LV.pF8-342.GFP delivery, compared to the full length LV.pF8-1175.GFP. (A) Representative pictures of liver sections stained for the endothelial marker (Lyve-1, in red) and the green fluorescent protein (GFP) using 400x magnification. (B) Liver of LV-injected mice decorated with the macrophage marker F4/80 (red) in combination with GFP (green). Nuclei are stained with 4',6-diamidino-2-phenylindole (DAPI) (blue). n=3-5 (mice); sections=3-6 per mouse. (for antibodies specifications refers to the Online Supplementary Appendix).

moter length. Specifically, in ECV-304, where Ets-1 is expressed, we observed a 3- to 6-fold increase in activity of each pF8 using the sgRNA F8.2, while no significant changes were observed with the sgRNA F8.1 (Figure 4B). In HEK293T cells, however, where Ets-1 is insignificant, we observed an upregulation in pF8 activity, ranging from a 20- to 40-fold, likely explained by the lack of competition for the BS involved (Figure 4C). Taken together, our results, highlight a central role of the sgRNA F8.2 in pF8 transactivation confirming the powerful role of the E2 site in promoter regulation.

In vivo maintenance of high endothelial specificity by shortened promoters

In order to assess the activity and specificity of the newly identified shortened pF8 sequences *in vivo*, we generated LV expressing GFP under the control of pF8-600, pF8-446 or pF8-342, and we administrated 5×10^8 TU to C57BL/6 mice. pF8-1175 was used as a control. Two weeks after injection, hepatic GFP expression was detected primarily in endothelial Lyve-1⁺ cells in all mice (Figure 5A), with rare F4/80⁺ macrophages GFP positive (GFP⁺) seen with the pF8-446 promoter (Figure 5B). Co-staining

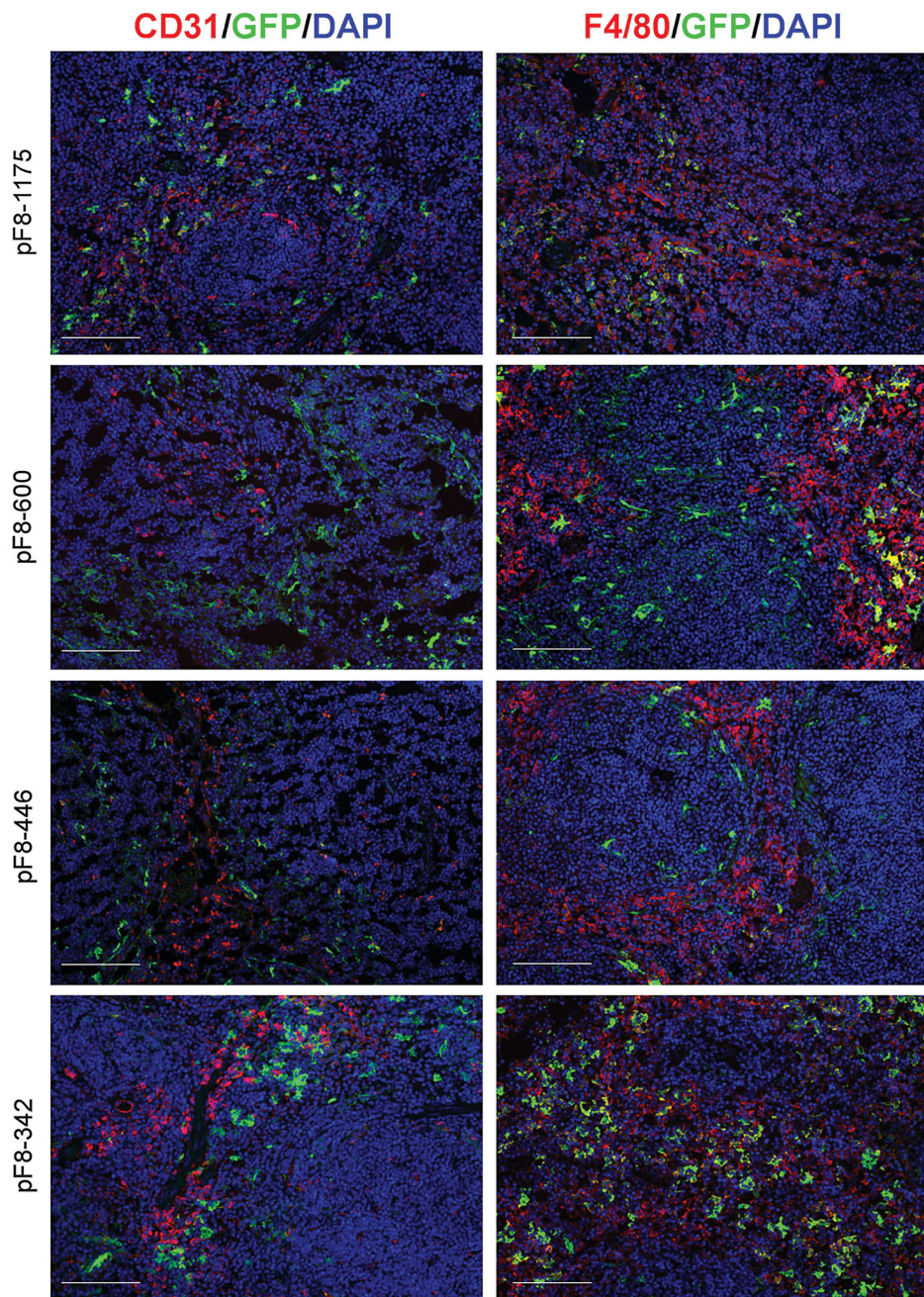


Figure 6. Green fluorescent protein expression in spleens under the control of pF8 shortened promoter sequences. Representative immunofluorescence images from mice spleens, 2 weeks following the delivery of lentiviral vector (LV) carrying different promoters. In red the endothelial marker CD31 (left side) or the macrophage marker F4/80 (right side) with green fluorescent protein (GFP) (green). Nuclei are stained with 4',6-diamidino-2-phenylindole (DAPI) (blue). Scale bars, 100 μ M. n=3-5 (mice); sections=5-7 per mouse.

with Lyve-1 was still visible 1 month post-injection, with a few F4/80⁺GFP⁺ cells appearing in the pF8-1175 and pF8-600 injected mice (Online Supplementary Figure S4A and B).

As previously observed for pF8-117523 in the spleen at 2 weeks, all pF8 short forms resulted in very low co-staining with the putative endothelial marker CD31 (Figure 6, left panel), while pF8-1,175, pF8-600 and pF8-446 showed a partial GFP expression in F4/80⁺ cells (Figure 6, right panel). Interestingly, in these mice several GFP⁺ cells were evident around the germinal centers (GC), resembling the EC lining in the marginal sinus of the spleen GC.³⁵ Unlike other promoters, the spleens of mice receiving the LV.pF8-342, showed a higher percentage of F4/80⁺/GFP⁺ cells (Figure 6, right panel) 2 weeks after the LV injection. The same GFP distribution pattern, but with a reduced expression, was confirmed in all treated mice at 1 and 2 months post LV-delivery. In particular, the LV.pF8-342.GFP-injected mice showed the most relevant reduction of GFP expression in F4/80⁺ cells over time (Online Supplementary Figures S5 and S6). Taken together, these results demonstrate that a significant reduction in pF8 size does not compromise its activity or specificity, suggesting that pF8-342 is enough for maintaining an endothelial-specific expression.

In vivo long-term recovery of factor VIII activity in a hemophilia A mouse model using the shortened F8 promoter

One of the major obstacles in HA gene therapy is represented by the large size of the FVIII expression cassette. As such, the choice of a suitable promoter to drive its expression is fundamental for success. In order to explore the ability of our new shortened promoters in rescuing FVIII expression *in vivo*, we generated LV carrying FVIII under their control and injected 1x10⁹ TU in B6/129 HA mice (n=4-6). pF8-1175 was used as a control. The FVIII activity promoted by pF8-600, pF8-446 resulted in a long-term (28 weeks) therapeutic correction (~10%), with no differences seen among them, and with respect to pF8-1175 (Figure 7A). Unexpectedly, despite the reduced response to Ets showed by luciferase assays, also the pF8-342 resulted in long-term therapeutic correction comparable to the other promoters tested. Importantly, independent of the size of the promoter used in the transfer construct, no anti-FVIII antibodies were detected in all treated mice, indicating the maintenance of specificity and, then, of an immunological profile similar to those observed for pF8-1175²³ (Figure 7B). High levels of anti-FVIII antibodies were instead detected

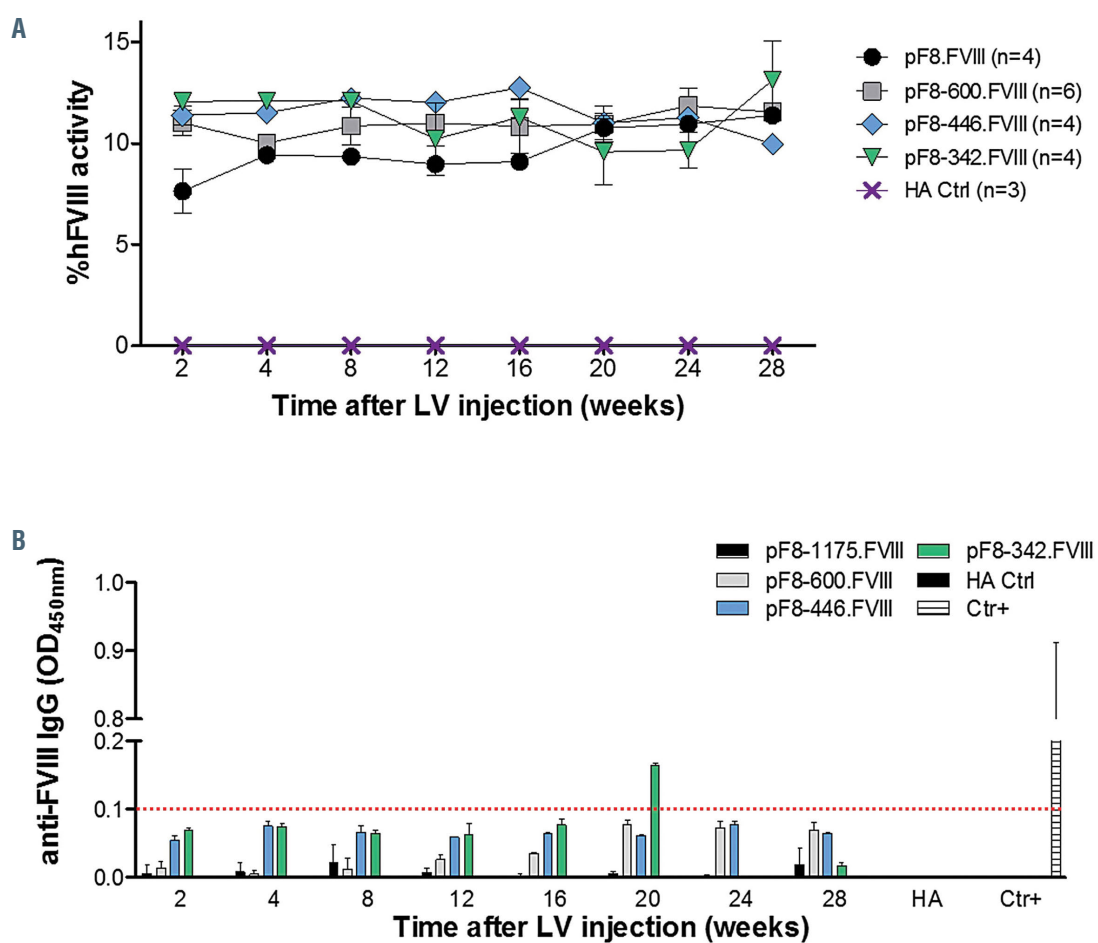


Figure 7. In vivo long-term correction of factor VIII activity with no immune response by F8 shortened promoters. (A) Graphic representation of factor VIII (FVIII) activity of B6/129 HA mice injected with lentiviral vector (LV).pF8-600.FVIII (grey square, n=6), LV.pF8-446.FVIII (light blue rhombus, n=4) or LV.pF8-342.FVIII (green triangle, n=4). pF8-1175.FVIII (black circle, n=4) were used as a control, while untreated hemophilia A (HA) mice were used as the negative control (violet X, n=3). No statistical differences in FVIII activity levels were observed among the four LV-injected experimental groups. (B) Enzyme-linked immunosorbent assay showing the absence of anti-FVIII antibodies in plasma of HA mice after LV delivery. Anti-FVIII positive HA mice injected with LV.PGK-FVIII served as positive control, while untreated HA mice were used as the negative control. Plasma dilution 1:2,000. Color bars were maintained according to the color scale used for FVIII activity graph.

in HA mice receiving FVIII under the control of the ubiquitous 3-phosphoglycerate kinase promoter, reinforcing the importance of a targeted expression of FVIII to avoid a specific immune response.

Discussion

One of the major challenges in the design of gene transfer vectors over the years, has involved the selection of cell type- or tissue-specific promoters suitable for restoring transgene expression in a defined disease setting. In gene therapy, transcriptional targeting represents a way to restrict mRNA and protein expression to a specific cell type, even if transduction of viral vectors is likely to occur in multiple cell types.³⁶ In the context of *F8* gene transfer, several attempts have been made to achieve a selective and stable gene expression in various cell types. This has been challenging due to the complexity of FVIII synthesis, its size and immunogenic behavior, therefore highlighting the need for novel approaches. Using previous *in silico* analyses performed on the native pF8,²⁵ we investigated in the present study the profile of TF potentially involved in promoting the expression of FVIII in EC. We identified and demonstrated *in vitro* that the Ets family of TF plays a fundamental role in the modulation of pF8 activity, offering regulatory elements that can be explored to promote FVIII expression in a targeted manner. Further, we defined a minimal pF8 required to efficiently drive FVIII expression *in vivo*, potentially overcoming a number of the current obstacles associated with *F8* gene delivery.³⁷

With LSEC now accepted as the main FVIII producing cells,^{15–18} understanding the key EC FVIII-specific regulatory elements is essential in promoting FVIII expression. The Ets-family of TF met our restricted criteria, with Ets-1 and -2 having the greatest number of BS across the pF8. More importantly, they are known to have essential roles in embryonic endothelial cell survival and in adult angiogenesis.²⁸ In adults the expression of Ets-1 is maintained at very low levels in the resting endothelium and is induced after specific stimuli. In particular, Ets-1 is reported to be up-regulated in response to pro-angiogenic and pro-inflammatory stimuli such as TNF- α , hepatocyte growth factor and platelet-derived growth factor.³⁸ In addition, hypoxia has been demonstrated to regulate Ets-1 expression through the hypoxia inducible factor-1.²⁹ Further, LSEC are known to be physiologically exposed to decreasing oxygen pressure along the liver lobule.³⁹

In our case, by overexpressing Ets-1 and Ets-2, both independently and collectively, we clearly demonstrate the involvement of Ets-1 in the regulation of pF8 activity. Interestingly, the transactivation efficiency of Ets-1 appeared to be potentiated by the presence of Ets-2, likely via protein-protein interactions. Co-operation between Ets-1 and -2 has been shown to be involved in the reactivation of the *TERT* gene in cancer.⁴⁰ In this context, the co-operative interaction of Ets-1 and Ets-2 promotes the recruitment of p52 to a mutant form of the *TERT* promoter enhancing *TERT* expression when the non-canonical NF- κ B signaling is activated. In our case, we observed this phenomenon in ECV-304 but not in HEK293T cells, suggesting the existence of cell-specific regulation with respect to *F8* expression. Both Ets-1 and Ets-2 are tightly regulated transcription factors,⁴¹ and it might be that in specific cells, like HEK293T, the forced expression of one

is able to bypass the establishment of a co-operative interaction. A similar regulation is not surprising for *F8* due to the necessity of a tight control, since it has been demonstrated that high expression of FVIII can cause cellular stress and increased immunogenicity.⁴²

In order to clarify the relevance of the Ets-BS for the regulation of pF8, we opted to generate several reduced sized pF8 progressively removing single or multiple Ets sites. This approach demonstrated that the -342 bp region, in which three Ets-1 and one Ets-2 sites were maintained, represented a minimal functional promoter *in vitro*. Further reduction of the pF8 to 246 bp, which excluded an additional Ets-BS, caused a strong suppression of basal pF8 activity and preserved a minimal response to Ets-1 and Ets-2 overexpression. Of note, we identified that the -223 to -217 Ets-1 (E2) site is the most relevant regulatory element needed to achieve the maximal up-regulation of pF8 activity. In recent years, several mutations targeting the nucleotide positions ranging from -218 to -221, encompassing the E2 site, have been described to be responsible for different degrees of HA.⁴³ It has been clearly shown that these nucleotides are part of a highly conserved region where any change compromises the functionality of the pF8. Our *in vitro* studies highlight the importance of the -218 to -221 sequence, identifying it as the most essential Ets-1 responsive element on pF8. The use of a CRISPRa system to transactivate pF8, reinforces this finding, highlighting the E2 site as being essential for pF8 regulation. While only a modest up-regulation of pF8 was detectable in ECV-304, it is likely that the physiological expression of Ets-1 hampers the efficient binding of the sgRNA to the E2 site. The use of CRISPRa also supports the concept of the binding of Ets to the E2 site.

The *in vivo* delivery of LV expressing the GFP or FVIII transgene under the control of each described shortened promoter, reinforces the results obtained *in vitro*. All LV-treated mice displayed GFP expression in liver Lyve-1 $^{+}$ cells, most likely LSEC,⁴⁴ resembling the pattern detectable using pF8-1175. Nevertheless, a few F4/80 $^{+}$ macrophages expressed GFP, especially with respects to the two longer pF8. This is not surprising because we previously described that the complete absence of macrophage targeting using an endothelial promoter, was only obtained by inserting a multiple miRNA target (mirT) sequence recognized by the hematopoietic-specific miRNA 142-3p (mirT-142-3p).⁴⁵

F8 gene transfer in HA mice confirmed the power of each tested promoter to drive long-term and stable FVIII expression without the appearance of inhibitors. Importantly, therapeutic levels of FVIII activity were detectable in all treated mice at similar levels to those observed in mice delivered with the control pF8-1,175 promoter. Such results are encouraging with respect to the current obstacles associated with the achievement of an efficient *F8* gene delivery.

There are some limitations in our study. While Ets TF seem to be involved in pF8 regulation, the direct binding of Ets-1 and Ets-2 to pF8, and their specific role in LSEC remains to be confirmed. Further, the difficulty to isolate and maintain primary LSEC for extended periods in culture,⁴⁶ limits the use of luciferase assays.

Taken together, our *in vitro* and *in vivo* results have identified the region from 0 to -342 as a minimal pF8 which preserves its activity and Ets-response and is comparable to the full-length pF8. Evidence for a role of Ets-1 and the

Ets-2 in pF8 regulation offers a new insight into the molecular mechanisms promoting FVIII expression in specific cell types. To date, *F8* has not been reported to be amongst the large number of genes shown to be direct targets of Ets-1 and Ets-2 regulation, such as *KDR*, *FLT1*, *ANGPT2*, *TEK*, *VWF*⁴⁷ and *CDH5*.⁴⁸ Interestingly, all these genes are normally expressed at different stages in EC, suggesting a common regulation with FVIII.

Establishing the minimal promoter sequence required for the maintenance of a regulated FVIII expression restricted to LSEC, offers new perspectives for developing novel approaches to cure HA. For example, it provides the possibility of inserting a pF8 into an AAV-FVIII construct. Currently, these classes of vectors are the safest and most extensively used for HA gene therapy,⁴⁹ however, they are limited by the size of the expression cassette, making it impossible to introduce both *F8* and its full-length promoter. The efficient pF8 size reduction (~70%) described herein, opens up the possibility of engineering shortened chimeric pF8 by including sequences enriched in TFBS (like Ets-1) which can enhance the pF8 activity, as has been described for the transthyretin promoter in hepatocytes.⁵⁰

Disclosures

AF, RF, SM, DZ are named inventors of the patent "PROMOTER FOR CELL-SPECIFIC GENE EXPRESSION AND USES THEREOF" (PCT/IB2017/053460).

Contributions

RF designed and performed most of the experiments; SM injected lentiviral vectors in mice, performed blood coagulation and enzyme-linked immunosorbent assays; EB designed, performed and analyzed immunofluorescence stainings; AC and SS helped with cloning experiments and luciferase assays; CA carried out statistical analyses; MP and SP generated and tested the impact of CRISPRa system on pF8; VB produced lentiviral vectors for in vivo experiments; SF and GP helped in planning and performing some in vitro experiments; GEW performed western blotting analysis and DC performed data analysis; AF conceived, supervised the study and generated funding; RF, GEW and AF wrote the paper; all authors critically revised the paper and approved the version to be published.

Acknowledgments

The authors thank Dr. Chiara Borsotti for help in revising the manuscript. Dr. Diego Zanolini for the contribution in planning some initial cloning experiments. Dr. Diego Cotella for providing the promoterless pNL1.1 plasmid and suggestions for luciferase experiments setting. Dr. Daniela Capello and Prof. Fabrizio Faggiano for contribution in luciferase assays data analysis. Dr. Silvia Buzzi for performing mice maintenance and coagulation assays.

Funding

This work was supported partly by European Research Council (ERC) #261178 and Horizon 2020 (HemAcure project #66742) to AF.

References

- Hoyer LW. Hemophilia A. *N Engl J Med*. 1994;330(1):38-47.
- Bolton-Maggs PHB, Pasi KJ. *Haemophilias A and B*. Lancet. 2003;361(9371):1801-1809.
- Mannucci PM, Tuddenham EG. The hemophilias—from royal genes to gene therapy. *N Engl J Med*. 2001;344(23):1773-1779.
- Weyand AC, Pipe SW. New therapies for hemophilia. *Blood*. 2019;133(5):389-398.
- Pipe SW. Gene therapy for hemophilia. *Pediatr Blood Cancer*. 2018;65(2).
- Lusher JM, Arkin S, Abildgaard CF, Schwartz RS. Recombinant factor VIII for the treatment of previously untreated patients with hemophilia A - safety, efficacy, and development of inhibitors. *N Engl J Med*. 2002;346(7):453-459.
- Lenting PJ, van Mourik JA, Mertens K. The life cycle of coagulation factor VIII in view of its structure and function. *Blood*. 1998;92(11):3983-3996.
- Aravalli RN, Belcher JD, Steer CJ. Liver-targeted gene therapy: approaches and challenges. *Liver Transplant*. 2015;21(2):718-737.
- Arruda VR. The search for the origin of factor VIII synthesis and its impact on therapeutic strategies for hemophilia A. *Haematologica*. 2015;100(7):849-850.
- Gitschier J, Wood WI, Goralka TM, et al. Characterization of the human factor VIII gene. *Nature*. 1984;312(5992):326-330.
- Ingerslev J, Christiansen BS, Heickendorff L, Petersen CM. Synthesis of factor VIII in human hepatocytes in culture. *Thromb Haemost*. 1988;60(3):387-391.
- Wion KL, Kelly D, Summerfield JA, Tuddenham EGD, Lawn RM. Distribution of factor VIII mRNA and antigen in human liver and other tissues. *Nature*. 1985;317(6039):726-729.
- Figueiredo MS, Brownlee GG. cis-acting elements and transcription factors involved in the promoter activity of the human factor VIII gene. *J Biol Chem*. 1995;270(20):11828-11838.
- McGlynn LK, Mueller CR, Begbie M, Notley CR, Lillicrap D. Role of the liver-enriched transcription factor hepatocyte nuclear factor 1 in transcriptional regulation of the factor V111 gene. *Mol Cell Biol*. 1996;16(5):1936-1945.
- Follenzi A, Benten D, Novikoff P, Faulkner L, Raut S, Gupta S. Transplanted endothelial cells repopulate the liver endothelium and correct the phenotype of hemophilic A mice. *J Clin Invest*. 2008;118(3):935-945.
- Shahani T, Covens K, Lavend'homme R, et al. Human liver sinusoidal endothelial cells but not hepatocytes contain factor VIII. *J Thromb Haemost*. 2014;12(1):36-42.
- Fahs SA, Hille MT, Shi Q, Weiler H, Montgomery RR. A conditional knockout mouse model reveals endothelial cells as the principal and possibly exclusive source of plasma factor VIII. *Blood*. 2014;123(24):3706-3713.
- Everett LA, Cleuren ACA, Khuriyan RN, Ginsburg D. Murine coagulation factor VIII is synthesized in endothelial cells. *Blood*. 2014;123(24):3697-3705.
- Zanolini D, Merlin S, Feola M, et al. Extrahepatic sources of factor VIII potentially contribute to the coagulation cascade correcting the bleeding phenotype of mice with hemophilia A. *Haematologica*. 2015;100(7):881-892.
- Madeira CL, Layman RE, De Vera ME, Fontes PA, Ragni M V. Extrahepatic factor VIII production in transplant recipient of hemophilia donor liver. *Blood*. 2009;113(21):5364-5365.
- Follenzi A, Raut S, Merlin S, Sarkar R, Gupta S. Role of bone marrow transplantation for correcting hemophilia A in mice (supplemental methods). *Blood*. 2012;120(23):1-17.
- Hollestelle MJ, Thines T, Crain K, et al. Tissue distribution of factor VIII gene expression in vivo—a closer look. *Thromb Haemost*. 2001;86(3):855-861.
- Merlin S, Famà R, Borroni E, et al. FVIII expression by its native promoter sustains long-term correction avoiding immune response in hemophilic mice. *Blood Adv*. 2019;3(5):825-838.
- Peyvandi F, Garagiola I. Clinical advances in gene therapy updates on clinical trials of gene therapy in haemophilia. *Haemophilia*. 2019;25(5):738-746.
- Farré D, Roset R, Huerta M, et al. Identification of patterns in biological sequences at the ALGGEN server: PROMO and MALGEN. *Nucleic Acids Res*. 2003;31(13):3651-3653.
- Follo C, Isidoro C. A fast and simple method for simultaneous mixed site-specific mutagenesis of a wide coding sequence. *Biotechnol Appl Biochem*. 2008;49(Pt 2):175-183.
- Pignani S, Zappaterra F, Barbon E, et al. Tailoring the CRISPR system to transactivate coagulation gene promoters in normal and mutated contexts. *Biochim Biophys Acta Gene Regul Mech*. 2019;1862(6):619-624.
- Wei G, Srinivasan R, Cantemir-Stone CZ, et al. Ets1 and Ets2 are required for endothelial cell survival during embryonic angiogenesis. *Blood*. 2009;114(5):1123-1130.
- Dittmer J. The biology of the Ets1 proto-oncogene. *Mol Cancer*. 2003;2:29.
- Oettgen P. Functional redundancy of Ets1 and Ets2. *Blood*. 2009;114(5):934-935.
- Sato Y, Teruyama K, Nakano T, et al. Role of transcription factors in angiogenesis: Ets-1

promotes angiogenesis as well as endothelial apoptosis. *Ann N Y Acad Sci.* 2001;947:117-123.

31. Takahashi K, Sawasaki Y, Hata J-I, Mukai K, Goto T. Spontaneous transformation and immortalization of human endothelial cells. *Vitr Cell Dev Biol.* 1990;26(3):265-274.

32. Basuyaux JP, Ferreira E, Stéphelin D, Butticé G. The Ets transcription factors interact with each other and with the c-Fos/c-Jun complex via distinct protein domains in a DNA-dependent and -independent manner. *J Biol Chem.* 1997;272(42):26188-26195.

34. Chavez A, Scheiman J, Vora S, et al. Highly efficient Cas9-mediated transcriptional programming. *Nat Methods.* 2015; 12(4):326-328.

35. Chen Y, Pikkariainen T, Elomaa O, et al. Defective microarchitecture of the spleen marginal zone and impaired response to a thymus-independent type 2 antigen in mice lacking scavenger receptors MARCO and SR-A. *J Immunol.* 2005;175(12):8173-8180.

36. Nicklin SA, Reynolds PN, Brosnan MJ, et al. Analysis of cell-specific promoters for viral gene therapy targeted at the vascular endothelium. *Hypertension.* 2001;38(1):65-70.

37. Pierce GF, Iorio A. Past, present and future of haemophilia gene therapy: from vectors and transgenes to known and unknown outcomes. *Haemophilia.* 2018;24 Suppl 6:60-67.

38. Dejana E, Taddei A, Randi AM. Foxs and Ets in the transcriptional regulation of endothelial cell differentiation and angiogenesis. *Biochim Biophys Acta.* 2007;1775(2):298-312.

39. Poisson J, Lemoine S, Boulanger C, et al. Liver sinusoidal endothelial cells: physiology and role in liver diseases. *J Hepatol.* 2017;66(1):212-227.

40. Li Y, Zhou QL, Sun W, et al. Non-canonical NF-κB signalling and ETS1/2 cooperatively drive C250T mutant TERT promoter activation. *Nat Cell Biol.* 2015;17(10):1327-1338.0

41. Poon GMK, Kim HM. Signatures of DNA target selectivity by ETS transcription factors. *Transcription.* 2017;8(3):193-203.

42. Lange AM, Altynova ES, Nguyen GN, Sabatino DE. Overexpression of factor VIII after AAV delivery is transiently associated with cellular stress in hemophilia A mice. *Mol Ther Methods Clin Dev.* 2016;3:16064.

43. Nougier C, Roualdes O, Fretigny M, et al. Characterization of four novel molecular changes in the promoter region of the factor VIII gene. *Haemophilia.* 2014;20(2):149-156.

44. Arimoto J, Ikura Y, Suekane T, et al. Expression of LYVE-1 in sinusoidal endothelium is reduced in chronically inflamed human livers. *J Gastroenterol.* 2010;45(3):317-325.

45. Merlin S, Cannizzo ES, Borroni E, et al. A novel platform for immune tolerance induction in hemophilia A mice. *Mol Ther.* 2017;25(8):1815-1830.

46. DeLeve L, Maretti-Mira A. Liver sinusoidal endothelial cell: an update. *Semin Liver Dis.* 2017;37(04):377-387.

47. Schwachtgren JL, Janel N, Barek L, et al. Ets transcription factors bind and transactivate the core promoter of the von Willebrand factor gene. *Oncogene.* 1997;15(25):3091-3102.

48. Lelièvre E, Mattot V, Huber P, Vandenbunder B, Soncin F. ETS1 lowers capillary endothelial cell density at confluence and induces the expression of VE-cadherin. *Oncogene.* 2000;19(20):2438-2446.

49. George LA, Ragni MV, Samelson-Jones BJ, et al. Spk-8011: preliminary results from a phase 1/2 dose escalation trial of an investigational AAV-mediated gene therapy for hemophilia a. *Blood.* 2017;130(Suppl 1):S604.

50. Chuah MK, Petrus I, De Bleser P, et al. Liver-specific transcriptional modules identified by genome-wide *in silico* analysis enable efficient gene therapy in mice and non-human primates. *Mol Ther.* 2014;22(9):1605-1613.



miR-146a is a pivotal regulator of neutrophil extracellular trap formation promoting thrombosis

Ana B. Arroyo,^{1*} María P. Fernández-Pérez,^{1*} Alberto del Monte,^{2*} Sonia Águila,¹ Raúl Méndez,³ Rebecca Hernández-Antolín,¹ Nuria García-Barberá,¹ Ascensión M. de los Reyes-García,¹ Paula González-Jiménez,³ María I. Arcas,⁴ Vicente Vicente,^{1,5} Rosario Menéndez,^{3,6} Vicente Andrés,^{2,7} Rocío González-Conejero^{1#} and Constantino Martínez^{1#}

¹Department of Hematology and Medical Oncology, Morales Meseguer University Hospital, Centro Regional de Hemodonación, Universidad de Murcia, IMIB-Arrixaca, Murcia; ²Centro Nacional de Investigaciones Cardiovasculares Carlos III (CNIC), Madrid;

³Servicio de Neumología, Hospital Universitario y Politécnico La Fe/Instituto de Investigación Sanitaria (IIS) La Fe, La Fe; ⁴Department of Pathology, Hospital Reina Sofía, Murcia; ⁵CIBER de Enfermedades raras (CIBER-ER), Murcia; ⁶Centro de Investigación en Red en Enfermedades Respiratorias (CIBER-ES, CB06/06/0028), Madrid and ⁷CIBER de Enfermedades Cardiovasculares (CIBER-CV), Madrid, Spain.

*ABA, MPF-P, and AdM contributed equally as co-first authors.

^{1#}RG-C and CM contributed equally as co-senior authors.

ABSTRACT

Neutrophil extracellular traps (NET) induce a procoagulant response linking inflammation and thrombosis. Low levels of miR-146a, a brake of inflammatory response, are involved in higher risk of cardiovascular events, but the mechanisms explaining how miR-146a exerts its function remain largely undefined. The aim of this study was to explore the impact of miR-146a deficiency in NETosis both in sterile and non-sterile models *in vivo*, and to investigate the underlying mechanism. Two models of inflammation were used: (i) *Ldlr*^{-/-} mice transplanted with bone marrow from *miR-146a*^{-/-} or wild-type mice were fed a high-fat diet, generating an atherosclerosis model; and (ii) an acute inflammation model was generated by injecting lipopolysaccharide (1 mg/kg) into *miR-146a*^{-/-} and wild-type mice. miR-146a deficiency increased NETosis in both models. Accordingly, *miR-146a*^{-/-} mice showed significantly reduced carotid occlusion time and elevated levels of NET in thrombi following FeCl₃-induced thrombosis. Infusion of DNase I abolished arterial thrombosis in both WT and *miR-146a*^{-/-} mice. Interestingly, miR-146a-deficient mice have aged, hyperreactive and pro-inflammatory neutrophils in their circulation which are more prone to form NET independently of the stimulus. Furthermore, we demonstrated that patients with community-acquired pneumonia with reduced miR-146a levels associated with the T variant of the functional rs2431697 had an increased risk of cardiovascular events due, in part, to an increased generation of NET.

Correspondence:

ROCÍO GONZÁLEZ-CONEJERO
rocio.gonzalez@carm.es, constant@um.es

Received: November 5, 2019.

Accepted: June 19, 2020.

Pre-published: June 25, 2020.

<https://doi.org/10.3324/haematol.2019.240226>

©2021 Ferrata Storti Foundation

Material published in *Haematologica* is covered by copyright. All rights are reserved to the Ferrata Storti Foundation. Use of published material is allowed under the following terms and conditions:
<https://creativecommons.org/licenses/by-nc/4.0/legalcode>. Copies of published material are allowed for personal or internal use. Sharing published material for non-commercial purposes is subject to the following conditions:
<https://creativecommons.org/licenses/by-nc/4.0/legalcode>, sect. 3. Reproducing and sharing published material for commercial purposes is not allowed without permission in writing from the publisher.



Introduction

Neutrophils play a crucial role in immunity and injury repair but also contribute to the development of several thrombo-inflammatory diseases.¹ The pathophysiological role of neutrophils has become more evident following the discovery of neutrophil extracellular traps (NET).² NET are large web-like structures released upon neutrophil activation, comprising a matrix of DNA and histones which are decorated with antimicrobial proteins, such as myeloperoxidase or neutrophil elastase (NE).³ These structures were first identified as a novel innate defense mechanism;³ however, NET also promote thrombosis through activation of platelets and the coagulation cascade.⁴ Therefore, NET interconnect immunity, inflammation, and thrombosis within a physiological process known as immunothrombosis.⁵ Thus,

uncontrolled or aberrant activation of immunothrombosis promotes thrombotic pathologies such as stroke, myocardial infarction, deep vein thrombosis, or disseminated intravascular coagulation during sepsis.^{5,6}

A large variety of infectious and sterile inflammatory stimuli have been described as triggers of NETosis. Interestingly, their consequences on neutrophil activation vary depending on the nature and duration of the stimulus.⁷ Two mechanisms resulting in NET formation have been described: lytic and vital NETosis.⁸ Specific microorganisms or lipopolysaccharides (LPS) induce vital NETosis directly or indirectly through toll-like receptors (TLR), via a TLR4-activated platelet interaction, by an oxidant-independent mechanism.^{9,10} This strategy aims to limit the spread of bacteria and keeps neutrophils alive for further functions.⁸ Alternatively, lytic NETosis can be induced by diverse sterile agonists such as phorbol 12-myristate 13-acetate,^{3,11} cholesterol crystals¹¹ or cytokines (interleukin-6,¹² interleukin-8,^{3,13} interferon- α ¹⁴). This drives NADPH oxidase activation via protein kinase C and Raf-MEK-ERK, which generates reactive oxygen species (ROS) inducing neutrophil death.¹⁵

MicroRNA (miRNA or miR) are a family of small non-coding RNA that regulate gene expression.¹⁶ Since their discovery, miRNA have been implicated as key modulators of numerous physiological and pathological processes.¹⁷⁻²⁰ In particular, miR-146a directly mediates thromboinflammatory processes as: (i) it inhibits several proinflammatory elements of the TLR-NF (nuclear factor)- κ B pathway^{21,22} and (ii) it is predominantly expressed in cells that promote thrombogenesis (monocytes/macrophages, platelets, neutrophils, and endothelial cells).^{23,24} Our group demonstrated that reduced levels of miR-146a, guided by the T variant of the functional miR-SNP rs2431697, are predictors of adverse cardiovascular events in patients with atrial fibrillation.²⁴ Interestingly, *in vitro* activation of rs2431697 TT neutrophils exacerbated NET release in accordance with elevated plasma NE levels found in T carriers, who also had a higher risk of adverse cardiovascular events.²⁵ Overall, our data suggest that miR-146a is crucially involved in linking inflammation, thrombosis, and NETosis. However, the role of miR-146a in immunothrombosis and NETosis is unknown. Here, we investigated the involvement of miR-146a in NET formation leading to arterial thrombosis in both sterile and non-sterile inflammatory murine models. Thus, we characterized the neutrophil phenotype to explain the exacerbated NETosis. Finally, we evaluated the association between low miR-146a levels, NETosis markers and the occurrence of thrombosis in septic patients.

Methods

Mice models

Atherosclerosis model

Irradiation and bone marrow (BM) transplantation were performed as previously described.²⁶ Briefly, *Ldlr*^{-/-} mice were irradiated and transplanted with BM cells obtained from wild-type (WT) or *miR-146a*^{-/-} mice. After 4 weeks on a standard diet, transplanted mice were fed an atherogenic diet for 8 weeks. Blood was collected from the facial vein into 3.2% citrate and plasma samples were stored at -80°C until analysis. Heart and aorta were extracted from euthanized mice after *in situ* perfusion with phosphate-buffered saline and fixed with 4% paraformaldehyde overnight

at 4°C. Tissue was embedded in paraffin and cross-sections from the aortic root were made.

Endotoxemia model

WT and *miR-146a*^{-/-} mice were injected intraperitoneally with a sublethal dose of LPS (1 mg/kg) (*E. coli* 0111/B4, Sigma-Aldrich, Madrid, Spain). For morphological analysis, lungs were fixed with 4% paraformaldehyde overnight at 4°C, embedded in paraffin and sectioned. Lung damage was evaluated in one section/mouse using a semi-quantitative score via a blind method following the pathologist's criteria.

Ferric chloride-induced arterial thrombosis

Animals were anesthetized by intraperitoneal injection (xylazine hydrochloride 10 mg/kg + ketamine hydrochloride 100 mg/kg). The carotid artery was isolated and the injury was generated by applying a piece of filter paper (5x1 mm) (GE Healthcare Whatman 1003917, Fisher, Madrid, Spain) soaked in a 7.5% ferric chloride (FeCl₃) solution for 2 min (Sigma-Aldrich, Madrid Spain). After washing the arterial surface with saline solution and removing residual FeCl₃, a Doppler ultrasound flow probe (Model 0.5 PSB, Transonic Systems, Ithaca, NY, USA) was applied. The probe was connected to a flow meter (Model TS420, Transonic Systems, Ithaca, NY, USA) that continuously registered the blood flow. Occlusion time was defined as the time elapsed from the withdrawal of FeCl₃ to the lack of blood flow (≤ 0.01 mL/min) for at least 3 consecutive minutes. Experiments were stopped after 30 min if no occlusion occurred. For the experiments with DNase I, mice were injected intravenously (tail vein) with 10 µg of Pulmozyme® (Roche Farma, Madrid, Spain) diluted in saline, 15 min before FeCl₃ treatment.

Patients and controls

The study (NEUMONAC study #2011/0219 [05/07/2011]) was approved by the Ethical Committee (ceic@iislafe.es) of our institution and performed in accordance with the ethical standards laid down in the 1964 Declaration of Helsinki and its subsequent amendments. Consecutive patients admitted with community-acquired pneumonia (CAP) were included from October 2015 to June 2018 at Hospital Universitario y Politécnico La Fe (Valencia, Spain). The patients' details are provided in the *Online Supplementary Methods*.

Healthy subjects were randomly selected among blood donors from our Transfusion Center and gave their informed consent to enrollment into the study.

Statistical analysis

All statistical analyses were conducted using GraphPad Prism 3.8 (GraphPad Software, Inc., La Jolla, CA, USA) and SPSS 22.0 for Windows (SPSS, Inc., Chicago, IL, USA). Differences between two groups were assessed by an unpaired Student *t*-test or Mann-Whitney U test, where appropriate. For multiple comparisons, one-way analysis of variance on ranks with the Bonferroni post-hoc test was used. Data are shown as mean \pm standard error of mean or as median (95% confidence interval), as appropriate. A *P*-value <0.05 was considered statistically significant.

Further details on the materials and methods are available in the *Online Supplementary Methods*.

Results

miR-146a deficiency promotes NET formation in an atherosclerosis model

Previous data from our laboratory demonstrated that

miR-146a deficiency upregulates NETosis in both murine and human *in vitro* models.²⁵ Thus, we aimed to extrapolate this finding to different *in vivo* models. We first utilized an atherosclerosis mouse model previously generated by our group.²⁶ Briefly, *Ldlr*^{-/-} mice were transplanted with BM from *miR-146a*^{-/-} or WT animals and fed a high-fat diet for 8 weeks (Figure 1A). As reported, transplant efficiency, body weight, circulating blood cell counts, plasma lipid profile, and atherosclerotic burden (atheroma, lesion, and necrotic core areas) were similar between the experimental groups.²⁶ No differences were found in cell-free (cf)DNA and NE plasma levels between the two groups of mice before they were fed the high-fat diet (*data not shown*). As expected, after 8 weeks of the atherogenic diet, notable differences in NET components between the two groups were observed. As shown in Figure 1B, plasma cfDNA levels were significantly higher in *Ldlr*^{-/-} BM *miR-146a*^{-/-} mice than in *Ldlr*^{-/-} BM WT littermates (348.1 ± 73.0 vs. 177.3 ± 39.4 ng/mL, respectively; $P < 0.05$). Similarly, plasma NE was almost 2-fold higher in BM *miR-146a*^{-/-} mice than in BM WT mice (228.6 ± 32.6 vs. 113.0 ± 14.2 ng/mL, respectively; $P < 0.05$) (Figure 1C). In addition, immunofluorescence analysis of aortic valves revealed that, although intact neutrophils were found in both cases (*Online Supplementary Figure S1*), there were substantial differences in the size and the amount of NET. DNA, and NE, and H2B staining revealed an increase of large NET in the atherosclerotic lesions and adhered to the vascular wall of BM *miR-146a*^{-/-} mice compared to BM WT mice, in which we only identified scattered NET throughout all the sections (Figure 1D). Quantification of NET in whole sections within aortic roots confirmed that *miR-146a*^{-/-} mice had more NET than had WT mice (ICorr values 0.78 ± 0.09 vs. 0.53 ± 0.07 , respectively; $P < 0.01$) (Figure 1E). In addition, zooming within NETotic areas demonstrated that H2B and NE co-localization was near to 100% ($R = 0.97$; Costes P -value = 1), in contrast to the low co-localization found in intact neutrophils ($R = 0.13$; Costes P -value = 1) (Figure 1F, *Online Supplementary Movies S1* and *S2*). Collectively, these results demonstrated a role for miR-146a in NET formation during the process of atherosclerosis.

miR-146a mediates NETosis and lung damage in an lipopolysaccharide-induced, sublethal model of inflammation

The molecular mechanisms leading to NETosis differ depending on the triggering stimulus.⁷ In order to investigate whether miR-146a may link different pathways provoking NETosis, we next examined the implication of miR-146a on NET formation using a non-sterile inflammatory mouse model generated by sublethal injection of LPS (1 mg/kg) for 4 h and 24 h. As expected, there was a significant progressive reduction in circulating leukocyte and platelet counts following induction of endotoxemia, although no relevant differences between *miR-146a*^{-/-} and WT animals (*Online Supplementary Figure S2*) were observed. As shown in Figure 2, basal plasma NET markers were similar between *miR-146a*^{-/-} and WT mice. However, following LPS administration at 4 h and 24 h, plasma cfDNA levels were higher in *miR-146a*^{-/-} mice than in WT mice, with the difference being statistically significant at 4 h (1653.0 ± 216.5 vs. 845.6 ± 294.4 ng/mL, respectively; $P < 0.01$) (Figure 2A). Similarly, LPS injection resulted in significantly higher levels of plasma NE in *miR-146a*^{-/-}

miR-146a^{-/-} mice when compared to WT mice, after 4 h (1671.3 ± 95.6 vs. 1206.1 ± 99.2 ng/mL, respectively; $P < 0.01$) and 24 h (2458.0 ± 57.1 vs. 1524.6 ± 61.2 ng/mL, respectively; $P < 0.001$) (Figure 2B). Higher NETosis in *miR-146a*^{-/-} mice following LPS challenge was confirmed by western blotting. Plasma citrullinated histone 3 (citH3) levels were higher in *miR-146a*^{-/-} mice than in WT mice at both 4 h and 24 h (Figure 2C). Finally, additional inflammatory and coagulation markers were analyzed. LPS-dependent ROS production at 24 h was significantly higher compared with basal levels only in *miR-146a*^{-/-} mice (178%; $P < 0.05$) (Figure 2D). Additionally, the amounts of thrombin-antithrombin (TAT) complexes were significantly greater 4 h after LPS injection than at baseline only in *miR-146a*^{-/-} mice (43%; $P < 0.05$) (Figure 2E).

Although all mice indistinctly survived sublethal LPS injection, we explored whether LPS challenge could differentially damage mice lungs. Staining of lung sections showed a notable increase of reticulin in samples from *miR-146a*^{-/-} mice compared with their WT littermates after 4 h of LPS (Figure 2F). According to the pathologist's criteria, the analysis showed that both reticulin score and global lung injury were increased in *miR-146a*^{-/-} mice compared to WT mice (Figure 2G). Therefore, miR-146a-deficient mice had higher NETosis, oxidative stress and activation of coagulation and consequently, greater lung damage after LPS injection.

miR-146a deficiency confers an aged, overactive, and pro-inflammatory phenotype to neutrophils

Although neutrophils have been considered to be a relatively homogeneous population, evidence demonstrating their heterogeneity is emerging.¹ To investigate whether the increased ability of *miR-146a*^{-/-} neutrophils to form NET in the above-mentioned models was related to a particular phenotype determined by miR-146a deficiency, we explored the aged/activated state of neutrophils by flow cytometry. miR-146a deficiency did not alter the total percentage of neutrophils in the circulation (*Online Supplementary Figures S2* and *S3*). Analysis of neutrophil surface markers revealed that *miR-146a*^{-/-} neutrophils exhibited significantly higher levels of Cxcr4 and CD11b, and lower levels of CD62L than WT neutrophils (Figure 3A). Our results also showed that neutrophils from *miR-146a*^{-/-} mice had significantly lower Cxcr1 levels than neutrophils from their WT littermates (Figure 3B), suggesting an additional pro-inflammatory ability for the *miR-146a*^{-/-} neutrophil phenotype.²⁷⁻²⁹ Tlr4 has been implicated in the process of aging³⁰ and is a target of miR-146a.³¹ Thus, we measured and compared its levels in *miR-146a*^{-/-} and WT neutrophils from whole blood and found that, as described before, aged neutrophils (defined by Cxcr4^{high} and CD62L^{low} surface expression) expressed higher levels of Tlr4 than the rest. Interestingly, aged *miR-146a*^{-/-} neutrophils expressed significantly more Tlr4 than aged WT neutrophils (Figure 3C). Moreover, miR-146a deficiency in isolated neutrophils produced significantly higher ROS levels (Figure 3D) and elevated oxygen consumption rate (Figure 3E) at basal state compared with those in neutrophils from WT mice. Thus, miR-146a deficiency seems to promote aging and hyperreactivity to neutrophils, a pro-inflammatory phenotype that could contribute to the exacerbated NETosis of these cells.

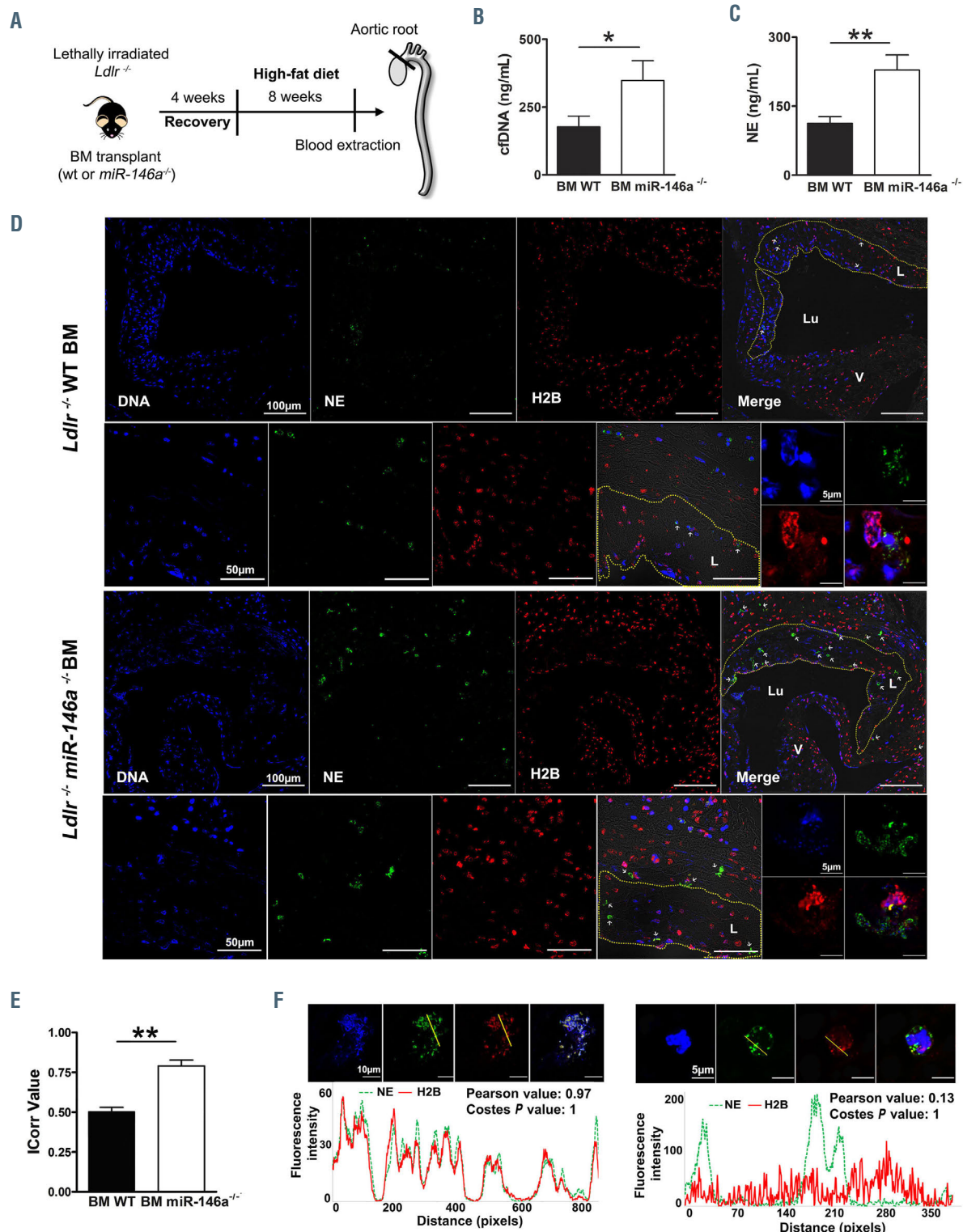


Figure 1. miR-146a deficiency enhances neutrophil extracellular trap formation in atherosclerosis. (A) *Ldlr*^{-/-} mice were transplanted with bone marrow (BM) from *miR-146a*^{-/-} or wild-type (WT) mice. After 4 weeks of recovery, mice were fed a high-fat diet for 8 weeks. Blood and aortic tissues were extracted for quantification of the formation of neutrophil extracellular traps (NET) (n=10-12/group). (B) Plasma cell-free (cf)DNA was measured using Sytox Green. (C) Plasma neutrophil elastase (NE) activity was quantified by enzyme-linked immunosorbent assay. (D) Representative confocal microscopy images of an aortic valve leaflet, an atherosclerotic area, and a NET detail from *Ldlr*^{-/-} BM WT, and *Ldlr*^{-/-} BM *miR-146a*^{-/-} mice immunostained for DNA (DAPI, blue), NE (green), and H2B (red). The dashed yellow line denotes an atherosclerotic lesion (L) boundary; the lumen (Lu), and valves (V) are also marked. White arrowheads point to NET. (E) NET quantification in aortic valve sections from *Ldlr*^{-/-} BM WT, and *Ldlr*^{-/-} BM *miR-146a*^{-/-} mice performed with the Colocalization Colormap Fiji plugin. The correlation index (ICorr) represents the fraction of positively correlated (co-localized) H2B and NE pixels in one representative section per mouse *in situ* WT and six *miR-146a*^{-/-} BM-transplanted *Ldlr*^{-/-} mice. (F) Fluorescence intensity plots of H2B and NE in a region of interest (yellow line) of a NET and a neutrophil found in the aortic valve from a *Ldlr*^{-/-} BM *miR-146a*^{-/-} and a *Ldlr*^{-/-} BM WT mouse, respectively. The correlation of H2B and NE fluorescence intensity was determined using the Pearson correlation coefficient and Costes method. In the Pearson correlation test, the R value ranges between -1 and 1, with 1 being a perfect correlation, 0 no linear correlation, and -1 a perfect negative linear correlation. Costes analysis compares pixel correlation for non-randomized with randomized images and calculates significance. The Costes P-value was 1 in both cases, indicating that the probability of random images correlating to real images is 0. P-value calculations were performed using the Mann-Whitney U test. Data represent mean \pm standard error of mean, *P<0.05, **P<0.01.

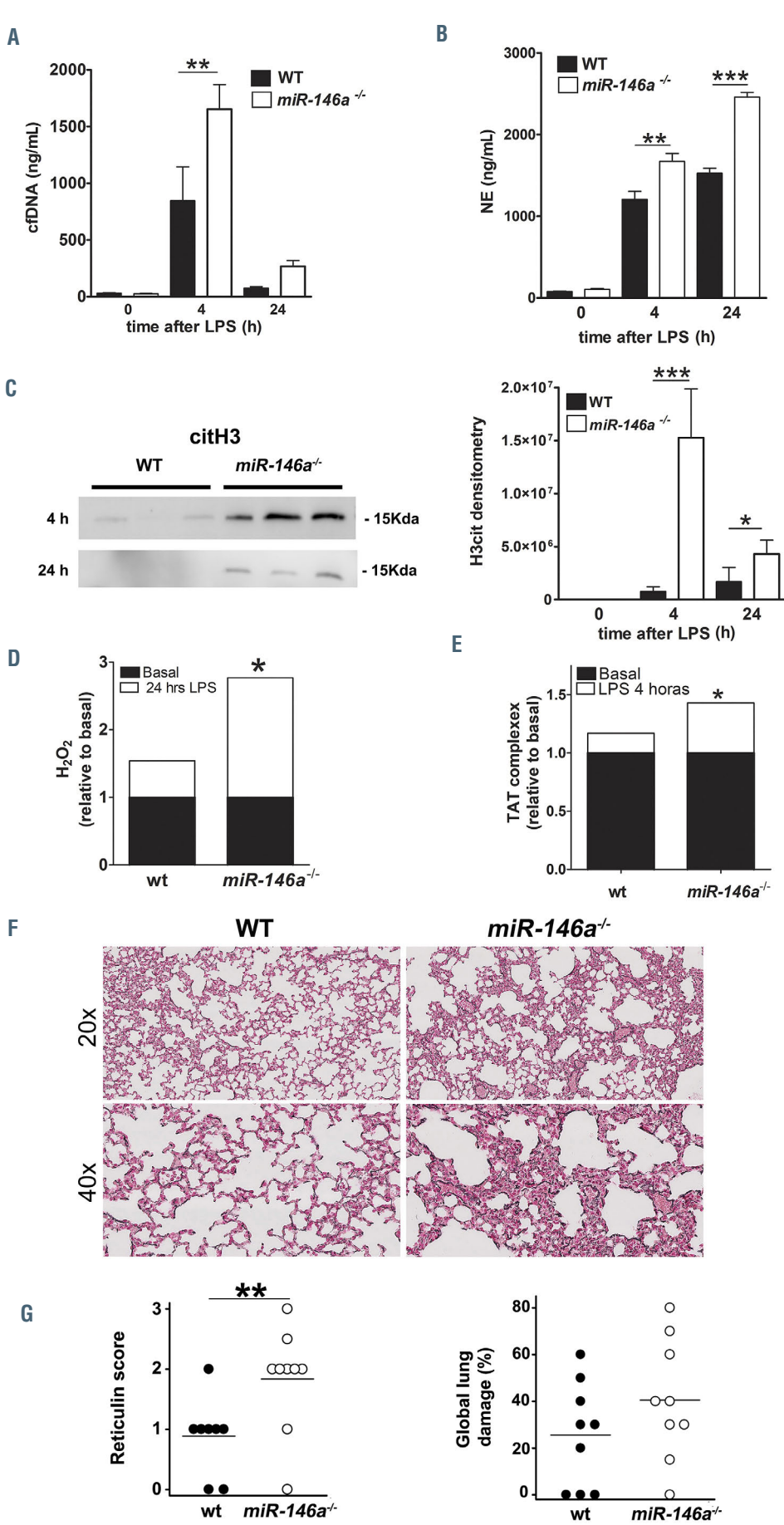


Figure 2. *miR-146a* deficiency mediates NETosis in endotoxemia. *miR-146a*^{-/-} and wild-type (WT) mice were injected intraperitoneally with a sub-lethal dose of lipopolysaccharide (LPS) (1 mg/kg). Plasma markers of neutrophil extracellular traps (NET) were measured 4 h and 24 h after LPS treatment (n=9/group). (A) Cell-free (cf)DNA levels were quantified by Sytox Green. (B) Neutrophil elastase (NE) levels were measured by enzyme-linked immunosorbent assay (ELISA). (C) Citrullinated histone 3 (CitH3) plasma levels were analyzed by western blot. (D) Reactive oxygen species (ROS) were quantified by fluorometry 24 h after treatment with LPS. (E) Thrombin-antithrombin (TAT) complex levels were detected by ELISA 4 h after LPS treatment. (F) Morphology of lungs from WT and *miR-146a*^{-/-} mice after LPS stimulation. Lung sections from WT and *miR-146a*^{-/-} mice treated 4 h with LPS (1 mg/kg) were stained for reticulin to observe tissue structure and global injury. Representative images of reticulin staining from WT and *miR-146a*^{-/-} lungs after LPS at 20x and 40x magnification. (G) Semi-quantitative analysis for reticulin and global lung damage according to the pathologist's criteria. One section/mouse was scored in a blinded fashion into four grades from 0 to 3 (0=normal, 1=mild, 2=moderate, 3=severe). P-value calculations were performed using one-way analysis of variance on ranks with the Bonferroni post-hoc test or the Mann-Whitney U test, where appropriate. Data represent mean \pm standard error of mean, *P<0.05, **P<0.01, ***P<0.001.

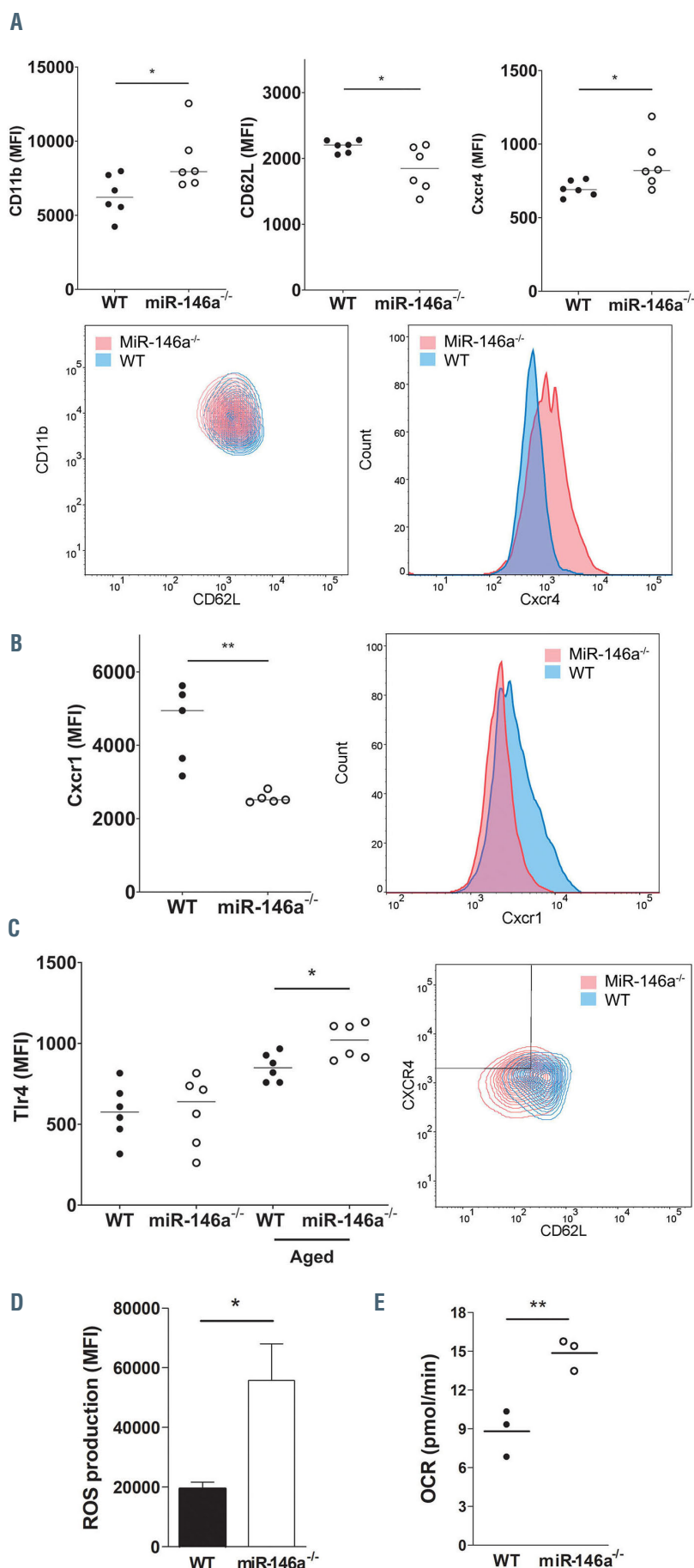


Figure 3. *miR-146a* determines neutrophil phenotype. (A) Flow cytometry analysis of CD11b, CD62L, and Cxcr4 ($P<0.05$ for all markers) on neutrophils (Ly6G-positive population) from blood of wild-type (WT) and *miR-146a*^{-/-} mice ($n=6$ mice in both groups). Contour plots from flow cytometry analysis of CD62L and CD11b on neutrophils from a representative WT mouse and an *miR-146a*^{-/-} mouse (bottom left panel). Comparison of Cxcr4 expression between WT and *miR-146a*^{-/-} representative mice (bottom right panel). (B) Flow cytometry analysis of Cxcr1 on neutrophils from blood of WT and *miR-146a*^{-/-} mice (left panel; $n=5$ mice in both groups; $P<0.01$). Comparison of Cxcr1 expression on a representative mouse with each genotype (right panel). (C) Tlr4 levels were measured in Cxcr4^{high} and CD62L^{low} (aged) neutrophil subpopulation versus the rest ($n=6$ mice in both groups; $P<0.05$). Contour plots from flow cytometry analysis of CD62L and Cxcr4 on peripheral blood pool neutrophils from six WT and six *miR-146a*^{-/-} mice (right panel). (D) Bone marrow (BM) isolated neutrophils were incubated with 10 μ M H₂DCFDA for 30 min at 37 °C and analyzed by flow cytometry ($n=3$ mice in both groups). (E) BM neutrophils were seeded on the plate and the oxygen consumption rate (OCR) was measured by a Seahorse Analyzer. (mean \pm standard deviation, $n=3$ mice for each group, samples in quadruplicate). Statistical analyses between groups of mice were performed using the Mann-Whitney test (A-C) or t-test (D, E); * $P<0.05$, ** $P<0.01$.

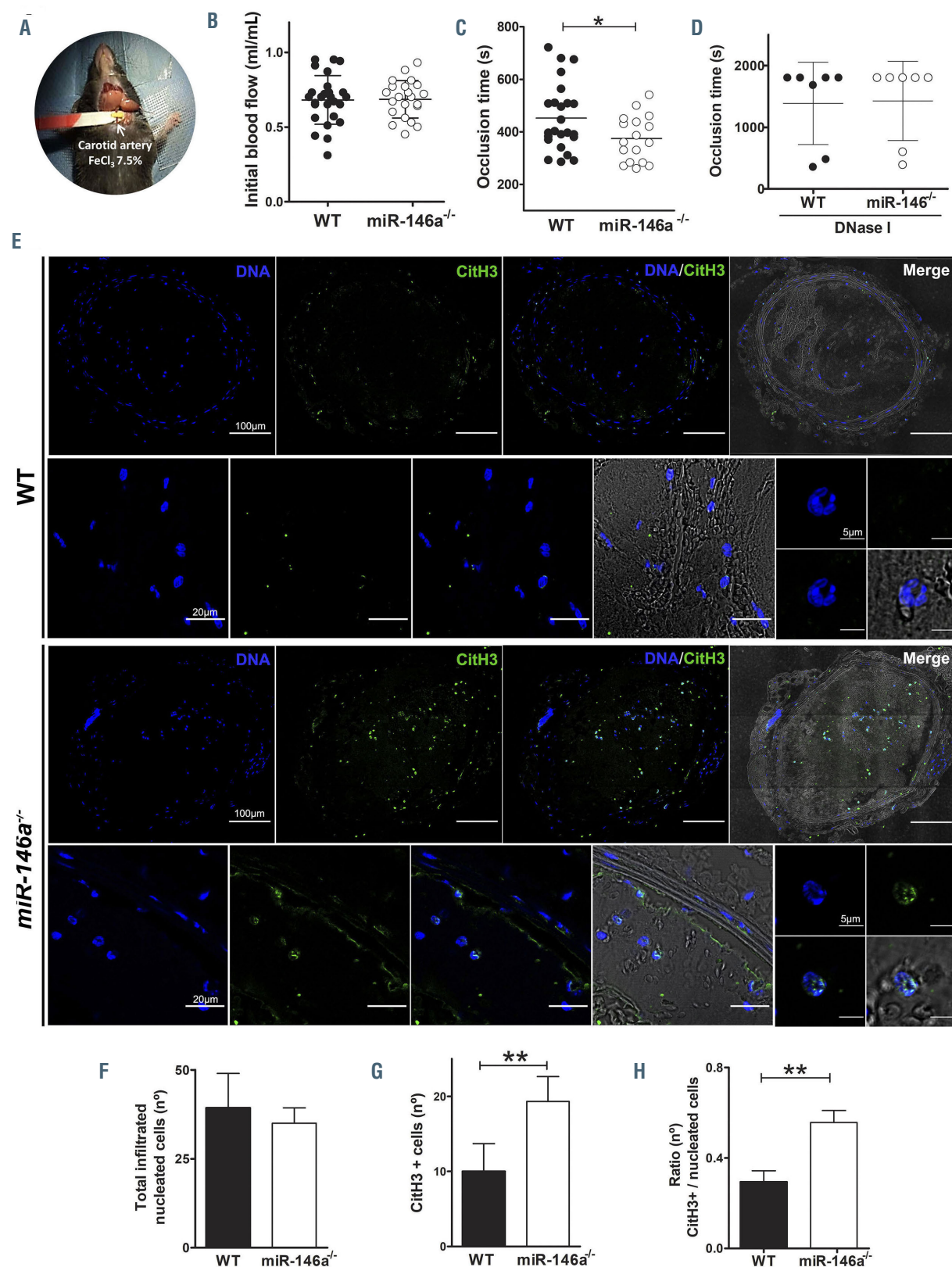


Figure 4. miR-146a deficiency accelerates carotid thrombotic occlusion. (A) Mouse model of FeCl₃-induced carotid arterial thrombosis. The carotid artery from wild-type (WT) and miR-146a^{-/-} mice was isolated and exposed to 7.5% FeCl₃ for 2 min (WT n=24, miR-146a^{-/-} n=17). A Doppler ultrasound flow probe registered the blood flow continuously. (B) Basal blood flow. (C) Time to carotid thrombotic occlusion. (D) Alternatively, WT (n=7) and miR-146a^{-/-} (n=7) mice were treated with DNase I (10 μg, i.v.) 15 min before vessel injury and the carotid occlusion time was measured for a maximum of 30 min. (E) Representative images of neutrophil extracellular traps (citrullinated histone 3 [CitH3]-positive nuclei) in the carotid thrombi from WT and miR-146a^{-/-} mice analyzed by immunofluorescence. For each genotype the upper row shows the complete cross-section of the thrombosed carotid artery (bar corresponds to 100 μm) and the lower row a higher magnification of the artery wall (bar corresponds to 20 μm) and the detail of a neutrophil (bar corresponds to 5 μm) (F-H) Quantification of total infiltrated nucleated cells, citH3-positive cells and the ratio of total nucleated to citH3-positive cells in the thrombi and the adventitial layer of carotid sections from WT and miR-146a^{-/-} mice (n=10/group). P-value calculations were performed using the unpaired Student t-test and Mann-Whitney U-test. Data represent mean ± standard error of mean, *P<0.05.

Loss of miR-146a accelerates time to carotid thrombotic occlusion by increasing NET release

Thus, we hypothesized that under a thrombotic stimulus, these neutrophils may favor the production of NET, thereby strongly contributing to thrombosis. To test this hypothesis, we induced carotid endothelial injury with FeCl₃ in *miR-146a*^{-/-} and WT mice (Figure 4A) and determined time to arterial occlusion. Although basal blood flow was similar between the two groups of animals (Figure 4B), *miR-146a*^{-/-} mice showed a significant reduction in time to occlusion compared to the time in WT littermates (374.5 ± 21.15 vs. 452.5 ± 26.14 s, respectively; $P<0.05$) (Figure 4C). The occlusion times of WT and *miR-146a*^{-/-} mice were similar upon treatment with DNase I (Figure 4D). Thus, DNase I treatment abolished arterial occlusion, supporting the concept that NET are essential for thrombus formation and stability upon FeCl₃ damage. To further analyze the association between thrombosis and NETosis, thrombi within carotids were isolated and immunofluorescence for citH3 was performed. FeCl₃-induced injury promoted similar infiltration of nucleated cells in both groups (Figure 4E-F); however, the number of DNA-citH3-positive cells within the carotid thrombi was significantly higher in *miR-146a*^{-/-} mice than in WT ones (19.3 ± 3.3 vs. 10.0 ± 3.6 cells, respectively; $P<0.05$) (Figure 4G). The ratio of citH3-positive to total nucleated cells found in the thrombi of carotid sections was significantly higher in *miR-146a*^{-/-} mice than in WT mice (Figure 4H, *Online Supplementary Figure S4*).

Of note, no relevant differences in F12 coagulation factor, recently implicated in NETosis,³² was observed between the two groups (*data not shown*). Thus, miR-146a deficiency may accelerate vessel occlusion due, in part, to increased NETosis associated with the presence of hyper-reactive neutrophils.

Low miR-146a levels in patients with community-acquired pneumonia are associated with an increased risk of cardiovascular events

In order to test the clinical impact of our *in vivo* results, we recruited 259 patients with CAP with a 30-day follow-up period. *Online Supplementary Table S1* shows the demographic and clinical characteristics of all 259 patients, as well as the frequencies and distribution of the rs2431697 genotype. We found no significant differences between the main cardiovascular risk factors and geno-

type (*Online Supplementary Table S1*). In addition, both Sepsis-related Organ Failure Assessment (SOFA) score and neutrophil count at entry were similar in all patients independently of their genotype (*Online Supplementary Table S1*). One hundred and twelve plasma samples were available for DNA-citH3 measurement. From these, 81 (72.3%) were considered as positive (optical density [OD] values >0.200 , the maximum OD value yielded for 30 healthy controls) (*Online Supplementary Figure S5, Online Supplementary Table S2*). As described for septic patients, plasma levels of DNA-citH3 correlated with clinical outcomes.^{33,34} Thus, plasma DNA-citH3 levels were significantly higher in septic patients (n=58) than in non-septic patients (n=23) ($P<0.001$). Furthermore, DNA-citH3 levels were significantly higher in patients in whom treatment failed or cardiovascular events occurred (n=18) than in the rest of the patients (n=63) ($P=0.028$) (*Online Supplementary Table S2*).

Interestingly, we observed significant differences between the occurrence of cardiovascular complications and rs2431697 genotype. As shown in Table 1, 30 of the 259 patients suffered from cardiovascular events when hospitalized and 29 of them were carriers of the T allele (relative risk [RR]=9.61, [95% CI]: 95% confidence interval: 1.28-72.15, $P=0.008$). The risk of cardiovascular events remained significantly higher for CT+TT patients 30 days after hospitalization (RR=2.85, 95% CI: 0.97-8.37, $P=0.049$) (Table 1). In addition, 21.4% of the carriers of the T allele developed a cardiovascular event and failed to respond to therapy (RR=2.89, 95% CI: 1.09-7.66, $P=0.027$) (Table 1). Finally, among patients with the highest DNA-citH3 plasma levels (≥ 0.406 OD units) we found a 3-fold higher frequency of T carriers individuals (30%) compared to CC homozygotes (9.5%; $P=0.061$) (Table 2).

Discussion

In the last years, the functional versatility of neutrophils has moved towards a fascinating area of research in which the inflammatory capacity of these cells is tightly linked to the development of cardiovascular diseases.³⁵ On the other hand, the pathophysiological role of NET in thrombogenesis is now firmly established.³⁶ In this process, known as immunothrombosis, the mechanisms leading to NETosis differ depending on the triggering stimulus.⁷ Identifying key regulators of NETosis³⁷ is a challenge to further contribute to the development of anti-thrombotic therapeutic tools that would not affect the essential role of NET fighting germs. In this work, we show that miR-146a, a well-known molecular brake to the NF-κB pathway, underlies NETosis-mediated thrombosis after both sterile and non-sterile stimulation.

First, we demonstrated that sterile inflammation in a

Table 1. Relationship between hospital cardiovascular complications and rs2431697 genotype in patients with community-acquired pneumonia (n=259).

	CC N=58	CT+TT N=201	P RR (95% CI)
CVE, N (%)	1 (1.7)	29 (14.4)	0.008 9.61 (1.28-72.15)
TF, N (%)	4 (6.9)	22 (10.9)	0.366 -
CVE+TF, N (%)	5 (8.6)	43 (21.4)	0.027 2.89 (1.09-7.66)
CVE-30, N (%)	4 (6.9)	35 (17.4)	0.049 2.85 (0.97-8.37)

RR: relative risk; 95% CI: 95% confidence interval; CVE: cardiovascular events during hospitalization, including pulmonary thromboembolism; TF: treatment failure during hospitalization; CVE+TF: occurrence of cardiovascular event and/or treatment failure; CVE-30: cardiovascular events 30 days after hospitalization.

Table 2. rs2431697 genotype frequencies according to DNA-citrullinated H3 plasma levels in patients with community-acquired pneumonia.

	DNA-citH3 < 4Q	DNA-citH3 > 4Q	P*
CC, N (%)	19 (90.5)	2 (9.5)	
CT+TT, N (%)	42 (70.0)	18 (30.0)	0.061

4Q indicates 4th quartile (≥ 0.406 optical density units). Measurements were performed in a total of 81 patients (OD ≥ 0.200). * χ^2 test.

model of miR-146a deficiency in the hematopoietic lineage caused greater NET formation. However, we previously showed that miR-146a deficiency in the hematopoietic lineage had no effect on atherosogenesis after 8 weeks of an atherogenic diet.²⁶ Here, our results suggest that miR-146a deficiency may participate in thrombosis rather than in atherosogenesis, through NETosis. This hypothesis is in accord with results published by Franck *et al.* demonstrating that NETosis does not alter atherosclerotic plaque formation but rather increases thrombosis in a model of plaque erosion.³⁸ Supporting this hypothesis, previous reports have shown that thrombosis induction increases NET deposition.^{39,40} Consistently, when arterial thrombosis was induced by FeCl₃ injury, we observed an increased generation of NET in the thrombi of *miR-146a*^{-/-} mice compared to WT mice, with a shorter time to vessel occlusion. The abolition of thrombosis by removal of NET with DNase I in *miR-146a*^{-/-} and WT mice, further supports the essential role of miR-146a in NET production. In this sense, Massberg *et al.* also found in a murine model of FeCl₃ injury that the inhibition of NET components, by infusion of anti-H2A-H2B-DNA antibody, prolonged the occlusion time and generated low stability thrombi in the carotid.³⁹

Next, we created a non-sterile model of inflammation by LPS injection into *miR-146a*^{-/-} mice. Indeed, *miR-146a*^{-/-} mice exhibit hyperreactivity to LPS, with an exacerbated inflammatory response, demonstrating miR-146a as a regulator of autoimmunity, myeloproliferation, and cancer.²³ Our results showed that miR-146a deficiency provokes higher rates of NETosis in LPS-challenged mice. Of note, no differences were found in the capacity of phagocytosis between *miR-146a*^{-/-} and WT neutrophils *in vitro* after LPS challenge (*data not shown*). In addition, miR-146a deficiency promotes a pro-coagulant phenotype with increased levels of thrombin-antithrombin complexes and ROS production and regulates the extent of organ damage following infection, as *miR-146a*^{-/-} mice developed greater lung damage than did WT mice. Although the use of murine models is considered useful for understanding the pathophysiology of sepsis, there are notable differences between these models and sepsis in humans.⁴¹ We therefore examined NETosis markers and their relationship with thrombosis in CAP patients. Plasma NETosis markers correlated with the incidence of sepsis in accordance with previously reported data,⁴² further supporting the concept that sepsis is a relevant model for investigating the role of NET in humans. Interestingly, we found a correlation between NETosis and thrombotic complications in CAP patients. Our group has previously described that the miR-SNP rs2431697 of *MIR146A* is associated with an increased risk of cardiovascular events in patients with atrial fibrillation.²⁴ Here, we have verified the role of rs2431697 genotype in cardiovascular events in patients with CAP. Supporting our findings, Xie *et al.* reported that activation of miR-146a expression decreased markers of myocardial injury in rats treated with LPS.⁴³ In addition, the injection of miR-146a has been described to play a protective role in the cardiac dysfunction induced by sepsis in a murine model, with longer survival of the mice.⁴⁴ Results from our cohort indicate that NETosis could be a functional path by which miR-146a levels lead to thrombosis in septic patients. Of note, we found that among patients with higher levels of NETosis markers, carriers of the T allele were 3-fold more

frequent than CC patients. The concept of sepsis and cardiovascular diseases sharing a common pathophysiology has been explored recently.⁴⁵ Common gene signaling pathways for both sepsis and cardiovascular diseases were investigated and genetic variations in miR-146a targets such as *IL6* or *IRAK1* were found to be shared in patients with both diseases.⁴⁵ Although the etiology of sepsis and cardiovascular disease is not identical, the two conditions share the same end-points of inflammation, coagulation, and endothelial activation.^{46,47} Overall our results demonstrate that miR-146a is involved in thrombogenesis of two diseases with cardiovascular events, atrial fibrillation and sepsis, *a priori* in two different models. Accordingly, miR-146a may be yet another regulator of immunothrombosis.

The mechanisms leading to the increased NET formation by miR-146a are still elusive. Interestingly, pro-inflammatory activity of neutrophils has been shown to correlate positively with aging.³⁰ Aged neutrophils are the

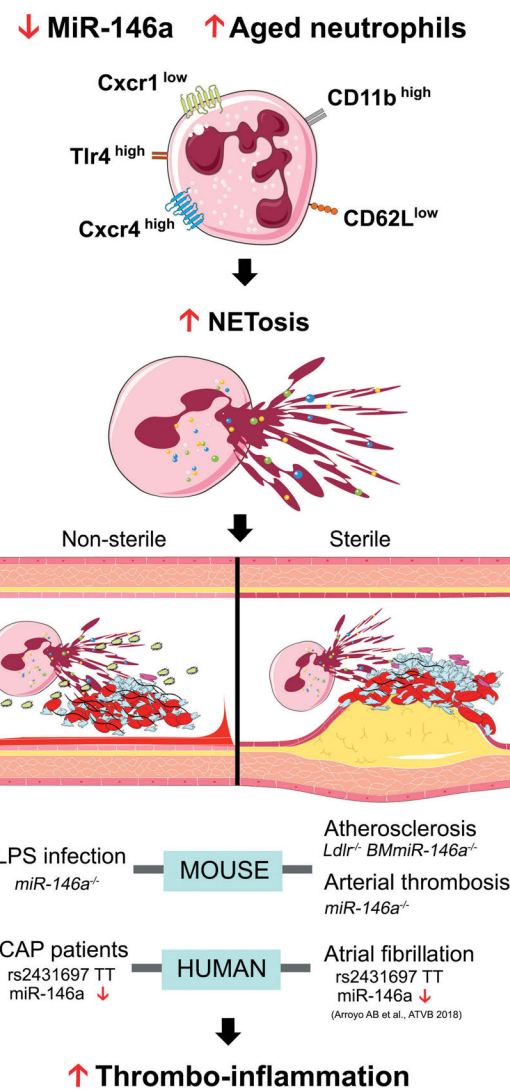


Figure 5. miR-146a plays a relevant role in thrombo-inflammation after sterile and non-sterile stresses. Low miR-146a levels promote an aging phenotype in neutrophils (CD62^{low} CD11b^{high} Cxcr4^{high} Tlr4^{high}) which primes these cells. Upon sterile or non-sterile stimuli, primed neutrophils would be more prone to NETosis leading to a thrombo-inflammatory process. MiR-146a: microRNA-146a; LPS: lipopolysaccharide; CAP: community-acquired pneumonia.

first line of defense in the context of acute inflammation since they do not return to the bone marrow, arrive first at the inflammatory tissues and infiltrate them in a TLR4/CD11b-dependent manner.⁴⁸ Thus, we investigated neutrophil phenotype in *miR-146a^{-/-}* mice in order to explain the greater NET formation observed in our different models. We found that *miR-146a^{-/-}* resting neutrophils have an aging phenotype CD62L^{low} CD11b^{high} Cxcr4^{high}, and a lower expression of Cxcr1.¹

Thus, we speculate that miR-146a deficiency could act as a priming effector on resting neutrophils so that, under any inflammatory stimulus, (sterile or non-sterile) these cells would reach higher activation rates than WT neutrophils. Our results show that Tlr4, which is a validated target of miR-146a, is overexpressed in aged *miR-146a^{-/-}* neutrophils in comparison with WT ones. One possible explanation for this finding may be that the deficiency of miR-146a favors a higher deregulation of the Tlr4/NF-κB axis in aged neutrophils than in non-aged ones. Thus, this hypothesis would also explain in part why circulating aged neutrophils are more prone to make NET, a previous indolent signal being necessary to prime these cells.^{49,50} Indeed, it has been shown that *Tlr4^{-/-}* mice or germ-free mice have less aged neutrophils than WT littermates.⁵⁰

In accord with our hypothesis, we observed higher ROS levels and oxygen consumption rate in neutrophils from *miR146^{-/-}* mice than WT mice, which may further suggest a primed status in *miR-146a^{-/-}* neutrophils. Importantly, the aging process is promoted in large part by ROS that produce cellular damage.⁵¹ ROS (mainly produced by NADPH oxidase) are also crucial to initiate the process of NET formation.⁵²

There are a few limitations in this study. First, for the *in vivo* inflammation models, we did not use a complex marker such as a granulocytic enzyme bound to DNA to measure NET. NET were quantified using cfDNA, NE, and citH3 for the LPS model and tissue immunofluorescence in the atherosclerotic model. Thus, we cannot rule out that part of the cfDNA and NE measured in plasma was due to neutrophil secretion or to apoptotic processes. Another point is that our study was performed in full *miR-146a^{-/-}* mice or BM transplanted mice. Given the interplay of other cells with neutrophils to promote NETosis, in particular platelets,^{9,10} it would be of interest in future studies to dissect the mechanisms implicating

miR-146a in the formation of NET using conditional models of miR-146a deficiency.

In summary, our results demonstrate that miR-146a deficiency promotes an aged neutrophil phenotype priming these cells for activation. Upon both sterile and non-sterile stimuli, such sensitized neutrophils are more prone to form NET, leading to thrombosis when physiological control is overwhelmed (Figure 5). Indeed, we demonstrate this hypothesis in a human disease, sepsis, in which patients with low miR-146a levels due to rs2431697 have increased plasma NET markers and a higher risk of cardiovascular events. These data not only strengthen the proposed interconnection between inflammation and thrombosis but also open new perspectives for the development of therapeutic tools against NETosis in different thrombo-inflammatory contexts.

Disclosures

No conflicts of interest to disclose.

Contributions

ABA, MPF-P, AdM, SA, RH-A, NG-B, AMR-P and MIA performed research; ABA, MPF-P, AdM, SA and MIA analyzed data; RaM, PG-J, and RoM collected samples/data from patients and analyzed patients' data; VV critically reviewed the paper; RG-C, and CM conceived and designed research; ABA, RG-C, and CM wrote the paper.

Acknowledgments

The authors thank Dr Juan José Cerón, Alberto Martínez, and Dr. Antonio Moscardó for technical assistance and Clive Drakeford and Javier Corral for reviewing the manuscript.

Funding

This work was supported by research grants from Instituto de Salud Carlos III (ISCIII), Fondo Europeo de Desarrollo Regional "Investing in your future" (PI17/00051 y PI17/01421) (PFI18/0045 to AdMIR-G) (CD18/00044: to SA), and Fundación Séneca (19873/GERM/15). The CNIC is supported by the ISCIII, the Ministerio de Ciencia, Innovación y Universidades (MCIU), and the Fundación Pro CNIC, and is a Severo Ochoa Center of Excellence (SEV-2015-0505). ABA has a research fellowship from Sociedad Española de Trombosis y Hemostasia (SETH). The MCIU supported AdM. (predoctoral contract BES-2014-067791).

References

1. Silvestre-Roig C, Hidalgo A, Soehnlein O. Neutrophil heterogeneity: implications for homeostasis and pathogenesis. *Blood*. 2016;127(18):2173-2181.
2. Papayannopoulos V. Neutrophil extracellular traps in immunity and disease. *Nat Rev Immunol*. 2017;18(2):134-147.
3. Brinkmann V, Reichard U, Goosmann C, et al. Neutrophil extracellular traps kill bacteria. *Science*. 2004;303(5663):1532-1535.
4. Martinod K, Wagner DD. Thrombosis: tangled up in NETs. *Blood*. 2014;123(18):2768-2776.
5. Engelmann B, Massberg S. Thrombosis as an intravascular effector of innate immunity. *Nat Rev Immunol*. 2013;13(1):34-45.
6. Laridan E, Martinod K, De Meyer S. Neutrophil extracellular traps in arterial and venous thrombosis. *Semin Thromb Hemost*. 2019;45(01):86-93.
7. Kenny EF, Herzig A, Krüger R, et al. Diverse stimuli engage different neutrophil extracellular trap pathways. *Elife*. 2017;6:e24437.
8. Jorch SK, Kubes P. An emerging role for neutrophil extracellular traps in noninfectious disease. *Nat Med*. 2017;23(3):279-287.
9. Clark SR, Ma AC, Tavener SA, et al. Platelet TLR4 activates neutrophil extracellular traps to ensnare bacteria in septic blood. *Nat Med*. 2007;13(4):463-469.
10. Maugeri N, Campana L, Gavina M, et al. Activated platelets present high mobility group box 1 to neutrophils, inducing autophagy and promoting the extrusion of neutrophil extracellular traps. *J Thromb Haemost*. 2014;12(12):2074-2088.
11. Desai J, Kumar S V, Mulay SR, et al. PMA and crystal-induced neutrophil extracellular trap formation involves RIPK1-RIPK3-MLKL signaling. *Eur J Immunol*. 2016;46(1):223-229.
12. Joshi MB, Lad A, Bharath Prasad AS, Balakrishnan A, Ramachandra L, Satyamoorthy K. High glucose modulates IL-6 mediated immune homeostasis through impeding neutrophil extracellular trap formation. *FEBS Lett*. 2013;587(14):2241-2246.
13. Kahlenberg JM, Carmona-Rivera C, Smith CK, Kaplan MJ. Neutrophil extracellular trap-associated protein activation of the NLRP3 inflammasome is enhanced in lupus macrophages. *J Immunol*. 2013;190(3):1217-1226.
14. Martinelli S, Urosevic M, Daryadel A, et al. Induction of genes mediating interferon-dependent extracellular trap formation during neutrophil differentiation. *J Biol Chem*. 2004;279(42):44123-44132.
15. Ley K, Hoffman HM, Kubes P, et al. Neutrophils: new insights and open questions. *Sci Immunol*. 2018;3(30):eaat4579.

16. Jonas S, Izaurrealde E. Towards a molecular understanding of microRNA-mediated gene silencing. *Nat Rev Genet.* 2015;16(7):421-433.

17. Bartel DP. MicroRNAs: target recognition and regulatory functions. *Cell.* 2009;136(2):215-233.

18. Barwari T, Joshi A, Mayr M. MicroRNAs in cardiovascular disease. *J Am Coll Cardiol.* 2016;68(23):2577-2584.

19. Essandoh K, Fan G-C. Role of extracellular and intracellular microRNAs in sepsis. *Biochim Biophys Acta.* 2014;1842(11):2155-2162.

20. Chen J-Q, Papp G, Szodoray P, Zeher M. The role of microRNAs in the pathogenesis of autoimmune diseases. *Autoimmun Rev.* 2016;15(12):1171-1180.

21. Taganov KD, Boldin MP, Chang KJ, Baltimore D. NF- κ B-dependent induction of microRNA miR-146, an inhibitor targeted to signaling proteins of innate immune responses. *Proc Natl Acad Sci U S A.* 2006;103(33):12481-12486.

22. Saba R, Sorensen DL, Booth SA. MicroRNA-146a: a dominant, negative regulator of the innate immune response. *Front Immunol.* 2014;5:578.

23. Boldin MP, Taganov KD, Rao DS, et al. miR-146a is a significant brake on autoimmunity, myeloproliferation, and cancer in mice. *J Exp Med.* 2011;208(6):1189-1201.

24. Roldan V, Arroyo AB, Salloum-Asfar S, et al. Prognostic role of MIR146A polymorphisms for cardiovascular events in atrial fibrillation. *Thromb Haemost.* 2014;112(4):781-788.

25. Arroyo AB, de los Reyes-García AM, Rivera-Caravaca JM, et al. MiR-146a regulates neutrophil extracellular trap formation that predicts adverse cardiovascular events in patients with atrial fibrillation. *Arterioscler Thromb Vasc Biol.* 2018;38(4):892-902.

26. del Monte A, Arroyo AB, Andrés-Manzano MJ, et al. miR-146a deficiency in hematopoietic cells is not involved in the development of atherosclerosis. *PLoS One.* 2018;13(6):e0198932.

27. Buckley CD, Ross EA, McGettrick HM, et al. Identification of a phenotypically and functionally distinct population of long-lived neutrophils in a model of reverse endothelial migration. *J Leukoc Biol.* 2006;79(2):303-311.

28. Hu N, Westra J, Rutgers A, et al. Decreased CXCR1 and CXCR2 expression on neutrophils in anti-neutrophil cytoplasmic autoantibody-associated vasculitides potentially increases neutrophil adhesion and impairs migration. *Arthritis Res Ther.* 2011;13(6):R201.

29. Xu R, Bao C, Huang H, et al. Low expression of CXCR1/2 on neutrophils predicts poor survival in patients with hepatitis B virus-related acute-on-chronic liver failure. *Sci Rep.* 2016;6:38714.

30. Zhang D, Chen G, Manwani D, et al. Neutrophil ageing is regulated by the microbiome. *Nature.* 2015;525(7570):528-532.

31. Wang J, Cui Z, Liu L, et al. MiR-146a mimics attenuates murine allergic rhinitis by down-regulating TLR4/TRAFF/NF- κ B pathway. *Immunotherapy.* 2019;11(13):1095-1105.

32. Stavrou EX, Fang C, Bane KL, et al. Factor XII and uPAR upregulate neutrophil functions to influence wound healing. *J Clin Invest.* 2018;128(3):944-959.

33. Hashiba M, Huq A, Tomino A, et al. Neutrophil extracellular traps in patients with sepsis. *J Surg Res.* 2015;194(1):248-254.

34. Hirose T, Hamaguchi S, Matsumoto N, et al. Presence of neutrophil extracellular traps and citrullinated histone H3 in the bloodstream of critically ill patients. *PLoS One.* 2014;9(11):e111755.

35. Bonaventura A, Montecucco F, Dallegri F, et al. Novel findings in neutrophil biology and their impact on cardiovascular disease. *Cardiovasc Res.* 2019;115(8):1266-1285.

36. Jiménez-Alcázar M, Kim N, Fuchs T. Circulating extracellular DNA: cause or consequence of thrombosis? *Semin Thromb Hemost.* 2017;43(06):553-561.

37. Khan MA, Palaniyar N. Transcriptional firing helps to drive NETosis. *Sci Rep.* 2017;7:41749.

38. Franck G, Mawson TL, Folco EJ, et al. Roles of PAD4 and NETosis in experimental atherosclerosis and arterial injury. *Circ Res.* 2018;123(1):33-42.

39. Massberg S, Grahl L, von Bruehl M-L, et al. Reciprocal coupling of coagulation and innate immunity via neutrophil serine proteases. *Nat Med.* 2010;16(8):887-896.

40. Knight JS, Luo W, O'Dell AA, et al. Peptidylarginine deiminase inhibition reduces vascular damage and modulates innate immune responses in murine models of atherosclerosis. *Circ Res.* 2014;114(6):947-956.

41. Liew PX, Kubes P. The neutrophil's role during health and disease. *Physiol Rev.* 2019;99(2):1223-1248.

42. Ebrahimi F, Giaglis S, Hahn S, et al. Markers of neutrophil extracellular traps predict adverse outcome in community-acquired pneumonia: secondary analysis of a randomised controlled trial. *Eur Respir J.* 2018;51(4):1701389.

43. Xie J, Zhang L, Fan X, Dong X, Zhang Z, Fan W. MicroRNA-146a improves sepsis-induced cardiomyopathy by regulating the TLR-4/NF- κ B signaling pathway. *Exp Ther Med.* 2019;18(1):779-785.

44. Gao M, Wang X, Zhang X, et al. Attenuation of cardiac dysfunction in polymicrobial sepsis by microRNA-146a is mediated via targeting of IRAK1 and TRAF6 expression. *J Immunol.* 2015;195(2):672-682.

45. Nakada T, Takahashi W, Nakada E, Shimada T, Russell JA, Walley KR. Genetic polymorphisms in sepsis and cardiovascular disease. *Chest.* 2019;155(6):1260-1271.

46. Montecucco F, Liberale L, Bonaventura A, Vecchiè A, Dallegri F, Carbone F. The role of inflammation in cardiovascular outcome. *Curr Atheroscler Rep.* 2017;19(3):11.

47. Ayoub KE, Pothineni NVK, Rutland J, Ding Z, Mehta JL. Immunity, inflammation, and oxidative stress in heart failure: emerging molecular targets. *Cardiovasc Drugs Ther.* 2017;31(5-6):593-608.

48. Uhl B, Vadlau Y, Zuchtrigel G, et al. Aged neutrophils contribute to the first line of defense in the acute inflammatory response. *Blood.* 2016;128(19):2327-2337.

49. Rosales C. Neutrophil: a cell with many roles in inflammation or several cell types? *Front Physiol.* 2018;9:113.

50. Ortmann W, Kolaczkowska E. Age is the work of art? Impact of neutrophil and organism age on neutrophil extracellular trap formation. *Cell Tissue Res.* 2018;371(3):473-488.

51. Davalli P, Mitic T, Caporali A, Lauriola A, D'Arca D. ROS, cell senescence, and novel molecular mechanisms in aging and age-related diseases. *Oxid Med Cell Longev.* 2016;2016:3565127.

52. Fuchs TA, Abed U, Goosmann C, et al. Novel cell death program leads to neutrophil extracellular traps. *J Cell Biol.* 2007;176(2):231-241.

Granulocyte colony-stimulating factor directly acts on mouse lymphoid-biased but not myeloid-biased hematopoietic stem cells

Miner Xie,¹ Shanshan Zhang,¹ Fang Dong,¹ Qingyun Zhang,¹ Jinhong Wang,¹ Chenchen Wang,¹ Caiying Zhu,¹ Sen Zhang,¹ Bingqing Luo,¹ Peng Wu¹ and Hideo Ema^{1,2,3}

¹State Key Laboratory of Experimental Hematology; ²National Clinical Research Center for Hematological Disorders and ³Department of Regenerative Medicine, Institute of Hematology and Blood Diseases Hospital, Chinese Academy of Medical Sciences and Peking Union Medical College, Tianjin, China



Ferrata Storti Foundation

Haematologica 2021
Volume 106(6):1647-1658

ABSTRACT

Granulocyte colony-stimulating factor (G-CSF) is widely used in clinical settings to mobilize hematopoietic stem cells (HSC) into the circulation for HSC harvesting and transplantation. However, whether G-CSF directly stimulates HSC to change their cell cycle state and fate is controversial. HSC are a heterogeneous population consisting of different types of HSC, such as myeloid-biased HSC and lymphoid-biased HSC. We hypothesized that G-CSF has different effects on different types of HSC. To verify this, we performed serum-free single-cell culture and competitive repopulation with cultured cells. Single highly purified HSC and hematopoietic progenitor cells (HPC) were cultured with stem cell factor (SCF), SCF + G-CSF, SCF + granulocyte/macrophage (GM)-CSF, or SCF + thrombopoietin (TPO) for 7 days. Compared with SCF alone, SCF + G-CSF increased the number of divisions of cells from the lymphoid-biased HSC-enriched population but not that of cells from the My-bi HSC-enriched population. SCF + G-CSF enhanced the level of reconstitution of lymphoid-biased HSC but not that of myeloid-biased HSC. Clonal transplantation assay also showed that SCF + G-CSF did not increase the frequency of myeloid-biased HSC. These data showed that G-CSF directly acted on lymphoid-biased HSC but not myeloid-biased HSC. Our study also revised the cytokine network at early stages of hematopoiesis: SCF directly acted on myeloid-biased HSC; TPO directly acted on myeloid-biased HSC and lymphoid-biased HSC; and GM-CSF acted only on HPC. Early hematopoiesis is controlled differentially and sequentially by a number of cytokines.

Introduction

Hematopoietic stem cells (HSC) are able to self-renew and differentiate into all blood lineages.¹ Granulocyte colony-stimulating factor (G-CSF) is widely used in clinical settings to mobilize HSC from the bone marrow (BM) to the peripheral blood (PB) for stem cell harvesting.² However, the effect of G-CSF on HSC is poorly understood. Several studies have reported that G-CSF drives dormant HSC into the cell cycle,³⁻⁵ whereas other studies have reported that G-CSF does not.^{6,7} Since *in vivo* G-CSF administration results in complex changes in the BM microenvironment, such as disruption of the SDF-1/CXCR4 axis,^{8,9} it may be difficult to determine the direct effect of G-CSF on HSC *in vivo*. To avoid this issue, Ogawa's research group combined *in vitro* culture with transplantation assay and reported that G-CSF can induce HSC self-renewal.¹⁰

The above studies are informative but quite controversial. This study aimed to clarify whether G-CSF acts directly on HSC and drives them into cycling, thus changing their fates. HSC are a heterogeneous population. Muller-Sieburg's research group was the first to classify HSC into myeloid-biased HSC (My-bi HSC), balanced HSC (Bala HSC), and lymphoid-biased HSC (Ly-bi HSC), based on the ratio of lymphoid to myeloid cells (the L/M ratio) in reconstituted mice.^{11,12} Given that G-CSF is a neutrophil-specific cytokine that is essential for granu-

Correspondence:

HIDEO EMA
hema@ihcams.ac.cn

Received: September 26, 2019.

Accepted: February 17, 2020.

Pre-published: February 20, 2020.

<https://doi.org/10.3324/haematol.2019.239251>

©2021 Ferrata Storti Foundation

Material published in *Haematologica* is covered by copyright. All rights are reserved to the Ferrata Storti Foundation. Use of published material is allowed under the following terms and conditions: <https://creativecommons.org/licenses/by-nc/4.0/legalcode>. Copies of published material are allowed for personal or internal use. Sharing published material for non-commercial purposes is subject to the following conditions: <https://creativecommons.org/licenses/by-nc/4.0/legalcode>, sect. 3. Reproducing and sharing published material for commercial purposes is not allowed without permission in writing from the publisher.



lopoiesis,^{13,14} we hypothesized that G-CSF acts directly on My-bi HSC but not on Ly-bi HSC.

To address this issue, we used a serum-free culture system, which enabled us to exclude the effect of unknown factors contaminated in the serum.¹⁵ To overcome the heterogeneity of HSC, we performed single-cell culture, single-cell transplantation, and single-cell reverse transcription-polymerase chain reaction (RT-PCR) on highly purified HSC and hematopoietic progenitor cells (HPC). Surprisingly, we found that G-CSF increased the number of divisions of Ly-bi HSC and maintained their repopulating activity after transplantation. SCF alone transiently activated My-bi HSC and increased their long-term reconstitution potential, but SCF + G-CSF did not show any additional effect on that potential. We conclude that G-CSF acts directly on Ly-bi HSC but not on My-bi HSC. This study suggested that My-bi HSC, which are more or less equivalent to long-term HSC, remain in the quiescent state after G-CSF injection in clinical settings.

Methods

Mice

C57BL/6 (CD45.2-B6) mice were purchased from Beijing HFK Bioscience Co. (Beijing, China). C57BL/6 mice congenic for the Ly5 locus (CD45.1-B6) were bred and maintained at the State Key Laboratory of Experimental Hematology. Animal experiments were approved by the Animal Care and Use Committees, Institute of Hematology and Blood Diseases Hospital, Chinese Academy of Medical Sciences and Peking Union Medical College.

Single-cell sorting

BM cells were isolated from 8- to 10-week old female CD45.1- or CD45.2-B6 mice, and c-Kit-positive cells were enriched using anti-c-Kit antibody-conjugated MACS beads (Miltenyi Biotechnology, catalog n. 130091224). Cell surface markers used for the identification of HSC1, HSC2, HPC1, HPC2, HPC3, and HPC4 are listed in *Online Supplementary Table S1*. Antibodies used for flow cytometry are listed in *Online Supplementary Table S2*.

Single-cell culture

Single cells were cultured in serum-free medium, supplemented with 50 ng/mL recombinant mouse SCF (Peprotech, 250-03) plus 50 ng/mL recombinant mouse thrombopoietin (TPO) (Peprotech, 315-14), 10 ng/mL recombinant human G-CSF (Peprotech, 300-23), or 10 ng/mL recombinant mouse GM-CSF (Peprotech, 315-03). Cells were cultured for 7 days at 37°C with 5% CO₂ in the air. Number of cells per well were counted daily under inverted microscope.

Serial competitive repopulation

Twenty HSC1 or HSC2 cells from CD45.1-B6 mice were cultured with cytokines for 7 days, and cells were transplanted into lethally irradiated CD45.2-B6 mice with 5×10⁵ BM competitor cells from CD45.2-B6 mice. As control, 20 freshly isolated HSC1 or HSC2 cells from CD45.1-B6 mice were similarly transplanted. For secondary transplantation of HSC1 cells, 2×10⁷ BM cells from primary recipients were transplanted into lethally irradiated CD45.2-B6 mice. PB cells were analyzed as previously described.¹⁶

Single-cell transplantation

Single HSC1 cells from CD45.1-B6 mice were cultured with SCF + TPO for 1 day, and the surviving single HSC1 cells were selected and transplanted into lethally irradiated CD45.2-B6 mice

with 5×10⁵ BM competitor cells from CD45.2-B6 mice (control). For the cultured cell group, single HSC1 cells were cultured with cytokines for 7 days, and cells of each well were transplanted into lethally irradiated CD45.2-B6 mice with 5×10⁵ BM competitor cells from CD45.2-B6 mice. PB cells were analyzed as previously described.¹⁶

Single-cell reverse transcription polymerase chain reaction

For single-cell RT-PCR, 48 single HSC1, HSC2, HPC1, HPC2, HPC3, and HPC4 cells were sorted into each well containing RT-STA master mix. For single-cell RT-PCR for cultured cells, single HSC1 cells were cultured with SCF, SCF+G-CSF, and SCF+TPO for 7 days. Single cells were randomly picked up from 48 wells by a micromanipulator and were placed into the RT-STA master mix. Freshly isolated 48 single HSC1 cells were used as a control. PCR was performed as previously described.¹⁶ The 48 genes set used for six populations and cultured cells are listed in *Online Supplementary Tables S3* and *S4*, respectively.

Statistical analysis

Statistical significance was assessed with the unpaired *t*-test and analysis of variance using GraphPad Prism 6.0 (GraphPad).

Results

Definitions of HSC1, HSC2, HPC1, HPC2, HPC3, and HPC4

HSC1 (CD201⁺CD150⁺CD48⁻CD41⁻CD34⁻KSL) and HSC2 (CD201⁺CD150⁺CD48⁻CD41⁻CD34⁻KSL) cells were defined as shown in Figure 1A. HSC1 were separated from HSC2 by expression of CD150.^{17,18} We previously showed that HSC1 cells are enriched in long-term (LT, >6 months) My-bi HSC (LT-My-bi HSC), while HSC2 cells are enriched in short-term (ST, <6 months) Ly-bi HSC (ST-Ly-bi HSC).^{16,18-21} HPC1 (CD201⁺CD150⁺CD48⁻CD41⁺CD34⁻KSL), HPC2 (CD150⁺Flt-3⁻CD34⁻KSL), HPC3 (CD150⁺Flt-3⁻CD34⁻KSL), and HPC4 (CD150⁺Flt-3⁺CD34⁻KSL) cells were defined as shown in Figure 1A and B. HPC1 cells are reportedly enriched in myeloid-restricted repopulating progenitors.¹⁹ HPC2, HPC3, and HPC4 cells were enriched in MPP2, MPP3, and MPP4/lymphoid-primed multipotent progenitor (LMPP), respectively (*Online Supplementary Figure S1*).

Cytokine receptor expression

Single-cell RT-PCR was performed on HSC1, HSC2, HPC1, HPC2, HPC3, and HPC4 cells to investigate the expression of cytokine receptors. Gene expression data are shown as heatmaps in *Online Supplementary Figure S2*. Figure 1C shows the percentage of gene-expressing cells. *c-Kit* and *Mpl* were detected in most cells examined. M-CSF receptor, *Csf1r*, was not expressed in >40% of cells in any of the populations examined. GM-CSF receptor comprises *Csf2ra* and *Csf2rb*. *Csf2ra* was not detected in >15% of cells in any of the populations examined. *Csf2rb* was also expressed in <15% of HSC1 cells, but was expressed in approximately from 40 to 60% of HSC2, HPC2, HPC3, and HPC4 cells, and in 100% of HPC1. G-CSF receptor, *Csf3r*, was detected in approximately 30% of HSC1 and HPC1 cells, while it was detected in >50% of HSC2 and HPC2, and >70% of HPC3 and HPC4 cells. *Cxcl12* was expressed in approximately from 20 to 40% of all populations. *Cxcr4* was expressed in approximately from 30 to

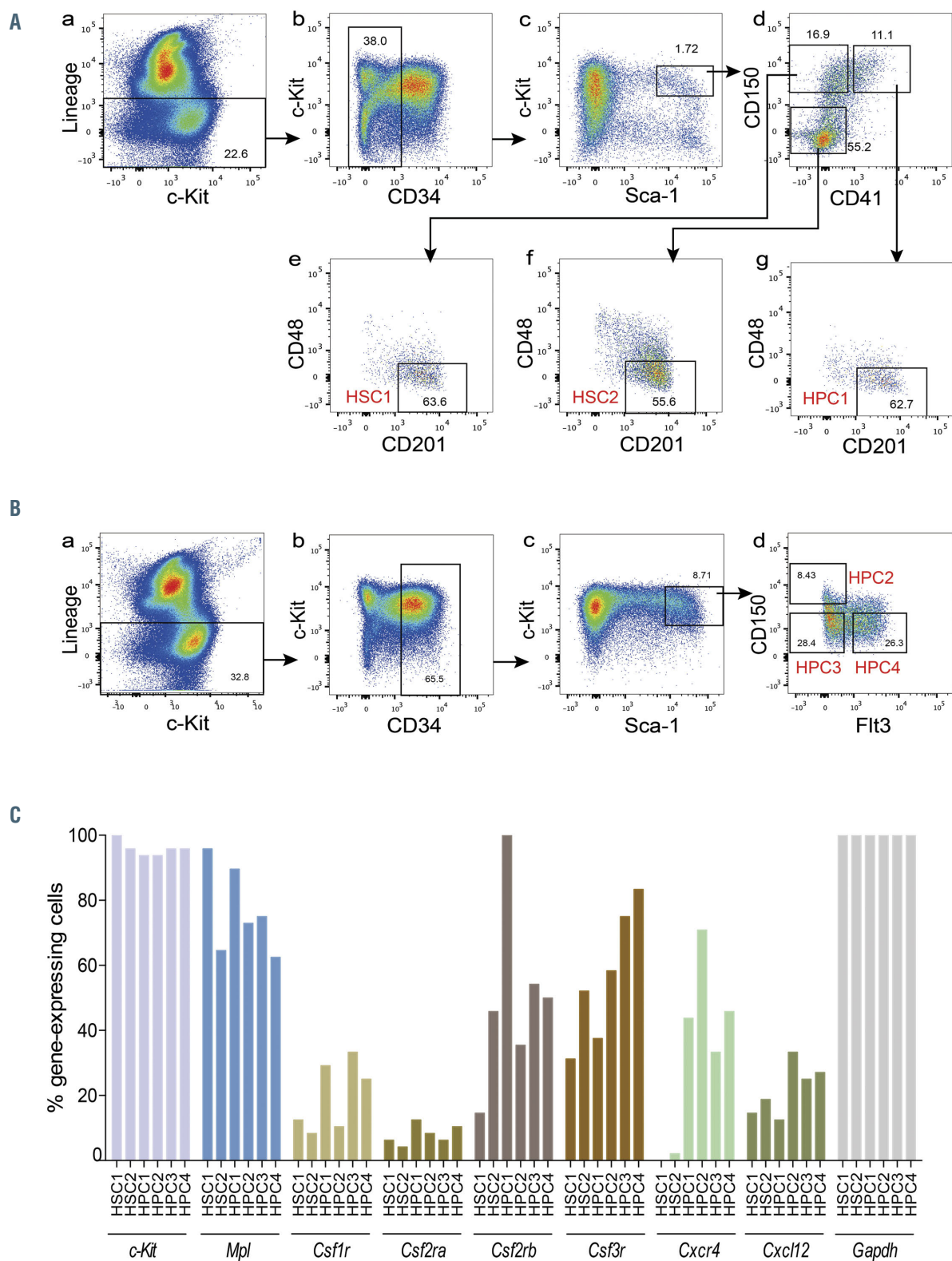


Figure 1. Gating strategy and single-cell real-time-polymerase chain reaction (RT-PCR) of HSC1, HSC2, HPC1, HPC2, HPC3, and HPC4 cells. (A) HSC1, HSC2, and HPC1 gating. Bone marrow (BM) cells were stained with antibodies and gated as follows. (a) Gating for lineage- cells (Lin- cells). (b) Gating for Lin-CD34+ cells. (c) Gating for CD34+ c-Kit+ Sca-1+ Lin- cells (CD34+ KSL cells). (d) Based on CD150 and CD41 expression, CD34+ KSL cells were divided into CD150+CD41+, CD150-CD41+, and CD150-CD41- cells. (e-g) CD201+CD48- cells were further selected from CD150+CD41+, CD150-CD41+, and CD150-CD41- cells. HSC1, HSC2, and HPC1 cells were defined as CD201+CD150+CD48- CD41+ CD34+ KSL cells, CD201+CD150+CD48+ CD41+ CD34+ KSL cells, and CD201+CD150+CD48+ CD41+ CD34+ KSL cells, respectively. (B) HPC2, HPC3, and HPC4 gating. BM cells were stained with antibodies and gated as follows. (a) Gating for lineage- cells (Lin- cells). (b) Gating for Lin-CD34+ cells. (c) Gating for CD34+ KSL cells. (d) CD34+ KSL cells were divided into CD150+Flt3+, CD150-Flt3+, and CD150-Flt3- cells. HPC2, HPC3 and HPC4 cells were defined as CD150+Flt3- CD34+ KSL cells, CD150-Flt3- CD34+ KSL cells, and CD150-Flt3+ CD34+ KSL cells, respectively. (C) Single-cell RT-PCR for six populations. The percentage of gene-expressing cells is shown. Gene-expressing cells are defined by a threshold cycle (Ct) value < 27.65.

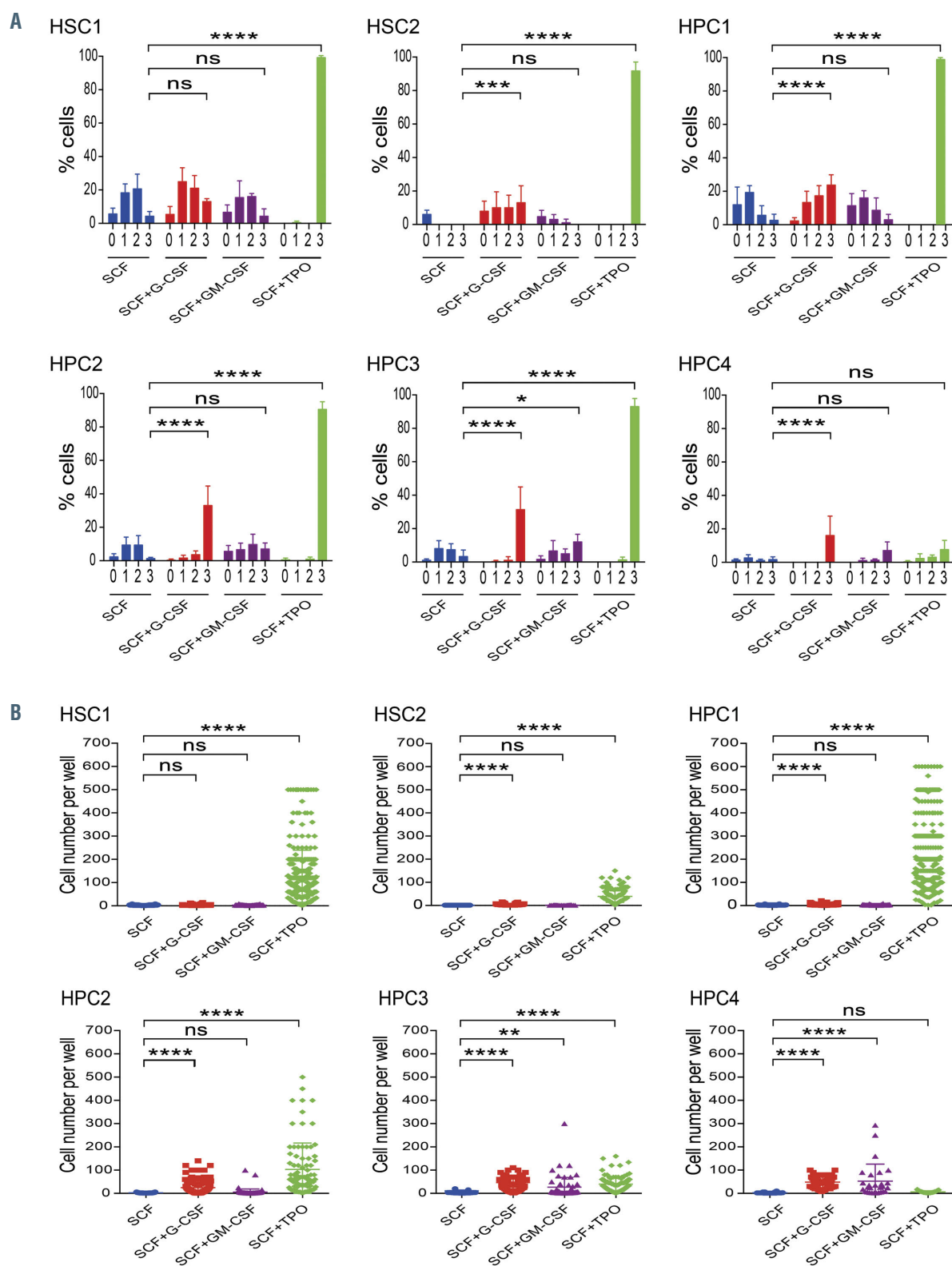


Figure 2. Single-cell culture of six populations. (A) Percentage of cells that underwent divisions is shown as mean±standard deviation (SD). (n=5). Number of cell division was estimated from the number of cells per well at days 1-7 of culture. When the number of cells per well was 1, 2, 3-4, or ≥5, single cells were considered to have undergone 0, 1, 2, or ≥3 division(s), respectively. Wells that had no cells were excluded from this analysis. Two-way ANOVA with Tukey's multiple comparisons test was used for statistical analysis. (B) Cell number per well at day 7 of culture is shown as mean±SD. (n=5). Unpaired t-test with Welch's correction was used for statistical analysis. *P<0.05; **P<0.01; ***P<0.001; and ****P<0.0001; ns: not significant.

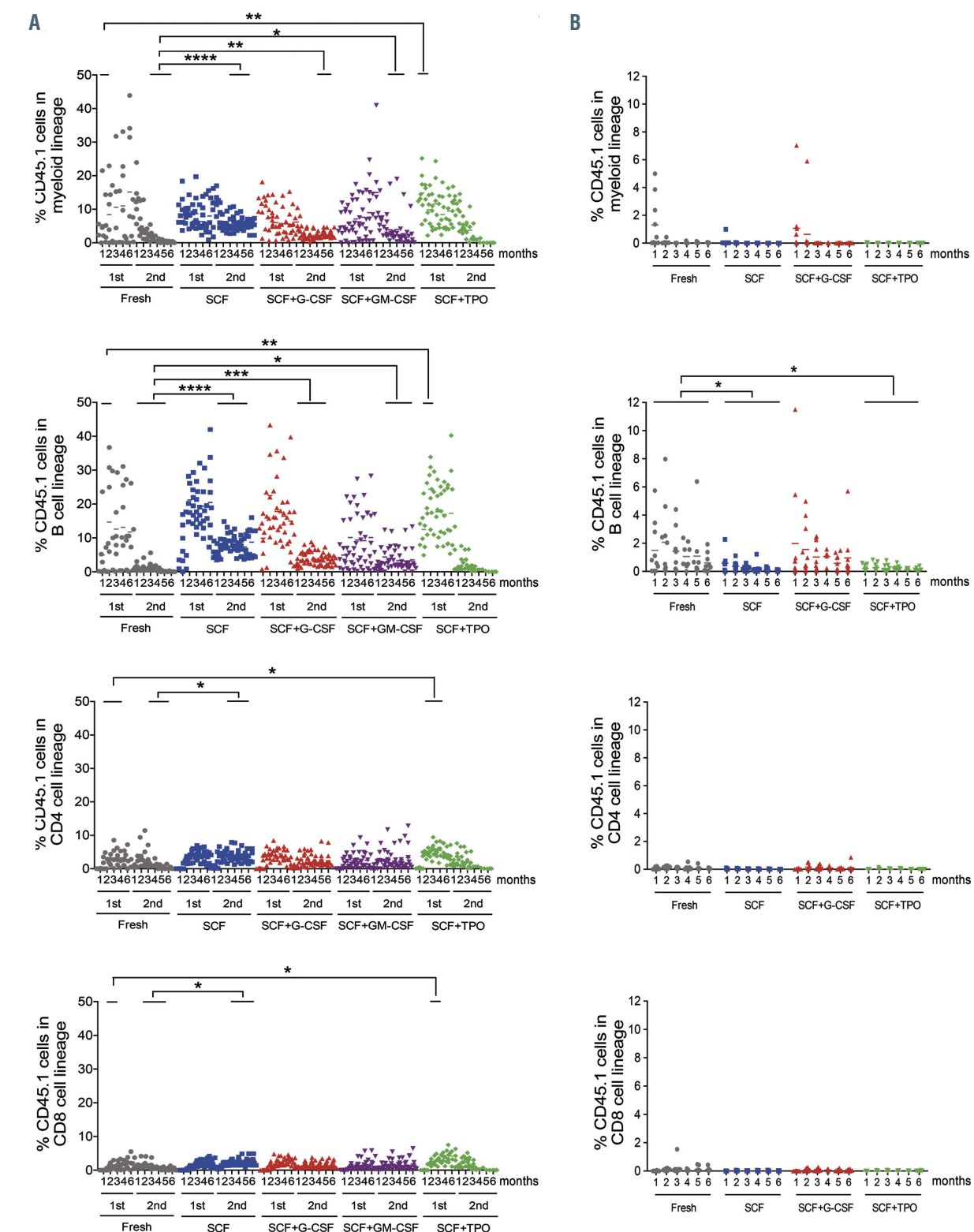


Figure 3. Repopulating activity of cultured HSC1 and HSC2 cells. (A) Percentages of CD45.1 cells derived from HSC1 cells are shown. Percentage of CD45.1 cells in the myeloid lineage, B-cell lineage, CD4 T-cell lineage, and CD8 T-cell lineage in the culture with stem cell factor (SCF) alone were greater than those of freshly isolated cells after secondary transplantation. Percentage of CD45.1 cells in the myeloid lineage and B-cell lineage in the culture with SCF + granulocyte colony-stimulating factor (G-CSF) or SCF + granulocyte/macrophage (GM-CSF) were greater than those of freshly isolated cells after secondary transplantation. Percentage of CD45.1 cells in the myeloid lineage, B-cell lineage, CD4 T-cell lineage, and CD8 T-cell lineage in the culture with SCF+ thrombopoietin (TPO) were greater than those of freshly isolated cells at early months after primary transplantation. (B) Percentages of CD45.1 cells derived from HSC2 cells are shown. Percentage of CD45.1 cells in the B-cell lineage of the culture with SCF or SCF + TPO was significantly smaller than that of freshly isolated cells. Dots represent % chimerism in myeloid lineage, B-cell lineage, CD4 T-cell lineage and CD8 T-cell lineage from individual mice at a time point after transplantation. The lines above dots indicate the time periods compared. The unpaired t-test with Welch's correction was used for statistical analysis between freshly isolated cells and cells in different culture conditions. *P<0.05; **P<0.01; ***P<0.001; ****P<0.0001.

50% of HPC1, 3, and 4 cells, and in 70% of HPC2 cells. Notably, *Cxcr4* was expressed in very few HSC1 and 2 cells.

Effect of granulocyte colony-stimulating factor and granulocyte/macrophage colony-stimulating factor on the division of single hematopoietic stem cells and hematopoietic progenitor cells

We next compared the effects of SCF alone, SCF + G-CSF, SCF + GM-CSF, and SCF + TPO on these six populations by single-cell culture. Figure 2A shows the percentage of cells that underwent divisions. Figure 2B shows the cell number per well at day 7 of culture. SCF supported the survival of a proportion of HSC1, HPC1, HPC2, and HPC3 cells, and induced their division 1-2 times. However, SCF alone did not support the survival of most HSC2 and HPC4 cells. SCF + G-CSF did not support division of HSC1 more than SCF alone. However, SCF + G-CSF significantly increased the number of divisions in HSC2, HPC1, HPC2, HPC3, and HPC4 cells, leading to a significant increase in the cell number per well. SCF + GM-CSF did not support the division of HSC1, HSC2, HPC1, and HPC2 cells but significantly increased the number of divisions of HPC3 and HPC4 cells, leading to an increase in the cell number per well. SCF + TPO significantly increased the number of divisions and cells per well in HSC1, HSC2, HPC1, HPC2, and HPC3 cells, but not in HPC4 cells. These data suggested that the target cells of G-CSF, GM-CSF, SCF, and TPO were different among HSC and HPC: SCF acted directly on HSC1, HPC1, HPC2, and HPC3 cells, but not on HSC2 and HPC4 cells. TPO acted on HSC1, HSC2, HPC1, HPC2, and HPC3 cells, but not on HPC4 cells. G-CSF acted directly on HSC2 and HPC1-4 cells, but not on HSC1 cells. GM-CSF acted directly on HPC3 and HPC4 cells.

Effect of granulocyte colony-stimulating factor on reconstitution potential

To examine the effect of the cytokines on the reconstitution potential in HSC1 and HSC2 cells, we performed competitive repopulation assay. Figure 3A shows the percentage of CD45.1 cells in the myeloid, B-cell, CD4 T-cell, and CD8 T-cell lineages after transplantation with HSC1 cells. Compared with freshly isolated cells, the levels of reconstitution of each lineage in the SCF culture were significantly increased after secondary transplantation. The levels of myeloid and B-cell lineages in SCF + G-CSF or SCF + GM-CSF cultures were also significantly increased after secondary transplantation. However, when we compared the reconstitution levels among cultured cells, there was no significant difference between SCF + G-CSF or GM-CSF and SCF cultures, suggesting that SCF, but neither G-CSF nor GM-CSF, increased the long-term reconstitution potential in HSC1 cells. The levels of reconstitution of each lineage in SCF + TPO culture were significantly increased in the early months after primary transplantation, suggesting that this combination of cytokines increased the short-term reconstitution potential in HSC1 cells.

Figure 3B shows the percentage of CD45.1 cells in myeloid, B-cell, CD4 T-cell and CD8 T-cell lineages after transplantation with HSC2 cells. Freshly isolated HSC2 cells showed B-lymphoid-biased reconstitution. The level of B-cell lineage reconstitution in SCF and SCF + TPO cultures was significantly lower than that in freshly isolated

cells, whereas that in SCF + G-CSF culture was comparable with that in freshly isolated cells. Taken together, these data suggested that SCF alone was sufficient to increase the long-term multilineage reconstitution potential. SCF + TPO increased the short-term multilineage reconstitution potential. SCF + G-CSF did not enhance the long-term myeloid lineage reconstitution potential but maintained the short-term lymphoid reconstitution potential.

Transplantation of clonally cultured cells

To further clarify the effect of G-CSF on HSC, we performed clonal transplantation assay. Eleven mice in the control group, 10 mice in the SCF group, 12 mice in the SCF + G-CSF group, and 4 mice in the SCF + TPO group were reconstituted (Figure 4). The percentage of chimerism and its lineage composition in single HSC1 cells varied from one another as reported.^{16,21} Similar to freshly isolated HSC1 cells, after one day culture single HSC1 cells showed a varying degree of reconstitution, indicating the heterogeneity of HSC.

We used the published criteria of My-bi, Bala, and Ly-bi HSC,^{11,12} and LT- and ST-HSC.²² In the control group of mice, 6 LT-My-bi HSC, 2 ST-Ly-bi HSC, and 3 HPC were detected (Figure 4A and *Online Supplementary Table S5*). After culture with SCF for 7 days, 1 LT-My-bi HSC, 1 ST-Bala HSC, 4 ST-Ly-bi HSC, and 4 HPC were detected (Figure 4B and *Online Supplementary Table S6*). After culture with SCF + G-CSF, 2 LT-My-bi HSC, 1 ST-Ly-bi HSC, 5 ST-Ly-bi HSC, and 4 HPC were detected (Figure 4C and *Online Supplementary Table S7*). After culture with SCF + TPO, 3 ST-Ly-bi HSC and 1 HPC were detected (Figure 4D and *Online Supplementary Table S8*). These data showed no difference in reconstitution potential between SCF and SCF + G-CSF cultures, but the significant reduction in reconstitution potential after culture with SCF + TPO.

To be more precise, LT-My-bi HSC activity was detected in the mouse transplanted with three cells from SCF culture (#1 mouse), and similarly, in the mice transplanted with three cells from SCF + G-CSF culture (#1 and #2 mice) (Figure 4B and C and *Online Supplementary Tables S6* and *S7*). ST-Ly-bi but not LT-My-bi HSC activity was detected in mice transplanted with >50 cells from SCF + TPO culture (#1, 2, and 3 mice) (Figure 4D and *Online Supplementary Tables S8*). These data suggested the similar effects of SCF and SCF + G-CSF on LT-My-bi HSC and the differentiation effect of SCF + TPO, associated with a number of divisions, on LT-My-bi HSC.

Gene expression of cultured cells

We examined the expression of cytokine receptors in day 7 cultured cells by single-cell RT-PCR. Gene expression data are shown as heatmaps in *Online Supplementary Figure S3*. Figure 5A depicts the gene expression in individual cells. Figure 5B depicts the relative expression level of genes. Consistent with the data in Figure 1C, both *c-Kit* and *Mpl* were expressed in the majority of freshly isolated HSC1 cells, while *Csf3r* was expressed in approximately 30% of the cells. After culture with SCF, the percentage of *c-Kit*- and *Mpl*-expressing cells slightly decreased but their relative expression levels significantly increased. However, neither the percentage of *Csf3r*-expressing cells nor the relative expression level of *Csf3r* changed. Interestingly, the percentage of *Csf3r*-expressing cells increased after culture with SCF + G-CSF or TPO. The rel-

ative expression level of *Csf3r* also increased after culture with SCF + TPO but not with SCF + G-CSF. Suppressor of cytokine signaling (SOCS) family are physiological regulators of several cytokine signaling.²³ Less than 50% of HSC1 expressed SOCS3 while most HSC1 expressed SOCS 2-6, approximately 30% of HSC1 expressed SOCS1, and <30% of HSC1 expressed SOCS7. Interestingly, the expression of SOCS3, but not the other SOCS, increased after culture with SCF + G-CSF or TPO (Online Supplementary Figure S4A and B) suggesting a positive correlation between *Csf3r* and SOCS3 expression in HSC. Members of early growth response gene (Egr) family, *Egr2* and *Egr3*, can directly induce SOCS3 expression.²⁴ *Egr3*, but neither *Egr1* nor *Egr2*, was detected in most cells (Online Supplementary Figure S4A and B). A very small number of freshly isolated HSC1 cells expressed *Cxcr4*, and the percentage of *Cxcr4*-expressing cells did not increase after culture with SCF, SCF + G-CSF, and SCF + TPO. These

data suggested that these cytokines cannot directly upregulate the expression of *Cxcr4*.

In culture with SCF or SCF + G-CSF, most HSC1 cells divided only 1-2 times and then stopped dividing. However, the multilineage reconstitution potential was maintained in these cells. To address the question of whether these cells returned to the quiescent state, we examined their cell cycle status by single-cell RT-PCR. *Mki-67* antigen is a nuclear protein exclusively expressed in proliferating cells during all phases of the cell cycle except G0.²⁵ *Mki67* was expressed in a small number of freshly isolated HSC1 cells. After culture, *Mki67* was expressed in approximately 50%, approximately 60%, and >95% of cells cultured with SCF, SCF + G-CSF, and SCF + TPO, respectively, and its relative expression level was also significantly increased. Both percentage of positive cells and relative expression level expressions for *Ccne1* and *Ccne2* increased in *Mki67*⁺ cultured cells. These

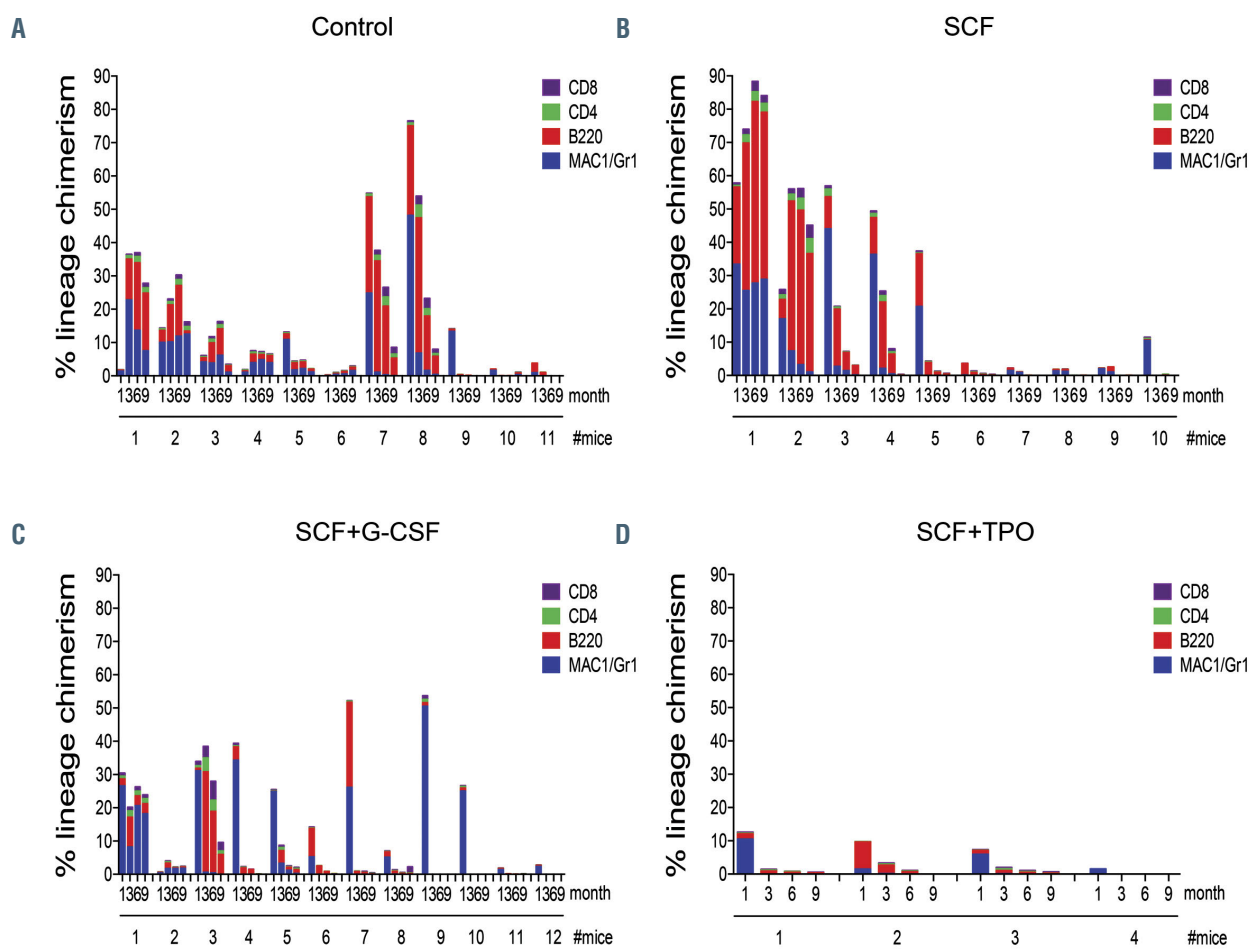


Figure 4. Transplantation of clonally cultured cells. (A) Lineage chimerism of single HSC1 cells. (B) Lineage chimerism of single-cell-derived cells in culture with stem cell factor (SCF). (C) Lineage chimerism of single-cell-derived cells in culture with SCF + granulocyte colony-stimulating factor (G-CSF). (D) Lineage chimerism of single-cell-derived cells in culture with SCF+ thrombopoietin (TPO). The percentage of the total chimerism was calculated as % (CD45.1⁺ cells) x 100% / (CD45.1⁺ cells + CD45.2⁺ cells). The percentage of myeloid lineage chimerism was calculated as (% CD45.1⁺ cells) x (Mac-1/Gr-1⁺ cells) / (Mac-1/Gr-1⁺ cells + B220⁺ cells + CD4⁺ cells + CD8⁺ cells), in which (Mac-1/Gr-1⁺ cells)/(Mac-1/Gr-1⁺ cells + B220⁺ cells + CD4⁺ cells + CD8⁺ cells) was derived from CD45.1⁺ cells. The percentage of B-cell lineage chimerism was calculated as (% CD45.1⁺ cells) x (B220⁺ cells)/(Mac-1/Gr-1⁺ cells + B220⁺ cells + CD4⁺ cells + CD8⁺ cells). The percentage of CD4 T-cell lineage chimerism was calculated as (% CD45.1⁺ cells) x (CD4⁺ cells)/(Mac-1/Gr-1⁺ cells + B220⁺ cells + CD4⁺ cells + CD8⁺ cells). The percentage of CD8 T-cell lineage chimerism was calculated as (% CD45.1⁺ cells) x (CD8⁺ cells)/(Mac-1/Gr-1⁺ cells + B220⁺ cells + CD4⁺ cells + CD8⁺ cells). Mice were considered to be reconstituted with donor cells when the percentage of donor-derived cells was ≥2.0%. My-bi, Bala, and Ly-bi hematopoietic stem cells (HSC) were defined by the ratio of lymphocytes to myeloid cells (L/M ratio) in the peripheral blood 6 months after transplantation. My-bi HSC were defined by the L/M ratio <3, Ly-bi HSC were defined by the L/M ratio >10, and Bala HSC were defined by 3 < L/M < 10. Long-term (LT)-HSC were defined when the percentage of myeloid cells maintained or increased by 6 months after transplantation. Short-term (ST)-HSC were defined when the percentage of myeloid cells decreased by 6 months, with myeloid, B-lymphoid, and T-lymphoid lineage reconstitution at a time after transplantation. HPC were defined when one or two lineages lacked from the definition of ST-HSC.

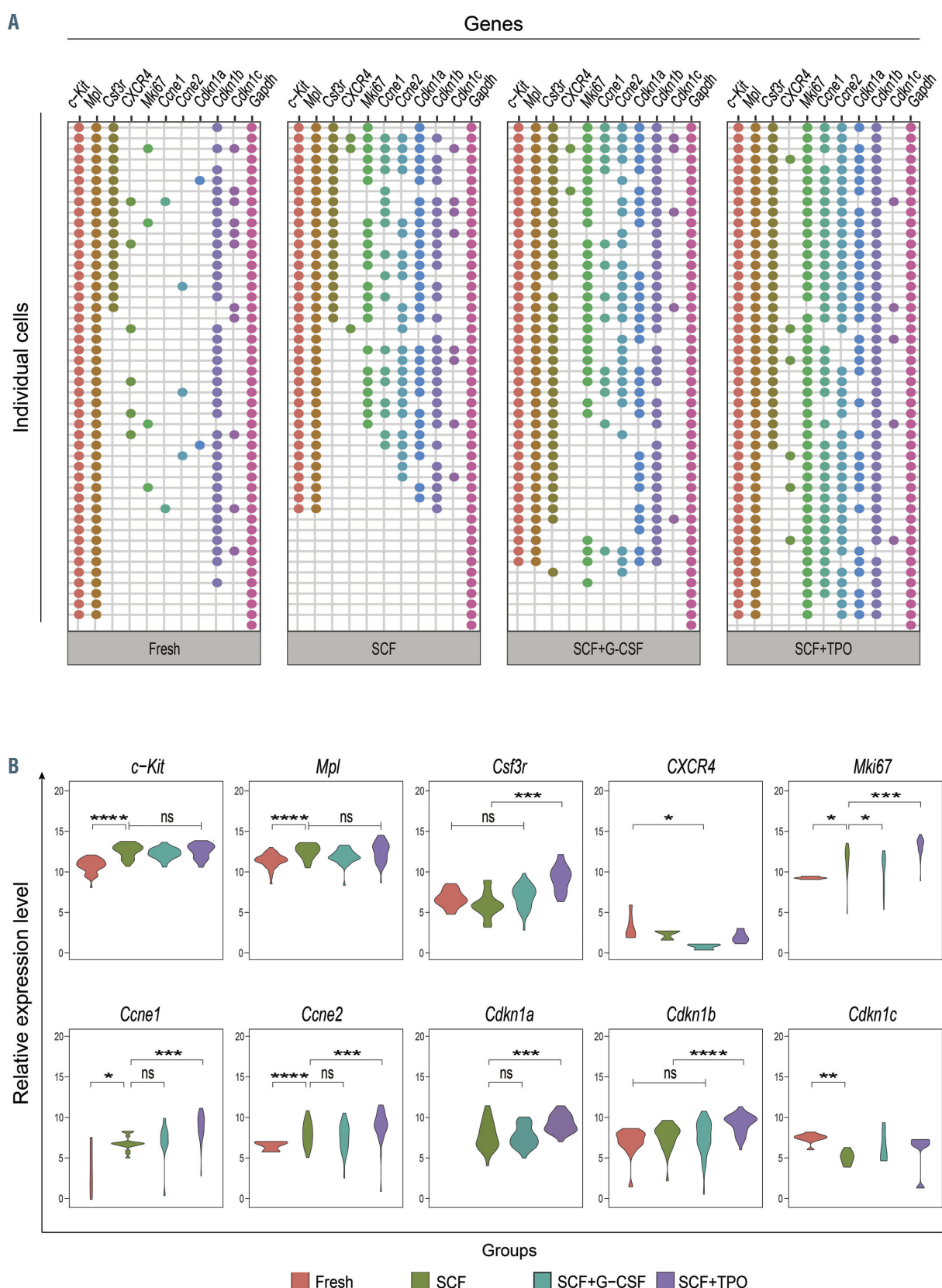


Figure 5. Single-cell real-time-polymerase chain reaction (RT-PCR) of cultured HSC1 cells. (A) Gene expression in a single cell. One column represents one gene, and a row represents a single cell. Gene-expressing cells are shown as dots, which are defined by the threshold cycle (Ct) value < 27.65 . (B) Violin density plots show the relative gene expression levels of gene-expressing cells. The relative expression level is defined as the $(27.65 - \text{Ct})$ values. Statistical significance was analyzed by ANOVA with Tukey's multiple comparisons test. * $P < 0.05$; ** $P < 0.01$; *** $P < 0.001$; **** $P < 0.0001$; ns: not significant.

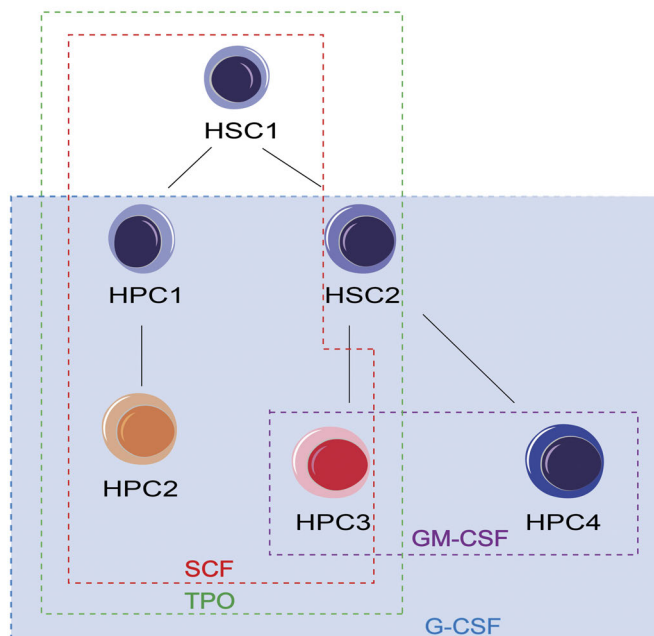


Figure 6. Cytokine network at the early stage of hematopoiesis. The model shows the cytokine network among HSC1, HSC2, HPC1, HPC2, HPC3, and HPC4. HSC1 cells respond to stem cell factor (SCF) and thrombopoietin (TPO). HSC2 cells respond to TPO and granulocyte colony-stimulating factor (G-CSF). HPC1 and HPC2 cells respond to SCF, TPO, and G-CSF. HPC3 cells respond to SCF, TPO, G-CSF, and GM-CSF. HPC4 cells respond to G-CSF and GM-CSF.

data suggested that HSC1 cells were quiescent in the steady state. After culture, most cells were continuously cycling in SCF + TPO, while approximately half of the cells were cycling in SCF or SCF + G-CSF.

Cell cycle progression is regulated by *Cdkn1a* (p21), *Cdkn1b* (p27), and *Cdk1c* (p57).²⁶ p21 was not expressed in the majority of freshly isolated *Mki67*⁻ cells (Figure 5) but p21 was expressed in most *Mki67*⁺ cells after culture; in particular, in SCF + TPO, its relative expression level was significantly increased. Interestingly, p27 was expressed in most freshly isolated *Mki67*⁻ cells as well as most *Mki67*⁺ cells after culture. p57 was expressed in some of freshly isolated *Mki67*⁻ cells, and also in some *Mki67*⁺ cells after culture; however, its relative expression level was decreased after culture. These data suggested that p21 was expressed in cycling cells while p57 was expressed in some quiescent cells. p27 was expressed in both quiescent cells and cycling cells.

Discussion

Functionally distinct HSC have been classified into My-bi, Bala, and Ly-bi HSC; α , β , and γ cells; or ST- and LT-HSC by different criteria. However, these classified cells overlap one another.²² Particularly, My-bi HSC overlap LT-HSC, and Ly-bi HSC overlap ST-HSC. In this study, by definition, we detected LT-My-bi HSC and ST-Ly-bi HSC at the single-cell level. We used HSC1 and HSC2 cells as highly purified HSC. HSC1 cells are significantly enriched in LT-My-bi HSC, while HSC2 cells are significantly enriched in ST-Ly-bi HSC.^{16,18-21} As shown in clonal transplantation, however, a small proportion of HSC1 contained ST-Ly-bi HSC (Figure 4A). Therefore, ST-Ly-bi HSC co-existed with LT-My-bi HSC in HSC1. We used HPC1, HPC2, HPC3, and HPC4 as highly purified HPC. We have recently shown that LT-HSC can be similarly detected in HSC1 and HPC1 cells.²¹ However, this study showed that *Csf2rb* expression in HPC1 was significantly greater than in HSC1 (Figure 1C), and HPC1 but not HSC1 cells responded to G-CSF in single-cell culture (Figure 2A).

HSC1 and HPC1 as populations remained functionally distinct.

Hematopoietic cytokines play a critical role in the regulation of hematopoiesis. In this study, we examined the effects of SCF, TPO, G-CSF, and GM-CSF on HSC1, HSC2, HPC1, HPC2, HPC3, and HPC4. SCF/c-Kit signaling plays an important role in hematopoiesis, particularly in the interaction of HSC and their niche, as shown by studies of W and Steel mutant mice.^{27,28} It has recently been reported that SCF is a niche factor from endothelial cells and perivascular stromal cells to maintain HSC.²⁹ Li and Johnson were the first to report that SCF is a survival factor of HSC in culture. We now confirmed their finding by transplantation assays (Figures 3 and 4). SCF alone was sufficient to support the survival of LT-HSC. Clonal transplantation assay showed that LT-HSC activity was detected in progeny from single LT-HSC. Therefore, self-renewal division took place in SCF culture (Figure 4B and *Online Supplementary Table S6*). Interestingly, HSC stopped dividing after 1-2 times in SCF culture (Figure 2). Single-cell RT-PCR suggested that some cells may be non-cycling, based on the expression of *Mki67* (Figure 5). The role of p57 in regulating HSC quiescence has been suggested.^{30,31} However, we showed that p57 was not upregulated in *Mki67*⁻ cells by SCF. p21 was expressed in the continuously cycling cells in *Mki67*⁺ cells from SCF + TPO culture, but not *Mki67*⁻ cells from freshly isolated cells. p21 expression was upregulated in *Mki67*⁺ cells after SCF culture, compared to *Mki67*⁻ cells from freshly isolated cells (Figure 5). These 'stop-dividing' cells may differ from the quiescent state *in vivo* at the molecular level. It would be interesting to see the functional difference between G0 and pseudo-G0 HSC.

Mpl was the second highly expressed receptor in HSC and HPC (Figure 1C). SCF and TPO synergistically acted on HSC1, HSC2, HPC1, HPC2, and HPC3, but they did not exert much action on HPC4 because the percentage of division and colony sizes in HPC4 were significantly smaller than those in the others (Figure 2B). Consistent with our data, it has been reported that deletion of TPO did not affect the number of CD34⁺FLT3⁺KSL cells but sig-

nificantly reduced that of CD34⁺/FLT3⁻ KSL cells.³² It also has been reported that deletion of TPO or Mpl results in the increase of cycling of HSC and subsequent reduction of the pool of quiescent HSC in mice.^{32,33}

TPO in synergy with SCF promoted rapid division of HSC *in vitro* (Figures 2 and 5). SCF + TPO transiently increased the level of ST reconstitution but this was substantially decreased in LT reconstitution (Figures 3A, 4D, and *Online Supplementary Table S8*). In this study, SCF + TPO supported the differentiation more than self-renewal in HSC. However, HSC may behave differently, depending on different culture conditions as recently reported.³⁴ It has also been recently reported that a low concentration of SCF and TPO can maintain HSC quiescent HSC *in vitro*.³⁵ TPO may have different roles in the regulation of HSC under different conditions.

About 30% of HSC1 expressed Csf3r, but either G-CSF alone or G-CSF + SCF did not induce their division at all (Figure 2A and *data not shown*). SCF + G-CSF did not increase LT reconstitution level more than did SCF alone (Figures 3A, 4B and C, and *Online Supplementary Tables S6 and S7*). *Csf3r* expression was upregulated in SCF + G-CSF culture (Figure 5). The percentage of SOCS3⁺ cells increased in *Csf3r*⁺ cells after SCF + G-CSF culture (*Online Supplementary Figure S4A*). SOCS3 may play a negative role in G-CSF signaling in LT-HSC as reported for G-CSF-driven granulopoiesis.^{36,37} As a result, most *Csf3r*⁺ LT-HSCs do not respond to G-CSF. Only approximately 10% of *Csf3r*⁺ cells responded to G-CSF and continuously divided more than three times and differentiated (Figure 2A), presumably escaping from the negative regulation by SOCS3. SCF + G-CSF maintained the reconstitution potential of HSC2 *in vitro* (Figure 3B), supporting a previous study demonstrating that SCF + G-CSF maintains B-lymphoid potential in culture.³⁸ Taken together, these data suggested that c-Kit and G-CSFR signaling in ST Ly-bi HSC is regulated differently from that in LT My-bi HSC.

Previously, HSC were stained with carboxyfluorescein diacetate succinimidyl ester (CFSE), their division was followed by CFSE intensity, and the function of CFSE-labeled HSC was examined through serial transplantation. This *in vivo* HSC division tracking study reported that G-CSF did not induce self-renewing division of HSC.⁶ Similarly, the other group, using H2B-GFP label retaining system, also reported that G-CSF did not stimulate LT-HSC.⁷ Supporting these studies, this study showed that G-CSF did not directly act on LT-My-bi HSC *in vitro*.

Our conclusions of the G-CSF effect may contradict previous studies.^{3-5,10} The levels of previous HSC purifications were not as high as ours, as they contained a mix of LT-My-bi HSC, ST-Ly-bi HSC, and HPC; serum was used in culture; some experiments lacked an appropriate control; the follow-up period after transplantation was not long enough to distinguish ST-Ly-bi HSC from LT-My-bi HSC by our definition; and experimental conditions differed. These differences may account for the discrepancies.

GM-CSF receptor is composed of two subunits, α and β . The α subunit binds GM-CSF with low affinity, while β subunit has no binding capacity by itself but forms a high affinity receptor with α subunit and plays a role in signal transduction.^{39,40} Our data showed that most HSC and HPC populations did not express *Csf2ra*, but most HPC1 and half of HSC2, HPC3, and HPC4 expressed *Csf2rb*. Only HPC2, HPC3 and HPC4 responded to GM-CSF. These data showed that target cells of GM-CSF differ

from those of G-CSF, and particular progenitors can receive signals from both G-CSF and GM-CSF.

Cxcl12 is also considered to be a niche factor synthesized by bone marrow stromal cells.^{9,41,42} Deletion of Cxcl12 from the BM, or its receptor, Cxcr4, from hematopoietic cells reduced HSC in the BM, indicating their roles in HSC retention.^{9,41-43} In agreement with this, successful mobilization of HSC and HPC from BM into the circulation has been achieved by the use of G-CSF or Cxcr4 antagonists through the disruption of the Cxcr4/Cxcl12 interaction.^{44,45} In this study, however, we detected little expression of *Cxcr4* in HSC (Figure 1C) even after stimulation with SCF, SCF + G-CSF, and SCF + TPO for 7 days (Figure 5). At least some HSC may not express Cxcr4 and be mobilized via Cxcr4-independent mechanism. As Cxcr7 has been reported as a new candidate receptor for Cxcl12.⁴⁶ Nevertheless, more precise mechanisms of HSC mobilization by G-CSF should be clarified.

Hematopoiesis is a blood formation process depicted as a hierarchy with self-renewing HSC ranking at the apex. In our model (Figure 6), HSC1 cells resides at the top rank, HSC2 and HPC1 cells reside at the second rank, and HPC2, HPC3, and HPC4 cells reside at the third rank. SCF, G-CSF, GM-CSF, and TPO act on different cell types, supporting the concept that cytokines exhibit multiple functions affecting cells at different developmental stages.⁴⁷ In addition, based on the cytokine responses, two major differentiation pathways from LT-HSCs are suggested: (1) the HSC1-HPC1-HPC2 pathway represents the myeloid differentiation pathway;¹⁹ and (2) the HSC1-HSC2-HPC3/4 pathway represents the lymphoid differentiation pathway. LT-HSC differentiated into either ST-HSC or myeloid progenitors like common myeloid progenitors. ST-HSC further give rise to LMPP which lose the response to SCF and TPO (Figure 2B), consistent with the decreased self-renewal ability and megakaryocyte potential in LMPP.⁴⁸ G-CSF is involved in both the myeloid and lymphoid differentiation pathways, regulating the proliferation of myeloid progenitors while maintaining Ly-bi HSC. In this regard, G-CSF works as a multipotent factor in hematopoiesis. Collectively, this cytokine network model indicates that different cytokines play a role in different differentiation pathways.

This study showed that LT-My-bi HSC do not respond to G-CSF, suggesting that HSC in healthy donors are protected from the proliferation and sequential exhaustion after G-CSF administration. G-CSF enhanced the efficacy of chemotherapy for eliminating leukemia stem cells without affecting the survival of normal HSC in the mouse acute myeloid leukemia (AML) model.⁴⁹ A large randomized clinical trial of G-CSF in AML patients showed that priming AML cells with G-CSF reduced the rate of relapse and improved disease-free survival without affecting hematologic recovery.⁵⁰ These studies together with our own suggested that normal HSC are protected from the cytotoxic effect of chemotherapy when G-CSF is injected before chemotherapy.

Disclosures

No conflicts of interest to disclose.

Contributions

MX performed the experiments, acquired and analyzed data, and wrote the manuscript; SZ helped with the transplantation

experiments; FD and QZ helped with the single-cell RT-PCR experiments; JW helped with the FACS operation; CW, CZ and PW helped with the PCR data analysis; SZ and BL helped with the culture experiments; HE designed and supervised the project and edited the manuscript.

Funding

This work was supported by grants from the National Key

Research and Development Program of China Stem Cell and Translational Research (2016YFA0100600, 2017YFA0104900, and 2019YFA0110203), CAMS Initiative for Innovative Medicine (CAMS-I2M) (2016-I2M-1-017 and 2017-I2M-1-015), CAMS Fundamental Research Funds for Central Research Institutes (2019PT320017), and the National Natural Science Foundation of China (81670105, 81970119, 81670106, 81421002).

References

- Till JE, McCulloch EA, Siminovitch L. A stochastic model of stem cell proliferation, based on the growth of spleen colony-forming cells. *Proc Natl Acad Sci U S A*. 1964; 51:29-36.
- Bensinger W, Singer J, Appelbaum F, et al. Autologous transplantation with peripheral blood mononuclear cells collected after administration of recombinant granulocyte stimulating factor. *Blood*. 1993;81(11):3158-3163.
- Morrison SJ, Wright DE, Weissman IL. Cyclophosphamide/granulocyte colony-stimulating factor induces hematopoietic stem cells to proliferate prior to mobilization. *Proc Natl Acad Sci U S A*. 1997; 94(5):1908-1913.
- Wright DE, Cheshier SH, Wagers AJ, Randall TD, Christensen JL, Weissman IL. Cyclophosphamide/granulocyte colony-stimulating factor causes selective mobilization of bone marrow hematopoietic stem cells into the blood after M phase of the cell cycle. *Blood*. 2001;97(8):2278-2285.
- Wilson A, Laurenti E, Oser G, et al. Hematopoietic stem cells reversibly switch from dormancy to self-renewal during homeostasis and repair. *Cell*. 2008;135(6): 1118-1129.
- Kovtonyuk LV, Manz MG, Takizawa H. Enhanced thrombopoietin but not G-CSF receptor stimulation induces self-renewing hematopoietic stem cell divisions in vivo. *Blood*. 2016;127(25):3175-3179.
- Bernitz JM, Daniel MG, Fstkhyan YS, Moore K. Granulocyte colony-stimulating factor mobilizes dormant hematopoietic stem cells without proliferation in mice. *Blood*. 2017;129(14):1901-1912.
- Pettit I, Szyper-Kravitz M, Nagler A, et al. G-CSF induces stem cell mobilization by decreasing bone marrow SDF-1 and up-regulating CXCR4. *Nat Immunol*. 2002; 3(7):687-694.
- Sugiyama T, Kohara H, Noda M, Nagasawa T. Maintenance of the hematopoietic stem cell pool by CXCL12-CXCR4 chemokine signaling in bone marrow stromal cell niches. *Immunity*. 2006;25(6):977-988.
- Abe T, Masuya M, Ogawa M. An efficient method for single hematopoietic stem cell engraftment in mice based on cell-cycle dormancy of hematopoietic stem cells. *Exp Hematol*. 2010;38(7):603-608.
- Muller-Sieburg CE, Cho RH, Karlsson L, Huang JF, Sieburg HB. Myeloid-biased hematopoietic stem cells have extensive self-renewal capacity but generate diminished lymphoid progeny with impaired IL-7 responsiveness. *Blood*. 2004;103(11):4111-4118.
- Muller-Sieburg CE, Cho RH, Thoman M, Adkins B, Sieburg HB. Deterministic regulation of hematopoietic stem cell self-renewal and differentiation. *Blood*. 2002;100(4): 1302-1309.
- Lieschke GJ, Grail D, Hodgson G, et al. Mice lacking granulocyte colony-stimulating factor have chronic neutropenia, granulocyte and macrophage progenitor cell deficiency, and impaired neutrophil mobilization. *Blood*. 1994;84(6):1737-1746.
- Cohen AM, Zsebo KM, Inoue H, et al. In vivo stimulation of granulopoiesis by recombinant human granulocyte colony-stimulating factor. *Proc Natl Acad Sci U S A*. 1987;84(8):2484-2488.
- Ieyasu A, Ishida R, Kimura T, et al. An all-recombinant protein-based culture system specifically identifies hematopoietic stem cell maintenance factors. *Stem Cell Reports*. 2017;8(3):500-508.
- Wang X, Dong F, Zhang S, et al. TGF-beta1 negatively regulates the number and function of hematopoietic stem cells. *Stem Cell Reports*. 2018;11(1):274-287.
- Kent DG, Copley MR, Benz C, et al. Prospective isolation and molecular characterization of hematopoietic stem cells with durable self-renewal potential. *Blood*. 2009; 13(25):6342-6350.
- Morita Y, Ema H, Nakauchi H. Heterogeneity and hierarchy within the most primitive hematopoietic stem cell compartment. *J Exp Med*. 2010;207(6):1173-1182.
- Yamamoto R, Morita Y, Oohara J, et al. Clonal analysis unveils self-renewing lineage-restricted progenitors generated directly from hematopoietic stem cells. *Cell*. 2013; 154(5):1112-1126.
- Dong F, Bai H, Wang X, et al. Mouse acute leukemia develops independent of self-renewal and differentiation potentials in hematopoietic stem and progenitor cells. *Blood Adv*. 2019;3(3):419-431.
- Wang J, Liu Z, Zhang S, et al. Lineage marker expression on mouse hematopoietic stem cells. *Exp Hematol*. 2019;76:13-23.e2.
- Ema H, Morita Y, Suda T. Heterogeneity and hierarchy of hematopoietic stem cells. *Exp Hematol*. 2014;42(2):74-82.e2.
- Alexander WS. Suppressors of cytokine signalling (SOCS) in the immune system. *Nat Rev Immunol*. 2002;2(6):410-416.
- Li S, Miao T, Sebastian M, et al. The transcription factors Egr2 and Egr3 are essential for the control of inflammation and antigen-induced proliferation of B and T cells. *Immunity*. 2012;37(4):685-696.
- Gerdes J, Lemke H, Baisch H, Wacker HH, Schwab U, Stein H. Cell cycle analysis of a cell proliferation-associated human nuclear antigen defined by the monoclonal antibody Ki-67. *J Immunol*. 1984;133(4):1710-1715.
- Pietras EM, Warr MR, Passegue E. Cell cycle regulation in hematopoietic stem cells. *J Cell Biol*. 2011;195(5):709-720.
- Barker JE, Sl/Sld hematopoietic progenitors are deficient in situ. *Exp Hematol*. 1994;22(2):174-177.
- Chabot B, Stephenson DA, Chapman VM, Besmer P, Bernstein A. The proto-oncogene c-kit encoding a transmembrane tyrosine kinase receptor maps to the mouse W locus. *Nature*. 1988;335(6185):88-89.
- Ding L, Saunders TL, Enikolopov G, Morrison SJ. Endothelial and perivascular cells maintain haematopoietic stem cells. *Nature*. 2012;481(7382):457-462.
- Matsumoto A, Takeishi S, Kanie T, et al. p57 is required for quiescence and maintenance of adult hematopoietic stem cells. *Cell Stem Cell*. 2011;9(3):262-271.
- Zou P, Yoshihara H, Hosokawa K, et al. p57(Kip2) and p27(Kip1) cooperate to maintain hematopoietic stem cell quiescence through interactions with Hsc70. *Cell Stem Cell*. 2011;9(3):247-261.
- Qian H, Buza-Vidas N, Hyland CD, et al. Critical role of thrombopoietin in maintaining adult quiescent hematopoietic stem cells. *Cell Stem Cell*. 2007;1(6):671-684.
- Kimura S, Roberts AW, Metcalf D, Alexander WS. Hematopoietic stem cell deficiencies in mice lacking c-Mpl, the receptor for thrombopoietin. *Proc Natl Acad Sci U S A*. 1998;95(3):1195-1200.
- Wilkinson AC, Ishida R, Kikuchi M, et al. Long-term ex vivo haematopoietic-stem-cell expansion allows nonconditioned transplantation. *Nature*. 2019;571(7763):117-121.
- Kobayashi H, Morikawa T, Okinaga A, et al. Environmental optimization enables maintenance of quiescent hematopoietic stem cells ex vivo. *Cell Rep*. 2019;28(1):145-158.e9.
- Kimura A, Kinjyo I, Matsumura Y, et al. SOCS3 is a physiological negative regulator for granulopoiesis and granulocyte colony-stimulating factor receptor signaling. *J Biol Chem*. 2004;279(8):6905-6910.
- Croker BA, Metcalf D, Robb L, et al. SOCS3 is a critical physiological negative regulator of G-CSF signaling and emergency granulopoiesis. *Immunity*. 2004;20(2):153-165.
- Hiyama F, Shih JP, Awgulewitsch A, Warr GW, Clark SC, Ogawa M. Clonal proliferation of murine lymphohemopoietic progenitors in culture. *Proc Natl Acad Sci U S A*. 1992;89(13):5907-5911.
- Nishinakamura R, Nakayama N, Hirabayashi Y, et al. Mice deficient for the IL-3/GM-CSF/IL-5 beta c receptor exhibit lung pathology and impaired immune response, while beta IL3 receptor-deficient mice are normal. *Immunity*. 1995;2(3):211-222.
- Hayashida K, Kitamura T, Gorman DM, Arai K, Yokota T, Miyajima A. Molecular cloning of a second subunit of the receptor for human granulocyte-macrophage colony-stimulating factor (GM-CSF): reconstitution of a high-affinity GM-CSF receptor. *Proc Natl Acad Sci U S A*. 1990;87(24):9655-9659.
- Ding L, Morrison SJ. Haematopoietic stem cells and early lymphoid progenitors occupy distinct bone marrow niches. *Nature*.

2013;495(7440):231-235.

42. Greenbaum A, Hsu YM, Day RB, et al. CXCL12 in early mesenchymal progenitors is required for haematopoietic stem-cell maintenance. *Nature*. 2013;495(7440):227-230.
43. Tzeng YS, Li H, Kang YL, Chen WC, Cheng WC, Lai DM. Loss of Cxcl12/Sdf-1 in adult mice decreases the quiescent state of hematopoietic stem/progenitor cells and alters the pattern of hematopoietic regeneration after myelosuppression. *Blood*. 2011;117(2):429-439.
44. Lévesque J-P, Hendy J, Takamatsu Y, Simmons PJ, Bendall LJ. Disruption of the CXCR4/CXCL12 chemotactic interaction during hematopoietic stem cell mobilization induced by GCSF or cyclophosphamide. *J Clin Invest*. 2003;111(2):187-196.
45. Broxmeyer HE, Orschell CM, Clapp DW, et al. Rapid mobilization of murine and human hematopoietic stem and progenitor cells with AMD3100, a CXCR4 antagonist. *J Exp Med*. 2005;201(8):1307-1318.
46. Burns JM, Summers BC, Wang Y, et al. A novel chemokine receptor for SDF-1 and ITAC involved in cell survival, cell adhesion, and tumor development. *J Exp Med*. 2006;203(9):2201-2213.
47. Ogawa M. Differentiation and proliferation of hematopoietic stem cells. *Blood*. 1993;81(11):2844-2853.
48. Adolfsson J, Månnsson R, Buza-Vidas N, et al. Identification of Flt3+ lympho-myeloid stem cells lacking erythro-megakaryocytic Potential. *Cell*. 2005;121(2):295-306.
49. Saito Y, Uchida N, Tanaka S, et al. Induction of cell cycle entry eliminates human leukemia stem cells in a mouse model of AML. *Nat Biotechnol*. 2010;28(3):275-280.
50. Löwenberg B, van Putten W, Theobald M, et al. Effect of priming with granulocyte colony-stimulating factor on the outcome of chemotherapy for acute myeloid leukemia. *N Engl J Med*. 2003;349(8):743-752.

Natural estrogens enhance the engraftment of human hematopoietic stem and progenitor cells in immunodeficient mice



Ferrata Storti Foundation

Sara Fañanas-Baquero,^{1,2} Israel Orman,^{1,2} Federico Becerra Aparicio,^{1,2} Silvia Bermudez de Miguel,^{1,2} Jordi Garcia Merino,^{1,2} Rosa Yañez,^{1,2} Yolanda Fernandez Sainz,^{1,2} Rebeca Sánchez,^{1,2} Mercedes Dassy-Rodríguez,^{1,2} Omaira Alberquilla,^{1,2} David Alfaro,³ Agustín Zapata,³ Juan A. Bueren,^{1,2} Jose Carlos Segovia^{1,2} and Oscar Quintana-Bustamante^{1,2}

¹Hematopoietic Innovative Therapies Division, Centro de Investigaciones Energéticas, Medioambientales y Tecnológicas (CIEMAT) and Centro de Investigación Biomédica en Red de Enfermedades Raras (CIBERER); ²Unidad Mixta de Terapias Avanzadas, Instituto de Investigación Sanitaria Fundación Jiménez Díaz and ³Department of Cell Biology, Faculty of Biology, Complutense University of Madrid, Madrid, Spain.

Haematologica 2021
Volume 106(6):1659-1670

ABSTRACT

Hematopoietic stem and progenitor cells (HSPC) are crucial in the maintenance of lifelong production of all blood cells. These stem cells are highly regulated to maintain homeostasis through a delicate balance between quiescence, self-renewal and differentiation. However, this balance is altered during the recovery after HSPC transplantation. Transplantation efficacy can be limited by inadequate hematopoietic stem cell number, poor homing, low level of engraftment, or limited self-renewal. As recent evidence indicates that estrogens are involved in regulating hematopoiesis, we sought to examine whether natural estrogens (estrone or E1, estradiol or E2, estriol or E3 and estetrol or E4) modulate human HSPC. Our results show that human HSPC subsets express estrogen receptors, and that signaling is activated by E2 and E4 on these cells. Additionally, these natural estrogens cause different effects on human progenitors *in vitro*. We found that both E2 and E4 expand human HSPC. However, E4 was the best tolerated estrogen and promoted cell cycling of human hematopoietic progenitors. Furthermore, we found that E2 and, more significantly, E4 doubled human hematopoietic engraftment in immunodeficient mice without altering other HSPC properties. Finally, the impact of E4 on promoting human hematopoietic engraftment in immunodeficient mice might be mediated through the regulation of mesenchymal stromal cells in the bone marrow niche. Collectively, our data demonstrate that E4 is well tolerated and enhances human reconstitution in immunodeficient mice directly, by modulating human hematopoietic progenitor properties, and indirectly, by interacting with the bone marrow niche. This might have particular relevance for improving hematopoietic recovery after myeloablative conditioning, especially when limited numbers of HSPC are available.

Correspondence:

OSCAR QUINTANA-BUSTAMANTE
oscar.quintana@ciemat.es

JOSE CARLOS SEGOVIA
jc.segovia@ciemat.es

Received: August 2, 2019.

Accepted: April 28, 2020.

Pre-published: April 30, 2020.

<https://doi.org/10.3324/haematol.2019.233924>

Introduction

Hematopoietic stem cells (HSC) are a rare cell population resident in the bone marrow (BM) of adult mammals and are at the top of a hierarchy of progenitors that become progressively restricted to several or a single blood lineage. HSC are capable of self-renewal and multipotent differentiation to all blood cell lineages,¹ and are crucial for the maintenance of lifelong production of all blood cells. They are homeostatically regulated through a delicate balance between quiescence, self-renewal and differentiation. Although HSC divide infrequently, they are activated to proliferate in response to BM injury to re-establish homeostasis.² Transplantation of hematopoietic stem and progenitor cells (HSPC) is routinely used to reconstitute hematopoiesis after myeloablative regimens to treat leukemia or hematopoietic genetic diseases. However, the efficacy of HSPC transplantation can be limited by inadequate cell

© 2021 Ferrata Storti Foundation

Material published in *Haematologica* is covered by copyright. All rights are reserved to the Ferrata Storti Foundation. Use of published material is allowed under the following terms and conditions: <https://creativecommons.org/licenses/by-nc/4.0/legalcode>. Copies of published material are allowed for personal or internal use. Sharing published material for non-commercial purposes is subject to the following conditions: <https://creativecommons.org/licenses/by-nc/4.0/legalcode>, sect. 3. Reproducing and sharing published material for commercial purposes is not allowed without permission in writing from the publisher.



numbers, poor homing, low engraftment, or differentiation stress of the HSPC. Different approaches have been attempted to solve these problems, such as using different sources of HSPC,³⁻⁵ *ex vivo* expansion of HSPC⁶⁻¹⁰ or stimulating the HSPC by accessory molecules^{11,12} or cells.¹³ However, these approaches require a profound understanding of HSPC regulation and how the properties of the cells can be boosted to maximize their efficacy at reconstituting a patient's blood system after HSPC transplantation.^{1,14}

Estrogen is the primary female sex hormone and, apart from its known role in the reproductive system, it is responsible for controlling many cellular and molecular processes, including growth and differentiation. Estrogens act through genomic or nuclear signaling and non-genomic or membrane-initiated steroid signaling (MISS), modulating intracellular second messengers.¹⁵ The four major naturally-occurring estrogens in women are estrone (E1), estradiol (E2), estriol (E3) and estetrol (E4). E1 is the predominant estrogen in postmenopausal women. E2 is considered the active estrogen during the estrous cycle. E3 and E4 are synthesized during pregnancy by the placenta and fetal liver, respectively, but their physiological roles are essentially unknown.¹⁶

Recent evidence indicates that E2 is involved in regulating the proliferation and lineage commitment of HSC,¹⁷ although the studies are few and their results are sometimes contradictory. E2 treatment was able to specifically increase the number of vascular HSC, but the long-term repopulating capacity of the HSC was limited.¹⁸ Additionally, this E2 was shown to promote the cell cycle of HSC and multipotent progenitors (MPP) and increase erythroid differentiation in females, also during pregnancy.¹⁹ Furthermore, E2 favors hematopoietic regeneration through the activation of telomerase activity²⁰⁻²² and the stimulation of the unfolded protein response on mouse HSC, which sustains protein homeostasis to favor hematopoietic regeneration.²³ In contrast, tamoxifen, whose active metabolite (4-hydroxytamoxifen) acts as an estrogen receptor antagonist, reduces the number of MPP and short-term HSC but activates the proliferation of long-term HSC.²⁴ In addition, E2 might modulate HSC indirectly through activating BM mesenchymal stromal cells (MSC). E2 treatment has been described to activate MSC osteogenic differentiation and also promotes the secretion of granulocyte-macrophage colony-stimulating factor and interleukin 6, which increased the number of HSC by modulating their niche.²⁵ Therefore, estrogen-mediated regulation of HSPC can also indirectly change the HSC BM niche. For that reason, a full understanding of the role of estrogens in HSC regulation is essential in order to be able to further develop the clinical potential of these hormones.

Here, we have examined the impact of natural estrogens on human HSPC. *Ex vivo*, E2 and E4 treatment expanded human HSPC and, more importantly, the administration of E4 to immunodeficient mice previously transplanted with human HSPC enhanced the level of engraftment of human hematopoietic cells.

Methods

Human cord blood-CD34⁺ cell samples and bone marrow mesenchymal stromal cells

Umbilical cord blood samples (CB) from healthy donors were provided by the Centro de Transfusión de la Comunidad de

Madrid. All samples were collected with written consent and agreement from the Centro de Transfusión de la Comunidad de Madrid's institutional review board (number PKDEFIN [SAF2017-84248-P]). Mononuclear cells were obtained by fractionation in Ficoll-hypaque according to the manufacturer's recommendations (GE Healthcare). Purified CB-CD34⁺ cells were obtained using a MACS CD34 Micro-Bead kit (Miltenyi Biotec). Cells were frozen in 10% dimethyl sulfoxide solution and stored in liquid nitrogen until their use.

Mononuclear cells from human BM were obtained by Ficoll-Paque Plus density gradient separation from heparinized BM samples obtained from healthy donors after informed consent. All the procedures were in accordance with the Helsinki Declaration of 1975, and its revision in 2000. Samples were cultured at 1.6×10^5 cells/cm² in MesenCult medium plus supplements for human cells (Stemcell Technologies). After 24 h, non-adherent cells were discarded. Fresh medium was added and replaced twice a week. At 80% confluence, adherent cells were trypsinized, washed, and seeded at 4×10^3 cells/cm². In all the experiments, BM-MSC were used at passages 5 to 8.

Hematopoietic cell transplant protocol in immunodeficient mice

All the mice were kept under standard pathogen-free conditions in the animal facility of CIEMAT. All animal experiments were performed in compliance with European and Spanish legislation and institutional guidelines. The protocol was approved by Consejería de Medio Ambiente y Ordenación del Territorio (protocol number PROEX 078/15).

CB-CD34⁺ cells were administered through the tail vein of female or male NOD.Cg-*Prkdc*^{scid} *Il2rg*^{tm1Wjl}/SzJ (NSG) mice sublethally irradiated the day before the transplant with 1.5 Gy. Three days later, the animals were treated with vehicle (olive oil) or daily doses of either E2 or E4 (2 µg of estrogen per day) intraperitoneally for 4 days. Four months after transplantation, the mice were sacrificed and BM was collected from the long bones of these animals. Additionally, when analysis of the hematopoietic niche was involved, the long bones were flushed, cut into small pieces and crushed before being digested with 200 U/mL collagenase IV/2 µg/mL DNaseI in Hanks balanced salt solution at 37°C for 45 min. Human engraftment was analyzed by flow cytometry (LSR Fortessa; BD). The cells were stained with hCD45-APCCy7 and hCD3-APC (BioLegend), hCD45-FITC, hCD33-PE, hCD19-FITC and hCD235a-FITC (Beckman Coulter), hCD34-Pecy5 (Immunotech), hCD38-PE, hCD90-APC, mCD45.1-PE, mCD45.1-Biotin and Ter119-Biotin (BD), mCD140a-APC (Pdgfra-APC, eBioscience) and mCD144-PE (VE-Cadherin-PE, eBioscience). DAPI-positive cells were excluded from the analysis. FlowJo software was used for the analyses.

Additionally, the hCD45⁺ population from primary mice was sorted in an Influx Cell Sorter (BD) and 1×10^6 hCD45⁺ cells were transplanted into sublethally irradiated female secondary NSG recipients. Four months later, the animals were sacrificed and analyzed as previously described.

Results

Engraftment of human cord blood CD34⁺ cells is favored in female immunodeficient mice

It has been previously described that the engraftment of highly purified human HSC (Lin⁻CD34⁺CD38⁻CD90⁺CD45RA⁺) is improved when these cells are transplanted into immunodeficient female recipients, as compared to male recipients.²⁶ To investigate whether this

enhanced engrafting potential in female recipients was also present in CB-CD34⁺ cells, we transplanted different amounts of HSPC into sublethally irradiated animals. As occurred when highly purified HSC were transplanted, we observed higher engraftment of human HSPC in female NSG animals than in their male counterparts (Figure 1A). Four months after the transplantation of 5×10^4 CB-CD34⁺ cells, human engraftment in mouse BM was $61.06 \pm 26.07\%$ (mean \pm standard deviation) in female mice and $18.94 \pm 13.93\%$ in male mice. Interestingly, this impairment in engrafting potential in males was even greater when only 5×10^3 CB-CD34⁺ cells were transplanted ($38.74 \pm 30.42\%$ BM cells were of human origin in female animals *versus* only $0.19 \pm 0.27\%$ in male animals) (Figure 1B). Therefore, engraftment of human cells was from 3.2- to >200 -fold greater in female recipients than in male recipients when 5×10^4 or 5×10^3 CB-CD34⁺ cells, respectively, were transplanted. Additionally, there were no differences in the percentages of myeloid, B, T cells or HSPC (hCD34⁺, hCD34⁺hCD38⁻ and hCD34⁺hCD38⁺hCD90⁺ cells) between the human engrafted cells (Online Supplementary Figure S1). These data highlight the importance of the gender of the NSG mouse recipients to facilitate the engraftment of human HSPC.

Human hematopoietic stem and progenitor cell subsets expressed both ESR1 and ESR2

To understand the potential role of sex hormones in the observed differences of human hematopoietic engraftment between male and female recipient mice, we analyzed the expression of the two main estrogen receptors, ESR1 and ESR2, in CB-CD34⁺ cells. As shown by immunostaining analysis (Figure 2A and B), most CD34⁺ cells were positive for ESR1, while ESR2 staining was dimmer in CD34⁺ cells (Figure 2A and B; Online Supplementary Figure S2A). Additionally, to investigate the differential

expression of these receptors in the hematopoietic progenitors, different populations of HSPC, such as HSC/MPP (CD34⁺CD38⁻CD45RA⁻), multilymphoid progenitors (MLP, CD34⁺CD38⁺CD45RA⁻) and committed hematopoietic progenitors (CD34⁺CD38⁺), were sorted out (Online Supplementary Figure S2B) and the expression of both estrogen receptors was determined by quantitative reverse transcriptase polymerase chain reaction (qRT-PCR). Both *ESR1* and *ESR2* were expressed in HSC, MLP and in more committed hematopoietic progenitors (Figure 2C and D; Online Supplementary Figure S2C). *ESR1* expression tended to be upregulated between HSC/MPP and MLP compartments to decrease again in the most committed hematopoietic progenitors (Figure 2C). In contrast, *ESR2* expression seemed to follow an opposite pattern with high values in both HSC/MPP and committed hematopoietic progenitors but reduced levels in the MLP cell population (Figure 2D). In both cases, although some tendencies were observed, no statistically significant differences were documented. Like *ESR1* and *ESR2*, the newly identified estrogen receptor, *GPER1*, was also detected by RT-PCR in CB-CD34⁺ cells from different donors (Online Supplementary Figure S2D). Consequently, human HSPC might respond to natural estrogens through any of the estrogen receptors.

Natural estrogens modified human hematopoietic stem and progenitor cells *in vitro*

Once we had demonstrated that both estrogen receptors were expressed in HSPC, we wanted to investigate a potential direct effect of estrogens on human HSPC. We cultured CB-CD34⁺ cells for 4 days with a range of concentrations, from 10 nM to 500 μ M, of the four natural estrogens (E1, E2, E3 and E4). As shown in Figure 3A, E1 and E3 reduced the expansion of the cells in culture prac-

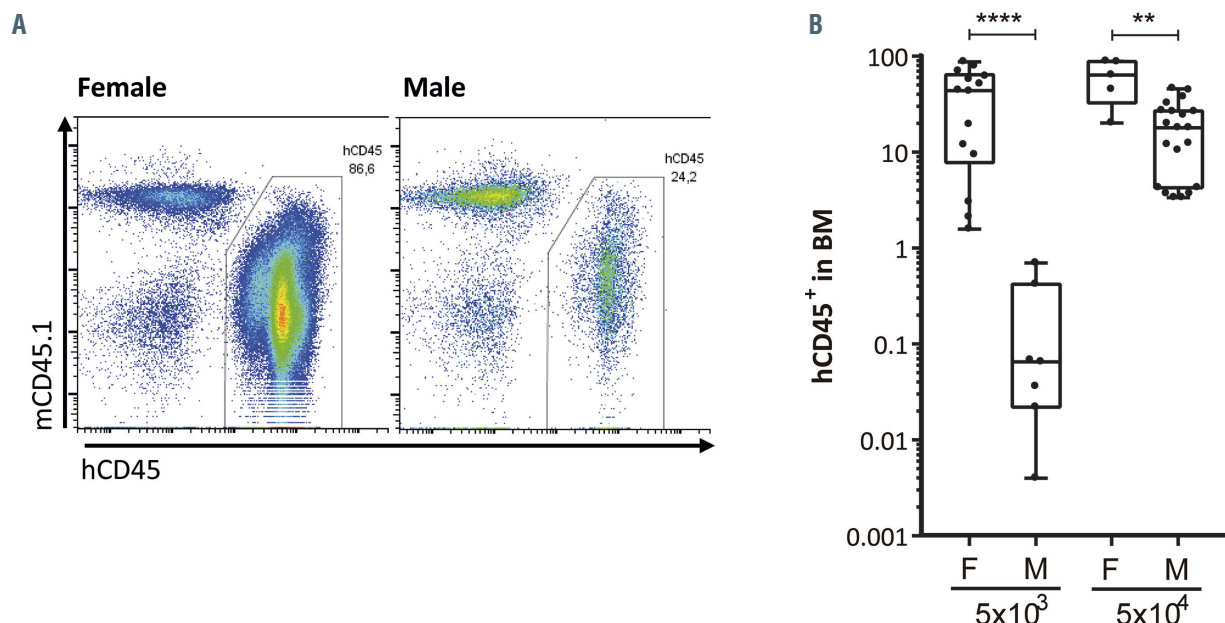


Figure 1. Human hematopoietic stem and progenitor cells show superior hematopoietic engraftment in female NSG mice than in male ones. (A) Representative flow cytometry analyses of human engraftment of 5×10^4 umbilical cord blood CD34⁺ (CB-CD34⁺) cells into sublethally irradiated female (left panel) and male (right panel) NOD.Cg-*Prkdc*^{sid} II2rg^{tm1Wjl}/SzJ (NSG) mice 4 months after transplantation. (B) Percentage of human hematopoietic cells, hCD45⁺, in the bone marrow of female (F) or male (M) animals transplanted with 5×10^3 or 5×10^4 CB-CD34⁺ cells. Data were obtained from six independent biological replicates and are presented by dots and box-plots that represent the interquartile range (p75, upper edge; p25, lower edge; p50, midline; p95, line above the box; and p5, line below the box). Statistical significance was analyzed by the Mann-Whitney U test; ** $P < 0.01$ and *** $P < 0.001$.

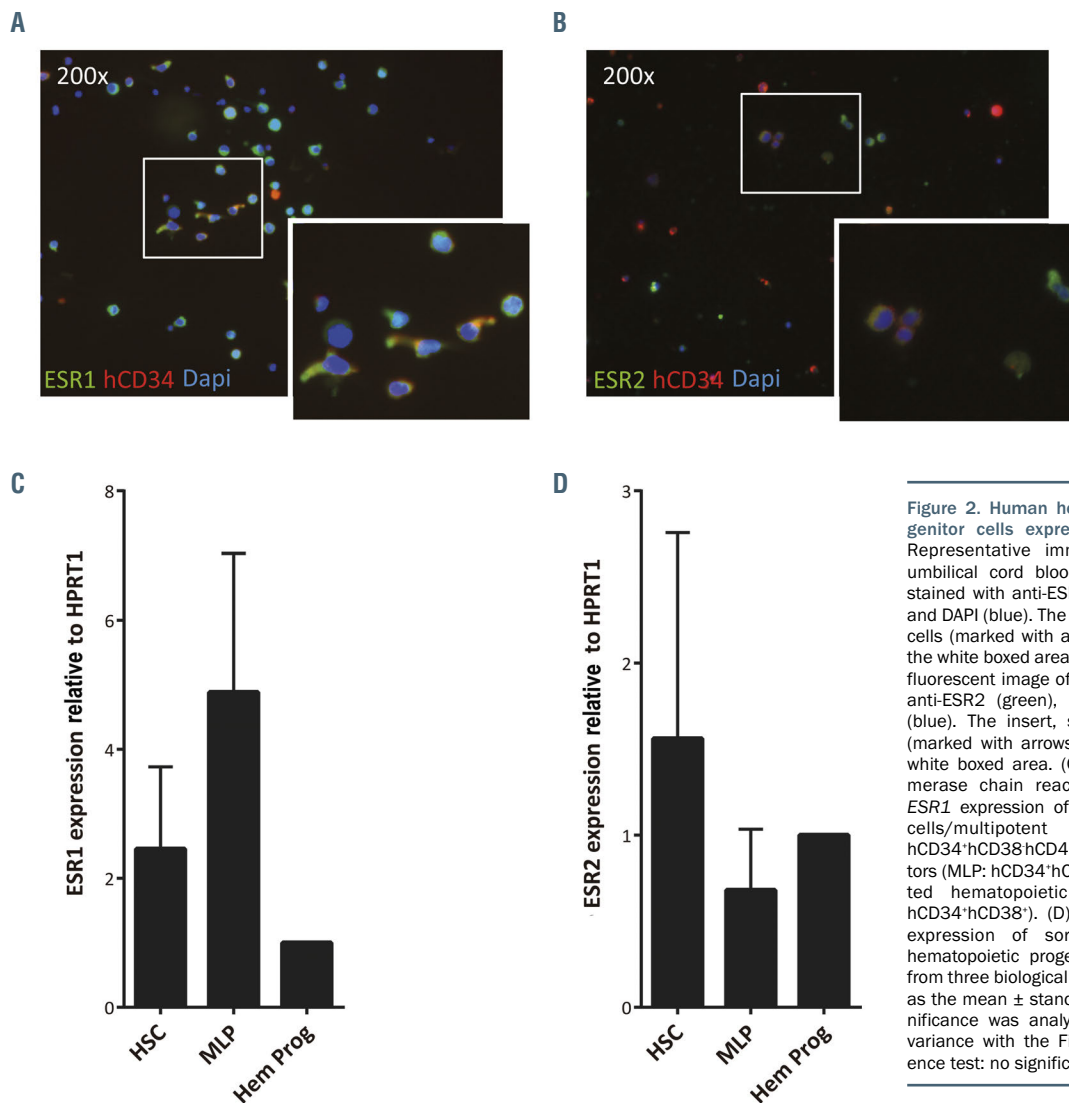


Figure 2. Human hematopoietic stem and progenitor cells express estrogen receptors. (A) Representative immunofluorescent image of umbilical cord blood CD34⁺ (CB-CD34⁺) cells stained with anti-ESR1 (green), anti-hCD34 (red) and DAPI (blue). The insert, showing ESR1⁺ CD34⁺ cells (marked with arrows), is an enlargement of the white boxed area. (B) Representative immunofluorescent image of CB-CD34⁺ cells stained with anti-ESR2 (green), anti-hCD34 (red) and DAPI (blue). The insert, showing ESR2⁺ CD34⁺ cells (marked with arrows), is an enlargement of the white boxed area. (C) Qualitative real-time polymerase chain reaction (qRT-PCR) analysis of ESR1 expression of sorted hematopoietic stem cells/multipotent progenitors (HSC/MPP: hCD34⁺hCD38⁺hCD45RA⁺), multi-lymphoid progenitors (MLP: hCD34⁺hCD38⁺hCD45RA⁺) and committed hematopoietic progenitors (Hem Prog: hCD34⁺hCD38⁺). (D) qRT-PCR analysis of ESR2 expression of sorted HSC/MPP, MLP and hematopoietic progenitors. Data were obtained from three biological replicates and are presented as the mean \pm standard deviation. Statistical significance was analyzed by one-way analysis of variance with the Fisher least significant difference test: no significant differences were found.

tically at any of the concentrations used. On the other hand, the lowest concentrations of E2 and E4 promoted the expansion of these cells, but at high doses they impaired cell growth. A similar behavior was detected when different subpopulations of hCD34⁺ cells were analyzed (Figure 3B; *Online Supplementary Figure S3A-E*). E1 prevented the expansion of hCD34⁺hCD38⁺ cells (*Online Supplementary Figure S3C*), MLP (*Online Supplementary Figure S3D*), MPP (hCD34⁺hCD38⁺hCD90⁺hCD45RA⁺) (*Online Supplementary Figure S3E*) and most primitive HSC (hCD34⁺hCD38⁺hCD90⁺hCD45RA⁺) (Figure 3B). The data for the rest of the tested estrogens showed an apparent amplification of these primitive populations when low concentrations of the hormones were used, but at the highest concentrations, they were toxic (Figure 3B; *Online Supplementary Figure S3C-E*). It is important to highlight that the best tolerated estrogen was E4. Concentrations up to 10 μ M of E4 seemed not to be detrimental to any of these HSPC subsets, including primitive HSC. In contrast, E2 induced apoptosis of HSPC at high doses (*Online Supplementary Figure S3F* and *G*), as previously described for this estrogen and tamoxifen.^{24,27} However, only human HSPC cultured in the presence of the highest concentration of E4 showed some induction of apoptosis. Furthermore, we analyzed the cell cycle of CB-CD34⁺ cells

after 4 days of culture in the presence of 100 nM E2 or E4. Estrogens, particularly E4, induced an increment of cells in G2/M phase (Figure 3C; *Online Supplementary Figure S3H*), which might explain the tendency of these two estrogens to expand human hematopoietic progenitors.

Previously, E2 was described to have a positive role in enhancing both CB-CD34⁺ cell proliferation and *in vitro* hematopoietic progenitor potential after more than week of *in vitro* treatment.²⁸ Hence, we cultured human HSPC in the presence of the lowest and best tolerated doses of E2 or E4 for 8 days. We detected a significant expansion of human progenitors with E4 at all the concentrations tested (Figure 3D). A similar effect was identified with 100 nM E2. The better tolerance of E4 over E2 was confirmed, since all the tested concentrations of E4 were non-toxic to CB-CD34⁺ cells (Figure 3D). The *in vitro* functionality of the estrogen-treated HSPC was assessed with colony-forming unit (CFU) assays. We did not observe any differences among the groups in CFU numbers or CFU types (*Online Supplementary Figure S3I*).

In order to assess which estrogen receptor was involved in the effect of these molecules in human HSPC, the cell cycle of CB-CD34⁺ was determined in the presence of these two estrogens together with either ESR1 antagonist (MPP), ESR2 antagonist (PHTPP) or GPER1 antagonist (G-

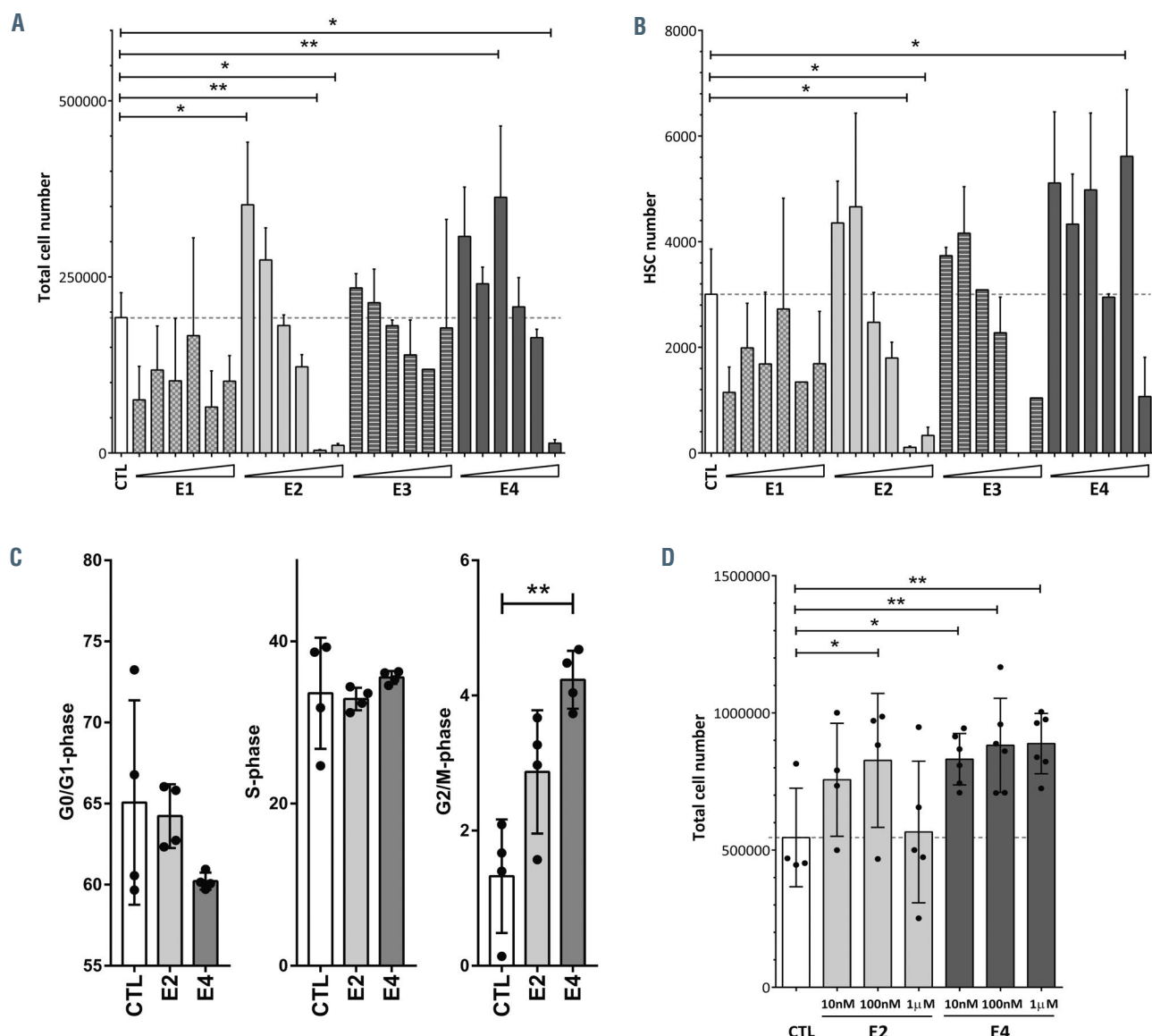


Figure 3. Natural estrogens affect human hematopoietic stem and progenitor cells differently. (A) Total number of estrogen-treated hematopoietic stem and progenitor cells (HSPC) after 4 days in culture. Different concentrations (10 nM, 100 nM, 1 μ M, 10 μ M, 100 μ M and 500 μ M) of the natural estrogens (E1, E2, E3 and E4) were used. (B) Total number of hematopoietic stem cells (HSC: hCD34⁺hCD38⁺hCD90⁺hCD45RA⁺) after 4 days in culture. Different concentrations (10 nM, 100 nM, 1 μ M, 10 μ M, 100 μ M and 500 μ M) of the natural estrogens (E1, E2, E3 and E4) were used. (C) Cell cycle analysis of HSPC treated with 100 nM E2 or E4. G0/G1-phase (left panel), S-phase (middle panel) and G2/M-phase (right panel). (D) Total cell number of estrogen-treated HSPC after 8 days in culture. Data were obtained from three to five biological replicates and are presented as mean \pm standard deviation. Statistical significance was analyzed by one-way analysis of variance with the Fisher least significant difference test: * P <0.05 and ** P <0.01.

15). Treatment with E2 or E4 alone tended to increase the percentage of cells in S/G2/M-phase as previously described; however, the addition of ESR2 antagonist seemed to block the increase of cells in S/G2/M-phase induced by E4 (Online Supplementary Figure S3j). Less clearly, ESR1 and GPER1 antagonists seemed to reduce the number of cells in S/G2/M-phase in E2-treated HSPC. We also assessed the expression of ESR1 and ESR2 in human HSPC cultured with estrogens for 4 days by immunofluorescence analysis (Online Supplementary Figure S3K and L). While ESR1 fluorescence intensity increased slightly but significantly with 100 nM of E2 or E4 (Online Supplementary Figure S3K and M), ESR2 expression was significantly increased in the presence of both E2 and E4 (Online Supplementary Figure S3L and N). Moreover, estro-

gen treatment increased the percentage of human HSPC showing a polarized localization of ESR1 at the membrane (Online Supplementary Figure S3K and O). Furthermore, the treatment with estrogens enhanced the percentage of hCD34⁺ cells with cytoplasmic localization of ESR2 (Online Supplementary Figure S3L and P).

Collectively, these data indicate that natural estrogens regulate human HSPC through the signaling of estrogen receptors.

E2 and E4 increased the number of human hematopoietic stem and progenitor cells in an *in vitro* model of human hematopoietic niche

Subsequently, we investigated the indirect effect of E2 and E4 on HSPC in an *in vitro* model of the human

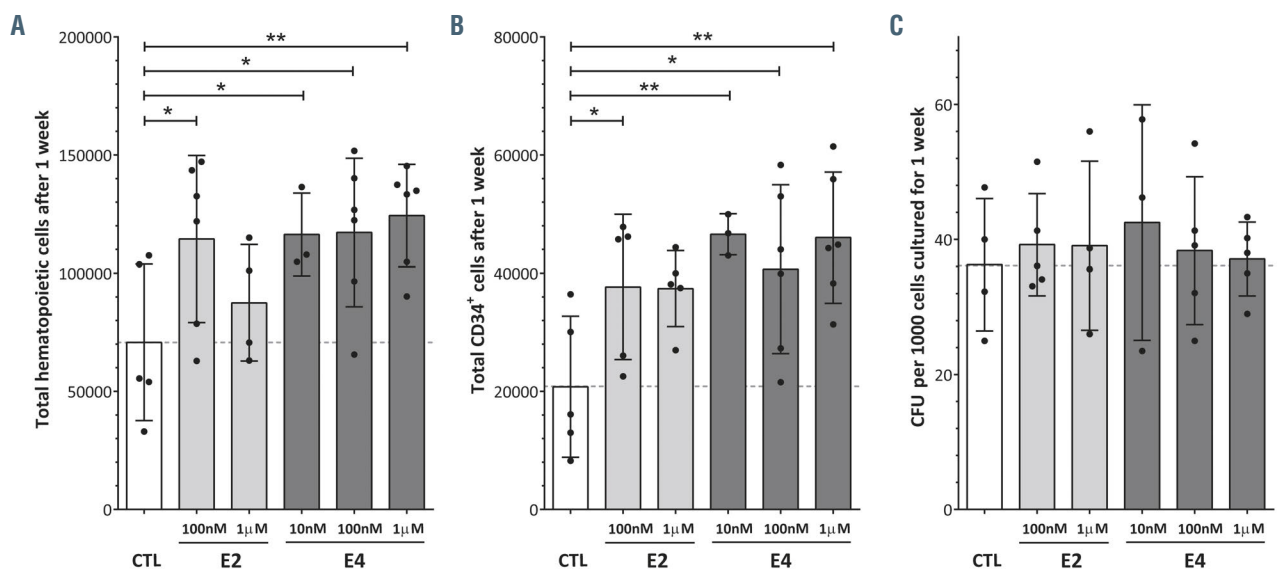


Figure 4. The impact of E2 and E4 on hematopoietic stem and progenitor cells in an *in vitro* model of the human hematopoietic niche. (A) Total hematopoietic cells after 1 week of co-culture with human bone marrow mesenchymal stromal cells (BM-MSC) in the presence of estrogens. (B) Total hCD34⁺ cells after 1 week of co-culture with human BM-MSC in the presence of estrogens. (C) Colony-forming units (CFU) derived from hematopoietic stem and progenitor cells after 1 week of co-culture with human BM-MSC in the presence of estrogens. Data were obtained from three to six biological replicates and are presented as the mean \pm standard deviation. The statistical significance was analyzed by one-way analysis of variance with the Fisher least significant difference test: * P <0.05 and ** P <0.01.

hematopoietic niche. CB-CD34⁺ cells were co-cultured on an irradiated human BM-MSC layer in the presence of 100 nM or 1 μ M of E2 and E4 (*Online Supplementary Figure S4A*). We analyzed the expansion of the hematopoietic cells in two ways: (i) after 1 week of co-culture (Figure 4), and (ii) after 4 weeks of co-culture with the estrogen present only during the first week (*Online Supplementary Figure S4C and D*). From 10 nM to 1 μ M of E4 and the lowest concentration of E2 increased the hematopoietic cells in the culture in the first week of co-culture (Figure 4A). Likewise, the number of hCD34⁺ cells in the co-culture was significantly higher following treatment with E4 or 10 nM E2 than in the control group (Figure 4B; *Online Supplementary Figure S4B*). However, we could not detect significant differences in the functionality of the hCD34⁺ cells in CFU assays (Figure 4C). Furthermore, the effect of these two estrogens on the expansion of human hematopoietic cells or hCD34⁺ cells did not seem to be enhanced after 4 weeks in co-culture with an initial single dose (*Online Supplementary Figure S4C and D*). Consequently, the positive effect of E2 and E4 on HSPC also occurs in an *in vitro* model of the human hematopoietic niche.

E2 and E4 boosted human hematopoietic engraftment in immunodeficient mice

To better evaluate the impact of E2 and E4 on the properties of HSPC, we transplanted 5×10^4 human CB-CD34⁺ cells into sublethally irradiated male NSG mice, in order to avoid any additional effects of endogenous estrogens of female recipient mice, and 3 days later treated the animals with vehicle or daily low doses of either E2 or E4 (2 μ g of estrogen per day) for 4 days (Figure 5A). Human hematopoietic engraftment was evaluated in the mouse BM by FACS analysis 4 months after transplantation (*Online Supplementary Figure S5A*). Surprisingly, the human hematopoietic contribution was significantly higher in the estrogen-treated animals than in vehicle-treated ones

(Figure 5B; *Online Supplementary Figure S5A*). None of the estrogens altered the normal distribution of human hematopoietic lineages within the hCD45⁺ population (*Online Supplementary Figure S5B-D*). More importantly, E4 administration significantly enhanced the hCD34⁺ cell population in male NSG mice (Figure 5C). No increase in the presence of the more primitive compartment, hCD34⁺hCD38⁺, was observed (Figure 5D). To explore the impact of the estrogen treatment on the long-term HSC, secondary transplants were performed. One million hCD45⁺ cells, purified from the BM of the primary recipients, were transplanted into sublethally irradiated female NSG mice. As shown in Figure 5E, the estrogen-treated human hematopoietic cells maintained their long-term engraftment potential without any observable problem in human hematopoietic reconstitution or any abnormal proliferation. This led us to conclude that these two estrogens, particularly E4, enhance *in vivo* human hematopoietic engraftment in male immunodeficient mice.

To study this finding in more depth, we transplanted limited numbers of human HSPC (5×10^3 CB-CD34⁺ cells/mouse), into male NSG mice, which were subsequently treated with vehicle, E2 or E4 as previously described. The percentage of mice positive for human engraftment, defined as animals in which hCD45⁺ cells constituted more than 0.1% of the cells in the mouse BM 4 months after transplantation, tended to increase after estrogen treatment (*Online Supplementary Figure S5E*). Moreover, the human hematopoietic chimerism of the positive animals seemed to be higher in the group treated with E4 than in the group given the vehicle (*Online Supplementary Figure S5F*). So, E2 and E4 might be able to improve the engraftment of human HSPC even when a very limited number of cells are transplanted.

To explore whether the enhancement of engraftment mediated by estrogens occurred in female recipients as well, we repeated the transplant of this very low number of CB-CD34⁺ cells into sublethally irradiated female NSG

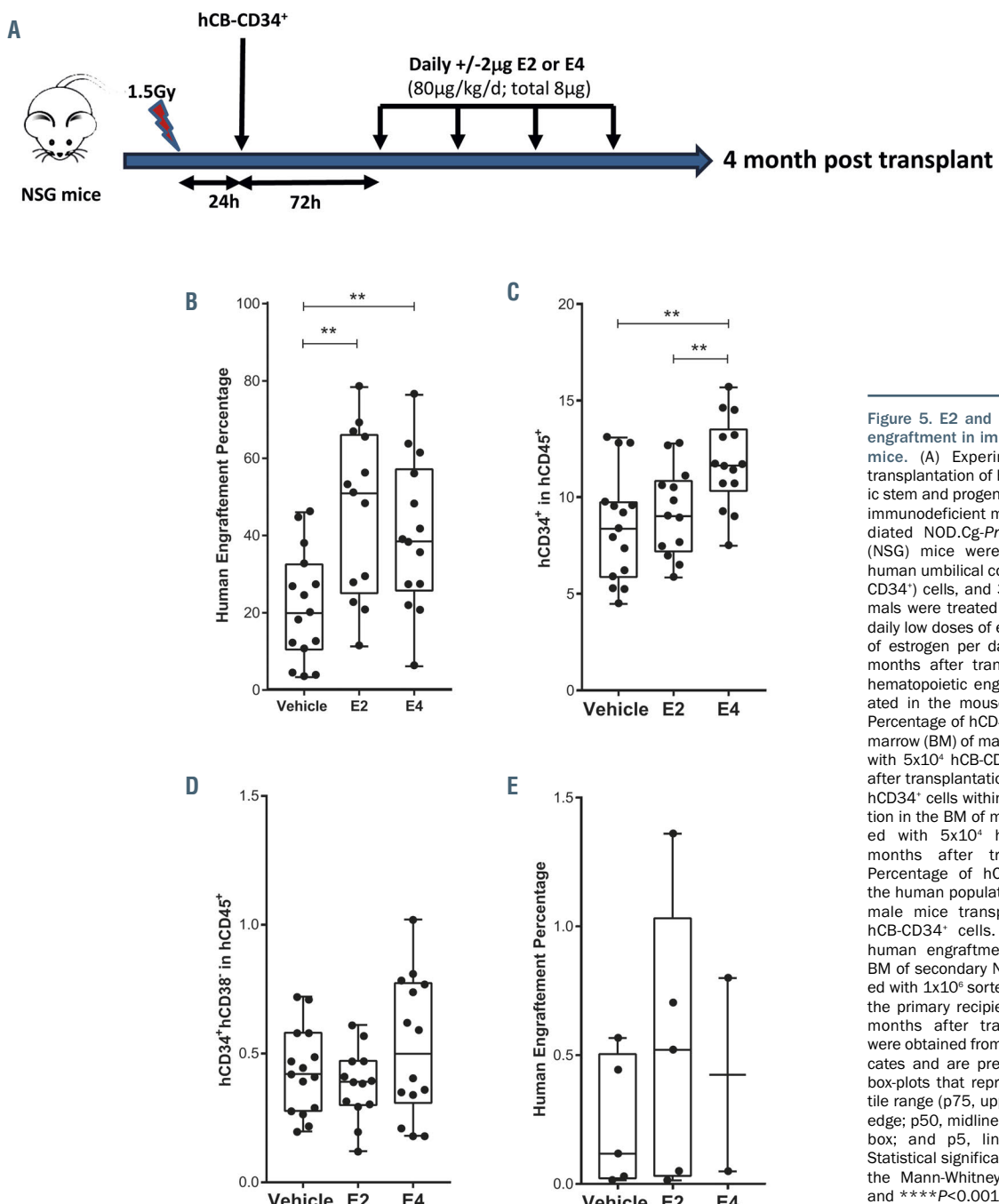


Figure 5. E2 and E4 enhance human engraftment in immunodeficient male mice. (A) Experimental scheme of transplantation of human hematopoietic stem and progenitor cells (HSPC) into immunodeficient mice. Sublethally irradiated NOD.Cg-Prkdc^{scid} Il2rg^{tm1Wj}/SzJ (NSG) mice were transplanted with human umbilical cord blood CD34⁺ (CB-CD34⁺) cells, and 3 days later the animals were treated with vehicle or with daily low doses of either E2 or E4 (2 µg of estrogen per day) for 4 days. Four months after transplantation, human hematopoietic engraftment was evaluated in the mouse bone marrow. (B) Percentage of hCD45⁺ cells in the bone marrow (BM) of male mice transplanted with 5×10^4 hCB-CD34⁺ cells 4 months after transplantation. (C) Percentage of hCD34⁺ cells within the human population in the BM of male mice transplanted with 5×10^4 hCB-CD34⁺ cells 4 months after transplantation. (D) Percentage of hCD34⁺hCD38⁻ within the human population in the BM of the male mice transplanted with 5×10^4 hCB-CD34⁺ cells. (E) Percentage of human engraftment (hCD45⁺) in the BM of secondary NSG mice transplanted with 1×10^6 sorted hCD45⁺ cells from the primary recipients and analyzed 4 months after transplantation. Data were obtained from four biological replicates and are presented by dots and box-plots that represent the interquartile range (p75, upper edge; p25, lower edge; p50, midline; p95, line above the box; and p5, line below the box). Statistical significance was analyzed by the Mann-Whitney U test: **P<0.01 and ****P<0.001.

nice. As shown in *Online Supplementary Figure S5G*, human engraftment 4 months after transplantation tended to increase in the female animals treated with either of the two estrogens, although differences between groups were not statistically significant. The percentages of hematopoietic progenitors within the human population did not show larger differences between vehicle- and estrogen-treated animals (*Online Supplementary Figure S5H*). Consequently, there is no clear effect of E2 or E4 on the engraftment of human HSPC in female animals.

E4 affects mesenchymal stromal cells within the mouse hematopoietic niche

To obtain further insight into the positive impact of estrogens on promoting human hematopoietic engraftment, we assessed whether estrogens act *in vivo* on human

HSPC to promote hematopoietic engraftment directly or indirectly through niche cells. We therefore cultured 5×10^4 CB-CD34⁺ cells with 100 nM of E2 or E4 for 4 days and transplanted the resulting cells after culture into NSG mice. As shown in Figure 6A, human engraftment of *in vitro* estrogen-treated HSPC was lower than that of vehicle-treated cells, which might indicate an indirect mechanism of estrogens in enhancing hematopoietic engraftment in NSG mice. Additionally, there was no difference in the percentage of lymphoid, myeloid or HSPC subpopulations among mice in the different groups (*Online Supplementary Figure S6A*). To gain a better understanding of the difference in engraftment between HSPC treated *in vitro* with estrogen and the *in vivo* effect of estrogens after HSC transplantation, we co-cultured 5×10^4 CB-CD34⁺ cells with human irradiated BM-MSC in the presence of

100 nM of E2 or E4 for 1 week and then transplanted the resulting cells into sublethally irradiated NSG mice. Human engraftment and lineage distribution were similar among mice in the different groups (Figure 6B; *Online Supplementary Figure S6B*), which indicated that the loss of engraftment ability due to *in vitro* estrogen-mediated expansion might be offset by the BM-MSC. Next, we examined the contribution of the hematopoietic niche to the engraftment of human HSPC after *in vivo* estrogen-treatment. To do this, we analyzed the mesenchymal and vascular endothelial compartments of the mouse BM niche 4 months after being transplanted and treated with E2 or E4. The percentages of mouse MSC (mCD140a⁺, also called Pdgfra⁺) and vascular endothelial cells (mCD144⁺, also called VE-Cadherin⁺) in the non-hematopoietic compartment were analyzed (*Online Supplementary Figure S6C*). Surprisingly, mCD140a⁺ cells, but not mCD144⁺ cells, were increased in the mice treated with E4 in comparison with vehicle-treated animals (Figure 6C and D). To focus on this finding, mice were sublethally irradiated and treated with estrogens without human HSPC transplantation. Surprisingly, there were more nucleated cells in the BM of mice treated with E4 (*Online Supplementary Figure S6F*). These mouse BM cells were cultured to study their ability to form fibroblast colony-forming units (CFU-F). We identified a tendency to more CFU-F in the BM of estrogen-treated mice than in the BM of vehicle-treated mice (Figure 6E; *Online Supplementary Figure S6G*), which might indicate a beneficial role of estrogens in improving the BM niche after irradiation.

We then evaluated whether human MSC might interact with these estrogens. So, we analyzed the expression of *ESR1* and *ESR2* in the human BM-MSC compartment by RT-PCR (Figure 6F) and immunofluorescence (Figure 6G; *Online Supplementary Figure S6H*). Both estrogen receptors were present in human BM-MSC, indicating that the presence of estrogens could influence the behavior of the human stromal cells and indirectly affect the biology and/or engraftment of human HSPC. To investigate the effect of estrogens on human BM-MSC, a limiting number of human BM-MSC were seeded and treated with estrogens and their CFU-F potential was assessed. As shown in *Online Supplementary Figure S6I*, the estrogens had no effect on human BM-MSC. The numbers of CFU-F dropped when the human BM-MSC had been previously irradiated. However, we observed an increase in the number of CFU-F when the BM-MSC were treated with estrogens after irradiation (*Online Supplementary Figure S6I*). In conclusion, estrogens, in particular E4, might facilitate and favor the hematopoietic engraftment of human progenitors through enhancing the mesenchymal compartment of the hematopoietic niche, in addition to having a direct effect on HSPC.

Discussion

The present study examines the potential use of estrogens to modify human HSPC engraftment in BM upon transplantation. On the basis of the differences in the level of human hematopoietic engraftment between female and male recipient mice (Figure 1; *Online Supplementary Figure S1*), and the expression of estrogen receptors in different subsets of human HSPC (Figure 2; *Online Supplementary*

Figure S2), we explored the impact of estrogen treatment on hematopoietic cells engraftment. E2 and E4 showed a positive effect on the expansion of these cells *in vitro* by activating the cell cycle (Figure 3; *Online Supplementary Figure S3*), with E4 being better tolerated than E2 (Figure 3; *Online Supplementary Figure S3*). Despite the modest role of these estrogens in modulating human progenitor activity *in vitro*, we found that E2, and even more E4, was able to boost human hematopoietic engraftment in immunodeficient mice (Figure 5; *Online Supplementary Figure S5*). This better performance of human HSPC in estrogen-treated animals might reflect observed gender differences. Furthermore, an apparent expansion of the mouse mesenchymal stromal compartment was identified in animals treated with E4, which may suggest an additional indirect regulation of the estrogens, enhancing human hematopoietic engraftment through niche regulation (Figure 6; *Online Supplementary Figure S6*). Thus, estrogens could act directly on HSPC as well as indirectly, through the modification of the BM stroma, or BM niche, to enhance CD34⁺ cell engraftment. These findings might be clinically relevant, since the use of E4 could facilitate HSPC transplantation when only a limited number of cells can be infused.

We have shown that estrogens improve the engraftment of human cells in immunodeficient mice, which reinforces the role of sex hormones in HSPC regulation and might explain the superior performance of female mice as recipients of hematopoietic transplants²⁶ (Figure 1). The importance of estrogens in regulating HSPC functions has been explored for a long time, without any clear conclusion being reached. E3 has been found to trap mouse hematopoietic progenitors in the liver.²⁹ E2 has been described as promoting the proliferation of very primitive mouse HSC. The increase of estrogen levels during pregnancy has also been associated with greater HSC division, higher HSC frequency and an increase in erythropoiesis.^{19,27} E2 has also been reported to expand human CB-CD34⁺ cells *in vitro*.²⁸ These data contrast with those previously described by Illing *et al.*, who found that long-term treatment of mice with E2 stimulated murine HSPC in the vascular niche but not in the endosteal niche, impairing long-term reconstitution potential.¹⁸ On the other hand, high doses of E2 suppressed hematopoiesis in mouse BM.³⁰ This negative effect caused by estrogens has also been shown by tamoxifen treatment, which increased mouse HSC proliferation, but not self-renewal, and induced apoptosis in short-term HSC and MPP.²⁴ Here, we found that human HSPC had different sensitivities to the four natural estrogens. E1 and, to a lesser extent, E2 and E3 were toxic for human HSPC (Figure 3; *Online Supplementary Figure S3*). E4 was better tolerated and was able to promote some degree of expansion of the human HSPC by activating their cell cycle and inducing less apoptosis (Figures 3 and 4; *Online Supplementary Figures S3 and S4*). These observations might explain the apparently divergent effects described previously for estrogens, since different doses and different estrogens were used in the above-mentioned reports.

We also observed that treatment with E2 or E4 *in vivo* enhanced human hematopoietic engraftment in male mice transplanted with 5×10^4 human HSPC (Figure 5B; *Online Supplementary Figure S5*), but only to a minor degree in animals transplanted with very limited numbers of CB-CD34⁺ cells (*Online Supplementary Figure 5E-G*). The apparent lack of effectiveness in female mice might be due to

the presence of endogenous estrogens in these female animals. Future experiments should be done with ovariectomized mice or taking the estrous cycle of female recipients into account to identify the real effect of estrogen treatment on HSPC in female recipients. Furthermore, E4 treatment enlarged the hCD34⁺ cell population in already boosted human hematopoietic engraftment, but it had

less impact on the hCD34⁺hCD38⁺ cell population and on secondary transplant (Figure 5D and E). Nevertheless, although the percentage of hCD34⁺hCD38⁺ cells was unmodified by estrogen treatment, the total cell number of this primitive population was increased since human engraftment was higher in estrogen-treated mice (Figure 5B and D).

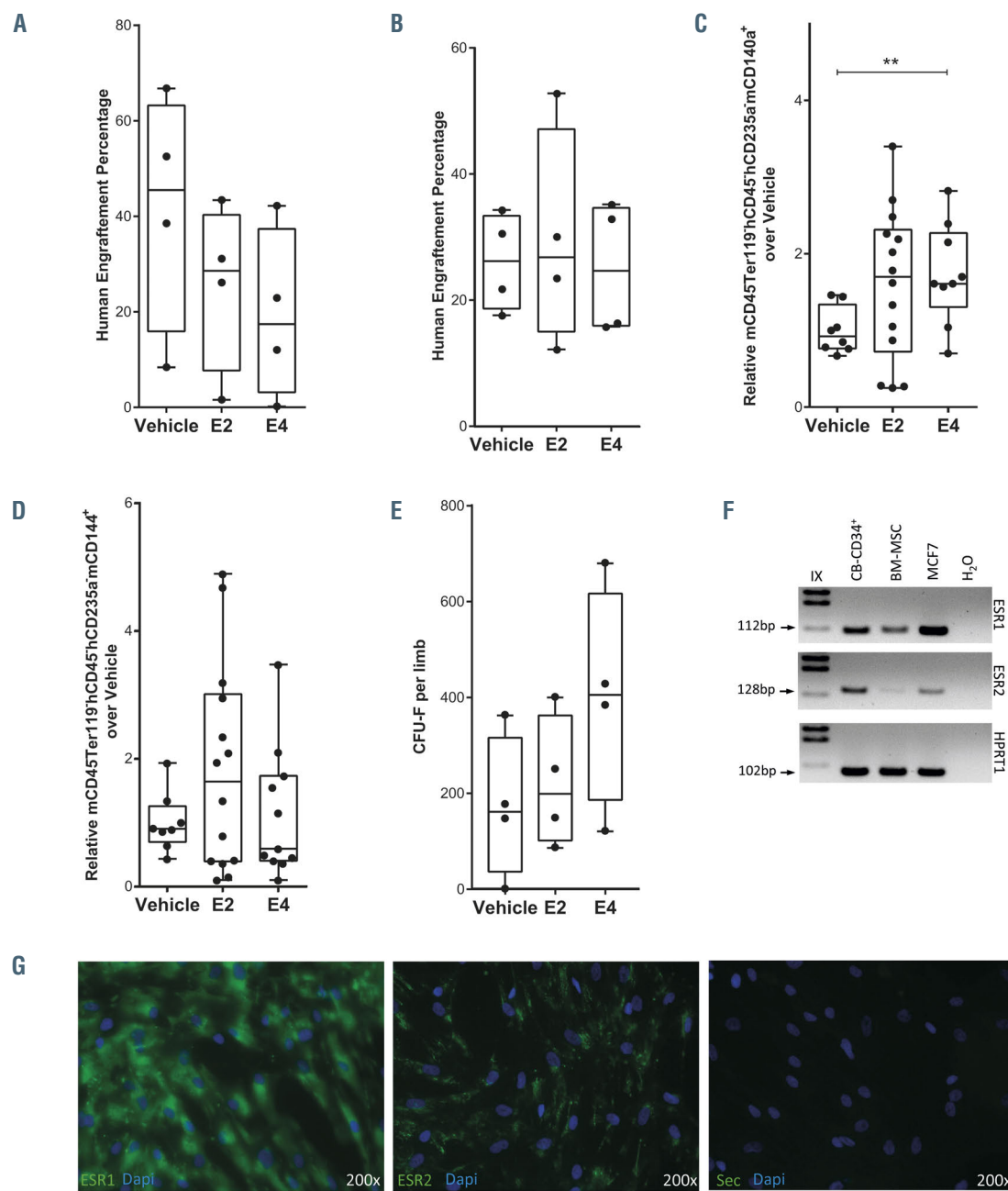


Figure 6. Estrogens modulate the hematopoietic niche. (A) Human engraftment in bone marrow (BM) of male mice transplanted with cells expanded from an initial dose of 5×10^4 hCB-CD34⁺ cells after 4 days in culture in the presence of 100 nM E2 or E4. Human engraftment was analyzed 2 months after transplantation. (B) Human engraftment in BM of male mice transplanted with cells expanded from an initial dose of 5×10^4 hCB-CD34⁺ cells after 1 week in co-culture with irradiated human BM-mesenchymal stromal cells (MSC) in the presence of 100 nM E2 or E4. Human engraftment was analyzed 3 months after transplantation. (C) Relative percentage of mouse MSC (mCD45Ter119hCD45hCD235amCD140a⁺) in the BM of male mice transplanted with 5×10^4 hCB-CD34⁺ cells, analyzed 4 months after transplantation. (D) Relative percentage of mouse vascular endothelial cells (mCD45Ter119hCD45hCD235amCD144⁺) in the BM of male mice transplanted with 5×10^4 hCB-CD34⁺ cells, analyzed 4 months after transplantation. (E) Number of fibroblast colony-forming units (CFU-F) derived from the BM of vehicle- or estrogen-treated mice after sublethal irradiation. (F) Representative agarose gel showing the quantitative real-time polymerase chain reaction products of ESR1 (top panel), ESR2 (middle panel) and HPRT1 (bottom panel) in human BM-MSC. (G) Representative immunofluorescence image of human BM-MSC stained with anti-ESR1 (green, left panel), anti-ESR2 (green, middle panel) or secondary antibody (green, right panel) and DAPI (blue). Data were obtained from three biological replicates and are presented by dots and box-plots that represent the interquartile range (p75, upper edge; p25, lower edge; p50, midline; p95, line above the box; and p5, line below the box). Statistical significance was analyzed by the Mann-Whitney U test: **p<0.01.

We have described a positive effect of E2 or E4 treatment on the engraftment of human cells, with the impact of E4 being more significant. It is important to note that E4 is synthesized exclusively by the human liver during pregnancy. It is detected at 9 weeks of pregnancy and reaches high levels in the second trimester, with concentrations rising steadily towards the end of pregnancy.¹⁶ The fetal liver is a hematopoietic organ during the last half of gestation. During the hematopoietic stage of the fetal liver, different signaling pathways are coordinated to promote both massive expansion of HSC through the activation of the HSC cycle and massive production of erythroid cells. After birth, the HSC migrate from the liver to the adult BM, where the most primitive HSC are largely quiescent.^{1,31} The concurrence of E4 synthesis in the fetal liver, when it is a hematopoietic organ, may suggest an indirect link between this estrogen and the expansion of human HSPC during pregnancy. The association between estrogens and hematopoietic development has previously been described during zebrafish development,³² in mice^{19,27} and in the hematopoietic differentiation of human induced pluripotent stem cells.²⁸ So estrogens have a clear impact on HSC emergence. Oguro *et al.* demonstrated coordination between E2 and 27-hydroxycholesterol in the regulation of hematopoiesis during pregnancy.²⁷ Consequently, we hypothesize that E4 likely plays a role in modulating early human hematopoiesis during embryonic development.

As previously reported, the observations could be attributed to an intricate regulation mediated by the estrogens.¹⁷ The complexity of estrogen signaling pathways starts with the existence of several estrogen receptors. Three of these receptors (ESR1, ESR2 and GPER³³) are expressed in hematopoietic cells, but only ESR1 has been described to play a role in the regulation of HSC.^{18,19,24} A second level of complexity is that the expression of these estrogen receptors tends to differ among hematopoietic subpopulations²⁴ (Figure 2). Moreover, different estrogens vary in their binding affinity for different estrogen receptors; for example, E2 has a 7-fold higher affinity for ESR1 (inhibition constant, $K_i=0.21$ nM) than for ESR2 ($K_i=0.015$ nM), and E4 has a 400-fold higher affinity for ESR1 ($K_i=4.9$ nM) than for ESR2 ($K_i=19$ nM).³⁴ Once the estrogen and receptor are bound, specific cell responses are triggered by two different mechanisms: (i) gene expression programs, which can be initiated through estrogen nuclear signaling, and (ii) the estrogens acting through membrane-initiated steroid signaling (MISS), which is a rapid extra-nuclear cellular response to the estrogen signal.¹⁵ These two types of estrogen signaling may also explain the differences we observed between the effects of E4 and E2, from their toxicity and expansion *in vitro* (Figure 3; *Online Supplementary Figure S3*) to their *in vivo* effects (Figure 6). E4 uncouples nuclear activation and MISS, in contrast to E2 which does not.¹⁵ For example, E4 acts as an estrogen antagonist on breast cancer cells.^{16,35} Moreover, the lower affinity of E4 for estrogen receptors, in comparison with the affinity of E2, might suggest a very limited effect of E4 on HSPC; however, the E4 doses, whose effects on HSPC were observed (Figures 3 and 4), were the same doses used by Abbot *et al.* for which ERE transcriptional activity could be detected.¹⁵ Furthermore, given that E4 lacks MISS activity, it is possible that the impact of E2 and E4 on human HSPC is due to their nuclear signaling, with similar transcriptional output, but this point will have to be analyzed in depth. Additionally, the presence of E2 or E4 increased the levels

of both ESR1 and ESR2 and modified their cellular localization. The increment of cells in S/G2/M-phase mediated by estrogens could be partially blocked by ESR1 and GPER antagonists in the case of E2, and by an ESR2 antagonist in the case of E4 (*Online Supplementary Figure S3J*). The implication of this is that different estrogen receptors in human HSPC might be involved in the signaling triggered by E2 or E4; however, this point will require more in-depth study. More interestingly, E2 might activate estrogen receptor-mediated MISS, since a clear polarized location of the estrogen receptors in the cytoplasm membrane was found (*Online Supplementary Figure S3O and P*). On the other hand, E4 might activate nuclear estrogen signaling, since E4 is unable to induce MISS¹⁵ and a clear increment of ESR2 in the cytoplasm was detected (*Online Supplementary Figure S3N*). The consequences of ESR1 and ESR2 upregulation and localization should be explored in future experiments. Additionally, Oguro *et al.*²⁷ described two different ESR1 ligands, E2 and 27-hydroxycholesterol, which regulated HSPC differently during pregnancy. Both ESR1 ligands collaborated to induce HSC proliferation, mobilization and extramedullary hematopoiesis. In a similar way, E2 and E4 might collaborate together with a differential impact on human HSPC.

We identified that the underlying mechanism mediated by estrogens is activation of the cell cycle *in vitro*, as previously described, which promotes the expansion of hematopoietic progenitors.^{19,24} However, estrogens might also have other effects, including the activation of telomerase activity to facilitate the expansion of HSPC,²⁰⁻²² or an increase of the unfolded protein response to promote hematopoietic regeneration after a proteotoxic stress, such as irradiation.^{23,36} In our *in vivo* model, E2 or E4 might activate the gene signaling involved in the cell cycle,^{19,24} telomerase activity²⁰⁻²² or unfolded protein response,²³ but these estrogens could also activate apoptosis^{24,27} when high doses are used (Figure 3; *Online Supplementary Figure S3G and H*). Surprisingly, the estrogen-mediated expansion observed *in vitro* was not enough to explain the improvement in human hematopoietic engraftment. Indeed, the *in vitro* proliferation of human HSPC induced by the estrogens was counterproductive to the enhancement of hematopoietic engraftment (Figure 6A). This might be due to the reduction of long-term engraftment ability of cycling HSPC, and the decoupling of HSPC expansion and stem cell properties *in vitro*.³⁷ As HSC quiescence, self-renewal and differentiation are controlled through intrinsic HSC signaling and extrinsic niche signaling and we observed that the co-culture of HSPC with human BM-MSC was able to expand hematopoietic cells (Figure 4) and maintain engraftment potential (Figure 6B), *in vitro* expansion of HSPC might be compensated by niche signaling. In accordance with this, estrogens could also modulate hematopoiesis by affecting the capacity of MSC to promote osteogenesis.^{30,38} Furthermore, osteogenic differentiation might favor the proliferation of HSPC.²⁵ The beneficial effect of E2 on the expansion of both HSPC and MSC was noted previously by Kitajima *et al.*³⁹ As shown in Figure 6, an increase in MSC was also detected in our *in vivo* model after E4 treatment. Besides, the presence of estrogen might favor the recovery of MSC after irradiation (Figure 6E; *Online Supplementary Figure S6E-G*), as previously described for HSPC.^{23,36} Consequently, the impact of estrogens on promoting human hematopoietic engraftment in immunodeficient mice might be mediated

through regeneration of the MSC compartment of the BM niche after irradiation, or a combined effect on human HSPC (Figures 2 and 3) and niche cells (Figure 6). We can, therefore, hypothesize that estrogens might coordinate HSPC proliferation and recovery of the BM niche in the context of HSC transplantation.

We suggest that the results reported could have some significant clinical implications. E4 has a safer therapeutic window than E2, which facilitates its clinical use.¹⁶ Additionally, E4 has been tested in several clinical trials and its safety and efficacy have been determined in different conditions, such as contraception,⁴⁰ menopause,⁴¹ osteoporosis⁴² and breast cancer.⁴³ The clinical application of E4 to modulate HSPC could, therefore, be considered for improving HSPC transplantation in the near future. The clinical use of E4 might potentially facilitate the transplantation of single cord blood units, the autologous transplantation of genetically modified HSPC to treat inherited hematopoietic diseases or in any situation in which a limited number of HSPC has to be infused. The administration of a clinically approved estrogen, such as E4, after HSPC transplantation could lead to an improvement in overall hematopoietic engraftment in the recipient.

Disclosures

JAB and JCS are consultants for Rocket Pharmaceuticals (NY,

USA). The other authors declare that they have no conflicts of interest to disclose.

Contribution

JCS and OQB conceived and designed the experiments. SFB, IO, FBA, SBM, JGM, MDR, RS, OA and OQB conducted the experiments. RY, YFS, DA and AZ provided reagents. AZ and JAB contributed with ideas. SFB, JCS and OQB wrote the manuscript.

Acknowledgments

The authors would like to thank Miguel A. Martin for the careful maintenance of NSG mice, and Norman Feltz for reviewing the manuscript.

Funding

This work was supported by grants from "Ministerio de Economía, Comercio y Competitividad y Fondo Europeo de Desarrollo Regional (FEDER)" (SAF2017-84248-P), "Fondo de Investigaciones Sanitarias, Instituto de Salud Carlos III" (RD16/0011/0011), TERCEL ("Red de Terapia Celular" of the "Instituto de Salud Carlos III") and AvanCell consortium of "Comunidad de Madrid". The authors also thank Fundación Botín for promoting translational research at the Hematopoietic Innovative Therapies Division of the CIEMAT. CIBERER is an initiative of the "Instituto de Salud Carlos III" and "Fondo Europeo de Desarrollo Regional (FEDER)".

References

- Orkin SH, Zon LI. Hematopoiesis: an evolving paradigm for stem cell biology. *Cell*. 2008;132(4):631-644.
- Wilson A, Laurenti E, Oser G, et al. Hematopoietic stem cells reversibly switch from dormancy to self-renewal during homeostasis and repair. *Cell*. 2008;135(6):1118-1129.
- Broxmeyer HE, Farag S. Background and future considerations for human cord blood hematopoietic cell transplantation, including economic concerns. *Stem Cells Dev*. 2013;22(Suppl 1):103-110.
- Lund TC, Boitano AE, Delaney CS, Shpall EJ, Wagner JE. Advances in umbilical cord blood manipulation-from niche to bedside. *Nat Rev Clin Oncol*. 2015;12(3):163-174.
- Smith AR, Wagner JE. Alternative haematopoietic stem cell sources for transplantation: place of umbilical cord blood. *Br J Haematol*. 2009;147(2):246-261.
- Zonari E, Desantis G, Petrillo C, et al. Efficient ex vivo engineering and expansion of highly purified human hematopoietic stem and progenitor cell populations for gene therapy. *Stem Cell Reports*. 2017;8(4):977-990.
- Wagner JEJ, Brunstein CG, Boitano AE, et al. Phase I/II trial of stemregenin-1 expanded umbilical cord blood hematopoietic stem cells supports testing as a stand-alone graft. *Cell Stem Cell*. 2016;18(1):144-155.
- Gori JL, Chandrasekaran D, Kowalski JP, et al. Efficient generation, purification, and expansion of CD34(+) hematopoietic progenitor cells from nonhuman primate-induced pluripotent stem cells. *Blood*. 2012;120(13):e35-44.
- Boitano AE, Wang J, Romeo R, et al. Aryl hydrocarbon receptor antagonists promote the expansion of human hematopoietic stem cells. *Science*. 2010;329(5997):1345-1348.
- Fares I, Chagraoui J, Gareau Y, et al. Cord blood expansion. Pyrimidoindole derivatives are agonists of human hematopoietic stem cell self-renewal. *Science*. 2014;345(6203):1509-1512.
- Cutler C, Multani P, Robbins D, et al. Prostaglandin-modulated umbilical cord blood hematopoietic stem cell transplantation. *Blood*. 2013;122(17):3074-3081.
- Goessling W, Allen RS, Guan X, et al. Prostaglandin E2 enhances human cord blood stem cell xenotransplants and shows long-term safety in preclinical nonhuman primate transplant models. *Cell Stem Cell*. 2011;8(4):445-458.
- Fernández-García M, Yáñez RM, Sánchez-Domínguez R, et al. Mesenchymal stromal cells enhance the engraftment of hematopoietic stem cells in an autologous mouse transplantation model. *Stem Cell Res Ther*. 2015;6(1):165.
- Perlin JR, Robertson AL, Zon LI. Efforts to enhance blood stem cell engraftment: Recent insights from zebrafish hematopoiesis. *J Exp Med*. 2017;214(10):2817-2827.
- Abot A, Fontaine C, Buscato M, et al. The uterine and vascular actions of estetrol delineate a distinctive profile of estrogen receptor α modulation, uncoupling nuclear and membrane activation. *EMBO Mol Med*. 2014;6(10):1328-1346.
- Coelingh Bennink HJT, Holinka CF, Diczfalusy E. Estetrol review: profile and potential clinical applications. *Climacteric*. 2008;11(Suppl)147-158.
- Heo H-R, Chen L, An B, Kim K-S, Ji J, Hong S-H. Hormonal regulation of hematopoietic stem cells and their niche: a focus on estrogen. *Int J Stem Cells*. 2015;8(1):18-23.
- Illing A, Liu P, Ostermay S, et al. Estradiol increases hematopoietic stem and progenitor cells independent of its actions on bone. *Haematologica*. 2012;97(8):1131-1135.
- Nakada D, Oguro H, Levi BP, et al. Oestrogen increases haematopoietic stem-cell self-renewal in females and during pregnancy. *Nature*. 2014;505(7484):555-558.
- Cha Y, Kwon SJ, Seol W, Park K-S. Estrogen receptor-alpha mediates the effects of estradiol on telomerase activity in human mesenchymal stem cells. *Mol Cells*. 2008;26(5):454-458.
- Calado RT, Yewdell WT, Wilkerson KL, et al. Sex hormones, acting on the TERT gene, increase telomerase activity in human primary hematopoietic cells. *Blood*. 2009;114(11):2236-2243.
- Yeap BB, Hui J, Knuiman MW, et al. Cross-sectional associations of sex hormones with leucocyte telomere length, a marker of biological age, in a community-based cohort of older men. *Clin Endocrinol (Oxf)*. 2019;90(4):562-569.
- Chapple RH, Hu T, Tseng Y-J, et al. ER α promotes murine hematopoietic regeneration through the Ire1 α -mediated unfolded protein response. *Elife*. 2018;7:e31159.
- Sánchez-Aguilar A, Arranz L, Martín-Pérez D, et al. Estrogen signaling selectively induces apoptosis of hematopoietic progenitors and myeloid neoplasms without harming steady-state hematopoiesis. *Cell Stem Cell*. 2014;15(6):791-804.
- Qiu X, Jin X, Shao Z, Zhao X. 17 β -estradiol induces the proliferation of hematopoietic stem cells by promoting the osteogenic differentiation of mesenchymal stem cells. *Tohoku J Exp Med*. 2014;233(2):141-148.
- Notta F, Doulatov S, Dick JE. Engraftment of human hematopoietic stem cells is more efficient in female NOD/SCID/IL-2R γ -null

recipients. *Blood*. 2010;115(18):3704-3707.

27. Oguro H, McDonald JG, Zhao Z, Umetani M, Shaul PW, Morrison SJ. 27-Hydroxycholesterol induces hematopoietic stem cell mobilization and extramedullary hematopoiesis during pregnancy. *J Clin Invest*. 2017;127(9):3392-3401.

28. Kim H-R, Lee J-H, Heo H-R, et al. Improved hematopoietic differentiation of human pluripotent stem cells via estrogen receptor signaling pathway. *Cell Biosci*. 2016;6(1):50.

29. Hayama T, Nawa Y, Ezaki T, Kotani M. Effects of estrogen on hepatic hemopoiesis in the adult mouse. *Exp Hematol*. 1983;11(7):611-617.

30. Perry MJ, Samuels A, Bird D, Tobias JH. Effects of high-dose estrogen on murine hematopoietic bone marrow precede those on osteogenesis. *Am J Physiol Endocrinol Metab* 2000;279(5):E1159-65.

31. Laird DJ, von Andrian UH, Wagers AJ. Stem cell trafficking in tissue development, growth, and disease. *Cell*. 2008;132(4):612-630.

32. Carroll KJ, Esain V, Garnaas MK, et al. Estrogen defines the dorsal-ventral limit of VEGF regulation to specify the location of the hemogenic endothelial niche. *Dev Cell*. 2014;29(4):437-453.

33. Di Vito C, Bergante S, Balduini A, et al. The oestrogen receptor GPER is expressed in human haematopoietic stem cells but not in mature megakaryocytes. *Br J Haematol*. 2010;149(1):150-152.

34. Coelingh Bennink, HJT; Bunschoten E. Pharmaceutical composition comprising estetrol derivatives for use in cancer therapy. United States Patent. 2015; US 9034854B2.

35. Gérard C, Blacher S, Communal L, et al. Estetrol is a weak estrogen antagonizing estradiol-dependent mammary gland proliferation. *J Endocrinol*. 2015;224(1):85-95.

36. Jin J, Wang Y, Wang J, et al. Impaired hematopoiesis and delayed thrombopoietic recovery following sublethal irradiation in SRC3 knockout mice. *Mol Med Rep*. 2014;9(5):1629-1633.

37. Tajer P, Pike-Overzet K, Arias S, Havenga M, Staal FJT. Ex vivo expansion of hematopoietic stem cells for therapeutic purposes: lessons from development and the niche. *Cells*. 2019;8(2):169.

38. Girasole G, Jilka RL, Passeri G, et al. 17 beta-estradiol inhibits interleukin-6 production by bone marrow-derived stromal cells and osteoblasts in vitro: a potential mechanism for the antiosteoporotic effect of estrogens. *J Clin Invest*. 1992;89(3):883-891.

39. Kitajima Y, Doi H, Ono Y, et al. Estrogen deficiency heterogeneously affects tissue specific stem cells in mice. *Sci Rep*. 2015;5:12861.

40. Kluft C, Zimmerman Y, Mawet M, et al. Reduced hemostatic effects with drospirenone-based oral contraceptives containing estetrol vs. ethinyl estradiol. *Contraception*. 2017;95(2):140-147.

41. Coelingh Bennink HJT, Verhoeven C, Zimmerman Y, Visser M, Foidart J-M, Gemzell-Danielsson K. Pharmacokinetics of the fetal estrogen estetrol in a multiple-rising-dose study in postmenopausal women. *Climacteric*. 2017;20(3):285-289.

42. Coelingh Bennink HJT, Verhoeven C, Zimmerman Y, Visser M, Foidart J-M, Gemzell-Danielsson K. Pharmacodynamic effects of the fetal estrogen estetrol in postmenopausal women: results from a multiple-rising-dose study. *Menopause*. 2017;24 (6):677-685.

43. Singer CF, Bennink HJTC, Natter C, et al. Antiestrogenic effects of the fetal estrogen estetrol in women with estrogen-receptor positive early breast cancer. *Carcinogenesis*. 2014;35(11):2447-2451.

Mobilization efficiency is critically regulated by fat via marrow PPAR δ

Tomohide Suzuki,¹ Shinichi Ishii,¹ Masakazu Shinohara,^{2,3} Yuko Kawano,^{1*} Kanako Wakahashi,^{1**} Hiroki Kawano,^{1*} Akiko Sada,¹ Kentaro Minagawa,^{1***} Michito Hamada,⁴ Satoru Takahashi,^{4,5,6,7} Tomoyuki Furuyashiki,⁸ Nguan Soon Tan,^{9,10} Toshimitsu Matsui¹¹ and Yoshio Katayama¹

¹Hematology, Department of Medicine, Kobe University Graduate School of Medicine, Kobe, Japan; ²Division of Epidemiology, Kobe University Graduate School of Medicine, Kobe, Japan; ³The Integrated Center for Mass Spectrometry, Kobe University Graduate School of Medicine, Kobe, Japan; ⁴Department of Anatomy and Embryology, Faculty of Medicine, University of Tsukuba, Tsukuba, Japan; ⁵Transborder Medical Research Center (TMRC), University of Tsukuba, Tsukuba, Japan; ⁶International Institute for Integrative Sleep Medicine (WPI-IIIS), University of Tsukuba, Tsukuba, Japan; ⁷Life Science Center, Tsukuba Advanced Research Alliance (TARA), University of Tsukuba, Tsukuba, Japan; ⁸Division of Pharmacology, Kobe University Graduate School of Medicine, Kobe, Japan; ⁹Lee Kong Chian School of Medicine, Nanyang Technological University Singapore, Singapore; ¹⁰School of Biological Sciences, Nanyang Technological University Singapore, Singapore and ¹¹Department of Hematology, Nishiwaki Municipal Hospital, Nishiwaki, Japan

Current affiliations:

^{*}YKaw and HK: Endocrine/Metabolism Division, Wilmot Cancer Institute, University of Rochester Medical Center, Rochester, NY, USA;

^{**}KW: Area of Cell and Developmental Biology, Centro Nacional de Investigaciones Cardiovasculares Carlos III (CNIC), Madrid, Spain;

^{***}KM: Hematology & Oncology Division, Penn State College of Medicine, Hershey, PA, USA.



Ferrata Storti Foundation

Haematologica 2021

Volume 106(6):1671-1683

ABSTRACT

The efficiency of mobilization of hematopoietic stem/progenitor cells from bone marrow into the circulation by granulocyte colony-stimulating factor (G-CSF) is extremely varied in humans and mice and a mechanistic explanation for poor mobilizers is lacking. A mechanism of regulating mobilization efficiency by dietary fat was assessed in mice. Compared to a normal diet, a fat-free diet for 2 weeks greatly increased mobilization. The bone marrow mRNA level of peroxisome proliferator-activated receptor δ (PPAR δ), a receptor for lipid mediators, was markedly upregulated by G-CSF in mice fed a normal diet and displayed a strong positive correlation with widely varied mobilization efficiency. It was hypothesized that the bone marrow fat ligand for PPAR δ might inhibit mobilization. A PPAR δ agonist inhibited mobilization in mice fed a normal diet and enhanced mobilization by a fat-free diet. Mice treated with a PPAR δ antagonist and chimeric mice with PPAR $\delta^{+/-}$ bone marrow showed enhanced mobilization. Immunohistochemical staining and flow cytometry revealed that bone marrow PPAR δ expression was enhanced by G-CSF mainly in mature/immature neutrophils. Analysis of bone marrow lipid mediators revealed that G-CSF treatment and a fat-free diet resulted in exhaustion of ω 3-polyunsaturated fatty acids such as eicosapentaenoic acid. Eicosapentaenoic acid induced the upregulation of genes downstream of PPAR δ , such as *Cpt1 α* and *Angptl4*, in mature/immature neutrophils *in vitro* and inhibited enhanced mobilization in mice fed with a fat-free diet *in vivo*. Treatment of wild-type mice with anti-Angptl4 antibody enhanced mobilization as well as bone marrow vascular permeability. Collectively, PPAR δ signaling in mature/immature bone marrow neutrophils induced by dietary fatty acids negatively regulates mobilization, at least partially, via Angptl4 production.

Correspondence:

YOSHIO KATAYAMA
katayama@med.kobe-u.ac.jp

Received: July 3, 2020.

Accepted: January 19, 2021.

Pre-published: February 4, 2021.

<https://doi.org/10.3324/haematol.2020.265751>

©2021 Ferrata Storti Foundation

Material published in *Haematologica* is covered by copyright. All rights are reserved to the Ferrata Storti Foundation. Use of published material is allowed under the following terms and conditions: <https://creativecommons.org/licenses/by-nc/4.0/legalcode>. Copies of published material are allowed for personal or internal use. Sharing published material for non-commercial purposes is subject to the following conditions: <https://creativecommons.org/licenses/by-nc/4.0/legalcode>, sect. 3. Reproducing and sharing published material for commercial purposes is not allowed without permission in writing from the publisher.



Introduction

Granulocyte colony-stimulating factor (G-CSF) is widely used in the clinic as a standard agent to induce the mobilization of hematopoietic stem/progenitor cells (HSPC) from bone marrow (BM) into the circulation. G-CSF-mobilized HSPC are currently a major source of cells for stem cell transplantation which is a curative therapeutic option for intractable hematologic diseases. According to the current understanding of the mechanism of G-CSF-induced mobilization, in addition to the cytokine's pharmacological effect of expanding BM neutrophils, its neurotropic action through the G-CSF receptor in the sympathetic nervous system (SNS) leads to the suppression of macrophages that support HSPC niche cell function,¹⁻³ reduction of stromal cell synthesis of factors retaining HSPC in the BM, such as CXCL12,⁴⁻⁶ and suppression of osteolineage cells through β_2 -adrenergic receptors (β_2 -AR),⁷⁻¹⁰ leading to the passive release of HSPC from the microenvironment rather than their expansion or active migration. Besides the mechanism of mobilization itself, two unfavorable clinical events in G-CSF-induced mobilization have long remained unexplained and unsolved since the clinical application of G-CSF for mobilization. First, donors/patients treated with G-CSF often complain of low-grade fever and bone pain, which can be relieved by the administration of non-steroidal anti-inflammatory drugs. Second, mobilization efficiency is widely variable, and 10% to 20% of healthy donors are poor mobilizers, such that the number of HSPC that can be harvested is insufficient for transplantation. As an explanation of the former problem, we have reported that low-grade fever (and likely bone pain) associated with the administration of G-CSF is due to prostaglandin E₂ (PGE₂) production from mature BM neutrophils stimulated by the SNS through β_3 -AR.¹¹ However, our understanding of the latter problem remains unacceptably inadequate. Poor mobilization is a particularly serious problem for healthy donors for allogeneic transplantation in the National Marrow Donor Program because they receive a certain dose of G-CSF without expected volunteer contribution to the patients. The wide range of mobilization efficiency, which occurs even in genetically identical mice, is currently unpredictable and uncontrollable. Mobilization efficiency may be partially determined by a balance between mobilization-promoting signals, such as SNS-mediated osteolineage suppression, and counteraction to mobilization, such as PGE₂ from neutrophils to support osteoblast activity.¹¹ Thus, it is clinically essential to elucidate the pathways that counteract mobilization during G-CSF treatment.

Analysis of lipid mediators in the BM lags behind that of other lipid-rich organs such as the liver and brain.^{12,13} BM fat has been suggested to modulate hematopoiesis.^{14,15} Evidence of lipid mediators of hematopoietic cells as inflammatory/resolving cells is accumulating.^{16,17} However, a precise evaluation of total BM fat contents had not been done before our previous report on PGE₂.¹¹ In addition to fat cells, the BM contains an enormous number of inflammatory cells, such as neutrophils, macrophages, and their precursors, which are constantly stimulated by many marrow factors on their way to maturation and peripheralization throughout the body. Red blood cells and their precursor erythroblasts could also be a significant reservoir of

lipid mediators.¹⁸ Given that all these cells are packed at high density in the marrow, they may actively exchange many lipid mediators to stimulate each other. This unique situation in BM makes it difficult to precisely evaluate lipid mediators in BM by flushing it with phosphate-buffered saline (PBS) or following pipetting, which immediately changes lipid metabolic cascades. We have developed a new procedure for sampling BM by flushing it directly with -20°C 100% methanol and preparing it for liquid chromatography-tandem mass spectrometry (LC-MS/MS) through which stable and precise evaluation of PGE₂ in BM was achieved.¹¹

In this study, we have applied this original method for the comprehensive analysis of marrow fat components, including not only $\omega 6$ -fatty acids/proinflammatory lipid mediators such as PGE₂ but also $\omega 3$ -fatty acids during G-CSF-induced mobilization. We found that mobilization efficiency can be enhanced by fat restriction in food. It also appeared that BM has a strong demand for certain ingested $\omega 3$ -fatty acids, which function as ligands for peroxisome proliferator-activated receptor δ (PPAR δ) in BM mature/immature neutrophils to suppress mobilization, at least partially, by regulating BM vascular permeability.

Methods

Mice

Mice were cared for in the Institute for Experimental Animals, Kobe University Graduate School of Medicine. PPAR $\delta^{-/-}$ mice were generated on a C57BL/6 background as described in the *Online Supplementary Methods*. Because all PPAR $\delta^{-/-}$ mice died *in utero*, PPAR $\delta^{+/-}$ and PPAR $\delta^{+/-}$ littermates at ages 6 to 8 weeks were used as transplant donors to generate chimeric mice. C57BL/6-CD45.1 congenic mice were purchased from The Jackson Laboratory (Bar Harbor, ME, USA) and used at ages 6 to 8 weeks. Wild-type (WT) C57BL/6 mice at ages 6 to 8 weeks were purchased from CLEA Japan (Chiba, Japan) and used for experiments after 2 weeks of acclimatization unless otherwise indicated. Male mice were used in all experiments. Mice were fed with a normal diet (ND; CE-2, CLEA Japan) consisting, on average, of 4.69% fat, 24.90% protein, and 51.00% carbohydrates, yielding a total calorie content of 3.45 kcal/g, except for fat-free diet (FFD; CLEA Japan) experiments. The FFD consisted of 0.72% fat, 17.60% protein, and 63.49% carbohydrates by weight, yielding the same total calorie value as the ND, and was started at ages 8 to 10 weeks after 2 weeks of acclimatization. Animals were maintained under specific pathogen-free conditions and on a 12 h light/12 h dark cycle. All animal studies were approved by the Animal Care and Use Committee of Kobe University.

Statistical analysis

All data were pooled from at least three independent experiments. All values were reported as the mean \pm standard error of the mean (SEM). The statistical analyses were conducted using a two-tailed unpaired Student *t*-test, the Mann-Whitney U test, a one-way analysis of variance (ANOVA) test with the Tukey *post-hoc* procedure, and Pearson correlation coefficient. No samples or animals were excluded from the analyses. Animals were randomly assigned to groups. Statistical significance was assessed with Prism (GraphPad Software, San Diego, CA, USA) and defined as *P*<0.05.

Detailed descriptions of the methods for the other procedures are provided in the *Online Supplementary Methods*.

Results

A short-term fat-free diet enhances mobilization efficiency

To examine the effect of insufficient fat intake on mobilization, WT C57BL/6 male mice were fed with a FFD, containing sufficient calories with protein and all known vitamins but without fat, or a ND for 2 weeks. The body weight of mice fed with the FFD for 2 weeks was comparable to that of the mice fed with the ND (24.71 ± 0.32 and 24.14 ± 0.35 g, respectively; $n=11$). The administration of either G-CSF (8 divided doses, every 12 h, 125 μ g/kg/dose, s.c.) or vehicle (PBS/bovine serum albumin [BSA]) was followed after this period with the continuation of the same diet. This period of fat restriction was reported to be safe with regard to sequelae associated with deficiency of essential fatty acids.^{19,20} This simple regimen had a dramatic effect, with the number of hematopoietic progenitor cells (HPC) being increased in the circulation compared to that in mice fed with a ND, as assessed by lineage Sca-1⁺c-kit⁺ (LSK) cells and colony-forming units in culture (CFU-C) (Figure 1A and B; *Online Supplementary Figure S1A*) with no alteration in BM HPC (*Online Supplementary Figure S1B*). Enhanced mobilization was also confirmed in hematopoietic stem cells (HSC), as assessed by long-term competitive repopulation for 6 months (Figure 1C). Thus,

a short-term deficit in fat intake is a promising method to enhance mobilization efficiency.

Marrow PPAR δ expression correlates with mobilization efficiency

Enhanced mobilization was unlikely due to the alteration of known key players in BM microenvironment for mobilization, such as osteolineage cell activity and a chemokine, because mRNA levels of Runx2, osteocalcin, and CXCL12 in BM cells after G-CSF treatment were comparable between animals fed the FFD or the ND (*Online Supplementary Figure S2*). According to this observation, we hypothesized that some lipid mediators from food intake might play a role in the BM to inhibit mobilization, and that a FFD led to a lack of these BM lipid mediators.

We first searched for a possible receptor that could induce this inhibitory signal. The PPAR family consists of fatty acid ligand-activated transcription factors.²¹ Among all three PPAR, α , γ , and δ (β/δ), in BM cells, PPAR α mRNA was unchanged. Consistent with the previously reported suppression of PPAR γ in CXCL12-abundant reticular cells by G-CSF,²² PPAR γ mRNA was significantly suppressed after G-CSF treatment (Figure 2A). Meanwhile, PPAR δ mRNA displayed the highest expression in the steady state and increased dramatically after G-CSF mobilization

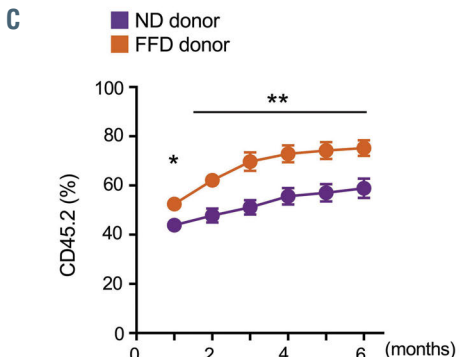
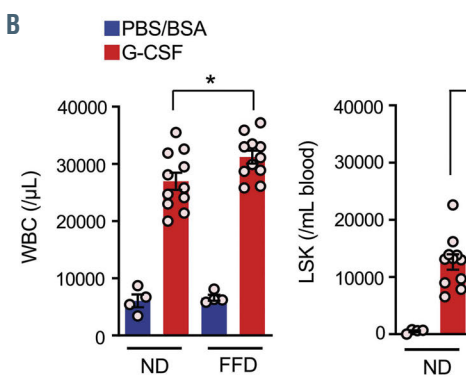
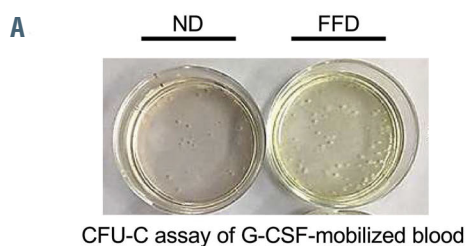


Figure 1. Short-term fat restriction enhanced hematopoietic stem/progenitor cell mobilization by granulocyte colony-stimulating factor. (A) Macrophotographs of culture dishes (35 mm) showing the results of the colony-forming units in culture (CFU-C) assay for mobilization of cells into the peripheral blood (20 μ L) following eight doses of granulocyte colony-stimulating factor (G-CSF). ND: normal diet, FFD: fat-free diet. (B) Mobilization efficiency assessed by the presence of white blood cells (WBC), lineage Sca-1⁺c-kit⁺ (LSK) cells, and CFU-C in the blood ($n=4$ for group treated with phosphate-buffered saline (PBS)/bovine serum albumin (BSA) and $n=10-11$ for the group treated with G-CSF). (C) Hematopoietic stem cell activity assessed by a long-term competitive repopulating assay of mobilized blood. Repopulating units (RU) were evaluated at 6 months after competitive transplantation ($n=6$). Representative pictures or combined data from at least three independent experiments are shown. Data are mean \pm standard error of mean. * $P<0.05$, ** $P<0.01$, *** $P<0.001$ (Student *t* test and Mann-Whitney *U* test).

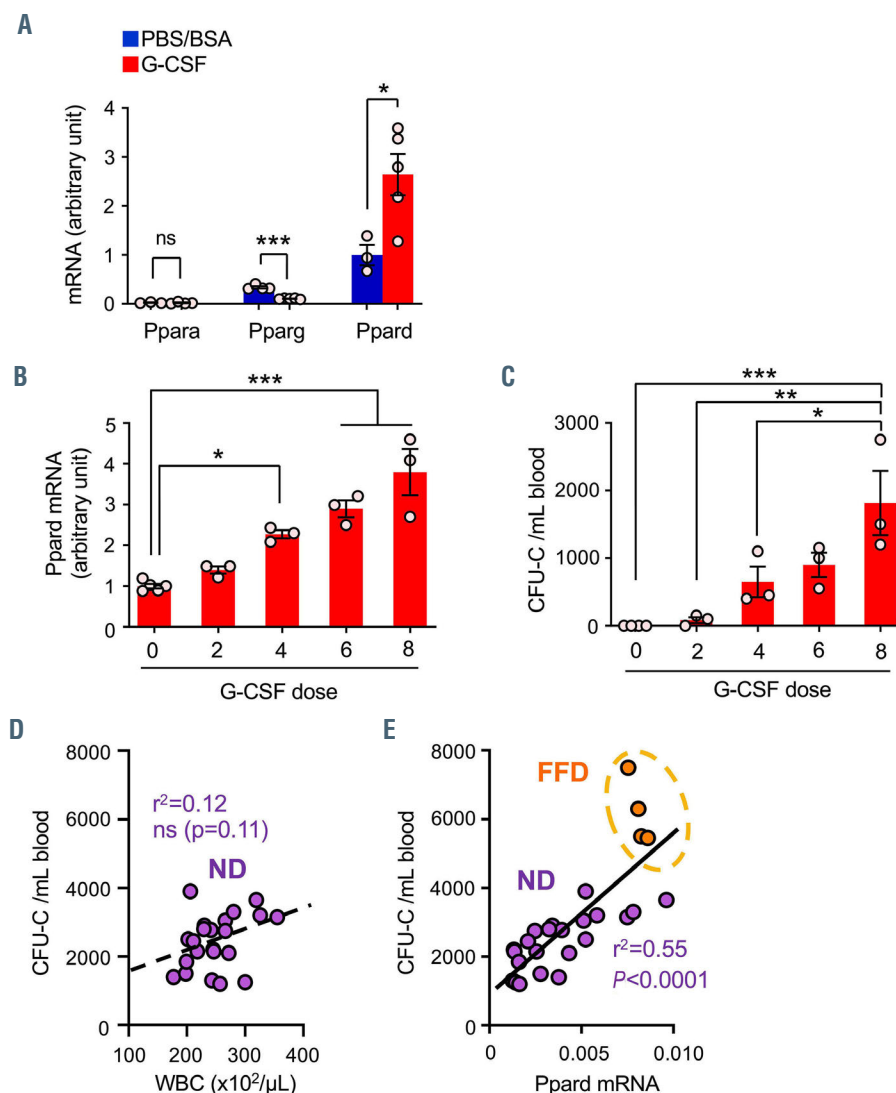


Figure 2. Strong correlation between bone marrow PPAR δ mRNA and mobilization efficacy. (A) Alteration of PPAR family mRNA in bone marrow (BM) cells during granulocyte colony-stimulating factor (G-CSF) mobilization ($n=3-5$). (B, C) Stepwise increase along with increasing G-CSF doses in (B) PPAR δ mRNA in BM cells and (C) colony-forming units in culture (CFU-C) in the blood ($n=3-5$). (D, E) Correlation of mobilization efficiency of CFU-C with (D) white blood cell (WBC) in the blood and (E) PPAR δ mRNA in BM cells in mice fed with a normal diet (ND, violet dots; $n=22$) or a fat-free diet (FFD, orange dots; $n=4$). ns: not significant. Combined data from at least three independent experiments are shown. Data are mean \pm standard error of mean. * $P<0.05$, ** $P<0.01$, *** $P<0.001$ (Student *t* test, analysis of variance, and Pearson correlation coefficient).

(Figure 2A). The increase in the expression of BM PPAR δ and mobilized HPC in the blood was dependent on the number of G-CSF doses (Figure 2B and C). Based on these data, we analyzed the correlation between mobilization efficiency and BM PPAR δ mRNA expression in a subset of C57BL/6 male mice fed with a ND after eight doses of G-CSF. The number of mobilized CFU-C varied greatly (range, 1200-3900/mL blood), and white blood cell count showed only a correlation trend (Figure 2D). Although the correlation between mobilized LSK cells and BM PPAR δ mRNA was weak and not statistically significant (*Online Supplementary Figure S3*), mobilization efficiency by CFU-C correlated strongly with BM PPAR δ mRNA (Figure 2E, violet dots). We also performed the same analysis in a subset of mice fed with the FFD. Consistent with this correlation, both mobilization efficiency and BM PPAR δ mRNA were higher than those of the best mobilizer mice fed the ND (Figure 2E, orange dots). Thus, in G-CSF mobilization, higher expression of BM PPAR δ is itself a marker of better mobilization. More importantly, this higher mobilization efficiency was likely due to the lack of signaling of this fatty acid ligand-activated transcription factor as a result of the insufficient supply of fat in the BM.

Next, we tried to identify the cell types that express

PPAR δ protein in BM. Immunohistochemical staining revealed clearly increased PPAR δ expression after eight doses of G-CSF treatment. Morphologically, myeloid lineage cells, which were relatively large with various segmental shaped nuclei, were positive, whereas small round lymphocytes with little cytoplasm were negative for PPAR δ (Figure 3A). PPAR δ protein and mRNA expression was also evaluated in sorted myeloid cell fractions. Flow cytometric analysis revealed that all three major myeloid populations in the BM, i.e., mature neutrophils ($CD11b^+Ly6G^{high}F4/80^{low}$) immature neutrophils ($CD11b^+Ly6G^{dull}F4/80^{low}$) and monocytes/macrophages ($CD11b^+Ly6G^{dull}F4/80^{high}$), showed high expression in steady-state, and both mature and immature neutrophils displayed a significant increase in PPAR δ protein and mRNA following G-CSF treatment (Figure 3B-D). In contrast, PPAR δ protein expression in these three myeloid fractions in peripheral blood was observed in only minor populations and it was not increased by G-CSF treatment (*Online Supplementary Figure S4*), indicating the marrow-specific role of PPAR δ .

Next, the alteration of BM PPAR δ mRNA expression by the depletion of mature neutrophils was examined using the anti-Ly6G antibody, 1A8 (*Online Supplementary Figures*

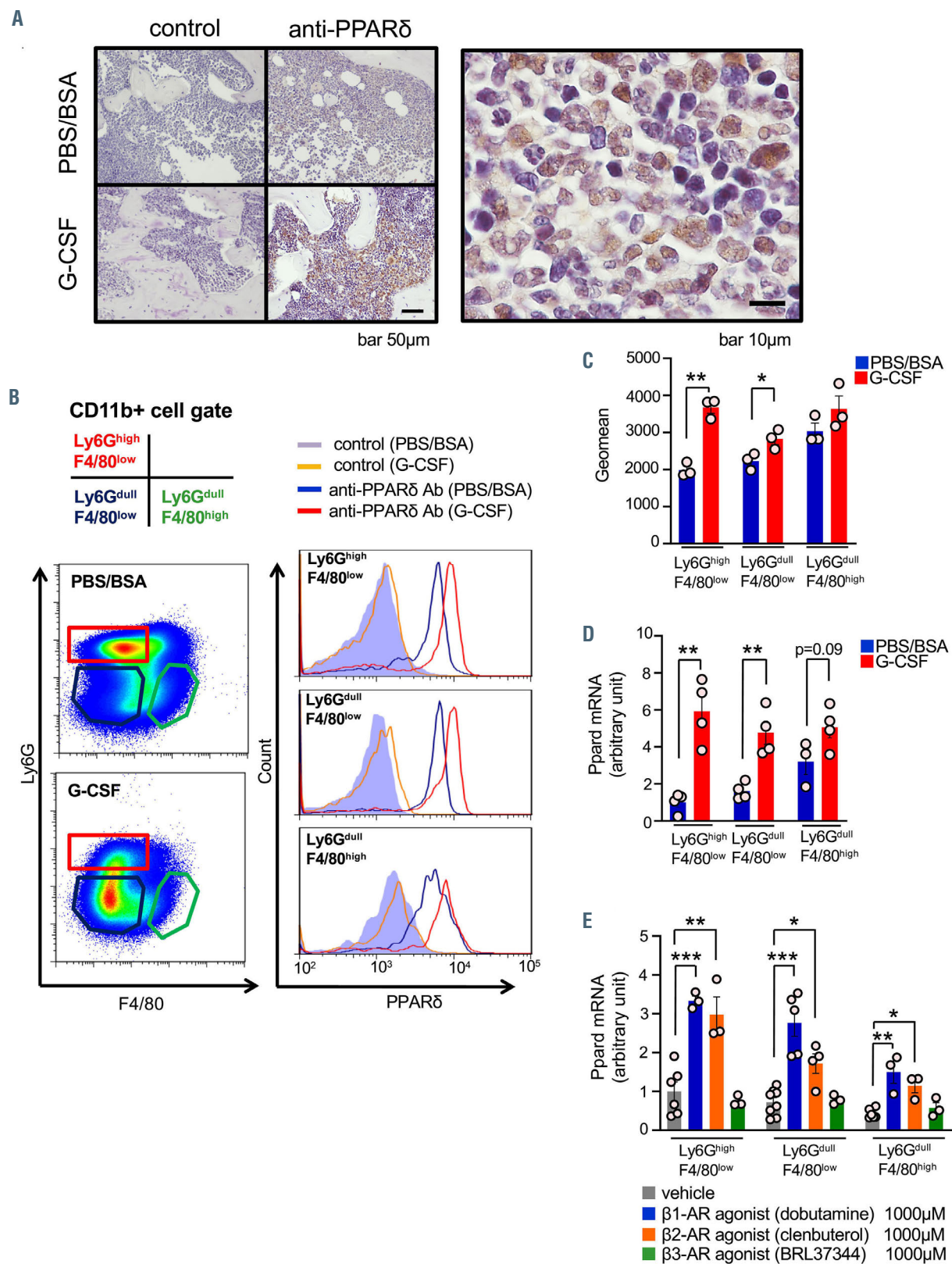


Figure 3. PPAR δ expression in bone marrow myeloid cells. (A) Immunohistochemical staining for PPAR δ in bone marrow (BM) sections from mice after treatment with eight doses of phosphate-buffered saline (PBS)/bovine serum albumin (BSA) or granulocyte colony-stimulating factor (G-CSF). Right panel shows BM PPAR δ staining after G-CSF at a higher magnification. (B, C) Flow cytometric analysis of PPAR δ in BM major myeloid populations (dot plot profiles) after treatment with eight doses of PBS/BSA or G-CSF shown in (B) as representative histograms and in (C) as geometric mean values (n=3-4). (D) PPAR δ mRNA expression in sorted BM major myeloid populations after treatment with eight doses of PBS/BSA or G-CSF (n=3-4). (E) Alteration of PPAR δ mRNA expression in sorted major myeloid populations from steady-state BM after *in vitro* treatment with selective agonists for each β -adrenergic receptor (β -AR) (dobutamine, clenbuterol, and BRL37344 for β_1 , β_2 , and β_3 -AR, respectively; n=3-8). Representative pictures or combined data from at least three independent experiments are shown. Data are mean \pm standard error of mean. *P<0.05, **P<0.01, ***P<0.001 (Student *t* test and analysis of variance).

S5 and *S6*). Without depletion, the absolute numbers of mature and immature neutrophils were comparable in steady-state BM, while the number of immature neutrophils was greatly increased and the number of mature neutrophils decreased by G-CSF treatment (*Online Supplementary Figure S6A*). The vast majority of increased neutrophils in peripheral blood following G-CSF treatment were also immature neutrophils (*Online Supplementary Figure S6B*). With selective depletion of mature neutrophils, the number of immature neutrophils in the BM was greatly increased without G-CSF treatment and the mobilization of both immature neutrophils and HPC (LSK cells and CFU-C) by G-CSF was slightly decreased (*Online Supplementary Figure S6A-H*), with no significant alteration of BM PPAR δ mRNA (*Online Supplementary Figure S6*). Thus, the cell population that mediated the increase of BM PPAR δ mRNA in response to G-CSF was not restricted to mature neutrophils.

In addition to myeloid cell fractions, the upregulation of PPAR δ mRNA was assessed in sorted BM CD45Ter119 $^+$ cells (non-hematopoietic [stromal] cells), LSK cells, B220 $^+$ B lymphocytes, and CD3 $^+$ T lymphocytes. These investigations suggested that some nonmyeloid cell fractions, such as stromal cells and T cells, might contribute partially to the increase of BM PPAR δ mRNA by G-CSF treatment (*Online Supplementary Figure S7*).

We assessed the signals that increase PPAR δ expression *in vitro* using the neutrophil precursor cell line 32D. As reported previously, BM is richly innervated with sympathetic nerves that regulate mobilization via suppression of the osteoblastic microenvironment through β_2 -AR stimulation by catecholamines and a marrow lipid mediator from mature neutrophils through β_3 -AR stimulation.⁷⁻¹¹ The pan- β -AR agonist isoproterenol, but not G-CSF, was an inducer of PPAR δ mRNA (*Online Supplementary Figure S8A*). Among all three β -AR (β_1 , β_2 , and β_3 -AR) agonists, the β_1 -AR agonist dobutamine recapitulated the effect of isoproterenol, significantly increasing PPAR δ mRNA, and the β_2 -AR agonist clenbuterol also showed a trend to induce PPAR δ mRNA, albeit to a lesser extent (*Online Supplementary Figure S8B*). This observation was further confirmed at the protein level by flow cytometry (*Online Supplementary Figure S8C*). The increase of PPAR δ mRNA by β_1 / β_2 -AR agonists was also confirmed in sorted BM mature/immature neutrophils and monocytes/macrophages (Figure 3E).

Thus, marrow PPAR δ expression strongly correlates with mobilization efficiency and is enhanced mainly in myeloid cells, particularly in neutrophil lineage cells, by G-CSF-induced high sympathetic tone, likely through β_1 / β_2 -AR.

Marrow PPAR δ signaling negatively regulates mobilization efficiency

Because FFD-G-CSF resulted in the upregulation of both BM PPAR δ expression and mobilization efficiency (Figure 2E, orange dots), greater mobilization was likely achieved via reduced PPAR δ activity due to the lack of natural fat ligands in the BM. In other words, marrow PPAR δ signaling might be a negative regulator of mobilization. We next sought to explore whether the modulation of PPAR δ signaling regulates HPC mobilization. The administration of the PPAR δ agonist GW501516 inhibited G-CSF-induced mobilization with no alteration in BM HPC (Figure 4A; *Online Supplementary Figure S9A*). In G-CSF-treated mice, mRNA

expression of major downstream genes of PPAR δ signaling such as carnitine palmitoyltransferase-1 α (Cpt1 α) and angiopoietin-like protein 4 (Angptl4) in BM was significantly increased by GW501516, suggesting that the PPAR δ agonist worked directly in BM cells (Figure 4B). Conversely, the administration of the PPAR δ antagonist GSK3787 enhanced G-CSF-induced mobilization through the inhibition of PPAR δ signaling in BM cells (Figure 4C and D; *Online Supplementary Figure S9B*). Furthermore, chimeric mice generated by the transplantation of BM cells from PPAR δ heterozygous deficient mice into lethally irradiated WT mice showed significantly increased mobilization and lower mRNA expression of Cpt1 α and Angptl4 in BM cells (Figure 4E and F; *Online Supplementary Figure S9C*). GW501516 also significantly inhibited the enhanced mobilization of CFU-C by the FFD (Figure 4G; *Online Supplementary Figure S9D*). These results suggest that PPAR δ signaling in BM cells is indeed a negative regulator of mobilization.

Certain ω 3-fatty acids are PPAR δ ligands

We have previously reported an original method of sampling BM in which lipids in the marrow can be stably and precisely evaluated.¹¹ Using this method combined with LC-MS/MS, a series of ω 3- and ω 6-polyunsaturated fatty acids (PUFA) in BM were enumerated in mice fed with the ND or FFD in G-CSF mobilization. In Figure 5A, ω 3-PUFA, such as eicosapentaenoic acid (EPA), docosahexaenoic acid (DHA), and their derivatives, were drastically decreased by eight doses of G-CSF and/or FFD, whereas ω 6-PUFA, including arachidonic acid and associated pro-inflammatory lipid mediators, were unchanged (Figure 5B). These observations suggest that BM requires a continuous supply of ω 3-fatty acids from diet, and that G-CSF treatment likely triggers strong consumption of ω 3-fatty acids in BM. Indeed, similarly to the PPAR δ agonist GW501516, EPA- and DHA-induced PPAR δ signaling in 32D cells upregulated Cpt1 α and Angptl4 mRNA expression (*Online Supplementary Figure S10A* and B). This effect, particularly with EPA, was significantly inhibited by the PPAR δ antagonist GSK3787 (*Online Supplementary Figure S10C*). Among sorted BM myeloid cells, EPA, but not DHA, significantly upregulated PPAR δ mRNA expression in mature/immature neutrophils *in vitro* (*Online Supplementary Figure S10D*). EPA, and to a lesser extent also DHA, upregulated Cpt1 α and Angptl4 mRNA expression in these cells, and this effect was inhibited by GSK3787 (Figure 6A). These results suggest that EPA (and/or its metabolites) may be a functional fatty acid ligand for PPAR δ in neutrophils and their precursors.

In concordance, EPA administration *in vivo* to normal mice partially attenuated the enhanced mobilization induced by a FFD (Figure 6B; *Online Supplementary Figure S11A*). We repeated the same experiment in chimeric mice with PPAR $\delta^{+/+}$ or PPAR $\delta^{-/-}$ BM. Consistently, in PPAR $\delta^{+/+}$ BM chimera, EPA administration showed a trend to partial reduction in CFU-C mobilization (Figure 6C; *Online Supplementary Figure S11B*). In PPAR $\delta^{-/-}$ BM chimera, however, mobilization efficiency in the FFD condition was further enhanced, and this effect was greatly inhibited by EPA (Figure 6C; *Online Supplementary Figure S11B*). These results suggest that BM in the FFD condition still contains lipid mediators that function as PPAR δ ligands, and that EPA may also use pathways other than PPAR δ to inhibit mobilization.

Thus, a certain ω 3-fatty acid, partially as a natural ligand

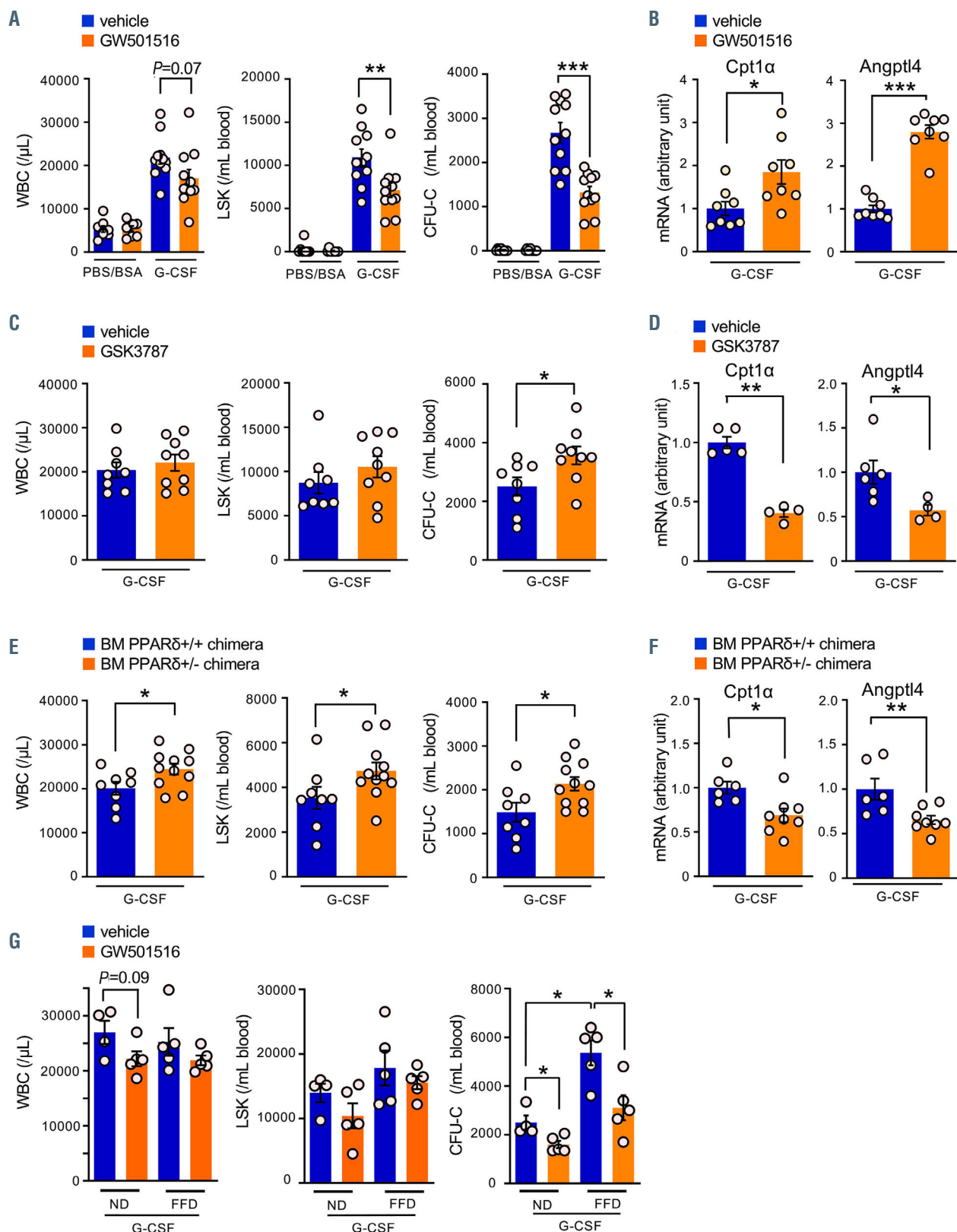


Figure 4. Regulation of granulocyte colony-stimulating factor-induced mobilization by PPAR δ signaling. (A, B) Mobilization efficiency modulated by the PPAR δ agonist (GW501516) of (A) white blood cells (WBC), lineageSca-1 $^+$ ckit $^+$ (LSK) cells, and colony-forming units in culture (CFU-C) in the blood (n=8 for the group treated with phosphate-buffered saline [PBS]/bovine serum albumin [BSA] and n=11 for the group treated with granulocyte colony-stimulating factor (G-CSF) and (B) mRNA expression of Cpt1 α and Angptl4 in bone marrow (BM) cells (n=8). (C, D) Mobilization efficiency modulated by the PPAR δ antagonist (GSK3787) in (C) WBC, LSK, and CFU-C in the blood (n=8-9) and (D) mRNA expression of Cpt1 α and Angptl4 in BM cells (n=4-6). (E, F) Mobilization efficiency in BM PPAR δ -/- chimeric mice in (E) WBC, LSK, and CFU-C in the blood (n=8-11) and (F) mRNA expression of Cpt1 α and Angptl4 in BM cells (n=6-8). (G) Modulation of mobilization (WBC, LSK, and CFU-C) by the PPAR δ agonist (GW501516) in mice fed with a normal diet (ND) or a fat-free diet (FFD) (n=4-5). Combined data from at least three independent experiments are shown. Data are mean \pm standard error of the mean. * $P<0.05$, ** $P<0.01$, *** $P<0.001$ (Student *t* test, analysis of variance, and Mann-Whitney *U* test).

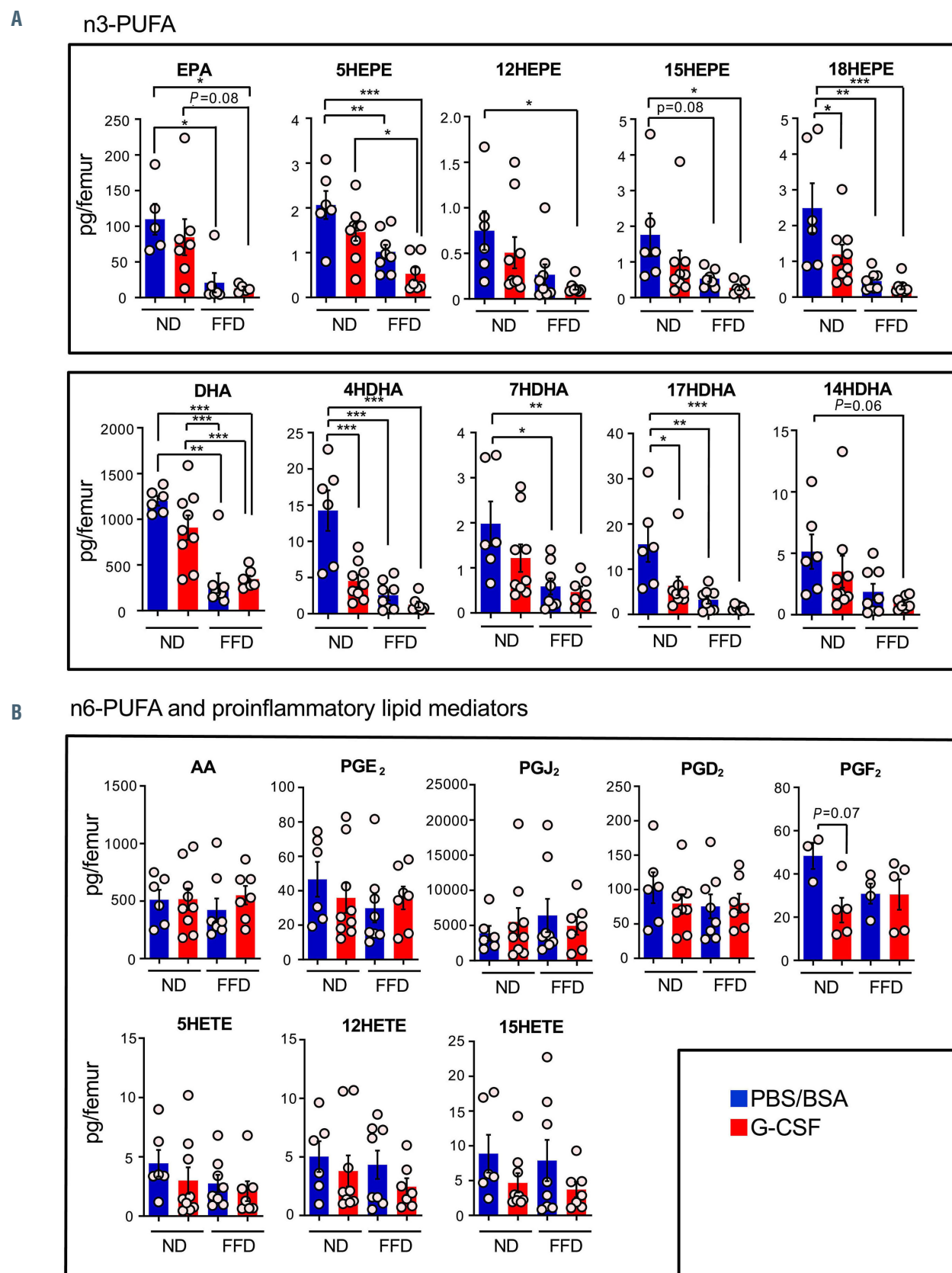


Figure 5. Lipid composition of whole bone marrow during mobilization. Analysis of lipid mediators in whole BM sampled at -20°C with 100% methanol by liquid chromatography and tandem mass spectroscopy after eight doses of phosphate-buffered saline (PBS)/bovine serum albumin (BSA) or granulocyte colony-stimulating factor (G-CSF) in mice fed a normal diet (ND) or fat-free diet (FFD) for representative (A) ω 3-fatty acids and (B) ω 6-fatty acids (n=3-9). Combined data from at least three independent experiments are shown. Data are mean \pm standard error of mean. *P<0.05, **P<0.01, ***P<0.001 (analysis of variance). PUFA: polyunsaturated fatty acids; EPA: eicosapentaenoic acid; HEPE: hydroxyeicosapentaenoic acid; DHA: docosahexaenoic acid; HDHA: hydroxydocosahexaenoic acid; AA: arachidonic acid; PG: prostaglandin, HETE: hydroxy-eicosatetraenoic acid

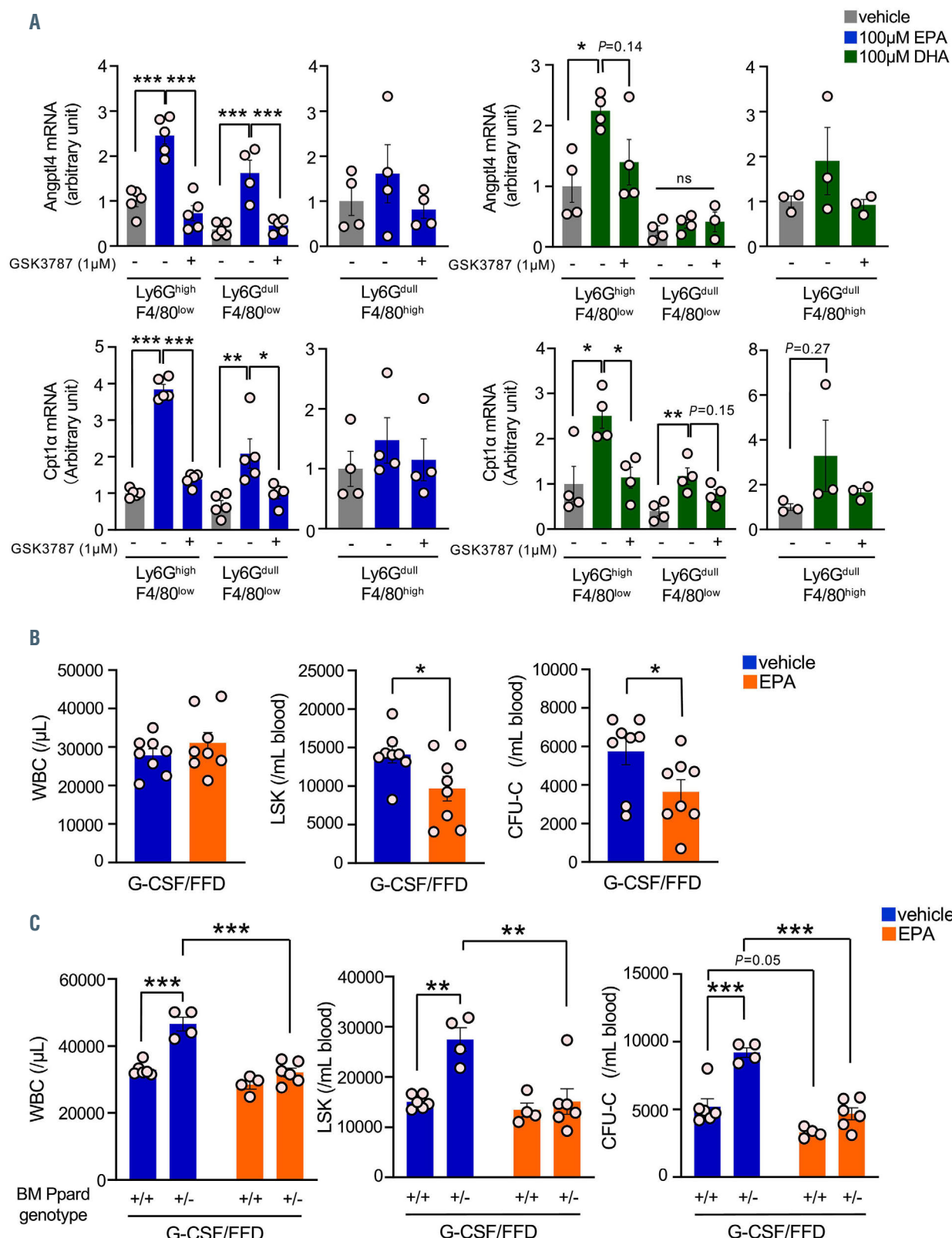


Figure 6. Function of ω -3-fatty acids as PPAR δ ligands *in vitro* and *in vivo*. (A) Alteration of PPAR δ downstream genes by eicosapentaenoic acid (EPA)/docosahexaenoic acid (DHA) in sorted major myeloid populations from steady-state bone marrow (BM) *in vitro* and its interference by the PPAR δ antagonist GSK3787 (n=3-5). (B) Modulation of granulocyte colony-stimulating factor (G-CSF)-induced mobilization by EPA administration in normal mice fed a fat-free diet (FFD) as assessed by white blood cells (WBC), lineageSca-1⁺c-kit⁺ (LSK) cells and colony-forming units in culture (CFU-C) in the blood (n=8). (C) Modulation of G-CSF-induced mobilization by EPA administration in chimeric mice with PPAR δ ^{+/+} or PPAR δ ^{-/-} BM fed a FFD as assessed by WBC, LSK and CFU-C in the blood (n=4-6). The FFD was started 8 weeks after BM transplantation and G-CSF was started 2 weeks after the initiation of the FFD. Combined data from at least three independent experiments are shown. Data are mean \pm standard error of mean. *P<0.05, **P<0.01, ***P<0.001 (Student *t* test and analysis of variance).

for BM PPAR δ , is a dietary component able to suppress mobilization.

PPAR δ -induced Angptl4 suppresses mobilization

As a downstream molecule of PPAR δ signaling, Angptl4 regulates blood vessel permeability leading to the modulation of cell migration, such as tumor metastasis.^{23,24} We first confirmed that G-CSF upregulated the level of Angptl4 protein in BM extracellular fluid, which showed a trend of further enhancement following treatment with the PPAR δ agonist GW501516 (Figure 7A). In contrast, the level of Angptl4 protein in the blood was not changed by G-CSF treatment (*Online Supplementary Figure S12A*). G-CSF treatment together with GW501516 significantly increased Angptl4 mRNA expression in BM myeloid cells (*Online Supplementary Figure S12B*). The analysis of BM samples from mice used in mobilization experiments with the FFD and GW501516, as shown in Figure 4G, revealed that Angptl4 and Cpt1 α mRNA levels in BM after G-CSF were decreased by the FFD but greatly increased by GW501516 treatment (*Online Supplementary Figure S12C*). Thus, the induction and suppression of Angptl4 mRNA expression in BM were likely associated with the suppression and enhancement of mobilization, respectively.

Indeed, this increase in Angptl4 protein in BM caused by G-CSF inhibited mobilization, because administration of the anti-Angptl4 neutralizing antibody (3F4F5)²⁵ significantly increased mobilization efficiency, as assessed by CFU-C, with a similar, but not statistically significant, trend of increased LSK cell mobilization (Figure 7B; *Online Supplementary Figure S12D*). BM vascular permeability, as assessed by Evans blue dye incorporation in BM, was decreased by GW501516 and/or G-CSF (*Online Supplementary Figure S13*), and significantly enhanced by the addition of the anti-Angptl4 antibody to G-CSF (Figure 7C), suggesting that Angptl4 may inhibit mobilization by, at least partially, suppressing BM vascular permeability. Therefore, these results suggest that Angptl4, produced mainly by BM neutrophils and their precursors via PPAR δ signaling, inhibits G-CSF mobilization.

Discussion

The functions of BM as a reservoir and consumer of orally ingested fat have not been thoroughly studied. In this study, we have demonstrated that BM fat is strongly influenced by diet. In particular, ω 3-PUFA and their derivatives are almost exhausted by a 2-week restriction of fat contents in food. BM myeloid cells such as neutrophils and their precursors have a strong demand for ω 3-PUFA, including EPA, which acts, at least partially, as a PPAR δ ligand to suppress HSC mobilization via Angptl4 production. A widely variable mobilization efficiency in response to G-CSF in healthy individuals, including a certain percentage of poor mobilizers, might partially originate from the BM fat profile in association with oral fat intake. Although it is not clear whether these findings in mice are applicable to mobilization in humans, the modulation of dietary fat might be a potential strategy to reduce the risk of poor mobilizers which could be examined in a future clinical study.

In this study, we demonstrated that neutrophils and their precursors, which are the major populations in BM, are strong consumers of ω 3-PUFA, particularly after G-

CSF treatment. It was reported that dietary ω 3-PUFA are rapidly incorporated into phospholipids, such as phosphatidylethanolamine and phosphatidylcholine, of human neutrophils²⁶ and inhibit these cells' inflammatory responses, such as leukotriene B₄ production and chemotaxis.^{27,28} However, the signaling receptor for ω 3-PUFA in this pathway is unclear. It was reported that certain ω 6-PUFA, 15d-PGJ₂, acted as ligands for PPAR γ to inhibit neutrophil chemotaxis by upregulating the sepsis-induced cytokines tumor necrosis factor- α and interleukin-4.²⁹ Interestingly, a biochemical study has shown that 15d-PGJ₂ can also stimulate PPAR δ to a similar magnitude as EPA.²¹ Based on our study in BM neutrophils and the reported strong interaction of EPA with PPAR δ ,^{21,30} neutrophils in circulation may also partially utilize ω 3-PUFA as PPAR δ ligands to diminish inflammation. EPA is also reported to prevent neutrophil migration across the endothelium as a supplier of PGD₃, which antagonizes PGD receptor DP-1 on neutrophils.³¹ This pathway might be one of the PPAR δ -independent EPA functions in the suppression of mobilization. In our current study, BM lipid mediators were assessed after eight doses of G-CSF, and the transition during the G-CSF treatment was not evaluated. Although no change was observed in BM ω 6-PUFA after eight doses of G-CSF, we have previously reported that the level of BM PGE₂ was increased after four doses.¹¹ These data are consistent with the transition of body temperature during G-CSF treatment, which increased after four doses and returned to normal levels at eight doses.¹¹ Thus, the contribution of BM ω 6-PUFA in mobilization cannot be excluded from the current study.

The signaling partners of the various PPAR are retinoid X receptors (RXR). PPAR-RXR are permissive heterodimers that can be activated by either PPAR ligands or RXR ligands.³² It was reported that RXR is activated during G-CSF-induced granulopoiesis. The synthetic RXR agonist bexarotene enhanced G-CSF-induced mobilization of neutrophils and CFU-C, but not of LSK cells, in circulation.²⁰ In contrast, PPAR δ ligands in our study suppressed the mobilization of both LSK cells and CFU-C. This difference may be because apo-PPAR δ , i.e., the absence of ligand, has been shown to reside on DNA or function as a transrepressor, unlike RXR.³³ It is also possible that RXR may not be a major signaling partner of PPAR δ in BM neutrophils and their precursors with ω 3-PUFA as PPAR δ ligands. Indeed, the promyelocytic leukemia-PPAR δ signaling pathway is important for HSC maintenance through the regulation of fatty acid oxidation and asymmetric division.³⁴ Although the contribution of PPAR is not clear, a very high level of fatty acids is the critical component for the *ex vivo* maintenance of HSC.³⁵ Thus, a continuous supply of fatty acids from the food is critically important for the maintenance of BM hematopoiesis in several different ways. BM in patients with anorexia nervosa commonly displays hypoplasia with gelatinous transformation.^{36,37} This may be partially due to the lack of oral intake of fatty acids, including ω 3-PUFA as PPAR δ ligands.

Hematopoietic Angptl4 deficiency in hyperlipidemic mice causes leukocytosis,³⁸ which suggests a potential role of Angptl4 from hematopoietic cells in the cells' intravasation from the BM cavity into the circulation. Angptl4 is known to have two major distinct roles. First, the N-terminal coiled-coil region (nAngptl4) regulates lipoprotein lipase leading to the control of lipid metabolism, insulin

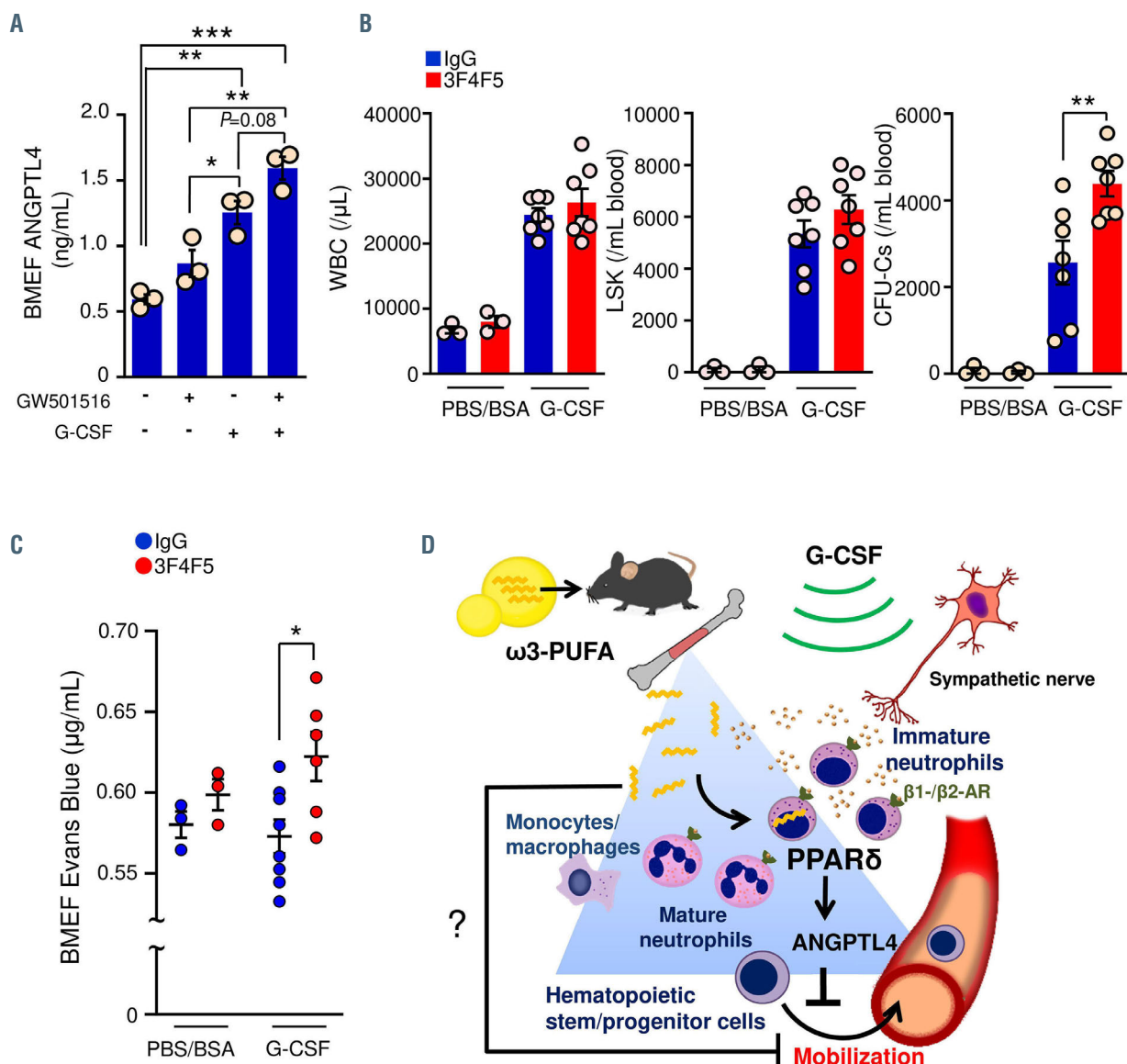


Figure 7. Angptl4 in bone marrow as a negative regulator of mobilization. (A) Angptl4 protein level in bone marrow (BM) extracellular fluid (BMEF) during granulocyte-stimulating factor (G-CSF)-induced mobilization with or without the PPAR δ agonist GW501516 (n=3). (B) G-CSF-induced mobilization in mice treated with the anti-Angptl4 antibody as assessed by white blood cells (WBC), lineage Sca-1 $^+$ c-kit $^+$ (LSK) cells and colony-forming units in culture (CFU-C) in the blood (n=3 for group treated with phosphate-buffered saline [PBS]/bovine serum albumin [BSA] and n=7 for group treated with G-CSF). (C) BM vascular permeability assessed by Evans blue dye concentration in BMEF during G-CSF mobilization with or without the anti-Angptl4 antibody (n=3-8). Combined data from at least three independent experiments are shown. Data are mean \pm standard error of mean. *P<0.05, **P<0.01, ***P<0.001 (Student *t* test and analysis of variance). (D) Schematic representation of the proposed role of dietary fat and PPAR δ in G-CSF-induced mobilization. High sympathetic tone induced by G-CSF stimulates β_1/β_2 -adrenergic receptors (β_1/β_2 -AR) to upregulate PPAR δ expression in BM myeloid cells. Dietary fatty acid ligands, such as ω_3 -polyunsaturated fatty acids (PUFA), bind to PPAR δ and promote Angptl4 expression to suppress the mobilization via, at least partially, inhibition of BM vascular permeability. The PPAR δ -independent pathway of ω_3 -PUFA to inhibit mobilization may also exist.

sensitivity, and glucose homeostasis. Second, the regulation of angiogenesis and vascular permeability is mediated by the COOH-terminal fibrinogen-like domain (cAngptl4).^{23,24} Among these effects, the regulation of vascular permeability seems to be the most relevant with respect to G-CSF-induced mobilization. The role of Angptl4 in regulating vascular permeability is context-dependent. Early studies suggested that Angptl4, although it was not shown whether cAngptl4 was used, decreased the leak of dye or extravasation of melanoma cells.^{39,40} In contrast, the promotion of vascular permeability and tumor metastasis by Angptl4 was reported in a breast

tumor model.⁴¹ Mechanistically, cAngptl4 was shown to activate $\alpha_5\beta_1$ integrin and subsequently decluster VE-cadherin and claudin-5 in primary human microvascular endothelial cells, leading to the induction of vascular leakiness and metastasis in a melanoma model.⁴² Angptl4-mediated increased vascular leakiness was also reported in nontumor pathological models such as influenza pneumonia and diabetic macular edema.^{25,43} It was also reported that altered post-translational modification, such as decreased sialylation, can augment the leakiness of the kidney glomerular epithelium.⁴⁴ In our study, Angptl4 inhibition led to increased BM vascular permeability and

increased trafficking of HPC from the BM cavity into the circulation. In addition to the consequences of using different models, proteolytic processing and post-translational modifications of Angptl4 may occur differently in each organ and each type of producer and effector cell, resulting in widely variable results.

BM is tightly regulated by the SNS, and a major step for HSPC mobilization by G-CSF is the strong suppression of osteolineage cells, such as osteoblasts and osteocytes, via β_2 -AR stimulation by catecholamines.^{7,9} G-CSF stimulation of sympathetic nerves inhibits the reuptake of released catecholamines at the synapse,¹⁰ leading to hyper-sympathetic tone in the BM. We have previously shown that BM neutrophils express all β_1 -, β_2 -, and β_3 -AR and that the selective β_3 -AR agonist activates the arachidonic acid cascade to increase PGE₂ production to protect osteoblast function.¹¹ In this study, induction of PPAR δ mRNA and protein by SNS signals was mainly through β_1 / β_2 -AR in mature/immature neutrophils. The β_1 / β_2 -AR-PPAR δ / ω 3-PUFA-Angptl4 pathway in BM myeloid cells counteracts the alteration of the BM microenvironment and suppresses mobilization upon G-CSF-induced marrow inflamma-

tion (Figure 7D). Our study has shed light on oral fat as an important regulator of interorgan communication between the nervous and hematopoietic systems.

Disclosures

No conflicts of interest to disclose.

Contributions

TS performed all the experiments and wrote the manuscript; SI, YKaw, KW, HK, AS, and KM helped with animal maintenance and tissue sample preparation; MS and TF performed the bone marrow lipid analysis; MH and ST supervised the study of PPAR δ -deficient mice; NST supervised the study with anti-Angptl4 antibody; TM supervised all experiments; and YKat supervised all experiments and wrote the manuscript.

Funding

This work was supported by PRESTO, the Japan Science and Technology Agency (#JPMJPR12M7; to YKat), CREST grant from AMED (#JP18gm0910012h2; to YKat), and Grants-in-Aid for Scientific Research (#15H04856 and #18H02837; to YKat) from the Japan Society for the Promotion of Science.

References

- Chow A, Lucas D, Hidalgo A, et al. Bone marrow CD169⁺ macrophages promote the retention of hematopoietic stem and progenitor cells in the mesenchymal stem cell niche. *J Exp Med.* 2011;208(2):261-271.
- Christopher MJ, Rao M, Liu F, Woloszynek JR, Link DC. Expression of the G-CSF receptor in monocytic cells is sufficient to mediate hematopoietic progenitor mobilization by G-CSF in mice. *J Exp Med.* 2011;208(2):251-260.
- Winkler IG, Sims NA, Pettit AR, et al. Bone marrow macrophages maintain hematopoietic stem cell (HSC) niches and their depletion mobilizes HSCs. *Blood.* 2010;116(23):4815-4828.
- Levesque JP, Hendy J, Takamatsu Y, Simmons PJ, Bendall LJ. Disruption of the CXCR4/CXCL12 chemotactic interaction during hematopoietic stem cell mobilization induced by G-CSF or cyclophosphamide. *J Clin Invest.* 2003;111(2):187-196.
- Petit I, Szyper-Kravitz M, Nagler A, et al. G-CSF induces stem cell mobilization by decreasing bone marrow SDF-1 and up-regulating CXCR4. *Nat Immunol.* 2002;3(7):687-694.
- Semerad CL, Christopher MJ, Liu F, et al. G-CSF potently inhibits osteoblast activity and CXCL12 mRNA expression in the bone marrow. *Blood.* 2005;106(9):3020-3027.
- Asada N, Katayama Y, Sato M, et al. Matrix-embedded osteocytes regulate mobilization of hematopoietic stem/progenitor cells. *Cell Stem Cell.* 2013;12(6):737-747.
- Katayama Y, Battista M, Kao WM, et al. Signals from the sympathetic nervous system regulate hematopoietic stem cell egress from bone marrow. *Cell.* 2006;124(2):407-421.
- Kawamori Y, Katayama Y, Asada N, et al. Role for vitamin D receptor in the neuronal control of the hematopoietic stem cell niche. *Blood.* 2010;116(25):5528-5535.
- Lucas D, Bruns I, Battista M, et al. Norepinephrine reuptake inhibition promotes mobilization in mice: potential impact to rescue low stem cell yields. *Blood.* 2012;119(17):3962-3965.
- Kawano Y, Fukui C, Shinohara M, et al. G-CSF-induced sympathetic tone provokes fever and primes antimobilizing functions of neutrophils via PGE2. *Blood.* 2017;129(5):587-597.
- Borgeson E, Johnson AM, Lee YS, et al. Lipoxin A4 attenuates obesity-induced adipose inflammation and associated liver and kidney disease. *Cell Metab.* 2015;22(1):125-137.
- Krashia P, Cordella A, Nobili A, et al. Blunting neuroinflammation with resolvin D1 prevents early pathology in a rat model of Parkinson's disease. *Nat Commun.* 2019;10(1):3945.
- Naveiras O, Nardi V, Wenzel PL, Hauschka PV, Fahey F, Daley GQ. Bone-marrow adipocytes as negative regulators of the haematopoietic microenvironment. *Nature.* 2009;460(7252):259-263.
- Zhou BO, Yu H, Yue R, et al. Bone marrow adipocytes promote the regeneration of stem cells and haematopoiesis by secreting SCF. *Nat Cell Biol.* 2017;19(8):891-903.
- Serhan CN. Pro-resolving lipid mediators are leads for resolution physiology. *Nature.* 2014;510(7503):92-101.
- Serhan CN, Levy BD. Resolvins in inflammation: emergence of the pro-resolving superfamily of mediators. *J Clin Invest.* 2018;128(7):2657-2669.
- Lankinen M, Uusitupa M, Schwab U. Genes and dietary fatty acids in regulation of fatty acid composition of plasma and erythrocyte membranes. *Nutrients.* 2018;10(11):1785.
- Chakravarthy MV, Pan Z, Zhu Y, et al. "New" hepatic fat activates PPAR α to maintain glucose, lipid, and cholesterol homeostasis. *Cell Metab.* 2005;1(5):309-322.
- Niu H, Fujiwara H, di Martino O, et al. Endogenous retinoid X receptor ligands in mouse hematopoietic cells. *Sci Signal.* 2017;10(503):eaan1011.
- Forman BM, Chen J, Evans RM. Hypolipidemic drugs, polyunsaturated fatty acids, and eicosanoids are ligands for peroxisome proliferator-activated receptors alpha and delta. *Proc Natl Acad Sci U S A.* 1997;94(9):4312-4317.
- Day RB, Bhattacharya D, Nagasawa T, Link DC. Granulocyte colony-stimulating factor reprograms bone marrow stromal cells to actively suppress B lymphopoiesis in mice. *Blood.* 2015;125(20):3114-3117.
- Fernandez-Hernando C, Suarez Y. ANGPTL4: a multifunctional protein involved in metabolism and vascular homeostasis. *Curr Opin Hematol.* 2020;27(3):206-213.
- Tan MJ, Teo Z, Sng MK, Zhu P, Tan NS. Emerging roles of angiopoietin-like 4 in human cancer. *Mol Cancer Res.* 2012;10(6):677-688.
- Li L, Chong HC, Ng SY, et al. Angiopoietin-like 4 increases pulmonary tissue leakiness and damage during influenza pneumonia. *Cell Rep.* 2015;10(5):654-663.
- Chilton FH, Patel M, Fonteh AN, Hubbard WC, Triggiani M. Dietary n-3 fatty acid effects on neutrophil lipid composition and mediator production. Influence of duration and dosage. *J Clin Invest.* 1993;91(1):115-122.
- Ferrante A, Goh D, Harvey DP, et al. Neutrophil migration inhibitory properties of polyunsaturated fatty acids. The role of fatty acid structure, metabolism, and possible second messenger systems. *J Clin Invest.* 1994;93(3):1063-1070.
- Sperling RI, Benincaso AI, Knoell CT, Larkin JK, Austen KF, Robinson DR. Dietary omega-3 polyunsaturated fatty acids inhibit phosphoinositide formation and chemotaxis in neutrophils. *J Clin Invest.* 1993;91(2):651-660.
- Reddy RC, Narala VR, Keshamouni VG, Milano JE, Newstead MW, Standiford TJ. Sepsis-induced inhibition of neutrophil chemotaxis is mediated by activation of peroxisome proliferator-activated receptor- γ . *Blood.* 2008;112(10):4250-4258.
- Xu HE, Lambert MH, Montana VG, et al. Molecular recognition of fatty acids by peroxisome proliferator-activated receptors. *Mol Cell.* 1999;3(3):397-403.
- Tull SP, Yates CM, Maskrey BH, et al. Omega-3 fatty acids and inflammation: novel interactions reveal a new step in neutrophil recruitment. *PLoS Biol.* 2009;7(8):e1000177.

32. Kliewer SA, Umesono K, Noonan DJ, Heyman RA, Evans RM. Convergence of 9-cis retinoic acid and peroxisome proliferator signalling pathways through heterodimer formation of their receptors. *Nature*. 1992;358(6389):771-774.

33. Tan NS, Vazquez-Carrera M, Montagner A, Sng MK, Guillou H, Wahli W. Transcriptional control of physiological and pathological processes by the nuclear receptor PPAR β/δ . *Prog Lipid Res*. 2016;64:98-122.

34. Ito K, Carracedo A, Weiss D, et al. A PML-PPAR δ pathway for fatty acid oxidation regulates hematopoietic stem cell maintenance. *Nat Med*. 2012;18(9):1350-1358.

35. Kobayashi H, Morikawa T, Okinaga A, et al. Environmental optimization enables maintenance of quiescent hematopoietic stem cells ex vivo. *Cell Rep*. 2019;28(1):145-158.

36. Cornbleet PJ, Moir RC, Wolf PL. A histochemical study of bone marrow hypoplasia in anorexia nervosa. *Virchows Arch A Pathol Anat Histol*. 1977;374(3):239-247.

37. Seaman JP, Kjeldsberg CR, Linker A. Gelatinous transformation of the bone marrow. *Hum Pathol*. 1978;9(6):685-692.

38. Aryal B, Rotllan N, Araldi E, et al. ANGPTL4 deficiency in haematopoietic cells promotes monocyte expansion and atherosclerosis progression. *Nat Commun*. 2016;7:12313.

39. Galau A, Cazes A, Le Jan S, et al. Angiopoietin-like 4 prevents metastasis through inhibition of vascular permeability and tumor cell motility and invasiveness. *Proc Natl Acad Sci U S A*. 2006;103(49):18721-18726.

40. Ito Y, Oike Y, Yasunaga K, et al. Inhibition of angiogenesis and vascular leakiness by angiopoietin-related protein 4. *Cancer Res*. 2003;63(20):6651-6657.

41. Padua D, Zhang XH, Wang Q, et al. TGF β primes breast tumors for lung metastasis seeding through angiopoietin-like 4. *Cell*. 2008;133(1):66-77.

42. Huang RL, Teo Z, Chong HC, et al. ANGPTL4 modulates vascular junction integrity by integrin signaling and disruption of intercellular VE-cadherin and claudin-5 clusters. *Blood*. 2011;118(14):3990-4002.

43. Sodhi A, Ma T, Menon D, et al. Angiopoietin-like 4 binds neuropilins and cooperates with VEGF to induce diabetic macular edema. *J Clin Invest*. 2019;129(11):4598-4608.

44. Clement LC, Avila-Casado C, Mace C, et al. Podocyte-secreted angiopoietin-like-4 mediates proteinuria in glucocorticoid-sensitive nephrotic syndrome. *Nat Med*. 2011;17(1):117-122.



Whole-slide image analysis of the tumor microenvironment identifies low B-cell content as a predictor of adverse outcome in patients with advanced-stage classical Hodgkin lymphoma treated with BEACOPP

Ron Daniel Jachimowicz,^{1,2,3*} Luise Pieper,^{4*} Sarah Reinke,^{4,*} Artur Gontarewicz,^{4,*} Annette Plütschow,¹ Heinz Haverkamp,¹ Leonie Frauenfeld,⁵ Falko Fend,⁵ Mathis Overkamp,⁵ Franziska Jochims,⁴ Christoph Thorns,⁶ Martin Leo Hansmann,⁷ Peter Möller,⁸ Andreas Rosenwald,⁹ Harald Stein,¹⁰ Hans Christian Reinhardt,^{2,3,11,12} Peter Borchmann,^{1,3} Bastian von Tresckow,^{1,3} Andreas Engert^{1,3} and Wolfram Klapper⁴

¹University of Cologne, Faculty of Medicine and University Hospital Cologne, Department I of Internal Medicine, Cologne; German Hodgkin Study Group, Cologne; ²Else Kröner Forschungskolleg Clonal Evolution in Cancer, University Hospital Cologne, Cologne;

³University of Cologne, Faculty of Medicine and University Hospital Cologne, Department I of Internal Medicine, Center for Integrated Oncology Aachen-Bonn-Cologne-Düsseldorf, Cologne; ⁴Department of Pathology, Hematopathology Section, University Hospital Schleswig-Holstein, Christian-Albrechts-University, Kiel; ^{5,18}Department of Pathology, University of Tübingen, Tübingen; ⁶Department of Pathology, University Hospital Schleswig-Holstein, University of Lübeck, Lübeck; ⁷Department of Pathology, University Hospital Frankfurt, Frankfurt; ⁸Department of Pathology, University Hospital Ulm, Ulm; ⁹Institute of Pathology, University of Würzburg, and Comprehensive Cancer Center Mainfranken, Würzburg; ¹⁰Pathodiagnostik, Berlin; ¹¹Cologne Excellence Cluster on Cellular Stress Response in Aging-Associated Diseases (CECAD), University of Cologne, Cologne and

¹²Center for Molecular Medicine Cologne (CMMC), University of Cologne, Cologne, Germany

*RDJ, LP, SR and AG contributed equally as co-first authors.

Correspondence:

RON D. JACHIMOWICZ
ron.jachimowicz@uk-koeln.de

WOLFRAM KLAPPER
wklapper@path.uni-kiel.de

Received: December 12, 2019.

Accepted: April 29, 2020.

Pre-published: May 7, 2020.

<https://doi.org/10.3324/haematol.2019.243287>

©2021 Ferrata Storti Foundation

Material published in *Haematologica* is covered by copyright. All rights are reserved to the Ferrata Storti Foundation. Use of published material is allowed under the following terms and conditions:
<https://creativecommons.org/licenses/by-nc/4.0/legalcode>. Copies of published material are allowed for personal or internal use. Sharing published material for non-commercial purposes is subject to the following conditions:
<https://creativecommons.org/licenses/by-nc/4.0/legalcode>, sect. 3. Reproducing and sharing published material for commercial purposes is not allowed without permission in writing from the publisher.



ABSTRACT

A subset of patients with advanced-stage classical Hodgkin lymphoma (cHL) relapse or progress following standard treatment. Given their dismal prognosis, identifying this group of patients upfront represents an important medical need. While prior research has identified characteristics of the tumor microenvironment, which are associated with cHL outcomes, biomarkers that are developed and validated in this high-risk group are still lacking. Here, we applied whole-slide image analysis (WSI), a quantitative, large-scale assessment of tumor composition that utilizes conventional histopathology slides. We conducted WSI on pre-treatment biopsies from 340 patients with advanced-stage cHL enrolled in the HD12 and HD15 trials of the German Hodgkin Study Group (GHSG), and tested our results in a validation cohort of 147 advanced-stage cHL patients within the GHSG HD18 trial. All patients were treated with BEACOPP-based regimens. By quantifying T cells, B cells, Hodgkin and Reed-Sternberg cells and macrophages with WSI, 80% of all cells in the tumor tissue were identified. Crucially, low B-cell count was associated with significantly reduced progression-free survival and overall survival, while the content of T cells, macrophages and Hodgkin and Reed-Sternberg cells was not associated with the risk of progression or relapse in the study cohort. We further validated low B-cell content as a prognostic factor for progression-free survival and overall survival in the validation cohort and demonstrated the good inter-observer agreement of WSI. WSI may represent a key tool for risk stratification of advanced-stage cHL and can easily be added to the standard diagnostic histopathology work-up.

Introduction

Classical Hodgkin lymphoma (cHL) is a B-cell-derived lymphoid malignancy, affecting 2.5-3/100,000 people per year. Depending on the clinical stage and associated risk factors, first-line treatment consists of poly-chemotherapy with or without consolidating radiotherapy, and results in long-term tumor control in 70-80% and overall survival of 80-90% of patients.^{1,2} Crucially, all patients with advanced-stage cHL currently continue to receive aggressive poly-chemotherapy within the German Hodgkin Study Group (GHSG) clinical trials. This treatment regimen is common practice because, to date, there is no reliable tool to distinguish, *a priori*, the subset of patients at high risk of relapse or progressive disease from those with lower risk. As a result, two groups of patients may be underserved by current treatment approaches: those who could be treated with less toxic treatment regimens; and those who are likely to relapse or progress after standard chemotherapy, as their prognosis is often very poor with less than 50% becoming long-term survivors.³ In contrast to non-Hodgkin lymphoma, clinical risk indices for cHL such as the International Prognostic Score (IPS) have not been successfully applied in treatment decision-making within the subgroup of patients with advanced stage cHL.⁴

Similarly, the commonly defined histological subtypes of cHL lack prognostic significance under the currently used standard treatment protocols. Four microenvironmental patterns reflect the basis of the histological subtypes in the current World Health Organization classification, namely nodular sclerosis, mixed cellularity, lymphocyte-rich and lymphocyte-depleted. In recent research, however, the tumor microenvironment of cHL has attracted interest as a predictor of disease outcome.⁵ cHL is characterized by the presence of neoplastic Hodgkin and Reed-Sternberg cells (HRSC) that constitute only a minority of cells within the affected lymph nodes. The tumor is mainly composed of non-neoplastic stromal and immune cells, which form a tumor microenvironment around HRSC. Depending on the cHL subtype, the cellular part of the tumor microenvironment is made up of variable proportions of macrophages, neutrophils, eosinophils, T cells, B cells, fibroblasts and plasma cells. The neoplastic HRSC is dependent on both endogenous- and exogenous signals, the latter stemming from crosstalk with the microenvironment, e.g., by the interaction between macrophages and tumor cells.⁶

The prognostic value of HRSC CD20 expression is controversial.⁷⁻¹⁰ Numerous studies utilizing quantitative assessment of mRNA or immunohistochemistry have suggested an adverse effect of increased macrophage infiltration¹¹⁻¹⁵ and a favorable effect for markers of normal B cells in the tumor microenvironment of cHL.¹⁶⁻¹⁸ However, the immunohistochemistry-based approaches used to assess the microenvironmental composition and the prognostic impact suffer from limitations hampering their integration into routine diagnostic procedures and clinical decision-making for cHL. Unlike gene expression analysis, which usually analyzes bulk tumor tissue, including the non-malignant microenvironment, classical immunohistochemical studies analyze a limited size of tumor regions and may be biased by intratumoral heterogeneity and observer-dependent selection of the areas analyzed. Moreover, validation of microenvironmental biomarkers has rarely been performed in large clinical trial cohorts. To

overcome these limitations and to test the prognostic role of the tumor microenvironment in advanced-stage cHL, we performed whole-slide-image analysis (WSI) of T cells (CD3), B cells (CD20), HRSC (CD30) and macrophages (CD68) in a study cohort and an independent validation cohort consisting of hundreds of patients treated within trials of the German Hodgkin Study Group (GHSG).

Methods

Study design and patients' samples

Between January 1999 and July 2017, 5,801 adult patients with primarily diagnosed and histologically confirmed advanced-stage cHL were randomized to receive first-line treatment with the BEACOPP regimen, containing bleomycin, etoposide, doxorubicin, cyclophosphamide, vincristine, procarbazine, and prednisone in standard or escalated (eBEACOPP) doses within the randomized GHSG clinical trials HD12, HD15, and HD18.¹⁹⁻²¹ Our cohort comprised trial patients with (cases) and without (controls) progression or relapse at the ratio of 1:2.

Inclusion criteria for the case-control cohort were documentation of the reference histology result and reference center and availability of a formalin-fixed paraffin-embedded lymph-node specimen obtained at first diagnosis as well as complete documentation of the presence or absence of prognostic factors. Inter-observer agreement of WSI was tested using randomly selected WSI slides analyzed by a second observer and a randomly selected cohort stained and analyzed in a second center (*Online Supplementary Methods*).

The WSI findings of the study cohort of patients (n=340) from HD12 and HD15 (Figure 1A) were matched with clinical data and analyzed for prognosis. The performance was subsequently tested using an independent validation cohort comprising HD18 patients (n=147) (Figure 1B). Median follow-up times were 66 months (95% confidence interval [95% CI]: 63-71) in the study cohort and 62 months (95% CI: 57-65) in the validation cohort.

Table 1 summarizes the clinical characteristics of the study and validation cohorts in relation to all randomized HD12 and HD15 patients or all randomized HD18 patients, respectively. Patients included in the study cohort were slightly younger compared to all patients from the HD12 and HD15 randomized cohorts (median age: 31 years [range, 24-40] vs. 33 years [25-42], respectively; $P=0.0093$). There were no differences in prognostically relevant laboratory parameters nor the IPS scores; however, more patients in the study cohort had ≥ 3 nodal areas affected and stage IV disease at diagnosis (Table 1A). The validation cohort did not differ from the HD18 randomized cohort regarding demographic and prognostic factors (Table 1B). The study was conducted in accordance with the recommendations of the ethics board of the Medical Faculty, University of Kiel.

Whole-slide image analysis

For each patient, the whole available tissue specimen/block was cut and subsequent slides were stained in the Department of Pathology at Kiel University for CD3 (clone SP7, Waltham, MA, USA), CD20 (clone L26, Dako, Glostrup, Denmark), CD30 (clone BerH2, maintained at the Department of Pathology, Kiel, Germany) and CD68 (clone PG-M1, Dako, Glostrup, Denmark), using a Leica-Bond-Max stainer (Leica Microsystems, Wetzlar, Germany). The slides were scanned (Hamamatsu Nanozoomer, Hamamatsu Photonics, Ammersee, Germany) and the resulting images were processed by TissueStudio 64, according to the manufacturer's recommendations (Definiens AG, Munich, Germany). The area ranged between 4-455 mm² (mean: 133.81 mm², standard

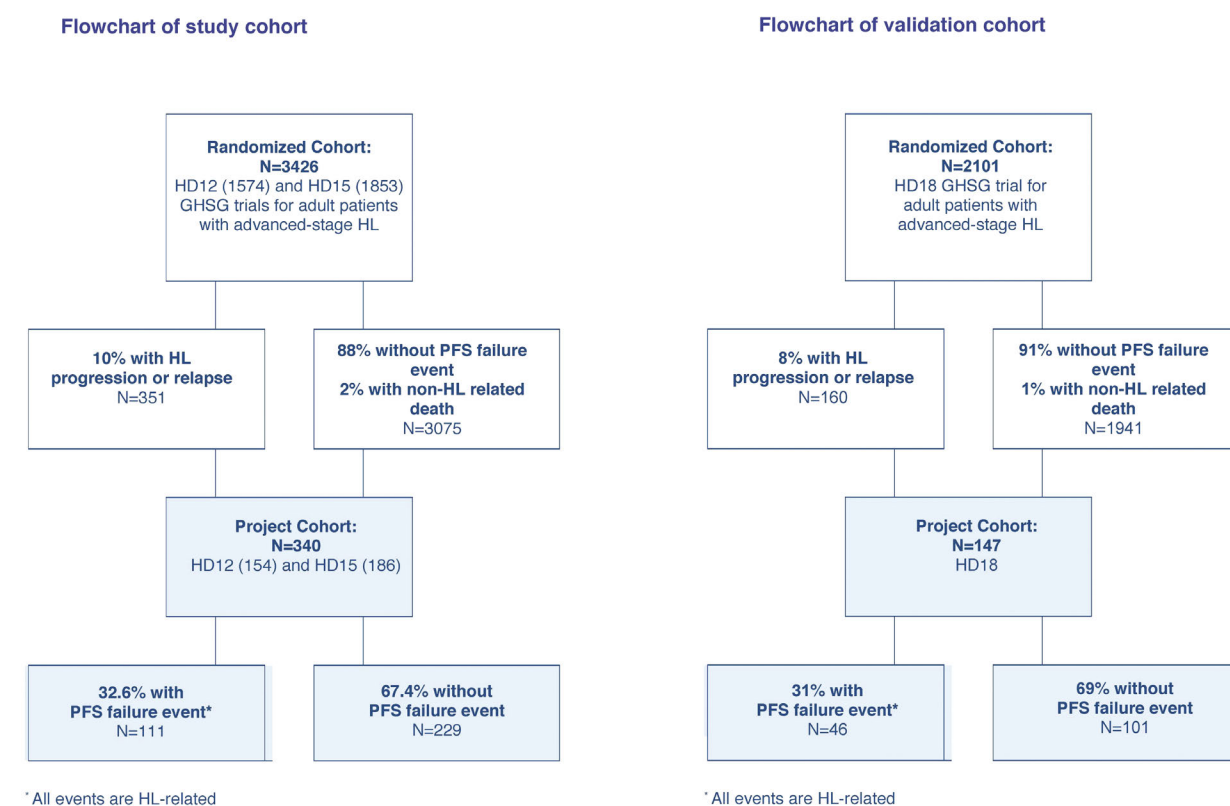


Figure 1. Flowchart of the study cohort and validation cohort. Average values of percentage of the respective cell types are indicated. For calculation of cell counts of macrophages (CD68) and Hodgkin and Reed-Sternberg cells (CD30) see the *Online Supplementary Methods*.

deviation [SD]: 80.84 mm²) (*Online Supplementary Figure S1*). Since we included the entire lymph node in the analysis, any heterogeneity of cell distribution did not influence our data. Cutting artifacts, and overstained or unstained areas were manually excluded from the analysis. Adjusting the threshold based on several representative locations on the sample also ensured that the setting for analysis for each sample had been selected to cover the specific staining of the lymph node. See the *Online Supplementary Methods* for a detailed description and statistics.

Results

Mapping the microenvironment in classical Hodgkin lymphoma through whole-slide image analysis in the study cohort

Within the study cohort, WSI detected a mean total cell count of 1,550,980 (SD: 949,004) for all analyzed lymph node specimens. The main cellular components of the tumor tissue (CD3⁺ T cells, CD20⁺ B cells, CD30⁺ HRSC and CD68⁺ macrophages) reflect the variable cell proportions dependent on the histological subtype (Figure 2). Overall, T cells, B cells, HRSC and macrophages accounted for a mean of 80% of all cells within the tumor tissue, highlighting the strength of WSI for comprehensively assessing cHL tumors. As expected, lymphocyte-rich cHL (n=9) showed high counts of B cells and T cells with concomitant low levels of HRSC and macrophages. Conversely, lymphocyte-depleted cHL (n=4) displayed the lowest counts of B cells and T cells while CD30 and CD68 levels were markedly elevated. The T-cell content displayed a moderate positive correlation with B-cell content

($\rho=0.42$; $P<0.001$), as well as a weak correlation with macrophage content ($\rho=0.15$; $P=0.0049$) and CD30 content ($\rho=0.15$; $P=0.0063$) (Table 2). We also observed a weak relationship between macrophage and HRSC content ($\rho=0.21$; $P=0.0001$). Of note, we did not detect a correlation between B-cell and macrophage content.

B-cell content was associated with risk of progression and relapse in the study cohort

We analyzed whether CD3, CD20, CD30 and CD68 differed between patients with lasting complete remission and patients with subsequent progression or relapse. While we did not observe any association of T-cell count, macrophage content or CD30-positivity with long-term remission status in our study cohort, B-cell content was significantly lower at the time of diagnosis in patients with later progression or relapse (mean 13.5%) than in patients with long-lasting complete remission (mean: 13.5% vs. 17.7%, respectively; $P=0.0079$) (Table 3). Further subgroup analyses revealed that patients with mixed cellularity and nodular sclerosis cHL had significantly lower B-cell counts when at risk for relapse and a similar trend was observed for patients with lymphocyte-depleted and lymphocyte-rich cHL (*data not shown*).

To further assess the association between B-cell content and progression-free survival, we performed explorative receiver operating characteristic (ROC) analyses in which a B-cell content of 21% or less was the best predictor of progression or relapse in the study cohort (ROC estimate – chance = 0.00959, $P<0.0001$). Utilizing this cut-off, both progression-free survival ($P=0.0004$, hazard ratio [HR]=2.479, 95% CI: 1.479-4.157) and overall survival

($P=0.04$, HR=2.372, 95% CI: 0.996-5.651) were significantly worse in patients presenting with low B-cell content (Figures 3A and 4A). We next examined the prognostic value of B-cell content in a multivariate model, including 11 known risk factors for progression-free survival and B-cell content as binary variables. Backward selection of effects with P -values <0.1 resulted in elimination of nine effects (extranodal disease, lymphopenia, stage IV disease, albumin <4 g/dL, leukocytosis, B-symptoms, elevated erythrocyte sedimentation rate, hemoglobin <10.5 g/dL, large mediastinal mass) and a final model including B-cell content $\leq 21\%$ ($P=0.0002$, odds ratio [OR]=3.133, 95% CI: 1.726-5.687), male sex ($P=0.0015$, OR=2.251, 95% CI: 1.363-3.720) and age ≥ 45 years ($P=0.056$, OR=1.837, 95% CI: 0.985-3.425) as risk factors for treatment failure.

B-cell content was associated with progression-free and overall survival in an Independent validation cohort

To validate whether low B-cell content at diagnosis, as determined by WSI, could predict survival in an independent validation cohort, we analyzed 147 patients treated within the HD18 trial.²¹ In line with the results observed in our study cohort, B-cell content at diagnosis was lower in patients who had progressive disease than in patients with long-lasting complete remission (mean 16.4% vs. 21.5%, respectively; $P=0.0616$) (Table 3). cHL patients in the validation cohort with a low B-cell content (most stringent cut-off value of 10%) had a worse progression-free survival ($P=0.04$, HR= 1.981, 95% CI: 1.104-3.557) (Figure 3B) and inferior overall survival ($P=0.01$, HR= 3.598, 95% CI: 1.205-10.739) compared to patients with a high B-cell count (Figure 4B).

Phenotype and distribution of B cell in classical Hodgkin lymphoma

B cells and macrophages were extremely unevenly distributed over lymph node tissues but did not reflect unaf-

fected tissue (*Online Supplementary Figures S2 and S3*). Visual inspection by experienced pathologists revealed non-infiltrated, pre-existing tissue in only 15% of cases (24/154) and the non-infiltrated tissues in these cases usually represented only a small fraction of the lymph node (median unaffected area in not-completely infiltrated cases, 10%). Furthermore, we did not detect an association of B-cell content by WSI and stage of disease for stages included in this cohort (stages II, III and IV; *data not shown*). Since WSI subsumes B cells in the whole lymph node, including B-cell nodules with considerable distance to HRSC (*Online Supplementary Figure S4*), we tested an association with B-cell content in the immediate vicinity of HRSC (<100 μ m radius) (see *Online Supplementary Methods*). Interestingly, despite the uneven distribution of B cells in the lymph node, we observed a correlation between B-cell content in the whole lymph node and immediate proximity to HRSC ($\rho=0.676$, $P<0.0001$, $n=41$) (*Online Supplementary Figure S5*). B cells at the borders of the nodular infiltration by HRSC are arranged in ill-defined follicles that lack germinal centers and are composed mainly of IgD-positive follicle mantle cells, some of

Table 1B. Patients' baseline characteristics comparing the validation cohort and all patients randomized into the HD18 GHSG trial.

Patients' characteristics	Validation cohort (N=147)	Randomized cohort (N=2101)	P
Age in years, median (IQR)	33 (25-42)	32 (24-43)	0.8322
GHSG risk factors, n(%)			
Extranodal disease	28 (19.0)	407 (19.4)	1
≥ 3 nodal areas	128 (87.1)	1809 (86.1)	0.8053
Large mediastinal mass	37 (25.2)	592 (28.2)	0.4473
Elevated ESR	93 (63.3)	1332 (63.4)	0.9295
IPS risk factors, n(%)			
Male sex	96 (66.0)	1278 (60.8)	0.1900
Age ≥ 45 years	26 (17.7)	437 (22.4)	0.2156
Clinical stage IV	53 (36.1)	765 (36.4)	1
Albumin <4 g/dL	85 (87.5)	1180 (56.2)	0.7305
Hemoglobin <10.5 g/dL	28 (19.0)	379 (18.0)	0.7390
Leukocytosis	30 (20.4)	436 (20.8)	1
Lymphopenia	10 (6.8)	151 (7.2)	1
IPS score, n(%)			
0 - 2	92 (63.0)	1206 (61.9)	0.8598
3 - 7	54 (37.0)	741 (38.1)	
Histological subtype - N/125 (%)			
Nodular sclerosis	72 (49.0)	747 (35.6)	0.0006
Mixed-cellularity	25 (17.0)	245 (11.7)	0.0447
Lymphocyte-rich	4 (2.7)	29 (1.4)	0.1402
Lymphocyte-depleted	0	8 (0.4)	1

HD12 trial: number of patients per arm (study cohort/randomized cohort): arm A 39/336, arm B 59/357, arm C 47/353, arm D 44/349. Chemotherapy: arms A and B: 8 cycles of escalated BEACOPP (eBEACOPP), arms C and D: 4 cycles of eBEACOPP + 4 cycles of baseline BEACOPP. Radiotherapy: arms A and D: 30 Gy to initial bulky sites and residual lymphoma. **HD15 trial:** number of patients per arm: arm A 64/677, arm B 69/680, arm C 73/674. Chemotherapy: arm A: 8 cycles of eBEACOPP; arm B: 6 cycles of eBEACOPP; arm C: 8 cycles of BEACOPP14. Radiotherapy: arms A, B, and C: 30 Gy consolidating radiotherapy to positron emission tomography (PET)-positive residues. **HD18 trial:** number of patients per arm (validation cohort/enrolled or randomized cohort): NULL 9/137, arm A 67/731, arm B 15/220, arm C 27/508, arm D 29/505. NULL not randomized arm; without PET result after 2 cycles of eBEACOPP. Chemotherapy for PET-positive arms A: 6-8 cycles of eBEACOPP and B: 6-8 cycles of eBEACOPP + rituximab; and for PET-negative arms C: 6-8 cycles of eBEACOPP and D: 4 cycles of eBEACOPP. Radiotherapy (30 Gy) was recommended for all arms with residual 18 F-FDG uptake and a mass with a largest diameter after chemotherapy of at least 2.5 cm. P values are for the comparison of patients included in the study or validation cohort *versus* patients not included. *Fisher exact test, if not stated otherwise, **Wilcoxon rank-sum test, IQR: interquartile range; ESR: erythrocyte sedimentation rate; IPS: International Prognostic Score; GHSG: German Hodgkin Study Group.

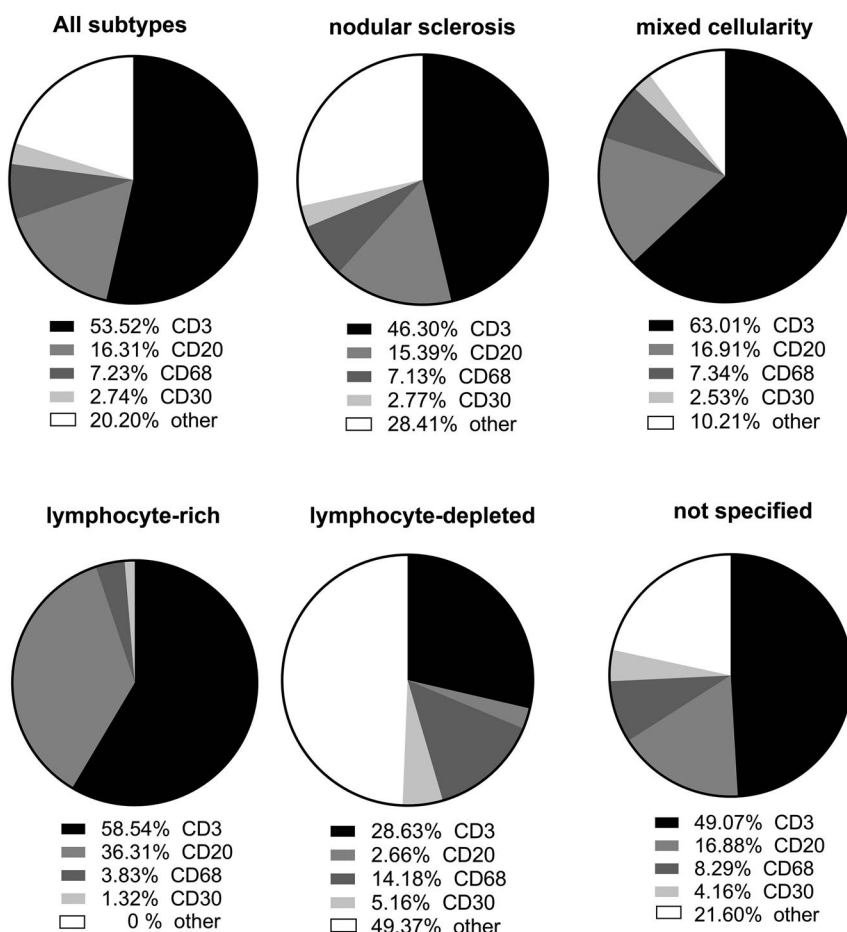


Figure 2. Cellular composition assessed by whole-slide imaging in the study cohort and according to histological subtypes of classical Hodgkin lymphoma. Average values of percentage of the respective cell types are indicated. For calculation of cell counts of macrophages (CD68) and Hodgkin and Reed-Sternberg cells (CD30) see the *Online Supplementary Methods*.

which express CD73 (*Online Supplementary Figure S4*). Thus, the vast majority of B cells seem to resemble naïve B cells. However, further subtyping of B cells in the microenvironment using appropriate methods is required to understand the nature of this population.

Inter-observer bias of whole-slide image analysis

To evaluate the inter-dependent bias of WSI, we took a two-pronged approach. First, we randomly selected CD20-stained whole slides that were re-analyzed by a second independent observer, using the same software. We found a high inter-observer concordance when the same or newly scanned images were processed in the image analysis software by a second observer (*Online Supplementary Figure S6*). Second, we randomly selected a cohort of 20 cases, for which the complete staining procedure for CD20 and WSI was performed in a second center (see *Online Supplementary Methods*). This approach revealed a correlation of results obtained at two independent centers ($r^2=0.6101$) (*Online Supplementary Figure S7*). Thus, WSI provides an unbiased approach for robust quantification of the global cellular composition of cHL tissue.

Discussion

Despite the overall outstanding treatment results in cHL, the *a priori* identification of a high-risk subset of patients remains a challenge in clinical practice. Studies

utilizing functional imaging influence clinical decision-making,²² but none of the previously proposed gene expression profiling or immunohistochemistry biomarkers has been incorporated into treatment protocols for cHL.⁴ So far, a comprehensive analysis of the cellular composition of the microenvironment in cHL is limited to gene expression studies.^{12,16,23} Here, we utilized WSI and achieved a comprehensive and robust quantification of the cellular composition of the cHL microenvironment throughout the whole tumor sample. To the best of our knowledge, this approach has not been applied to cHL previously and opens a novel conceptual window into the assessment of cellular composition of tumor tissue.

In contrast to previously reported studies,^{11,17,24} but in line with several other studies,^{25,26} we did not observe a correlation of macrophage content with outcome in cHL. The discrepancy between our results and previously published studies with respect to macrophage counts may be explained in multiple ways. First, the technology to assess macrophage counts differs. We cannot rule out that gene expression analysis utilizing mRNA expression level of multiple genes assesses macrophages in a different manner than our WSI approach. However, comparing conventional immunohistochemistry image analysis or even visual inspection of small fields of view, we consider WSI a more accurate measure of macrophage content. Second, there is a difference between the population of patients in our study and those in previous publications. Patients in our study were treated with rather intensive chemotherapy (BEACOPP/eBEACOPP), which is known to achieve

Table 2. Correlation analyses of whole-slide image analysis-determined CD3, CD20, CD30 and CD68 content in the study cohort.

	CD68-positive area rate Rho / P	CD20-positive cell rate Rho / P	CD3-positive cell rate Rho / P	CD30-positive area rate Rho / P
CD68-positive area rate	1	-0.05289 0.3389	0.15472 0.0049	0.21218 0.0001
CD20-positive cell rate	-0.05289 0.3389	1	0.42374 / <0.0001	-0.07154 / 0.1956
CD3-positive cell rate	0.15472 0.0049	0.42374 / <0.0001	1	0.15024 / 0.0063
CD30-positive area rate	0.21218 0.0001	-0.07154 / 0.1956	0.15024 / 0.0063	1

Rho: Pearson correlation coefficients; P= probability > 1/2 under the null hypothesis: Rho=0.

Table 3. Whole-slide image analysis-determined CD20-positive cell rates at baseline according to progression-free survival-failure status.

	CD20-positive cell rates (%)				Validation cohort				
	PFS failure	N (%)	Study cohort Group mean	P-value	PFS failure	N (%)	Group mean	P-value	
All patients	no	229 (67.4)	17.7	0.0079	no	201 (69.4)	21.5	0.0616	
	yes	111 (32.6)	13.5		yes	45 (30.6)	16.4		
CD20-negative	no	184 (67.4)	18.1	0.0002	no	not available			
	yes	89 (32.6)	12.4		yes				
CD20-positive	no	45 (67.2)	16.3	n.s.	no	not available			
	yes	22 (32.8)	17.9		yes				
Mixed cellularity	no	70 (70.0)	19.5	0.0064	no	20 (80)	20.8	0.2529	
	yes	30 (30.0)	13.3		yes	5 (20)	14.4		
Nodular sclerosis	no	145 (65.6)	16.9	0.0033	no	145 (65.6)	16.9	0.0274	
	yes	76 (34.4)	12.1		yes	76 (34.4)	12.1		
Lymphocyte-depleted	no	3 (0.75)	2.4	n.s.	no	0	0	not applicable	
	yes	1 (0.25)	5.5		yes	0	0		
Lymphocyte rich	no	6 (0.67)	32.2	n.s.	no	4 (100)	18.2	not applicable	
	yes	3 (0.33)	55.7		yes	0			

PFS: progression-free survival.

higher levels of event-free survival than the levels achieved with ABVD-based regimens.²¹ However, the prognostic relevance of macrophage content was absent despite the fact that we enriched the cohort for patients who had events signifying progression. It is important to mention that we excluded all non-cHL and all non-treatment-related deaths (n=55 in the study cohort) from all the analyses in order to identify a biomarker of lymphoma aggressiveness that was not biased by unrelated deaths. However, inclusion of those 55 patients as progression-free survival failures did not affect the overall results obtained within this study (*data not shown*).

One might speculate that the BEACOPP regimen reduced lymphoma-related events and that biomarkers established in patients treated with ABVD might lose their prognostic power. Recently published results on the prognostic range of the IPS in patients with advanced-stage cHL enrolled on the Eastern Cooperative Oncology Group 2496 trial do in fact argue for such an interpretation.²⁷ In the aforementioned study, two factors (age and stage) were significantly associated with freedom from progression in a multivariate analysis.²⁷ Similarly, we found that apart from low B-cell content, only male sex and age were predictive of treatment failure in a multivariate analysis. Similar findings were reported by the Spanish Hodgkin Lymphoma Study Group in an analysis of patients with advanced-stage cHL treated with ABVD.²⁸ We thus believe that our study cohort is representative of the population of

advanced-stage cHL patients and the absence of a prognostic significance of macrophage content is most likely due to the effective treatment applied.

In light of the fact that the BEACOPP-treated populations analyzed in our study had very few lymphoma-related events (progression or relapse), the value of CD20 content by WSI as a prognostic tool appears to be even higher. B-cell content in the microenvironment of cHL has been identified in several previous studies as a prognostic tool if analyzed by gene expression profiling or immunohistochemistry.^{12,16,17,29,30} However, this biomarker has so far attracted less attention compared to the macrophage count. Gene expression profiling of the cHL microenvironment is a laborious technology that is not widely available. In addition, gene expression analysis is dependent on the technology applied, leading to the different prognostic expression patterns in multiple studies.^{12,16,31} Unfortunately, immunohistochemistry techniques, which are theoretically easy to apply in a routine diagnostic setting, are mostly used to analyze small areas or even hotspots of B cells, making this approach prone to observer-dependent bias.^{17,30} Nevertheless, several groups previously noted that the expression of B-cell cluster genes was related to a favorable outcome in cHL.^{12,16,17,29,30} In contrast to previous findings, we did not identify a correlation between B-cell and macrophage content, which might also be related to the methodology used.

In view of the recent demonstration of variable pheno-

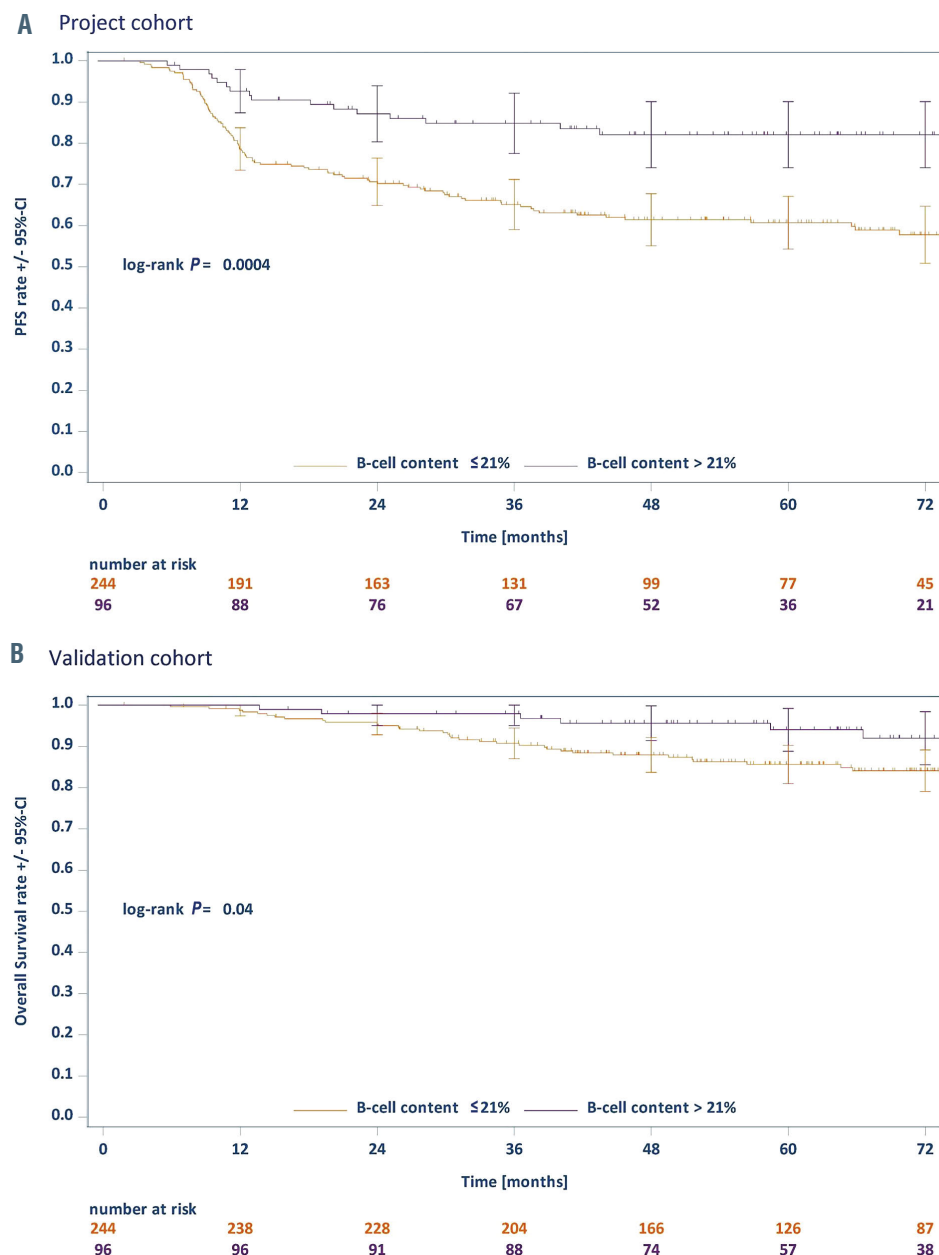


Figure 3. Progression-free survival according to CD20 content. (A) Kaplan-Meier plots of progression-free survival (PFS) in the study cohort for the two risk groups according to B-cell content (CD20-positive cell rate: $\leq 21\%$ or $> 21\%$). (B) Kaplan-Meier plots of PFS in the validation cohort for the two risk groups according to B-cell content (CD20-positive cell rate: $\leq 10\%$ or $> 10\%$).

types of tumor-infiltrating B cells populating the microenvironment of solid cancers,³² the adoption of a broader panel of B-cell/plasma-cell-associated antigens, T-cell subsets and correlation with PD-1 staining should be performed in future WSI applications and could include, among others, CD4, CD8, CD19, CD27, CD5, CD38 and CD138. However, WSI on large cohorts, as performed in our study, will probably have to be focused on a limited number of markers.

Nevertheless, WSI has several advantageous features, compared to gene expression profiling and conventional immunohistochemistry studies, by combining the diagnostic accuracy of digital image analysis and a large-scale approach. By providing cell counts (e.g., the number of B cells) independently of relative expression levels of biomarkers for cell subtypes (e.g., CD20 mRNA), WSI reflects a direct read-out for the cellular composition and consequently a direct measure for therapeutic targets of

immunological therapy. Since CD20 staining is performed at virtually any diagnosis of cHL, WSI makes use of existing histology data without any additional molecular procedures. CD20-stained slides of cHL can be digitalized at any pathology center and moved via the worldwide web in a timely manner to allow centralized assessment. We thus envision this technology to be highly suitable for incorporation into future clinical trials.

The cellular composition of the microenvironment of cHL is complex and its analysis has so far been restricted to a limited number of lymphoma specimens.³³ WSI of multiplexed-stains allows the number of cellular markers to be increased and might help in the translation of findings obtained in a few patients' specimens into large cohorts of patients. Moreover, novel analytic tools beyond the plain assessment of relative amount of cell types can potentially be applied to WSI data.³⁴ In summary, B-cell content assessed by WSI in advanced-stage cHL allows for

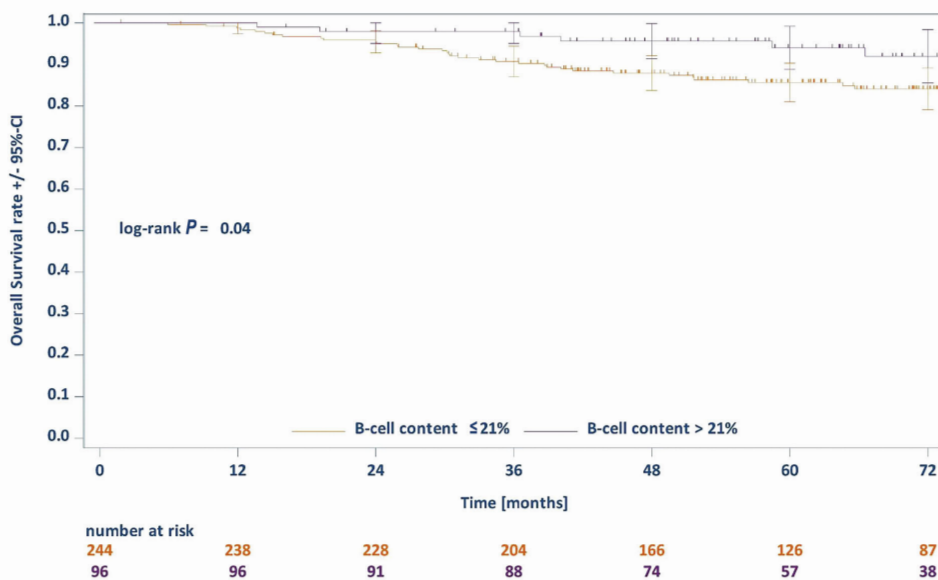
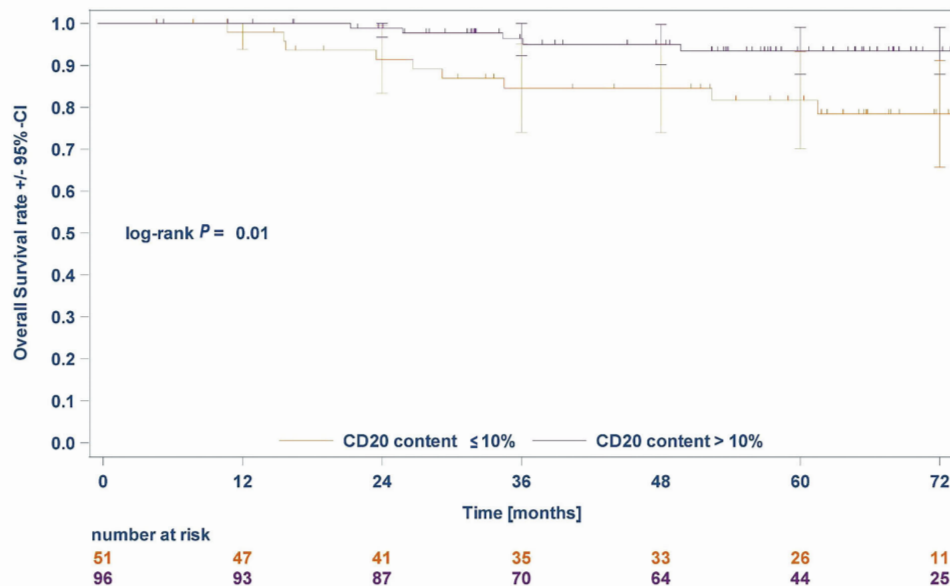
A Project cohort

Figure 4. Overall survival according to CD20 content. (A) Kaplan-Meier plots of overall survival in the study cohort for the two risk groups according to B-cell content (CD20-positive cell rate: $\leq 21\%$ or $> 21\%$). (B) Kaplan-Meier plots of overall survival in the validation cohort for the two risk groups according to B-cell content (CD20-positive cell rate: $\leq 10\%$ or $> 10\%$).

B Validation cohort

a robust discrimination of patients at high risk of experiencing relapse or progressive disease and thus identifies a population of patients who may qualify for novel first-line treatment strategies. Furthermore, we envision that WSI may also be applied to identify patients in whom de-escalation of treatment intensity may be possible. We thus anticipate the use of WSI in all future GHSG studies. Even though additional testing is required to define cut-off values, this approach is close to clinical application since the data required (CD20 staining) are generated in the standard diagnostic workup of any cHL around the world. We cannot imagine any other technology with such a broad potential for application, considering that even in less well-developed countries access may be affordable.

Finally, this is a unique opportunity to establish a risk model looking specifically at the microenvironment in prospective clinical trials.

Disclosures

AE: consultancy or advisory services for and honoraria from Takeda and BMS; research funding from Takeda, BMS and Affimed; honoraria. HCR: consultancy or advisory services for Abbvie and AstraZeneca; research funding from Gilead Sciences. BvT: consultancy or advisory services for Amgen, Pfizer, Takeda and MSD; honoraria from Roche, Takeda and MSD; research funding from Novartis, MSD and Takeda. WK: consultancy or advisory services for and honoraria from Takeda; research funding from Takeda, Amgen, Regeneron and Roche.

Contributions

RDJ, AP, HH, SR, AE and WK designed the research. RDJ, LP, SR, AG, AP, HH, LF, FF, MO, FJ, CT, MLH, PM, AR, HS, HCR, PB, BvT, AE and WK collected and assembled the data. RDJ, SR, AP, AE and WK analyzed and interpreted the data. RDJ and WK wrote the first draft and all authors approved the paper.

Acknowledgments

The authors thank all patients enrolled in GHSG clinical trials,

all clinicians and pathologists supporting the clinical trials and the translational research program of the GHSG.

Funding

This work was supported by a grant from German Cancer Aid (Deutsche Krebshilfe n. 70112502), the Else Kröner-Fresenius Stiftung (2016-Kolleg-19 to RDJ) and the Stiftung Kölner Krebsforschung (to RDJ). Image analysis software was supported by the Kinderkrebsinitiative Buchholz, Holm-Seppensen.

References

1. Diehl V, Franklin J, Pfreundschuh M, et al. Standard and increased-dose BEACOPP chemotherapy compared with COPP-ABVD for advanced Hodgkin's disease. *N Engl J Med.* 2003;348(24):2386-2395.
2. Sjöberg J, Halthur C, Kristinsson SY, et al. Progress in Hodgkin lymphoma: a population-based study on patients diagnosed in Sweden from 1973-2009. *Blood.* 2012;119(4):990-996.
3. Goodman KA, Riedel E, Serrano V, et al. Long-term effects of high-dose chemotherapy and radiation for relapsed and refractory Hodgkin's lymphoma. *J Clin Oncol.* 2008;26(32):5240-5247.
4. Eichenauer DA, Engert A, Andre M, et al. Hodgkin's lymphoma: ESMO Clinical Practice Guidelines for diagnosis, treatment and follow-up. *Ann Oncol.* 2014;25(Suppl 3):iii70-75.
5. Aoki T, Steidl C. Novel biomarker approaches in classic Hodgkin lymphoma. *Cancer J.* 2018;24(5):206-214.
6. Condeelis J, Pollard JW. Macrophages: obligate partners for tumor cell migration, invasion, and metastasis. *Cell.* 2006;124(2):263-266.
7. Vassallo J, Metze K, Traina F, et al. Further remarks on the expression of CD20 in classical Hodgkin's lymphomas. 2002;87(3):ELT17.
8. Rassidakis GZ, Medeiros LJ, Viviani S, et al. CD20 expression in Hodgkin and Reed-Sternberg cells of classical Hodgkin's disease: associations with presenting features and clinical outcome. *J Clin Oncol.* 2002;20(5):1278-1287.
9. Aldred V, Vassallo J, Froes MCAH, Augusto Soares F. CD20 expression by Hodgkin-Reed-Sternberg cells in classical Hodgkin lymphoma is related to reduced overall survival in young adult patients. *Leuk Lymphoma.* 2008;49(11):2198-2202.
10. Portlock CS, Donnelly GB, Qin J, et al. Adverse prognostic significance of CD20 positive Reed-Sternberg cells in classical Hodgkin's disease. *Br J Haematol.* 2004;125(6):701-708.
11. Steidl C, Farinha P, Gascoyne RD. Macrophages predict treatment outcome in Hodgkin's lymphoma. *Haematologica.* 2011;96(2):186-189.
12. Steidl C, Lee T, Shah SP, et al. Tumor-associated macrophages and survival in classic Hodgkin's lymphoma. *N Engl J Med.* 2010;362(10):875-885.
13. Tzankov A, Matter MS, Dimhofer S. Refined prognostic role of CD68-positive tumor macrophages in the context of the cellular micromilieu of classical Hodgkin lymphoma. *Pathobiology.* 2010;77(6):301-308.
14. Kamper P, Bendix K, Hamilton-Dutoit S, et al. Tumor-infiltrating macrophages correlate with adverse prognosis and Epstein-Barr virus status in classical Hodgkin's lymphoma. *Haematologica.* 2011;96(2):269-276.
15. Panico L, Ronconi F, Lepore M, et al. Prognostic role of tumor-associated macrophages and angiogenesis in classical Hodgkin lymphoma. *Leuk Lymphoma.* 2013;54(11):2418-2425.
16. Chetaille B, Bertucci F, Finetti P, et al. Molecular profiling of classical Hodgkin lymphoma tissues uncovers variations in the tumor microenvironment and correlations with EBV infection and outcome. *Blood.* 2009;113(12):2765-2775.
17. Greaves P, Clear A, Coutinho R, et al. Expression of FOXP3, CD68, and CD20 at diagnosis in the microenvironment of classical Hodgkin lymphoma is predictive of outcome. *J Clin Oncol.* 2013;31(2):256-262.
18. Tudor CS, Distel LV, Eckhardt J, et al. B cells in classical Hodgkin lymphoma are important actors rather than bystanders in the local immune reaction. *Hum Pathol.* 2013;44(11):2475-2486.
19. Borchmann P, Haverkamp H, Diehl V, et al. Eight cycles of escalated-dose BEACOPP compared with four cycles of escalated-dose BEACOPP followed by four cycles of baseline-dose BEACOPP with or without radiotherapy in patients with advanced-stage Hodgkin's lymphoma: final analysis of the HD12 trial of the German Hodgkin Study Group. *J Clin Oncol.* 2011;29(32):4234-4242.
20. Engert A, Haverkamp H, Kobe C, et al. Reduced-intensity chemotherapy and PET-guided radiotherapy in patients with advanced stage Hodgkin's lymphoma (HD15 trial): a randomised, open-label, phase 3 non-inferiority trial. *Lancet.* 2012;379(9828):1791-1799.
21. Borchmann P, Goergen H, Kobe C, et al. PET-guided treatment in patients with advanced-stage Hodgkin's lymphoma (HD18): final results of an open-label, international, randomised phase 3 trial by the German Hodgkin Study Group. *Lancet.* 2018;390(10114):2790-2802.
22. Hutchings M, Loft A, Hansen M, et al. FDG-PET after two cycles of chemotherapy predicts treatment failure and progression-free survival in Hodgkin lymphoma. *Blood.* 2006;107(1):52-59.
23. Scott DW, Chan FC, Hong F, et al. Gene expression-based model using formalin-fixed paraffin-embedded biopsies predicts overall survival in advanced-stage classical Hodgkin lymphoma. *J Clin Oncol.* 2013;31(6):692-700.
24. Tan KL, Scott DW, Hong F, et al. Tumor-associated macrophages predict inferior outcomes in classic Hodgkin lymphoma: a correlative study from the E2496 Intergroup trial. *Blood.* 2012;120(16):3280-3287.
25. Azambuja D, Natkunam Y, Biasoli I, et al. Lack of association of tumor-associated macrophages with clinical outcome in patients with classical Hodgkin's lymphoma. *Ann Oncol.* 2012;23(3):736-742.
26. Sanchez-Espiridon B, Martin-Moreno AM, Montalban C, et al. Immunohistochemical markers for tumor associated macrophages and survival in advanced classical Hodgkin's lymphoma. *Haematologica.* 2012;97(7):1080-1084.
27. Diefenbach CS, Li H, Hong F, et al. Evaluation of the International Prognostic Score (IPS-7) and a Simpler Prognostic Score (IPS-3) for advanced Hodgkin lymphoma in the modern era. *Br J Haematol.* 2015;171(4):530-538.
28. Guisado-Vasco P, Arranz-Saez R, Canales M, et al. Stage IV and age over 45 years are the only prognostic factors of the International Prognostic Score for the outcome of advanced Hodgkin lymphoma in the Spanish Hodgkin Lymphoma Study Group series. *Leuk Lymphoma.* 2012;53(5):812-819.
29. Sanchez-Aguilera A, Montalban C, de la Cueva P, et al. Tumor microenvironment and mitotic checkpoint are key factors in the outcome of classic Hodgkin lymphoma. *Blood.* 2006;108(2):662-668.
30. Panico L, Tenneriello V, Ronconi F, et al. High CD20+ background cells predict a favorable outcome in classical Hodgkin lymphoma and antagonize CD68+ macrophages. *Leuk Lymphoma.* 2015;56(6):1636-1642.
31. Sanchez-Espiridon B, Montalban C, Lopez A, et al. A molecular risk score based on 4 functional pathways for advanced classical Hodgkin lymphoma. *Blood.* 2010;116(8):e12-17.
32. Griss J, Bauer W, Wagner C, et al. B cells sustain inflammation and predict response to immune checkpoint blockade in human melanoma. *Nat Commun.* 2019;10(1):4186.
33. Cader FZ, Schackmann RCJ, Hu X, et al. Mass cytometry of Hodgkin lymphoma reveals a CD4(+) regulatory T-cell-rich and exhausted T-effector microenvironment. *Blood.* 2018;132(8):825-836.
34. Carey CD, Guseleinert D, Lipschitz M, et al. Topological analysis reveals a PD-L1-associated microenvironmental niche for Reed-Sternberg cells in Hodgkin lymphoma. *Blood.* 2017;130(22):2420-2430.

Whole exome sequencing reveals NOTCH1 mutations in anaplastic large cell lymphoma and points to Notch both as a key pathway and a potential therapeutic target

Hugo Larose,^{1,2} Nina Prokoph,^{1,2} Jamie D. Matthews,¹ Michaela Schleiderer,³ Sandra Höglar,⁴ Ali F. Alsulami,⁵ Stephen P. Ducray,^{1,2} Edem Nugloze,⁶ Mohammad Feroze Fazaludeen,⁷ Ahmed Elmouna,⁶ Monica Ceccon,^{2,8} Luca Mologni,^{2,8} Carlo Gambacorti-Passerini,^{2,8} Gerald Hoefler,⁹ Cosimo Lobello,^{2,10} Sarka Pospisilova,^{2,10,11} Andrea Janikova,^{2,11} Wilhelm Woessmann,^{2,12} Christine Damm-Welk,^{2,12} Martin Zimmermann,¹³ Alina Fedorova,¹⁴ Andrea Malone,¹⁵ Owen Smith,¹⁵ Mariusz Wasik,^{2,16} Giorgio Inghirami,¹⁷ Laurence Lamant,¹⁸ Tom L. Blundell,⁵ Wolfram Klapper,¹⁹ Olaf Merkel,^{2,3} G. A. Amos Burke,²⁰ Shahid Mian,⁶ Ibraheem Ashankty,²¹ Lukas Kenner^{2,3,22} and Suzanne D. Turner^{1,2,10}



Ferrata Storti Foundation

Haematologica 2021
Volume 106(6):1693-1704

¹Department of Pathology, University of Cambridge, Cambridge, UK; ²European Research Initiative for ALK Related Malignancies (ERIA; www.ERIALCL.net); ³Department of Pathology, Medical University of Vienna, Vienna, Austria; ⁴Unit of Laboratory Animal Pathology, University of Veterinary Medicine Vienna, Vienna, Austria; ⁵Department of Biochemistry, University of Cambridge, Tennis Court Road, Cambridge, UK; ⁶Molecular Diagnostics and Personalised Therapeutics Unit, Colleges of Medicine and Applied Medical Sciences, University of Ha'il, Ha'il, Saudi Arabia; ⁷Neuroinflammation Research Group, Department of Neurobiology, A.I Virtanen Institute for Molecular Sciences, University of Eastern Finland, Finland; ⁸University of Milano-Bicocca, Monza, Italy; ⁹Diagnostic and Research Institute of Pathology, Medical University of Graz, Graz, Austria; ¹⁰Center of Molecular Medicine, CEITEC, Masaryk University, Brno, Czech Republic; ¹¹Department of Internal Medicine - Hematology and Oncology, University Hospital Brno, Czech Republic; ¹²University Hospital Hamburg-Eppendorf, Pediatric Hematology and Oncology, Hamburg, Germany; ¹³Department of Pediatric Hematology/Oncology and Blood Stem Cell Transplantation, Hannover Medical School, Hannover, Germany; ¹⁴Belarusian Center for Pediatric Oncology, Hematology and Immunology, Minsk, Belarus; ¹⁵Our Lady's Children's Hospital, Crumlin, Ireland; ¹⁶Perelman School of Medicine, Philadelphia, PA, USA; ¹⁷Department of Pathology and Laboratory Medicine, Cornell University, New York, NY USA; ¹⁸Institut Universitaire du Cancer Toulouse, Oncopole et Université Paul-Sabatier, Toulouse, France; ¹⁹Department of Pathology, Hematopathology Section, UKSH Campus Kiel, Kiel, Germany; ²⁰Department of Paediatric Oncology, Addenbrooke's Hospital, Cambridge, UK; ²¹Department of Medical Technology Laboratory, College of Applied Medical Sciences, King Abdulaziz University, Jeddah, Saudi Arabia and ²²Ludwig-Boltzmann Institute for Cancer Research, Vienna, Austria

ABSTRACT

Patients diagnosed with anaplastic large cell lymphoma (ALCL) are still treated with toxic multi-agent chemotherapy and as many as 25-50% of patients relapse. To understand disease pathology and to uncover novel targets for therapy, we performed whole-exome sequencing of anaplastic lymphoma kinase (ALK)⁺ ALCL, as well as gene-set enrichment analysis. This revealed that the T-cell receptor and Notch pathways were the most enriched in mutations. In particular, variant T349P of NOTCH1, which confers a growth advantage to cells in which it is expressed, was detected in 12% of ALK⁺ and ALK⁻ ALCL patients' samples. Furthermore, we demonstrated that NPM-ALK promotes NOTCH1 expression through binding of STAT3 upstream of NOTCH1. Moreover, inhibition of NOTCH1 with γ -secretase inhibitors or silencing by short hairpin RNA leads to apoptosis; co-treatment *in vitro* with the ALK inhibitor crizotinib led to additive/synergistic antitumor activity suggesting that this may be an appropriate combination

Correspondence:

SUZANNE D. TURNER
sdt36@cam.ac.uk

Received: September 19, 2019.

Accepted: April 9, 2020.

Pre-published: April 23, 2020.

<https://doi.org/10.3324/haematol.2019.238766>

©2021 Ferrata Storti Foundation

Material published in *Haematologica* is covered by copyright. All rights are reserved to the Ferrata Storti Foundation. Use of published material is allowed under the following terms and conditions: <https://creativecommons.org/licenses/by-nc/4.0/legalcode>. Copies of published material are allowed for personal or internal use. Sharing published material for non-commercial purposes is subject to the following conditions: <https://creativecommons.org/licenses/by-nc/4.0/legalcode>, sect. 3. Reproducing and sharing published material for commercial purposes is not allowed without permission in writing from the publisher.



therapy for future use in the circumvention of ALK inhibitor resistance. Indeed, crizotinib-resistant and -sensitive ALCL were equally sensitive to γ -secretase inhibitors. In conclusion, we show a variant in the extracellular domain of NOTCH1 that provides a growth advantage to cells and confirm the suitability of the Notch pathway as a second-line druggable target in ALK⁺ ALCL.

Introduction

Systemic anaplastic large cell lymphoma (ALCL) is a T-cell malignancy accounting for approximately 15% of all cases of pediatric lymphoma and 1-2% of adult lymphomas.¹ The majority of pediatric cases (>90%) express NPM-ALK, the result of the t(2;5)(p23;q35) translocation, creating a fusion between the nucleolar phosphoprotein gene *nucleophosmin1* (*NPM1*) and *anaplastic lymphoma kinase* (*ALK*), leading to the ALK⁺ ALCL diagnostic entity, although other ALK fusion proteins also exist.^{2,3} ALK fusion proteins induce the activation of several downstream signaling pathways involved in oncogenesis, including PI3K, ERK1/2 MAP kinase, and JAK-STAT.

Genetic studies conducted to date have not revealed consistent genetic abnormalities among ALK⁺ ALCL, although a higher frequency of genomic gains and losses has been associated with a poorer prognosis.⁴⁻⁶ Genomic gains include the region encoding the *NOTCH1* locus,⁴ which may explain why *NOTCH1* is expressed in the majority of ALK⁺ ALCL and in some ALK⁻ ALCL.^{7,8} In contrast, for ALK-ALCL, mutations in the JAK1/STAT3 pathway have been described.⁹

ALK⁺ ALCL is largely a chemosensitive malignancy, although despite good initial responses, the relapse rate reaches 50% independently of the chemotherapy regimen used;¹⁰⁻¹⁴ therefore, new therapies are needed for patients who do not respond to standard chemotherapy. There is also a need for less toxic treatment schedules for low-risk patients. Crizotinib, a small molecule ATP-competitive inhibitor of ALK/MET/ROS1 which is currently in clinical trials (NCT01606878, NCT02034981) for pediatric ALK⁺ lymphoid malignancies, given as monotherapy produces remission in more than 80% of relapsed patients, although rapid relapse on discontinuation of therapy has been reported.^{11,15-17} As such, second-line treatment and combination therapies for relapsed patients are still required. We therefore conducted whole exome sequencing (WES) of 25 ALK⁺ ALCL tumors, validating data in a further 78 cases of ALCL to understand disease pathology and to uncover novel targets for therapy. Beside the T-cell receptor (TCR) pathway, the most commonly affected signaling axis is that involving NOTCH1, of which a T349P variant provides a growth advantage to cells. Furthermore, *NOTCH1* is expressed as a consequence of NPM-ALK-driven STAT3 activity, a key signaling node in ALCL. Accordingly, the NOTCH1 pathway provides a target for second-line therapy, whereby γ -secretase inhibitors (GSI) show synergistic activity with inhibitors of ALK, and are efficacious as single agents in ALK-inhibitor resistant cell lines. Finally, we show evidence that NOTCH1 is a biomarker predictive of relapse risk.

Methods

Patients' samples

Patients' tumor tissues (at initial presentation) and matched peripheral blood DNA were obtained following patient/parental

consent according to both the Declaration of Helsinki and local guidelines from the following institutions: Children's Cancer and Leukaemia Group tissue bank, Newcastle, UK (*Online Supplementary Table S1*); Institut Universitaire du Cancer Toulouse, France; University Hospital Brno, Czech Republic; Biobank of the Medical University of Graz, Austria; Belarusian Center for Pediatric Oncology, Hematology and Immunology, Minsk, Belarus; Justus-Liebig University, Giessen, Germany; and Our Lady's Children's Hospital, Crumlin, Ireland (*Online Supplementary Table S2*). All tissues were obtained and processed with full ethical approval (NHS Research ethics committee reference numbers 07/Q0104/16, 06/MRE04/90 and 08/H0405/22+5).

The patient tissue microarray used here has been described elsewhere.¹⁸ Briefly, formalin-fixed paraffin-embedded (FFPE) tissue specimens from pediatric, patients with NPM-ALK⁺ ALCL treated in the Berlin-Frankfurt-Münster (BFM) group study NHL-BFM90, NHL-BFM95 or patients enrolled in the European intergroup trial ALCL99 between August 1998 and December 2008 were obtained from both male and female children (*Online Supplementary Table S3*) with informed consent and in accordance with the Declaration of Helsinki. Eligibility was confirmed by demonstration of NPM-ALK positivity of the tumor either by NPM-ALK polymerase chain reaction, two-color fluorescence *in situ* hybridization for the t(2;5), or nuclear and cytoplasmic staining for ALK. The inclusion criteria were fulfilled by 89 patients.

Whole exome sequencing

DNA was extracted from fresh-frozen tissue from patients (n=18; with a tumor content >90%) and matched peripheral blood from four patients using the QIAgen DNAeasy Blood and Tissue Kit (Qiagen, Hilden, Germany), following the manufacturer's instructions. Library preparation was conducted using the Nextera Rapid Capture Exome Kit before samples were sequenced, at either the Washington State University Core (Illumina HiSeq2500) or the Molecular Diagnostics and Personalized Therapeutics Unit, University of Ha'il (Illumina MiSeq) (*Online Supplementary Table S4*). Sequencing data are available at the Sequence Read Archive (<https://www.ncbi.nlm.nih.gov/sra>) under accession number PRJNA491296. The bioinformatic processing is detailed in the *Online Supplementary Methods*.

Immunohistochemistry, pathology and quantification

Immunohistochemistry was performed on FFPE sections with the conventional avidin-biotin-peroxidase method. Heat antigen retrieval was performed using citrate buffer, pH 6.1. Endogenous peroxidases were quenched by incubating sections in 3% H₂O₂ in phosphate-buffered saline (PBS) for 10 min. An avidin/biotin and a protein block were subsequently performed. Primary antibodies (*Online Supplementary Table S5*) were added in 1% bovine serum albumin/PBS at 4°C overnight. Slides were incubated with biotin-conjugated secondary antibodies and then with horse radish peroxidase (HRP) using the IDetect Super Stain System – HRP and developed under visual control using aminoethyl carbazole. Hemalaun counterstaining was performed and slides mounted with AquaTex. Sections were washed with PBS three times in between each step. Stained slides were assessed for cleaved NOTCH1 staining by an experienced pathologist (blinded with respect to clinicopathological parameters and patients' outcome)

using the histoscore system. Stained slides were scored qualitatively for the intensity of staining and classified as showing negative, weak, moderate or strong staining (to qualify for 'moderate' or 'strong' staining, at least 10% of cells had to stain positive). Analysis of event-free survival was performed as described previously,¹⁹ grouping negative and weak staining into 'low cleaved NOTCH1 expression' and moderate and strong into 'high cleaved NOTCH1 expression'.

Statistical analyses

All experiments were executed in biological triplicates. The MTT, RealTimeGlo, apoptosis, cell cycle and quantitative polymerase chain reaction assays were additionally executed with technical triplicates. All plots are representative of the mean of the biological replicates, while the error bars represent the standard deviation. Two-tailed *t*-tests were used to calculate the *P*-value when comparing two samples (multiple comparisons were corrected using the Holm-Sidak method); when comparing more than two samples, two-way analysis of variance (ANOVA) was used (again, multiple comparisons were corrected using the Holm-Sidak method). Statistical tests were conducted using GraphPad PRISM 8 (Graphpad).

Results

The genomic profile of anaplastic large cell lymphoma

Eighteen ALK⁺ ALCL exomes sequenced in this study in addition to seven previously sequenced samples⁹ (*Online Supplementary Table S1*) were analyzed. The samples comprised 17 pediatric cases (≤ 18 years) and eight adult cases (*Online Supplementary Table S4*); a flowchart illustrating the cohorts of patients is shown in *Online Supplementary Figure S1*. All patient samples were collected at diagnosis. Data regarding variants found in at least a quarter of the patients are summarized in Figure 1, which shows that the most commonly mutated genes in both adult and pediatric cases were *TYW1B*, *DEFB132* and *KCNJ18* (the full list of variants can be found in *Online Supplementary Table S6*). None of the variants in these genes has been reported previously in hematologic malignancies and were not studied further here. Two patients presented with one mutation each in *TP53* (COSMIC ID: COSM3958801 and COSM9969). We also studied copy number variations, but found no novel events larger than 100,000 bp present consistently in more than one sample at a sequencing depth of at least 50x (*Online Supplementary Figure S2A*, *Online Supplementary Table S7*), as previously observed.⁴ Among previously reported alterations in ALCL, a single copy gain on chromosome 7 was observed in three patient tumor samples (S3, S9 and S15)⁵ and a single copy loss on chromosome 17p was also seen in three patients (S9, S14 and S57).⁶

The most predominant single nucleotide variants are non-synonymous and are present at higher levels in patients who subsequently relapsed

The majority of somatic variants detected in the 25 tumor samples were non-synonymous single nucleotide variants (39.4%), in keeping with a previous publication reporting that the ALK⁺ ALCL genome is largely stable.⁴ Single nucleotide variants were followed in frequency by frameshift and non-frameshift deletions and splice variants (24.1%, 10.8% and 10.6%, respectively), while the germline genome of ALCL patients points to an overwhelming presence of single nucleotide polymorphisms

(89.3%) (*Online Supplementary Figure S2B*). The proportion of each type of variant detected differed between patient tumors (Figure 2B), although in general, pediatric patients known to have relapsed (n=9) had a significantly higher proportion of non-synonymous single nucleotide variants than patients who did not (n=9; *P*<0.0001) (Figure 2B), suggesting that a high percentage of non-synonymous single nucleotide variants at diagnosis may be indicative of relapse, although this requires validation in a larger dataset of patients treated with comparable treatment protocols.

Deficiency of DNA repair mechanisms and spontaneous deamination of 5-methyl cytosine are identified as signatures of anaplastic large cell lymphoma

Online Supplementary Figure S2C shows the prevalence, in representative patient S57, of the 96 variant types that were used to derive the mutational signatures (*Online Supplementary Figure S2D*). Examining the type of mutations in the patients for whom matched peripheral blood was available (n=11), showed an enrichment for mutational signatures 1, 3, 12 and 26²⁰ (Figure 2C). Interestingly, 1A is a signature based on the prevalence of C>T transitions at NpCpG trinucleotides and is associated with spontaneous deamination of 5-methyl-cytosine,²¹ whereas signature 3 has its roots in homologous recombination deficiency during DNA double-strand break repair.²⁰ The etiology of signature 12 has not yet been identified, although signature 26 is associated with a breakdown in DNA mismatch repair. The combination of signatures 3 and 26 may indicate, from an evolutionary perspective, how ALCL tumors accumulate mutations. Comparable patterns were found when comparing signatures to the COSMIC signature database²² (*data not shown*). There was no detectable difference between the mutational signature of pediatric (n=4) or adult (n=7) ALK⁺ ALCL patients (data not shown).

Gene set enrichment analysis confirms the importance of T-cell receptor signaling, but also of the Notch pathway in ALK⁺ anaplastic large cell lymphoma pathobiology

Gene set enrichment analysis (GSEA) of mutated genes showed that TCR signaling and Notch pathways are enriched across all five databases used (Figure 2D; *Online Supplementary Table S8*). Further analysis of the domains frequently found in the mutated genes revealed an enrichment in proteins with epidermal growth factor (EGF)-like or calcium-ion binding domains (Figure 2E), two features of the NOTCH1 protein, and indeed the locus of both of the *NOTCH1* mutations identified in this study (see below). Twenty of the 25 patient tumors carry mutations in proteins of the Notch pathway with a range of one to four and a median of two mutations per patient (*Online Supplementary Table S8*). Furthermore, reactome network clustering analysis²³ showed TP53 as a key node, which is not unexpected as TP53 has been reported to play a key role in the pathogenesis of ALCL²⁴ (*Online Supplementary Figure S2E*). Given the importance of the Notch pathway in T-cell biology, particularly in the developing thymus, which we proposed to be the origin of ALK⁺ ALCL,²⁵ and the previous implication of the NOTCH1 pathway in the pathogenesis of ALCL,⁸ the *NOTCH1* mutations detected and the NOTCH1 pathway were explored for their role in the pathogenesis of ALK⁺ ALCL.

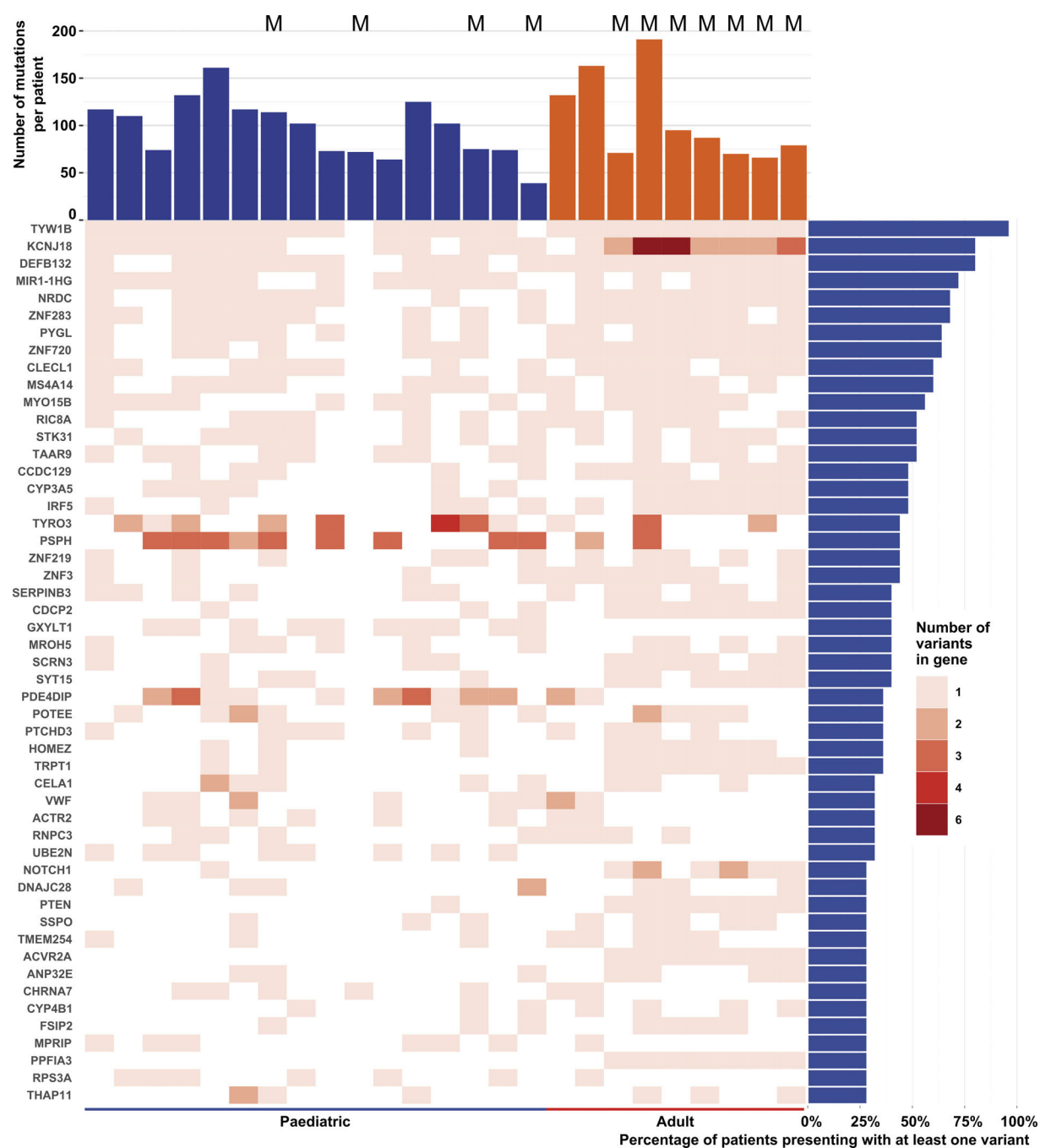


Figure 1. Summary of whole exome sequencing data. Individual results for each patient presented as a heatmap for genes found to be mutated in at least a quarter of patients. The number of different variants presenting in each gene is displayed for individual patients. The total number of variants identified for individual patients is also displayed above the graph. The panel on the right shows the percentage of patients presenting with at least one variant of the indicated gene. Pediatric and adult patients are separated. Patients for whom matched peripheral blood was sequenced are labeled with an 'M'.

NOTCH1 variant T349P provides a growth advantage to cells

Of the 25 ALK⁺ ALCL tumor samples analyzed by WES, 24% presented with the NOTCH1 variant T349P, while 12% had the T311P variant. These data were validated by Sanger sequencing of a further 78 samples (including 18 of the samples previously analyzed by WES with a total of 55 ALK⁺ ALCL, and 23 ALK⁻ ALCL) (Online Supplementary Table S2). In this validation cohort, the T349P variant was detected in 12% of patients (n=78;

15% of ALK⁻ patients and 9.3% of ALK⁺ patients) (Online Supplementary Figure S3A) and the T311P variant was found in 7.6% of patients (n=78; 10.2% of ALK⁺ patients, none in ALK⁻ patients) (Online Supplementary Figure S3B). In the majority of cases, tumors presented with a mutation at either T311P or T349P and therefore the overall incidence of patients with at least one mutation of the EGF-like domain was 18% (n=78), although one patient presented with both mutations. We detected two additional NOTCH1 mutations, H1190P and G1503S,

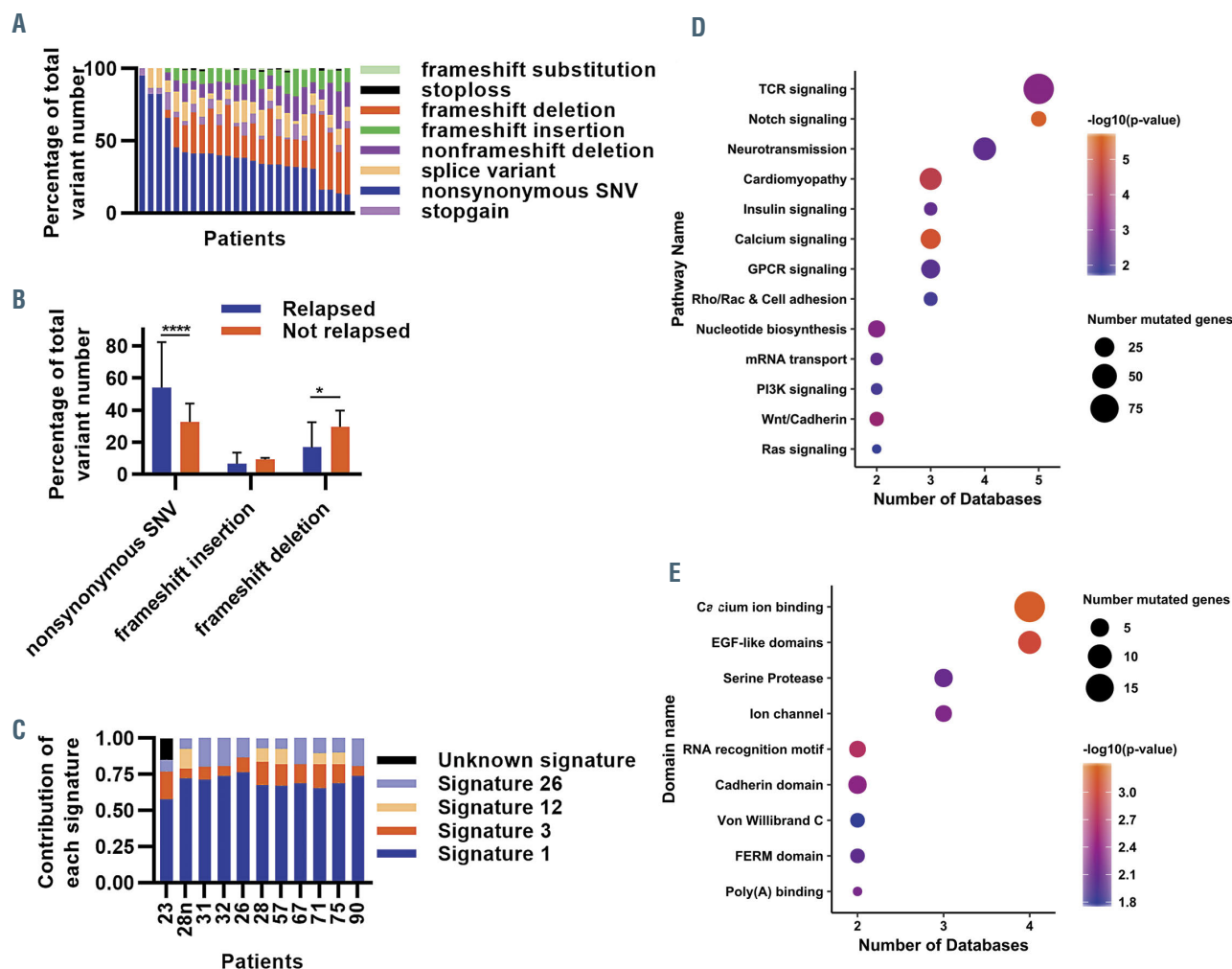


Figure 2. Analysis of whole exome sequencing data yields insights into the ALK+ anaplastic large cell lymphoma genomic landscape. (A) Proportion of variant type for each patient. (B) Mean and standard deviation of the proportion of variant types for patients who did (n=9) or did not (n=9) relapse within 5 years after diagnosis (****P<0.0001). (C) Mutational signatures²⁰ derived from the variant profiles of each of the 11 patients for whom we hold sequenced matched peripheral blood. (D, E) Scatter plots of the pathways (D) or domains (E) found to be enriched in our dataset, displaying the number of databases in which each hit was found to be enriched, along with the $-\log_{10}$ of the statistical enrichment P-value of the software in which each hit was found to be most enriched, and the corresponding number of genes involved. SNV: single nucleotide variant.

although these were only detected in one patient each and so were not studied further. Of note, there was no significant difference in prognosis for patients presenting with NOTCH1 T349P and/or T311P over those with wild-type (WT) NOTCH1 when considering the whole cohort of patients (*Online Supplementary Table S9*, *Online Supplementary Figure S3J*). However, if adult patients were considered in isolation, there was a significant reduction in overall survival for those with NOTCH1 mutations ($P<0.05$) but these data are based on just three patients and so should be interpreted with caution.

Variant T349P, at position 1045, is within the sixth of 34 exons of NOTCH1, which encodes one of the numerous EGF-like domains that make up the extracellular domain of NOTCH1 (EGF-like domain 9 of 36, which is a calcium-binding domain). NOTCH1 T349P was predicted to be a function-altering mutation by variant effect prediction software including SIFT (score=0.01) and PolyPhen (score=0.999), among others.²⁶⁻³⁰ Furthermore, the COSMIC database shows that T311 and T349 are the two most frequently reported mutated amino acids at the presumed NOTCH1/JAG1 interface across a range of

cancers (including chronic myelomonocytic leukemia,³¹ chronic lymphocytic leukemia,³² T-cell acute lymphoblastic leukemia,³³ rhabdomyosarcoma³⁴ and squamous cell carcinoma³⁵) (Figure 3A).

To determine the impact of the detected NOTCH1 mutants on cell proliferation, WT, T349P or T311P mutants of NOTCH1 were expressed in HEK293FT cells (Figure 3B and C). These cells were chosen because of their low levels of endogenous NOTCH1 expression. In comparison, ALCL cell lines express high levels of WT NOTCH1. A significant increase in ATP production, suggestive of enhanced cell proliferation (as determined by a RealTime-Glo assay), was observed at 72 h for cells expressing the NOTCH1 T349P mutant as compared to WT NOTCH1 in the absence of exogenously applied ligand (Figure 3D). The T311P mutant also led to an increase in proliferation, although this was not statistically significant when compared to WT NOTCH1. However, a significant increase in proliferation was detected when using an MTT assay (*Online Supplementary Figure S3J*). In addition, the transcriptional targets of NOTCH1 activity, HES1 and HEY1, were expressed at higher levels in the

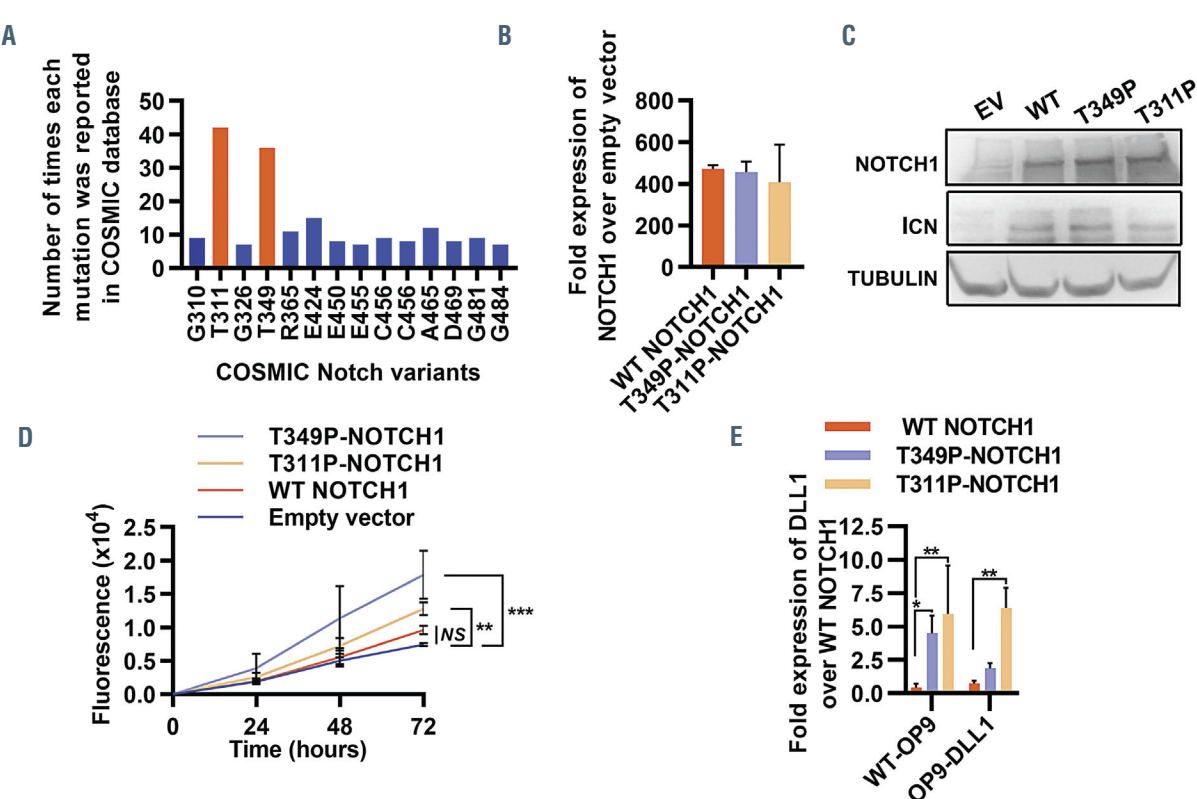


Figure 3. NOTCH1 T349P and T311P mutants confer a growth advantage to cells. (A) The most frequent variants (of the amino acids involved in the NOTCH1-JAG1 interface) of NOTCH1 reported on COSMIC, and the frequency at which they have been reported. (B) Quantitative polymerase chain reaction (qPCR) showing the fold increase in transcript levels of NOTCH1 compared to that in cells transduced with an empty vector (n=3). (C) Western blot for full-length and cleaved intracellular NOTCH1 (ICN) and α -tubulin in HEK293FT cells 48 h after transfection to express wild-type (WT) or mutant (T349P or T311P) NOTCH1, or an empty vector (EV). Only the relevant sections of the whole blot are shown and the contrast of the whole image was modified in order to improve legibility. Data are representative of three biological repeats. (D) Proliferation of HEK293FT cells expressing the indicated proteins or empty vector control as measured by the Real Time Glo assay at 24, 48 and 72 h after transfection (**P<0.001; n=3). (E) Fold-change in expression of DLL1 over the WT NOTCH1 control as assessed by qPCR in HEK293FT cells expressing the indicated proteins and co-cultured with either WT or DLL1-expressing OP9 cells (*P<0.05; **P<0.01; n=3). All bar plots display the mean of biological replicates, and error bars represent the standard deviation.

HEK293FT cells expressing NOTCH1 mutants compared to those transfected with either an empty vector or WT NOTCH1 (*Online Supplementary Figure S3F* and *S3G*). These data are suggestive of increased NOTCH1 activity as a consequence of the NOTCH1 T349P mutation compared to WT NOTCH1.

To determine why the T349P NOTCH1 mutant led to enhanced cell proliferation, *in silico* modeling was performed to predict the effects of the mutation on protein conformation using a published crystal structure of NOTCH1 bound to one of its ligands (Jagged1; PDBID 5UK5) (*Online Supplementary Figure S3C* and *S3D*).³⁶ The model demonstrated that NOTCH1 residues 349 and 311 mediate binding to NOTCH1 ligands. Therefore, to determine whether increased cell proliferation (Figure 3D) was dependent on NOTCH1 ligand, NOTCH1 WT or mutant-expressing HEK293FT cells were co-cultured with OP9 cells expressing or not the NOTCH1 ligand DLL1. There was no discernible difference in proliferation between cells co-cultured with wild-type OP9, or OP9-DLL1 cells (*Online Supplementary Figure S3E*). However, increased transcription of endogenous DLL1 was observed on expression of the mutant forms of NOTCH1 compared to WT protein, suggesting that the mutant proteins might themselves lead to transcription of ligand in an autonomous fashion (Figure 3E). In an

attempt to validate this, we silenced DLL1 using a specific siRNA (*Online Supplementary Figure S3H*), which reduced the proliferation advantage induced by the NOTCH1 T349P mutant (*Online Supplementary Figure S3I*).

NPM-ALK induces expression of NOTCH1 via STAT3 transcriptional activity in anaplastic large cell lymphoma

Given that ALCL cell lines express high levels of WT NOTCH1,⁸ the mechanism of NOTCH1 expression was investigated. NPM-ALK activity was inhibited by incubation with the ALK/ROS/MET inhibitor crizotinib (Figure 4A) or expression silenced with a specific shRNA (Figure 4D) in three and two cell lines, respectively. In both cases, a significant decrease in transcripts for NOTCH1 (Figure 4B and E) and its transcriptional target HES1 (Figure 4C and F), was observed, suggesting that NOTCH1 transcription and NOTCH1 activity are dependent on NPM-ALK. Given that STAT3 is a key nodal downstream target of NPM-ALK, STAT3 expression was inhibited by employing specific shRNA in ALCL cell lines (Figure 4G). As predicted, transcript levels of NOTCH1 (Figure 4H), HES1 (Figure 4I) and HEY1 (Figure 4J) were all significantly downregulated as a result of STAT3 silencing in both ALK⁺ and ALK⁻ ALCL cell lines (Figure 4H-J, *Online Supplementary Figure S4A*). Analysis of published chro-

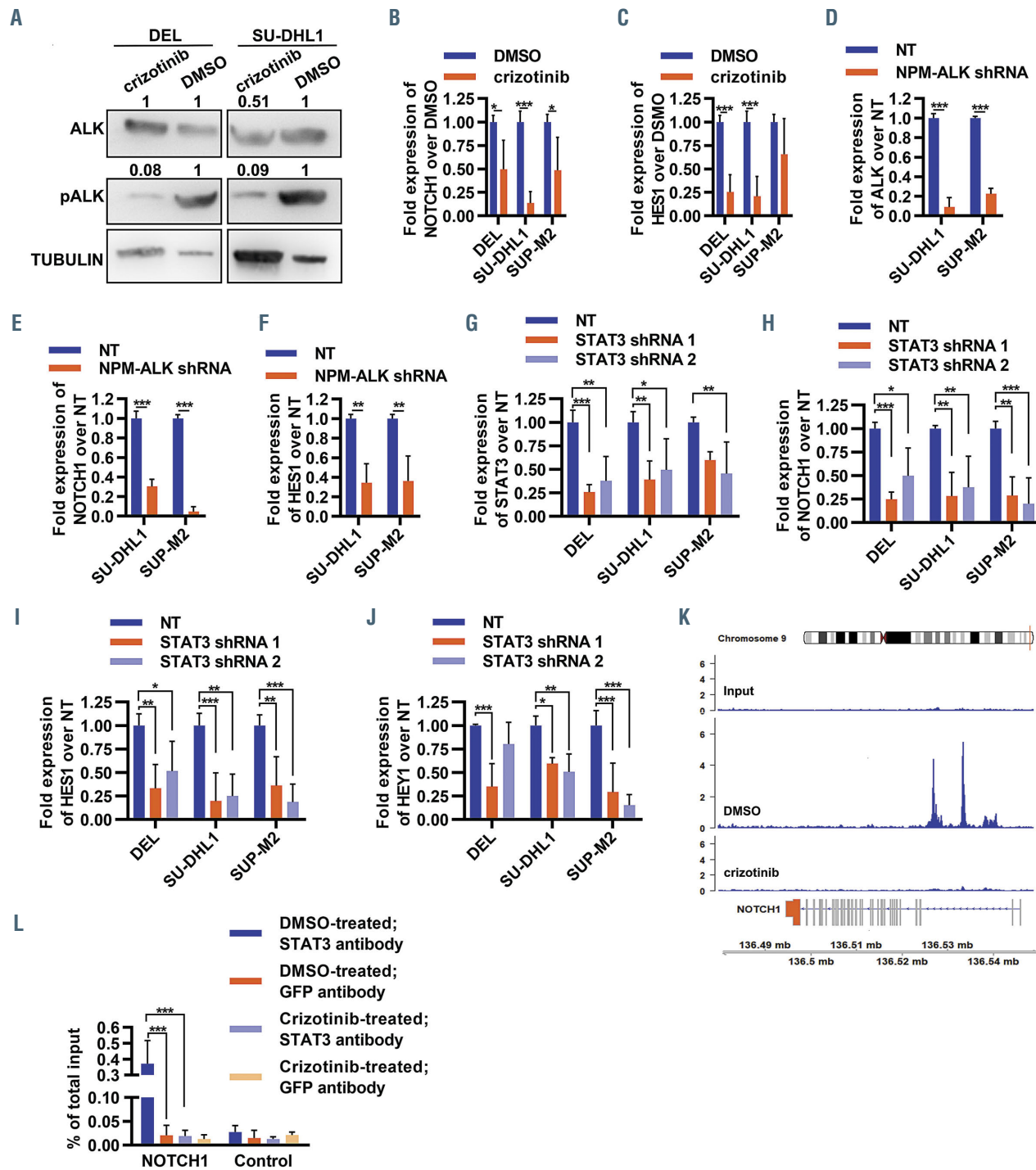


Figure 4. STAT3-mediated regulation of NOTCH1 by NPM-ALK in ALK⁺ anaplastic large cell lymphoma. (A) Representative western blot for ALK, phospho-ALK and α-tubulin in ALK⁺ anaplastic large cell lymphoma (ALCL) cell lines when treated with 300 nM crizotinib or a vehicle control (dimethylsulfoxide, DMSO) for 6 h. Only the relevant sections of the whole blot are shown and the contrast of the whole image was modified in order to improve legibility. Data are representative of three biological replicates. Densitometry is included, as fold-change over the vehicle control and loading control. (B, C) Fold-change expression of NOTCH1 (B) and HES1 (C) over vehicle control in the indicated ALK⁺ ALCL cell lines 48 h after treatment with crizotinib, as determined by quantitative polymerase chain reaction (qPCR) (*P<0.05; **P<0.01; ***P<0.001; n=3). (D-F) Fold-change expression of NPM-ALK (D), NOTCH1 (E) and HES1 (F) over non-targeting control in ALK⁺ ALCL cell lines 48 h after transduction with control non-targeting (NT) shRNA, or a shRNA targeting NPM-ALK, as determined by qPCR (**P<0.01; ***P<0.001; n=3). (G-J) Fold-change expression of STAT3 (G), NOTCH1 (H), HES1 (I) and HEY1 (J) over non-targeting NT control in ALK⁺ ALCL cell lines 48 h after transduction with control NT shRNA, or one of two shRNA targeting STAT3, as determined by qPCR (**P<0.01; ***P<0.001; n=3). (K) Binding of STAT3 to the promoter regions of NOTCH1 in SU-DHL1 cells treated with a vehicle control (middle track) or crizotinib (lower track); the upper track is the input for two separate cell lines, data were obtained by analyzing previously published data.³⁷ (L) Chromatin immunoprecipitation-qPCR binding of STAT3 and GFP at the NOTCH1 promoter region, or at a negative control intergenic region, in SUP-M2 cells treated with either a vehicle control or crizotinib (300 nM) for 6 h, as determined by qPCR (****P<0.0001; n=3), expressed as the percentage of the total input. All measures of expression by qPCR were normalized to GAPDH and PPIA. All bar charts display the mean of biological replicates, and error bars represent standard deviations.

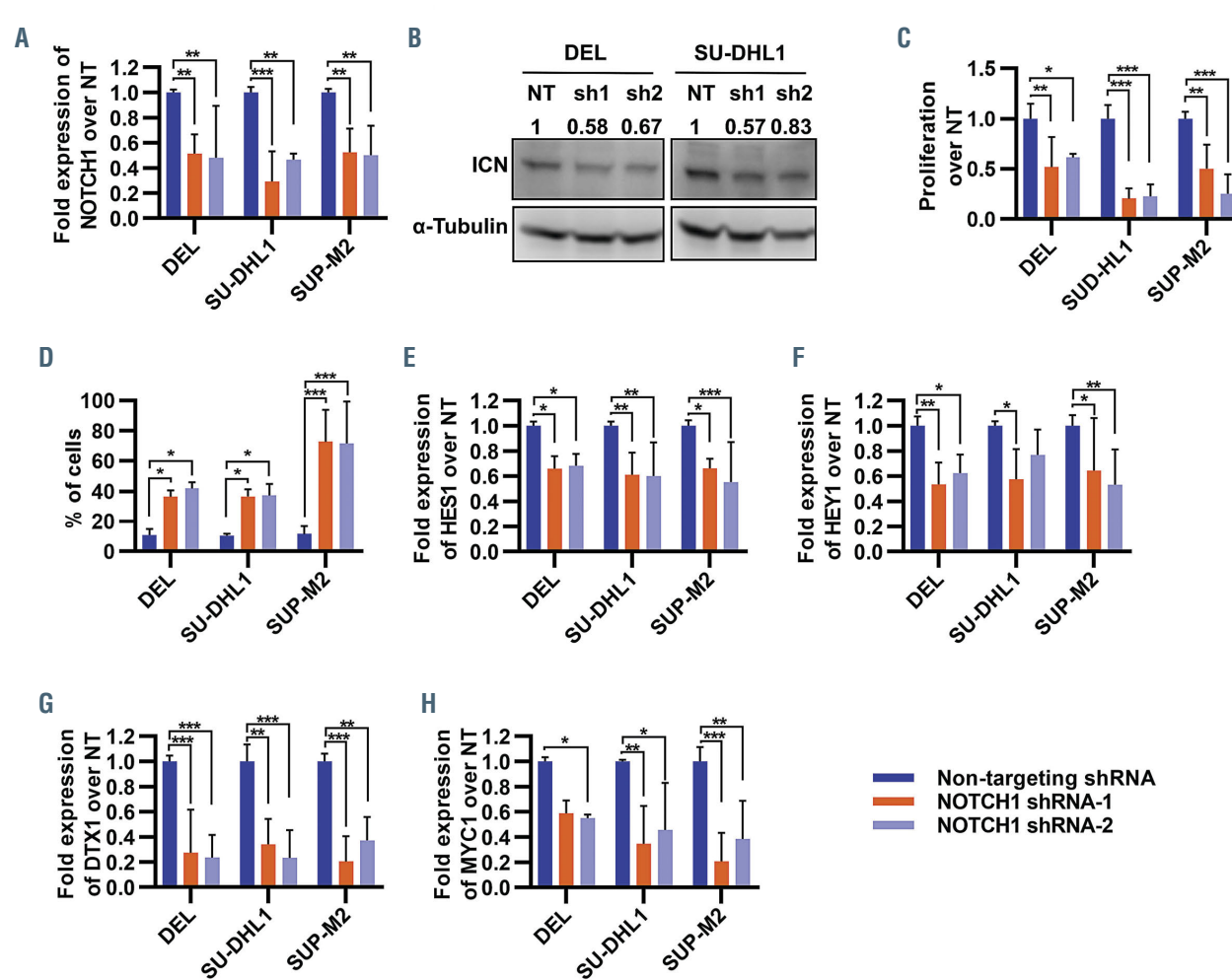


Figure 5. Silencing NOTCH1 expression in anaplastic large cell lymphoma cell lines inhibits cell proliferation and induces cell death. (A) Fold change expression of NOTCH1 over non-targeting (NT) control (normalized to GAPDH and PPIA) in the indicated ALK⁺ anaplastic large cell lymphoma (ALCL) cell lines 48 h after transduction with control non-targeting (NT) shRNA, or one of two shRNA targeting NOTCH1 as determined by quantitative polymerase chain reaction (**P<0.01; ***P<0.001; n=3). (B) Representative western blot for cleaved intracellular NOTCH1 (ICN) and α -tubulin in ALK⁺ ALCL cell lines 48 h after transduction with NT control shRNA, or one of three shRNA targeting NOTCH1. Only the relevant sections of the whole blot are shown and the contrast of the whole image was modified in order to improve legibility. Data are representative of three biological repeats. Densitometry is included as fold-change over the vehicle control and loading control. (C) Proliferation of ALK⁺ ALCL cell lines over the NT control shRNA, determined using an MTT assay 48 h after transduction with NT control shRNA, or one of two shRNA targeting NOTCH1 (*P<0.05; **P<0.01; ***P<0.001; n=3). (D) Quantification of the percentage of cells positive for annexin V and/or propidium iodide 48 h after transduction with NT control shRNA (left panel), or two shRNA targeting NOTCH1 (middle and right panels) (*P<0.05; ***P<0.001; n=3). (E-H) Fold-change of expression of HES1 (E), HEY1 (F), DTX1 (G) or MYC (H) over NT control shRNA transduced cells (normalized to GAPDH and PPIA) in the indicated ALK⁺ ALCL cell lines 48 h after transduction with NT control shRNA, or one of two shRNA targeting NOTCH1, as determined by quantitative polymerase chain reaction (*P<0.05; **P<0.01; ***P<0.001; n=3). All bar plots display the mean of biological replicates, and error bars represent standard deviations; the bar plots are color-coded as indicated in the Figure.

matin immunoprecipitation sequencing data³⁷ of STAT3 binding sites in the ALCL cell lines SU-DHL1 and JB6, treated with either crizotinib or a vehicle control, showed a significant decrease in binding of STAT3 at the NOTCH1 gene in crizotinib-treated cells (Figure 4K, *Online Supplementary Figure S4B*). These data were validated by chromatin immunoprecipitation-quantitative polymerase chain reaction analysis whereby a significant decrease in binding of STAT3 at the NOTCH1 gene upon crizotinib treatment in the SUP-M2 cell lines was observed (Figure 4L).

NOTCH1 is a therapeutic target in ALK⁻ and ALK⁺ anaplastic large cell lymphoma

Given the expression and activity of NOTCH1 in ALCL, its utility as a therapeutic target was investigated. Expression of NOTCH1 was inhibited at both transcript

(Figure 5A, *Online Supplementary Figure S5A*) and protein levels (Figure 5B) by shRNA in both ALK⁺ and ALK⁻ ALCL cell lines leading to a significant decrease in cell proliferation at 48 h, as measured by the MTT assay, in all four cell lines (Figure 5C, *Online Supplementary Figure S5B*) concomitant with a significant increase in the percentage of cells staining positive for either annexin-V or propidium iodide, suggestive of cell death by apoptosis (Figure 5D). As expected, NOTCH1's transcriptional targets HES1 and HEY1 (Figures 5E and 5F, *Online Supplementary Figure S5A*) were also downregulated upon NOTCH1 silencing by shRNA. To further determine the signaling cascade downstream of NOTCH1, we made use of published microarray data examining the effect of GSI treatment on gene expression in T-cell acute lymphoblastic leukemia,³⁸⁻⁴⁰ and found genes such as MYC and DTX1 to be potential targets of NOTCH1 signaling (*Online Supplementary Figure*

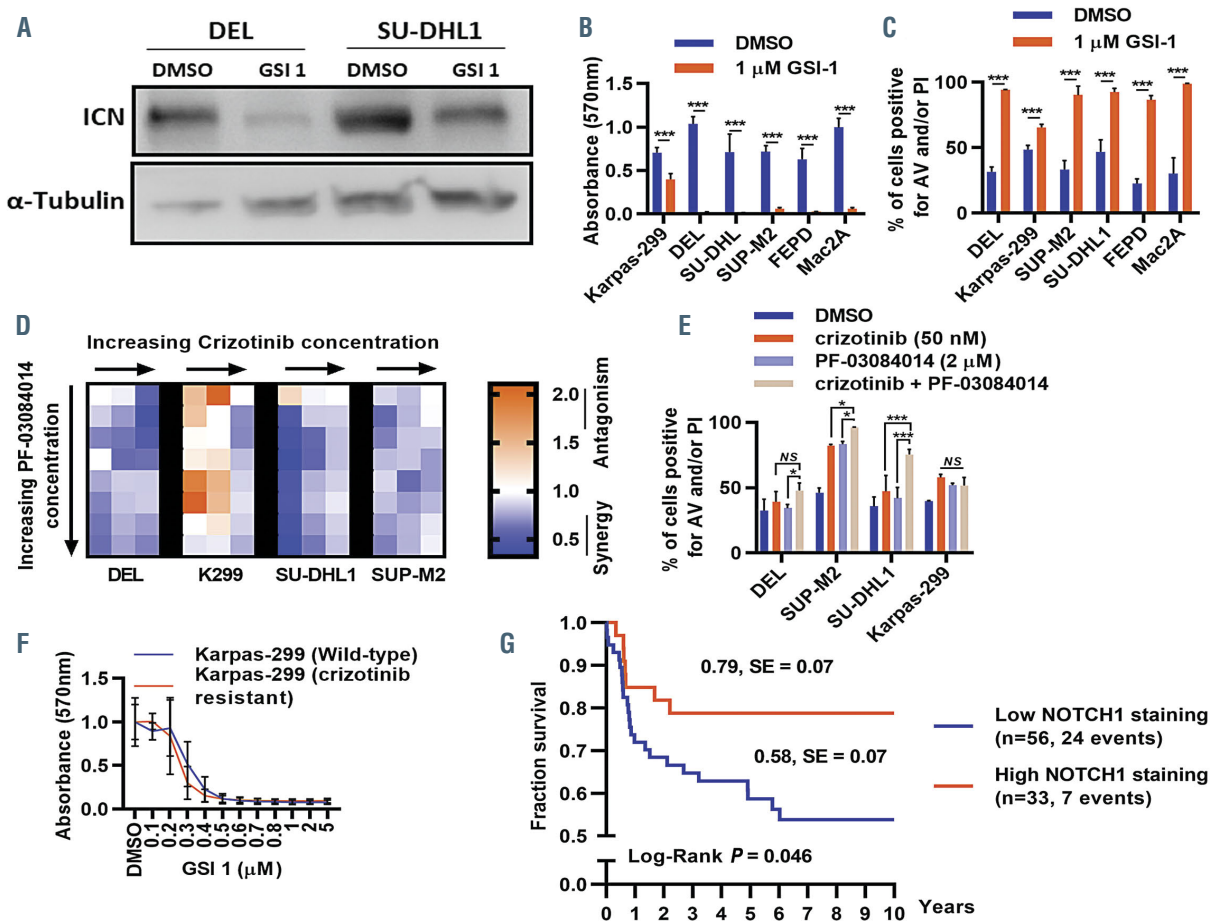


Figure 6. ALK inhibitor sensitive and resistant anaplastic large cell lymphoma cell lines are sensitive to γ -secretase inhibitors. (A) Western blot for cleaved intracellular NOTCH1 (ICN) and α -tubulin in ALK⁺ anaplastic large cell lymphoma (ALCL) cell lines when treated with 1 μ M GSI-1 for 48 h. Only the relevant sections of the whole blot are shown and the contrast of the whole image was modified in order to improve legibility. Data are representative of three biological repeats. (B) Proliferation of a panel of ALK⁺ and ALK⁻ ALCL cell lines treated with 1 μ M of GSI-1 for 48 h, compared to vehicle control, as measured by the MTT assay (**P<0.0001; n=3). (C) Quantification of the percentage of cells positive for annexin V (AV) and/or propidium iodide (PI) when treated with either vehicle control or 1 μ M GSI-1 for 48 h (**P<0.001; n=3). (D) BLISS matrix showing the combination index on treating the indicated ALK⁺ ALCL cell lines with crizotinib and PF-03084014 for 72 h (using a range of concentrations from 25 to 100 nM for crizotinib, and from 100 nM to 10 μ M for PF-03084014). A combination index of <1 indicates synergy between drugs, 1 indicates additive effects, >1 indicates antagonistic effects (n=3). (E) Quantification of the percentage of cells positive for AV and/or PI when treated with either vehicle control, 50 nM crizotinib, 2 μ M PF-03084014 or a combination of PF-03084014 and crizotinib for 48 h (NS: not significant; *P<0.05; **P<0.00; n=3). (F) Proliferation over vehicle control of wild-type or crizotinib-resistant Karpas-299 cells when treated with increasing concentrations of GSI-1, as measured by the MTT assay (n=3). (G) Ten-year event-free survival of patients with ALK⁺ anaplastic large cell lymphoma showing either little or no (n=56), or strong (n=33) NOTCH1 expression. All bar plots display the mean of biological replicates and error bars represent standard deviations.

S5C). In keeping with these data, we show that silencing NOTCH1 by shRNA in the ALK⁺ ALCL cell lines DEL, SU-DHL1 and SUP-M2 (and the ALK⁻ ALCL cell line FEPD) leads to significant decreases in both MYC and DTX1 transcript levels (Figure 5G and H, *Online Supplementary Figure S5A*) and protein levels (*Online Supplementary Figure S5D*), suggesting that NOTCH1 in ALCL signals through a number of pathways beyond HES1 and HEY1. Indeed, analysis of published microarray data suggests that the expression of MYC and NOTCH1, and DTX1 and NOTCH1 correlates in both ALK⁺ and ALK⁻ ALCL, but not in reactive lymph nodes (*Online Supplementary Figure S5E-J*).

Given the reduced cell proliferation and increased cell death observed on shRNA-mediated knockdown of NOTCH1 expression, ALCL cell lines were incubated with two different GSI: GSI-1 (Z-LLNle-CHO) and PF-03084014.⁴¹ GSI-1 inhibited NOTCH1 cleavage, as shown by a decrease in expression of the intracellular domain of

NOTCH1 (ICN) 48 h after drug treatment (Figure 6A), concomitant with a decrease in cell proliferation, as shown by the MTT assay (Figure 6B), and an increase in apoptosis, as determined by positive cell surface staining for annexin V and/or intracellular propidium iodide (Figure 6C, *Online Supplementary Figure S6A*). In contrast, PF-03084014 did not significantly affect cell proliferation or apoptosis on its own at any of the concentrations assessed, ranging from 10 nM to 10 μ M for up to 72 h of incubation (*data not shown*). None of the ALCL cell lines used in the research described here carries either the NOTCH1 T311P or T349P mutation.

Gamma secretase inhibitors synergize with ALK inhibitors to induce cell death

Co-incubation of three of four ALCL cell lines with either PF-03084014 or GSI-1 with crizotinib led to additive to synergistic activity in reducing cell proliferation, as indicated by a Bliss Independence Index of less than one

across several concentrations (Figure 6D, *Online Supplementary Figure S6B*). Karpas 299 cells have different genetic defects, which may explain the antagonistic results in this cell line.⁴² Indeed, a significant increase in apoptotic cells was observed following 48 h of treatment with a combination of 50 nM crizotinib and 2 μ M PF-03084014 (Figure 6E, *Online Supplementary Figure S6C*).

Ideally, a single-agent ALK inhibitor would provide a less toxic frontline treatment approach in the future, although resistance would be expected to develop. Therefore, crizotinib-resistant ALCL cell lines were assessed for their sensitivity to GSI which led to a significant decrease in cell proliferation (Figure 6F, *Online Supplementary Figure S6D-F*). These data suggest the potential use of GSI as either second-line treatment for ALK inhibitor-resistant disease, or frontline therapy in combination with ALK tyrosine kinase inhibitors.

NOTCH1 is a potential biomarker predictive of relapse in ALK⁺ anaplastic large cell lymphoma

A clinically annotated FFPE tissue microarray of 89 ALK⁺ ALCL patient samples, biopsied at the time of the patients' initial presentation, was analyzed for cleaved NOTCH1 protein expression (*Online Supplementary Figure S6G*). Of the 89 patient tumors assessed, 88.8% showed high cleaved NOTCH1 staining (moderate and strong staining categories), in keeping with previously published results.^{7,8,43} Interestingly, patients with low cleaved NOTCH1 staining (negative and weak staining categories) are more likely to relapse (based on the 10-year event-free survival) and have a significantly worse prognosis ($P<0.05$) (Figure 6G).

Discussion

The genetics underlying ALK⁺ ALCL at the level of somatic mutations remains largely unknown. Being a relatively rare cancer with a common, well-characterized driving oncogenic event, more could be done to uncover other genetic alterations. We therefore sequenced 18 ALK⁺ ALCL tumors and analyzed their genome together with seven previously reported ALK⁺ cases⁹ in order to uncover pathogenic mechanisms and novel therapeutic targets. Mutational signature analysis showed signatures 1, 3 and 26 in all our patient samples. The latter two signatures have their roots in homologous recombination DNA double-strand-break repair and mismatch DNA repair deficiency.²⁰ This suggests that DNA damage repair mechanisms might be impaired in these patients, predisposing them to ALCL, perhaps through germline mutations in DNA repair proteins (such as a BRCA2 variant K3326X, COSM4984873, found in germline sample 67B⁴⁴). In contrast, signature 1, accounting for the majority of the total contribution, is associated with a prevalence of C>T transitions at NpCpG trinucleotides and spontaneous deamination of 5-methyl-cytosine, considered an age-related phenomenon due to endogenous mutational processes.²¹ In general, 5-methyl cytosine residues are unstable within DNA and are prone to mutation, representing hotspots for this activity.⁴⁵ This is paradoxical with the young age range of ALK⁺ ALCL patients, with the majority being young adults, and suggests that the mechanism(s) leading to such mutations may be 'speeded up'. Indeed, CpG transitions may be a consequence of secondary factors that promote deamination, such as exogenous mutagens and carcinogens, for example polycyclic aromatic hydrocarbons.⁴⁵

To identify pathways that are key to ALCL biology, GSEA was employed and revealed a number of pathways commonly affected by mutations in ALK⁺ ALCL. Interestingly, the TCR signaling pathway was prominent in our analysis. It has previously been shown that NPM-ALK can substitute for key TCR-induced distal signaling pathways and silencing of proximal proteins has been shown in ALCL.⁴⁶ Another key pathway identified was NOTCH1; gain-of-function mutations in *NOTCH1* have previously been identified in a number of other cancers, most notably in approximately 50 to 60% of T-cell acute lymphoblastic leukemia.^{47,48} However, most of these mutations are in the intracellular domains of the protein, with few reported in the extracellular domains.⁴⁹⁻⁵¹ In contrast, novel mutations in the EGF-like domain of extracellular NOTCH1 were detected in 9.3% (T349P) and 10.2% (T311P) of ALK⁺ ALCL patients analyzed in this study. Predicted to be deleterious, the functional significance of these mutations was investigated using bioinformatics analysis. It has previously been shown that EGF-like domains 8 to 12 are important for NOTCH1 binding to its ligands.⁵² Specifically, threonine bases, lost in T349P and T311P, within the EGF-like domains are post-translationally modified by O-linked glycosylation which is necessary for ligand-engaged NOTCH1 signaling.⁵³⁻⁵⁵ Mutations to proline, a rigid and bulky amino acid, result in a change in tertiary structure, often forcing a change in β -sheet conformation (EGF-like domains are made of β -sheets among others). We demonstrated the positive impact of the T349P mutant on NOTCH1 activity, as shown by enhanced cell proliferation when expressed in HEK293 cells. We theorize that NOTCH1 T349P could modulate ligand binding (either directly or through modulation of calcium binding, particularly as calcium signaling is thought to be dysregulated in ALCL and calcium ions play an important role in NOTCH1 ligand binding^{56,57}).

Regardless of the presence of NOTCH1 mutations, NOTCH1 constitutes a therapeutic target in ALCL independently of ALK status; suppression of NOTCH1 expression or activity led to an increase in apoptosis, in keeping with previous reports.^{7,8,58} Intriguingly, NPM-ALK has previously been shown to be sufficient to induce NOTCH1 expression.²⁵ Not only did we confirm this by silencing NPM-ALK in ALCL, but we also showed that NPM-ALK acts through STAT3, which binds to the *NOTCH1* promoter. This could explain why we observed synergistic effects between crizotinib and GSI in inducing cell death despite our evidence that NPM-ALK promotes NOTCH1 expression. Indeed, studies have shown that crizotinib synergizes with brentuximab vedotin, which targets CD30-expressing cells, despite NPM-ALK having been shown to drive CD30 expression.⁵⁹ ALK inhibitors are now being added to frontline therapy⁶⁰ (e.g., in trial NCT01979536) although this combination has led to some unexpected toxicity.¹¹ NOTCH1 inhibition may therefore serve as a second-line treatment. Indeed, although GSI have suffered from gastrointestinal-related toxicity, isoform-specific GSI or antibody-based treatments that target NOTCH1 directly (NCT03422679) have shown more promise.⁶¹ Published studies variously describe that GSI-1 (both as a single treatment and in combination) and PF-03084014 are relatively well tolerated.⁶²⁻⁶⁴

Ultimately, our data show that GSI and ALK inhibitors act additively/synergistically and induce apoptosis of ALCL cell lines, and furthermore that ALK inhibitor-resis-

tant cell lines remain sensitive to NOTCH1 inhibition. Hence, inhibition of NOTCH1 via GSI might represent a therapeutic option for both treatment-naïve and ALK inhibitor-resistant ALCL – while NOTCH1 expression may be a viable biomarker predictive of relapse.

Disclosures

No conflicts of interest to disclose.

Contributions

HL: conceptualization, methodology, investigations, writing of the original draft, and visualization. NP: conceptualization, investigations, writing, review and editing. JDM: software, visualization, formal analysis, writing, review and editing. MS, SH, EN, MFM, AE, MC, LM, CGP, GH, CL, SP, AJ, AF, AM, OW, GI, LL, OM, WK, SM, IA, MW, GAAB and LK: resources. AFA: investigations, software. SPD: investigation, writing, review and editing. WW and CDW: resources, writing, review and editing. MZ: software and formal analysis. TLB: conceptualization, methodology, software, writing, review and editing. SDT: conceptualization, resources, writing, review, editing, supervision, project administration, and acquisition of funding.

Acknowledgments

The authors would like to thank Professor Christopher Aster

and Dr Johnson (Harvard Medical School) for providing the full-length NOTCH1 cDNA. We also thank: the Cambridge NIHR BRC Cell Phenotyping Hub; Medical Research Laboratories Core for Sanger sequencing; Washington State University Genomic Sequencing for library preparation, quality control and sequencing; the CCLG Tissue Bank, the CCLG centers and the ECMC Pediatric Network for the collection and provision of tissue samples. We especially thank the patients and families who voluntarily donated the samples.

Funding

This work was supported by grants from the Ministry of Science, Kingdom of Saudi Arabia to SDT, AI and SM (grant number 74497) and Bloodwise to SDT (grant number 12065). HL is supported by a Department of Pathology, University of Cambridge Pathology Centenary Fund PhD studentship. SDT, LK, OM, SK, NP, SPD, CGP, WW, CDW and CL are recipients of funds from a European Union Horizon 2020 Marie Skłodowska-Curie Innovative Training Network (ITN-ETN) grant, award n. 675712. CL is supported by a Czech Science Foundation research grant n. 19-23424Y and by research infrastructures EATRIS-CZ (LM2015064) and the NCMG (LM2015091) funded by MEYS CR. WK is supported by the KinderkrebsInitiative Buchholz, Holm-Seppensen. The CCLG Tissue Bank is funded by Cancer Research UK and CCLG.

References

- Alessandri AJ, Pritchard SL, Schultz KR, Massing BG. A population-based study of pediatric anaplastic large cell lymphoma. *Cancer*. 2002;94(6):1830-1835.
- Lamant L, Dastugue N, Pulford K, et al. A new fusion gene TPM3-ALK in anaplastic large cell lymphoma created by a (1;2)(q25;p23) translocation. *Blood*. 1999;93(9):3088-3095.
- Morris SW, Kirstein MN, Valentine MB, et al. Fusion of a kinase gene, ALK, to a nucleolar protein gene, NPM, in non-Hodgkin's lymphoma. *Science*. 1994;263(5151):1281-1284.
- Youssif C, Goldenbogen J, Hamoudi R, et al. Genomic profiling of pediatric ALK-positive anaplastic large cell lymphoma: a Children's Cancer and Leukaemia Group study. *Genes Chromosom. Cancer*. 2009;48(11):1018-1026.
- Salaverria I, Beà S, Lopez-Guillermo A, et al. Genomic profiling reveals different genetic aberrations in systemic ALK-positive and ALK-negative anaplastic large cell lymphomas. *Br J Haematol*. 2008;140(5):516-526.
- Boi M, Rinaldi A, Kwee I, et al. PRDM1/BLIMP1 is commonly inactivated in anaplastic large T-cell lymphoma. *Blood*. 2013;122(15):2683-2693.
- Kamstrup MR, Biskup E, Gjerdrum LMR, et al. The importance of Notch signaling in peripheral T-cell lymphomas. *Leuk Lymphoma*. 2014;55(3):639-644.
- Jundt F, Anagnostopoulos I, Förster R, et al. Activated Notch1 signaling promotes tumor cell proliferation and survival in Hodgkin and anaplastic large cell lymphoma. *Blood*. 2002;99(9):3398-3403.
- Crescenzo R, Abate F, Lasorsa E, et al. Convergent mutations and kinase fusions lead to oncogenic STAT3 activation in anaplastic large cell lymphoma. *Cancer Cell*. 2015;27(4):516-532.
- Brugières L, Pacquement H, Le Deley M-C, et al. Single-drug vinblastine as salvage treatment for refractory or relapsed anaplastic large-cell lymphoma: a report from the French Society of Pediatric Oncology. *J Clin Oncol*. 2009;27(30):5056-5061.
- Prokoph N, Larose H, Lim MS, Burke GAA, Turner SD. Treatment options for paediatric anaplastic large cell lymphoma (ALCL): current standard and beyond. *Cancers (Basel)*. 2018;10(4):99.
- Minard-Colin V, Brugières L, Reiter A, et al. Non-Hodgkin lymphoma in children and adolescents: progress through effective collaboration, current knowledge, and challenges ahead. *J Clin Oncol*. 2015;33(27):2963-2974.
- Le Deley M-C, Rosolen A, Williams DM, et al. Vinblastine in children and adolescents with high-risk anaplastic large-cell lymphoma: results of the randomized ALCL99-vinblastine trial. *J Clin Oncol*. 2010;28(25):3987-3993.
- Gritt G, Boschini C, Rossi A, et al. Primary treatment response rather than front line stem cell transplantation is crucial for long term outcome of peripheral T-cell lymphomas. *PLoS One*. 2015;10(3):e0121822.
- Gambacorti-Passerini C, Mussolini L, Brugières L. Abrupt relapse of ALK-positive lymphoma after discontinuation of crizotinib. *N Engl J Med*. 2016;374(1):95-96.
- Gambacorti-Passerini C, Messa C, Pogliani EM. Crizotinib in anaplastic large-cell lymphoma. *N Engl J Med*. 2011;364(8):775-776.
- Mossé YP, Voss SD, Lim MS, et al. Targeting ALK with crizotinib in pediatric anaplastic large cell lymphoma and inflammatory myofibroblastic tumor: a Children's Oncology Group study. *J Clin Oncol*. 2017;35(28):3215-3221.
- Abramov D, Oschlies I, Zimmermann M, et al. Expression of CD8 is associated with non-common type morphology and outcome in pediatric anaplastic lymphoma kinase-positive anaplastic large cell lymphoma. *Haematologica*. 2013;98(10):1547-1553.
- Ait-Tahar K, Damm-Welk C, Burkhardt B, et al. Correlation of the autoantibody response to the ALK oncoantigen in pediatric anaplastic lymphoma kinase-positive anaplastic large cell lymphoma with tumor dissemination and relapse risk. *Blood*. 2010;115(16):3314-3319.
- Alexandrov LB, Nik-Zainal S, Wedge DC, et al. Signatures of mutational processes in human cancer. *Nature*. 2013;500(7463):415-421.
- Helleday T, Eshtad S, Nik-Zainal S. Mechanisms underlying mutational signatures in human cancers. *Nat Rev Genet*. 2014;15(9):585-598.
- <https://cancer.sanger.ac.uk/cosmic/signatures>.
- Fabregat A, Jupe S, Matthews L, et al. The reactome pathway knowledge base. *Nucleic Acids Res*. 2018;46(D1):D649-D655.
- Cui Y-X, Kerby A, McDuff FKE, Ye H, Turner SD. NPM-ALK inhibits the p53 tumor suppressor pathway in an MDM2 and JNK-dependent manner. *Blood*. 2009;113(21):5217-5227.
- Malcolm TIMM, Villarese P, Fairbairn CJ, et al. Anaplastic large cell lymphoma arises in thymocytes and requires transient TCR expression for thymic egress. *Nat Commun*. 2016;7:10087.
- Adzhubei IA, Schmidt S, Peshkin L, et al. A method and server for predicting damaging missense mutations. *Nat Methods*. 2010;7(4):248-249.
- Kumar P, Henikoff S, Ng PC. Predicting the effects of coding non-synonymous variants on protein function using the SIFT algorithm. *Nat Protoc*. 2009;4(7):1073-1082.

28. Chun S, Fay JC. Identification of deleterious mutations within three human genomes. *Genome Res.* 2009;19(9):1553-1561.

29. Schwarz JM, Cooper DN, Schuelke M, Seelow D. Mutationtaster2: mutation prediction for the deep-sequencing age. *Nat Methods.* 2014;11(4):361-362.

30. Choi Y, Sims GE, Murphy S, Miller JR, Chan AP. Predicting the functional effect of amino acid substitutions and indels. *PLoS One.* 2012;7(10):e46688.

31. Mason CC, Khorashad JS, Tantravahi SK, et al. Age-related mutations and chronic myelomonocytic leukemia. *Leukemia.* 2016;30(4):906-913.

32. Ljungström V, Cortese D, Young E, et al. Whole-exome sequencing in relapsing chronic lymphocytic leukemia: clinical impact of recurrent RPS15 mutations. *Blood.* 2016;127(8):1007-1016.

33. Neumann M, Vosberg S, Schlee C, et al. Mutational spectrum of adult T-ALL. *Oncotarget.* 2015;6(5):2754-2766.

34. Kohsaka S, Shukla N, Ameur N, et al. A recurrent neomorphic mutation in MYOD1 defines a clinically aggressive subset of embryonal rhabdomyosarcoma associated with PI3K-AKT pathway mutations. *Nat Genet.* 2014;46(6):595-600.

35. Martin D, Abba MC, Molinolo AA, et al. The head and neck cancer cell oncogene: a platform for the development of precision molecular therapies. *Oncotarget.* 2014;5(19):8906-8923.

36. Luca VC, Kim BC, Ge C, et al. Notch-Jagged complex structure implicates a catch bond in tuning ligand sensitivity. *Science.* 2017;355(6331):1320-1324.

37. Menotti M, Ambrogio C, Cheong T-C, et al. Wiskott-Aldrich syndrome protein (WASP) is a tumor suppressor in T cell lymphoma. *Nat Med.* 2019;25(1):130-140.

38. Choi SH, Severson E, Pear WS, et al. The common oncogenic program of NOTCH1 and NOTCH3 signaling in T-cell acute lymphoblastic leukemia. *PLoS One.* 2017;12(10):e0185762.

39. Sanchez-Martin M, Ambesi-Impiombato A, Qin Y, et al. Synergistic antileukemic therapies in NOTCH1-induced T-ALL. *Proc Natl Acad Sci U S A.* 2017;114(8):2006-2011.

40. Wang H, Zou J, Zhao B, et al. Genome-wide analysis reveals conserved and divergent features of Notch1/RBPJ binding in human and murine T-lymphoblastic leukemia cells. *Proc Natl Acad Sci U S A.* 2011;108(36):14908-14913.

41. Locatelli MA, Aftimos P, Dees EC, et al. Phase I study of the gamma secretase inhibitor PF-03084014 in combination with docetaxel in patients with advanced triple-negative breast cancer. *Oncotarget.* 2017;8(2):2320-2328.

42. Turturro F, Frist AY, Arnold MD, Seth P, Pulford K. Biochemical differences between SUDHL-1 and KARPAS 299 cells derived from t(2;5)-positive anaplastic large cell lymphoma are responsible for the different sensitivity to the antiproliferative effect of p27(Kip1). *Oncogene.* 2001;20(33):4466-4475.

43. Kamstrup MR, Ralfkjaer E, Skovgaard GL, Gniadecki R. Potential involvement of Notch1 signalling in the pathogenesis of primary cutaneous CD30-positive lymphoproliferative disorders. *Br J Dermatol.* 2008;158(4):747-753.

44. Meeks HD, Song H, Michailidou K, et al. BRCA2 polymorphic stop codon K3326X and the risk of breast, prostate, and ovarian cancers. *J Natl Cancer Inst.* 2015;108(2): djv315.

45. Pfeifer GP. Mutagenesis at methylated CpG sequences. *Curr Top Microbiol Immunol.* 2006;301:259-281.

46. Turner SD, Yeung D, Hadfield K, Cook SJ, Alexander DR. The NPM-ALK tyrosine kinase mimics TCR signalling pathways, inducing NFAT and AP-1 by RAS-dependent mechanisms. *Cell Signal.* 2007;19(4):740-747.

47. Aster JC, Blacklow SC, Pear WS. Notch signalling in T-cell lymphoblastic leukaemia/lymphoma and other haematological malignancies. *J Pathol.* 2011;223(2): 262-273.

48. Breit S, Stanulla M, Flohr T, et al. Activating NOTCH1 mutations predict favorable early treatment response and long-term outcome in childhood precursor T-cell lymphoblastic leukemia. *Blood.* 2006;108(4):1151-1157.

49. Wang NJ, Sanborn Z, Arnett KL, et al. Loss-of-function mutations in Notch receptors in cutaneous and lung squamous cell carcinoma. *Proc Natl Acad Sci U S A.* 2011;108(43):17761-17766.

50. Vollbrecht C, Mairinger FD, Koitzsch U, et al. Comprehensive analysis of disease-related genes in chronic lymphocytic leukemia by multiplex PCR-based next generation sequencing. *PLoS One.* 2015;10(6): e0129544.

51. Athanasakis E, Melloni E, Rigolin GM, et al. The p53 transcriptional pathway is preserved in ATM-mutated and NOTCH1-mutated chronic lymphocytic leukemias. *Oncotarget.* 2014;5(24):12635-12645.

52. Rebay I, Fleming RJ, Fehon RG, et al. Specific EGF repeats of Notch mediate interactions with Delta and Serrate: implications for notch as a multifunctional receptor. *Cell.* 1991;67(4):687-699.

53. Stanley P, Okajima T. Roles of glycosylation in notch signaling. *Curr Top Dev Biol.* 2010;92:131-164.

54. Haines N, Irvine KD. Glycosylation regulates Notch signalling. *Nat Rev Mol Cell Biol.* 2003;4(10):786-797.

55. Pakkiriswami S, Couto A, Nagarajan U, Georgiou M. Glycosylated Notch and cancer. *Front Oncol.* 2016;6:37.

56. Rand MD, Grimm LM, Artavanis-Tsakonas S, et al. Calcium depletion dissociates and activates heterodimeric notch receptors. *Mol Cell Biol.* 2000;20(5):1825-1835.

57. Rust R, Visser L, Van Der Leij J, et al. High expression of calcium-binding proteins, S100A10, S100A11 and CALM2 in anaplastic large cell lymphoma. *Br J Haematol.* 2005;131(5):596-608.

58. Dang Q, Chen L, Xu M, et al. The γ -secretase inhibitor GSI-I interacts synergistically with the proteasome inhibitor bortezomib to induce ALK+ anaplastic large cell lymphoma cell apoptosis. *Cell Signal.* 2019;59:76-84.

59. Hudson S, Wang D, Middleton F, et al. Crizotinib induces apoptosis and gene expression changes in ALK+ anaplastic large cell lymphoma cell lines; brentuximab synergizes and doxorubicin antagonizes. *Pediatr Blood Cancer.* 2018;65(8):e27094.

60. Larose H, Burke GAA, Lowe EJ, Turner SD. From bench to bedside: the past, present and future of therapy for systemic paediatric ALCL, ALK. *Br J Haematol.* 2019;185 (6):1043-1054.

61. Habets RA, de Bock CE, Serneels L, et al. Safe targeting of T cell acute lymphoblastic leukemia by pathology-specific NOTCH inhibition. *Sci Transl Med.* 2019;11(494): eaau6246.

62. Papayannidis C, DeAngelo DJ, Stock W, et al. A phase 1 study of the novel gamma-secretase inhibitor PF-03084014 in patients with T-cell acute lymphoblastic leukemia and T-cell lymphoblastic lymphoma. *Blood Cancer J.* 2015;5:e350.

63. Samon JB, Castillo-Martin M, Hadler M, et al. Preclinical analysis of the γ -secretase inhibitor PF-03084014 in combination with glucocorticoids in T-cell acute lymphoblastic leukemia. *Mol Cancer Ther.* 2012;11(7): 1565-1575.

64. Wei P, Walls M, Qiu M, et al. Evaluation of selective gamma-secretase inhibitor PF-03084014 for its antitumor efficacy and gastrointestinal safety to guide optimal clinical trial design. *Mol Cancer Ther.* 2010;9(6): 1618-1628.



Brentuximab vedotin in combination with rituximab, cyclophosphamide, doxorubicin, and prednisone as frontline treatment for patients with CD30-positive B-cell lymphomas

Jakub Svoboda,¹ Steven M. Bair,¹ Daniel J. Landsburg,¹ Sunita Dwivedy Nasta,¹ Sarah J. Nagle,² Stefan K. Barta,¹ Nadia Khan,³ Joanne Fillicko-O'Hara,⁴ Sameh Gaballa,⁴ Lauren Strelec,¹ Elise Chong,¹ Sheryl Mitnick,¹ Terease S. Waite,¹ Cara King,¹ Hatcher Ballard,¹ Matthew Youngman,¹ James Gerson,¹ John P. Plastaras,¹ Amit Maity,¹ Agata M. Bogusz,¹ Stacy S. Hung,⁵ Hisae Nakamura,⁵ Reza Nejati,³ Christian Steidl,⁵ Megan Lim,¹ Marco Ruella¹ and Stephen J. Schuster¹

¹University of Pennsylvania, Philadelphia, PA, USA; ²Oregon Health and Science University, Portland, OR, USA; ³Fox Chase Cancer Center, Philadelphia, PA, USA;

⁴Thomas Jefferson University, Philadelphia, PA, USA and ⁵Centre for Lymphoid Cancer, Vancouver, British Columbia, Canada

Haematologica 2021
Volume 106(6):1705-1713

ABSTRACT

We conducted a phase I/II multicenter trial using six cycles of brentuximab vedotin (BV) in combination with rituximab, cyclophosphamide, doxorubicin, and prednisone (R-CHP) for treatment of patients with CD30-positive B-cell lymphomas. Thirty-one patients were evaluable for toxicity and 29 for efficacy including 22 with primary mediastinal B-cell lymphoma, five with diffuse large B-cell lymphoma, and two with gray zone lymphoma. There were no treatment-related deaths; 32% of patients had non-hematologic grade 3/4 toxicities. The overall response rate was 100% (95% confidence interval [95% CI]: 88-100) with 86% (95% CI: 68-96) of patients achieving complete response at the end of systemic treatment. Consolidative radiation following end-of-treatment response assessment was permissible and used in 52% of all patients including 59% of the patients with primary mediastinal B-cell lymphoma. With a median follow-up of 30 months, the 2-year progression-free survival and overall survival rates were 85% (95% CI: 66-94) and 100%, respectively. In the cohort with primary mediastinal B-cell lymphoma, the 2-year progression-free survival rate was 86% (95% CI: 62-95). In summary, BV-R-CHP with or without consolidative radiation is a feasible and active frontline regimen for CD30-positive B-cell lymphomas (ClinicalTrials.gov identifier: NCT01994850).

Introduction

Brentuximab vedotin (BV) is an immunoconjugate consisting of a CD30-directed antibody linked to the anti-microtubule agent auristatin.¹ BV is highly active in relapsed and refractory (r/r) classical Hodgkin lymphoma and in CD30-expressing T-cell lymphomas.^{2,3} In the frontline setting, BV combined with chemotherapy has been recently approved for advanced classical Hodgkin lymphoma and CD30-positive (CD30⁺) T-cell lymphomas based on results of randomized trials showing benefit of the BV-containing arms.^{4,5}

BV targets the cell membrane protein CD30 that is expressed not only by classical Hodgkin lymphoma and some T-cell lymphomas, but at various frequencies also by B-cell non-Hodgkin lymphomas including up to 80% of primary mediastinal B-cell lymphomas (PMBCL).^{6,9} PMBCL is a mature large B-cell lymphoma of thymic origin which usually presents with mediastinal masses. It occurs predominantly in young adults and represents about 5% of aggressive B-cell lymphomas.¹⁰ While previous classifications considered it as a subtype of diffuse large B-cell lymphoma (DLBCL), PMBCL is now thought of as a distinct clinicopathological entity with clinical features and also a molecular signature that share similarities with

Correspondence:

JAKUB SVOBODA
jakub.svoboda@pennmedicine.upenn.edu

Received: September 19, 2019.

Accepted: May 14, 2020.

Pre-published: May 15, 2020.

<https://doi.org/10.3324/haematol.2019.238675>

©2021 Ferrata Storti Foundation

Material published in *Haematologica* is covered by copyright. All rights are reserved to the Ferrata Storti Foundation. Use of published material is allowed under the following terms and conditions: <https://creativecommons.org/licenses/by-nc/4.0/legalcode>. Copies of published material are allowed for personal or internal use. Sharing published material for non-commercial purposes is subject to the following conditions: <https://creativecommons.org/licenses/by-nc/4.0/legalcode>, sect. 3. Reproducing and sharing published material for commercial purposes is not allowed without permission in writing from the publisher.



those of classical Hodgkin lymphoma.¹¹ Recent efforts using gene expression profiling have aimed at better defining PMBCL at the molecular level and distinguishing it from other aggressive B-cell lymphomas with mediastinal presentation. In particular, the NanoString® based Lymph3Cx assay measures expression of 58 genes and allows precise identification of PMBCL cases.¹²

Presently, the optimal frontline management of patients with PMBCL remains controversial. Traditionally, PMBCL was included in clinical trials regarding aggressive B-cell lymphomas and regimens designed for DLBCL were found to be effective.¹³⁻¹⁷ Rituximab in combination with cyclophosphamide, doxorubicin, vincristine and prednisone (R-CHOP) results in event-free survival rates of about 80% when followed by consolidative radiation therapy.^{14,16} In 2013, in a phase II trial by Dunleavy *et al.* including 51 PMBCL patients treated at the National Cancer Institute, dose-adjusted etoposide, prednisone, vincristine, cyclophosphamide, and doxorubicin, plus rituximab (DA-EPOCH-R) without radiotherapy achieved an event-free survival of 93%.¹⁵ Many centers in the USA now use this dose-intense DA-EPOCH-R approach for frontline treatment of all PMBCL patients without considering any risk stratification.¹⁵ Some patients with r/r PMBCL, can be salvaged by high-dose chemotherapy with autologous stem cell transplant or radiation, but outcomes tend to be poor.^{18,19} Recently, pembrolizumab and axicabtagene ciloleucel were approved for the treatment of r/r PMBCL.²⁰⁻²² While the activity of BV as monotherapy in r/r PMBCL has been disappointing, results of a phase II trial using nivolumab in combination with BV are very encouraging.^{23,24}

To test the tolerability and make a preliminary assessment of the efficacy of BV in frontline treatment of B-cell lymphomas, we designed a phase I/II trial using BV in combination with rituximab, cyclophosphamide, doxorubicin, and prednisone (R-CHP) for the treatment of CD30⁺ PMBCL, DLBCL, and gray zone lymphoma (GZL) in adult patients (ClinicalTrials.gov identifier: NCT01994850).

Methods

Study design and patient eligibility

This multicenter, single arm, phase I/II study enrolled patients aged 18 years and over with untreated histologically confirmed CD30⁺ PMBCL, DLBCL, or GZL. Patients with any stage, measurable disease, and an Eastern Cooperative Oncology Group Performance Status of 3 or less were eligible. The diagnostic biopsy had to demonstrate at least 1% or higher expression of CD30 on the lymphoma B cells by immunohistochemistry and was assessed independently by two pathologists. Patients with active central nervous system involvement and uncontrolled systemic infections were excluded. Enrollment began in January 2014 and was completed in April 2017. The primary objective of the phase I portion was to determine the safety of the combination and the maximum tolerated dose of BV in combination with R-CHP using a de-escalation design. The primary objective of the phase II portion was the overall response rate at the end of systemic treatment as determined by investigator assessment using International Working Group response criteria for non-Hodgkin lymphoma.²⁵ Secondary endpoints were 2-year progression-free survival and 2-year overall survival for all patients and by each lymphoma subtype (PMBCL, DLBCL, and GZL).

With regard to the toxicity assessment, the study had 90% power to detect any unforeseen toxicity that occurred in 7% or

Table 1. The study regimen: brentuximab vedotin in combination with rituximab, cyclophosphamide, doxorubicin, and prednisone (BV-R-CHP).

Agent	Route	Dose	Cycle 1	Cycles 2-6
Prednisone (or equivalent)	PO (or IV equivalent)	100 mg	Days 1-5	Days 1-5
Rituximab	IV	375 mg/m ² [†]	Day 1 and 2 [†]	Day 1
Cyclophosphamide	IV	750 mg/m ²	Day 2	Day 1
Doxorubicin	IV	50 mg/m ²	Day 2	Day 1
Brentuximab vedotin [‡]	IV	1.8 mg/kg or 1.2 mg/kg	Day 2	Day 1

Consolidative radiation following the end-of-treatment response assessment was permissible.

[†]The rituximab dose was split into 100 mg/m² and 275 mg/m² on day 1 and day 2, respectively of cycle 1. [‡]The maximum dose of brentuximab vedotin was 180 mg. PO: *per os*; IV: intravenous.

more of patients. The number of patients required for the trial was determined based on the following assumptions for an optimal two-stage design in order to detect and minimize enrollment if the overall response rate was not greater than 50% but also to minimize the likelihood of failing to reject the null hypothesis if the overall response rate was at least 70%. Sample size calculations for the stopping rules were based upon a type I error rate of 10% and type II error rate of 20%. The number of subjects enrolled and evaluable in the phase I cohort was defined as at least six and a maximum of 12. For the phase II cohort, using the null hypothesis of a 50% overall response rate, the study required a sample size of 20 patients. Since the phase I subjects were recruited, treated, and followed in the same way as the phase II subjects, the phase I subjects accrued at the phase II dose were included in the efficacy analysis.

The study was conducted in three academic centers in the USA and was run in accordance with the Declaration of Helsinki. Approval from the institutional review board of each center was obtained before initiating the study at each site. All patients signed a written informed consent form before enrollment into the trial.

Treatment protocol and response assessment

As shown in Table 1, the study treatment protocol consisted of six cycles of BV administered with the R-CHOP regimen without vincristine, including: rituximab 375 mg/m², cyclophosphamide 750 mg/m², and doxorubicin 50 mg/m² on day 1 and prednisone 100 mg (or equivalent) daily on days 1 through 5 of each 21-day cycle. For cycle 1, rituximab was split into two doses (100 mg/m² on day 1 and 275 mg/m² on day 2) to reduce risks of an infusion reaction to rituximab. We also aimed to separate the initial rituximab infusion from the first exposure to BV to avoid any potential confusion about attribution of infusion reactions. The rest of the agents were given on day 2 (cyclophosphamide, doxorubicin, BV). In cycles 2 through 6, rituximab was administered at a dose of 375 mg/m² on day 1 together with the rest of the agents.

For phase I, the starting dose of BV was 1.8 mg/kg (maximum dose of 180 mg) with a 3+3 de-escalation design to 1.2 mg/kg (maximum dose of 120 mg) should dose-limiting toxicities occur during the first 21-day cycle. A dose-limiting toxicity was defined as any grade 3 or 4 non-hematologic toxicity requiring a dose delay over 14 days from the planned day 1 of cycle 2 or any hematologic toxicity not returning to baseline or ≤ grade 2 by 21 days from the planned day 1 of cycle 2. By protocol, at least six patients had to be enrolled and complete one cycle of dosing at the final recommended BV dose in phase I prior to beginning enrollment of patient in phase II. Dose modifications during cycle 2 through 6 for treatment-associated toxicity were specified in the protocol and based on the grade using the Common Terminology Criteria for Adverse Events (CTCAE) version 4.0.

The use of granulocyte-colony stimulating factor (G-CSF) was

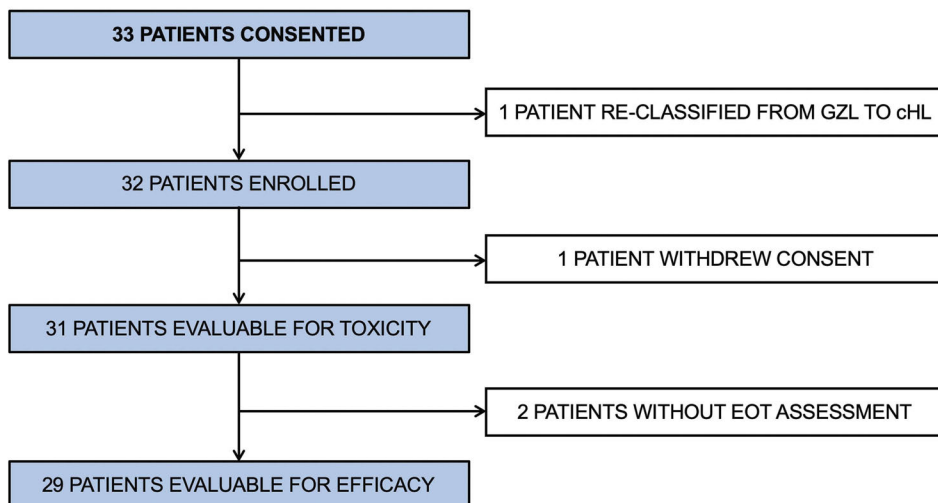


Figure 1. CONSORT diagram. GZL: gray zone lymphoma; cHL: classical Hodgkin lymphoma; EOT: end of treatment.

allowed as per institutional policy. Consolidative radiation therapy was permitted after completion of all systemic therapy and only after end-of-treatment imaging at the discretion of the treating physician.

Treatment response was assessed by imaging with fluorodeoxyglucose-positron emission tomography/computed tomography (FDG-PET/CT) using the revised response criteria for malignant lymphoma described by Cheson *et al.*²⁵ Computed tomography scans were performed after cycles 2 and 4 to monitor for interim response. End-of-treatment imaging was performed 3–5 weeks after completion of systemic therapy using FDG-PET/CT. Consolidative radiation following end-of-treatment response assessment was permissible at the discretion of the treating physician.

Correlative studies

CD30 expression was determined on the diagnostic tissue biopsies using immunohistochemistry though visual inspection by two independent pathologists. The gene expression analysis (Lymph3Cx) was performed on archival formalin-fixed, paraffin-embedded tissue from pre-treatment biopsies. The tissue was examined by a hematopathologist for adequate tumor amount and nucleic acids were extracted from formalin-fixed paraffin-embedded scrolls or unstained slides. The Lymph3Cx assay was previously described and validated to aid in the molecular distinction of PMBCL *versus* DLBCL.²⁶ The gene expression assay on the diagnostic tissue was performed in a blinded fashion, and once the assignment of diagnosis by Lymph3Cx was made, a correlation with investigator-based diagnosis (PMBCL *vs.* DLBCL *vs.* GZL) was performed.

Statistical analysis

The overall response rate and complete response rate with a two-sided 95% exact confidence intervals (95% CI) were calculated using the Clopper-Pearson method. Two-year progression-free and overall survival rates were estimated using the Kaplan-Meier method. The median follow-up was estimated by the reverse Kaplan-Meier method.²⁷ The data cut-off for analysis was January 1, 2019.

Results

Patients' characteristics

Thirty-three patients gave consent to enrollment in the

Table 2. Patients' characteristics.

All patients (N=31)

Age, years	
Median	37
Range	18–76
Female	15 (48%)
Elevated LDH	21 (68%)
Stage III–IV	13 (42%)
Lymphoma subtype	
PMBL	23 (74%)
DLBCL	6 (19%)
GZL	2 (7%)
ECOG PS	
Median	1
Range	0–2
IPI risk category	
Low	15 (48%)
Low-intermediate	11 (36%)
High-intermediate	4 (13%)
High	1 (3%)

LDH: lactate dehydrogenase; PMBCL: primary mediastinal B-cell lymphoma; DLBCL: diffuse large B-cell lymphoma; GZL: gray zone lymphoma; ECOG PS: Eastern Cooperative Oncology Group Performance Status; IPI: International Prognostic Index.

trial (Figure 1). One of these patients was subsequently reclassified from having GZL to having classical Hodgkin lymphoma and was taken off the study before starting therapy. Thus, 32 patients were enrolled and received at least one cycle of therapy. One patient withdrew from the study after cycle 1 to receive R-CHOP therapy closer to home. The characteristics of the patients evaluable for toxicity (n=31) are presented in Table 2. The median age was 37 years (range, 18–76), 50% of the patients were female, 42% had stage III/IV disease and 17% were classified in high-intermediate or high International Prognostic Index (IPI) risk group.²⁸ Using traditional clinicopathological criteria, 23 patients had a diagnosis of PMBCL, six were diagnosed as having DLBCL, and two as having GZL. For the PMBCL cohort, 91% of patients had large mediastinal masses over 7.5 cm in maximal transverse diameter and 35% had stage III/IV disease. Two patients were removed from the study (1 patient because of non-compliance and 1 in complete remission because of a regimen violation). Therefore, a total of 29 patients were

evaluable for efficacy. Of those, 15 patients (52%) received consolidative radiation after completing BV-R-CHP and final end-of-treatment response assessment. This number included 13 (59%) of 22 evaluable PMBCL patients. Of those, 8 patients received radiation using protons. Twenty-six patients had archival formalin-fixed paraffin-embedded diagnostic tissue available for Lymph3Cx gene expression analysis.

Safety and feasibility

Toxicities of this outpatient regimen are listed in Table 3A and B. There were no treatment-related or on-study deaths. Using a de-escalation design during the phase I portion of the trial, the first six patients were treated with the initial dose of 1.8 mg/kg (maximum 180 mg) in com-

bination with standard dose R-CHP with plans to reduce BV to 1.2 mg/kg (maximum 120 mg) should there be dose-limiting toxicities. As there were no dose-limiting toxicities during phase I, the BV dose of 1.8 mg/kg (maximum 180 mg) was used as the phase II dose. Overall in all patients (combining phase I and phase II cohorts), any grade 3 or 4 toxicity occurred in 84% of study patients. Hematologic adverse events of any grade were recorded in the majority of patients and in 77% of patients with grade 3 or 4 toxicities. Of note, 16% of patients received no G-CSF and 6% had G-CSF support for only one or two of the six cycles. Non-hematologic grade 3 and 4 toxicities were seen in 32% of patients, including infections in 15% of patients (Table 3B). Toxicities occurring in over 10% of patients included peripheral sensory neuropathy in 19 patients (61%) which were either grade 1 (48%) or grade 2 (13%) (Table 3A). Three patients (10%) reported motor neuropathy, two with grade 1 (6%) and one with grade 2 (3%). One patient discontinued protocol treatment after cycle 4 because of sepsis and grade 3 cardiomyopathy. One patient discontinued BV after cycle 5 because of transient grade 2 pneumonitis which was deemed at least possibly related to BV. Only three patients required BV dose reductions to 1.2 mg/kg because of persistent grade 2 peripheral sensory neuropathy outside of the period of dose-limiting toxicities. In total, two patients enrolled on the study died in the follow-up period. One PMBCL patient developed acute myeloid leukemia 2 years after completion of study treatment and mediastinal radiation therapy and ultimately died of acute myeloid leukemia 39 months after completing study treatment. One patient died of progressive lymphoma 40 months after completing study treatment.

Thromboembolic events were noted in eight patients (36%) in the PMBCL cohort. Pulmonary embolism was seen in three patients and upper extremity deep vein thrombosis in five patients. Of those, three events were diagnosed prior to initiating BV-R-CHP and five events were diagnosed while patients were on study treatment. Three of the five patients who had on-treatment events were asymptomatic and thrombosis was reported as an incidental finding on their first computed tomography with intravenous contrast (1 with pulmonary embolism and 1 with internal jugular vein thrombosis). Two of the five patients with on-treatment events had line-associated thromboses.

Table 3A. All adverse events at least possibly related to the BV-R-CHP regimen.

All AE	Total (%)	G1 (%)	G2 (%)	G3 (%)	G4 (%)
Hematologic AE					
Leukopenia	77	13	32	16	16
Lymphopenia	84	6	32	23	23
Neutropenia	58	3	13	19	23
Febrile neutropenia	23			23	
Anemia	68	48	16	3	
Thrombocytopenia	23	13	6		3
Non hematologic AE*					
Abdominal pain	16	10	3	3	
ALT elevation	16	13		3	
ALKP elevation	13	10	3		
Allergic rhinitis	13	13			
Anorexia	13	6	6		
Anxiety	13	13			
Arthralgia	10	10			
AST elevation	19	19			
Chills	10	10			
Constipation	52	52			
Cough	19	19			
Diarrhea	42	29	13		
Dizziness	29	29			
Dyspnea	16	16			
Fatigue	65	58	6		
Fever	26	19	6		
GERD	19	16	3		
Headache	35	32	3		
Hot flashes	13	13			
Hyperglycemia	16	10	3	3	
Hypoalbuminemia	10	3	6		
Hypocalcemia	10	6	3		
Hypokalemia	10	6		3	
Hyponatremia	32	32			
Infusion reaction	13	10	3		
Insomnia	10	10			
Motor neuropathy	10	6	3		
Mucositis	29	26	3		
Myalgia	10	10			
Nausea	68	52	16		
Pain	16	16			
Sensory neuropathy	61	48	13		
Thromboembolic event	16	3	6	6	
Urinary frequency	10	10			
Urinary tract infection	16	9	6		
Vomiting	13	9	3		

*In $\geq 10\%$ of patients. AE: adverse events; G: grade; ALT: alanine transaminase; ALKP: alkaline phosphatase; AST: aspartate transaminase; GERD: gastro-esophageal reflux disease.

Table 3B. Grade 3 or 4 adverse events at least possibly related to the BV-R-CHP regimen.

Grade 3/4 AE	% Total (n=31)
All*	84
Hematologic	77
Non-hematologic	32
Infections	15
Thromboembolic event	6
ALT elevation	3
Abdominal pain	3
LV dysfunction	3
Hypokalemia	3
Muscle weakness	3
Lactic acidosis	3
Hyperglycemia	3

*Some patients experienced multiple grade 3/4 toxicities so the percentages do not add up. AE: adverse events; ALT: alanine transaminase; LV: left ventricular.

Efficacy

In the combined phase I/II cohort with 29 evaluable patients, the overall response rate was 100% (95% CI: 88-100) with 86% (95% CI: 68-96) of patients achieving a complete response and 14% (95% CI: 4-32) achieving a partial response according to FDG-PET/CT imaging at the end of treatment. All four patients with a partial response had a diagnosis of PMBCL and had a low or low-intermediate IPI risk classification. Only two of the four patients with a partial response ultimately progressed. At a median follow-up of 30 months (95% CI: 26-46), four patients (14%) progressed: three with PMBCL and one with GZL. The 2-year progression-free survival rate was 85% (95% CI: 66-94) and the 2-year overall survival was 100% (Figure 2). Of three patients who were not evaluable per study criteria, two remain progression-free at last follow-up and the status of one patient is unknown.

In the PMBCL cohort of 22 evaluable patients with a median follow-up of 30 months (95% CI: 23-46), the 2-year progression-free survival rate was 86% (95% CI: 62-95) with a 2-year overall survival of 100% (Figure 2). Of the three PMBCL patients who progressed, two had bulky advanced stage disease with expression of CD30 $\leq 10\%$ and one had bulky stage I disease with CD30 expression of 1%. There was no statistically significant difference in progression-free survival between the PMBCL patients who received consolidative radiation therapy (n=13) and those who did not (n=9) ($P=0.95$).

CD30 expression as determined by immunohistochemistry and response to therapy

While all cases expressed CD30 in at least 1% of the lymphoma B cells in the tumor biopsy by immunohistochemistry, it was challenging to capture CD30 expression as a single metric since there was great heterogeneity of CD30 expression patterns, as depicted in Figure 3. Additionally, given the 100% overall response rate and low number of relapses, we could not make any conclusions about correlations between efficacy of the BV-containing regimen and CD30 expression as determined by immunohistochemistry.

Gene expression analysis to improve diagnostic accuracy of primary mediastinal B-cell lymphoma

Of 29 evaluable patients with CD30⁺ B-cell lymphoma, 26 had a pre-treatment biopsy available (11 excisional biopsies and 15 core needle biopsies). Of the 26 samples, five core needle biopsies did not have adequate tumor content or amounts of extractable RNA for the Lymph3Cx assay. The biopsies of the remaining 21 patients (11 excisional and 10 core needle biopsies) were tested. All three subtypes of CD30⁺ B-cell lymphomas as assessed by investigator assessment were tested in blinded fashion by the Lymph3Cx assay and comprised 14 cases of PMBCL, six of DLBCL, and one case of GZL. Of 14 patients with PMBCL by investigator assessment alone, 11 patients (79%) had Lymph3Cx probability scores >0.9 which were

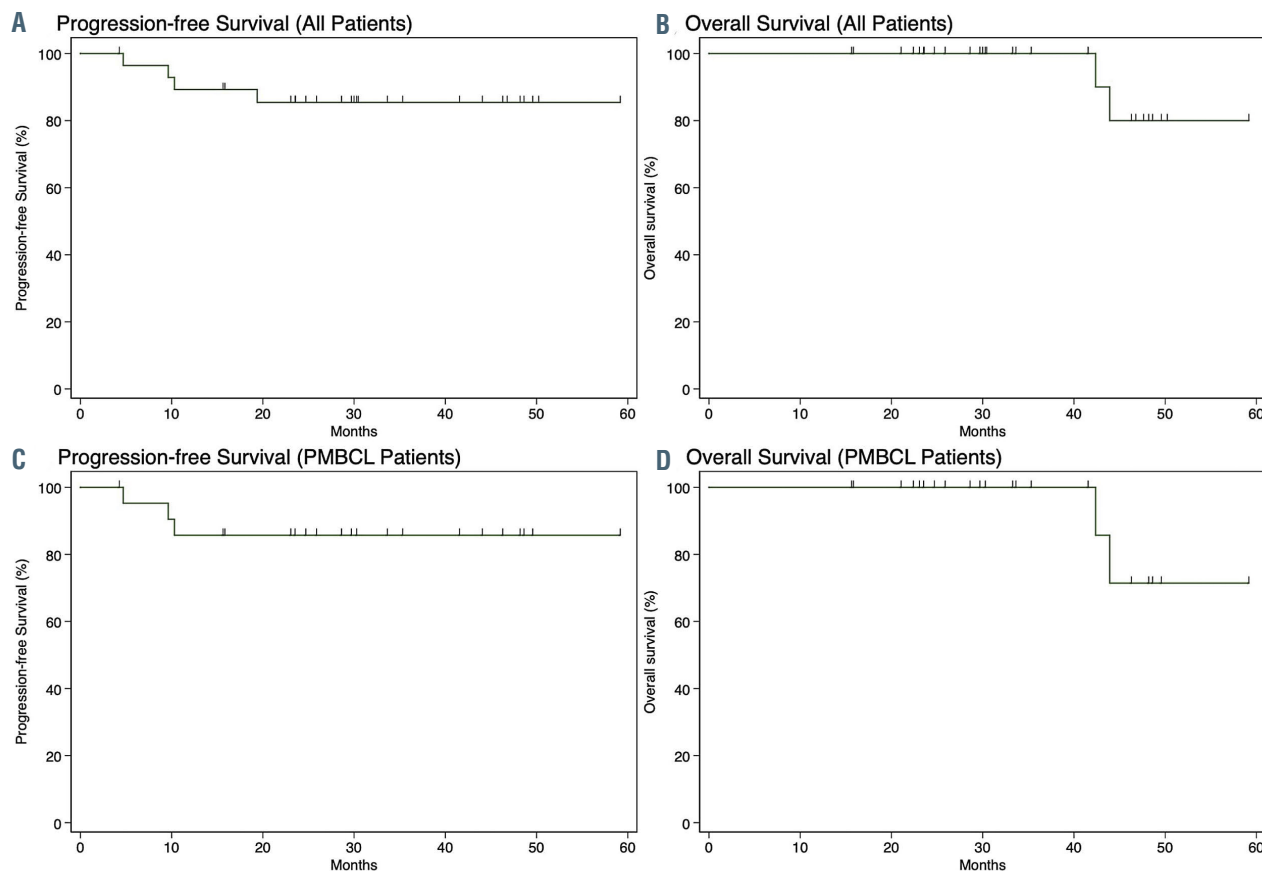


Figure 2. Survival curves for patients who received the BV-R-CHP treatment regimen. (A, B) Progression-free survival (A) and overall survival (B) of all evaluable patients enrolled in the trial (n=29). (C, D) Progression-free survival (C) and overall survival (D) of evaluable patients with primary mediastinal B-cell lymphoma (PMBCL) (n=22).

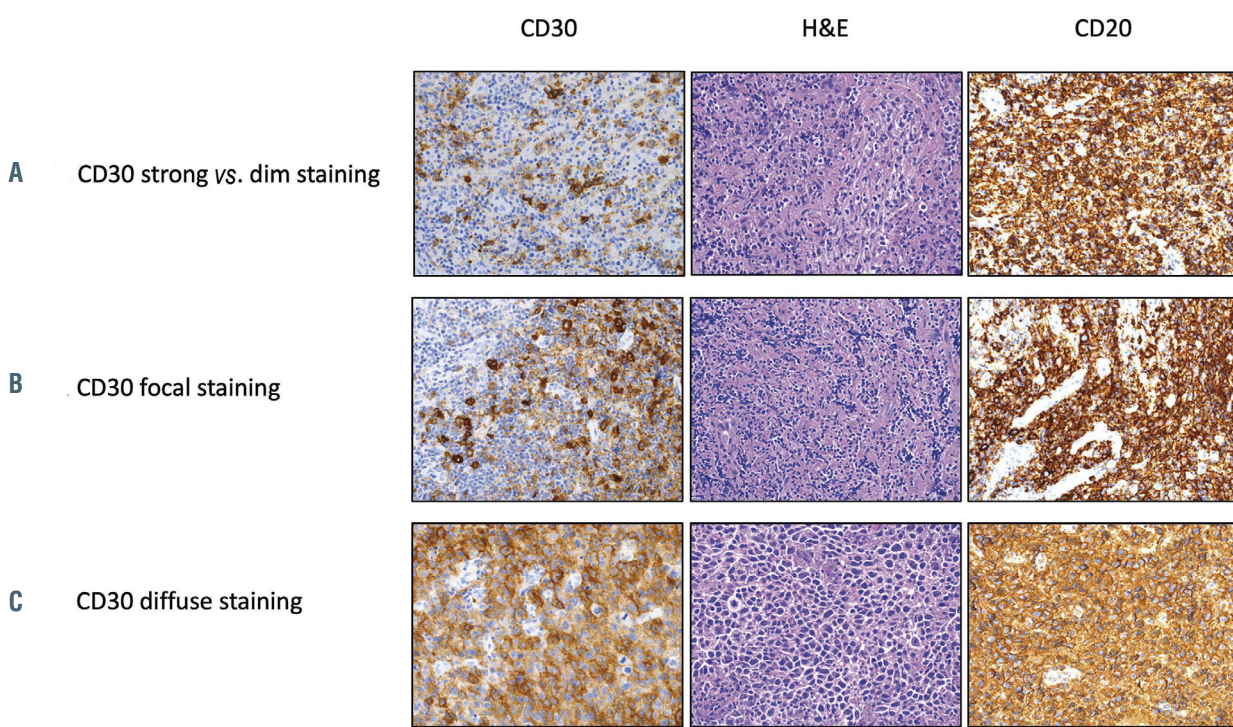


Figure 3. Examples of different CD30 staining patterns by immunohistochemistry in three representative patients with primary mediastinal B-cell lymphoma enrolled on the trial. (A) Heterogeneous staining pattern with strong and dim staining in different areas of the same tumor. (B) Focal staining in one area of the tumor. (C) Diffuse staining throughout the tumor. The antibodies used were CD20 (ready to use, DAKO) and CD30 (ready to use, Leica) and they were detected using a chromogenic substrate, diaminobenzene (Leica). An original magnification x200 was used for all images. H&E: hematoxylin & eosin.

consistent with a molecular diagnosis of PMBCL (mPMBCL) by gene expression; two patients scored in the indeterminate category (0.1 to 0.9); and one patient scored as having a molecular diagnosis of DLBCL (< 0.1) (Figure 4). None of the CD30⁺ B-cell lymphoma samples that were felt to be DLBCL by investigator assessment scored as having a molecular diagnosis of PMBCL by Lymph3Cx.

Discussion

There is a strong rationale for replacing vincristine with BV in the standard R-CHOP regimen for the treatment of CD30⁺ aggressive B-cell lymphomas. BV specifically delivers the antimicrotubule agent auristatin to CD30-expressing cells, which could result in improved efficacy from BV and reduced toxicity due to the omission of vincristine. While BV displayed only limited clinical activity as monotherapy in aggressive r/r B-cell lymphomas, it has not been widely studied in the frontline setting or in combination with chemotherapy.^{24,29} In our phase I/II study, we showed that a frontline regimen using BV at a dose of 1.8 mg/kg in combination with R-CHP for patients with CD30⁺ B-cell lymphomas has an acceptable toxicity profile and is highly active.

Our study included a heterogeneous group of B-cell lymphomas, but the majority of the patients had a clinicopathological diagnosis of PMBCL. For many reasons, this is a challenging population to study in a frontline setting. PMBCL is a rare and clinically heterogeneous lymphoma. Patients with this type of lymphoma often present with an acute onset of pulmonary symptoms necessitating urgent therapy which may lead to a selection bias in non-

randomized studies. While several frontline treatment approaches are effective in PMBCL, there are unique challenges in this population of patients. DA-EPOCH-R is a highly active dose-intense regimen, but it requires central venous access, use of growth factors, frequent blood testing, and inpatient admission at some institutions. R-CHOP is easier to administer, but the excellent outcomes in PMBCL are achieved using consolidative radiation therapy, which may cause long-term toxicities.^{14,16,30,31} While a recently published phase III trial comparing R-CHOP *versus* DA-EPOCH-R in DLBCL included a small cohort of PMBCL cases (n=35), it was not statistically powered to detect the differences in this lymphoma subtype.¹⁷

We recognize that it is difficult to compare regimens across different trials, but outcomes within the PMBCL cohort in our study are comparable to previously published results for patients treated with R-CHOP with radiotherapy or dose-intense regimens such as DA-EPOCH-R.^{14-16,19,30,32} For lymphoma subtypes other than PMBCL, the numbers of patients were too small to make any efficacy conclusions regarding BV-R-CHP. One of two patients with GZL relapsed after achieving a complete response and none of the five patients with CD30⁺ DLBCL relapsed, which is encouraging. Interestingly, preliminary results from another phase II trial (ClinicalTrial.gov identifier: NCT01925612) using BV-R-CHOP in DLBCL (without any requirement for CD30 staining) documented an overall response rate of 97% in the initial 30 evaluable patients. None of the CD30⁺ DLBCL patients in the preliminary report relapsed, but the median follow-up of 5 months was short.³³

Regarding toxicity of the BV-R-CHP regimen, there were no study-related deaths. With the caveats about

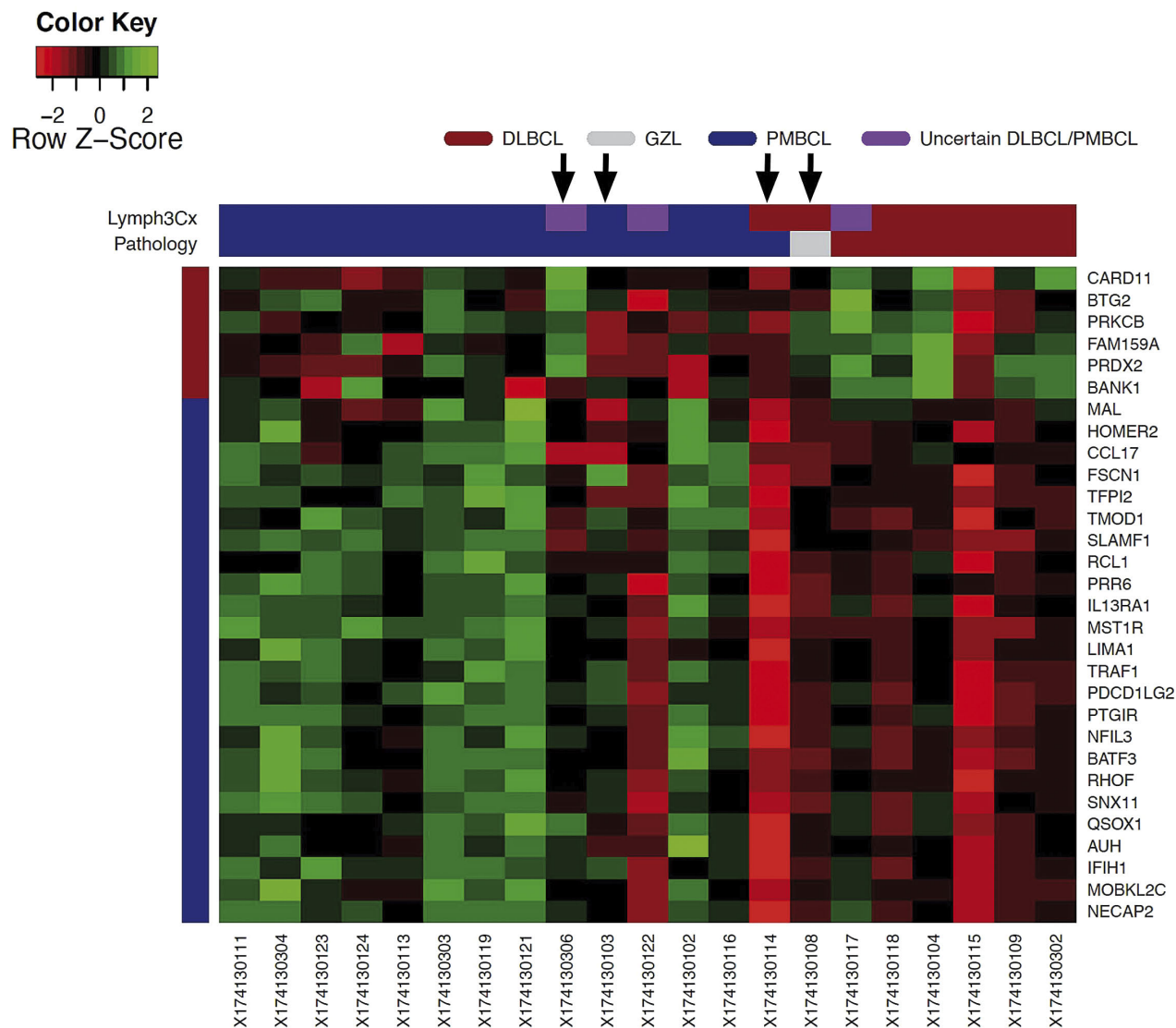


Figure 4. Correlation of Lymph3Cx results with standard clinicopathological diagnoses made by the investigators. DLBCL: diffuse large B-cell lymphoma; GZL: gray zone lymphoma; PMBCL: primary mediastinal B-cell lymphoma. Patients who progressed are labeled by an arrow. Of 14 patients with PMBCL diagnosed by investigator assessment alone, 11 patients (79%) had Lymph3Cx probability scores >0.9, which were consistent with a molecular diagnosis of PMBCL by gene expression analysis, two patients (14%) scored in the indeterminate category (0.1 to 0.9), and one patient (7%) scored as having DLBCL (< 0.1).

cross-trial comparisons of studies, the rate of grade 3 or 4 hematologic and non-hematologic toxicities was similar or lower compared to the rates reported for R-CHOP.^{17,34} When compared to the DA-EPOCH-R arm from the recently published randomized trial in DLBCL, there appears to be less toxicity with BV-R-CHP in our study.¹⁷ However, one limitation of this comparison is the younger median age of patients in our cohort. Neuropathy is of particular concern with a BV-containing regimen and was closely monitored in our study. While peripheral sensory neuropathy was reported in 61% of patients, no patient experienced grade 3 or 4 neuropathy. This lack of severe peripheral neuropathy may again relate to the young age of our patients and the fact that our BV-containing regimen did not contain additional vinca alkaloids, in contrast to some of the other BV-containing combinations used frontline.^{4,33} There were no unexpected opportunistic infections using the combination of rituximab and BV. The administration of G-CSF was not consistent across the participating institutions in our study, but over 20% of

patients did not require G-CSF at all or its use was limited to one or two cycles. However, considering that 23% of patients experienced febrile neutropenia, empiric use of G-CSF should be considered in patients being treated with BV-R-CHP. With regard to long-term toxicities, one patient developed acute myeloid leukemia 2 years after completing the trial therapy and radiation. It is not possible to determine the association between the protocol treatment and her leukemia, but the fact that the patient's mother died of acute myeloid leukemia and the patient had normal cytogenetics (rare in secondary leukemias) is suggestive of other contributing factors.

The high rate of thrombosis in the PMBCL cohort is of special interest. Thromboses were found in over one third of PMBCL patients and approximately 50% were diagnosed prior to initiation of therapy. This high risk of thrombosis in PMBCL patients was described with similar frequency in retrospective studies and is not likely to be related to BV-R-CHP.^{19,35} This finding warrants further investigations about screening, the potential contribution

of central lines to thrombosis, and any possible role for prophylactic anticoagulation in PMBCL patients.

We also attempted to define clinical and pathological factors which would correlate with outcomes of patients receiving BV-R-CHP therapy for CD30⁺ B-cell lymphomas. IPI risk group, which is well-established as a prognostic factor for outcomes of frontline treatments in DLBCL, did not clearly correlate with complete response rate, progression-free survival or overall survival in our study. This could be due to the small number of patients in the high or high-intermediate IPI risk category. Furthermore, the majority of our patients had PMBCL and the utility of the IPI has some limitations as most patients are young and present with limited stage disease. For our ancillary studies, we planned an analysis of CD30 expression by immunohistochemistry and correlation with outcomes as there is controversy over the impact of CD30 status on the efficacy of BV.^{33,36,37} However, this proved difficult because of the very low number of relapses and heterogeneity of CD30 staining patterns in neoplastic cells (Figure 3). Additional studies beyond a simple determination of the percentage of CD30⁺ cells by immunohistochemistry and visual assessment will need to be applied and other groups have attempted this with some success.^{37,38}

Among 21 patients who had pre-treatment tissue analyzed by LymphC3x, we found that there was discordance between the protocol-specified standard clinicopathological diagnosis of PMBCL and the gene expression-based method. These findings are thought-provoking since, in small trials of PMBCL, even a few misclassified patients may have a great impact on interpretation of the results. We believe that developing objective diagnostic criteria based on quantitative methods, such as gene expression signatures, will be an important step in designing treatment strategies for B-cell lymphoma patients with mediastinal lesions and for comparing results across PMBCL trials.

This trial is limited by the small number of evaluable patients and diagnostic heterogeneity. However, the entities included are rare, and we involved three institutions to enroll 32 patients. One of the challenges when interpreting the clinical efficacy and progression-free/overall survival data of patients treated with the BV-R-CHP regimen is the fact that consolidative radiation was used in about 50% of all patients enrolled on this trial. The protocol was designed in 2011-2012 when R-CHOP followed by consolidative radiation therapy was utilized by most centers for PMBCL patients. Therefore, the protocol allowed investigators to use consolidative radiotherapy after completion of BV-R-CHP. It is important to note that the end-of-treatment response assessment was performed before radiation. Interestingly, there were no statistically significant differences in progression-free or overall survival between patients who received consolidative radiation and those who did not. There were no clear differences in patients' characteristics between those who received consolidative radiotherapy and those who did not other than institutional practice differences. Of the four patients who did not achieve metabolic complete response on end-of-treatment imaging, two received consolidative radiation therapy and two did not. Longer follow-up will be necessary to determine whether

there are any long-term toxicities of radiation in the study participants (with the majority of patients having received proton radiation). Of note, an ongoing randomized trial in patients with PMBCL may allow us to determine whether consolidative radiation therapy after frontline chemoimmunotherapy is necessary in patients who achieve metabolic complete response after systemic treatment (ClinicalTrial.gov identifier: NCT01599559).

BV in combination with R-CHP with or without consolidative radiation therapy is a feasible and active frontline treatment in patients with CD30⁺ B-cell lymphomas. The safety profile of this regimen, ease of administration and preliminary efficacy data appear promising. The next generation of trials in CD30⁺ B-cell lymphomas and PMBCL should take into consideration the clinical and biological heterogeneity of these lymphomas. Ultimately, developing treatment regimens that will be tailored to unique tumor and patient characteristics will result in improved outcomes and will minimize treatment-related toxicities.

Disclosures

JS has received research funding from Seattle Genetics, BMS, Merck, Celgene, Incyte, and Pharmacyclics and honoraria for consultancy from Seattle Genetics, BMS, Kite, Kyowa, and Astra-Zeneca. DL has received research funding from Curis, Takeda, and Triphase and honoraria for consultancy from Curis and Celgene and for participation in a speakers' bureau from Seattle Genetics. SDN has received research funding from Roche, Incyte, Rafael, Atleron, Takeda/Millenium, Debiopharm, and Atara and honoraria for consultancy from Merck. SKB has received research funding from Seattle Genetics, Merck, Celgene, Takeda, and Bayer, and honoraria for consultancy from Janssen, for educational activity from Mundipharma, and for advisory board work from Seattle Genetics. NK has received research funding from BMS and Janssen and honoraria for consultancy from Seattle Genetics and for participation in a speakers' bureau from Genentech. EAC has received honoraria for consultancy from Novartis. JG has received honoraria for consultancy from Seattle Genetics. CS has received research funding from BMS and Tioma and honoraria for consultancy from Seattle Genetics, Roche, Bayer, and Curis; CS is also named as an inventor on a patent filed by the National Cancer Institute "Methods for determining lymphoma type". SJS has received research funding from Celgene, Genentech, Merck, and Novartis and honoraria for consultancy from Celgene, Dava Oncology, Merck, Nordic Nanovector, Novartis, Genentech, Gilead, and Pfizer. AM has received research funding from Merck. MSL has received honoraria for consultancy from Seattle Genetics. SMB, SJN, JEF, SG, LS, SM, TSW, CK, HJB, MY, JPP, AMB, SSH, HK, RN, and MR have no conflicts of interest to disclose.

Contributions

JS and SJS designed the study; JS analyzed the data and wrote the manuscript; SMB, SJN, LS, HJB, MY and SM performed research and analyzed the data; DL, SDN, SKB, NK, JEF, SG, EAC, JG, TSW, CK, JPP and AM provided treatment and follow-up for patients on the study; AMB, SSH, RN, CS, MSL and MR were involved in research design and analysis of the correlative studies. All authors read, critically reviewed and approved the manuscript. The authors would like to thank Dr. Elena Gitelson, in memoriam, who was involved with the initial trial conception and protocol discussions.

References

- Younes A, Yasothan U, Kirkpatrick P. Brentuximab vedotin. *Nat Rev Drug Discov*. 2012;11:19.
- Younes A, Gopal AK, Smith SE, et al. Results of a pivotal phase II study of brentuximab vedotin for patients with relapsed or refractory Hodgkin's lymphoma. *J Clin Oncol*. 2012;30(18):2183-2189.
- Pro B, Advani R, Brice P, et al. Brentuximab vedotin (SGN-35) in patients with relapsed or refractory systemic anaplastic large-cell lymphoma: results of a phase II study. *J Clin Oncol*. 2012;30(18):2190-2196.
- Connors JM, Jurczak W, Straus DJ, et al. Brentuximab vedotin with chemotherapy for stage III or IV Hodgkin's lymphoma. *N Engl J Med*. 2018;378(4):331-344.
- Horwitz S, O'Connor OA, Pro B, et al. Brentuximab vedotin with chemotherapy for CD30-positive peripheral T-cell lymphoma (ECHELON-2): a global, double-blind, randomised, phase 3 trial. *Lancet*. 2019;393(10168):229-240.
- Hu S, Xu-Monet ZY, Balasubramanyam A, et al. CD30 expression defines a novel subgroup of diffuse large B-cell lymphoma with favorable prognosis and distinct gene expression signature: a report from the International DLBCL Rituximab-CHOP Consortium Program Study. *Blood*. 2013;121(14):2715-2724.
- Lu T-X, Liang J-H, Miao Y, et al. Epstein-Barr virus positive diffuse large B-cell lymphoma predict poor outcome, regardless of the age. *Sci Rep*. 2015;5:12168.
- Slack GW, Steidl C, Sehn LH, Gascoyne RD. CD30 expression in de novo diffuse large B-cell lymphoma: a population-based study from British Columbia. *Br J Haematol*. 2014;167(5):608-617.
- Higgins JP, Warnke RA. CD30 expression is common in mediastinal large B-cell lymphoma. *Am J Clin Pathol*. 1999;112(2):241-247.
- Barth TF, Leithauser F, Joos S, Bentz M, Moller P. Mediastinal (thymic) large B-cell lymphoma: where do we stand? *Lancet Oncol*. 2002;3(4):229-234.
- Rosenwald A, Wright G, Leroy K, et al. Molecular diagnosis of primary mediastinal B cell lymphoma identifies a clinically favorable subgroup of diffuse large B cell lymphoma related to Hodgkin lymphoma. *J Exp Med*. 2003;198(6):851-862.
- Mottok A, Steidl C. Biology of classical Hodgkin lymphoma: implications for prognosis and novel therapies. *Blood*. 2018;131(15):1654-1665.
- Zinzani PL, Stefoni V, Finolezzi E, et al. Rituximab combined with MACOP-B or VACOP-B and radiation therapy in primary mediastinal large B-cell lymphoma: a retrospective study. *Clin Lymphoma Myeloma*. 2009;9(5):381-385.
- Rieger M, Österborg A, Pettengell R, et al. Primary mediastinal B-cell lymphoma treated with CHOP-like chemotherapy with or without rituximab: results of the Mabthera International Trial Group study. *Ann Oncol*. 2010;22(3):664-670.
- Dunleavy K, Pittaluga S, Maeda LS, et al. Dose-adjusted EPOCH-rituximab therapy in primary mediastinal B-cell lymphoma. *N Engl J Med*. 2013;368(15):1408-1416.
- Gleeson M, Hawkes EA, Cunningham D, et al. Rituximab, cyclophosphamide, doxorubicin, vincristine and prednisolone (R-CHOP) in the management of primary mediastinal B-cell lymphoma: a subgroup analysis of the UK NCRI R-CHOP 14 versus 21 trial. *Br J Haematol*. 2016;175(4):668-672.
- Bartlett NL, Wilson WH, Jung S-H, et al. Dose-adjusted EPOCH-R compared with R-CHOP as frontline therapy for diffuse large B-cell lymphoma: clinical outcomes of the phase III Intergroup Trial Alliance/CALGB 50303. *J Clin Oncol*. 2019;37(21):1790-1799.
- Kuruvilla J, Pintile M, Tsang R, Nagy T, Keating A, Crump M. Salvage chemotherapy and autologous stem cell transplantation are inferior for relapsed or refractory primary mediastinal large B-cell lymphoma compared with diffuse large B-cell lymphoma. *Leuk Lymphoma*. 2008;49(7):1329-1336.
- Giulino-Roth L, O'Donohue T, Chen Z, et al. Outcomes of adults and children with primary mediastinal B-cell lymphoma treated with dose-adjusted EPOCH-R. *Br J Haematol*. 2017;179(5):739-747.
- Armand P, Rodig SJ, Melnichenko V, et al. Pembrolizumab in patients with relapsed or refractory primary mediastinal large B-cell lymphoma (PMBCL): data from the Keynote-013 and Keynote-170 studies. *Blood*. 2018;132(Suppl 1):228.
- Neelapu SS, Locke FL, Bartlett NL, et al. Axicabtagene ciloleucel CAR T-cell therapy in refractory large B-cell lymphoma. *N Engl J Med*. 2017;377(26):2531-2544.
- Zinzani PL, Ribrag V, Moskowitz CH, et al. Safety and tolerability of pembrolizumab in patients with relapsed/refractory primary mediastinal large B-cell lymphoma. *Blood*. 2017;130(3):267-270.
- Moskowitz AJ, Santoro A, Gritti G, et al. Nivolumab combined with brentuximab vedotin for relapsed/refractory primary mediastinal large B-cell lymphoma: preliminary results from the phase 2 CheckMate 436 trial. *Blood*. 2018;132(Suppl 1):1691.
- Zinzani PL, Pellegrini C, Chiappella A, et al. Brentuximab vedotin in relapsed primary mediastinal large B-cell lymphoma: results from a phase 2 clinical trial. *Blood*. 2017;129(16):2328-2330.
- Cheson BD, Pfistner B, Juweid ME, et al. Revised response criteria for malignant lymphoma. *J Clin Oncol*. 2007;25(5):579-586.
- Mottok A, Wright G, Rosenwald A, et al. Molecular classification of primary mediastinal large B-cell lymphoma using routinely available tissue specimens. *Blood*. 2018;132(22):2401-2405.
- Schemper M, Smith TL. A note on quantifying follow-up in studies of failure time. *Control Clin Trials*. 1996;17(4):343-346.
- International Non-Hodgkin's Lymphoma Prognostic Factors Project. A predictive model for aggressive non-Hodgkin's lymphoma. *N Engl J Med*. 1993;329(14):987-994.
- Jacobsen ED, Sharman JP, Oki Y, et al. Brentuximab vedotin demonstrates objective responses in a phase 2 study of relapsed/refractory DLBCL with variable CD30 expression. *Blood*. 2015;125(9):1394-1402.
- Shah NN, Szabo A, Huntington SF, et al. R-CHOP versus dose-adjusted R-EPOCH in frontline management of primary mediastinal B-cell lymphoma: a multi-centre analysis. *Br J Haematol*. 2018;180(4):534-544.
- Soumerai JD, Hellmann MD, Feng Y, Sohani AR, Toomey CE, Barnes JA. Treatment of primary mediastinal B-cell lymphoma with rituximab, cyclophosphamide, doxorubicin, vincristine and prednisone is associated with a high rate of primary refractory disease. *Leuk Lymphoma*. 2014;55(3):538-543.
- Martelli M, Ceriani L, Zucca E, et al. [18F]fluorodeoxyglucose positron emission tomography predicts survival after chemoimmunotherapy for primary mediastinal large B-cell lymphoma: results of the International Extranodal Lymphoma Study Group IELSG-26 study. *J Clin Oncol*. 2014;32(17):1769-1775.
- Bartlett NL, Farber CM, Yasenchak CA, et al. Updated results of a phase II trial of brentuximab vedotin combined with R-CHOP in frontline treatment of patients (pts) with high-intermediate/high-risk diffuse large B-cell lymphoma (DLBCL). *J Clin Oncol*. 2015;33(15_suppl):8506.
- Vitolo U, Trněný M, Belada D, et al. Obinutuzumab or rituximab plus cyclophosphamide, doxorubicin, vincristine, and prednisone in previously untreated diffuse large B-cell lymphoma. *J Clin Oncol*. 2017;35(31):3529-3537.
- Lekovic D, Milijc P, Mihaljevic B. Increased risk of venous thromboembolism in patients with primary mediastinal large B-cell lymphoma. *Thromb Res*. 2010;126(6): 477-480.
- Duvic M, Tetzlaff MT, Gangar P, Clos AI, Sui D, Talpur R. Results of a phase II trial of brentuximab vedotin for CD30+ cutaneous T-cell lymphoma and lymphomatoid papulosis. *J Clin Oncol*. 2015;33(32):3759-3765.
- Kim YH, Prince HM, Whitaker S, et al. Outcomes by CD30 expression in patients with CTCL receiving brentuximab vedotin (BV) vs physician's choice (PC) in the phase 3 ALCANZA study. *J Clin Oncol*. 2017;35(15_suppl):7517.
- Sabattini E, Pizzi M, Tabanelli V, et al. CD30 expression in peripheral T-cell lymphomas. *Haematologica*. 2013;98(8):e81-e82.



Molecular profiling reveals a hypoxia signature in breast implant-associated anaplastic large cell lymphoma

Naoki Oishi,^{1,2} Tanya Hundal,¹ Jessica L. Phillips,¹ Surendra Dasari,¹ Guangzhen Hu,¹ David S. Viswanatha,¹ Rong He,¹ Ming Mai,¹ Hailey K. Jacobs,¹ Nada H. Ahmed,^{1,3} Sergei I. Syrbu,⁴ Youssef Salama,¹ Jennifer R. Chapman,⁵ Francisco Vega,^{5,6} Jagmohan Sidhu,⁶ N. Nora Bennani,⁷ Alan L. Epstein,⁸ L. Jeffrey Medeiros,⁹ Mark W. Clemens,¹⁰ Roberto N. Miranda^{9#} and Andrew L. Feldman^{1#}

¹Department of Laboratory Medicine and Pathology, Mayo Clinic, Rochester, MN, USA;

²Department of Pathology, University of Yamanashi, Chuo, Yamanashi, Japan;

³Department of Clinical Pathology, Suez Canal University, Ismailia, Egypt; ⁴Department of Pathology, University of Iowa, Iowa City, IA, USA; ⁵Department of Pathology, University of Miami, Miami, FL, USA; ⁶Department of Pathology and Laboratory Medicine, United Health Services, Binghamton, NY, USA; ⁷Division of Hematology, Mayo Clinic, Rochester, MN, USA; ⁸Department of Pathology, University of Southern California Keck School of Medicine, Los Angeles, CA, USA; ⁹Department of Hematopathology, MD Anderson Cancer Center, Houston, TX, USA and ¹⁰Department of Plastic Surgery, MD Anderson Cancer Center, Houston, TX, USA

⁵Current affiliation: Department of Hematopathology, MD Anderson Cancer Center, Houston, TX, USA

⁹MWC, RNM, and ALF contributed equally as co-senior authors.

ABSTRACT

Breast implant-associated anaplastic large cell lymphoma (BIA-ALCL) is a recently characterized T-cell malignancy that has raised significant patient safety concerns and led to worldwide impact on the implants used and clinical management of patients undergoing reconstructive or cosmetic breast surgery. Molecular signatures distinguishing BIA-ALCL from other anaplastic large cell lymphomas have not been fully elucidated and classification of BIA-ALCL as a World Health Organization entity remains provisional. We performed RNA sequencing and gene set enrichment analysis comparing BIA-ALCL to non-BIA-ALCL and identified dramatic upregulation of hypoxia signaling genes including the hypoxia-associated biomarker CA9 (carbonic anhydrase-9). Immunohistochemistry validated CA9 expression in all BIA-ALCL, with only minimal expression in non-BIA-ALCL. Growth induction in BIA-ALCL-derived cell lines cultured under hypoxic conditions was proportional to upregulation of CA9 expression, and RNA sequencing demonstrated induction of the same gene signature observed in BIA-ALCL tissue samples compared to non-BIA-ALCL. CA9 silencing blocked hypoxia-induced BIA-ALCL cell growth and cell cycle-associated gene expression, whereas CA9 overexpression in BIA-ALCL cells promoted growth in a xenograft mouse model. Furthermore, CA9 was secreted into BIA-ALCL cell line supernatants and was markedly elevated in human BIA-ALCL seroma samples. Finally, serum CA9 concentrations in mice bearing BIA-ALCL xenografts were significantly elevated compared to those in control serum. Together, these findings characterize BIA-ALCL as a hypoxia-associated neoplasm, likely attributable to the unique microenvironment in which it arises. These data support classification of BIA-ALCL as a distinct entity and uncover opportunities for investigating hypoxia-related proteins such as CA9 as novel biomarkers and therapeutic targets in this disease.

Correspondence:

ANDREW L. FELDMAN
feldman.andrew@mayo.edu

Received: December 20, 2019.

Accepted: May 14, 2020.

Pre-published: May 15, 2020.

<https://doi.org/10.3324/haematol.2019.245860>

©2021 Ferrata Storti Foundation

Material published in *Haematologica* is covered by copyright. All rights are reserved to the Ferrata Storti Foundation. Use of published material is allowed under the following terms and conditions:

<https://creativecommons.org/licenses/by-nc/4.0/legalcode>. Copies of published material are allowed for personal or internal use. Sharing published material for non-commercial purposes is subject to the following conditions:

<https://creativecommons.org/licenses/by-nc/4.0/legalcode>, sect. 3. Reproducing and sharing published material for commercial purposes is not allowed without permission in writing from the publisher.



Introduction

Anaplastic large cell lymphomas (ALCL) are a heterogeneous group of CD30-positive T-cell lymphomas with varying clinical presentation, prognosis, and molecular pathogenesis.¹ Breast implant-associated (BIA)-ALCL is a rare form of ALCL arising in association with breast implants placed for reconstructive or cosmetic purposes.² It typically occurs in the peri-implant capsule and/or effusion an average of 9 years after implant placement. The cytological and immunophenotypic features of BIA-ALCL are similar to those of systemic and primary cutaneous ALK-negative ALCL, including the presence of hallmark cells, CD30 positivity, and frequent loss of T-cell markers such as CD3 and CD5. The prognosis of patients with BIA-ALCL is associated with clinical stage, particularly the presence or absence of a mass-forming lesion and/or locoregional lymph node involvement, which influence the therapeutic approach.^{3,4} Complete surgical excision of the peri-implant fibrous capsule is essential and sufficient in patients without a mass or lymph node involvement, whereas systemic chemotherapy is recommended in those with advanced disease.^{3,5} Based on these distinct clinical features, the revised World Health Organization (WHO) classification recognizes BIA-ALCL as a provisional entity.²

The molecular pathogenesis of BIA-ALCL remains incompletely understood. Recent studies have suggested a possible relationship to underlying chronic allergic reaction and bacterial biofilm infection.^{6,7} Rearrangements of *ALK*, *DUSP22*, and *TP63* are consistently absent, referred to as the triple-negative (TN) genetic subtype.^{8,9} Recurrent *JAK1* and *STAT3* gene mutations have been identified⁹⁻¹² and, like many other ALCL,^{13,14} BIA-ALCL shows consistent activation of the JAK-STAT3 pathway as detected by immunohistochemistry for Tyr705-phosphorylated STAT3.^{9,12,15} *In vivo* studies have demonstrated that inhibition of JAK-STAT signaling by sunitinib or ruxolitinib effectively suppresses growth of TLBR cell lines derived from BIA-ALCL,^{15,16} suggesting potential therapeutic utility of these drugs for patients with advanced disease. In addition to mutations affecting the JAK-STAT signaling pathway, gene alterations in epigenetic modifiers are also frequent in BIA-ALCL.¹⁷

However, these findings have not identified a molecular profile of BIA-ALCL that is unique to the peri-implant

microenvironment in which it originates. Identification of unique molecular features specific for BIA-ALCL could lead to discovery of biomarkers that improve early detection, diagnosis, and follow-up; identify candidate targets for therapy or preventive strategies; and provide justification to upgrade the WHO classification of BIA-ALCL from a provisional to a definite entity. We therefore interrogated the gene expression profile of BIA-ALCL.

Methods

Gene expression profiling

Human studies were conducted with approval of the Institutional Review Boards at Mayo Clinic and The University of Texas MD Anderson Cancer Center. We performed RNA sequencing on formalin-fixed paraffin-embedded tumor tissue from 11 patients with BIA-ALCL (Table 1). All were female and their mean age was 55 years (range, 44-73 years). All had received textured implants. As described previously,¹⁴ RNA from AllPrep extraction was used to prepare sequencing libraries (TruSeq RNA Access, Illumina) and sequenced on a HiSeq 4000 (Illumina). Reads were aligned to hg38 with MAP-RSeq¹⁸ modified to use the STAR aligner.¹⁹ Gene-level read counts based on Ensembl version 78 were transformed into reads per kilobase per million mapped reads (RPKM). Gene expression data were compared to those of 24 previously sequenced non-BIA-ALCL of TN genetic subtype (10 primary cutaneous ALCL and 14 systemic ALK-negative ALCL¹⁴). Gene set enrichment analysis (GSEA) was performed using GSEA software (Broad Institute) as described previously.¹⁴

Immunohistochemistry

Immunohistochemistry for CA9 was carried out on formalin-fixed paraffin-embedded sections of 17 BIA-ALCL and 48 non-BIA-ALCL (from patients with a mean age of 54 years). The WHO subtypes of these latter were primary cutaneous ALCL (n=13), ALK-negative ALCL (n=24), and ALK-positive ALCL (n=11). Genetic subtypes included 11 ALK-positive, ten with *DUSP22* rearrangements, two with *TP63* rearrangements, and 25 TN. Deparaffinized tissue sections were heated in pH 6.0 citric acid buffer in a steam cooker for 30 min. After incubation with 3% hydrogen peroxide for 10 min and 5% bovine serum albumin for 10 min, the slides were incubated with anti-CA9 rabbit monoclonal antibody (1:100 dilution, clone D47G3; Cell Signaling Technology) at 4°C overnight. Sections were then incubated with horseradish peroxidase-conjugated anti-rabbit secondary antibody

Table 1. Clinical and pathological features of 11 patients with breast implant-associated anaplastic large cell lymphoma.

Patient #	Age	Sex	ALK	<i>DUSP22</i> -R	<i>TP63</i> -R	T*	N*	M*	Stage*	Subtype†
151	46	F	Neg.	Neg.	Neg.	T1	N0	M0	IA	<i>In situ</i>
224	55	F	Neg.	Neg.	Neg.	T2	N0	M0	IB	Tumor type
403	47	F	Neg.	Neg.	Neg.	T1	N0	M0	IA	<i>In situ</i>
425	45	F	Neg.	Neg.	Neg.	T2	N2	M0	IIB	Tumor type
2680	74	F	Neg.	Neg.	Neg.	T1	N0	M0	IA	<i>In situ</i>
2896	65	F	Neg.	Neg.	Neg.	T4	N0	M0	IIA	Tumor type
3176	61	F	Neg.	Neg.	Neg.	T4	N0	M0	IIA	Tumor type
3177	57	F	Neg.	Neg.	Neg.	T1	N0	M0	IA	<i>In situ</i>
3181	76	F	Neg.	Neg.	Neg.	T2	N0	M0	IB	Tumor type
3183	63	F	Neg.	Neg.	Neg.	T4	N0	M0	IIA	Tumor type
3184	41	F	Neg.	Neg.	Neg.	T4	N0	M0	IIA	Tumor type

Age in years. F: female; Neg.: negative; R: rearrangement. *TNM (tumor-node-metastasis) staging according to Clemens *et al.*⁴⁹ †Histological subtype according to Laurent *et al.*¹⁷

(Biocare Medical), developed with 3,3'-diaminobenzidine, and counterstained with hematoxylin. Stains were scored in a blind fashion by two hematopathologists (NO and ALF). For CA9, scoring was based on percentage of tumor cells with membranous staining.

BIA-ALCL xenograft models

Studies were approved by the Mayo Clinic Institutional Animal Care and Use Committee (IACUC) under protocol A00002776. Five-week-old female NOD.Cg-Prkdcscid Il2rgtm1Wjl/SzJ (NSG) mice were purchased from The Jackson Laboratory and maintained under standard laboratory conditions. Cell lines TLBR-1, TLBR-2, and TLBR-3 were established from BIA-ALCL by one of the authors (ALE).^{15,20} and were maintained in RPMI-1640 (Gibco) supplemented with 10% fetal bovine serum (Clontech), 1% penicillin/streptomycin (Gibco), and 100 U/mL interleukin-2 (R&D 202-IL-050). TLBR-1, -2, and -3 cells were cultured at a concentration of 0.5×10^6 /mL for 72 h and resuspended in phosphate-buffered saline. Mice were injected subcutaneously in the right flank with TLBR-1, -2, or -3 cells. Tumor volumes were calculated in mm³ using the formula $P \times L/2$, where P and L represent the shortest and longest dimensions, respectively.

Additional methods are described in the *Online Supplementary Material*.

Results

Increased expression of hypoxia signaling pathway genes is a hallmark of BIA-ALCL

We performed RNA sequencing to identify gene expression signatures that might distinguish BIA-ALCL from other types of ALCL. Since BIA-ALCL are consistently of TN genetic subtype,⁹ we compared BIA-ALCL to other TN ALCL to avoid bias from the distinct expression profiles of other genetic subtypes¹⁴ (Figure 1A). A distinct cluster of genes was upregulated in BIA-ALCL, which formed the basis for subsequent analyses. Two clusters of genes were expressed only in non-BIA cases: one was enriched for keratin genes and consisted of biopsies at epithelial sites (skin and tongue) and the other contained Y-linked genes and represented male patients.

We then performed GSEA to identify candidate molecular signatures for genes upregulated in BIA-ALCL (Figure 1B, *Online Supplementary Table S1*). We focused on the second highest ranking gene set, HALLMARK HYPOXIA (normalized enrichment score [NES], 2.727; false discovery rate q -value [FDR], 0.000), as a candidate molecular feature distinctive of BIA-ALCL. The highest ranking gene set, HALLMARK EPITHELIAL MESENCHYMAL TRANSITION (NES, 2.963; FDR, 0.000) and other subsequent pathways mostly related to collagen formation and extracellular matrix organization, likely reflecting stromal components in the fibrous capsule surrounding the breast implant and seroma in BIA-ALCL samples.²¹ Supporting these GSEA results, examination of differential expression of genes and absolute RPKM values between BIA-ALCL and non-BIA-ALCL revealed significantly higher expression levels of downstream target genes of the hypoxia signaling pathway such as *VEGFA*, *VEGFB*, *SLC2A3* (encoding GLUT3), and *CA9* (carbonic anhydrase-9; RPKM, mean \pm standard deviation: 16.5 ± 20.2 vs. 0.4 ± 0.7 ; $P < 0.001$, *t*-test) (*Online Supplementary Figure S1*). Among genes associated with hypoxia, *CA9* showed the highest fold-change between BIA-ALCL and non-BIA-ALCL

($FC = 5.296$, FDR, 3.07×10^{-9}) (Figure 1C). Collectively, these results suggest that increased expression of hypoxia signaling pathway genes is a transcriptional hallmark of BIA-ALCL. We did not identify a significant difference in *CA9* expression between *in situ* and tumor-type BIA-ALCL as described by Laurent *et al.*¹⁷ (Table 1), or distinct gene signatures associated with clinical stage; associations between gene expression and clinicopathological features should be evaluated in future, larger studies.

CA9 protein is consistently expressed in BIA-ALCL but not in other ALCL

CA9 is a well-established biomarker of hypoxia and tumoral expression of *CA9* is widely used in the histopathological diagnosis of hypoxia-related cancers.²² Therefore, having identified a hypoxia-associated signature and high *CA9* mRNA expression in BIA-ALCL, we performed immunohistochemistry to investigate *CA9* protein expression in BIA-ALCL and non-BIA-ALCL. *CA9* was expressed on the cell membrane of BIA-ALCL cells (% positive staining, mean \pm standard deviation, $91 \pm 15\%$) but not in admixed inflammatory cells, validating the RNA sequencing data at the protein level (Figure 2A). A relatively narrow range of protein scores was observed by immunohistochemistry, compared to a wide range of *CA9* gene expression values. The correlation between the two was not statistically significant, likely due to gene expression values reflecting contributions from non-neoplastic cells whereas immunohistochemistry was scored only in the tumor cells. Conversely, *CA9* was mostly negative in non-BIA-ALCL (ALK-positive, $2 \pm 6\%$; ALK-negative, $5 \pm 11\%$; cutaneous, $3 \pm 5\%$; $P < 0.0001$, Dunn multiple comparison test) (Figure 2B). We also stratified *CA9* protein expression by genetic subtype of ALCL (Figure 2C). BIA-ALCL (all TN) showed significantly more *CA9* expression than ALK-positive ALCL, *DUSP22*-rearranged ALCL, and TN non-BIA-ALCL, suggesting that high *CA9* expression in BIA-ALCL is attributable to BIA presentation rather than TN genetic subtype. Taken together, these data indicate that *CA9* is specifically expressed in BIA-ALCL at the mRNA and protein levels.

Hypoxia-induced *CA9* expression drives growth of BIA-ALCL cells

We next examined *CA9* expression in BIA-ALCL cell lines under normoxic and hypoxic conditions. Expression of *HIF-1α* was evaluated to confirm the response to hypoxia. Western blotting of TLBR-1, -2, and -3 cells cultured under normoxic or hypoxic conditions revealed distinct patterns of *CA9* expression in each cell line, providing unique models for further study (Figure 3A). In TLBR-1, *CA9* was expressed under baseline normoxic conditions, suggesting constitutive expression of the hypoxic program. *CA9* expression was further induced by hypoxia. In TLBR-2, *CA9* was absent under normoxic conditions but was induced under hypoxic conditions, consistent with a canonical hypoxia response. In contrast, *CA9* expression in TLBR-3 was absent under normoxic conditions and only minimally induced by hypoxia.

To explore the functional significance of these distinct patterns of *CA9* expression, we evaluated the effects of hypoxia with or without siRNA-mediated silencing of *CA9* on BIA-ALCL cell growth (Figure 3B). In TLBR-1, which showed evidence of a constitutive hypoxia program under normoxic conditions, hypoxia induced only a

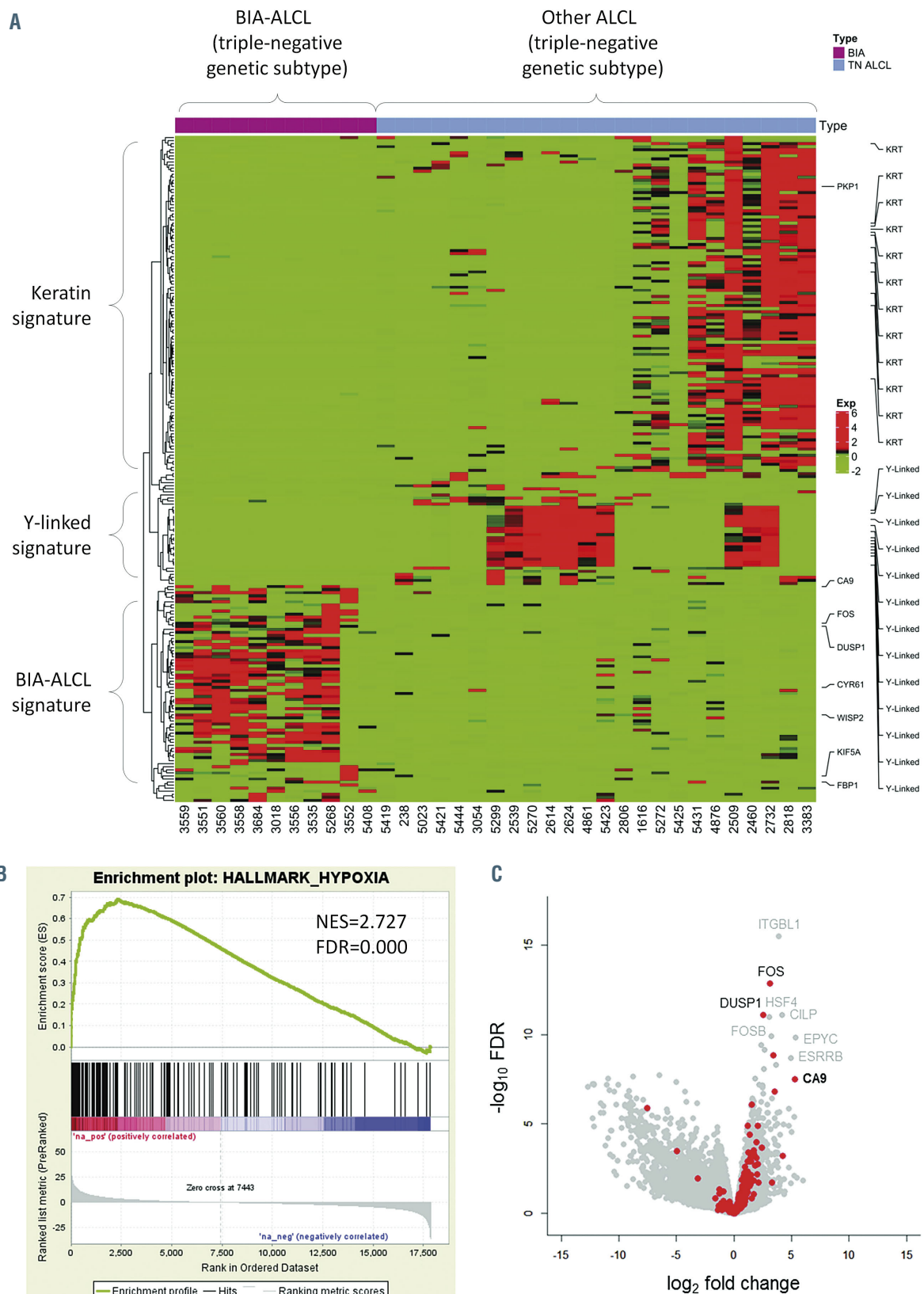


Figure 1. Breast implant-associated anaplastic large cell lymphomas show upregulation of hypoxia-associated genes. (A) Heatmap of genes differentially expressed between breast implant-associated (BIA) anaplastic large cell lymphomas (ALCL) and other ALCL of triple-negative (TN) genetic subtype (lacking rearrangements of ALK, DUSP22 and TP63). A distinct signature of genes overexpressed in BIA-ALCL is seen. Signatures in subgroups of non-BIA ALCL include a keratin (KRT) signature seen in biopsies at epithelial sites (skin and tongue) and a Y-linked signature seen in male patients. See also *Online Supplementary Figure S1*. (B) Gene set enrichment analysis shows upregulation of genes associated with hypoxia in BIA-ALCL. See also *Online Supplementary Table S2*. NES: normalized enrichment score; FDR: false discovery rate. (C) A volcano plot indicating differentially expressed genes between BIA-ALCL and other TN ALCL. Hypoxia-related genes from HALLMARK_HYPOXIA and SEMENZA HIF1 TARGETS gene sets are indicated in red.

slight increase in growth ($14 \pm 13\%$ above normoxic baseline, $P < 0.05$, Mann-Whitney test). Silencing *CA9* inhibited this growth to $77 \pm 6\%$ of normoxic baseline ($P < 0.001$). In TLBR-2, a proposed model of canonical hypoxia response, hypoxia substantially increased growth by $281 \pm 79\%$ ($P < 0.0001$) and this increase was reversed nearly to nor-

moxic baseline by *CA9* silencing ($P < 0.001$ vs. control siRNA). In TLBR-3, which was resistant to hypoxia-induced *CA9* expression, no significant increase in growth was induced by hypoxia. In summary, these data indicate that hypoxia-induced growth in BIA-ALCL cell lines follows a pattern similar to that of hypoxia-induced expres-

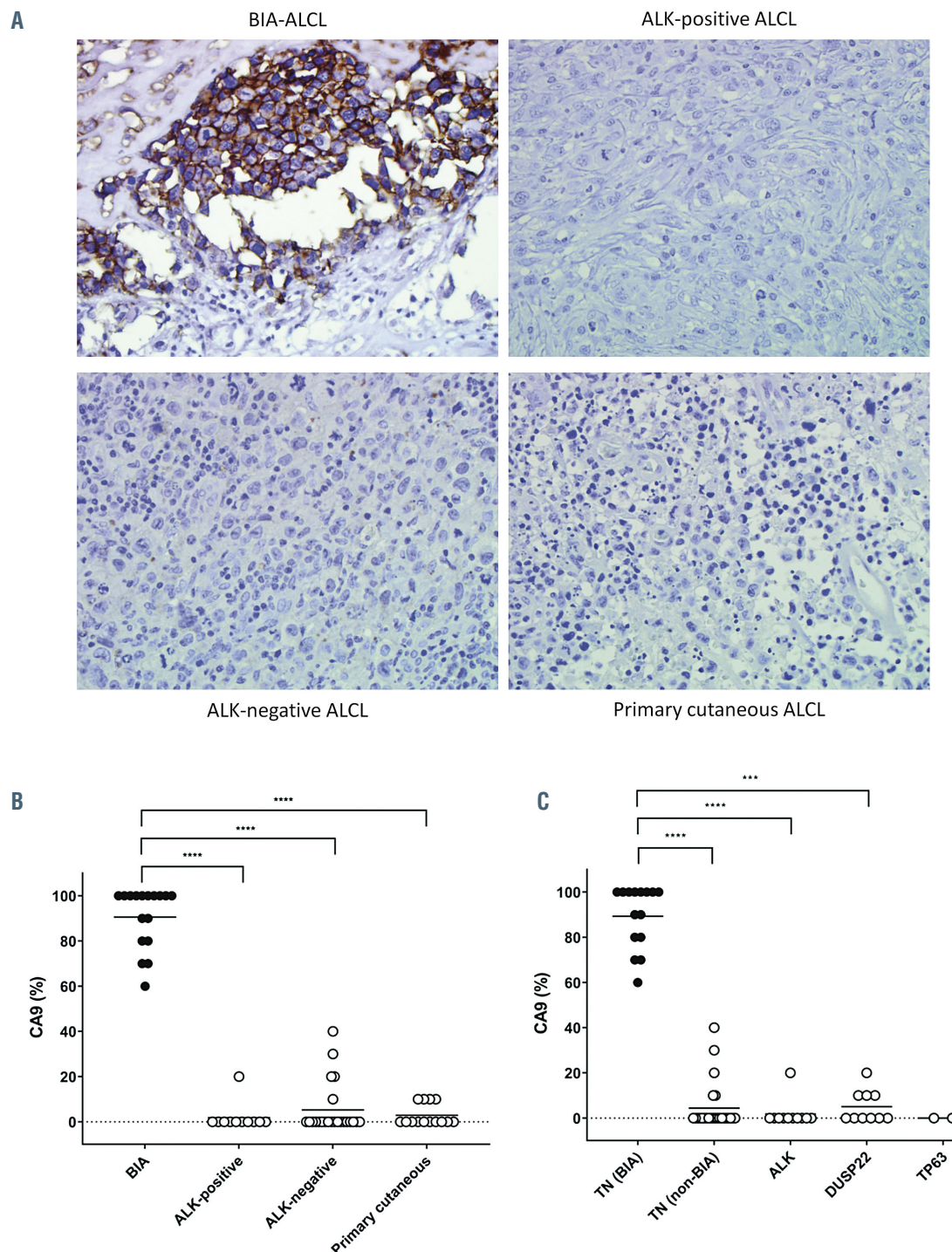


Figure 2. Breast implant-associated anaplastic large cell lymphomas consistently express CA9. (A) Representative microscopic images of immunohistochemistry for CA9 in breast implant-associated (BIA) anaplastic large cell lymphoma (ALCL), systemic ALK-positive ALCL, systemic ALK-negative ALCL, and primary cutaneous ALCL (40 \times original magnification). (B) BIA-ALCL show significantly higher CA9 expression than other forms of ALCL. (C) The increased expression of CA9 in BIA-ALCL is independent of genetic subtype. All BIA-ALCL tested have triple-negative (TN) genetics (lacking rearrangements of ALK, DUSP22, and TP63). BIA-ALCL show significantly higher CA9 expression than ALCL with any of these rearrangements, as well as TN non-BIA-ALCL. *** $P < 0.001$; **** $P < 0.0001$.

sion of CA9 and that CA9 drives BIA-ALCL cell growth under hypoxic conditions.

Hypoxia and CA9 expression drive unique gene signatures in BIA-ALCL cells

We examined the effects of hypoxia and CA9 knockdown on gene expression in BIA-ALCL cells by performing RNA sequencing in TLBR-2 cells, which showed evidence of a canonical hypoxia response in the preceding experiments. As anticipated, CA9 mRNA was markedly upregulated under hypoxic conditions and effectively downregulated by CA9 siRNA (both, $P<0.0001$) (Figure 4A). A heatmap of genes whose expression varied significantly showed clusters of genes with unique expression patterns as well as clusters of genes with expression patterns shared between two of the three conditions (Figure 4B). We used GSEA to explore these findings further (Figure 4C). Notably, the set of genes overexpressed in BIA-ALCL tissue samples as compared with TN non-BIA-ALCL (Figure 1A) was markedly enriched in TLBR-2 cells cultured under hypoxic conditions (NES=2.325; FDR=0.000), providing *in vitro* validation of the tissue-based finding that BIA-ALCL are characterized by a hypoxia signature. Furthermore, the HALLMARK HYPOXIA gene set identified in BIA-ALCL *versus* non-BIA-ALCL tissue samples (Figure 1B) was also significantly enriched in hypoxic TLBR-2 cells (NES=2.151, FDR=0.000), among other gene sets related to metabolic pathways such as HALLMARK GLYCOLYSIS, REACTOME METABOLISM OF CARBOHYDRATES, and REACTOME GLUCOSE METABOLISM (Online Supplementary Table S2). In contrast, siRNA-mediated CA9 knockdown was associated with significant depletion of cell cycle pathways, including REACTOME S PHASE (NES=-2.214; FDR=0.000) as well as MYC target gene sets and multiple other cell cycle-associated gene sets (Online Supplementary Table S3). These findings corroborate previous data showing that CA9 inhibition induced cell cycle arrest in glioblastoma cells, and specifically a marked reduction of cells in S phase.²³ We also performed an exploratory analysis comparing RNA sequencing data in TLBR cell lines. Although only TLBR-1 significantly expressed CA9 at baseline, other hypoxia-related genes were relatively overexpressed in TLBR-2 or TLBR-3 (Online Supplementary Figure S5), suggesting heterogeneity that merits investigation in larger future studies.

CA9 overexpression drives BIA-ALCL growth in a xenograft model

We evaluated the effects of CA9 on BIA-ALCL cell growth further by using a lentiviral system to overexpress CA9 in TLBR-3 cells, which lack both baseline and hypoxia-inducible CA9 expression (Figure 3A). Corroborating CA9 siRNA data from TLBR-1 and -2 cells, CA9 overexpression in TLBR-3 augmented cell growth *in vitro* (Online Supplementary Figure S2). We then examined the effect of CA9 overexpression in a xenograft model. The median time after inoculation to establishment of palpable subcutaneous tumors was 17 days in the CA9 group and 26 days in the control (empty vector-transduced) group ($P=0.004$, log-rank test) (Figure 5A). At 38 days, when the first animal required euthanasia because of tumor size, tumors were $1,764 \pm 1,526 \text{ mm}^3$ in the CA9 group and $126 \pm 130 \text{ mm}^3$ in the control group (Figure 5B); differences in tumor growth were highly significant ($P<0.0001$, two-

way repeated measure analysis of variance with the Geisser-Greenhouse correction). Using this protocol-defined euthanasia endpoint, median overall survival was 47 days in the CA9 group and 76 days in the control group ($P=0.0008$, log-rank test) (Figure 5C). Thus, CA9 accelerates tumor growth in the TLBR-3 BIA-ALCL xenograft model.

Secreted CA9 in BIA-ALCL cell line models and patients' samples

Secreted CA9 has been proposed as a biomarker for CA9-expressing malignancies.^{22,24-26} We therefore evaluated secretion of CA9 into the supernatants of BIA-ALCL cell lines. Secreted CA9 could be detected in culture supernatants of TLBR-1, -2, and -3 cells at concentrations mir-

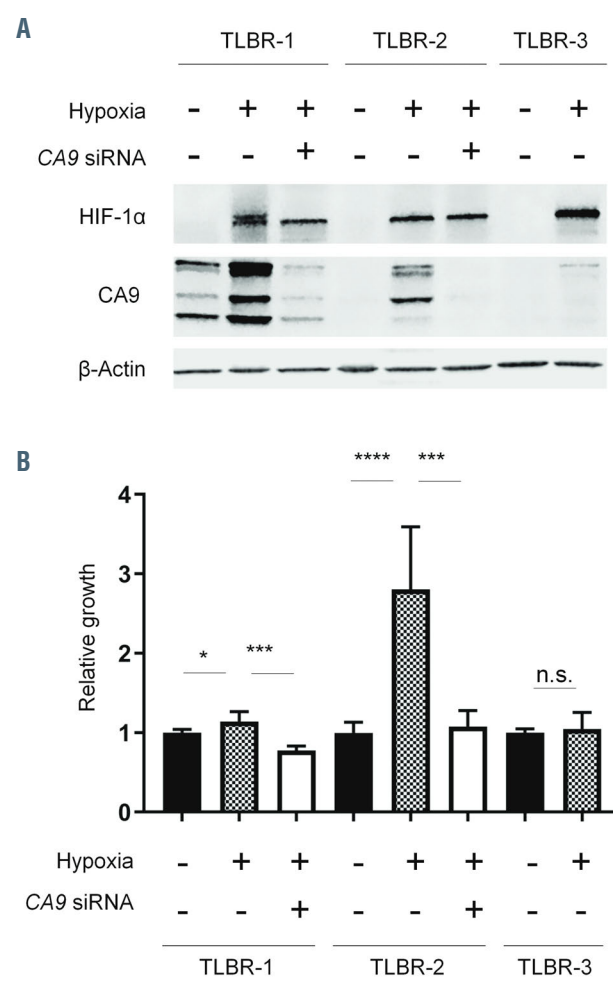


Figure 3. CA9 expression and growth of breast implant-associated anaplastic large cell lymphoma cell lines. (A) TLBR-1, -2, and -3 breast implant-associated (BIA) anaplastic large cell lymphoma (ALCL) cell lines show distinct patterns of CA9 expression under normoxic and hypoxic conditions. HIF-1 α serves as a positive control for hypoxia. TLBR-1 shows constitutive CA9 expression under normoxic conditions, which is further enhanced by hypoxia. TLBR-2 lacks constitutive CA9 expression but CA9 is induced by hypoxia (canonical hypoxia response). TLBR-3 shows minimal hypoxia-induced CA9 expression. The effects of siRNA-mediated CA9 silencing are shown. Representative data from three independent experiments. (B) Growth of TLBR-1, -2, and -3 cells mirrors CA9 expression. TLBR-1 cells, which constitutively express CA9, show only slight growth induction by hypoxia. Growth is inhibited by CA9 silencing. TLBR-2 cells, which show a canonical hypoxia response, have marked hypoxia-induced growth which is almost completely reversed by CA9 silencing. Hypoxia does not induce either growth or CA9 expression in TLBR-3 cells. * $P<0.05$; ** $P<0.001$; *** $P<0.0001$; n.s., not statistically significant.

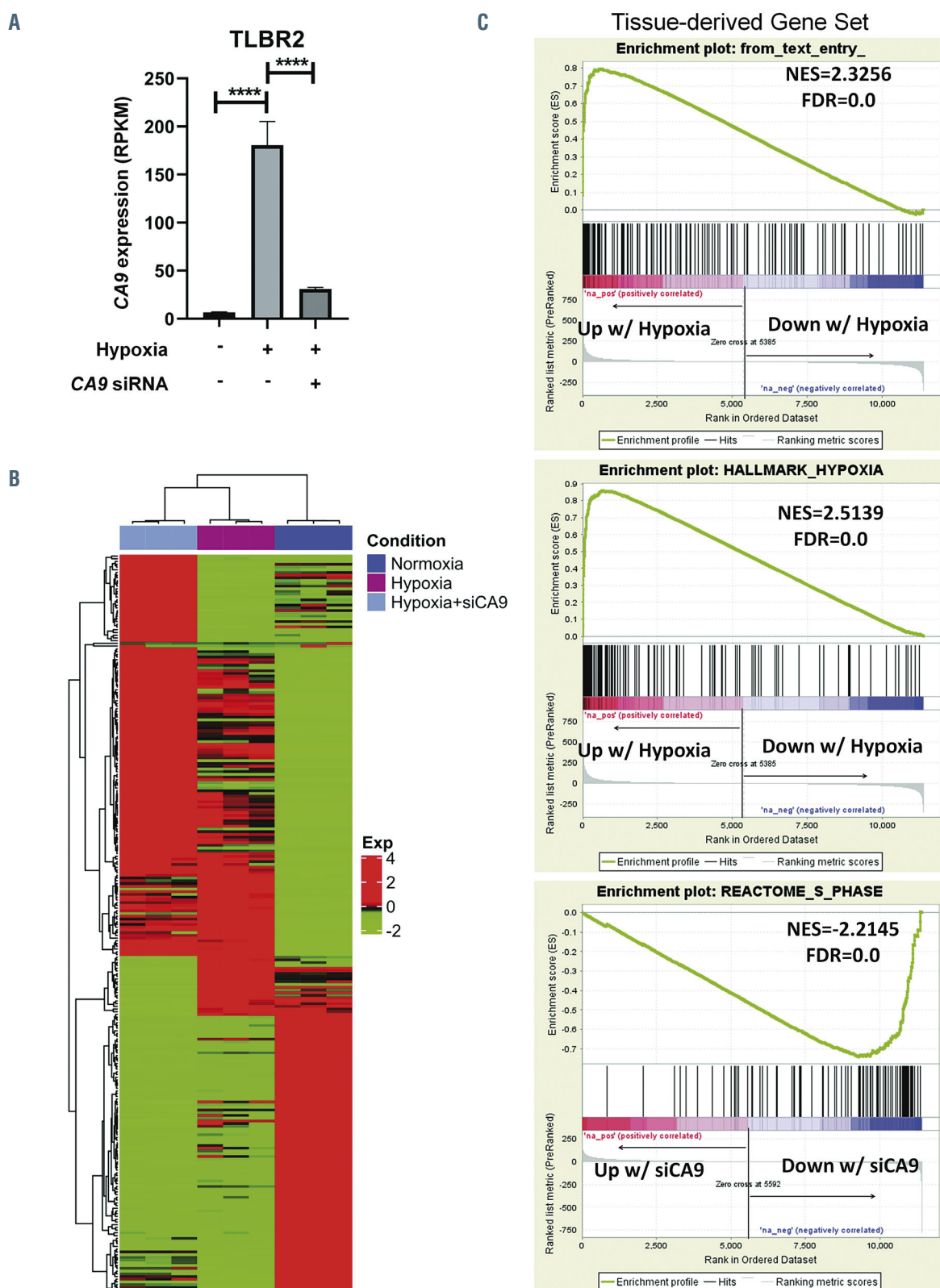


Figure 4. Gene signatures associated with hypoxia and CA9 expression in breast implant-associated anaplastic large cell lymphoma cells. (A) CA9 mRNA expression is induced by hypoxia and inhibited by CA9 siRNA in TLBR-2 breast implant-associated (BIA) anaplastic large cell lymphoma (ALCL) cells. RPKM: reads per kilobase per million mapped reads; **** $P<0.0001$. (B) Heatmap showing relative gene expression in TLBR-2 for each of the three conditions shown in panel A. RNA sequencing was performed in triplicate for each condition. (C) **Top panel:** TLBR-2 cells cultured under hypoxic conditions show significant enrichment for the set of genes overexpressed in BIA- versus non-BIA-ALCL tissue samples ("tissue-derived gene set," defined as $\log_2 FC > 1$ and $FDR \leq 0.05$; cf. Figure 1A). **Middle panel:** the HALLMARK_HYPOXIA gene set identified by gene set enrichment analysis in BIA- versus non-BIA-ALCL tissue samples is also significantly enriched in hypoxic TLBR-2 cells. See also *Online Supplementary Table S2*. **Bottom panel:** hypoxic TLBR-2 cells treated with CA9 siRNA show marked depletion of REACTOME S PHASE and other gene sets related to cell cycle and MYC targets. See also *Online Supplementary Table S3*. FC: fold change; NES: normalized enrichment score; FDR: false discovery rate.

oring their cellular expression levels (Figure 6A). Since BIA-ALCL cells can secrete CA9, we next examined whether CA9 could be detected in peri-implant seroma specimens involved by BIA-ALCL. Indeed, all ten BIA-ALCL seroma specimens evaluated contained detectable CA9, with a mean concentration of $84,046 \pm 118,695$ pg/mL (range, 423-360,262 pg/mL) (Figure 6B). In contrast, seromas lacking involvement by BIA-ALCL showed a mean concentration of 502 ± 390 pg/mL (range, 9-887 pg/mL; $P < 0.0001$, Mann-Whitney test).

Four serum and/or plasma samples from BIA-ALCL were available to evaluate CA9 concentrations (Online Supplementary Figure S3). While the CA9 concentration in normal human serum or plasma is < 25 pg/mL,^{24,26} the plasma CA9 concentration was 128 pg/mL in one BIA-ALCL patient. Because the number of human blood samples available for testing was limited, we examined whether CA9 secreted from BIA-ALCL cells might be detectable in serum samples using mouse xenograft models. We harvested subcutaneous TLBR-1, -2, and -3 tumors when each tumor reached a volume of $1,000 \text{ mm}^3$ and obtained simultaneous serum samples. Tumor lysate CA9 concentrations from TLBR-1, -2, and -3 were $108,175 \pm 39,252$ pg/mL, $231,070 \pm 88,185$ pg/mL, and $6,903 \pm 1,871$ pg/mL, respectively, based on standardized total protein concentrations of $1 \mu\text{g}/\mu\text{L}$; all pairwise comparisons showed significant differences (Online Supplementary Figure S4). A similar pattern of serum CA9 concentrations was observed, with mean values for TLBR-1, -2, and -3 tumor-bearing mice of 170 ± 46 pg/mL, 183 ± 170 pg/mL, and 122 ± 119 pg/mL; values in all groups were significantly higher than CA9 concentrations in serum obtained from non-tumor-bearing mice (46 ± 11 pg/mL) (Figure 6C). Taken together, these findings indicate that CA9 can be secreted from BIA-ALCL cells and is detectable in peri-implant seroma fluid involved by BIA-ALCL. Serum CA9 concentrations are elevated in sera from BIA-ALCL xenograft-bearing mice and serum levels in BIA-ALCL patients should be evaluated in larger cohorts.

Discussion

In this gene expression profiling study comparing BIA-ALCL to their non-BIA counterparts, we found that BIA-ALCL demonstrate a hypoxia signature, likely attributable to the unique microenvironment in which they arise. Notably, the carbonic anhydrase CA9 was expressed consistently in BIA-ALCL and only minimally in non-BIA-ALCL. CA9 promoted hypoxia-induced growth in BIA-ALCL cell lines *in vitro* and in mouse xenograft models. In addition, CA9 was significantly elevated in human seroma samples involved by BIA-ALCL and in serum from BIA-ALCL xenograft-bearing mice. These findings identify unique biological features of BIA-ALCL, support its classification as a WHO entity distinct from other forms of ALCL, and uncover opportunities to explore hypoxia-related proteins and pathways in novel diagnostic, preventive, or therapeutic strategies for patients with this disease.

RNA sequencing with transcriptomic analysis and GSEA revealed enhanced expression of hypoxia signaling pathway genes as a hallmark of BIA-ALCL. A recent study by Di Napoli *et al.* also compared the transcriptome of BIA-ALCL to that of other peripheral T-cell lymphomas including non-ALCL.²⁷ The authors identified a number of

notable findings, including upregulation of genes involved in cell motility (e.g., *CCR6*, *MET*, and *HGF*), myeloid cell differentiation (e.g., *PPARG* and *JAK2*), and viral gene transcription (e.g., *RPS10*), and downregulation of T-cell receptor signaling genes. Differentially expressed genes reported by Di Napoli *et al.* tended to show similar changes in our dataset (Online Supplementary Figure S6). However, the gene ontology analysis of Di Napoli *et al.* compared BIA-ALCL to non-neoplastic T cells, whereas our study was designed to identify differences between

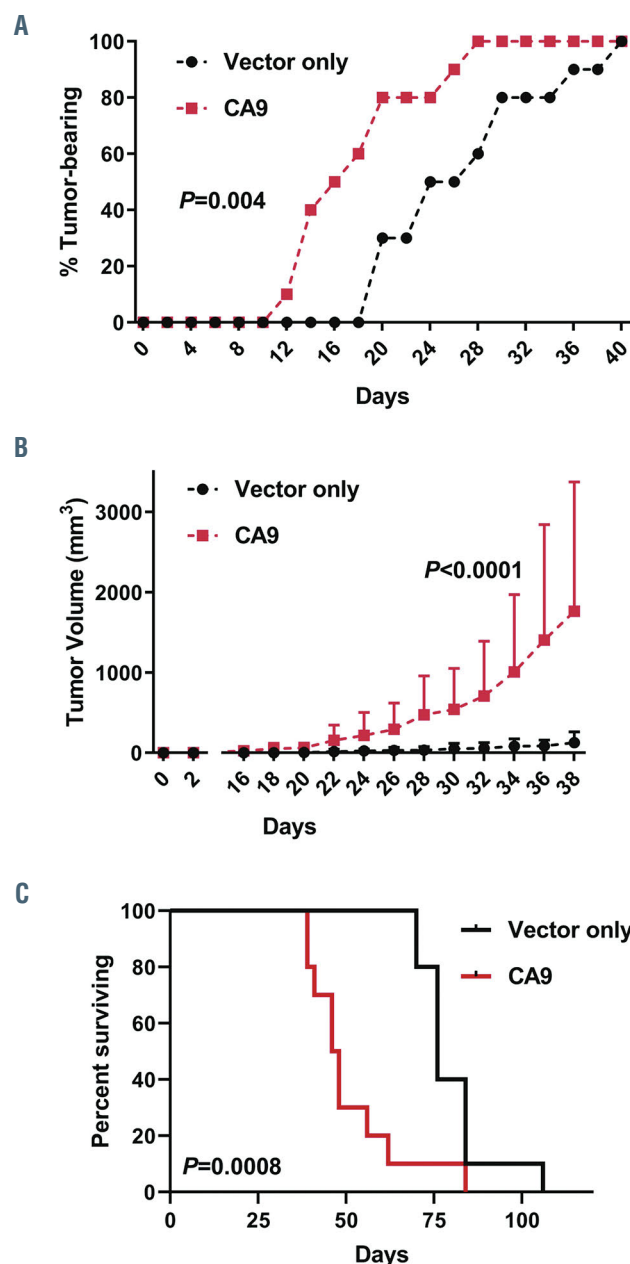


Figure 5. CA9 accelerates breast implant-associated anaplastic large cell lymphoma growth in a mouse xenograft model. (A) Mice inoculated with TLBR-3 breast implant-associated anaplastic large cell lymphoma cells stably transduced with a CA9 lentiviral vector develop palpable tumors faster than mice inoculated with cells transduced with vector control. (B) Mice inoculated with TLBR-3 cells overexpressing CA9 develop larger tumors than mice inoculated with control-transduced TLBR-3 cells. (C) Overall survival is shorter in mice bearing CA9-overexpressing TLBR-3 tumors than in those bearing control-transduced tumors.

BIA-ALCL and TN ALCL arising at other anatomic sites. Therefore, these two studies are complementary and emphasize different aspects of BIA-ALCL pathogenesis for further study. Of note, occasional non-BIA-ALCL (especially with TN genetics) showed a moderate degree of CA9 expression, highlighting the need for additional future study of hypoxia-associated pathways in T-cell neoplasms other than BIA-ALCL.²⁸

BIA-ALCL arises in a unique tumor microenvironment consisting of the breast prosthesis, seroma fluid, and surrounding fibrous capsule. Local hypoxia is a well-established factor promoting the development of tissue fibrosis,^{29,30} and tissues with artificial prostheses are postulated to be hypoxic.^{31,32} For example, Kim *et al.* showed that the thickness of the fibrous capsule around silicone implants in rats was reduced by stem cell-derived endothelial precursor cell conditioned medium, which promotes wound healing at least in part by reducing tissue ischemia, suggesting the peri-implant microenvironment is hypoxic even in the non-neoplastic setting.³³ The ability to tolerate low oxygen tension may be critical for pre-neoplastic cells situated between the prosthesis and peri-implant fibrous capsule to survive and proliferate in the early stages of BIA-ALCL lymphomagenesis. Since most patients with implants do not develop BIA-ALCL, however, future studies should examine possible interplay between hypoxia and recurrent genetic events reported in this disease, such as mutations in JAK-STAT and epigenetic modifier genes.¹⁷ Furthermore, it would be of interest to compare the molecular signature of BIA-ALCL with that of other effusion-associated malignancies such as primary effusion lymphomas of B-cell origin, in which targetable hypoxic metabolic pathways have been reported previously.^{34,35}

Among genes within the hypoxic signature, we identified CA9 as being most robustly overexpressed in BIA-ALCL, a finding we validated at the protein level by immunohistochemistry. CA9 is a hypoxia-inducible enzyme that catalyzes reversible hydration of carbon dioxide to bicarbonate ions and protons.²² CA9 is expressed in a variety of solid cancers and has been associated with poor prognosis.³⁶⁻³⁸ Overexpression of CA9 represents an adaptive response to hypoxia by which cancer cells control intracellular and extracellular pH, facilitating survival and growth in an acidic tumor microenvironment.^{22,39-44} Our data on silencing CA9 expression in hypoxia-inducible TLBR-2 cells and overexpressing CA9 in hypoxia-insensitive TLBR-3 cells indicate that CA9 promotes growth of BIA-ALCL cells. Although CA9 inhibitors have been developed,²³ the direct therapeutic implications of our findings for BIA-ALCL are unclear since disease limited to the hypoxic seroma and surrounding capsule is adequately managed by surgery alone in most cases.³ We did not have adequate tissue material from disseminated BIA-ALCL to evaluate whether CA9 expression is retained outside its native microenvironment. Nevertheless, understanding the role of CA9 and other hypoxic signaling pathways in early BIA-ALCL could lead to less invasive strategies to manage localized disease and/or novel prosthetic approaches that decrease the risk of its development.

Our findings also suggest that CA9 could be useful as a biomarker for screening, detection, and/or follow-up of BIA-ALCL. CA9 expression in normal human tissues is limited to gastric, colonic, and gallbladder epithelium.²² Clear cell renal cell carcinoma is a prototypic malignancy expressing high CA9, in which recurrent *VHL* mutations

lead to increased expression of hypoxia-associated genes including CA9; accordingly, CA9 is a widely-used immunohistochemical marker to distinguish clear cell renal cell carcinoma from other renal tumors.⁴⁵ In addition, serum CA9 levels are associated with tumor size, grade,

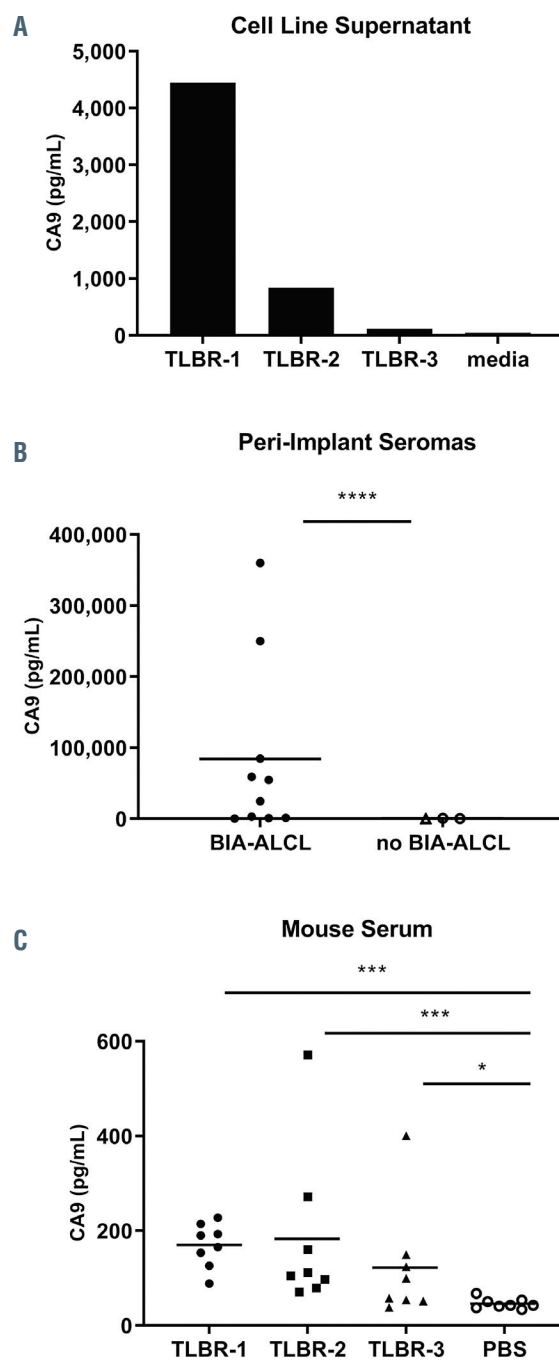


Figure 6. CA9 as a candidate biomarker in breast implant-associated anaplastic large cell lymphoma. (A) TLBR-1, -2, and -3 cell lines secrete CA9 into culture supernatant proportionally to their cellular expression, as determined by western blot (cf. Figure 3A). Data represent three replicates measured by CA9 enzyme-linked immunosorbent assay. (C) Peri-implant seroma samples involved by breast implant-associated (BIA) anaplastic large cell lymphoma (ALCL) have significantly higher CA9 concentrations than those not involved by BIA-ALCL. (C) Serum samples obtained from mice bearing 1000 mm³ subcutaneous TLBR-1, -2, and -3 tumors have significantly higher CA9 concentrations than those from non-tumor-bearing mice. *P<0.05; **P<0.01; ***P<0.001; ****P<0.0001 (Mann-Whitney test). PBS: phosphate-buffered saline.

and metastatic status of clear cell renal cell carcinoma and high preoperative levels are associated with postoperative recurrence.²⁶ We demonstrated that CA9 is readily secreted by BIA-ALCL cells *in vitro* and that significantly elevated CA9 concentrations are present in peri-implant seromas involved by BIA-ALCL. Various inflammatory conditions can cause peri-implant seromas,^{46,47} and the diagnosis of BIA-ALCL in seroma fluid can be a significant challenge if neoplastic cells are rare. Hanson *et al.* recently reported specificity of an enzyme-linked immunosorbent assay for CD30 in seroma specimens involved by BIA-ALCL,⁴⁸ while Kadin *et al.* reported that BIA-ALCL cell lines secrete a unique cytokine profile that includes interleukin-13.⁷ A multi-analyte approach incorporating CA9 that evaluates these proteins in seroma fluid could greatly facilitate the diagnosis of BIA-ALCL when few atypical cells are present and could potentially guide the decision regarding implant removal in suspicious cases in which definite neoplastic cells cannot be identified. This prospect should encourage international collaboration and standardized seroma collection protocols to facilitate progress given the rarity of BIA-ALCL. The role of serum CA9 measurement in BIA-ALCL remains unclear because limited samples were available for analysis. However, we identified elevated CA9 concentrations in serum samples from BIA-ALCL xenograft-bearing mice, and the role of serum CA9 as a possible biomarker to predict or monitor disease activity should be evaluated in larger human studies.

Disclosures

No conflicts of interest to disclose.

Contributions

NO performed research, analyzed and interpreted data, and wrote the manuscript. TH, JLP and GH performed research and analyzed and interpreted data. SD performed bioinformatic and statistical analysis and interpreted data. DSV and RH interpreted data. MM, HKJ and NHA performed research. SIS, JRC, FV, JS, NNB and LJM provided samples and interpreted data. YS analyzed data. ALE contributed TLBR cell lines and vital reagents. MWC and RNM designed the study, provided samples, and interpreted data. ALF designed the study, analyzed and interpreted data, and wrote the manuscript. All authors approved the final manuscript.

Funding

This work was supported by Award Numbers R01 CA177734 (ALF), P30 CA15083 (Mayo Clinic Cancer Center), P50 CA97274 (University of Iowa/Mayo Clinic Lymphoma SPORE), and UL1 TR002377 (Mayo Clinic Center for Clinical and Translational Science) from the National Institutes of Health; by Award Number CI-48-09 from the Damon Runyon Cancer Research Foundation (ALF); by a grant from the Plastic Surgery Foundation, American Society of Plastic Surgeons (MD Anderson Cancer Center); and by the Department of Laboratory Medicine and Pathology and the Center for Individualized Medicine, Mayo Clinic.

References

- Xing X, Feldman AL. Anaplastic large cell lymphomas: ALK positive, ALK negative, and primary cutaneous. *Adv Anat Pathol*. 2015;22(1):29-49.
- Feldman AL, Harris NL, Stein H, et al. Breast implant-associated anaplastic large cell lymphoma. In: Swerdlow SH, Campo E, Harris NL, et al., eds. WHO Classification of Tumours of Haematopoietic and Lymphoid Tissues. Revised 4th ed. Lyon: International Agency for Research on Cancer, 2017:421-422.
- Miranda RN, Aladily TN, Prince HM, et al. Breast implant-associated anaplastic large-cell lymphoma: long-term follow-up of 60 patients. *J Clin Oncol*. 2014;32(2):114-120.
- Ferrufino-Schmidt MC, Medeiros LJ, Liu H, et al. Clinicopathologic features and prognostic impact of lymph node involvement in patients with breast implant-associated anaplastic large cell lymphoma. *Am J Surg Pathol*. 2018;42(3):293-305.
- Clemens MW, Medeiros LJ, Butler CE, et al. Complete surgical excision is essential for the management of patients with breast implant-associated anaplastic large-cell lymphoma. *J Clin Oncol*. 2016;34(2):160-168.
- Hu H, Johani K, Almatroudi A, et al. Bacterial biofilm infection detected in breast implant-associated anaplastic large-cell lymphoma. *Plast Reconstr Surg*. 2016;137(6):1659-1669.
- Kadin ME, Morgan J, Xu H, et al. IL-13 is produced by tumor cells in breast implant-associated anaplastic large cell lymphoma: implications for pathogenesis. *Hum Pathol*. 2018;78:54-62.
- Laurent C, Delas A, Gaulard P, et al. Breast implant-associated anaplastic large cell lymphoma: two distinct clinicopathological variants with different outcomes. *Ann Oncol*. 2016;27(2):306-314.
- Oishi N, Brody GS, Ketterling RP, et al. Genetic subtyping of breast implant-associated anaplastic large cell lymphoma. *Blood*. 2018;132(5):544-547.
- Blombery P, Thompson E, Ryland GL, et al. Frequent activating STAT3 mutations and novel recurrent genomic abnormalities detected in breast implant-associated anaplastic large cell lymphoma. *Oncotarget*. 2018;9(90):36126-36136.
- Di Napoli A, Jain P, Duranti E, et al. Targeted next generation sequencing of breast implant-associated anaplastic large cell lymphoma reveals mutations in JAK/STAT signalling pathway genes, TP53 and DNMT3A. *Br J Haematol*. 2018;180(5):741-744.
- Letourneau A, Maerevoet M, Milowich D, et al. Dual JAK1 and STAT3 mutations in a breast implant-associated anaplastic large cell lymphoma. *Virchows Arch*. 2018;473(4):505-511.
- Crescenzo R, Abate F, Lasorsa E, et al. Convergent mutations and kinase fusions lead to oncogenic STAT3 activation in anaplastic large cell lymphoma. *Cancer Cell*. 2015;27(4):516-532.
- Luchtel RA, Dasari S, Oishi N, et al. Molecular profiling reveals immunogenic cues in anaplastic large cell lymphomas with DUSP22 rearrangements. *Blood*. 2018;132(13):1386-1398.
- Lechner MG, Megiel C, Church CH, et al. Survival signals and targets for therapy in breast implant-associated ALK- anaplastic large cell lymphoma. *Clin Cancer Res*. 2012;18(17):4549-4559.
- Chen J, Zhang Y, Petrus MN, et al. Cytokine receptor signaling is required for the survival of ALK- anaplastic large cell lymphoma, even in the presence of JAK1/STAT3 mutations. *Proc Natl Acad Sci U S A*. 2017;114(15):3975-3980.
- Laurent C, Nicolae A, Laurent C, et al. Gene alterations in epigenetic modifiers and JAK-STAT signaling are frequent in breast implant-associated ALCL. *Blood*. 2020;135(5):360-370.
- Kalari KR, Nair AA, Bhavsar JD, et al. MAP-Seq: Mayo analysis pipeline for RNA sequencing. *BMC Bioinformatics*. 2014;15:224.
- Dobin A, Davis CA, Schlesinger F, et al. STAR: ultrafast universal RNA-seq aligner. *Bioinformatics*. 2013;29(1):15-21.
- Lechner MG, Lade S, Liebertz DJ, et al. Breast implant-associated, ALK-negative, T-cell, anaplastic, large-cell lymphoma: establishment and characterization of a model cell line (TLBR-1) for this newly emerging clinical entity. *Cancer*. 2011;117(7):1478-1489.
- Aladily TN, Medeiros LJ, Amin MB, et al. Anaplastic large cell lymphoma associated with breast implants: a report of 13 cases. *Am J Surg Pathol*. 2012;36(7):1000-1008.
- Pastorek J, Pastorekova S. Hypoxia-induced carbonic anhydrase IX as a target for cancer therapy: from biology to clinical use. *Semin Cancer Biol*. 2015;31:52-64.
- Boyd NH, Walker K, Fried J, et al. Addition of carbonic anhydrase 9 inhibitor SLC-0111 to temozolamide treatment delays glioblastoma growth in vivo. *JCI Insight*. 2017;2(24):e92928.
- Zavada J, Zavadova Z, Zat'ovicova M, Hyrsil L, Kawaciuk I. Soluble form of carbonic anhydrase IX (CA IX) in the serum and urine of renal carcinoma patients. *Br J Cancer*. 2003;89(6):1067-1071.
- Smith AD, Truong M, Bristow R, Yip P, Milosevic MF, Joshua AM. The utility of serum CA9 for prognostication in prostate cancer. *Anticancer Res*. 2016;36(9):4489-4492.

26. Li G, Feng G, Gentil-Perret A, Genin C, Tostain J. Serum carbonic anhydrase 9 level is associated with postoperative recurrence of conventional renal cell cancer. *J Urol.* 2008;180(2):510-513; discussion 513-514.

27. Di Napoli A, De Cecco L, Piccaluga PP, et al. Transcriptional analysis distinguishes breast implant-associated anaplastic large cell lymphoma from other peripheral T-cell lymphomas. *Mod Pathol.* 2019;32(2):216-230.

28. Nasu K, Yamaguchi K, Takanashi T, et al. Crucial role of carbonic anhydrase IX in tumorigenicity of xenotransplanted adult T-cell leukemia-derived cells. *Cancer Sci.* 2017;108(3):435-443.

29. Higgins DF, Kimura K, Iwano M, Haase VH. Hypoxia-inducible factor signaling in the development of tissue fibrosis. *Cell Cycle.* 2008;7(9):1128-1132.

30. Lokmic Z, Musyoka J, Hewitson TD, Darby IA. Hypoxia and hypoxia signaling in tissue repair and fibrosis. *Int Rev Cell Mol Biol.* 2012;296:139-185.

31. de Araujo MF, Etchebehere RM, de Melo MLR, et al. Analysis of CD15, CD57 and HIF-1alpha in biopsies of patients with peri-implantitis. *Pathol Res Pract.* 2017;213(9): 1097-1101.

32. Rommelt C, Munsch T, Drynda A, Lessmann V, Lohmann CH, Bertrand J. Periprosthetic hypoxia as consequence of TRPM7 mediated cobalt influx in osteoblasts. *J Biomed Mater Res B Appl Biomater.* 2019;107(6):1806-1813.

33. Kim CH, Kim DH, Oh SH, Song SY. Human embryonic stem cell-derived endothelial precursor cell conditioned medium reduces the thickness of the capsule around silicone implants in rats. *Ann Plast Surg.* 2015;75(3): 348-352.

34. Mediani L, Gibellini F, Bertacchini J, et al. Reversal of the glycolytic phenotype of primary effusion lymphoma cells by combined targeting of cellular metabolism and PI3K/Akt/ mTOR signaling. *Oncotarget.* 2016;7(5):5521-5537.

35. Shrestha P, Davis DA, Veeranna RP, Carey RF, Viollet C, Yarchoan R. Hypoxia-inducible factor-1 alpha as a therapeutic target for primary effusion lymphoma. *PLoS Pathog.* 2017;13(9):e1006628.

36. Brennan DJ, Jirstrom K, Kronblad A, et al. CA IX is an independent prognostic marker in premenopausal breast cancer patients with one to three positive lymph nodes and a putative marker of radiation resistance. *Clin Cancer Res.* 2006;12(21):6421-6431.

37. Hussain SA, Ganesan R, Reynolds G, et al. Hypoxia-regulated carbonic anhydrase IX expression is associated with poor survival in patients with invasive breast cancer. *Br J Cancer.* 2007;96(1):104-109.

38. Kon-no H, Ishii G, Nagai K, et al. Carbonic anhydrase IX expression is associated with tumor progression and a poor prognosis of lung adenocarcinoma. *Lung Cancer.* 2006;54(3):409-418.

39. Lee SH, McIntyre D, Honess D, et al. Carbonic anhydrase IX is a pH-stat that sets an acidic tumour extracellular pH in vivo. *Br J Cancer.* 2018;119(5):622-630.

40. Svastova E, Witarski W, Csaderova L, et al. Carbonic anhydrase IX interacts with bicarbonate transporters in lamellipodia and increases cell migration via its catalytic domain. *J Biol Chem.* 2012;287(5):3392-3402.

41. Chiche J, Ilc K, Brahimi-Horn MC, Pouyssegur J. Membrane-bound carbonic anhydrases are key pH regulators controlling tumor growth and cell migration. *Adv Enzyme Regul.* 2010;50(1):20-33.

42. Chiche J, Ilc K, Laferriere J, et al. Hypoxia-inducible carbonic anhydrase IX and XII promote tumor cell growth by counteracting acidosis through the regulation of the intracellular pH. *Cancer Res.* 2009;69(1): 358-368.

43. Lou Y, McDonald PC, Olumi A, et al. Targeting tumor hypoxia: suppression of breast tumor growth and metastasis by novel carbonic anhydrase IX inhibitors. *Cancer Res.* 2011;71(9):3364-3376.

44. Sansone P, Piazzesi G, Paterini P, et al. Cyclooxygenase-2/carbonic anhydrase-IX up-regulation promotes invasive potential and hypoxia survival in colorectal cancer cells. *J Cell Mol Med.* 2009;13(9B):3876-3887.

45. Kuroda N, Tanaka A, Ohe C, Nagashima Y. Recent advances of immunohistochemistry for diagnosis of renal tumors. *Pathol Int.* 2013;63(8):381-390.

46. Gabriel SE, Woods JE, O'Fallon WM, Beard CM, Kurland LT, Melton LJ 3rd. Complications leading to surgery after breast implantation. *N Engl J Med.* 1997;336(10):677-682.

47. Spear SL, Rottman SJ, Glicksman C, Brown M, Al-Attar A. Late seromas after breast implants: theory and practice. *Plast Reconstr Surg.* 2012;130(2):423-435.

48. Hanson SE, Hassid VJ, Branch-Brooks C, et al. Validation of a CD30 enzyme-linked immunosorbant assay for the rapid detection of breast implant-associated anaplastic large cell lymphoma. *Aesthet Surg J.* 2019;40(2):149-153.

49. Clemens MW, Horwitz SM. NCCN consensus guidelines for the diagnosis and management of breast implant-associated anaplastic large cell lymphoma. *Aesthet Surg J.* 2017;37(3):285-289.

Subcutaneous daratumumab in patients with relapsed or refractory multiple myeloma: part 2 of the open-label, multicenter, dose-escalation phase Ib study (PAVO)



Ferrata Storti Foundation

Jesus San-Miguel,¹ Saad Z. Usmani,² Maria-Victoria Mateos,³ Niels W.C.J. van de Donk,⁴ Jonathan L. Kaufman,⁵ Philippe Moreau,⁶ Albert Oriol,⁷ Torben Plesner,⁸ Lotfi Benboubker,⁹ Kevin Liu,¹⁰ Peter Hellermans,¹¹ Tara Masterson,¹² Pamela L. Clemens,¹² Man Luo,¹² Andrew Farnsworth,¹³ Hareth Nahi¹⁴ and Ajai Chari¹⁵

¹Clínica Universidad de Navarra-CIMA, IDISNA, CIBERONC, Pamplona, Spain; ²Levine Cancer Institute/Atrium Health, Charlotte, NC, USA; ³University Hospital of Salamanca/IBSAL, Salamanca, Spain; ⁴Amsterdam UMC, Vrije Universiteit Amsterdam, Department of Hematology, Amsterdam, the Netherlands; ⁵Winship Cancer Institute, Emory University, Atlanta, GA, USA; ⁶University Hospital of Nantes, Nantes, France; ⁷Institut Català d'Oncologia, HGTiP, Barcelona, Spain; ⁸Vejle Hospital and University of Southern Denmark, Vejle, Denmark; ⁹Service d'Hématologie et Thérapie Cellulaire, Hôpital Bretonneau, Centre Hospitalier Régional Universitaire (CHRU), Tours, France; ¹⁰Janssen Research & Development, LLC, Raritan, NJ, USA; ¹¹Janssen Research & Development, Beerse, Belgium; ¹²Janssen Research & Development, LLC, Spring House, PA, USA; ¹³Janssen Research & Development, LLC, High Wycombe, UK; ¹⁴Karolinska Institute, Department of Medicine, Division of Hematology, Karolinska University Hospital at Huddinge, Stockholm, Sweden and ¹⁵Tisch Cancer Institute, Mount Sinai School of Medicine, New York, NY, USA

Haematologica 2021
Volume 106(6):1725-1732

ABSTRACT

Intravenous daratumumab is approved for the treatment of multiple myeloma. In part 1 of the PAVO study, a mix-and-deliver subcutaneous formulation of daratumumab with recombinant human hyaluronidase PH20 (rHuPH20) was well tolerated, with low rates of infusion-related reactions and an efficacy similar to that of intravenous daratumumab. Part 2 of PAVO evaluated a concentrated, pre-mixed co-formulation of daratumumab and rHuPH20 (DARA SC). Patients who had received two or more prior lines of therapy, including a proteasome inhibitor and an immunomodulatory drug, were given daratumumab (1,800 mg) and rHuPH20 (30,000 U) in 15 mL subcutaneously over 3 to 5 minutes as per the approved intravenous monotherapy dosing schedule. Primary endpoints were daratumumab trough concentration at the end of weekly dosing (just prior to the day 1 dose of cycle 3) and safety. Twenty-five patients were enrolled in PAVO part 2. DARA SC achieved daratumumab trough concentrations similar to or greater than those achieved with intravenous daratumumab 16 mg/kg. The adverse event profile of DARA SC was consistent with that of intravenous daratumumab, with no new safety concerns and a lower infusion-related reaction rate. At a median follow-up of 14.2 months, the overall response rate was 52%, the median duration of response was 15.7 months, and the median progression-free survival was 12.0 months. DARA SC 1,800 mg was well tolerated in relapsed/refractory multiple myeloma, with a low infusion-related reaction rate and reduced administration time. Daratumumab serum concentrations following DARA SC were consistent with those following intravenous dosing, and deep and durable responses were observed. Based on these results, ongoing studies are investigating DARA SC in the treatment of multiple myeloma and other conditions. (ClinicalTrials.gov identifier: NCT02519452).

Correspondence:

JESUS SAN-MIGUEL
sanmiguel@unav.es

Received: November 26, 2019.

Accepted: April 29, 2020.

Pre-published: April 30, 2020.

<https://doi.org/10.3324/haematol.2019.243790>

©2021 Ferrata Storti Foundation

Material published in *Haematologica* is covered by copyright. All rights are reserved to the Ferrata Storti Foundation. Use of published material is allowed under the following terms and conditions: <https://creativecommons.org/licenses/by-nc/4.0/legalcode>. Copies of published material are allowed for personal or internal use. Sharing published material for non-commercial purposes is subject to the following conditions: <https://creativecommons.org/licenses/by-nc/4.0/legalcode>, sect. 3. Reproducing and sharing published material for commercial purposes is not allowed without permission in writing from the publisher.



Introduction

Daratumumab is a human IgG_κ monoclonal antibody targeting CD38 with a direct on-tumor¹⁻⁴ and immunomodulatory⁵⁻⁷ mechanism of action. The direct on-tumor actions of daratumumab are mediated by complement-dependent cytotoxicity

city, antibody-dependent cell-mediated cytotoxicity, antibody-dependent cellular phagocytosis, and apoptosis.^{1,4} The immunomodulatory actions of daratumumab lead to modulation of the tumor microenvironment, including the depletion of CD38⁺ immunosuppressive cells, which may explain the clonal expansion of cytotoxic T cells, increase in helper T cells, and increase in granzyme B⁺ CD8⁺ T cells observed following exposure to this drug.^{5,7}

Intravenous (IV) daratumumab 16 mg/kg is approved as a monotherapy and in combination with bortezomib/dexamethasone, lenalidomide/dexamethasone, or pomalidomide/dexamethasone (in the USA) in patients with relapsed or refractory (RR) multiple myeloma (MM).^{8,9} Daratumumab 16 mg/kg IV is also approved in combination with bortezomib/melphalan/prednisone or lenalidomide/dexamethasone (in the USA) for the treatment of patients with newly diagnosed MM who are ineligible for autologous stem cell transplantation, and in combination with bortezomib/thalidomide/dexamethasone (in the USA) for patients with newly diagnosed MM who are eligible for autologous stem cell transplantation.^{8,9} In clinical studies of daratumumab, the median durations of the first, second, and subsequent daratumumab IV infusions were 7.0, 4.3, and 3.4 hours (h), respectively.⁸ For the convenience of patients and healthcare providers, the first daratumumab 16 mg/kg IV dose may be split over 2 days (8 mg/kg administered on days 1 and 2 of cycle 1), which is associated with a shorter median infusion duration of 4.2 h on day 1 of cycle 1.^{8,10,11} In addition to split-dose administration of daratumumab, alternative approaches to reducing the duration of the first daratumumab infusion include administering a low priming dose on day 1 of cycle 1 and the remainder of the 16 mg/kg IV dose on day 2, or giving an 8 mg/kg IV dose on day 1 of cycle 1 before proceeding with the 16 mg/kg IV dose from day 8 of cycle 1 onwards.¹² Furthermore, a shorter, 90-minute (min) infusion for subsequent (day 15 of cycle 1 and beyond) 16 mg/kg IV administrations of daratumumab was shown to be well tolerated.¹³ Infusion-related reactions (IRR) occur in approximately 50% of patients treated with IV daratumumab; these reactions are manageable and occur primarily during the first infusion.⁸

Given the infusion time required for IV administration and the incidence of IRR associated with daratumumab, a subcutaneous (SC) delivery method is in development, with the goal of shortening the duration of infusion without compromising the safety or efficacy of the drug. SC administration of daratumumab may be associated with a lower risk of IRR, improved tolerability due to a more gradual systemic absorption of the drug, and greater convenience for both patients and healthcare providers by reducing infusion times.

Recombinant human hyaluronidase PH20 (rHuPH20; ENHANZE® drug delivery technology, Halozyme, Inc., San Diego, CA, USA) depolymerizes hyaluronan in the SC space, allowing rapid administration of large volumes of injected drugs, thus facilitating SC delivery.¹⁴ A mix-and-deliver formulation of daratumumab (20 mg/mL) and rHuPH20 (DARA-MD), given SC by means of a syringe pump at two dose levels (DARA-MD 1,200 mg and DARA-MD 1,800 mg) over 20 to 30 min, was evaluated in part 1 of PAVO, a phase Ib study in patients with RRMM.¹⁵ Results from part 1 showed that SC administration of daratumumab is feasible in patients with MM. DARA-MD was well tolerated, with low rates of IRR (23%). The

serum concentrations achieved with the 1,800 mg dose of DARA-MD were consistent with those observed for daratumumab 16 mg/kg IV in patients with RRMM. Moreover, the efficacy of the 1,800 mg dose of DARA-MD was comparable to that of daratumumab 16 mg/kg IV in a similar population of patients.¹⁶ At the 1,800 mg dose level of DARA-MD, the overall response rate (ORR) was 42%, and responses were deep and durable, with four (9%) patients achieving a stringent complete response.¹⁵

Based on the results from part 1 of the PAVO study, a concentrated, pre-mixed co-formulation of daratumumab 1,800 mg (120 mg/mL) and rHuPH20 (DARA SC) with a smaller injection volume (15 mL for DARA SC vs. 60 mL for DARA-MD 1,200 mg and 90 mL for DARA-MD 1,800 mg) and shorter injection time was developed, enabling manual SC injection into the abdomen.¹⁷ This report describes part 2 of PAVO, which investigated the safety, pharmacokinetics (PK), and efficacy of DARA SC in patients with RRMM.

Methods

Study design and patients

PAVO (MMY1004) is a phase Ib, open-label, multicenter, dose-finding, proof-of-concept study. Detailed eligibility criteria have already been published.¹⁵ Briefly, patients were ≥ 18 years of age, had RRMM and had received two or more prior lines of treatment, including a proteasome inhibitor (PI) and an immunomodulatory drug (IMiD), and were naïve to anti-CD38 therapy. In part 1, DARA-MD was administered by SC infusion over 20 to 30 min through a syringe pump to determine the recommended dose for part 2. In part 2, a concentrated co-formulation of the selected daratumumab dose (1,800 mg) and rHuPH20 concentration (30,000 U; in 15 mL) in a single, pre-mixed vial was administered over 3 to 5 min by manual SC injection (DARA SC) at alternating locations in the periumbilical area of the abdominal wall. Treatment was given in 28-day cycles: once weekly during cycles 1 and 2, every 2 weeks during cycles 3 through 6, and every 4 weeks thereafter until disease progression or unacceptable toxicity. All patients remained in the hospital for observation for at least 24 h after the end of the SC injection on day 1 of cycle 1. Inpatient observation after subsequent doses was implemented if deemed necessary based on safety observations.

Endpoints and assessments

The primary endpoints were daratumumab trough concentration (C_{trough}) at the end of weekly dosing (just prior to administration of the day 1 dose of cycle 3) and safety. Secondary endpoints included ORR and complete response rate.

Blood samples for PK analysis were collected on days 1, 2, 3, 4, 8, 15, and 22 of cycle 1; days 1, 8, 15, 22, 23, and 25 of cycle 2; day 1 of cycles 3, 4, 6, and 8; and 4 and 8 weeks after the final dose of study medication. Blood samples collected prior to dosing on days 1 and 15 of cycle 1, day 22 of cycle 2, and day 1 of cycle 4 as well as 4 and 8 weeks after the end of treatment were assessed for anti-daratumumab antibodies and anti-rHuPH20 antibodies.

Safety assessments included adverse-event monitoring, physical examinations, electrocardiograms, injection-site evaluations, clinical laboratory parameters, vital sign measurements, and Eastern Cooperative Oncology Group Performance Status. Adverse events were assessed using National Cancer Institute Common Terminology Criteria for Adverse Events Version 4.03.¹⁸

Responses were assessed according to International Myeloma Working Group consensus recommendations^{19,20} at the beginning

of each cycle. Disease evaluations were performed by a central laboratory until disease progression or end of treatment.

Statistical analyses

The primary endpoint of C_{trough} at the end of weekly dosing (prior to the day 1 dose of cycle 3) was evaluated in patients who received all eight weekly doses of DARA SC and provided a pre-dose PK sample on day 1 of cycle 3 (PK-evaluable population). All other PK analyses were performed on the PK-analysis population, which included patients who received at least one dose of study drug and provided one or more post-infusion PK samples. The safety population included all patients who received at least one dose of study drug.

The study protocol was approved by the clinical study sites' institutional review boards or ethics committees. Additional details on the study design, statistical analyses, and study supervision are provided in the *Online Supplementary Appendix*.

Results

Patients and treatment

At the clinical cutoff date of December 14, 2018, 25 patients had been enrolled in part 2 of the study and had received DARA SC 1,800 mg. The patients' median age was 68 (range, 51–85) years, and 24% of patients were ≥ 75 years of age (Table 1). The median number of prior lines of therapy was three (range, 2–9); 96% and 92% of patients had received prior treatment with bortezomib and lenalidomide, respectively. Fifty-six percent of patients were refractory to both a PI and an IMiD, and 76% of patients were refractory to the last line of therapy. Of the 16 patients with available cytogenetic data, four (25%) had a high-risk cytogenetic abnormality at baseline: two had del17p, one had t(4;14), and one had t(14;16).

Of the 25 patients treated with DARA SC during part 2 of the study, 19 (76%) discontinued treatment: 17 (68%) due to progressive disease and two (8%) due to physicians' decision (both had unconfirmed progressive disease). At the clinical cutoff date, the median duration of follow-up was 14.2 (range, 2.4–18.5) months.

Pharmacokinetics and immunogenicity

PK results for C_{trough} on day 1 of cycle 3 are presented for the PK-evaluable population (n=22); all other PK data are presented based on the PK-analysis population (n=25). The linear mean daratumumab serum concentration profiles after cycle 1 (first dose) and after the last weekly dose (eighth dose) are shown in Figure 1. Daratumumab serum concentrations after SC administration were sustained from 48 h post-dose onwards until the end of the dosing interval (Figure 1A). SC administration of daratumumab was followed by slow systemic absorption as opposed to the immediate systemic availability following IV administration (Figure 1A). However, the maximum C_{trough} was similar or higher following DARA SC 1,800 mg than after the 16 mg/kg IV dosing of daratumumab (Figure 1B and Table 2).

Simulation of mean concentration-time profiles of daratumumab following SC and IV dosing revealed that the C_{trough} following DARA SC 1,800 mg dosing remained higher than after 16 mg/kg IV dosing throughout the dosing regimen (Figure 2). For SC dosing, the mean maximum concentration (C_{max}) was lower during early weekly dosing but was higher at the end of weekly dosing and during

every-2-week dosing (Figure 2). After reaching every-4-week dosing, the C_{max} for DARA SC 1,800 mg was similar to that for the 16 mg/kg IV dosing of daratumumab overall (Figure 2). The mean and median C_{trough} values for end of weekly dosing (day 1 of cycle 3) in PAVO part 2, as well as in patients receiving daratumumab 16 mg/kg IV as monotherapy in the GEN501 part 2 and SIRIUS studies, are summarized in Table 2.

Of the 25 patients, one (4%) patient was positive for anti-daratumumab antibodies; the antibodies were neutralizing and transient (detected only at week 4 after treatment). This patient experienced no IRR and had a best response of stable disease. One (4%) patient was positive for anti-rHuPH20 antibodies at baseline, and four (16%) patients were positive for anti-rHuPH20 antibodies during treatment; all the antibodies were non-neutralizing. Among the four patients who were positive for anti-

Table 1. Baseline demographics and clinical characteristics of the all-treated population.

Characteristic	DARA SC 1,800 mg (n=25)
Age, years	
Median (range)	68 (51–85)
≥ 75 , n (%)	6 (24.0)
Median (range) weight, kg	70.9 (52.0–104.8)
Baseline ECOG Performance Status, n (%)	
0	11 (44.0)
1	13 (52.0)
2	1 (4.0)
ISS stage, n ^a	24
I, n (%)	13 (54.2)
II, n (%)	5 (20.8)
III, n (%)	6 (25.0)
Median (range) time from diagnosis, years	5.9 (2.1–12.8)
Type of myeloma, n	24
IgG, n (%)	13 (54.2)
Cytogenetic risk, n ^b	16
Standard risk, n (%)	12 (75.0)
High risk, n (%)	4 (25.0) ^c
t(4;14)	1 (6.3)
t(14;16)	1 (6.3)
del17p	2 (12.5)
Prior lines of therapy, n (%)	
Median (range)	3 (2–9)
≤ 3	17 (68.0)
>3	8 (32.0)
Prior ASCT, n (%)	17 (68.0)
Prior PI, n (%)	25 (100)
Bortezomib	24 (96.0)
Prior IMiD, n (%)	25 (100)
Lenalidomide	23 (92.0)
Refractory to, n (%)	
Bortezomib	16 (64.0)
Lenalidomide	14 (56.0)
Both PI and IMiD	14 (56.0)
Last line of therapy	19 (76.0)

DARA: daratumumab; SC: subcutaneous; ECOG: Eastern Cooperative Oncology Group; ISS: International Staging System; ASCT: autologous stem cell transplantation; PI: proteasome inhibitor; IMiD: immunomodulatory drug. ^aISS stage is derived based on the combination of serum β_2 -microglobulin and albumin. ^bAssessed by fluorescence *in situ* hybridization or karyotyping. ^cConsists of two patients with del17p, one patient with t(4;14), and one patient with t(14;16).

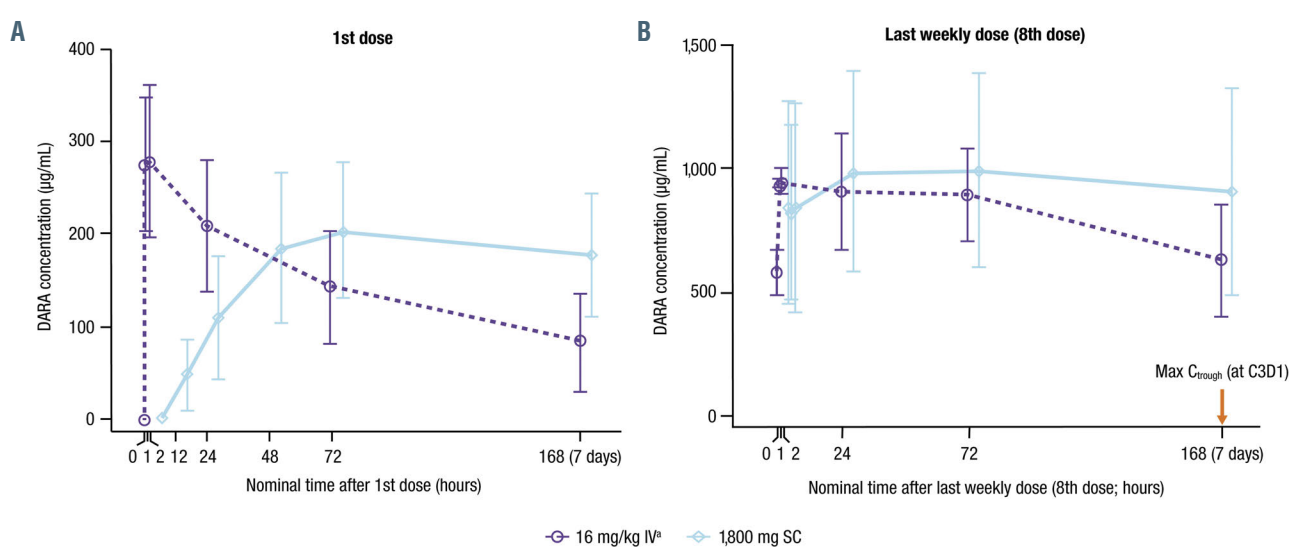


Figure 1. Serum concentrations of daratumumab over time. The mean (\pm standard deviation) serum concentrations of daratumumab over time (A) after the first dose and (B) after the last weekly dose (eighth dose). DARA: daratumumab; C_{trough} : trough concentration; C3D1: day 1 of cycle 3; IV: intravenous; SC: subcutaneous. ^aFrom the GEN501 study.¹⁶

Table 2. C_{trough} for end of weekly daratumumab dosing (day 1 of cycle 3) for DARA SC 1,800 mg and historical data for daratumumab 16 mg/kg IV.

Study	Dose/route	n	Daratumumab cycle 3, day 1 C_{trough} ($\mu\text{g}/\text{mL}$)		
			Mean	Median	CV%
PAVO ^a	1,800 mg SC	22	932	860	42%
GEN501 part 2	16 mg/kg IV	27	617	714	51%
SIRIUS	16 mg/kg IV	73	573 ^b	560	58%

C_{trough} : trough concentration; DARA: daratumumab; SC: subcutaneous; IV: intravenous; CV: coefficient of variation. ^aBased on the pharmacokinetic-evaluable population.

^bAs reported by Clemens *et al.*²²

rHuPH20 antibodies during treatment, one patient experienced a mild IRR on day 1 of cycle 1, and best responses were partial response (1 patient), stable disease (2 patients), and progressive disease (1 patient).

Safety

The adverse event profile of DARA SC was consistent with the known safety and tolerability profile of IV daratumumab. The most frequently reported treatment-emergent adverse events (TEAE) were lymphopenia (32%), arthralgia (28%), back pain (28%), and thrombocytopenia, diarrhea, and nasopharyngitis (24% each) (Table 3). The most common grade 3/4 TEAE was lymphopenia (20%) (Table 3). No treatment discontinuations due to TEAE were observed. Serious TEAE were reported in six (24%) patients who received DARA SC but were not considered related to the study drug. One patient died during part 2 of the study due to disease progression in the context of MM-related amyloid light chain (AL) amyloidosis (clinically significant cardiac involvement was not present); this death was not considered related to DARA SC. A secondary primary malignancy was observed in one patient (metastatic adenocarcinoma of prostate). There were no reports of tumor lysis syndrome or intravascular hemolysis.

The incidence and severity of IRR was low with DARA SC 1,800 mg. Among the 25 patients who received DARA SC 1,800 mg, four (16%) reported IRR, the majority of which occurred on day 1 of cycle 1. The median time to onset of an IRR was 70 (range, 9-80) min. Patient 1 experienced grade 3 hypertension, grade 2 chills, and grade 2 dys-

pnea. Patient 2 experienced grade 1 allergic rhinitis, patient 3 experienced grade 1 sneezing, and patient 4 experienced grade 3 hypertension. Patients 1, 2, and 3 experienced their IRR following the first injection (day 1 of cycle 1), whereas patient 4 experienced the IRR following the ninth injection (day 1 of cycle 3). The IRR of grade 3 hypertension were reversible, and both occurred in patients with a medical history of hypertension. There were no grade 4 IRR and no discontinuations due to IRR.

Injection-site TEAE were observed in three (12%) patients; these included injection-site induration, injection-site discoloration, erythema, and hematoma (n=1 each; all grade 1 severity). Erythema and induration were objectively measured for all injections, regardless of attribution as a TEAE. Measurable erythema (24%) and measurable induration (4%) at the injection site resolved within 1 h.

Efficacy

At a median follow-up of 14.2 months, the ORR with DARA SC 1,800 mg was 52%, which included a complete response in one (4%) patient, very good partial responses in seven (28%) patients, and partial responses in five (20%) patients (Figure 3A). The median time to best response was 1.02 (range, 1.0-12.1) months, and the median duration of response was 15.7 (range, 4.6-not estimable) months. Among 13 responders, three responses deepened over time (Figure 3B); one patient with an initial partial response at month 2 went on to achieve a complete response at month 12, and two patients who achieved initial partial responses at month 1 went on to achieve very good partial responses

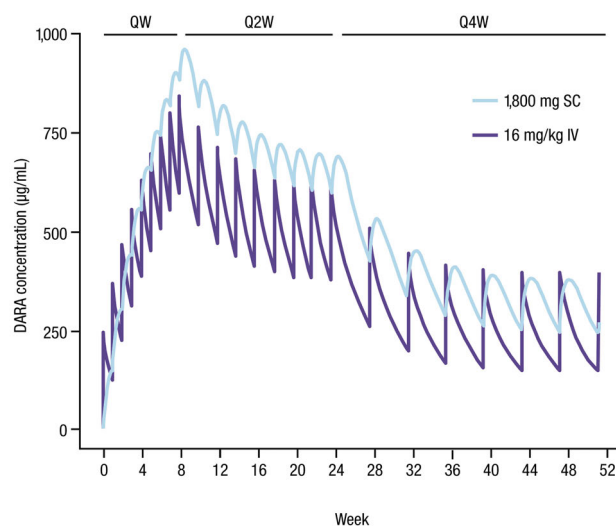


Figure 2. Simulation of mean concentration-time profiles of daratumumab following subcutaneous and intravenous dosing.^{18,20} QW: weekly; Q2W: every 2 weeks; Q4W: every 4 weeks; SC: subcutaneous; IV: intravenous; DARA: daratumumab. ^aThe dosing schedule is once weekly in cycles 1 and 2, every 2 weeks in cycles 3 through 6, and every 4 weeks thereafter. ^bSimulations were conducted based on a population pharmacokinetic (PK) model developed for daratumumab following SC and IV administration using scheduled dosing and estimated individual PK parameters. Serum concentration-time data (from the PAVO, GEN501, and SIRIUS studies) were used for the population PK model development using a nonlinear mixed-effects modeling (NONMEM®, version 7.2) approach with the first-order conditional estimation with interaction method. The daratumumab SC model was based on a previous population PK model for daratumumab IV²¹ except for the absorption, which was described by a first-order process and a relative bioavailability parameter.

at month 2. At the clinical cutoff, the median progression-free survival was 12.0 (range, 5.6–16.6) months among all-treated patients and 11.7 (range, 2.8–13.8) months among patients refractory to both PI and IMiD.

Discussion

PAVO is the first clinical study to evaluate the safety, PK, and efficacy of SC administration of daratumumab in combination with rHuPH20. The results from this study demonstrate that daratumumab co-formulated with rHuPH20 is well tolerated, has an acceptable PK profile, and achieves deep and durable responses in patients with RRMM. In part 1 of the study, dose escalation of a first-generation mix-and-deliver formulation of daratumumab and rHuPH20 (DARA-MD) showed that daratumumab SC administration is feasible in patients with RRMM.¹⁵ DARA-MD 1,800 mg had a PK profile and produced clinical responses that were consistent with those of IV infusion of daratumumab 16 mg/kg and was well tolerated, with a low rate of IRR. Based on the promising safety and efficacy observed with DARA-MD during part 1 of PAVO, a pre-mixed co-formulation of daratumumab 1,800 mg with rHuPH20 (DARA SC), which has a smaller injection volume and is administered over 3 to 5 min, was investigated in part 2 of the study.

Population PK and exposure-response analyses of daratumumab IV monotherapy in patients with MM revealed that the daratumumab maximum C_{trough} is strongly related to ORR.²¹ In these studies, the maximum C_{trough} occurred prior to daratumumab dosing on day 1 of cycle 3 with daratumumab monotherapy administered with the same dosing

Table 3. Treatment-emergent adverse events.

TEAE, n (%)	DARA SC 1,800 mg (n=25)	
	All grades >10%	Grade 3 or 4 >1 patient
Hematologic		
Lymphopenia	8 (32.0)	5 (20.0)
Thrombocytopenia	6 (24.0)	2 (8.0)
Anemia	4 (16.0)	1 (4.0)
Leukopenia	3 (12.0)	1 (4.0)
Neutropenia	2 (8.0)	2 (8.0)
Non-hematologic		
Arthralgia	7 (28.0)	0
Back pain	7 (28.0)	0
Diarrhea	6 (24.0)	1 (4.0)
Nasopharyngitis	6 (24.0)	0
Hypertension	5 (20.0)	2 (8.0)
Fatigue	5 (20.0)	1 (4.0)
Asthenia	5 (20.0)	1 (4.0)
Insomnia	5 (20.0)	1 (4.0)
Nausea	5 (20.0)	0
Headache	5 (20.0)	0
Upper RTI	5 (20.0)	0
Pyrexia	5 (20.0)	0
Cough	5 (20.0)	0
Vomiting	4 (16.0)	0
Constipation	4 (16.0)	0
Musculoskeletal pain	4 (16.0)	0
Oropharyngeal pain	4 (16.0)	0
Bone pain	3 (12.0)	1 (4.0)
Chills	3 (12.0)	0
Peripheral edema	3 (12.0)	0
Musculoskeletal chest pain	3 (12.0)	0
Musculoskeletal discomfort	3 (12.0)	0
Dyspnea	3 (12.0)	0

TEAE: treatment-emergent adverse event; DARA: daratumumab; SC: subcutaneous; RTI: respiratory tract infection.

schedule used in the PAVO study.²² Based on these findings, C_{trough} at the end of weekly dosing (just prior to the dose on day 1 of cycle 3) was selected as the primary PK endpoint for the PAVO study. DARA SC 1,800 mg achieved similar or greater maximum C_{trough} values compared with those of standard IV dosing (16 mg/kg) at day 1 of cycle 3 (i.e., at the end of weekly dosing). The mean C_{trough} at day 1 of cycle 3 (pre-dose) was 932 μ g/mL after eight weekly doses of DARA SC 1,800 mg compared with 617 μ g/mL (GEN501 part 2) and 573 μ g/mL (SIRIUS) after weekly dosing with IV daratumumab.^{16,22} Daratumumab serum concentrations were sustained from 48 h post-dose onwards until the end of the dosing interval. Although DARA SC is administered at a fixed dose, while IV daratumumab is administered by weight-based dosing, interpatient PK variability of the two dosing methods was comparable.^{23,24} Due to the small sample size in part 2 of PAVO, the relationship between the PK of DARA SC and patients' body weight could not be assessed. However, in a body-weight-based subgroup analysis of the phase III COLUMBA study (NCT03277105), DARA SC achieved adequate exposure that was consistent with that of IV daratumumab, regardless of body weight.²⁵ In patients weighing \leq 65 kg, the higher mean maximum C_{trough} observed with DARA SC versus IV daratumumab did not have a clinically relevant effect on safety, and the ORR in all subgroups were consistent with the overall population. These results suggest that dose individualization of DARA SC on the basis of body weight is not necessary.

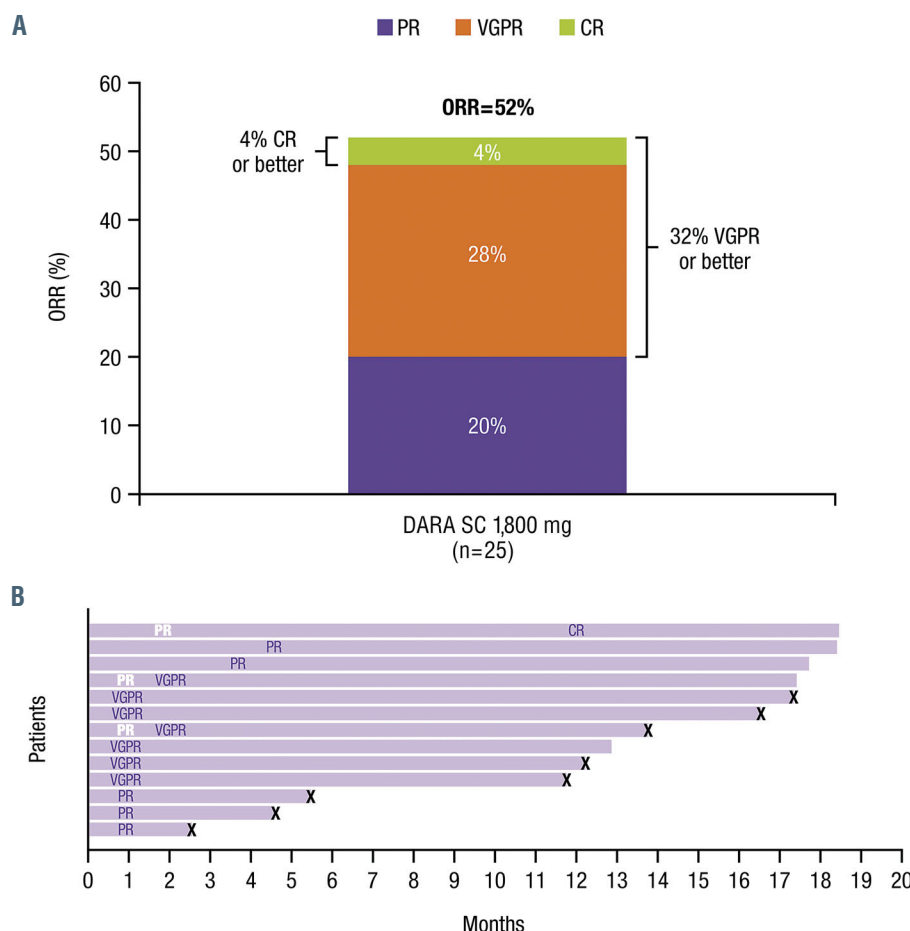


Figure 3. Responses to DARA SC 1,800 mg. (A) Summary of responses. Responses were evaluated in the all-treated population, which included all patients who received at least one dose of the study drug. (B) Swim lane plot of responders. White text indicates the first response and pink text indicates the best response. 'X' indicates disease progression. DARA: daratumumab; SC: subcutaneous; ORR: overall response rate; CR: complete response; VGPR: very good partial response; PR: partial response.

There was a low incidence of anti-daratumumab antibodies with DARA SC, indicating a low risk of daratumumab immunogenicity following SC administration. Few patients (16%) were positive for treatment-emergent or treatment-induced anti-rHuPH20 antibodies; this rate is consistent with the immunogenicity rates reported for other rHuPH20-containing treatments (SC rituximab [9%], trastuzumab [20%], and immune globulin infusion HYQVIA [18%]).²⁶⁻²⁸

The safety profile of DARA SC was consistent with the known profile of IV daratumumab; however, the frequency of IRR was lower with the SC administration than with the IV administration. The IRR rate with DARA SC was 16%, while IRR rates for IV administration of daratumumab range from 45% to 56% in monotherapy and combination regimens for RRMM.²⁹⁻³⁴ The majority of IRR occurred on day 1 of cycle 1. Only two patients experienced grade 3 IRR, and no cases of grade 4 IRR were reported. There were no discontinuations due to IRR or other TEAE. DARA SC injections in the perumbilical area were well tolerated; few injection-site TEAE were observed, and all objectively measured cases of erythema and induration were fully reversible and resolved within 1 h after the end of the injection.

Durable clinical responses were observed with DARA SC during this study, with a median duration of response of 15.7 months. Over time, the ORR improved, increasing from 44% to 52% after a median follow-up of 4.6¹⁷ versus 14.2 months, respectively, and responses deepened, with one patient achieving a complete response with longer follow-up. Despite the sample size of 25 patients, the median progression-free survival was 12.0 months among all-treat-

ed patients and 11.7 months among patients refractory to both PI and IMiD. An ORR of 52% is noteworthy in this population, with patients having received a median of three (range, 2-9) prior lines of therapy and 56% of patients being refractory to both PI and IMiD and 76% of patients being refractory to their last line of therapy. Clinical response rates achieved with DARA SC 1,800 mg were comparable to those achieved with daratumumab 16 mg/kg IV.^{16,35} In a pooled analysis of 148 patients with RRMM who received daratumumab 16 mg/kg IV in the monotherapy studies GEN501 and SIRIUS, the ORR was 31%, with 14% of patients achieving a very good partial response or better and 5% achieving a complete response or better.³¹ After a median follow-up of 20.7 months, the median progression-free survival was 4.0 months.³¹ The pooled patient population received a median of five (range, 2-14) prior lines of therapy, 87% were considered double refractory to a PI and an IMiD, and 91% were considered refractory to the last line of therapy.

In part 1 of PAVO, DARA-MD was administered by means of an infusion pump over a period of approximately 20 to 30 min.¹⁵ Compared with DARA-MD, the DARA SC formulation contains a higher concentration of daratumumab in a smaller injection volume (15 mL), thus enabling drug delivery through a single SC injection with a handheld syringe and needle by manual push into the abdominal wall over 3 to 5 min. As the median durations of the first, second, and subsequent daratumumab IV infusions in clinical studies were 7.0, 4.3, and 3.4 hours, respectively,⁸ DARA SC substantially shortens the duration of administration, thereby reducing the treatment

burden for patients and healthcare providers.

Findings from PAVO on the safety, PK, and efficacy profile of DARA SC informed four ongoing phase III studies of DARA SC 1,800 mg.³⁶⁻³⁹ In the randomized, multicenter, open-label, non-inferiority study, COLUMBA, DARA SC demonstrated non-inferiority to DARA 16 mg/kg IV in terms of ORR and maximum C_{trough} on day 1 of cycle 3, with a similar safety profile and a significantly reduced IRR rate, in patients with RRMM.³⁶ Patient-reported outcome data from COLUMBA indicated that patients receiving DARA SC were more satisfied with their cancer therapy and had more positive perceptions of their treatment than patients receiving IV daratumumab.⁴⁰ The efficacy and safety of DARA SC are also being investigated in combination with standard-of-care regimens in the phase II PLEIADES study, and results from this study demonstrate the feasibility of administering DARA SC in combination with standard-of-care regimens containing SC bortezomib. In PLEIADES, DARA SC in combination with SC bortezomib plus lenalidomide/dexamethasone and with SC bortezomib plus melphalan/prednisone in patients with newly diagnosed MM demonstrated comparable clinical activity and safety to the corresponding IV daratumumab regimens, with lower rates of IRR and shorter durations of administration.⁴¹ Although the dose of DARA SC on day 1 of cycle 1 should not be given at home, at-home administration of subsequent doses of DARA SC by a healthcare provider is a possibility for future consideration; however, additional safety follow-up is needed, particularly to further confirm that the risk of severe IRR with administration beyond the first day of cycle 1 is very low or absent.

Taken together, these findings show that DARA SC is well tolerated, with a low rate of IRR and a shortened administration time. No new safety concerns were identified, and the overall adverse event profile with SC administration was comparable to that reported with IV administration of daratumumab at the approved dose level (16 mg/kg).^{16,35} DARA SC achieved maximum C_{trough} values that were similar to or greater than the maximum C_{trough} observed for the approved 16 mg/kg IV dose following the same dosing schedule. DARA SC demonstrated robust clinical efficacy, producing deep and durable responses with a rapid onset. Collectively, these data indicate that, compared to the current IV formulation, DARA SC reduces administration time as well as IRR rates without compromising safety or efficacy. Based on these results, ongoing studies are actively investigating DARA SC in MM and other disease states.

Disclosures

JS-M has acted as a consultant for Amgen, Bristol Myers Squibb, Celgene, Janssen, Merck, Novartis, Takeda, Sanofi, and Roche. SZU has acted as a consultant for AbbVie, GlaxoSmithKline, Celgene, Amgen/Onyx, Takeda/Millennium, Sanofi, Seattle Genetics, Skyline, Merck, and Janssen; has received research funding from Celgene, Amgen/Onyx, Takeda/Millennium, Sanofi, Seattle Genetics, Skyline, Merck, Janssen, Array BioPharma, and

Pharmacyclics; has served on speakers' bureaus for Celgene, Amgen, Janssen, Sanofi, and Takeda; and has received travel expenses from Janssen, Celgene, Amgen, and Takeda. M-VM has received honoraria from and has acted as a consultant for Celgene, Janssen, Takeda, and Amgen. NWCJvdD has received research support from Janssen Pharmaceuticals, Amgen, Celgene, Novartis, and Bristol Myers Squibb and has served on advisory boards for Janssen Pharmaceuticals, Amgen, Celgene, Bristol Myers Squibb, Novartis, Bayer, Takeda, and Servier. JLK has acted as a consultant or served in an advisory role for Janssen, Takeda, Celgene, Bristol Myers Squibb, Karyopharm Therapeutics, TG Therapeutics, Sanofi, Amgen, and Tecnofarma; has received research funding (institutional) from Merck, Celgene, Janssen, Sutro Biopharma, Fortis Therapeutics, Amgen, AbbVie/Genentech, and Bristol Myers Squibb; and has received travel and accommodation expenses from Janssen, Celgene, Bristol Myers Squibb, Sanofi, Amgen, and Takeda. PM has acted as a consultant for and received honoraria from Celgene, Takeda, and Janssen. AO has acted as a consultant for and received honoraria from Amgen, Takeda, and Janssen and has served on speakers' bureaus for Amgen, Celgene, and Janssen. TP has received research support from Janssen Pharmaceuticals and served on advisory boards for Janssen Pharmaceuticals, Celgene, Takeda, and Behring. LB has acted as a consultant for and received honoraria from Takeda, Celgene, Janssen, and Amgen and has received travel expenses from Janssen, Celgene, and Amgen. KL, PH, TM, PLC, ML, and AF are employees of Janssen. PH, TM, PLC, ML, and AF hold stock in Johnson & Johnson. AC has acted as a consultant for Amgen, Array BioPharma, Celgene, Janssen, Millennium, Takeda, and Novartis and has received research funding from Amgen, Array BioPharma, Celgene, Janssen, Millennium, Takeda, Novartis, and Pharmacyclics. HN has no conflicts of interest to report.

Contributions

All authors developed the manuscript, provided final submission approval, and confirmed that the protocol was followed and that the data were accurate and complete.

Acknowledgments

This study was sponsored by Janssen Research & Development, LLC. The authors would like to thank the patients who participated in this study and their families, as well as the study co-investigators, research nurses, and coordinators at each of the clinical sites. Medical writing and editorial support were provided by Kristin Runkle, PhD, of MedErgy, and were funded by Janssen Global Services, LLC.

Funding

The study was registered at ClinicalTrials.gov (NCT02519452) and was sponsored by Janssen Research & Development, LLC. Medical writing and editorial support were funded by Janssen Global Services, LLC. The data-sharing policy of Janssen Pharmaceutical Companies of Johnson & Johnson is available at <https://www.janssen.com/clinical-trials/transparency>. As noted on this site, requests for access to the study data can be submitted through the Yale Open Data Access (YODA) Project site at <http://yoda.yale.edu>.

References

1. de Weers M, Tai YT, van der Veer MS, et al. Daratumumab, a novel therapeutic human CD38 monoclonal antibody, induces killing of multiple myeloma and other hematologi-
- cal tumors. *J Immunol.* 2011;186(3):1840-1848.
2. Lammerts van Bueren J, Jakobs D, Kaldenhoven N, et al. Direct in vitro comparison of daratumumab with surrogate analogs of CD38 antibodies MOR03087, SAR650984 and Ab79. *Blood.* 2014;124(21):3474.
3. Overdijk MB, Verploegen S, Bogels M, et al. Antibody-mediated phagocytosis contributes to the anti-tumor activity of the therapeutic antibody daratumumab in lymphoma and multiple myeloma. *MAbs.*

2015;7(2):311-321.

- Overdijk MB, Jansen JH, Nederend M, et al. The therapeutic CD38 monoclonal antibody daratumumab induces programmed cell death via Fc_Y receptor-mediated cross-linking. *J Immunol*. 2016;197(3):807-813.
- Krejcik J, Casneuf T, Nijhof IS, et al. Daratumumab depletes CD38+ immune-regulatory cells, promotes T-cell expansion, and skews T-cell repertoire in multiple myeloma. *Blood*. 2016;128(3):384-394.
- Chiu C, Casneuf T, Axel A, et al. Daratumumab in combination with lenalidomide plus dexamethasone induces clonality increase and T-cell expansion: results from a phase 3 randomized study (POLLUX). Presented at: the 58th American Society of Hematology (ASH) Annual Meeting & Exposition; December 3-6, 2016; San Diego, CA. Abstract 4531.
- Adams HC III, Stevenaert F, Krejcik J, et al. High-parameter mass cytometry evaluation of relapsed/refractory multiple myeloma patients treated with daratumumab demonstrates immune modulation as a novel mechanism of action. *Cytometry A*. 2019;95(3):279-289.
- DARZALEX® (daratumumab) injection, for intravenous use [package insert]. Horsham, PA: Janssen Biotech, Inc; 2019.
- European Medicines Agency. Summary of opinion (post authorisation). DARZALEX (daratumumab). https://www.ema.europa.eu/en/documents/smop/chmp-post-authorisation-summary-positive-opinion-darzalexii-11_en.pdf. Published July 2018. Accessed August 2019.
- Jakubowiak A, Chari A, Lonial S, et al. Daratumumab (DARA) in combination with carfilzomib, lenalidomide, and dexamethasone (KRd) in patients (pts) with newly diagnosed multiple myeloma (MMY1001): an open-label, phase 1b study. Presented at: the Annual Meeting of the American Society of Clinical Oncology (ASCO); June 2-6, 2017; Chicago, IL. Abstract 8000.
- Chari A, Martinez-Lopez J, Mateos MV, et al. Daratumumab in combination with carfilzomib and dexamethasone (D-Kd) in lenalidomide-refractory patients with relapsed multiple myeloma: subgroup analysis of MMY1001. Presented at: the Annual Meeting of the American Society of Clinical Oncology (ASCO); June 1-5, 2018; Chicago, IL. Abstract 8002.
- Scheid C, Munder M, Salvender H, Engelhardt M. Infusion of daratumumab in combination therapies - practical information for the outpatient area. *Dtsch Med Wochenschr*. 2018;143(16):1201-1206.
- Barr H, Dempsey J, Waller A, et al. Ninety-minute daratumumab infusion is safe in multiple myeloma. *Leukemia*. 2018;32(11):2495-2518.
- Halozyme Therapeutics. Mechanism of action for Hylenex recombinant (hyaluronidase human injection). www.hylenex.com/mechanism-of-action. Accessed August 2019.
- Usmani SZ, Nahi H, Mateos MV, et al. Subcutaneous delivery of daratumumab in relapsed or refractory multiple myeloma. *Blood*. 2019;134(8):668-677.
- Lokhorst HM, Plesner T, Laubach JP, et al. Targeting CD38 with daratumumab monotherapy in multiple myeloma. *N Engl J Med*. 2015;373(13):1207-1219.
- Chari A, Nahi H, Mateos MV, et al. Subcutaneous delivery of daratumumab in patients (pts) with relapsed or refractory multiple myeloma (RRMM): PAVO, an open-label, multicenter, dose escalation phase 1b study. Presented at: the 59th American Society of Hematology (ASH) Annual Meeting & Exposition; December 9-12, 2017; Atlanta, GA. Abstract 838.
- US Department of Health and Human Services, National Institutes of Health, National Cancer Institute. Common terminology criteria for adverse events (CTCAE): Version 4.03. https://evs.nci.nih.gov/ftp1/CTCAE/CTCAE_4_03/CTCAE_4_03_2010-06-14_QuickReference_5x7.pdf. Accessed August 2019.
- Durie BGM, Harousseau JL, Miguel JS, et al. International uniform response criteria for multiple myeloma. *Leukemia*. 2006;20(9):1467-1473.
- Rajkumar SV, Harousseau JL, Durie B, et al. Consensus recommendations for the uniform reporting of clinical trials: report of the International Myeloma Workshop Consensus Panel 1. *Blood*. 2011;117(18):4691-4695.
- Xu XS, Yan X, Puchalski T, et al. Clinical implications of complex pharmacokinetics for daratumumab dose regimen in patients with relapsed/refractory multiple myeloma. *Clin Pharmacol Ther*. 2017;101(6):721-724.
- Clemens PL, Yan X, Lokhorst HM, et al. Pharmacokinetics of daratumumab following intravenous infusion in relapsed or refractory multiple myeloma after prior proteasome inhibitor and immunomodulatory drug treatment. *Clin Pharmacokinet*. 2017;56(8):915-924.
- Wang DD, Zhang S, Zhao H, Men AY, Parivar K. Fixed dosing versus body size-based dosing of monoclonal antibodies in adult clinical trials. *J Clin Pharmacol*. 2009;49(9):1012-1024.
- Bai S, Jorga K, Xin Y, et al. A guide to rational dosing of monoclonal antibodies. *Clin Pharmacokinet*. 2012;51(2):119-135.
- Mateos MV, Usmani SZ, Grosicki S, et al. Randomized, open-label, non-inferiority, phase 3 study of subcutaneous (SC) versus intravenous (IV) daratumumab (DARA) administration in patients (pts) with relapsed or refractory multiple myeloma (RRMM): body weight subgroup analysis of COLUMBA. Presented at: the 61st American Society of Hematology (ASH) Annual Meeting & Exposition; December 7-10, 2019; Orlando, FL. Abstract 1906.
- European Medicines Agency. MabThera: EPAR – product information; 2008.
- European Medicines Agency. Herceptin: EPAR – product information; 2010.
- HYQVIA [Immune Globulin Infusion 10% (Human) With Recombinant Human Hyaluronidase] Solution for subcutaneous administration [package insert]. Westlake Village, CA: Baxalta US Inc.; 2016.
- Palumbo A, Chanan-Khan A, Weisel K, et al. Daratumumab, bortezomib, and dexamethasone for multiple myeloma. *N Engl J Med*. 2016;375(8):754-766.
- Dimopoulos MA, Oriol A, Nahi H, et al. Daratumumab, lenalidomide, and dexamethasone for multiple myeloma. *N Engl J Med*. 2016;375(14):1319-1331.
- Usmani SZ, Weiss BM, Plesner T, et al. Clinical efficacy of daratumumab monotherapy in patients with heavily pretreated relapsed or refractory multiple myeloma. *Blood*. 2016;128(1):37-44.
- Plesner T, Arkenau HT, Gimsing P, et al. Phase 1/2 study of daratumumab, lenalidomide, and dexamethasone for relapsed multiple myeloma. *Blood*. 2016;128(14):1821-1828.
- Chari A, Mark TM, Krishnan A, et al. Use of montelukast to reduce infusion reactions in an early access treatment protocol of daratumumab in United States patients with relapsed or refractory multiple myeloma. Presented at: the 58th American Society of Hematology (ASH) Annual Meeting & Exposition; December 3-6, 2016; San Diego, CA. Abstract 2142.
- Chari A, Suvannasankha A, Fay JW, et al. Daratumumab plus pomalidomide and dexamethasone in relapsed and/or refractory multiple myeloma. *Blood*. 2017;130(8):974-981.
- Lonial S, Weiss BM, Usmani S, et al. Daratumumab monotherapy in patients with treatment-refractory multiple myeloma (SIRIUS): an open-label, randomised, phase 2 trial. *Lancet*. 2016;387(10027):1551-1560.
- Mateos MV, Nahi H, Legieb W, et al. Efficacy and safety of the randomized, open-label, non-inferiority, phase 3 study of subcutaneous (SC) versus intravenous (IV) daratumumab (DARA) administration in patients (pts) with relapsed or refractory multiple myeloma (RRMM): COLUMBA. Presented at: the Annual Meeting of the American Society of Clinical Oncology (ASCO); May 31-June 4, 2019; Chicago, IL. Abstract 8005.
- Sonneveld P, Terpos E, Dimopoulos M, et al. Pomalidomide and dexamethasone (pom-dex) with or without daratumumab (DARA) in patients (pts) with relapsed or refractory multiple myeloma (RRMM): a multicenter, randomized, phase 3 study (APOLLO). Presented at: the Annual Meeting of the American Society of Clinical Oncology (ASCO); June 1-5, 2018; Chicago, IL. Abstract TPS8059.
- Rajkumar SV, Voorhees PM, Goldschmidt H, et al. Randomized, open-label, phase 3 study of subcutaneous daratumumab (DARA SC) versus active monitoring in patients (pts) with high-risk smoldering multiple myeloma (SMM): AQUILA. *J Clin Oncol*. 2018;36(15 Suppl):TPS8062.
- Comenzo RL, Kastritis E, Mauer M, et al. Subcutaneous daratumumab + cyclophosphamide, bortezomib, and dexamethasone (CyBorD) in patients with newly diagnosed amyloid light chain (AL) amyloidosis: updated safety run-in results of ANDROMEDA. Presented at: the 24th European Hematology Association (EHA) Annual Congress; June 13-16, 2019; Amsterdam, The Netherlands. Abstract S875.
- Usmani SZ, Mateos MV, Hungria V, et al. Greater treatment satisfaction in patients receiving subcutaneous versus intravenous daratumumab for relapsed or refractory multiple myeloma: COLUMBA. Presented at: the 17th International Myeloma Workshop (IMW); September 12-15, 2019; Boston MA. Abstract SP-084.
- Chari A, San-Miguel J, McCarthy H, et al. Subcutaneous (SC) daratumumab (DARA) in combination with standard multiple myeloma (MM) treatment regimens: an open-label, multicenter phase 2 study (PLEIADES). Presented at: the 17th International Myeloma Workshop (IMW); September 12-15, 2019; Boston, MA. Abstract OAB-022.

The survival impact of maintenance lenalidomide: an analysis of real-world data from the Canadian Myeloma Research Group national database

Multiple myeloma (MM) is an incurable malignancy of mature plasma cells. Treatment of MM focuses on obtaining a deep and durable remission to improve overall and progression-free survival (PFS). Patients with good functional status ≤ 70 years of age are generally considered eligible for treatment with bortezomib-based induction chemotherapy followed by autologous stem cell transplant (ASCT) which has demonstrated a PFS and overall survival (OS) benefit in large, randomized controlled trials.¹⁻⁶ The use of lenalidomide maintenance (LM) following ASCT is based on four large randomized control trials and a meta-analysis demonstrating improvement in both PFS and OS.^{2,5,7-9}

Currently, data validating the use of LM in the real-world, Canadian landscape, in which LM is publicly funded, is limited.¹⁰⁻¹³ An analysis of the survival impact

and adverse effects of LM in large, real-world cohorts is of considerable importance. In order to address this knowledge gap, we conducted a retrospective, observational study of patients meeting International Myeloma Working Group (IMWG) criteria for MM who were treated with upfront bortezomib-based induction chemotherapy followed by ASCT.¹⁴ Data was collected from the Canadian Myeloma Research Group Database (CMRG-DB), a comprehensive collaborative data-sharing platform that pools data from academic cancer centers across Canada and includes legacy data dating back to 2007. The project was approved by Health Research Ethics Board of Alberta. We included patients receiving either lenalidomide monotherapy as maintenance or no maintenance (non-LM). Charts were reviewed with regard to demographics, response and adverse effects. The primary outcomes of this analysis were PFS, OS and progression-free survival 2 (PFS2) defined as time from initiation of second line chemotherapy to death, relapse or last follow-up. Progression was defined as per the IMWG criteria with an additional endpoint of near complete

Table 1. Baseline characteristics of lenalidomide maintenance and non-lenalidomide maintenance groups.

Characteristic	No maintenance N	Maintenance N	P
Patients	533	723	
Age at diagnosis, median (range) in years	57.9 (32.4 – 71.4)	58.1 (30.4 – 72.2)	0.711
Male (%)	332 (62.3)	443 (61.3)	0.714
Laboratory values at diagnosis, median (range)			
Hemoglobin (g/L)	104 (39-169)	107.5 (53-173)	0.0012
Platelets (x10 ⁹ /L)	221 (20-576)	219 (10-740)	0.7758
Neutrophils (x10 ⁹ /L)	3.4 (0.3-15.3)	3.3 (0.3-17.3)	0.3659
Calcium (mmol/L)	2.5 (1.6-4.4)	2.4 (1.7-5.7)	0.9322
Creatinine level (mmol/L)	96 (42-2,705)	84 (32-2,700)	0.0112
ISS, Median	II	II	
ISS I (%)	122 (26.8)	232 (35.9)	
ISS II (%)	167 (36.6)	252 (39.0)	
ISS III (%)	167 (36.6)	162 (25.1)	<0.0001
Missing (%)	77	77	
High risk cytogenetics	56/315 (17.8)	137/567 (24.2)	0.028
del 17p* (%)	26/307 (8.5)	76/560 (13.6)	0.026
t(4:14) (%)	30/302 (9.9)	58/545 (10.6)	0.746
t(14:16) (%)	8/176 (4.6)	13/451 (2.9)	0.298
Missing (%)	218	156	
Immunoglobulin subtype			
IgG (%)	283/483 (58.6)	386/696 (55.5)	
IgA (%)	101/483 (20.9)	148/696 (21.2)	
IgD (%)	1/483 (0.21)	0/696 (0)	0.542 [‡]
IgM (%)	1/483 (0.21)	2/696 (0.29)	
Light chain (%)	97/483 (20.1)	160/696 (23)	
Induction regimen used			
CyBor/CyBorD/P (%)	646 (89.4)	370 (69.4)	<0.001
RVD / RVDD* / VTD (%)	9 (1.24)	18 (3.38)	0.017 [‡]
VD/P (%)	68 (9.41)	135 (25.3)	<0.001
VD-PACE (%)	0 (0)	1 (0.19)	–
Bortezomib monotherapy (%)	0 (0)	9 (1.7)	<0.001 [‡]

[‡]Fisher's exact test. Ig: immunoglobulin; ISS: injury severity score; Cy: cyclophosphamide; V: bortezomib (also abbreviated as Bor in standard combination regime). P: prednisone; D: dexamethasone; D*: doxil; R: lenalidomide; T: thalidomide; PACE: cisplatin, adriamycin, cyclophosphamide & etoposide.

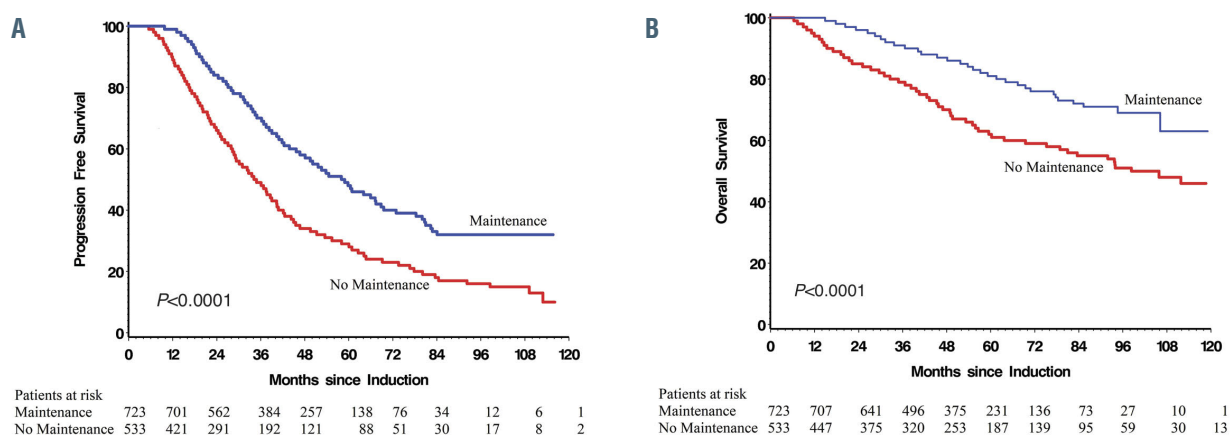


Figure 1. Survival outcomes in patients treated with and without lenalidomide maintenance post autologous stem cell transplant. (A) Progression free survival. (B) Overall survival.

Table 2. Survival and response outcomes in lenalidomide maintenance and non-lenalidomide maintenance groups.

	No maintenance Group	Maintenance Group	P
Median OS			
High risk cytogenetics	45.3 months	NYR	<0.0001
Standard risk cytogenetics	NYR	NYR	<0.0001
Median PFS			
High risk cytogenetics	22.0 months	53.0 months	<0.0001
Standard risk cytogenetics	38.6 months	59.9 months	<0.0001
Response			
nCR & CR	145 (45.2%)	297 (52%)	0.05 <0.01
VGPR	114 (35.5%)	239 (41.9%)	0.06
PR	49 (15.3%)	24 (4.2%)	<0.01
SD or less	13 (4.1%)	11 (1.9%)	0.08

NYR: Not yet reached; CR: complete response; nCR: near complete response; VGPR: very good partial response; PR: partial response; SD: stable disease.

response (nCR) in whom complete response (CR) status was not confirmed by bone marrow biopsy.¹⁵ Data was analyzed using version 9.4 of the SAS system for Windows with Kaplan-Meier curves to evaluate PFS and OS. χ^2 analysis was used for dichotomous variables. A P -value of <0.05 was considered statistically significant.

We included 1,256 patients beginning induction treatment between January 2007 and January 2016. Seven hundred and twenty-three patients (57.6%) received LM and 533 (42.4%) did not. All relevant baseline characteristics of each group are illustrated in Table 1.

The median follow-up was 49.1 months in the LM group (range, 8.6–124.8 months) and 45.3 months in the non-LM group (range, 4.5–141.1 months). At the time of analysis, 397 (54.9%) of the LM group had not yet progressed compared to 198 (37.2%) of patients in the non-LM group.

The median PFS was 58.2 months (95% Confidence Interval [CI]: 52.0–64.0) in the LM group compared to 34.6 months in the non-LM group (95%CI: 30.7–37.7, $P < 0.0001$), Figure 1A. The 5-year OS was 81% in the LM group compared to 61.5% in the non-LM cohort. The median OS was 98.3 months in the non-LM cohort (95%CI: 83.5) but not reached (>124 months) in the LM group ($P < 0.0001$, Figure 1B). There was no difference in PFS ($P = 0.66$) or OS ($P = 0.75$) between 21/28 day and 28/28 lenalidomide dosing schedules. Median PFS2 was NYR in the LM cohort compared to 64.2 months (95%CI: 55.3–74.8, $P < 0.0001$). Response rates were deeper in the

LM cohort including nCR/CR (52.0% vs. 45.2%, $P = 0.05$) and \geq VGPR (93.9% vs. 80.7%, $P < 0.01$). The PFS benefit of lenalidomide persisted in those achieving a nCR/CR ($P < 0.0001$), VGPR ($P = 0.0006$) and PR ($P = 0.03$). The presence of high-risk cytogenetics was associated with reduced PFS and OS in all patients (Table 2). While the worse outcome could not be overcome entirely with the use of maintenance both median PFS and OS were improved regardless of cytogenetic risk (Table 2).

In further data available for 226 patient in Edmonton, Alberta common indication for dose reduction or medication discontinuation were cytopenias (27.7%), rash (10.8%), infection (9.5%) and fatigue (8.1%). 19.6% discontinued therapy prior to relapse. Venous and arterial thrombosis during frontline treatment was not significantly different between the groups at 2.6% in the non-LM group compared to 5.4% in the LM group ($P = 0.5$). Rates of secondary primary malignancy (SPM) were observed in 6.4% of the non-LM group and 3.4% of the LM patients ($P = 0.32$). Primary sites included skin, lung, bladder and prostate in the non-LM group and breast, brain, lung, kidney and one case of CLL in the LM group.

This analysis from the CMRG-DB is the first dataset analyzing the use of LM following ASCT in the real-world Canadian landscape. Our data validates findings of large, phase 3 randomized controlled trials illustrating a positive impact of LM on PFS and OS in a real-world setting.^{2,4,7,9} The median PFS data demonstrated a clear advantage for LM. The median OS data also strongly

favored the use of LM. The disease control and survival advantage of LM persisted in patients with standard- or high-risk cytogenetics. Interestingly, patients with high-risk cytogenetics treated with LM had superior PFS and OS compared with standard-risk patients in the non-LM cohort, a finding that supports using LM even in patients anticipated to have the poorer survival outcomes associated with these cytogenetic abnormalities. Lastly, the improved PFS2 outcomes in LM patients demonstrates that non-LM patients do not "catch up" to their maintenance counterparts with second-line therapy.

LM further improved survival outcomes in each response category, including those in the nCR/CR group. This suggests that the impact of LM on PFS and OS goes beyond simply improving patients' response criteria and offers additional survival advantages even in those who achieve a nCR/CR, perhaps through an immune as well as a cytotoxic effect.

Although most patients required a dose reduction or medication discontinuation at some point during their treatment, only 19.6% of patients discontinued therapy prior to relapse. This suggests that LM is well-tolerated.

Limitations of our study include its retrospective, observational nature. Patients were enrolled who started chemotherapy prior to 2016 and significant changes have emerged in the field of myeloma in recent years, particularly with regards to novel chemotherapeutic agents in the setting of relapsed disease. These may have influenced the OS data which depends in part on treatment received for disease recurrence. Given that the non-LM cohort largely comprises of those starting chemotherapy prior to 2012, these patients may not have had the same access to clinical trials or novel combination therapy as their LM counterparts. On the other hand, patients progressing on LM might be expected to experience poorer results with second-line therapy, which was not the case based on PFS2 data. However, the similarity of our data when compared to large scale, randomized, controlled trials suggests that the impact of this temporal relationship between the LM and non-LM groups may not significantly impact our results. Further, the availability of additional agents only affects the PFS2 and OS outcomes. The cohort presented here is still reflective of the impact of LM on disease control in the post-ASCT setting as measured by PFS.

Lastly, the recent adoption of LM limits our ability to see its full impact on survival outcomes as many of LM patients have not yet experienced their first relapse. Longer follow-up will allow further assessment of the impact of maintenance therapy, particularly in the era of improved therapy for relapsed disease.

Despite the limitations of retrospective data, large multicenter datasets have undeniable merits as they allow for evaluation of the generalizability of new treatments in patients who would not meet eligibility criteria for a clinical trial. Such datasets also provide lengthy and detailed follow-up of real-world data beyond the line of treatment in question, which can be challenging to collect in prospective randomized control trials.^{2,5,9-11} Furthermore, those with early relapse as well as long-term disease-free survivors are easily identified in these large, retrospective datasets. Examination of their data will be useful in the determination of contributing and prognosticating factors in these, and other, patient subsets.

In summary, our retrospective cohort validates the data seen in large phase 3 trials demonstrating the positive impact LM has had on PFS, OS and response in the real-world setting. This data supports the ongoing use of LM as a current standard of care.

Hannah M. Cherniawsky,¹ Vishal Kukreti,² Donna Reece,² Esther Masih-Khan,^{2,3} Arleigh McCurdy,⁴ Victor H. Jimenez-Zepeda,⁵ Michael Sebag,⁶ Kevin Song,⁷ Darrell White,⁸ Julie Stakiw,⁹ Richard LeBlanc,¹⁰ Anthony Reiman,¹¹ Muhammad Aslam,¹² Martha Louzada,¹³ Rani Kotb,¹⁴ Engin Gul,³ Eshetu Atenafu,³ and Christopher P. Venneri¹⁵

¹University of Alberta, Edmonton, Alberta; ²Medical Oncology and Hematology, Princess Margaret Cancer Center, Toronto, Ontario; ³Canadian Myeloma Research Group, Toronto, Ontario;

⁴The Ottawa Hospital, Ottawa, Ontario; ⁵Tom Baker Cancer Center, Calgary, Alberta; ⁶Department of Oncology, Division of Hematology, McGill University, Montreal, Quebec; ⁷BC Cancer, Vancouver General Hospital, Vancouver, British Columbia;

⁸Queen Elizabeth II Health Sciences Center, Dalhousie University, Halifax, Nova Scotia; ⁹Saskatoon Cancer Center, University of Saskatchewan, Saskatoon, Saskatchewan; ¹⁰Maisonneuve-Rosemont Hospital Research Center, University of Montreal, Montreal, Quebec; ¹¹Department of Oncology, Saint John Regional Hospital, Saint John, New Brunswick; ¹²Allan Blair Cancer Center, Regina, Saskatchewan; ¹³London Regional Cancer Center, London, Ontario; ¹⁴Cancer Care Manitoba, Winnipeg, Manitoba and ¹⁵Cross Cancer Institute, University of Alberta, Edmonton, Alberta, Canada

Correspondence:

ESTHER MASIH-KHAN - esther.masih-khan@uhnresearch.ca

doi:10.3324/haematol.2020.259093

Received: June 15, 2020.

Accepted: September 30, 2020.

Pre-published: October 13, 2020.

Disclosures: VK received honoraria from Amgen, Takeda and Celgene; DC received research funding from Otsuka, Celgene, Janssen, Takeda, Merck, BMS, and Millennium, acts as a consultant for Celgene, Jansen, Amgen, Karyopharm and Takeda, and received honoraria from Celgene, Janssen, Amgen and Takeda; AmcC received honoraria and acts as a consultant for Celgene, Janssen, Amgen, Takeda; JVHJ-Z received honoraria from Celgene, Janssen, Takeda, Merck and BMS; MS is a member on an entity's Board of Directors or advisory committees of Janssen Inc., Amgen, Takeda, Celgene; KS received research funding from Celgene, honoraria from Celgene, Janssen, Amgen and Takeda; DW received honoraria from Amgen, Antengene, Celgene, Janssen, Karyopharm, Sanofi and Takeda; RLB is a member on an entity's Board of Directors or advisory committees of Celgene Canada, Janssen Inc., Amgen, Takeda, Sanofi and received research funding from Celgene (co-investigator); ML received honoraria from Janssen, Celgene, Amgen, Pfizer; CPV received honoraria from Janssen, Amgen, Takeda and research funding Celgene Amgen; all remaining authors declare non conflicts of interest.

Contributions: HMC, CPV, VK, DR, and EMK designed research, performed research, collected, analyzed, interpreted data and wrote the manuscript. EA performed statistical analysis, analyzed, interpreted data and wrote the manuscript; All authors designed research, analyzed and interpreted data.

Acknowledgments: the authors would like to thank the Canadian Myeloma Research Group for their support and our patients for generously donating their data for analysis.

References

1. Attal M, Harousseau JL, Stoppa AM, Sotto JJ, et al. A prospective, randomized trial of autologous bone marrow transplantation and chemotherapy in multiple myeloma. *Intergroupe Français du Myélome. N Engl J Med.* 1996;335(2):91-97.
2. McCarthy PL, Holstein SA, Petrucci MT, et al. Lenalidomide maintenance after autologous stem-cell transplantation in newly diagnosed multiple myeloma: a meta-analysis. *J Clin Oncol.* 2017;35(29):3279-3289.

3. Morgan GJ, Davies FE, Hawkins K, et al. Follow up analysis for MRC Myeloma VII Trial. *Blood*. 2004;104(11):927.
4. Palumbo A, Bringhen S, Petrucci MT, et al. Intermediate-dose melphalan improves survival of myeloma patients aged 50 to 70: results of a randomized controlled trial. *Blood*. 2004;104(10):3052-3057.
5. Palumbo A, Cavallo F, Gay F, et al. Autologous transplantation and maintenance therapy in multiple myeloma. *N Engl J Med*. 2014;371(10):895-905.
6. Palumbo A, Gay F, Falco P, et al. Bortezomib as induction before autologous transplantation, followed by lenalidomide as consolidation-maintenance in untreated multiple myeloma patients. *J Clin Oncol*. 2010;28(5):800-807.
7. Attal M, Lauwers-Cances V, Marit G, et al. Lenalidomide maintenance after stem-cell transplantation for multiple myeloma. *N Engl J Med*. 2012;366(19):1782-1791.
8. Jackson GH, Davies FE, Pawlyn C, et al. Lenalidomide maintenance versus observation for patients with newly diagnosed multiple myeloma (Myeloma XI): a multicentre, open-label, randomised, phase 3 trial. *Lancet Oncol*. 2019;20(1):57-73.
9. McCarthy PL, Owzar K, Hofmeister CC, et al. Lenalidomide after stem-cell transplantation for multiple myeloma. *N Engl J Med*. 2012;366(19):1770-1781.
10. Cherniawsky H, Sandhu I, Chu MP, et al. The survival impact of lenalidomide maintenance chemotherapy in multiple myeloma patients treated with autologous stem cell transplant and bortezomib-based induction: an analysis of real world data. *Blood*. 2017;130(Suppl 1):S3132.
11. Cote J, Phillips M, Atenafu EG, et al. Pattern of first relapse in multiple myeloma (MM) patients (Pts) after a cybord induction regimen and autologous stem cell transplantation (ASCT): impact of maintenance therapy in the real-world setting. *Blood*. 2016;128(22):2137.
12. Yang C, Jiang H, Masih-Khan E, et al. Tolerability and efficacy of post transplant lenalidomide maintenance therapy in multiple myeloma: a real world single centre experience. *Blood*. 2017;130(Suppl 1):S3462.
13. Lonial S, Anderson KC. Association of response endpoints with survival outcomes in multiple myeloma. *Leukemia*. 2014;28(2):258-268.
14. Rajkumar SV, Dimopoulos MA, Palumbo A, et al. International Myeloma Working Group updated criteria for the diagnosis of multiple myeloma. *Lancet Oncol*. 2014;15(12):e538-e548.
15. Kumar S, Paiva B, Anderson KC, et al. International Myeloma Working Group consensus criteria for response and minimal residual disease assessment in multiple myeloma. *Lancet Oncol*. 2016;17(8):e328-e346.

No association between *ECSIT* germline mutations and hemophagocytic lymphohistiocytosis in natural killer/T-cell lymphoma

Hemophagocytic lymphohistiocytosis (HLH) is a clinical syndrome of excessive immune activation with fever, cytopenia, and organ infiltration by activated macrophages. Secondary HLH associated with natural killer (NK)/T-cell lymphoma (NKTCL) has extremely poor prognosis,¹ and biomarkers that may predict patients who are more likely to develop HLH are lacking. Wen *et al.*² recently showed an association between a somatic gene mutation in the evolutionarily conserved signaling intermediate in Toll pathway (*ECSIT*) gene (c.T419C; p.V140A) and HLH in NKTCL. The variant *ECSIT* protein triggered NF- κ B signaling pathway more potently, leading to aberrant secretion of proinflammatory cytokines by *ECSIT*-T419C-transfected NKTCL cell lines. They found that the *ECSIT*-T419 mutation was significantly enriched in individuals with NKTCL-associated HLH, which developed in nine of 17 patients with and five of 36 patients without the mutation, respectively. Patients with *ECSIT*-T419 had elevated expression of proinflammatory cytokines and poorer prognosis. While intriguing, the prevalence of *ECSIT*-T419 and relation with HLH has not been assessed in independent cohorts. We therefore sought to examine whether the *ECSIT*-T419 mutation predisposes to HLH in multiple cohorts of patients with NKTCL and correlates its presence with clinical outcomes.

First, we studied the mutational profile of *ECSIT* in 25 subjects with sporadic NKTCL from China with available whole exome sequencing of paired tumour-blood samples.³ Samples were sequenced with Illumina HiSeq X and NextSeq 6000, and variant-calling was performed by Strelka2 using default single-sample settings.⁴ We found the *ECSIT*-T419 mutation in five of 25 subjects, but they were all germline mutations; heterozygously mutated in both matching tumour (variant allele frequency [VAF], mean, 43.8%, 95% Confidence Interval [CI]: 38.8-48.9) and blood (VAF mean, 53.8%, 95%CI: 51.5-56.2) samples from these five subjects (Figure 1A). The reported prevalence of somatic *ECSIT*-T419 mutation in Wen *et al.*'s study was 19.3% (17 of 88), similar to the mutation frequency of Jiang *et al.*'s cohort, but were all germline mutations.

In order to further verify whether *ECSIT*-T419 is a germline or somatic mutation, we studied 67 patients with NKTCL who provided written informed consent under respective institutions' Institutional Review Boards (IRB) from Singapore local hospitals and Sun Yat-Sen University Cancer Center in Guangzhou, China. We Sanger sequenced matched tumor- buccal swab (representative Sanger sequence in Figure 1B) or peripheral blood (representative Sanger sequence in Figure 1C) samples from NKTCL patients and *ECSIT*-T419 was validated in 7.5% (five of 67) of both the tumor and matching non-tumor samples. Targeted resequencing using next-generation sequencing method revealed the mean VAF of *ECSIT*-T419 to be 52.2%, 95%CI: 42.8-61.6 in the five tumors, 52.2%, 95%CI: 48.5-56.0 in four matched blood samples, and 53% in a matched buccal swab sample ($P=0.90$, 2-tailed Wilcoxon Rank-sum test, VAF of *ECSIT*-T419 between tumors and non-tumoral samples). The near 50% VAF, and the presence of *ECSIT*-T419 mutation observed in all matching tumor, blood and buccal swab DNA indicate that this is a germline heterozygous single-nucleotide polymorphism

(SNP), with a report SNP ID of rs145036301. Among the five patients with *ECSIT*-T419 mutation, HLH information was available for three patients and none developed HLH, as defined by the HLH 2004 criteria.⁵

Given the discrepant findings, we re-analyzed the initial discovery cohort of paired tumor-normal exome data (n=5) from Wen *et al.*² In the sample where *ECSIT*-T419 mutation was reported as a somatic mutation, VAF was 52% in the tumor (150 of 288; alternate allele depth/reference allele depth) and 10% (5 of 51) in the matched normal sample (Figure 1D). Furthermore, the VAF exceeded the thresholds of 30% in tumor and 5% in matched normal sample as specified by Wen *et al.*² Thus, this variant should not be considered as a somatic mutation as based on the authors' analysis criteria.

Notwithstanding the false somatic call, we wanted to examine whether the germline *ECSIT*-T419 mutation is associated with HLH in two independent cohorts of patients with NKTCL in Singapore and Taiwan. In Singapore, the cases were identified using local databases from two teaching hospitals and all samples and clinical information were collected after IRB approval. Cases were reviewed by a central pathologist and HLH was defined according to the HLH 2004 criteria. Sixty-four cases of NKTCL were identified between 2007-2017, and *ECSIT*-T419 mutations were found in 15.4% (two of 13) and 5.9% (two of 51) patients with and without HLH respectively. Out of the 13 patients with HLH, four were women. Median age was 43 (range, 18-60 years). At time of the last follow-up in December 2018, all patients had died. Seven of 12 patients received polychemotherapy, while one was treated with the HLH-2004 protocol (with dexamethasone, etoposide, cyclosporin), and two received steroids. Median survival was only 33 days (range, 1-389 days). Causes of death were lymphoma (n=6), HLH (n=6), and infection (n=1). The two individuals with *ECSIT* mutation succumbed at day 1 and day 89. Within these NKTCL patients with HLH in our Singapore cohort, there was no significant association of the *ECSIT* mutation with them ($P=0.18$, Fisher's exact test, *Online Supplementary Table S1*).

In the Taiwanese cohort of 85 NKTCL cases with clinical and sequencing data from the Chang Gung Memorial Hospital, *ECSIT*-T419 mutation frequency was observed at 11.8% (ten of 85). Nine cases developed HLH, and none of these samples harboured the *ECSIT*-T419C mutation. When both Singapore and Taiwan cohorts were combined for analysis, we did not find any statistical association between *ECSIT*-T419C mutation and HLH (OR=1.48, 95%CI: 0.38-5.76, $P\approx 1.0$, Fisher's exact test, *Online Supplementary Table S2*). There were also no significant associations between the *ECSIT*-T419C mutation with clinical characteristics such as sex, stage, Eastern Cooperative Oncology Group (ECOG) performance status and international prognostic index (Figure 1E; *Online Supplementary Table S3*). Overall survival (*Online Supplementary Figure S1A*) and progression-free survival (*Online Supplementary Figure S1B*) were also not significantly associated with *ECSIT*-T419 mutation.

Given the rarity and fulminant nature of malignancy-associated HLH hindering the collection of biopsy specimens, we combined data from multiple cohorts to examine associations between *ECSIT*-T419 and HLH in NKTCL in the largest study to date. Strict diagnostic inclusion criteria were used for both HLH and NKTCL. Some possible explanations for the discordant results between Wen *et al.* and our study need consideration. Patients in Singapore and Taiwan developed HLH at around the time of diagnosis or relapse, as opposed to

Wen *et al.*'s cohort which developed HLH 3 to 6 months after diagnosis of NKTCL, during or after treatment. The onset of HLH might be triggered by the initiation of chemotherapy that leads to loss of immune homeostasis and further aggravates T-cell dysfunction which may further lower the threshold for triggering HLH in lymphoma

patients.⁶ It is possible that in the absence of chemotherapy in our patients, the activating effect of the *ECSIT*-T419 mutation on the NF- κ B pathway is not strong enough to drive HLH. However, there were four *ECSIT* wild-type patients from Singapore who developed HLH again after chemotherapy initiation.

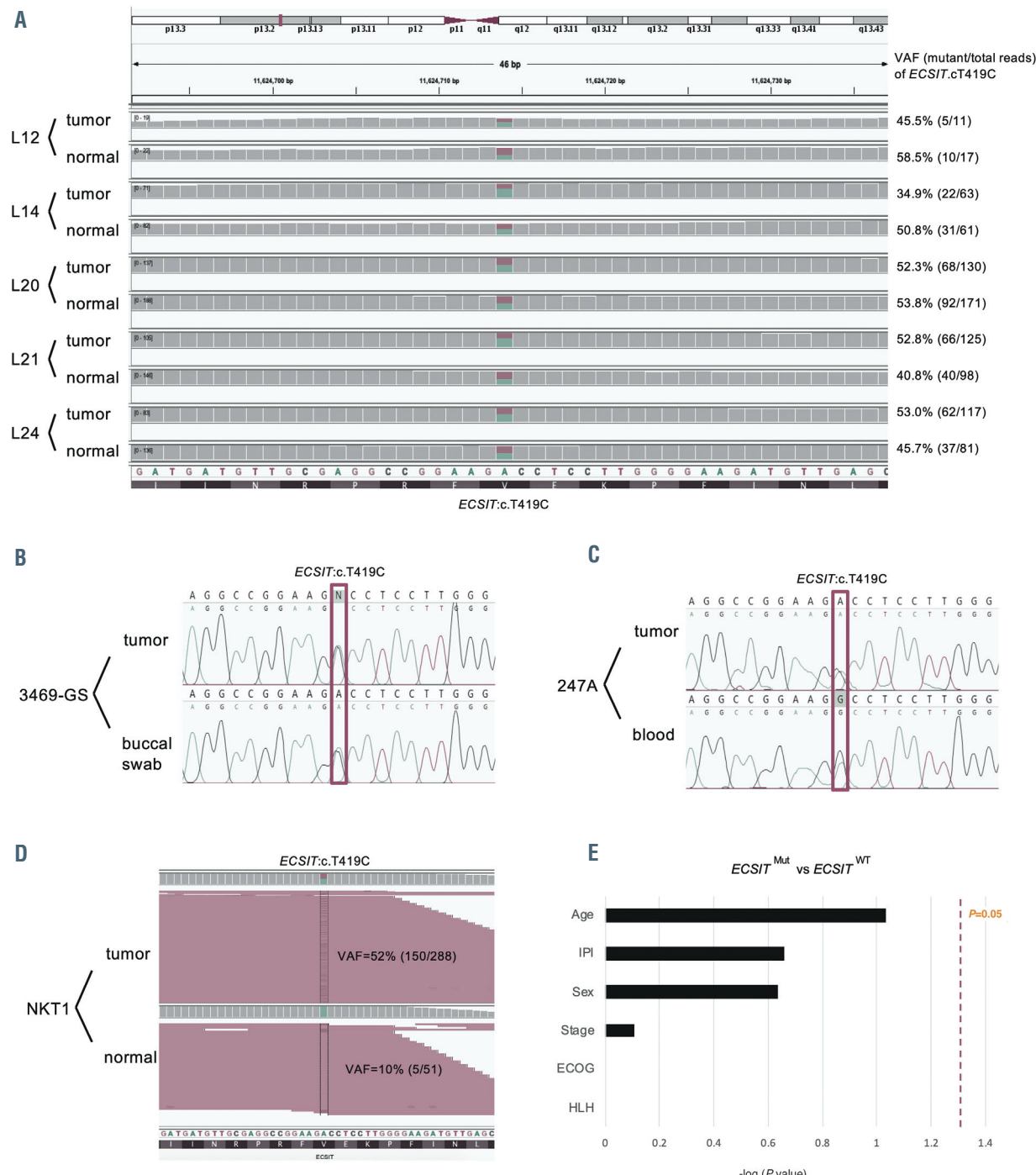


Figure 1. *ECSIT*-T419C is a germline mutation not associated with hemophagocytic lymphohistiocytosis in natural killer/T-cell lymphoma patients. (A) Sanger sequencing electropherogram profile for tumor-normal paired samples with heterozygous *ECSIT*-V140A mutation, identified as L12, L14, L20, L21, and L24 in Jiang *et al.*³ (B and C) Representative Sanger sequencing electropherogram profile for two tumor- peripheral blood (B) and buccal swab (C) samples for the *ECSIT*-V140A mutation from Singapore local hospitals and the Sun Yat-Sen University Cancer Center in Guangzhou, China. (D) Integrative Genomics Viewer (IGV) snapshot centered around heterozygous germline *ECSIT*-T419C mutation of the paired tumor-normal exome sequencing data of sample NKT1 from Wen *et al.*² Variant allele frequencies (VAF) were calculated from the number of variant-supporting/total read-counts at *ECSIT*-T419C. Aligned reads were colored pink according to the read-strand that they were aligned with onto the human reference genome. (E) No association between *ECSIT* mutation and clinical characteristics of natural killer/T-cell lymphoma patients in Singapore and Taiwan. *ECSIT*: evolutionarily conserved signaling intermediate in Toll pathway; IPI: international prognostic index; ECOG: Eastern Cooperative Oncology Group, HLH: hemophagocytic lymphohistiocytosis, Mut: mutant; WT: wild-type.

Differences in other patient characteristics may also explain the discordance (e.g., patients with HLH in Singapore had stage III or IV disease, while most patients with HLH in Wen *et al.*'s cohort had early stage disease).

In summary, our data from multiple cohorts do not support the risk effect of *ECSIT*-T419 mutation (SNP rs145036301) on HLH in NKTCL. Furthermore, this is a germline rather than somatic mutation that appears in SNP database (dbSNP v153) and has now been flagged as a common polymorphic variant by Catalogue of Somatic Mutations in Cancer (COSMIC v90) databases.^{7,8} Additionally, there were no differences in clinical characteristics or prognosis between NKTCL patients with and without *ECSIT*-T419 mutation. One limitation of our study is not being able to examine whether germline variants in genes associated with familial HLH are enriched in patients with NKTCL-associated HLH. However, recent studies have not shown an association of biallelic pathogenic variants in HLH-associated genes with adult HLH, albeit in cohorts that comprise a mixture of lymphoma and non-lymphoma subtypes.^{9,10} Ultimately, additional efforts to define disruptive variants in a larger number of genes, in expanded cohorts of adults with lymphoma associated HLH, may further refine our understanding and treatment of this devastating condition.¹

Shin Yeu Ong,¹ Jing Quan Lim,^{2,3} Nicholas Grigoropoulos,¹ Yurike Laurensia,² Dachuan Huang,^{2,3} Burton Kuan Hui Chia,² Daryl Cheah Ming Zhe,² Sahil Ajit Saraf,⁴ Chee Leong Cheng,⁴ Wen-Yu Chuang,⁵ Ming-Chung Kuo,⁶ Yi-Jiun Su,⁶ Colin Phipps,¹ Chandramouli Nagarajan,¹ Yuh Shan Lee,¹ Daryl Tan Chen Lung,¹ Lee-Yung Shih,⁶ Yeow Tee Goh,¹ Soon Thye Lim^{2,3#} and Choong Kiat Ong^{2,3,7#}*

¹Department of Haematology, Singapore General Hospital, Singapore; ²National Cancer Center, Singapore; ³Duke-NUS Medical School, Singapore; ⁴Department of Pathology, Singapore General Hospital, Singapore; ⁵Department of Pathology, Chang Gung Memorial Hospital at Linkou and Chang Gung University, Taoyuan, Taiwan; ⁶Division of Hematology-Oncology, Chang Gung Memorial Hospital at Linkou, and Chang Gung University, Taoyuan, Taiwan and ⁷Genome Institute of Singapore, A*STAR, Singapore.

*SYO and JQL contributed equally as co-first authors.

#STL and CKO contributed equally as co-senior authors.

Correspondence:

CHOON KIAT ONG - cmrock@nccs.com.sg

SOON THYE LIM - lim.soon.thye@singhealth.com.sg

doi:10.3324/haematol.2020.269209

Received: August 12, 2020.

Accepted: September 30, 2020.

Pre-published: October 13, 2020.

Disclosures: no conflicts of interest to disclose.

Contributions: CKO conceived the project and designed the study; SYO drafted the initial manuscript; CCL, SAS, and WYC performed pathological studies; YL performed sequencing studies; JQL and BKHC performed the bioinformatics analysis; SYO, JQL, DCH, DCMZ, CP, CN, YSL, DTCL, STL, MCK, YJS, and LYS recruited participants, managed subject information and tissue samples, and contributed to data analysis; CKO, JQL, NG and YTC participated in critical revision of the manuscript.

Funding: the study was supported by grants from the Singapore Ministry of Health's National Medical Research Council (NMRC-OFLCG-18May0028 and NMRC-ORIRG16nov090), Tanoto Foundation Professorship in Medical Oncology, New Century International Pte Ltd, Ling Foundation, and Chang Gung Memorial Hospital (OMRPCG3C0021), Taiwan.

References

1. Jin Z, Wang Y, Wang J, et al. Multivariate analysis of prognosis for patients with natural killer/T cell lymphoma-associated hemophagocytic lymphohistiocytosis. *Hematology*. 2018;23(4):228-234.
2. Wen H, Ma H, Cai Q, et al. Recurrent *ECSIT* mutation encoding V140A triggers hyperinflammation and promotes hemophagocytic syndrome in extranodal NK/T cell lymphoma. *Nat Med*. 2018; 24(2):154-164.
3. Jiang L, Gu ZH, Yan ZX, et al. Exome sequencing identifies somatic mutations of *DDX3X* in natural killer/T-cell lymphoma. *Nat Genet*. 2015;47(9):1061-1066.
4. Kim S, Scheffler K, Halpern AL, et al. Strelka2: fast and accurate calling of germline and somatic variants. *Nat Methods*. 2018;15(8):591-594.
5. Henter JI, Horne A, Arico M, et al. HLH-2004: diagnostic and therapeutic guidelines for hemophagocytic lymphohistiocytosis. *Pediatr Blood Cancer*. 2007;48(2):124-131.
6. Dauer N, McClain K, Allen CE, et al. A consensus review on malignancy-associated hemophagocytic lymphohistiocytosis in adults. *Cancer*. 2017;123(17):3229-3240.
7. Smigelski EM, Sirotkin K, Ward M, et al. dbSNP: a database of single nucleotide polymorphisms. *Nucleic Acids Res*. 2000;28(1):352-355.
8. Tate JG, Bamford S, Jubb HC, et al. COSMIC: the Catalogue of Somatic Mutations In Cancer. *Nucleic Acids Res*. 2019; 47(D1):D941-D947.
9. Miller PG, Niroula A, Ceremsak JJ, et al. Identification of germline variants in adults with hemophagocytic lymphohistiocytosis. *Blood Adv*. 2020;4(5):925-929.
10. Carvelli J, Piperoglou C, Farnarier C, et al. Functional and genetic testing in adults with HLH reveals an inflammatory profile rather than a cytotoxicity defect. *Blood*. 2020;136(5):542-552.

Pituitary iron and factors predictive of fertility status in transfusion-dependent thalassemia

Long-term survival of patients with transfusion-dependent thalassemia (TDT) raises hopes of attaining a decent quality of life, having a family and maintaining reproductive potential. However, for many these remain significant challenges despite advances in the management of iron overload. While pregnancies are possible, there is inadequate information to guide patients on their reproductive ability and on markers that predict when they will have infertility issues. Preservation of fertility and timely interventions remain pervasive concerns. Although the association of iron toxicity with cardiac and pancreatic dysfunction has been investigated extensively, the progression of iron deposition in the anterior pituitary leading to hypogonadotropic hypogonadism and infertility has not been adequately explored.¹

To address these issues, we sought to investigate pituitary dysfunction and stratify the risk of infertility utilizing reproductive data and information on systemic iron load. We also evaluated the progression of pituitary dysfunction and systemic iron parameters and their effect on reproductive capacity. Magnetic resonance imaging (MRI) measurements of anterior pituitary iron (R2) and volume have established reference data in normal controls and proved an adequate method to predict clinical hypogonadism in thalassemia.^{2,4} Identifying risk thresholds could assist in establishing the timing and effectiveness of intensifying chelation treatment to halt further damage and potentially restore function.

The study was approved by institutional review boards and all patients provided written informed consent to participation.

Fifty-three TDT patients, 10 years and older, and 12 healthy subjects (age 12–40 years) underwent MRI (Philips Achieva[®], 1.5 T) to determine cardiac iron (T2*), anterior pituitary iron (R2) and three-dimensional volume.⁵ Levels of non-transferrin bound iron, labile plasma iron (LPI), and ferritin were measured in blood samples, and liver iron concentration (LIC) and myocardial iron were quantified by MRI and a superconducting quantum interference device (SQUID), respectively. In order to assess fertility, plasma gonadotropins (luteinizing hormone [LH] and follicular-stimulating hormone [FSH]), estradiol and testosterone levels were assayed. Anti-Müllerian hormone (AMH) levels were determined in women in order to evaluate ovarian reserve and inhibin B levels were measured in men to assess impairment of spermatogenesis.^{6,7} In 17 patients these measures were repeated 2–3 years later to assess for changes over time. The patients' pubertal and reproductive history was recorded. Z scores for anterior pituitary iron accumulation, Z(R2), and volume, Z(V), were calculated for each patient.⁸ Parametric statistics were applied to characterize patients: mean \pm standard deviation, *t*-test, and Pearson correlation. Associations of Z(R2) and Z(V) with age and LH and FSH levels were demonstrated by boxplots and linear regression. Receiver operating characteristic (ROC) curve analysis was used in patients for categorization into Z(R2) ≤ 4 and > 4 to examine the sensitivity and specificity for systemic iron parameters.

Moderate-severe pituitary iron deposition Z(R2) > 2 , mean 5.4) was observed in 33 patients (62%, age 26 \pm 7 years), a rate comparable to that in the report by Noetzli *et al.*⁴ The rest of the patients (32%, age 23 \pm 8 years) had no iron accumulation (mean Z(R2) of 0.03). Thirty-two patients (60%) had a Z(V) < -2 (mean -2.8) indicating sig-

nificant gland shrinkage; the remaining 40% had a Z(V) of -0.7. There was a negative correlation between Z(R2) and Z(V): $r=-0.36$, $P=0.02$ (Figure 1A). We found that a Z(R2) value > 4.0 predicted pituitary volume loss: Z(V) < -2.0 was present in 17/20 patients with a Z(R2) > 4 and in only 16/33 with a Z(R2) < 4.0 ($P<0.009$).

Twenty-three patients (43%, 28 \pm 6 years) simultaneously had Z(R2) > 4 and Z(V) < -2 , of whom ten (43%) were splenectomized. Overall, patients who underwent splenectomy had higher pituitary R2, smaller gland volume and a significantly higher cardiac iron in comparison to the non-splenectomized patients ($P<0.004$) while LIC was similar (Table 1). This supports the notion that

Table 1. Patients' disease characteristics.

Characteristics	N (%) or mean \pm SD
Study patients	
Females:males	53* 27:26
Age (years)	25 \pm 8 (range 10–45)
β^0 thalassemia	34
E/ β^0 thalassemia	18
Hb H-Constant Spring	1
Years on regular transfusions	18.7 \pm 6
β^0 thalassemia major (mean age 24 \pm 6)	19.7 \pm 6
E/ β^0 thalassemia (mean age 28 \pm 6)	17 \pm 5
Chelation treatment	
Mono therapy (DFX)	29 (55%)
Combination therapy (DFX & DFO)	24 (45%)
Systemic iron measures	
LIC (mg/g dw)	15 \pm 11
Cardiac T2* (ms)	27.2 \pm 10
Mean annual ferritin (μ g/L)	2620 \pm 2332
NTBI (μ mol/L)	1.9 \pm 1.3
LPI (μ mol/L)	0.25 \pm 0.5
Anterior pituitary	
R2 (s ⁻¹)	14.5 \pm 3
Z score of R2: Z(R2)	3.4 \pm 3.6
Pituitary Z(R2) > 2 (n=33; 62%)	5.4
Females' Z(R2)	3.2 \pm 4.4
Males' Z(R2)	3.7 \pm 4.5
Volume (mm ³)	377 \pm 110
Z score of volume: Z(V)	-2.0 \pm 1.2
Pituitary Z(V) < -2 (n=32; 60%)	-2.8
Females' Z(V)	-2.3 \pm 1.1
Males' Z(V)	-1.7 \pm 1.3
Spleen status	
Group I: splenectomized	17
Age (years)	31 \pm 6
Age at splenectomy (years)	15 \pm 8
Years since splenectomy	17 \pm 6
Z(R2) score	5.2 \pm 3
Z(V) score	-2.7 \pm 1
Cardiac T2* (ms)	21 \pm 11
LIC (mg/g dw)	17 \pm 11
Mean annual ferritin (μ g/L)	2982 \pm 2800
Group II: non-splenectomized	35
Age (years)	21 \pm 6
Z(R2) score	2.6 \pm 3
Z(V) score	-1.6 \pm 1
Cardiac T2* (ms)	30 \pm 9
LIC (mg/g dw)	14 \pm 11
Mean annual ferritin (μ g/L)	2450 \pm 2050

Two individuals died from iron overload complications during the study period. SD: standard deviation; DFX: deferasirox; DFO: deferoxamine; LIC: liver iron concentration; dw: dry weight; NTBI: non-transferrin bound iron; LPI: labile plasma iron; LIC and cardiac iron (T2) were obtained within 6 months of laboratory studies. Normal NTBI and LPI: not detectable.

splenectomy accelerates iron loading in the pituitary gland as previously reported to occur in the myocardium.³ To assess for a possible confounding effect of older age (mean 31±6 and 21±6 years in splenectomized *versus* non-splenectomized patients, respectively) a multivariable general linear model predicting $Z(V)$ was constructed. It showed that splenectomy was significant while age was not ($P=0.002$ and $P=0.218$, respectively).

Patients in the third decade of age had significantly higher pituitary iron accumulation than those in their second decade ($Z(R2)$ 4.9±3 vs. 1.1±2, $P<0.002$), paralleled by a decrease in pituitary volume, most apparent in the fourth decade of life (*Online Supplementary Figure S1*). These findings appear to be a decade later than in a prior study.⁴ It is possible that this difference is the consequence of improved adherence to treatment or greater efficacy of the oral chelation drug, deferasirox, used for extended periods by most of our patients. Indeed, two studies have shown stabilization of pre-existing hypogonadism, and a low rate of new endocrine disorders with long-term (5 and 6.5 years) chelation with deferasirox.^{9,10} However, further longitudinal study is needed to assess the effect of chelation regimens on pituitary iron.

Pituitary MRI findings in the 12 control patients were consistent with the published reference data used in this study.

The levels of gonadotropins (LH and FSH) were inversely correlated with pituitary iron load, $Z(R2)$, and directly correlated with anterior pituitary volume, $Z(V)$; LH/FSH levels declined with gland shrinkage (*Online Supplementary Figure S2*). Ten of 24 post-pubertal women reported regular menstrual periods (group I) and 14 had primary or secondary amenorrhea (group II). LH and FSH concentrations were normal in group I and significantly lower in group II ($P<0.04$ and $P<0.005$, respectively). Pituitary iron load and pituitary volume also differed significantly between the two groups ($P<0.03$ and $P<0.006$, respectively) (Figure 1B). These findings suggest low reproductive potential among women in group II, as also indicated by low AMH levels (Table 2), signifying compromised oocyte count⁶ and diminished reproductive potential. AMH, a key marker of ovarian reserve, has been reported to be positively associated with pregnancy and live birth rates after assisted reproduction. Its validity in TDT women was demonstrated and it serves as a prognostic factor for the probability of pregnancy when gonadotropin secretion is compromised.^{11,12}

Men who received testosterone supplementation (group II) had lower LH and FSH levels compared to men who did not (group I); $P<0.03$ and $P<0.001$, respectively. Although testosterone treatment could contribute to the low levels, our findings indicate that the main causes are pituitary iron toxicity and volume loss since $Z(R2)$ and $Z(V)$ differed significantly between the two groups ($P<0.02$ and $P<0.0002$, respectively). Such low FSH levels, as observed in group II (1.3 mIU), are associated with low spermatogenesis as also shown in thalassemic men with severe iron overload.¹³ Furthermore, the levels of inhibin B, a sensitive marker for male infertility, differed significantly between these two cohorts ($P<0.03$) and were lower than the reported mean level in men with normal fertility parameters. The concentration of inhibin B was below the 10th percentile in 8/26 men (31%), in a range that considerably decreases the likelihood of retrieving testicular spermatozoa.¹⁴

Cardiac iron, in addition to strongly correlating with pituitary iron, had an optimal cutoff for predicting a pituitary iron threshold associated with reduced volume and

loss of function; area under the curve (AUC) = 0.96, $P=0.009$ (Figure 1C). The close association between cardiac and pituitary iron might be caused by the additional cellular iron uptake through L-type Ca^{2+} channels.¹⁵ Fifteen of 16 patients with a $T2^*<20$ ms had a $Z(R2)>4.0$ while only 5/35 with a $T2^*>20$ ms had a $Z(R2)>4.0$ ($P<0.006$). Therefore, adult patients with a $T2^*<20$ ms are at risk of a decline in fertility potential, but assessing fertility markers even before this cardiac $T2^*$ threshold is recommended. LIC and ferritin concentration were less predictive of pituitary iron load; the AUC for these were 0.76 and 0.80, respectively, possibly because of the greater variation in liver and plasma iron. We found no correlation of pituitary iron with non-transferrin bound iron or labile plasma iron.

The effect of chelation over time has not been examined before. We conducted a second measurement ($n=17$) after an interval of 2.6±1 years which demonstrated decreases in systemic iron: LIC by 46±20%, ferritin by 44±21% and cardiac iron by 34±30% in 11, 10 and 12

Table 2. Patients' fertility and hormone data.

Characteristics	N (%) or mean (± SD)
Females[^]	24
Group I: regular menses	10 (42%)
Age (years)	20±5
LH/FSH (mIU/mL)	8±7.5±2
Estradiol (pg/mL)	84±75
AMH (ng/mL)	4±3.5
Pituitary $Z(R2)$ score	1.3
Pituitary $Z(V)$ score	-1.7
Cardiac $T2^*$ (ms)	28±7
Group II: amenorrhea	14 (58%)
Age (years)	31±5
LH/FSH (mIU/mL)	2±2/2.9±3
Estradiol (pg/mL)	40±47
AMH (ng/mL)	1.6±1
Pituitary $Z(R2)$ score	5.1
Pituitary $Z(V)$ score	-2.9
Cardiac $T2^*$ (ms)	20±9
Pregnancies/live children	5/4
With assistant reproductive therapy	2
Males[^]	26
Group I: no testosterone treatment	16 (62%)
Age (years)	22±7
LH/FSH (mIU/mL)	3.7±2.7/4.5±2.4
Inhibin B (pg/mL)	140±69
Testosterone (ng/dL)	385±240
Pituitary $Z(R2)$ score	2.3
Pituitary $Z(V)$ score	-1.0
Cardiac $T2^*$ (ms)	30±7
Father of a child	3
With assistant reproductive therapy	3
Group II: on testosterone replacement treatment	10 (38%)
Age (years)	28±6
LH/FSH (mIU/mL)	1.5±1.8/1.3±1.6
Inhibin B (pg/mL)	80±55
Pituitary $Z(R2)$ score	5.7
Pituitary $Z(V)$ score	-2.7
Cardiac $T2^*$ (ms)	23±8

[^]Levels of estradiol and testosterone from patients receiving hormone replacement were excluded from analysis. LH: luteinizing hormone; FSH: follicle-stimulating hormone; AMH: anti-Müllerian hormone. Normal ranges: AMH in fertile women, 1.0–4.0 ng/mL; Inhibin B in adult men, 125–215 pg/mL (both change with age)

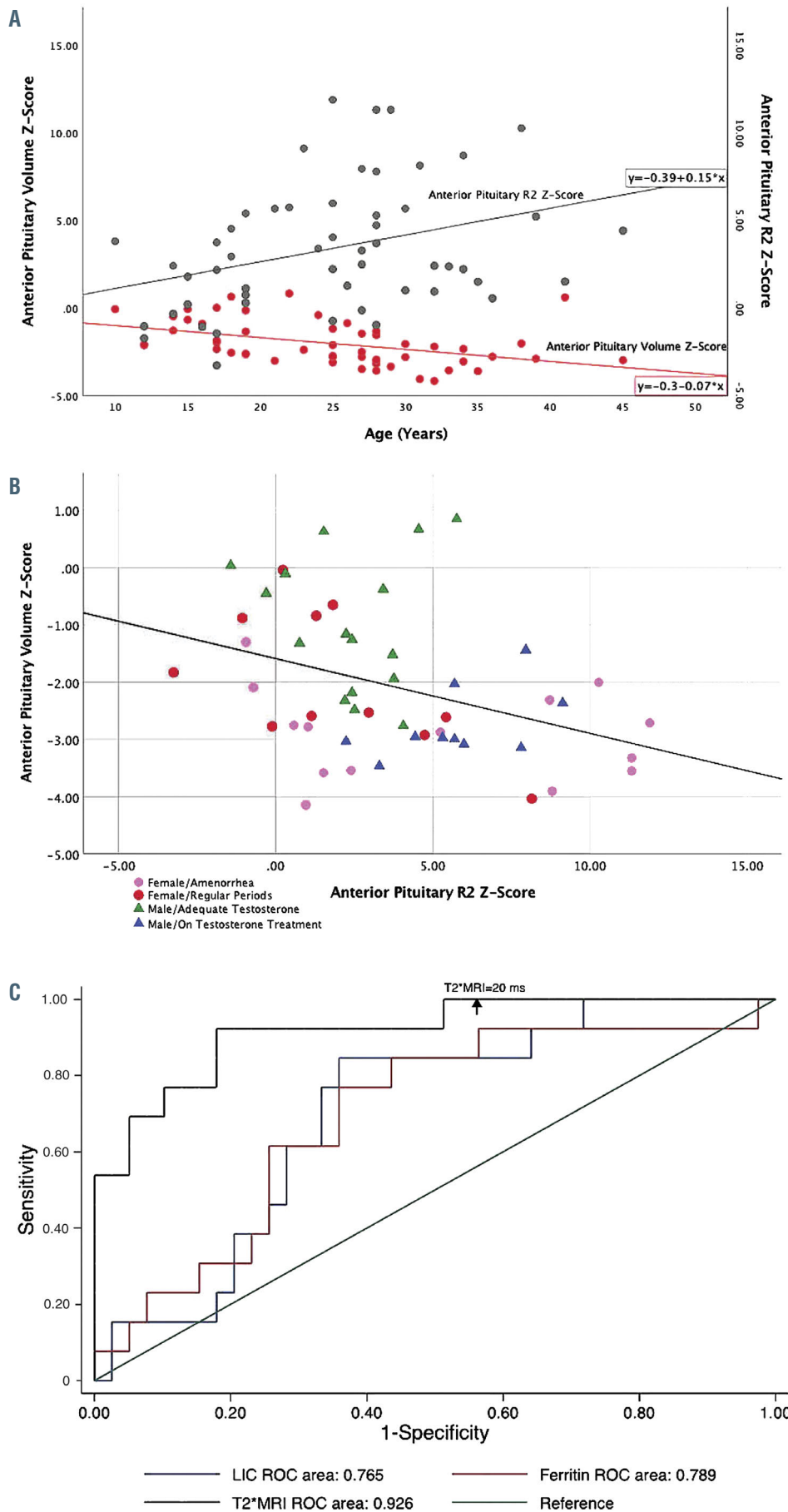


Figure 1. Pituitary iron and volume, relation to hormonal status and to systemic iron. (A) Z scores of pituitary R2 and volume (V) as a function of age in the 53 chronically transfused patients. Pituitary iron and volume are inversely correlated ($r = -0.36$; $P < 0.02$). (B) Distribution by gender and hormonal/reproductive status (based on groups I and II shown in the Tables). The majority of group I patients (men with adequate endogenous testosterone and women with regular periods, represented as green triangles and red circles, respectively) have only moderately elevated pituitary iron accumulation and small changes in pituitary volume; Z scores 0 to 5.0 and 0 to -3.0, respectively. Men requiring testosterone treatment (blue triangles) and women with amenorrhea (pink circles) (group II) had more severe pituitary iron loading and more notable gland shrinkage. (C) Receiver-operating characteristic (ROC) curves for the prediction of pituitary iron show that cardiac T2* correlates strongly with pituitary iron. Liver iron and ferritin concentrations are weakly predictive, the cardiac T2* is superior to both of these measures. The point of cardiac T2* = 20 ms is shown. This value was the optimal cutoff for predicting abnormal pituitary iron; ROC area = 0.93.

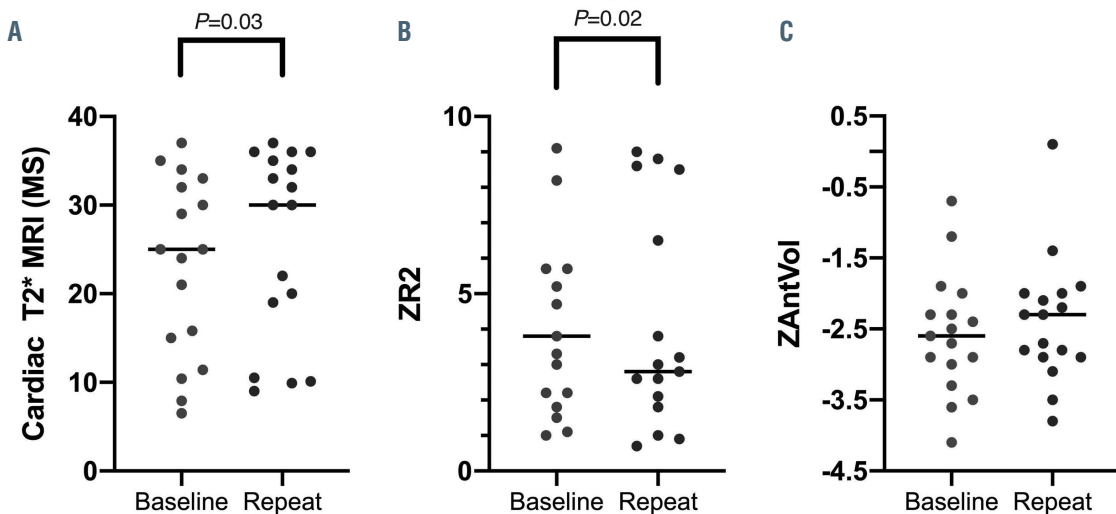


Figure 2. Effect of chelation on pituitary iron and volume. A longitudinal study (mean 2.6 years) showed a significant decrease in pituitary iron ($P<0.02$) correlating with an improvement in cardiac iron ($P<0.03$). The change in pituitary volume was minimal, as expected to be irreversible, and not statistically significant.

patients, respectively. Results were stable or worse in the remaining ones. A parallel improvement in pituitary $Z(R2)$ was noted in 9/17 (53%) individuals, whose mean baseline $Z(R2)$ was 6.4 (Figure 2). The change was modest in those with a baseline $Z(R2) > 8$, suggesting chelation failure in severe pituitary iron load. Eight of the nine patients with improved $Z(R2)$ also had a decrease in cardiac iron, again showing a good correlation of these two measures. Pituitary volume remained abnormally low in subsequent testing. The mean $Z(V)$ was -2.6 at baseline and -2.4 upon repeat imaging, confirming the irreversible cell destruction in patients with high iron burden. LH/FSH concentrations decreased by a mean of 28% at repeat testing in 7/8 women. AMH levels remained stable overall, supporting reports on preserved gonadal function and successful ovulation induction despite low LH and FSH levels. Longitudinal studies on a larger scale are needed to further explore these findings.

In summary, our data confirm previous pituitary MRI findings of iron and volume changes and risk thresholds for hypogonadism. Our study further highlights the high prevalence and progressive nature of pituitary iron loading, despite advances in chelation therapy, causing irreversible volume loss and deleterious effects on reproductive status. Splenectomy and older age are risk factors for these effects.

Our findings also validate cardiac T2*MRI as a proxy for pituitary $R2$, which can be used where pituitary MRI is not available. The findings also have implications for modifying chelation treatment, which is effective in mild-moderate cases in preventing or delaying infertility.¹⁶ Discussion of reproductive status, utilizing these hormonal and MRI findings, and informing patients of higher risk of infertility are prudent for proper planning of fertility preservation.

Sylvia T. Singer,¹ Roland Fischer,² Isabel Allen,³ Ashutosh Lal,¹ Elliott Vichinsky,¹ Qing Yuan⁴ and Zhiyue J. Wang⁴

¹Division of Hematology-Oncology, Department of Pediatrics, University of California San Francisco, UCSF Benioff Children's Hospital Oakland, Oakland, CA, USA; ²University Medical Center Hamburg-Eppendorf (UKE), Hamburg, Germany; ³University of California San Francisco, San Francisco, CA, USA and ⁴University of Texas Southwestern Medical Center, Texas, TX, USA

Correspondence:

SYLVIA T. SINGER - *sylvia.singer@UCSF.edu*

doi:10.3324/haematol.2020.252726

Received: March 23, 2020.

Accepted: October 9, 2020.

Pre-published: October 29, 2020.

Disclosures: no conflicts of interest to disclose.

Contributions: STS designed and performed the study, analyzed results and wrote the paper; ZJW and QY analyzed patients' images and pituitary data; RF reviewed and analyzed the data and reviewed and revised the manuscript; IEA performed the statistical analysis; AL and EV reviewed and revised the paper.

References

1. Wood JC. Estimating tissue iron burden: current status and future prospects. *Br J Haematol*. 2015;170(1):15-28.
2. Wood JC. Use of magnetic resonance imaging to monitor iron overload. *Hematol Oncol Clin North Am*. 2014;28(4):747-764, vii.
3. Noetzli LJ, Panigrahy A, Hyderi A, Dongelyan A, Coates TD, Wood JC. Pituitary iron and volume imaging in healthy controls. *AJNR Am J Neuroradiol*. 2012;33(2):259-265.
4. Noetzli LJ, Panigrahy A, Mittelman SD, Hyderi A, Dongelyan A, Coates TD, et al. Pituitary iron and volume predict hypogonadism in transfusional iron overload. *Am J Hematol*. 2012;87(2):167-171.
5. Wang ZJ, Wang DJ, Chia JM, Yuan Q, Morris MC, Rollins NK. A software tool for semi-automated quantification of pituitary volumes. International society of magnetic resonance imaging in medicine (ISMRM) 19th meeting. Montreal, Canada, 2011:4247.
6. La Marca A, Broekmans FJ, Volpe A, Fauzer BC, Macklon NS. Anti-Müllerian hormone (AMH): what do we still need to know? *Hum Reprod*. 2009;24(9):2264-2275.
7. Yalçı S, Gurbuz B, Fıcicioğlu C. Serum levels of inhibin B in men and their relationship with gonadal hormones, testicular volume, testicular biopsy results and sperm parameters. *J Obstet Gynaecol*. 2002;22(6):649-654.
8. Aydinok Y, Bayraktaroglu S, Yıldız D, Alper H. Myocardial iron loading in patients with thalassemia major in Turkey and the potential role of splenectomy in myocardial siderosis. *J Pediatr Hematol Oncol*. 2011;33(5):374-378.
9. Poggi M, Sorrentino F, Pugliese P, et al. Longitudinal changes of endocrine and bone disease in adults with beta-thalassemia major receiving different iron chelators over 5 years. *Ann Hematol*. 2016;95(5):757-763.
10. Casale M, Citarella S, Filosa A, et al. Endocrine function and bone disease during long-term chelation therapy with deferasirox in patients with beta-thalassemia major. *Am J Hematol*. 2014;89(12):1102-1106.

11. Singer ST, Vichinsky EP, Gildengorin G, van Disseldorp J, Rosen M, Cedars MI. Reproductive capacity in iron overloaded women with thalassemia major. *Blood*. 2011;118(10):2878-2881.
12. Chang HH, Chen MJ, Lu MY, et al. Iron overload is associated with low anti-mullerian hormone in women with transfusion-dependent beta-thalassaemia. *BJOG*. 2011;118(7):825-831.
13. Singer ST, Killilea D, Suh JH, et al. Fertility in transfusion-dependent thalassemia men: effects of iron burden on the reproductive axis. *Am J Hematol*. 2015;90(9):E190-192.
14. Grunewald S, Glander HJ, Paasch U, Kratzsch J. Age-dependent inhibin B concentration in relation to FSH and semen sample qualities: a study in 2448 men. *Reproduction*. 2013;145(3):237-244.
15. Oudit GY, Trivieri MG, Khaper N, Liu PP, Backx PH. Role of L-type Ca²⁺ channels in iron transport and iron-overload cardiomyopathy. *J Mol Med (Berl)*. 2006;84(5):349-364.
16. Farmaki K, Tzoumari I, Pappa C, Chouliaras G, Berdoukas V. Normalisation of total body iron load with very intensive combined chelation reverses cardiac and endocrine complications of thalassemia major. *Br J Haematol*. 2010;148(3):466-475.

Antimicrobial resistance is a risk factor for mortality in adults with sickle cell disease

Sickle cell disease (SCD), an inherited red blood cell disorder caused by homozygous or compound heterozygous inheritance of mutations in the β -globin gene, affects 1 in 365 African Americans.¹ SCD is considered an immunodeficient state² and infectious complications are a major contributor to the morbidity and mortality.³ Newborn screening, penicillin prophylaxis, and pneumococcal vaccination have led to reductions in sepsis-related mortality and > 95% of children with SCD living in high-resource settings now survive into adulthood.⁴ Despite these measures, high rates of hospitalizations in SCD patients are characterized by fevers⁵ and 14–18% of deaths are attributed to infectious causes in contemporary SCD cohorts.³

Antimicrobial-resistant infections are a global public health crisis associated with high rates of morbidity, health-related costs, and death in the general population.⁶ Penicillin prophylaxis may be leading to changes in antimicrobial resistance patterns in SCD. In a cohort of SCD children, 71% of whom were receiving penicillin prophylaxis, nasopharyngeal carriage of penicillin-resistant *Streptococcus pneumoniae* was observed in 55% of isolates.⁷ Antimicrobial resistance patterns in SCD adults are less clear and their impact on survival are not well understood.

We conducted a longitudinal study to i) identify risk factors for multidrug resistant (MDR) infections in adults with SCD, ii) compare antimicrobial resistance patterns to 16,000 propensity score-matched African Americans,

and iii) determine the association of MDR infections on survival in SCD adults enrolled in a prospective registry at the University of Illinois at Chicago (UIC).

We analyzed 320 SCD patients receiving medical care at UIC Hospital between January 1, 2017 and April 14, 2020. The protocol was approved by the Institutional Review Board and all subjects provided written informed consent.

Baseline demographic, clinical, and laboratory variables were obtained at each patient's first outpatient visit during the study period from the Cerner Medical Systems. Central venous catheterizations and diabetes diagnosis were queried using pertinent 9th and 10th Procedure Coding system editions of the International Classification of Disease (ICD-9-PCS and ICD-10-PCS) during the study period (*Online Supplementary Table S1*). Pneumococcal conjugate vaccine (PCV13) and pneumococcal polysaccharide vaccine (PPSV23) administration were queried during the 5 years prior to and including the study period. A blood culture contaminant was defined as a blood culture isolating coagulase-negative *Staphylococcus*, *Bacillus* species, *Corynebacterium* species, *Propionibacterium* species, or *Streptococcus viridans* group in less than 50% of simultaneously ordered cultures or in only one positive culture result.⁸ Organisms were considered to be multidrug resistant if the isolate organism was non-susceptible to three or more categories of antibiotics according to the European Center for Disease Prevention and Control (ECDC) and the Centers for Disease Control and Prevention (CDC) guidelines.⁹

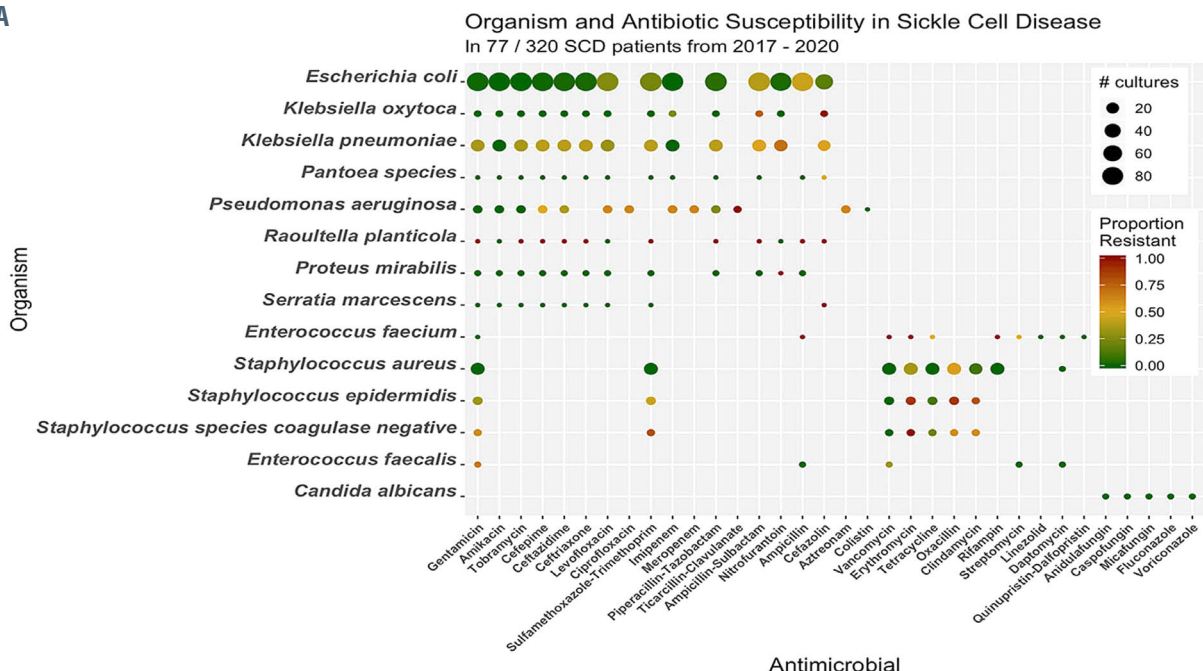
Between January 1, 2017 and April 14, 2020, 34,612 adults with culture data and race classified as "black" or

Table 1. Clinical and laboratory values stratified by infection status in patients with sickle cell disease.

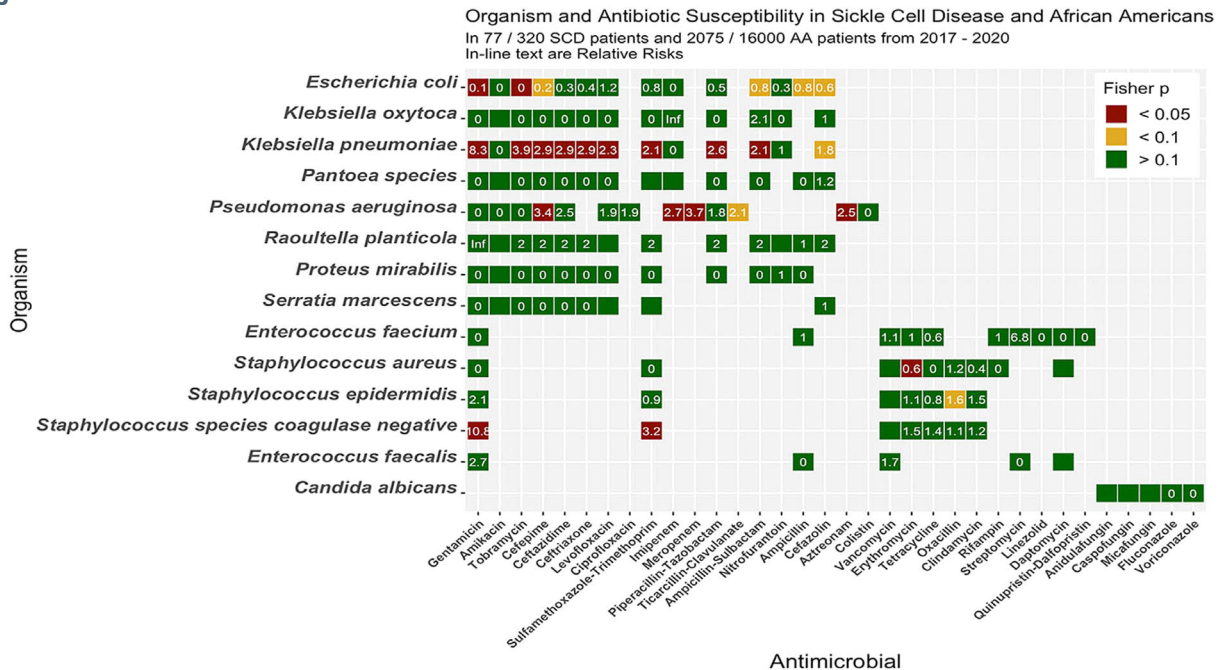
	n	No or non-MDR Infection	n	MDR Infection	P
Age at first encounter (years)	299	37 (29 - 48)	21	36 (31 - 50)	0.8
Male (%) / Female (%)	299	124 (41%) / 175 (59%)	21	3 (14%) / 18 (86%)	0.014
HbSS/SB0-thalassemia genotype	299	225 (75%)	21	18 (86%)	0.3
Hydroxyurea use (%)	299	130 (43%)	21	9 (43%)	0.9
Diabetes diagnosis (%)	299	23 (8%)	21	3 (14%)	0.3
Leg ulcer diagnosis (%)	295	35 (12%)	21	1 (5%)	0.3
Avascular necrosis diagnosis (%)	295	93 (32%)	21	10 (48%)	0.1
Pneumococcal vaccinations (%) [*]					
13-valent	299	189 (63%)	21	15 (71%)	0.4
23-valent		179 (60%)		7 (33%)	0.017
Systolic blood pressure (mmHg)	274	124 (113 - 135)	20	120 (112 - 131)	0.4
White blood cell count ($\times 10^3/\mu\text{L}$)	260	9.4 (7.0 - 12.3)	18	11.2 (9.1 - 12.4)	0.1
Hemoglobin (g/dL)	260	9.3 (8.1 - 10.6)	18	9.0 (8.4 - 9.4)	0.5
Hemoglobin F (%)	165	5.8 (2.2 - 11.0)	15	2.3 (1.9 - 4.2)	0.05
Platelet count ($\times 10^3/\mu\text{L}$)	260	295 (207 - 374)	18	400 (244 - 439)	0.1
Reticulocyte count ($\times 10^3/\mu\text{L}$)	250	174 (120 - 271)	16	234 (156 - 354)	0.07
Lactate dehydrogenase (u/L)	184	305 (230 - 405)	13	333 (287 - 428)	0.3
Ferritin (ng/mL)	182	339 (89 - 1076)	12	839 (332 - 2779)	0.08
eGFR (ml/min/1.73 m ²)	253	124 (95 - 141)	17	106 (55 - 141)	0.6
Central venous catheters (n)	299	64 (21%)	21	10 (48%)	0.006
Vaso-occlusive crises (n/year)	299	2 (0 - 4)	21	3 (1 - 6)	0.1
Acute chest syndrome history (%)	299	213 (71%)	21	18 (86%)	0.2
Heart failure (%)	186	6 (3%)	13	0 (0%)	0.5

Heart failure was defined as an ejection fraction < 50%; *The prevalence of pneumococcal vaccinations was assessed within the last 5 years of the study period. $P < 0.003$ was considered statistically significant after the Bonferroni correction. MDR: multi-drug resistant; eGFR: estimated glomerular filtration rate.

A



B



C

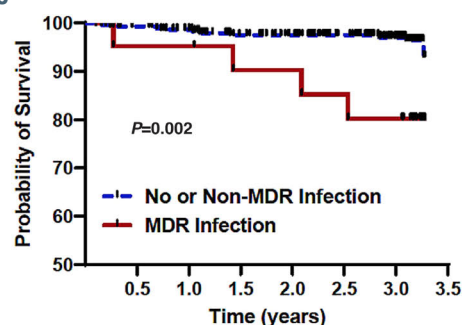


Figure 1. Antibiotic resistance patterns and its effect on survival patterns in patients with sickle cell disease. (A) Antibiotic resistance patterns in patients with sickle cell disease (SCD); (B) a comparison of antibiotic resistance patterns in patients with SCD versus African Americans without SCD (relative risks are provided in each box); (C) survival patterns by infection status in patients with SCD.

“African American” were identified through the UIC Cerner Medical Systems. Those with an ICD-9/10 code of SCD were excluded from this cohort. The African American cohort of 16,000 patients used in our analyses were chosen by propensity score, matched to the SCD cohort at a 50:1 ratio for age, sex, and follow-up time using the Matchit R analytic software package by the nearest-neighbor matching algorithm.¹⁰

Baseline characteristics at the time of study initiation were compared by MDR status using the Kruskal-Wallis and Chi-square or Fisher’s exact test for linear and categorical variables, respectively. Median and interquartile range (IQR) are provided. A final multivariate logistic regression model was fit by stepwise variable selection of variables with $P<0.1$ in the univariate analysis, adjusting for the following covariates: age, sex, sickle cell genotype, and hydroxyurea use. Fisher’s exact test was used to compare MDR status between SCD and AA patients for each specific antimicrobial-organism pair. Relative risk (RR) was calculated as the ratio of the proportional resistance between the SCD and AA groups. Survival was analyzed by MDR status using Kaplan-Meier curves and Cox Proportional Hazards models, adjusting for the following covariates: age, sex, SCD genotype, and hydroxyurea use. For patients lost to follow-up, MDR status and survival were censored at the date of last known contact. The survival time was defined as the period between January 1, 2017 and either the date of patient’s death or last known encounter up to April 14, 2020.

Baseline characteristics of the SCD and AA cohort were similar for age, sex, and follow-up time (Online Supplementary Table S2). Between January 1, 2017 and April 14, 2020, we observed 176 non-recurrent positive cultures, defined as not occurring within 30 days of a previous culture with an identical organism and source,¹¹ in 77 of 320 (24.1%) SCD patients (Online Supplementary Table S3). The total infection rate in SCD patients was 205.0 infections per 1,000-person-years. We observed 3,968 non-recurrent positive cultures in 2,075 of 16,000 (13.0%) AA patients, for a total infection rate of 92.8 infections per 1,000-person-years ($P<0.001$).

An MDR infection was observed in 27.3% (21 of 77) of SCD and 33.3% (692 of 2,075) of AA patients ($P=0.3$) with an infection. Baseline differences in the SCD patients by MDR status are provided in Table 1. There were no SCD adults on penicillin prophylaxis during the study period. Female sex (OR 5.9, 95% Confidence Interval [CI]: 1.6–21.7; $P=0.007$) and central venous catheter placement (OR 4.3, 95%CI: 1.6–11.5; $P=0.004$) were independently associated with an increased MDR infection risk and PPSV23 vaccination was associated with a reduced risk (OR 0.2, 95%CI: 0.1–0.6; $P=0.003$), adjusting for age, SCD genotype and hydroxyurea use.

Antimicrobial resistance patterns for antimicrobial-organism pairs in SCD patients are provided in Figure 1A and Online Supplementary Table S4. Antimicrobial resistance was observed in 11.4% (135 of 1,050) of unique *Escherichia coli* infections, including 26.1% (23 of 88 tested) resistant to levofloxacin, 22.7% (20 of 88 tested) to sulfamethoxazole-trimethoprim, and 2.4% (2 of 82 tested) to nitrofurantoin. *Klebsiella pneumoniae* and *Pseudomonas aeruginosa* were highly resistant to several antibiotic groups, with the exception of amikacin and imipenem for *Klebsiella pneumoniae* and amikacin for *Pseudomonas aeruginosa*. Oxacillin-resistant *Staphylococcus aureus* was observed in 53.8% of infections. Both coagulase-negative *Staphylococcus epidermidis* and *Staphylococcus* species were highly resistant to most antibiotic groups except for vancomycin. We observed

only one *Staphylococcus pneumoniae* infection, which was resistant to penicillin.

A comparison of resistance patterns between SCD and AA patients are provided in Figure 1B. *Escherichia coli* infections were less commonly resistant, while *Klebsiella pneumoniae* and *Pseudomonas aeruginosa* infections were typically more resistant to antibiotics in SCD versus AA patients.

During the 3-year study period, 14 of 320 (4.4%) SCD patients died; ten of 299 (3.3%) without and four of 21 (19.0%) with an MDR infection (Figure 1C). Sepsis was a contributing factor to the cause of mortality in eight of ten deaths with a known etiology. Developing an MDR infection was an independent risk factor for death (Hazard Ratio [HR] 4.9, 95%CI: 1.5–16.4; $P=0.009$), adjusting for age, sex, SCD genotype and hydroxyurea use.

In the era of penicillin prophylaxis, we observed higher rates of infection but a similar prevalence of MDR infections in SCD adults compared to AA. This suggests that penicillin prophylaxis may be altering colonization and infection patterns but not drug resistance patterns for gram-positive infections in SCD adults. Vaccination with PPSV23 reduces exposure to antimicrobial drugs and is associated with less resistance to erythromycin, trimethoprim-sulfamethoxazole, and cephalosporins in the general population.¹² We observed high rates of resistance to trimethoprim-sulfamethoxazole and erythromycin in gram-positive bacterial infections. Furthermore, vaccination with PPSV23 was associated with a 5-fold lower risk of having an MDR infection. In the general population, approximately 20–67% of central-line associated infections are MDR infections.¹³ In our cohort, central venous catheter line placement, which is often required for pain management or for exchange transfusion therapy in SCD, was associated with a 4-fold greater risk of developing an MDR infection. Alternative strategies for administering pain medications, such as inhaled routes, and better implementation of protective measures, such as the use of chlorhexidine for skin preparation, avoiding femoral vein catheters, and the use of anti-septic barrier caps,¹⁴ may help reduce MDR infection rates in SCD. The association of female sex with a higher MDR infection rate may be due to the increased risk for urinary tract infections in females. Other potential biological differences, such as the effects of sex hormones and X-chromosome genes on immune response regulation, may also be contributing to the observed differences.¹⁵

Limitations of our study include being a single-center study and not taking into account the specific antimicrobial therapies used to treat the infections. Investigating the effects of socioeconomic status and health behavior may highlight modifiable risk factors to improve vaccination rates in SCD. Health care utilization is a likely contributor to developing antibiotic resistance, and therapies that reduce hospitalizations may be another approach to reduce MDR infections. Future strategies to reduce the spread of antibiotic resistance, such as greater implementation of PPSV23 and strategies to reduce central venous catheter placement, may help decrease the morbidity and early mortality observed in SCD.

Andrew Srisuwananukorn,¹ Jin Han,^{1,2} Rasha Raslan,³ Michel Gowhari,¹ Faiz Hussain,¹ Franklin Njoku,¹ Robert E. Molokie,^{1,4} Victor R. Gordeuk¹ and Santosh L. Saraf¹

¹Sickle Cell Center, Department of Medicine, University of Illinois at Chicago, Chicago, IL, USA; ²Department of Pharmacy Practice, College of Pharmacy, University of Illinois at Chicago, Chicago, IL,

USA; ³Department of Internal Medicine, Virginia Commonwealth University Medical Center, Richmond, VA, British Columbia, Canada and ⁴Department of Medicine, Jesse Brown VA Medical Center, Chicago, IL, USA

Correspondence: SANTOSH L. SARAF - ssara@uic.edu
doi:10.3324/haematol.2020.267872

Received: July 23, 2020.

Accepted: October 12, 2020.

Pre-published: October 29, 2020.

Disclosures: no conflicts of interest to disclose.

Contributions: AS and SLS designed and performed research, analyzed the data, and wrote the paper; JH, RR, MG, FH, FN, REM, and VRG designed and performed research and wrote the paper.

Funding: the project described was supported by the National Institutes of Health through grants R03 HL-146788, and R01 HL-153161 (SLS). The content is solely the responsibility of the authors and does not necessarily represent the official views of the NIH.

References

1. Hassell KL. Population estimates of sickle cell disease in the U.S. *Am J Prev Med.* 2010;38(4 Suppl):S512-521.
2. Battersby AJ, Knox-Macaulay HH, Carroll ED. Susceptibility to invasive bacterial infections in children with sickle cell disease. *Pediatr Blood Cancer.* 2010;55(3):401-406.
3. Darbari DS, Wang Z, Kwak M, et al. Severe painful vaso-occlusive crises and mortality in a contemporary adult sickle cell anemia cohort study. *PLoS One.* 2013;8(11):e79923.
4. Quinn CT, Rogers ZR, McCavit TL, Buchanan GR. Improved survival of children and adolescents with sickle cell disease. *Blood.* 2010; 115(17):3447-3452.
5. Rogovik AL, Friedman JN, Persaud J, Goldman RD. Bacterial blood cultures in children with sickle cell disease. *Am J Emerg Med.* 2010; 28(4):511-514.
6. CDC. Antibiotic resistance threats in the United States. www.cdc.gov/DrugResistance/Biggest-Threatshtml. 2019.
7. Daw NC, Wilimas JA, Wang WC, et al. Nasopharyngeal carriage of penicillin-resistant *Streptococcus pneumoniae* in children with sickle cell disease. *Pediatrics.* 1997;99(4):e7.
8. Chulamokha L, Scholand SJ, Riggio JM, Ballas SK, Horn D, DeSimone JA. Bloodstream infections in hospitalized adults with sickle cell disease: a retrospective analysis. *Am J Hematol.* 2006; 81(10):723-728.
9. Magiorakos AP, Srinivasan A, Carey RB, et al. Multidrug-resistant, extensively drug-resistant and pandrug-resistant bacteria: an international expert proposal for interim standard definitions for acquired resistance. *Clin Microbiol Infect.* 2012;18(3):268-281.
10. Ho DE, Imai K, King G, Stuart EA. MatchIt: nonparametric preprocessing for parametric causal inference. *J Stat Softw.* 2011;42(8):1-28.
11. Woudt SHS, de Greeff SC, Schoffelen AF, Vlek ALM, Bonten MJM. Infectious Diseases Surveillance Information System-Antimicrobial Resistance Study Group. Antibiotic resistance and the risk of recurrent bacteremia. *Clin Infect Dis.* 2018;66(11):1651-1657.
12. Centers for Disease Control and Prevention. Prevention of pneumococcal disease: recommendations of the Advisory Committee on Immunization Practices (ACIP). 1997 Apr 4;46(RR-8):1-24.
13. Burnham JP, Rojek RP, Kollef MH. Catheter removal and outcomes of multidrug-resistant central-line-associated bloodstream infection. *Medicine.* 2018;97(42):e12782.
14. Chaftari AM, Hachem R, Jiang Y, et al. Changing epidemiology of catheter-related bloodstream infections in cancer patients. *Infect Control Hosp Epidemiol.* 2018;39(6):727-729.
15. van Lunzen J, Altfeld M. Sex differences in infectious diseases-common but neglected. *J Infect Dis.* 2014;209(Suppl 3):S79-80.

Rapid decline in estimated glomerular filtration rate in sickle cell anemia: results of a multicenter pooled analysis

Chronic kidney disease (CKD), typically defined as kidney damage or decreased kidney function for 3 or more months, is common in sickle cell disease (SCD).¹ Increasing evidence suggests that the glomerulopathy of SCD is progressive.² CKD is associated with increased mortality in SCD.³ Based on single center studies, we previously reported on the high prevalence of rapid decline in kidney function, defined as estimated glomerular filtration rate (eGFR) loss >3.0 mL/min/1.73 m² per year, in SCD.^{4,6} In the present study, we further examine rapid eGFR decline in sickle cell anemia, using a pooled analysis of patients to better characterize factors associated with such decline and its association with mortality.

Patients from four centers, University of North Carolina at Chapel Hill (UNC), Duke University Medical Center (Duke), University of Illinois at Chicago (UIC), and St. Jude Children's Research Hospital/Methodist University Comprehensive Sickle Cell Center (Methodist) were analyzed.^{4,5,7,8} Patients, at least 18 years old, with sickle cell anemia, were evaluated during routine visits while in "steady state". Baseline visit was defined as the first available serum creatinine measurement during the study period. Only patients with two or more measures of kidney function over the observation period were included. Mortality during the observation period was assessed by medical record review and/or by utilizing the US Social Security Death Index. Approvals were obtained from Institutional Review Boards at each institution.

Estimated GFR was calculated using the creatinine-based chronic kidney disease epidemiology collaboration (CKD-EPI) equation.⁹ Rapid decline of kidney function was defined as eGFR loss of >3.0 mL/min/1.73 m² per year¹⁰ or eGFR loss of >5.0 mL/min/1.73 m² per year.¹¹ Rapid decline of kidney function, using these thresholds, was ascertained based on the slope in a linear model, with eGFR as the response and time as the covariate, using all available observations from a patient. The slope was defined as the estimate of the regression coefficient for time. CKD progression was defined as a decline in eGFR to <90 mL/min/1.73m² and at least 25% decline from baseline,¹¹ or eGFR decline to <90 mL/min/1.73m² and at least 50% decline from baseline or requiring renal replacement therapy.¹²

Variables of interest were summarized by median and interquartile ranges (IQR) if continuous, or by counts and percentages if categorical. In order to evaluate eGFR change over time, a linear mixed effects model with subject level random effects for intercept and slope for time was fitted, adjusting for baseline age, sex and cohort. Stratified analyses according to hyperfiltration at baseline were conducted. Logistic regression analyses were employed to evaluate variables associated with rapid decline in eGFR. In multivariable analyses, variables associated with rapid decline in eGFR with P-values <0.3 in individual analyses, but without an excess of missing data (<20% missing data), were included in the initial model. Cox regression analyses were employed to evaluate the association of rapid decline in eGFR with mortality, from the period of first eGFR assessment to the last assessment.

The analysis included 606 individuals with sickle cell anemia (HbSS, HbSβ⁰), 236 from UNC (followed from 2004 – 2013), 203 from Duke (followed from 2002 –

2016), 94 from UIC (followed from 2009 – 2017) and 73 from Methodist (followed from 2006 – 2017). The median observation period was 5.20 years (IQR: 1.56-7.53), with 31,286 patient-years of observation. The median patient age in the pooled analysis was 27 years (IQR: 20-38) and 327 (54.0%) were female (Table 1). Baseline laboratory and clinical data in individual cohorts are shown in the *Online Supplementary Table S1*. In evaluating the change in eGFR over time in the pooled analysis, only the main cohort effect was retained as the time-cohort interaction was not significant ($P=0.19$). For all patients, the change in eGFR over time, adjusted for baseline age, sex and main cohort effect, was -2.36 mL/min/1.73 m² per year (95% Confidence Interval [CI]: -2.68 to -2.04; $P<0.0001$) (Figure 1A). In patients with hyperfiltration, the time-cohort interaction was significant ($P=0.008$), so both main cohort and interaction effects were retained. The estimated change in eGFR over time for patients with hyperfiltration, without consideration of the time-cohort interaction, was -2.09 mL/min/1.73 m² per year (95% CI: -2.50 to -1.69; $P<0.0001$). In patients without hyperfiltration, the time-cohort interaction was not significant ($P=0.97$),

Table 1. Baseline demographic, laboratory and clinical variables in pooled patient cohorts with sickle cell anemia.

Variable	Total Number	Median (IQR) /Number (%)
Age (years)	606	27 (20, 38)
Sex (female)	606	327 (54.0)
Weight (kg)	556	65.8 (57.7, 75.3)
Height (cm)	246	169.5 (163.0, 175.5)
White Blood Cell Count (x10 ⁹ /L)	564	10.5 (7.9, 13.0)
Hemoglobin (g/dL)	564	8.8 (7.8, 9.9)
Hematocrit (%)	562	26.0 (22.8, 29.0)
Reticulocyte Count (x10 ⁹ /L)	464	258.7 (179.0, 364.6)
Platelet Count (x10 ⁹ /L)	558	416 (310.7, 523.0)
Baseline eGFR (mL/min/1.73m ²)	606	143.9 (120.4, 159.7)
Blood Urea Nitrogen (mg/dL)	320	8.0 (6.0, 11.0)
Total Bilirubin (mg/dL)	530	2.4 (1.5, 4.0)
Direct Bilirubin (mg/dL)	214	0.3 (0.2, 0.5)
Ferritin (ng/mL)	328	524.5 (159.5, 1308.0)
Hemoglobinuria (Yes)	363	70 (19.3)
Proteinuria* (Yes)	305	73 (23.9)
Albumin-Creatinine Ratio (mcg/mg)	20	82.5 (23.5, 295.5)
Hemoglobin F (%)	370	7.7 (3.6, 14.2)
H/O Acute Chest Syndrome (Yes)	568	416 (73.2)
H/O Stroke (Yes)	555	104 (18.7)
H/O Leg Ulcers (Yes)	533	88 (16.5)
H/O Priapism** (Yes)	201	81 (40.3)
H/O Avascular Necrosis (Yes)	426	152 (35.7)
Systolic Blood Pressure (mm Hg)	578	118 (109, 128)
Diastolic Blood Pressure (mm Hg)	578	68 (61, 74)
H/O Diabetes (Yes)	558	11 (2.0)
Chronic RBC Transfusion (Yes)	577	58 (10.1)
Hydroxyurea Therapy (Yes)	604	321 (53.2)
RAAS Blocking Agents (Yes)	329	38 (11.6)

*Proteinuria – at least 1+ by dipstick urinalysis; **Male patients only. eGFR: estimated glomerular filtration rate; RAAS: blocking agents: renin-angiotensin-aldosterone system blocking agents (Angiotensin-converting enzyme inhibitors and angiotensin receptor blockers); IQR: interquartile range.

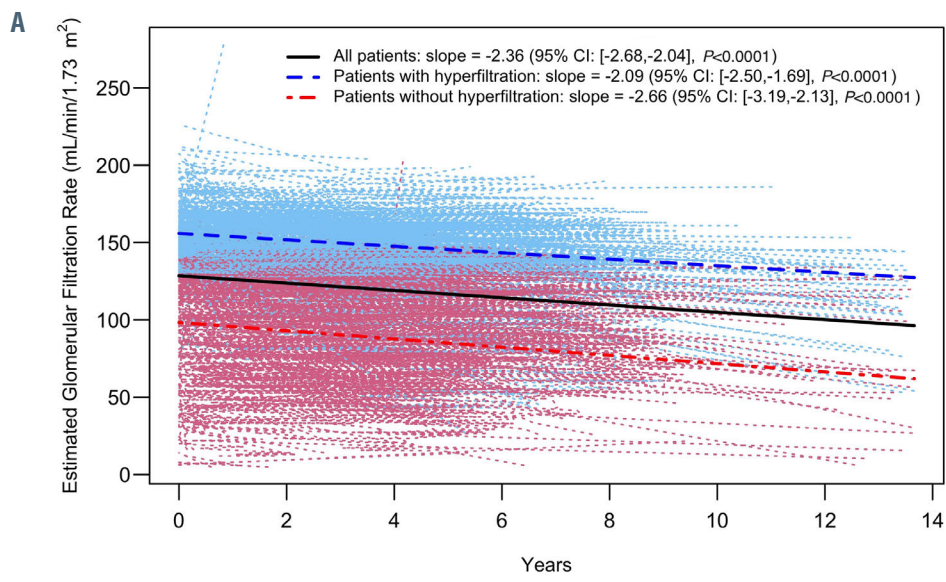
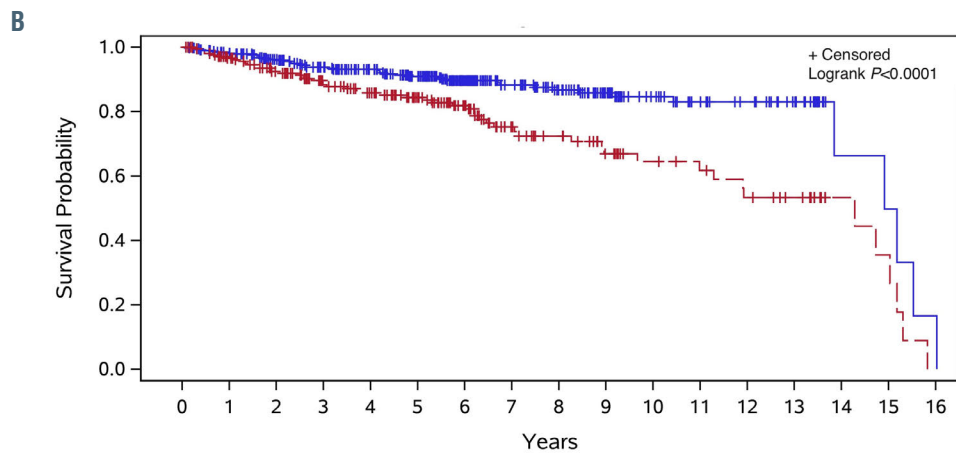
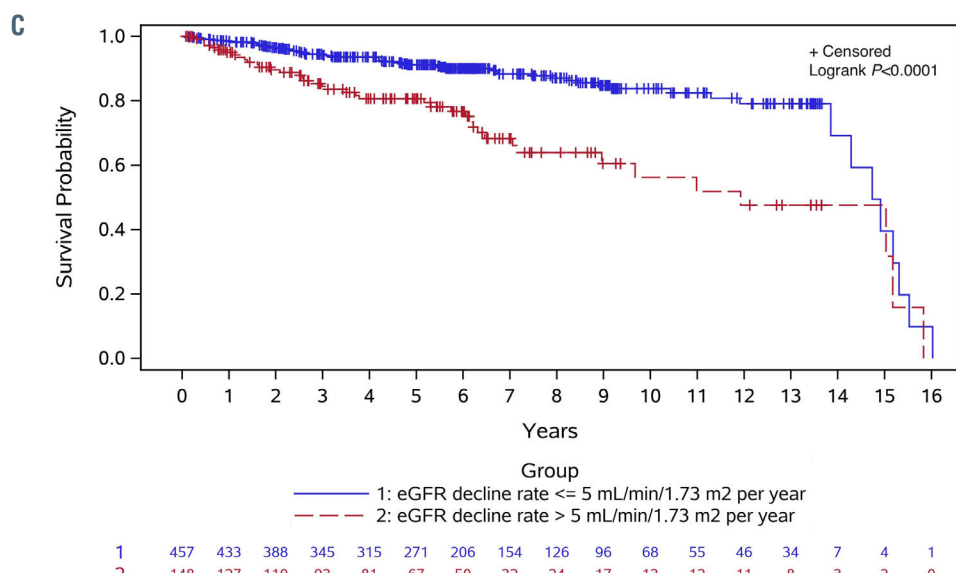


Figure 1. The slope of estimated glomerular filtration rate (eGFR) decline in sickle cell anemia and the association of rapid eGFR decline with mortality in the pooled population are shown. (A) The change in eGFR over time, adjusted for baseline age, sex and main cohort effect, was $-2.36 \text{ mL/min}/1.73 \text{ m}^2$ per year (95% Confidence Interval [CI]: -2.68 to -2.04 ; $P < 0.0001$). (B) Kaplan-Meier estimates of the survival probabilities for rapid ($>3.0 \text{ mL/min}/1.73 \text{ m}^2$ per year) and non-rapid eGFR decline groups (log-rank test; $P < 0.0001$). (C) Kaplan-Meier estimates of the survival probabilities for rapid ($>5.0 \text{ mL/min}/1.73 \text{ m}^2$ per year) and non-rapid eGFR decline groups (log-rank test; $P < 0.0001$). The number of patients at risk at each time point are shown in (B) and (C).



1	390	368	327	294	267	231	172	131	105	79	55	44	38	27	4	3	1
2	215	192	171	144	129	107	84	55	45	34	26	23	19	15	6	4	0



1	457	433	388	345	315	271	206	154	126	96	68	55	46	34	7	4	1
2	148	127	110	93	81	67	50	32	24	17	13	12	11	8	3	3	0

hence only the main cohort effect was retained. The change in eGFR over time was $-2.66 \text{ mL/min/1.73 m}^2 \text{ per year}$ (95%CI: -3.19 to -2.13 ; $P<0.0001$).

Rapid decline of kidney function, defined as eGFR loss $>3.0 \text{ mL/min/1.73 m}^2 \text{ per year}$, was observed in 216 patients (35.6%), and in 149 patients (24.6%) when defined as eGFR loss $>5.0 \text{ mL/min/1.73 m}^2 \text{ per year}$ (*Online Supplementary Table S2*). CKD progression was observed in 130 of 606 patients (21.5%), defined as eGFR decline to $<90 \text{ mL/min/1.73 m}^2$ and at least 25% decline from baseline, and in 55 of 606 patients (9.1%) defined as eGFR decline to $<90 \text{ mL/min/1.73 m}^2$ and at least 50% decline from baseline. Using a threshold of $>3.0 \text{ mL/min/1.73 m}^2 \text{ per year}$, 96 of 216 patients (44.4%) with rapid decline had CKD progression defined as $\geq 25\%$ eGFR decline from baseline, while 48 of 216 patients (22.2%) had CKD progression defined as $\geq 50\%$ eGFR decline from baseline. Using a threshold of $>5.0 \text{ mL/min/1.73 m}^2 \text{ per year}$, 76 of 149 patients (51.0%) with rapid decline had CKD progression defined as $\geq 25\%$ eGFR decline from baseline, while 43 of 149 patients (28.9%) had CKD progression defined as $\geq 50\%$ eGFR decline from baseline.

The association of baseline variables with rapid eGFR decline ($>3.0 \text{ mL/min/1.73 m}^2 \text{ per year}$) in the pooled population was examined (Table 2). Adjusted for cohort, we observed significantly increased odds of rapid decline with increasing age and male sex. Adjusted for age, sex, and cohort, there were significantly lower odds of rapid decline with higher hemoglobin and hematocrit. The odds of rapid decline in kidney function were significantly increased with higher levels of direct bilirubin and ferritin, as well as hemoglobinuria, history of stroke and use of ACE inhibitors/angiotensin receptor blockers.

Adjusted for cohort, we similarly observed significantly increased odds of rapid decline, using a threshold of $>5.0 \text{ mL/min/1.73 m}^2 \text{ per year}$, with increasing age (Table 2). Adjusted for age, sex, and cohort, there were lower odds of rapid decline with higher hemoglobin and hematocrit. The odds of rapid decline were significantly increased with higher baseline blood urea nitrogen, direct bilirubin and ferritin, as well as hemoglobinuria, proteinuria, and history of stroke. Associations of covariates with rapid decline in individual cohorts are shown in the *Online Supplementary Table S3*. Using a

Table 2. Association of clinical and laboratory variables with rapid decline of eGFR in pooled patient cohorts with sickle cell anemia.

Variable*	Rapid decline based on $>3.0 \text{ mL/min/1.73 m}^2$ threshold		Rapid decline based on $>5.0 \text{ mL/min/1.73 m}^2$ threshold	
	Odds ratio (95% CI)	P	Odds ratio (95% CI)	P
Age**	1.03 (1.01, 1.04)	0.0011	1.02 (1.003, 1.04)	0.02
Sex (Male)**	1.40 (1.0, 1.96)	0.05	1.25 (0.86, 1.82)	0.24
White Blood Cell Count	0.99 (0.94, 1.03)	0.52	0.99 (0.95, 1.04)	0.80
Hemoglobin	0.89 (0.79, 0.996)	0.042	0.80 (0.70, 0.92)	0.0012
Hematocrit	0.96 (0.92, 0.995)	0.029	0.93 (0.89, 0.98)	0.0029
Reticulocyte Count	1.0 (0.999, 1.001)	0.99	1.001 (0.999, 1.002)	0.39
Platelet Count	0.999 (0.998, 1.0)	0.14	0.999 (0.998, 1.001)	0.36
Baseline eGFR	1.0 (0.99, 1.01)	0.91	0.997 (0.991, 1.004)	0.44
Blood Urea Nitrogen	1.04 (0.99, 1.08)	0.054	1.06 (1.01, 1.098)	0.0089
Total Bilirubin	1.02 (0.95, 1.09)	0.58	1.05 (0.98, 1.13)	0.21
Direct Bilirubin	1.74 (1.01, 2.97)	0.044	1.99 (1.15, 3.43)	0.013
Indirect Bilirubin	1.02 (0.90, 1.16)	0.72	0.98 (0.85, 1.13)	0.79
Ferritin*	1.02 (1.01, 1.03)	0.0037	1.02 (1.01, 1.03)	0.0037
Hemoglobinuria	2.16 (1.24, 3.78)	0.007	3.20 (1.79, 5.73)	<0.0001
Proteinuria*	1.68 (0.94, 2.99)	0.08	2.48 (1.34, 4.58)	0.0037
Albumin-Creatinine Ratio**	1.0 (0.998, 1.003)	0.80	1.0 (0.998, 1.003)	0.77
Hemoglobin F	0.99 (0.96, 1.02)	0.42	0.99 (0.96, 1.02)	0.48
Weight	1.0 (0.99, 1.01)	0.94	0.996 (0.98, 1.01)	0.55
H/O Acute Chest Syndrome	1.25 (0.82, 1.92)	0.30	1.45 (0.90, 2.35)	0.13
H/O Stroke	2.13 (1.36, 3.34)	0.001	1.77 (1.09, 2.88)	0.021
H/O Leg Ulcers	1.29 (0.77, 2.17)	0.33	1.31 (0.74, 2.32)	0.35
H/O Avascular Necrosis	0.92 (0.59, 1.43)	0.70	0.77 (0.47, 1.28)	0.32
Systolic Blood Pressure	1.01 (0.99, 1.02)	0.31	1.01 (0.99, 1.02)	0.33
Diastolic Blood Pressure	1.01 (0.99, 1.02)	0.44	1.01 (0.99, 1.02)	0.60
H/O Diabetes	0.95 (0.26, 3.47)	0.94	0.65 (0.13, 3.19)	0.60
Chronic RBC Transfusion	1.47 (0.81, 2.68)	0.20	1.39 (0.74, 2.64)	0.31
Hydroxyurea Therapy	1.28 (0.90, 1.83)	0.18	1.20 (0.81, 1.79)	0.37
RAAS Blocking Agents	2.17 (1.04, 4.53)	0.04	1.88 (0.86, 4.09)	0.11

*Results adjusted for age, sex and cohort effects, except that **are adjusted only for cohort effects; RAAS blocking agents: renin-angiotensin-aldosterone system blocking agents (Angiotensin-converting enzyme inhibitors and angiotensin receptor blockers); *proteinuria (at least 1+ by dipstick urinalysis); **available in only the UIC cohort; *odds ratio is provided for 100 ng/mL increase in ferritin.

threshold of >3.0 mL/min/1.73 m² per year, multivariable analysis showed significant associations of rapid decline with age (odds ratio [OR]: 1.03, 95%CI: 1.01-1.04; $P=0.003$), male sex (OR: 1.58, 95%CI: 1.09-2.29; $P=0.016$), and history of stroke (OR: 1.99, 95%CI: 1.25-3.15; $P=0.004$). Using a threshold of >5.0 mL/min/1.73 m² per year, significant associations were observed between rapid decline and hemoglobin (OR: 0.83, 95%CI: 0.72-0.96; $P=0.009$) as well as history of stroke (OR: 1.72, 95%CI: 1.03-2.86; $P=0.038$).

Ninety-eight of 605 patients died during the observation period. Adjusted for age, sex, white blood cell count, hemoglobin, baseline eGFR and use of hydroxyurea, rapid eGFR decline, at thresholds of >3.0 mL/min/1.73 m² per year and >5.0 mL/min/1.73 m² per year, was associated with increased mortality risk (hazard ratio [HR]: 2.41, 95%CI: 1.57-3.69; $P<0.0001$ and HR: 2.90, 95%CI: 1.87-4.48; $P<0.0001$, respectively). Kaplan-Meier estimates showed significantly lower survival probabilities for patients with rapid eGFR decline using both decline thresholds (log-rank test; $P<0.0001$) (Figures 1B and C).

In this multicenter analysis, we confirm accelerated eGFR loss over time in adults with sickle cell anemia, with an average eGFR loss of 2.36 mL/min/1.73 m² per year, representing a faster kidney function decline than is reported in African American adults.¹³ The observed decline in this pooled cohort is similar to that in patients with diabetes, who have reported eGFR declines of 2.1 and 2.7 mL/min/1.73 m² per year, respectively, for women and men.¹⁴ We also confirm the high prevalence of rapid eGFR decline, as well as its impact on survival. Regardless of the threshold, >3.0 mL/min/1.73 m² or >5.0 mL/min/1.73 m² per year, rapid decline is more frequent in sickle cell anemia than the reported prevalence of 10.5% after 12 years in the African American population.¹³ Much like in patients with diabetes,¹⁵ male sex was a significant risk factor for rapid eGFR decline. This is consistent with the finding in a multicenter, observational study, which reported faster kidney function decline in males with SCD.¹⁶

In age-, sex- and cohort-adjusted analysis, we observed an association of proteinuria with rapid decline of kidney function. However, proteinuria was not included in the multivariable analysis due to severe lack of data. Albuminuria is a known risk factor for progression of CKD.²

Increased hemoglobin was associated with a lower risk of rapid eGFR decline. Although not evaluated in the multivariable analysis due to substantial missing data, hemoglobinuria has previously been shown to be associated with albuminuria and CKD progression, suggesting an important role for intravascular hemolysis in the pathogenesis of SCD-related kidney disease.¹⁷ Based on the role of intravascular hemolysis, drugs that decrease hemolysis may prevent or slow the progression of kidney disease in SCD.

Our study is limited by lack of data for several important variables. Approximately 40% of patients had only two eGFR evaluations, which may have had an impact on the estimated change in eGFR over time. Most patients did not have urine albumin-creatinine ratios, limiting assessment of the role of albuminuria.

In conclusion, this pooled analysis confirms the high prevalence of rapid decline in kidney function in adults with sickle cell anemia. The association of rapid decline in kidney function with increased mortality highlights the need for early identification of individuals at risk for such decline.

Kenneth I. Ataga,¹ Qingning Zhou,² Vimal K. Derebail,³ Santosh L. Saraf,⁴ Jane S. Hankins,⁵ Laura R. Loehr,⁶ Melanie E. Garrett,⁷ Allison E. Ashley-Koch,⁷ Jianwen Cai⁸ and Marilyn J. Telen⁹

¹Center for Sickle Cell Disease, University of Tennessee Health Sciente Center, Memphis, TN; ²Department of Mathematics and Statistics, University of North Carolina, Charlotte, NC; ³Division of Nephrology and Hypertension, University of North Carolina, Chapel Hill, NC; ⁴Division of Hematology/Oncology, University of Illinois, Chicago, IL; ⁵Department of Hematology, St. Jude Children's Research Hospital, Memphis, TN; ⁶Division of General Medicine and Clinical Epidemiology, University of North Carolina, Chapel Hill, NC; ⁷Duke Molecular Physiology Institute, Duke University Medical Center, Durham, NC; ⁸Department of Biostatistics, University of North Carolina, Chapel Hill, NC and ⁹Division of Hematology, Duke University Medical Center, Durham, NC, USA

Correspondence: KENNETH I. ATAGA - kataga@uthsc.edu

doi:10.3324/haematol.2020.267419

Received: July 17, 2020.

Accepted: October 23, 2020.

Pre-published: November 12, 2020.

Disclosures: KIA has received funding from the US FDA (R01FD006030), Novartis, and Global Blood Therapeutics, served on advisory boards for Novartis, Global Blood Therapeutics, Novo Nordisk and Editas Medicine, and as a consultant for Roche. Dr. Derebail has received funding from the US FDA (R01FD006030), has served on advisory boards for Novartis and Retrophin. SLF has received research funding from Novartis, Global Blood Therapeutics and Pfizer and served as a consultant role for Global Blood Therapeutics and advisory board for Novartis. JSH receives research funding from Global Blood Therapeutics, and consultant fees from Global Blood Therapeutics and MJ Lifesciences. MJT has served on steering committees and advisory committees for Pfizer, GlycoMimetics, Novartis, and Forma Therapeutics. JC has received funding from the FDA (R01FD006030). KIA, VKD, LL, JC received funding for the study from the US Food and Drug Administration (R01FD006030).

Contributions: KIA designed the study, analyzed the data and wrote the manuscript; QZ and JC analyzed the data, and assisted in study design and manuscript preparation; MEG assisted in data analysis and manuscript preparation; VKD, SLS, JSH, LRL, AEA-K and MJT assisted in study design, data analysis and manuscript preparation.

Funding: funding for the study was provided by the US Food and Drug Administration, R01FD006030 (KIA, VKD, LL, JC).

References

1. Ataga KI, Derebail VK, Archer DR. The glomerulopathy of sickle cell disease. *Am J Hematol*. 2014;89(9):907-914.
2. Gosmanova EO, Zaidi S, Wan JY, Adams-Graves PE. Prevalence and progression of chronic kidney disease in adult patients with sickle cell disease. *J Investig Med*. 2014;62(5):804-807.
3. Thrower A, Ciccone EJ, Maitra P, et al. Effect of renin-angiotensin-aldosterone system blocking agents on progression of glomerulopathy in sickle cell disease. *Br J Haematol*. 2019;184(2):246-252.
4. Xu JZ, Garrett ME, Soldano KL, et al. Clinical and metabolomic risk factors associated with rapid renal function decline in sickle cell disease. *Am J Hematol*. 2018;93(12):1451-1460.
5. Derebail VK, Ciccone EJ, Zhou Q, et al. Progressive decline in estimated GFR in patients with sickle cell disease: an observational Cohort Study. *Am J Kidney Dis*. 2019;74(1):47-55.
6. Derebail VK, Zhou Q, Ciccone EJ, et al. Rapid decline in estimated glomerular filtration rate is common in adults with sickle cell disease and associated with increased mortality. *Br J Haematol*. 2019;186(6):900-907.
7. Saraf SL, Viner M, Rischall A, et al. HMOX1 and acute kidney injury in sickle cell anemia. *Blood*. 2018;132(15):1621-1625.

8. Hankins JS, Estepp JH, Hodges JR, et al. Sickle Cell Clinical Research and Intervention Program (SCCRIP): a lifespan cohort study for sickle cell disease progression from the pediatric stage into adulthood. *Pediatr Blood Cancer*. 2018;65(9):e27228.
9. Levey AS, Stevens LA, Schmid CH, et al. A new equation to estimate glomerular filtration rate. *Ann Intern Med*. 2009;150(9):606-612.
10. Rifkin DE, Shlipak MG, Katz R, et al. Rapid kidney function decline and mortality risk in older adults. *Arch Intern Med*. 2008;168(20):2212-2218.
11. Levin A, Stevens PE. Summary of KDIGO 2012 CKD Guideline: behind the scenes, need for guidance, and a framework for moving forward. *Kidney Int*. 2014;85(1):49-61.
12. Feldman HI, Appel LJ, Chertow GM, et al. The Chronic Renal Insufficiency Cohort (CRIC) Study: design and methods. *J Am Soc Nephrol*. 2003;14(7 Suppl 2):S148-153.
13. Young BA, Katz R, Boulware LE, et al. Risk factors for rapid kidney function decline among African Americans: the Jackson Heart Study (JHS). *Am J Kidney Dis*. 2016;68(2):229-239.
14. Hemmelgarn BR, Zhang J, Manns BJ, et al. Progression of kidney dysfunction in the community-dwelling elderly. *Kidney Int*. 2006;69(12):2155-2161.
15. de Hauteclercque A, Ragot S, Slaoui Y, et al. The influence of sex on renal function decline in people with Type 2 diabetes. *Diabet Med*. 2014;31(9):1121-1128.
16. Olaniran KO, Allegretti AS, Zhao SH, et al. Kidney function decline among black patients with sickle cell trait and sickle cell disease: an observational cohort study. *J Am Soc Nephrol*. 2020;31(2):393-404.
17. Saraf SL, Zhang X, Kanas T, et al. Haemoglobinuria is associated with chronic kidney disease and its progression in patients with sickle cell anaemia. *Br J Haematol*. 2014;164(5):729-739.

Serum monoclonal component in chronic lymphocytic leukemia: baseline correlations and prognostic impact

The first report analyzing the presence of a serum monoclonal component (sMC) in patients with lymphoid malignancies was published in 1957.¹ Since then, the identification of a sMC in other lymphoid neoplasms has awakened interest, mainly due to its relationship with B-cell biology and its adverse prognostic impact in some entities, such as diffuse large B-cell lymphoma.²⁻⁴ To date, five reports have employed serum immunofixation electrophoresis (sIFE) to study the presence of a sMC in chronic lymphocytic leukemia (CLL).⁵⁻¹⁰ In the largest of these studies, containing 133 patients, Xu and colleagues reported a prevalence of 20%, and correlated the presence of a sMC with advanced stage, adverse prognostic features, and worse overall survival (OS).⁹ To our knowledge, the present study represents the largest series analyzing the prevalence and prognostic impact of a sMC in CLL. Found in 30% of patients at diagnosis, it is associated with clinical, biological and genetic adverse prognostic features, and shorter OS and relative survival, with a comparable time to first treatment (TTFT), risk of Richter syndrome (RRS), and risk of second malignancies (RSM).

We studied 548 patients diagnosed with CLL (n=340), CLL-type monoclonal B-cell lymphocytosis (MBL, n=108), or small lymphocytic lymphoma (SLL, n=93) at a single institution between 1997 and 2018, with available data on sIFE at diagnosis. The study was conducted according to the Hospital Clínic de Barcelona Institutional Review Board and in accordance with the Declaration of Helsinki. Serum protein electrophoresis

(sPEP) and sIFE were performed at diagnosis in all patients. A non-measurable sMC was defined as a positive sIFE but normal sPEP. A biclonal sIFE was defined as the presence of two heavy or light chains on the sIFE. Immunoparesis was defined as a decreased level of at least one of the three immunoglobulin (Ig) classes. Light chains were considered concordant if the light chains of the sIFE matched the light chain restriction by flow cytometry of the peripheral blood and/or bone marrow.

In order to estimate TTFT, RRS and RSM, in which death without the primary event is possible, cumulative incidence was calculated (cmprsk package, R software, Vienna, Austria) and compared by use of Gray's test. In order to compare the OS observed in our cohort with that of the general population, patients were matched by age and sex with Spanish individuals from the Human Mortality Database,¹¹ which provides an estimate of the cause-specific survival through relative survival analysis (relsurv package, R software, Vienna, Austria). Excess mortality (also called survival reduction), expressed as a percentage, was calculated with the following formula: [1-(cohort survival/population survival)] x 100, and was intended to reflect the reduction in life expectancy with respect to the general population. Variables that had a significant impact on OS were used to construct a multi-variate Cox proportional hazards regression model. *P*-values <0.05 were considered to indicate statistical significance.

Baseline characteristics of the patients are shown in Table 1. One hundred and sixty-five patients (30%) had a +sIFE at diagnosis. Patients with a +sIFE were significantly older (median age 70 years [y] vs. 66 y, *P*=0.007), and the prevalence of a +sIFE increased with age. Patients diagnosed with SLL had a higher prevalence of a +sIFE

Table 1. Baseline characteristics of the patients

Characteristic	All patients (n=548)	Negative (n=383, 70%)	Serum immunofixation Positive (n=165, 30%)	<i>P</i>
Age in years, median (range)	67 (30-97)	66 (30-92)	70 (32-97)	0.007
Male sex, n (%)	324 (59)	223 (58)	101 (61)	NS
ECOG PS ≥1, n (%)	44 (9)	19 (5)	25 (16)	<0.001
Lymphadenopathy (CT), n (%)	191 (57)	125 (52)	66 (70)	0.003
B symptoms, n (%)	20 (4)	13 (4)	7 (5)	NS
Binet stage C, n (%)	26 (5)	12 (3)	14 (9)	0.007
Rai stage III-IV, n (%)	30 (6)	12 (3)	18 (11)	<0.001
β2-microglobulin above ULN, n (%)	257 (48)	158 (42)	99 (62)	<0.001
FISH [n=493 (90%)]				0.032
normal, n (%)	145 (29)	105 (31)	40 (26)	
del(13q), n (%)	203 (41)	146 (43)	57 (37)	
+12, n (%)	75 (15)	51 (15)	24 (16)	
del(11q), n (%)	49 (10)	229 (9)	20 (13)	
del(17p), n (%)	21 (4)	9 (3)	12 (8)	
Unmutated <i>IGHV</i> genes, n (%) [n=333 (61%)]	139 (42)	87 (37)	52 (53)	0.009
Abnormal <i>ATM</i> gene, n (%) [n=237 (43%)]	17 (7)	11 (6)	6 (9)	NS
Mutated <i>NOTCH1</i> gene, n (%) [n=288 (53%)]	31 (11)	19 (9)	12 (15)	NS
Mutated <i>SF3B1</i> gene, n (%) [n=276 (50%)]	26 (9)	17 (9)	9 (12)	NS
Abnormal <i>TP53</i> gene, n (%) [n=268 (49%)]	20 (8)	14 (7)	6 (8)	NS
Abnormal <i>BIRC3</i> gene, n (%) [n=102 (19%)]	1 (1)	1 (1)	0	NS
Mutated <i>MYD88</i> gene, n (%) [n=102 (19%)]	4 (4)	3 (4)	1 (3)	NS

ECOG PS: Eastern Cooperative Oncology Group Performance Status; CT: computed tomography; ULN: upper limit of normal; FISH: fluorescence *in situ* hybridization; NS: not statistically significant.

(45% vs. 27% and 25% for CLL and MBL, respectively). The presence of a +sIFE was associated with a worse Eastern Cooperative Oncology Group performance status (ECOG PS), higher frequency of lymphadenopathy, more advanced Binet and Rai stages, and higher β_2 -microglobulin (B2M) levels (62 vs. 42%, $P<0.001$). The distribution of fluorescence *in situ* hybridization (FISH) abnormalities was significantly different according to the sIFE, with a higher frequency of favorable-risk FISH in -sIFE patients, and of high-risk abnormalities in +sIFE patients ($P=0.032$). Likewise, the proportion of patients with unmutated immunoglobulin heavy chain gene (IGHV) genes was significantly higher among patients with a +sIFE (53 vs. 37%, $P=0.009$). No significant differences were seen in the mutation/deletion rate of *ATM*, *NOTCH1*, *SF3B1*, *TP53*, *MYD88*, or *BIRC3* according to the sIFE.

The proportion of patients with immunoparesis did not differ according to the sIFE. Among the 165 patients with a +sIFE at diagnosis, IgM- κ was the most common isotype (25%), followed by IgG- κ (22%), and IgG- λ (21%). The frequency of other isotypes was: IgM- λ (8%), IgA- κ (2%), IgA- λ (2%), κ free-light chains (κ -FLC, 1%), λ -FLC (6%), and bi/tryclonal (11%). Among the cases in which the quantification of the sMC was available for review, most had a non-measurable sMC (positive sIFE but normal sPEP). In the remaining eight cases, the median sMC was 4.3 g/L (range, 2–9.8). The information between the light chain of the serum Ig and the light chain restriction by flow cytometry was compared in 132 cases with a +sIFE: 72% were concordant and 28% were discordant. When concordance was further analyzed considering the sIFE isotype, it was found to be higher for IgM cases (89%). Protein and immunochemical features

Table 2. Treatment, response, and outcomes.

Characteristic	All patients	Serum immunofixation		P
		Negative	Positive	
10-y probability of requiring treatment, % (95% CI)	49 (44–54)	48 (42–53)	52 (43–60)	NS
Frontline treatment [n=230 (42%)], n (%)				NS
Alkylating agents +/- rituximab	62 (27)	44 (29)	18 (24)	
Purine analogs	41 (18)	27 (18)	14 (19)	
Purine analogs + rituximab	64 (28)	42 (28)	22 (29)	
Novel agents	26 (11)	16 (11)	10 (13)	
Others	35 (15)	24 (16)	11 (15)	
Complete response, n (%)	101 (56)	67 (55)	34 (58)	NS
10-y overall survival, % (95% CI)	52 (47–58)	57 (51–64)	42 (34–52)	0.003
10-y risk of Richter syndrome, % (95% CI)	3 (2–5)	3 (2–6)	3 (1–7)	NS
10-y risk of second malignancies, % (95% CI)	23 (19–28)	23 (18–28)	24 (17–32)	NS

CI: confidence interval; NS: not statistically significant. y: years.

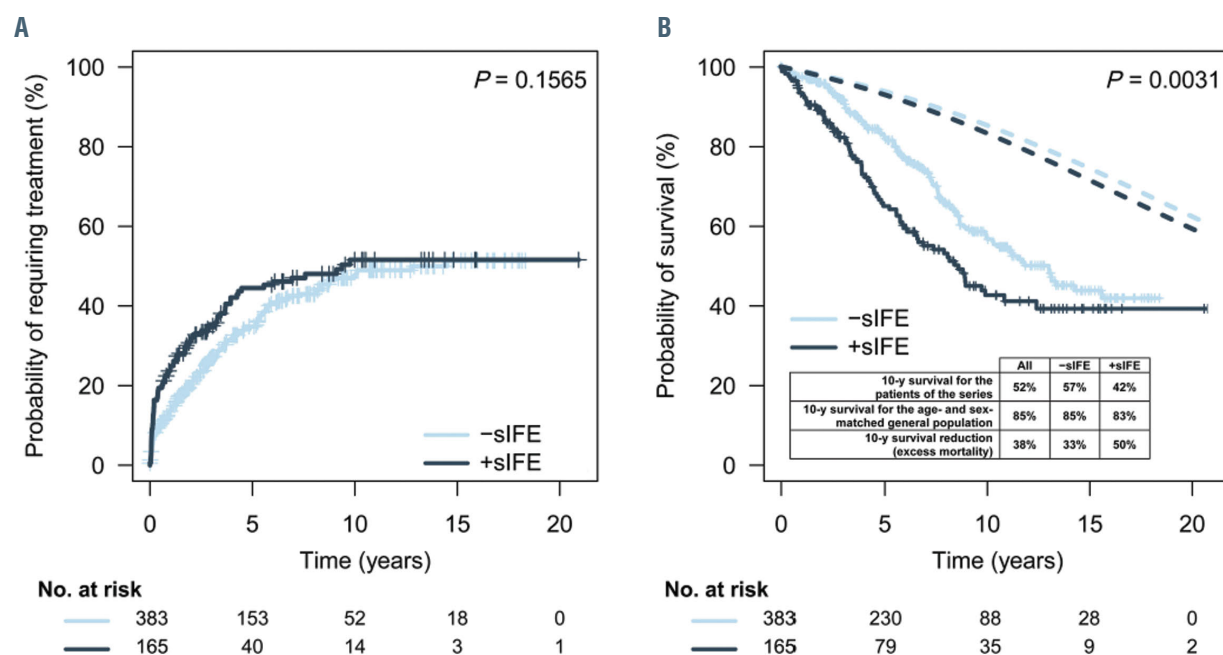


Figure 1. Outcomes according to serum immunofixation. (A) Time to first treatment. (B) Overall survival (continuous lines), and survival of the sex- and age-matched general population (dashed lines).

of the 165 patients with a +sIFE can be found in the *Online Supplementary Table S1*.

Frontline treatment, response, and outcomes are depicted in Table 2. Two-hundred and thirty (42%) patients received some treatment during follow-up. The median TTFT was 10 years, and no significant differences were seen according to the sIFE (Figure 1A). Frontline regimens were comparable between patients with a negative and positive sIFE, as was the proportion of patients achieving a complete response after treatment.

With a median follow-up of 6.7 years, median OS for the entire cohort was 10.9 years, being significantly shorter for +sIFE compared with -sIFE patients (8.5 vs. 11.9 years; 10-year OS: 42 vs. 57%; $P=0.003$, Figure 1B). When a two-variable Cox regression, including age (as a quantitative variable) and sIFE, was performed, we observed that both parameters retained independent prognostic impact on OS. Furthermore, despite being significantly older, relative survival analysis showed that excess mortality (survival reduction) with respect to the sex- and age-matched general population was more prominent for patients with a +sIFE (50% at 10 years) compared to that of patients with a -sIFE (33% at 10 years). In a multivariate model for OS, with 286 cases and 108 events (including age >60 years, ECOG PS ≥ 1 , elevated B2M, Rai stage III-IV, unmutatedIGHV genes, del(17p), CD38 expression $>30\%$, and a +sIFE), only age, ECOG PS, B2M, and IGHV status retained prognostic impact on OS.

When evaluating OS among patients with a +sIFE according to the heavy chain isotype, no global statistically significant differences were seen. However, when pairwise combinations were performed, biclonal cases had a significantly poorer OS (*Online Supplementary Figure S1A*), whereas the light chain isotype did not have a significant impact on OS (*Online Supplementary Figure S1B*). The presence of immunoparesis was evaluated in patients with +sIFE and -sIFE, and it was not an adverse prognostic factor for OS in either of the groups (*Online Supplementary Figure S2*). No significant differences were found between light chain-concordant and discordant cases with regard to OS. Richter syndrome was seen in 15 patients (3%). For the entire series, the 10-year RRS was 3% (95% Confidence Interval [CI]: 2–5%), without significant differences according to the sIFE (*Online Supplementary Figure S3A*). A second tumor was identified in 104 patients (19%), and no patient developed multiple myeloma. The 10-year risk of developing a SM was of 23% for all patients, with similar rates irrespective of sIFE (*Online Supplementary Figure S3B*).

In conclusion, we found a 30% prevalence of a +sIFE in our cohort of CLL patients, which is in line with previous studies.^{5–10} Patients with a +sIFE had a more advanced stage and clinical, radiological, biochemical, and genetic poor prognostic markers, as already reported.^{5,9,10} Contrary to previous data,^{9,10} however, we observed a clear relationship between a +sIFE and age. In our series, IgM-κ constituted the most common isotype, which is in accordance with the report by Xu and colleagues.⁹ Eleven percent of cases were biclonal, a finding that has been previously interpreted as: i) the malignant transformation occurring at the time of isotype switching from IgM to IgG,¹² ii) the persistent isotype switching capability of CLL cells, independently of IGHV mutation,¹³ iii) the presence of multiple simultaneous clonal lymphoproliferative disorders,¹⁴ or iv) the emergence of a subclone secreting a different Ig isotype, due to clonal evolution. The light chain concordance rate was 72%, pointing to

the fact that, in most cases, the sMC is a product directly secreted by the tumor population. It had been suggested that concordance was higher in the case of IgM proteins,¹⁵ and we obtained similar findings. Despite comparable TTFT, frontline regimens, and response, we demonstrated that a +sIFE is a predictor of a poorer OS and relative survival, irrespective of age. However, due to its association with other clinical and biological adverse prognostic features, the sIFE did not retain its negative impact in the multivariate analysis. Biclonal cases had a poorer prognosis, possibly reflecting a higher degree of immunological dysfunction.

The sIFE is positive in one in three CLL patients at diagnosis, and this finding is associated with adverse prognostic baseline features and shorter survival. The study of the sMC in CLL could be an aid to advance in the understanding of B-cell malignancies, anticipate patient outcomes, and eventually tailor therapy.

Pablo Mozas,^{1*} Juan A. Piñeyroa,^{1*} Ferran Nadeu,^{2,3} Laura Magnano,^{1,2} Andrea Rivero,¹ Alfredo Rivas-Delgado,¹ Alex Bataller,¹ Aleix Fabregat,⁴ Eva Giné,^{1,2} Tycho Baumann,¹ Neus Villamor,^{2,3,5} Juan Ignacio Aróstegui,⁶ Marta Aymerich,⁵ Armando López-Guillermo,^{1,2,3,7} Elías Campo,^{2,3,5,7} and Julio Delgado^{1,2,3}

¹Department of Hematology, Hospital Clínic, Barcelona; ²Institut d'Investigacions Biomèdiques August Pi i Sunyer (IDIBAPS), Barcelona; ³Centro de Investigación Biomédica en Red de Cáncer (CIBERONC), Madrid; ⁴Department of Biochemistry and Molecular Biology, Hospital Clínic, Barcelona; ⁵Hematopathology Unit, Department of Pathology, Hospital Clínic, Barcelona;

⁶Department of Immunology, Hospital Clínic, Barcelona and

⁷Universitat de Barcelona, Barcelona, Spain

*PM and JAP contributed equally as co-first authors.

Correspondence: PABLO MOZAS - mozas@clinic.cat

doi:10.3324/haematol.2020.263228

Received: June 17, 2020.

Accepted: October 23, 2020.

Pre-published: November 5, 2020.

Disclosures: no conflicts of interest to disclose.

Contributions: PM and JAP designed the study, collected and analyzed the data, and wrote the manuscript; FN, LM, AR, ARD, AB, AF, EG, TB, NV, JIA, MA, ALG, EC and JD contributed to data collection and reviewed the manuscript.

Funding: this study was supported by "Becas de Investigación de la FEHH" (Fundación Española de Hematología y Hemoterapia) to PM; FN received a pre-doctoral fellowship of the Ministerio de Economía y Competitividad (MINECO, BES-2016-076372); LM received the PI19/00925 grant (Instituto de Salud Carlos III); AL-G and EG received the PI19/00887 grant (Instituto de Salud Carlos III); EC is supported by grants from "La Caixa" Foundation (CLLEvolution-LCF/PR/HR17/52150017), the Instituto de Salud Carlos III, the European Regional Development Fund (FEDER – "Una Manera de Hacer Europa") (PMP15/00007), and is an Academia Researcher of the Institució Catalana de Recerca i Estudis Avançats (ICREA) of the Generalitat de Catalunya.

References

- Azar HA, Hill WT, Osserman EF. Malignant lymphoma and lymphatic leukemia associated with myeloma-type serum proteins. *Am J Med*. 1957;23(2):239–249.
- Cox MC, Di Napoli A, Scarpino S, et al. Clinicopathologic characterization of diffuse-large-B-cell lymphoma with an associated serum monoclonal IgM component. *PLoS One*. 2014;9(4):e93903.
- Li Y, Wang L, Zhu HY, et al. Prognostic significance of serum immunoglobulin paraprotein in patients with diffuse large B cell

lymphoma. *Br J Haematol.* 2018;182(1):131-134.

4. Papageorgiou SG, Thomopoulos TP, Spathis A, et al. Prognostic significance of monoclonal gammopathy in diffuse large B-cell lymphoma. *Hematol Oncol.* 2019;37(5):634-637.

5. Deegan M, Abraham J, Sawdyk M, Van Slyck E. High incidence of monoclonal proteins in the serum and urine of chronic lymphocytic leukemia patients. *Blood.* 1984;64(6):1207-1211.

6. Pangalis GA, Moutsopoulos HM, Papadopoulos NM, Costello R, Kokkinou S, Fessas P. Monoclonal and oligoclonal immunoglobulins in the serum of patients with b-chronic lymphocytic leukemia. *Acta Haematol.* 1988;80(1):23-27.

7. Hansen DA, Robbins BA, Bylund DJ, Piro LD, Saven A, Ellison DJ. Identification of monoclonal immunoglobulins and quantitative immunoglobulin abnormalities in hairy cell leukemia and chronic lymphocytic leukemia. *Am J Clin Pathol.* 1994;102(5):580-585.

8. Bernstein ZP, Fitzpatrick JE, O'Donnell A, Han T, Foon KA, Bhargava A. Clinical significance of monoclonal proteins in chronic lymphocytic leukemia. *Leukemia.* 1992;6(12):1243-1245.

9. Xu W, Wang YH, Fan L, et al. Prognostic significance of serum immunoglobulin paraprotein in patients with chronic lymphocytic leukemia. *Leuk Res.* 2011;35(8):1060-1065.

10. El-Hussiny, Ibrahim L, Azmy E, Shamaa S. Prognostic significance of serum monoclonal immunoglobulin in B-chronic lymphocytic leukemia. *Egypt J Haematol.* 2012;37(4):240.

11. University of California, Berkeley (USA) and MPI for DR (Germany). Human Mortality Database. Available at www.mortality.org

12. Sahota SS, Garand R, Bataille R, Smith AJ, Stevenson FK. V(H) gene analysis of clonally related IgM and IgG from human lymphoplasmacytoid B-cell tumors with chronic lymphocytic leukemia features and high serum monoclonal IgG. *Blood.* 1998;91(1):238-243.

13. Efremov DG, Ivanovski M, Batista FD, Pozzato G, Burrone OR. IgM-producing chronic lymphocytic leukemia cells undergo immunoglobulin isotype-switching without acquiring somatic mutations. *J Clin Invest.* 1996;98(2):290-298.

14. Sanchez ML, Almeida J, Gonzalez D, et al. Incidence and clinicobiologic characteristics of leukemic B-cell chronic lymphoproliferative disorders with more than one B-cell clone. *Blood.* 2003;102(8):2994-3002.

15. Qian GX, Fu SM, Solanki DL, Rai KR. Circulating monoclonal IgM proteins in B cell chronic lymphocytic leukemia: their identification, characterization and relationship to membrane IgM. *J Immunol.* 1984;133(6):3396-3400.

Homozygous Southeast Asian ovalocytosis in five live-born neonates

Southeast Asian ovalocytosis (SAO) is an autosomal dominant inherited red blood cell (RBC) membrane disorder caused by the heterozygous deletion of codons 400–408 in SLC4A1/band 3/anion exchanger 1 (AE1).¹ This deletion leads to misfolding of the protein, creating an inactive anion-transporter and altering the mechanical stability of the RBC. Heterozygous SAO is characterized by the presence of stomatocytes, theta cells (RBC with two stomas), macro-ovalocytes and ≥25% ovalocytes in the peripheral blood smears.² Although heterozygous SAO carriers are generally asymptomatic, homozygous SAO was considered to be lethal.³ However, one successful birth of a homozygous SAO individual, born to asymptomatic heterozygous SAO Comorian parents, was reported in 2014 showing an association with severe dyserythropoietic anemia.⁴ Here, we report the birth of five unrelated homozygous SAO babies in Malaysia showing that homozygous SAO is not as rare as previously thought. These babies belong to an SAO cohort collected from January 2007 to March 2020 at University Sains Malaysia (USM), which includes a total of 68 patients. The study was instigated to further understand the physiological implications of heterozygous SAO within the Malay population. The detection of numerous homozygous SAO births has highlighted the need for the development of good practice to support the survival of these babies.

SAO has a distinctive geographical distribution, occurring mostly in areas of Southeast Asia including neighboring regions of the Malay Peninsula, coastal regions of Papua New Guinea, Thailand, Indonesia, Taiwan and even Madagascar in the western Indian Ocean.^{5,6} Investigations into the high incidence of SAO in malarious areas revealed that the SAO mutation confers protection from severe malaria caused by *Plasmodium vivax* and *Plasmodium falciparum*.^{7,8}

AE1 is the most abundant RBC membrane protein and mediates the efficient transport of carbon dioxide in the blood.¹ Heterozygous SAO individuals have only 50% normal RBC anion transport activity and thus less efficient gas transport. The heterozygous expression of the SAO AE1 in the red cell membrane not only affects the folding and structure of AE1 but also affects the structure of other red cell membrane proteins depressing a relatively high number of red cell antigens.⁹ Neonatal anemia has also been reported in SAO families.²

A truncated form of AE1 is expressed in the α -intercalated cells of the kidneys and is essential for acid secretion in the urine.¹ Loss of AE1 anion-transport activity in the kidney causes distal renal tubular acidosis (dRTA) and occurs when AE1 expression is severely reduced as in hereditary spherocytosis (HS)^{10,11} or when kidney AE1 activity is severely reduced¹ or trafficking of kidney AE1 is impeded in the α -intercalated cell.¹ Many dRTA mutations are recessive. When SAO AE1 is inherited in trans to a recessive dRTA AE1 mutation then the compound heterozygote will completely lack AE1 anion transport activity. This phenomenon explains the prevalence of dRTA in South East Asia where there are a number of recessive dRTA AE1 mutations maintained in the population.¹²

Homozygous SAO individuals, with no functioning AE1, and homozygous HS individuals, with no AE1, suffer from hemolytic anemia, dRTA and failure to thrive.^{3,10,11} An in-depth study of homozygous SAO cells,¹³

showed expression of SAO AE1 during erythropoiesis (*in vitro*) affected trafficking and cytokinesis resulting in numerous multinucleated erythroblasts and reduced proliferation and enucleation. Unexpectedly, even the *in vitro* cultured heterozygous SAO erythroblasts displayed multinuclearity and reduced enucleation, with an intermediate phenotype part way between the homozygous and control cells,¹³ suggesting that heterozygous SAO individuals may have a mild dyserythropoiesis. Mature homozygous SAO RBC show signs of altered membrane composition, oxidative damage, are very large, oval and unstable.^{4,13} AE1 null HS individuals sometimes have a mild dyserythropoiesis¹⁰ and their RBC are unstable.¹¹ Extensive clinical management of AE1 null individuals, including splenectomy, has improved the survival of these children, some of whom have now reached adolescence. Similarly, the Comorian homozygous SAO child is now 10 years old and quite well, receiving regular transfusions, iron chelation and acidosis treatment.^{4,13} From Malaysia, a live-born homozygous SAO neonate with dRTA was reported in 2015 but the child failed to thrive after 2 years.¹⁴

In Malaysia, where the prevalence of SAO is around 4% within the Malay ethnic group,¹⁵ SAO diagnostic tests are performed mostly upon still birth or recurring miscarriages of the mother. Several heterozygous SAO mothers in this cohort have a history of past miscarriages and complications during pregnancy such as hydrops fetalis as well as intrauterine death (Figure 1). Furthermore, SAO was identified in 18 of 22 dRTA patients (81.8%) when the association between SAO and dRTA was studied in the Malaysian dRTA cohort.¹⁵ Here, we provide an overview of a Malaysian heterozygous SAO cohort and describe the clinical characteristics of five live-born homozygous SAO cases in Malaysia.

This SAO cohort includes a total of 107 patients whose blood samples were tested for the 27 base pair deletion of AE1 using polymerase chain reaction (PCR) and blood smears (Online Supplementary Appendix; Online Supplementary Table S1). Among the 107 tested patients, 68 cases were positive where 93% (63 of 68 cases) of SAO positive cases belonged to Malay ethnicity. Within this Malaysian SAO cohort, 81 cases studied belong to a total of 28 families. Among these 28, 23 families had at least one heterozygous SAO family member. The remaining 26 samples were from individual cases, of which 15 were heterozygous SAO. The majority of the SAO positive cases (43%, n=29) are from Penang, followed by Kuala Lumpur (22%, n=15), Johor (10%, n=7), Sabah (9%, n=6), Kedah (9%, n=6), and Melaka (7%, n=5) (Online Supplementary Figure S3). A variety of RBC morphologies were observed from peripheral blood film examinations of the SAO positive cases, which includes macro-ovalocytes, stomatocytes, theta cells, spherocytes and target cells (Online Supplementary Table S1; Online Supplementary Figure S1).

Surprisingly, a total of six homozygous SAO were found in our cohort, five of whom were live-born (Figure 1, Table 1, Online Supplementary Appendix, and Homozygous SAO case histories). All parents of live-born homozygous SAO cases, with the exception of one (GO 009/16), were confirmed heterozygous for the SAO AE1 deletion; case GO 012/19 was a homozygous fetus that suffered intra-uterine death at 29 weeks. All the five live-born cases were delivered prematurely, at 30 to 35 weeks of gestation. Similar to previous homozygous SAO live-borns, our five homozygous SAO live-borns suffered a severe phenotype requiring intra-uterine transfusions, post-delivery transfusions and ventilation sup-

port. Despite efforts to manage their condition, two of the five patients reported here died, one during the neonatal period and one at 2 months. Even though the other two cases survived during the neonatal period, one of them (GO 012/13) succumbed during infancy due to complications of anemia and the other is not traceable after 2 months. Further details of the obstetric history of

these families are provided in Figure 1 and the *Online Supplementary Table S2*.

Among the five live-born homozygous SAO cases, three of them had severe anemia at birth and two of them developed it at 26 weeks (GO/01/10) and 25 weeks (GO 012/13). All except GO 001/14 had hydrops fetalis and hepatosplenomegaly (Table 1). Physical examination

Table 1. Comparison of five Malaysian live-born homozygous Southeast Asian ovalocytosis (SAO) cases with a previously reported Comorian homozygous SAO case.

Case	GO 003/10	GO 010/10	GO 001/14	GO 009/16	GO 012/13 ¹⁴	Comorian SAO homozygote ^{4,13}
Gestation (weeks)	34	35	33	30	35	29
Age at diagnosis	Newborn	15 days old	3 months old	Newborn	4 months old	No data
Sex	Male	Male	Male	Male	Male	Male
Race/nationality	Malay	Malay	Malay	Malay	Malay	Comorian
Living status	Died at 6 hours of life	Died at 2 months old	Not known	Died within few hours of life	Died at 24 months old	Alive, 10 years old (2020)
Anemia	Severe anemia at birth (Hb 4.9 g/dL)	Severe anemia at 26 weeks gestation (Hb 2.4 g/dL)	Severe anemia at birth (Hb 5.0 g/dL)	Severe anemia at birth (Hb 2.0 g/dL)	Severe anemia at 25 weeks gestation (Hb 3.0 g/dL); Hb 7.4 g/dL at 4 months old	Severe anemia at 22 weeks gestation (Hb 2.9 g/dL)
Hydrops fetalis	Yes	Yes	No	Yes	Yes	Yes
Hepatosplenomegaly	Yes	Yes	No	Yes	Yes	No data
Physical examination	Pale	Bronzed	Pale, jaundiced	Very pale, born not vigorous, poor APGAR score, umbilical bleeding	Good APGAR, very pale, jaundiced, tachypnoeic	No data
Full blood picture	Many elliptocytes, stomatocytes, and NRBC.	Many spherocytic RBC, crenated RBC, fragmented RBC, NRBC, many spherocytes and microspherocytes.	Severe anemia with marked reticulocytosis, NRBC, many spherocytes and microspherocytes.	Spherocytosis with polychromasia. Severe anemia with marked reticulocytosis, NRBC, many spherocytes and microspherocytes.	Hypochromic microcytic cells, elliptocytes as well as teardrop cells were observed.	Rich erythroid lineage. Large ovalocytes, large reticulocytes and macrocytes. Normal myeloid and megakaryocyte lineages.
Normal platelet count. Leucoerythroblastic picture and neutrophilia	NRBC, and reticulocytes.	Slightly reduced platelet (adequate for hemostasis, no clumping noted).	Theta cells also observed.	Theta cells also seen. Normal platelets.		
Patient genetics	Homozygous SAO deletion	Homozygous SAO deletion	Homozygous SAO deletion	Homozygous SAO deletion	Homozygous SAO deletion	Homozygous SAO deletion, β globin "La De'sirade", α thalassemia
Complication and management	1. Required intubation (ventilatory and inotropic support). 2. Packed cell transfusion after birth but died within few hours of life.	1. Intrauterine transfusion twice due to fetal anemia at 26 weeks. 2. Ventilated after birth. 3. Packed cell transfusion at day 5 of life.	1. Ventilated after birth. 2. Exchange transfusion at 5 hours of life. 3. Six episodes of hemolysis within 42 days of life (all required packed cell transfusion). 4. Hematinic prescribed.	1. Ventilated after birth. 2. Weekly transfusions from 1 month old. 3. Developed renal tubular acidosis type I due to persistent metabolic acidosis and hypokalemia.	1. Intrauterine transfusion at 25 weeks due to fetal anemia and hydrops fetalis. 2. 2-weekly transfusions from 1 month old. 3. Developed renal tubular acidosis type I due to persistent metabolic acidosis and hypokalemia.	1. Monthly transfusions since birth. 2. dRTA (3 months old) treated with oral sodium bicarbonate and potassium gluconate. 3. High ferritinemia (6 months old) treated with deferoxamine mesilate. 4. 10 years old (2020): still undergoing regular transfusions, iron chelation, and acidosis treatment.

DRTA: distal renal tubular acidosis; Hb: hemoglobin; NRBC: nucleated red blood cell; PCR: polymerase chain reaction; RBC: red blood cell; SAO: Southeast Asian ovalocytosis; APGAR score: appearance, pulse, grimace, activity, and respiration score.

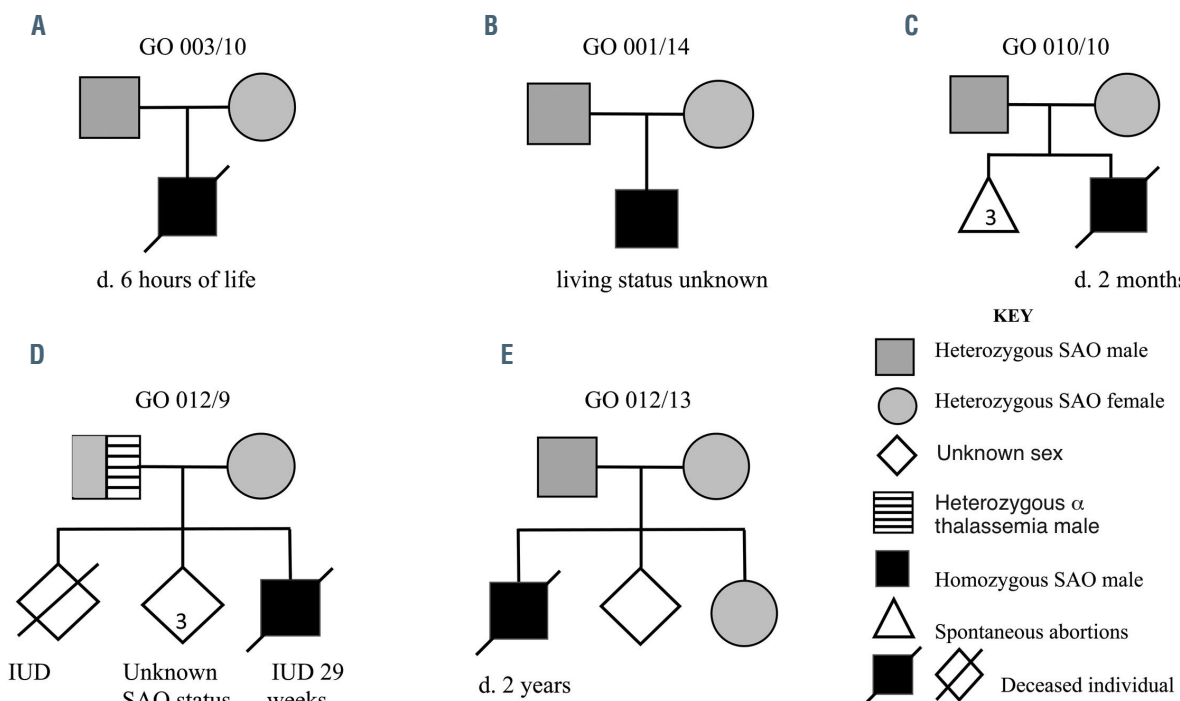


Figure 1. Family pedigree charts of five homozygous Southeast Asian ovalocytosis cases. Families of each homozygous Southeast Asian ovalocytosis (SAO) cases are represented: (A) GO 003/10, (B) GO 001/14, (C) GO 010/10, (D) GO 012/19, and (E) GO 012/13. Squares and circles denote male and females, respectively, with filled ones (grey or black) showing members affected with SAO. The numbered triangle (C) shows number of spontaneous abortions that occurred in the couple's past pregnancies. Parents of two SAO homozygous children (GO 012/19 and GO 010/10) had multiple unsuccessful pregnancies. The mother of GO 012/19 suffered two intra-uterine deaths (including GO 012/19), while the mother of GO 010/10 suffered three spontaneous abortions. None of these other unsuccessful pregnancies were investigated further. On the other hand, parents of GO 012/13 have two living children among whom one is SAO heterozygous, while parents of GO 012/19 have three living children with unknown SAO status (see the *Online Supplementary Table S2*). d: died; IUD: intra-uterine death.

revealed pale appearance, distended abdomen due to hepatosplenomegaly, and jaundice in all five cases. One of the five cases was reported to have dRTA diagnosed in the third month¹⁴ but the other four were not tested. Despite medical interventions, all five homozygous SAO children failed to thrive. This could be due to hepatosplenomegaly, severe anemia or lack of appropriate clinical management. It is difficult to gain more insights into the implications of the SAO homozygous cases as incomplete clinical data of the SAO cohort was collected, lacking data on hemoglobin abnormalities and blood group compatibility. It is also not known whether prenatal diagnosis and termination of pregnancy were offered. These services are not always available, and/or not acceptable to parents. It is now evident that careful clinical management can improve the life of homozygous SAO individuals.⁴ The long-standing assumptions that homozygous SAO is lethal, and that heterozygous SAO is asymptomatic should be re-assessed.

Several point mutations in AE1 that result in a wide range of complications have been reported, many of them leading to anemia and dRTA.^{2,12} Hemolytic anemia is recorded in children with homozygous G701D or compound heterozygous G701D/SAO, V850/SAO, A858D/SAO and V850/A858D mutations.¹ Therefore, homozygous SAO and other AE1 null individuals, who show disparity in survival, may be indicating the cumulative result of hemolysis, acidosis and other hematological abnormalities influenced by the co-occurrence of additional mutations.

To our knowledge, this preliminary Malaysian SAO cohort study, for the first-time reports five homozygous

SAO live-born cases. Since Malaysia and Southeast Asia have a high prevalence of SAO it would be beneficial to screen for SAO at antenatal clinics, at least for parents with a history of hydropic or stillborn fetuses. It is also essential to investigate the impact of heterozygous mutant SAO AE1 on other pathological conditions and ageing. Development of international and national guidelines for assessing a number of hematological, renal, and hepatic conditions in combination with genetic mutation markers to improve survival of homozygous AE1 null probands is needed.

Amanda A. Lavinya,¹ Ruzzieatul A. Razali,² Munirah A. Razak,³ Rashidah Mohamed,⁴ Emmanuel J. Moses,⁵ Meera Soundararajan,⁶ Lesley J. Bruce,⁷ Jeyanthi Eswaran^{1,8} and Narazah Mohd Yusoff¹

¹*Newcastle University Medicine Malaysia, Johor, Malaysia;*
²*Clinical Genetics Section, Advanced Medical and Dental Institute (AMDI), University Sains Malaysia, Penang, Malaysia;*

³*Pathology Department, Hospital Kuala Lumpur, Kuala Lumpur, Malaysia;*
⁴*Pathology Department, Hospital Ampang, Selangor, Malaysia;*
⁵*Cluster of Regenerative Medicine, Advanced Medical and Dental Institute (AMDI), University Sains Malaysia, Penang, Malaysia;*
⁶*Department of Applied Sciences, Northumbria University, Newcastle upon Tyne, UK;*
⁷*Bristol Institute for Transfusion Sciences, NHS Blood and Transplant, Bristol, UK and*
⁸*Institute of Clinical and Translational Research, Faculty of Medicine, Newcastle University, Newcastle upon Tyne, UK*

Correspondence:

NARAZAH MOHD YUSOFF - *narazah@usm.my*

JEYANTHY ESWARAN - jeyanthy.eswaran@newcastle.ac.uk
doi:10.3324/haematol.2020.268581

Received: August 9, 2020.

Accepted: October 28, 2020.

Pre-published: November 12, 2020.

Disclosures: no conflicts of interest to disclose.

Contributions: RR, MR and RM contributed to the data and samples; NY performed the blood smear and PCR tests, analyzed results and collected the cohort; NY, MS, AL, EJM and JE analyzed the cohort data, and prepared the figures and tables; LJB, MS and JE wrote the manuscript.

Acknowledgments: the authors would like to thank the patients and their families for their full cooperation without which this report would not have been possible.

References

1. Wrong O, Bruce LJ, Unwin RJ, Toye AM, Tanner MJA. AE1 mutations, distal renal tubular acidosis, and Southeast Asian ovalocytosis. *Kidney Int.* 2002;62(1):10-19.
2. Laosombat V, Dissaneevate S, Wongchanchailert M, Satayasevanaa B. Neonatal anemia associated with Southeast Asian ovalocytosis. *Int J Hematol.* 2005;82(3):201-205.
3. Liu SC, Jarolim P, Rubin HL, et al. The homozygous state for the AE1 protein mutation in Southeast Asian ovalocytosis may be lethal. *Blood.* 1994;84(10):3590-3591.
4. Picard V, Proust A, Eveillard M, et al. Homozygous Southeast Asian ovalocytosis is a severe dyserythropoietic anemia associated with distal renal tubular acidosis. *Blood.* 2014;123(12):1963-1965.
5. Wilder JA, Stone JA, Preston EG, Finn LE, Ratcliffe HL, Sudoyo H. Molecular population genetics of SLC4A1 and Southeast Asian ovalocytosis. *J Hum Genet.* 2009;54(3):182-187.
6. Rabe T, Jambou R, Rabarijaona L, et al. South-East Asian ovalocytosis among the population of the Highlands of Madagascar: a vestige of the island's settlement. *Trans R Soc Trop Med Hyg.* 2002;96(2):143-144.
7. Allen SJ, O'Donnell A, Alexander ND, et al. Prevention of cerebral malaria in children in Papua New Guinea by Southeast Asian ovalocytosis AE1. *Am J Trop Med Hyg.* 1999;60(6):1056-1060.
8. Rosanas-Urgell A, Lin E, Manning L, et al. Reduced risk of *Plasmodium vivax* malaria in Papua New Guinean children with Southeast Asian Ovalocytosis in two cohorts and a case-control study. *PLoS Med.* 2012;9(9):e1001305.
9. Bruce LJ, Beckmann R, Ribeiro ML, et al. A AE1-based macrocomplex of integral and peripheral proteins in the RBC membrane. *Blood.* 2003;101(10):4180-4188.
10. Kager L, Bruce LJ, Zeithofer P, et al. AE1 null (VIENNA), a novel homozygous SLC4A1 p.Ser477X variant causing severe hemolytic anemia, dyserythropoiesis and complete distal renal tubular acidosis. *Pediatr Blood Cancer.* 2017;64(3).
11. Ribeiro ML, Alloisio N, Almeida H, et al. Severe hereditary spherocytosis and distal renal tubular acidosis associated with the total absence of AE1. *Blood.* 2000;96(4):1602-1604.
12. Khositseth S, Bruce LJ, Walsh SB, et al. Tropical distal renal tubular acidosis: clinical and epidemiological studies in 78 patients. *QJM.* 2012;105(9):861-877.
13. Flatt JF, Stevens-Hernandez CJ, Cogan NM, et al. Expression of South East Asian ovalocytic AE1 disrupts erythroblast cytokinesis and reticulocyte maturation. *Front Physiol.* 2020;11:357.
14. Asnawi AW, Sathar J, Nasir SF, Mohamed R, Jayaprakasam KV, Vellapandian ST. Homozygous Southeast Asian hereditary ovalostomatocytosis: management dilemma. *Pediatr Blood Cancer.* 2015;62(10):1872-1873.
15. Yusoff NM, Van Rostenberghe H, Shirakawa T, et al. High prevalence of Southeast Asian ovalocytosis in Malays with distal renal tubular acidosis. *J Hum Genet.* 2003;48(12):650-653.

Structural aberrations are associated with poor survival in patients with clonal cytopenia of undetermined significance

Many patients referred to the hematological department with unexplained cytopenia are diagnosed with idiopathic cytopenia of undetermined significance (ICUS) when diagnostic bone marrow (BM) morphological findings or cytogenetic abnormalities defining myelodysplastic syndromes (MDS) are absent.¹ Approximately half of ICUS patients harbor MDS-related somatic mutations, a condition known as clonal cytopenia of undetermined significance (CCUS), associated with a >13-fold higher risk of progression to MDS or acute myeloid leukemia (AML) than ICUS patients without detectable mutations (i.e., ICUS non-clonal).^{1,2} Still, the natural history of ICUS varies considerably; thus, additional prognostic markers remain to be identified.

Single nucleotide polymorphism-based array analysis (SNP-A) in patients with myeloid malignancies allows the identification of chromosomal aberrations beyond the resolution of metaphase cytogenetics (≤ 5 Mb), i.e., focal copy number aberrations (CNA) and copy-neutral loss of heterozygosity (CNLOH) (*Online Supplementary Figure S1*), that correlate with clinical features and outcome (reviewed by Kanagal-Shamanna *et al.*,³ Xu *et al.*⁴ and Ronaghy *et al.*⁵).

In this study, we investigated whether CNA and CNLOH were also present in ICUS patients and, if so, whether they had prognostic impact.

Patients (n=153) diagnosed with ICUS after routine work-up in Denmark between 2009-2017 were included upon first visit to the Department of Hematology and followed prospectively until death or study cut-off date (*Online Supplementary Methods*).

The study was approved by the Danish Science Ethics Committee and conducted in accordance with the

Table 1. Structural aberrations, including relevant genes affected, in the cohort of 153 patients with idiopathic cytopenia that are also recurrently detected in myeloid malignancies.

A		Chromosomal Region	Abnormality type	Relevant gene(s) (if known)*	No. and disorder of cases		Relation*	
1p34		CNLOH	<i>MPL</i>		1 (CCUS)		MDS, MDS/MPN, MPN, AML	
1q		CNLOH			1 (ICUS non-clonal)		MDS, MPN	
2p23		Deletion	<i>DNMT3A</i>		1 (ICUS non-clonal)		MDS, AML	
4q12-q24		CNLOH, Deletion	<i>TET2, PDGFRA, FIP1L1</i>		2, CNLOH (CCUS); 1, Deletion (CCUS)		MDS, MDS/MPN, MPN, AML	
7q22		Deletion	<i>CUX1</i>		1 (CCUS)		MDS, MDS/MPN, MPN, AML	
11q13-q23		CNLOH	<i>CBL, CCND1</i>		1 (CCUS)		MDS, MDS/MPN, MPN, AML	
19p13		CNLOH	<i>DNMT1, PRDX2</i>		1 (ICUS non-clonal)		MDS	
20q		CNLOH			1 (CCUS)		MDS	
B		Gene	Chr	Start, bp	End, bp	OMIM	Abnormality	Patient ID [†]
							Disorder of patient	Relation
<i>TET2</i> [‡]		4	106,067,032	106,200,973	612839	612839	Deletion CNLOH	36 22, 34
<i>CUX1</i>		7	101,458,959	101,927,250	116896	116896	Deletion	34
<i>DNMT3A</i> [‡]		2	25,455,845	25,565,459	602769	602769	Deletion	6
<i>IDH2</i> [‡]		15	90,626,277	90,645,736	147650	147650	CNLOH [§]	11
<i>CALR</i>		19	13,049,392	13,055,304	109091	109091	CNLOH	13
<i>GNAS</i>		20	57,414,773	57,486,250	139320	139320	CNLOH	1
<i>CBL</i> [‡]		11	119,076,752	119,178,859	165360	165360	CNLOH	1
<i>MLL</i>		11	118,307,205	118,397,539	159555	159555	CNLOH	1
<i>SFI</i>		11	64,532,076	64,546,316	601516	601516	CNLOH	1
<i>GNB1</i>		1	1,716,725	1,822,526	139380	139380	CNLOH	14
<i>MPL</i>		1	43,803,475	43,820,135	159530	159530	CNLOH	14
<i>FBXW7</i>		4	153,242,410	153,457,253	606278	606278	CNLOH	22, 34
<i>KIT</i>		4	55,524,085	55,606,881	164920	164920	CNLOH	34
-Y						[10 patients]	ICUS	MDS, MPN, AML non-clonal/CCUS

(A) List of copy number aberrations (CNA) and copy neutral loss of heterozygosity (CNLOH) in our study cohort of patients with idiopathic cytopenia of undetermined significance (ICUS), that are also recurrently detected in patients with myeloid malignancies. These include ten CNA and CNLOH in eight chromosomal regions identified in eight patients (two patients had more than one). The cases listed in this table are all included in (B) except for chromosome 1q abnormality, as the gene(s) at this location that relevant for myeloid malignancies is unknown. (B) List of genes recurrently affected in myelodysplastic syndromes, myeloproliferative neoplasms and/or acute myeloid leukemia that were involved in CNA and/or CNLOH in the ICUS patients. The cases listed in this table are all included in (A), except for the one marked by a section sign (§) as CNLOH(15q) is not reported as a recurrent lesion in myeloid malignancies.*From reviews by Kanagal-Shamanna *et al.*³ and Xu *et al.*⁴ †Patient ID in accordance with *Online Supplementary Tables S2, S3*. [‡]Genes included in the 20-gene panel and sequenced in the study. [§]Not included in (A). CNLOH: copy-neutral loss of heterozygosity; CCUS: clonal cytopenia of undetermined significance; ICUS: idiopathic cytopenia of unknown significance; MDS: myelodysplastic syndromes; MPN: myeloproliferative neoplasms; AML: acute myeloid leukemia; Chr: chromosome; bp: base pairs; OMIM: online Mendelian inheritance in man.

Helsinki Declaration. All patients provided written informed consent.

Targeted next-generation sequencing of diagnostic samples was performed using a custom-designed multiplex Ion Ampliseq panel (Thermo Fisher Scientific, Waltham, MA, USA) including 20 genes recurrently mutated in MDS (*Online Supplementary Appendix*). SNP-

A was performed on diagnostic samples using the Infinium CytoSNP-850K v1.1 BeadChip (Illumina, San Diego, CA, USA). Illumina intensity files (.idat files) were analyzed visually with the GenomeStudio software version 2011.1 (Illumina) (*Online Supplementary Appendix*).

Patient characteristics at baseline are presented in the *Online Supplementary Table S1* and the *Online*

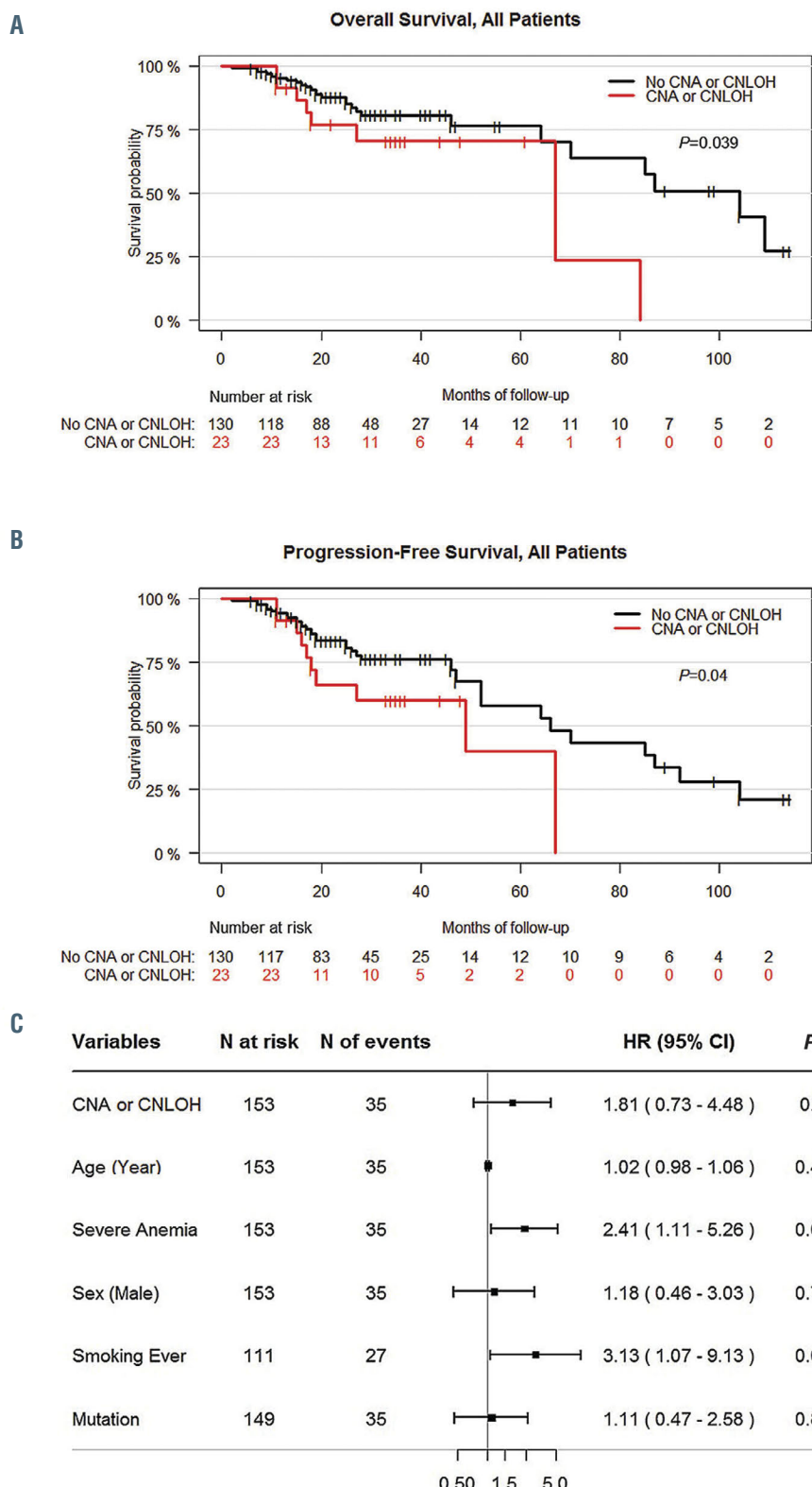


Figure 1. Single nucleotide polymorphism-based array analysis-detected structural aberrations demarcate survival in patients with idiopathic cytopenia of undetermined significance but are not an independent adverse prognostic factor. Kaplan-Meier estimates of (A) overall survival and (B) progression-free survival of the group of idiopathic cytopenia of undetermined significance (ICUS) patients with copy number aberrations (CNA) or copy neutral loss of heterozygosity (CNLOH) (excluding loss of the Y chromosome; red curve) and the group of ICUS patients without CNA or CNLOH (black curve). (C) Forest plot of hazard ratios (HR) including 95% Confidence intervals (CI) for all-cause mortality in multivariable analysis in ICUS patients (n=109 with complete data). Overall survival was measured from first bone marrow investigation (=inclusion) to death from any cause. Progression-free survival was measured from first bone marrow investigation to progression to a myeloid cancer or death from any cause. Annotated P-values are from two-sided log-rank tests. Severe anemia was defined as hemoglobin <100 g/L. Mutations were identified by targeted next generation sequencing using a 20-gene panel with a lower limit of detection at 2%.

Supplementary Figure S2 illustrates the workflow. Median age was 69 years (range, 17-94 years) and two-thirds were male. Sixty-four patients (42%) had ≥ 1 mutation(s) in MDS-related genes with the most commonly affected genes being *TET2*, *DNMT3A* and *SRSF2* (Online Supplementary Table S2).

SNP-A identified a total of 25 structural aberrations (excluding loss of the Y chromosome [LOY]); 12 deletions, eight CNLOH and five gains, in 23 of 153 patients (15%) (Online Supplementary Table S3, Online Supplementary Figure S3).

Median sizes of the aberrations were deletions: 248 Kb (range, 131.6-2,867.5 Kb), CNLOH: 82.9 Mb (range, 11.6-137.1 Mb) and gains: 1.3 Mb (range, 0.6-2.6 Mb) ranging from minor genomic segments to entire chromosomes.

Mutations in MDS-related genes were present in 12 of

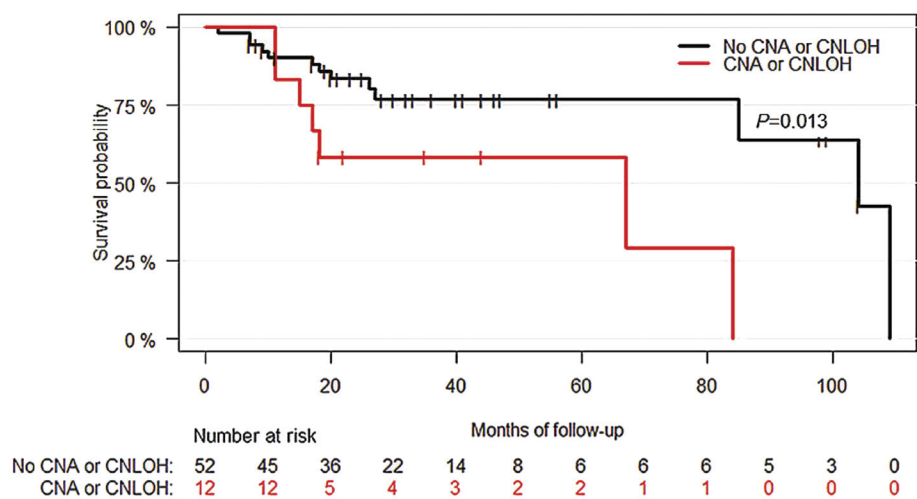
23 patients (52%) with CNA/CNLOH (Online Supplementary Table S3). Thus, a marker of clonal hematopoiesis was identified in 11 of 85 ICUS patients (13%) in whom no abnormalities were detected by conventional cytogenetics or targeted sequencing (Online Supplementary Figure S4).

The CNA/CNLOH identified in the ICUS patients were largely overlapping with recurrent CNA/CNLOH of known or likely clinical significance in patients with myeloid malignancies (10 of 25 CNA/CNLOH; 40%) (Table 1A).^{3,4,6} Correspondingly, many genes frequently mutated in MDS, myeloproliferative neoplasms and/or AML were located within the sites of CNA/CNLOH (Table 1B; Online Supplementary Figure S5).

Mean corpuscular volume (median, 97 vs. 90 fL; $P=0.014$) and ferritin level (median, 260 vs. 173 μ g/L;

A

Overall Survival, CCUS Patients



B

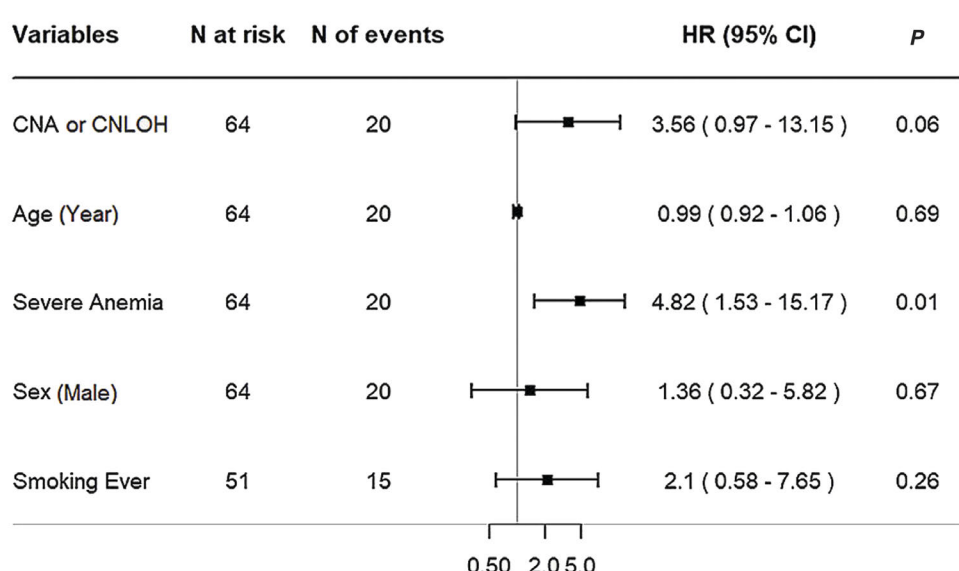


Figure 2. In patients with clonal cytopenia of undetermined significance, the presence of additional structural aberrations is associated with an increased hazard of all-cause mortality in univariable and multivariable analysis. (A) Kaplan-Meier estimates of overall survival of the group of clonal cytopenia of undetermined significance (CCUS) patients with copy number aberrations (CNA) or copy neutral loss of heterozygosity (CNLOH) (excluding loss of the Y chromosome; red curve) and the group of CCUS patients without CNA or CNLOH (black curve). (B) Forest plot of hazard ratios (HR) including 95% Confidence Intervals (CI) for all-cause mortality in multivariable analysis in CCUS patients ($n=51$ with complete data). Overall survival was measured from first bone marrow investigation (=inclusion) to death from any cause. Patients alive at the last date of follow-up were censored at that time. Annotated P-values are from two-sided log-rank tests. Severe anemia was defined as hemoglobin <100 g/L.

$P=0.043$) were significantly higher in ICUS patients with CNA/CNLOH, and LOY was more preponderant (29% vs. 8% of males; $P=0.028$) than in ICUS patients without CNA/CNLOH (*Online Supplementary Table S4*). Notably, there was no significant correlation between the presence of CNA/CNLOH and the mutational profile.

Of utmost importance for the clinical relevance is whether the presence of chromosomal lesions translates to more precise prognostication in ICUS patients. Median follow-up time was 25 months (range, 2-114 months). No patients were lost to follow-up, the only censoring was administrative at the study cut-off date. Twenty patients had a follow-up BM investigation performed for suspected MDS. A total of 15 of 153 patients (10%) progressed to myeloid malignancy (MDS, $n=12$; AML, $n=2$; chronic myelomonocytic leukemia, $n=1$), and 35 died (23%) of any cause. All patients but one who progressed carried somatic mutation(s).

Survival of ICUS patients with CNA/CNLOH was significantly shorter than of patients without CNA/CNLOH for overall survival (OS) (median, 67 vs. 104 months; $P=0.039$; hazard ratio [HR]=2.26; 95% Confidence Interval [CI]: 1.04-4.93), and progression-free survival (PFS) (median, 49 vs. 66 months; $P=0.04$; HR=2.07; 95%CI: 1.04-4.14) (*Figure 1A and B; Online Supplementary Table S5*). In multivariable analysis adjusting for age, sex, severe anemia, mutational status and smoking, CNA/CNLOH were not associated with adverse outcomes in ICUS patients (*Figure 1C; Online Supplementary Figure S6; Online Supplementary Table S5*).

The presence of somatic mutation(s) was significantly associated with inferior PFS (HR=2.40; 95%CI: 1.30-4.43; $P=0.004$), but not OS (HR=1.60; 95%CI: 0.82-3.16; $P=0.2$) in univariable analysis. Somatic mutation(s) was a borderline significant independent factor for inferior PFS (adjusted HR=2.03; 95%CI: 0.97-4.26; $P=0.06$) (*Online Supplementary Figure S6*).

When we analyzed CCUS patients ($n=64$) as a subgroup the adverse effect of CNA/CNLOH on OS was more pronounced than in the entire study population of ICUS non-clonal and CCUS patients. After a median follow-up of 24 months (range, 2-109 months), median OS was 67 months in the group of CCUS patients with CNA/CNLOH compared with 104 months in the group of CCUS patients without CNA/CNLOH ($P=0.013$) (*Figure 2A*). The corresponding HR was 3.22 (95%CI: 1.22-8.51) for all-cause mortality in CCUS patients with CNA/CNLOH. Notably, also in multivariable analysis the presence of CNA/CNLOH in CCUS patients conferred a more than three times higher hazard of death, which was borderline significant (adjusted HR=3.56; 95%CI: 0.97-13.15; $P=0.056$) (*Figure 2B*). Interestingly, this increased mortality hazard was not driven by progression to overt myeloid malignancy as an association with PFS was less evident (*Online Supplementary Figure S7*).

On the other hand, in a separate analysis of the patients with non-clonal ICUS, the presence of CNA/CNLOH was not associated with shorter survival (*Online Supplementary Figure S8*).

CCUS patients with CNA/CNLOH had a significantly higher variant allele frequency of somatic mutations than CCUS patients without CNA/CNLOH (median 36% vs. 24%; $P=0.039$) and were more likely to have LOY ($P=0.035$) and macrocytosis ($P=0.022$) (*Online Supplementary Table S6*). There was no significant difference between the two CCUS groups with respect to age, sex, adverse mutations, number of mutations, smoking or hematological parameters.

Multiple studies have demonstrated worse survival of

patients with myeloid malignancies harboring cryptic chromosomal lesions compared with patients without cryptic lesions.^{3,4} Akin to our findings, the impact of CNA/CNLOH was generally more pronounced on OS than PFS, and SNP-A improved prognostic stratification in primarily lower-risk MDS patients including patients with a normal karyotype.^{7,8}

To our knowledge, only three smaller previous studies have reported on CNA/CNLOH in patients with ICUS/pre-MDS with frequencies at 15-32%.⁹⁻¹¹ However, their study designs did not enable distinction between ICUS non-clonal and CCUS or correlation to clinical outcomes.

SNP-A in large patient cohorts from genome-wide association studies including healthy controls showed that the frequency of mosaic CNA/CNLOH in peripheral blood increases to approximately 2-3% for age >75 years.¹² Even when only considering clonal mosaicism (*Online Supplementary Table S3*), the frequency of autosomal mosaic CNA/CNLOH was 2-3-fold higher in our study population. This suggests that the loss of chromosomal integrity found by SNP-A in the ICUS patients was related to their disorder, rather than their advanced age.

Our study has certain limitations. Firstly, follow-up was relatively short given the cohort size and the life expectancy of ICUS/CCUS patients. This may have influenced the lack of statistical significance in multivariable analysis. Obviously, our findings need validation in an independent cohort.

Secondly, DNA from BM was not available for SNP-A in all patients, hence, granulocytes from peripheral blood were the source of DNA in these cases (*Online Supplementary Methods*). We considered this feasible as previous studies have shown a high concordance (95%) for SNP-A karyotype between peripheral blood and BM as also seen for somatic mutations.^{8,13}

Thirdly, germline DNA was not available as matched DNA reference to allow definitive distinction between acquired and constitutional aberrations. Some aberrations, especially small CNA, appeared to be fully clonal (i.e., not mosaic) (*Online Supplementary Table S3*) and therefore could be germline variants potentially predisposing to disease development. However, extensive MDS-associated aberrations and LOY were also present in a fully clonal state, as observed previously.¹⁴ Furthermore, it has been demonstrated that large (≥ 25 Mb) and/or telomeric CNLOH do not require verification as they do not occur in non-clonal control DNA.^{7,15}

Finally, due to the scarcity of surplus sample material we were unable to proceed with sequencing of myeloid malignancy-associated genes that were not included in our 20-gene panel and were found to be affected by deletion or CNLOH in a subset of patients (Table 1B). Sequencing of these genes was compelling as regions of acquired CNLOH may pinpoint homozygous loss of tumor suppressor genes or oncogenes with homozygosity of mutations.^{3,15}

Besides these limitations, our data document that additional structural aberrations detected by SNP-A may influence the variability in the clinical course among CCUS patients and distinguish patients with a markedly worse OS. By contrast, in the group of ICUS non-clonal patients, CNA/CNLOH had no impact on survival. Newer technologies such as whole-genome sequencing, capable of simultaneously detecting mutations and CNA, are increasingly being used in the diagnostic setting. We believe our study emphasizes the importance of the compound analysis of mutations and structural aberrations in CCUS patients.

*Srine U. Mikkelsen,^{1,2} Setareh Safavi,³
Konstantinos Dimopoulos,⁴ Colm J. O'Rourke,²
Mette K. Andersen,³ Mette S. Holm,⁵ Claus W. Marcher,⁶
Jesper B. Andersen,² Jakob W. Hansen^{1,2,7#}
and Kirsten Grønbæk^{1,2,7#}*

¹Department of Hematology, Rigshospitalet, Copenhagen; ²Biotech Research and Innovation Center (BRIC), Department of Health and Medical Sciences, University of Copenhagen, Copenhagen; ³Department of Clinical Genetics, Rigshospitalet, Copenhagen; ⁴Department of Clinical Biochemistry, Rigshospitalet, Copenhagen; ⁵Department of Hematology, Aarhus University Hospital, Aarhus; ⁶Department of Hematology, Odense University Hospital, Odense and ⁷DanStem, University of Copenhagen, Copenhagen, Denmark

[#]JWH and KG contributed equally as co-senior authors.

Correspondence:

KIRSTEN GROENBAEK - kirsten.groenbaek@regionh.dk

doi:10.3324/haematol.2020.263319

Received: June 13, 2020.

Accepted: November 2, 2020.

Pre-published: November 12, 2020.

Disclosures: no conflicts of interest to disclose.

Contributions: SUM wrote the manuscript, collected patient data, performed laboratory analysis (SNP-A), performed analysis of SNP-A data, performed statistical analyses, prepared the tables and figures and applied for funding; SS performed analysis of SNP-A data; KD performed statistical analyses and prepared the figures. CJR performed laboratory analysis (SNP-A); MKA performed genetic and chromosomal analyses; MSH recruited patients; CWM recruited patients. JBA supervised the study; JWH designed the study, managed the biobank, extracted the DNA, collected patient data, performed targeted next generation sequencing, supervised the study and applied for funding; KG designed the study, managed the biobank, supervised the study and applied for funding. All authors contributed to the critical reviewing and editing of the manuscript.

Acknowledgments: the authors would like to thank the Danish Cancer Society (grant no. R204-A12363), the administrators of Rigshospitalet's Research Funds and Greater Copenhagen Health Science Partners who provided grants that covered the salary for SUM. The authors would also like to thank Aase og Ejnar Danielsens Fond and the administrators of Frk. Amalie Jørgensens Mindelegat for research grants to SUM and JWH, respectively.

Funding: the project is part of the Danish Research Center for Precision Medicine in Blood Cancers funded by the Danish Cancer Society (grant no. R223-A13071) and Greater Copenhagen Health Science Partners. The Novo Nordisk Foundation Center for Stem Cell Biology (DanStem) is supported by a Novo Nordisk Foundation grant (grant no. NNF17CC0027852).

References

1. Kwok B, Hall JM, Witte JS, et al. MDS-associated somatic mutations and clonal hematopoiesis are common in idiopathic cytopenias of undetermined significance. *Blood*. 2015;126(21):2355-2361.
2. Malcovati L, Galli A, Travaglino E, et al. Clinical significance of somatic mutation in unexplained blood cytopenia. *Blood*. 2017;129(25):3371-3378.
3. Kanagal-Shamanna R, Hodge JC, Tucker T, et al. Assessing copy number aberrations and copy neutral loss of heterozygosity across the genome as best practice: an evidence based review of clinical utility from the cancer genomics consortium (CGC) working group for myelodysplastic syndrome, myelodysplastic/myeloproliferative and myeloproliferative neoplasms. *Cancer Genet*. 2018;228-229:197-217.
4. Xu X, Bryke C, Sukhanova M, et al. Assessing copy number abnormalities and copy-neutral loss-of-heterozygosity across the genome as best practice in diagnostic evaluation of acute myeloid leukemia: an evidence-based review from the cancer genomics consortium (CGC) myeloid neoplasms working group. *Cancer Genet*. 2018;228-229:218-235.
5. Ronagh A, Yang RK, Khouri JD, Kanagal-Shamanna R. Clinical applications of chromosomal microarray testing in myeloid malignancies. *Curr Hematol Malig Rep*. 2020;15(3):194-202.
6. Bernard E, Nannya Y, Hasserjian RP, et al. Implications of TP53 allelic state for genome stability, clinical presentation and outcomes in myelodysplastic syndromes. *Nat Med*. 2020;26(10):1549-1556.
7. Tiu RV, Gondek LP, O'Keefe CL, et al. Prognostic impact of SNP array karyotyping in myelodysplastic syndromes and related myeloid malignancies. *Blood*. 2011;117(17):4552-4560.
8. Starczynowski DT, Vercauteren S, Telenius A, et al. High-resolution whole genome tiling path array CGH analysis of CD34+ cells from patients with low-risk myelodysplastic syndromes reveals cryptic copy number alterations and predicts overall and leukemia-free survival. *Blood*. 2008;112(8):3412-3424.
9. Evans AG, Ahmad A, Burack WR, Iqbal MA. Combined comparative genomic hybridization and single-nucleotide polymorphism array detects cryptic chromosomal lesions in both myelodysplastic syndromes and cytopenias of undetermined significance. *Mod Pathol*. 2016;29(10):1183-1199.
10. Cargo CA, Rowbotham N, Evans PA, et al. Targeted sequencing identifies patients with preclinical MDS at high risk of disease progression. *Blood*. 2015;126(21):2362-2365.
11. Xiao X, He X, Li Q, et al. Single-nucleotide polymorphism array technique generating valuable risk-stratification information for patients with myelodysplastic syndromes. *Front Oncol*. 2020;10:962.
12. Laurie CC, Laurie CA, Rice K, et al. Detectable clonal mosaicism from birth to old age and its relationship to cancer. *Nat Genet*. 2012;44(6):642-650.
13. Mohamedali AM, Gäken J, Ahmed M, et al. High concordance of genomic and cytogenetic aberrations between peripheral blood and bone marrow in myelodysplastic syndrome (MDS). *Leukemia*. 2015;29(9):1928-1938.
14. Thiel A, Beier M, Ingenhag D, et al. Comprehensive array CGH of normal karyotype myelodysplastic syndromes reveals hidden recurrent and individual genomic copy number alterations with prognostic relevance. *Leukemia*. 2011;25(3):387-399.
15. O'Keefe C, McDevitt MA, Maciejewski JP. Copy neutral loss of heterozygosity: a novel chromosomal lesion in myeloid malignancies. *Blood*. 2010;115(14):2731-2739.

Minimal residual disease monitoring in acute myeloid leukemia with non-A/B/D *NPM1* mutations by digital polymerase chain reaction: feasibility and clinical use

In patients with acute myeloid leukemia (AML), treatment stratification is primarily based on pre-therapeutic factors, including cytogenetic and molecular aberrations and measurable/minimal residual disease (MRD) during treatment.¹ Sequential MRD monitoring allows for assessment of the response to chemotherapy and early detection of relapses, possibly identifying patients who need pre-emptive or more intensive therapy.² In clinical practice, MRD monitoring is based on molecular real-time quantitative reverse transcriptase-polymerase chain reaction (RT-qPCR) and/or flow cytometry.³ Currently available molecular markers are basically represented by fusion transcripts (especially *CBFB-MYH11*, *RUNX1-RUNX1T1* and *PML-RARA*)^{4,5} or mutations, mainly *NPM1* mutations.⁶ However, 60 to 70% of AML patients lack these leukemia-specific MRD targets and their samples are not informative for MRD detection by RT-qPCR.³ Additionally, RT-qPCR assays require the generation of standard curves covering the cycling threshold range of patients' samples to ensure the linearity of the assay at the measured MRD level. This implies the maintenance of plasmid standards for each molecular target, limiting widespread use of this technique for rare markers in clinical practice. In this context, digital polymerase chain reaction (dPCR) is a promising approach to validate new MRD markers in AML patients. dPCR provides absolute quantification of nucleic acid target sequences with high sensitivity. Notably, it avoids the absolute quantification of plasmid standards and the pitfalls associated with variations in reaction efficiencies (e.g., number of technical replicates performed, effect of the volume transferred throughout the dilution series).⁷ This makes dPCR more convenient for quantifying rare molecular markers and an

accurate alternative method for monitoring MRD. Briefly, the sample is divided into thousands of partitions (wells or droplets depending on the technology) containing amplification reagents in which the targets are randomly distributed. Each partition is analyzed and classified in a positive or negative category depending on the initial presence of the target. The absolute quantification is then estimated by modeling the measured number of positive fractions as a Poisson distribution model that estimates how many compartments contained one, two or more targets before amplification.

NPM1 mutations are one of the most frequent genetic abnormalities in adult AML, being detected in approximately 35% of all patients with AML and in 50 to 60% of those with cytogenetically normal AML, in whom they are a major prognostic factor.^{1,8} Since their discovery in 2005, more than 50 different mutations located in exon 11 of *NPM1* have been identified.⁹ Type A (c.860_863dupTCTG), B (c.863_864insCATG) and D (c.863_864insCCTG) mutations predominate in approximately 90% of *NPM1*-mutated AML patients.¹⁰ While RT-qPCR could be effectively used to monitor all *NPM1*-mutated transcripts,^{11,12} in clinical practice, RT-qPCR analysis is mostly restricted to type A, B and D mutations for which commercial plasmid standards are available. Recently, in a study focused on *NPM1*-type A, B or D mutation quantification by RT-qPCR, the Acute Leukemia French Association (ALFA) group supported the strong prognostic significance of post-induction *NPM1*-based MRD on outcome, independently of additional molecular or cytogenetic aberrations.⁶ Patients who did not achieve a 4-log reduction (poor responders) in *NPM1*-based MRD in peripheral blood were shown to have a higher cumulative incidence of relapse and shorter survival. Additionally, *NPM1*-based MRD was shown to be a good predictive factor for the indication of allogeneic stem cell transplantation in poor responders.

The purpose of the present study was to define the

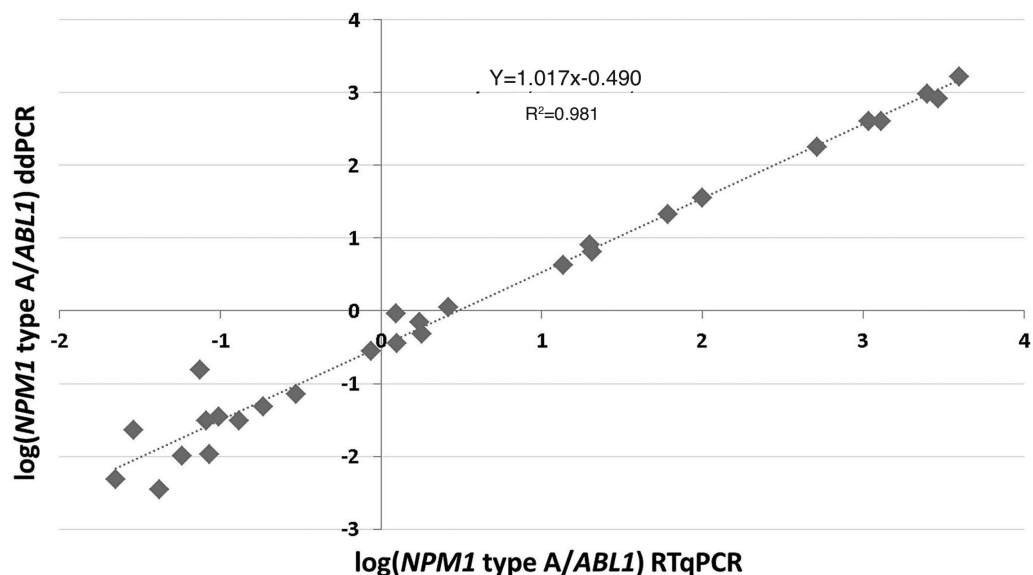


Figure 1. Correlation between the quantification of levels of *NPM1* type A mutation transcripts determined by real-time quantitative reverse transcriptase-polymerase chain reaction and droplet digital polymerase chain reaction. *NPM1* type A mutation transcript levels were quantified in samples from 28 patients with acute myeloid leukemia using both real-time quantitative reverse transcriptase-polymerase chain reaction (RT-qPCR) with a TaqMan chemistry assay and a droplet digital polymerase chain reaction (ddPCR) assay. The correlation between the ddPCR and RT-qPCR results was assessed using least squares regression after logarithmic transformation.

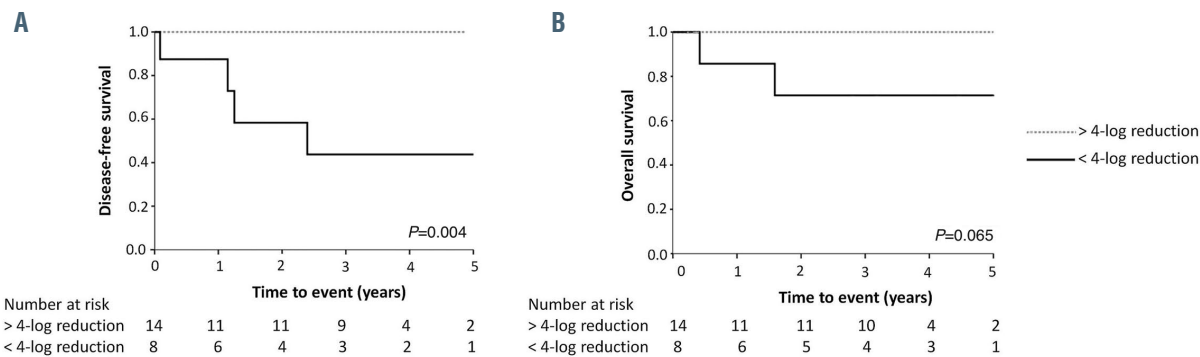


Figure 2. Outcomes according to *NPM1*-based minimal residual disease. (A) Disease-free survival and (B) overall survival in acute myeloid leukemia patients with rare *NPM1* mutations according to post-induction log reduction in minimal residual disease in peripheral blood (<4-log reduction or >4-log reduction). Disease-free and overall survival were censored at allogeneic stem cell transplantation.

ability of droplet dPCR to quantify non-A/B/D *NPM1* mutations and to retrospectively evaluate the prognostic impact of post-induction *NPM1*-based MRD in AML patients with a “rare” *NPM1* mutation (i.e. non-A/B/D) enrolled in the ALFA-0702 trial.

From March 2009 to September 2013, 713 patients aged 18–59 years old with *de novo* AML were included in the phase II randomized multicenter ALFA-0702 trial (Eudra-CT, 2008-000668-18; ClinicalTrials.gov, NCT00932412).¹⁵ The study was approved in December 2008 by the Institutional Review Board of the French Regulatory Agency and the Ethics Committee Sud-Est IV, France. All patients gave informed consent for both treatment and genetic analyses, according to the Declaration of Helsinki. *NPM1* mutations and *FLT3*-internal tandem duplications (ITD) were determined by fragment analysis and Sanger sequencing as part of the patients’ care.¹³ Overall, *NPM1*-mutated AML accounted for 36% of the cases of AML (234 patients), of which 13% (31 patients) had non-A/B/D mutations. Among them, 22 patients with available RNA-complementary DNA (cDNA) extracted from peripheral blood after induction therapy were selected for this study. Additionally, 28 AML patients with a *NPM1*-type A mutation were selected to compare the performance of droplet dPCR *versus* standard RT-qPCR performed as previously described.⁶

Peripheral blood samples were collected at diagnosis and after induction (MRD1) for patients in complete remission. Droplet dPCR was performed on cDNA using the Bio-Rad QX200™ droplet dPCR system with FAM- and HEX-labeled probes (Online Supplementary Figure S1, Online Supplementary Table S1). *NPM1* mutations and *ABL1* transcripts were quantified in multiplex. Each sample was partitioned into 20,000 uniform droplets allowing a random distribution of the target cDNA. End-point PCR amplification of the nucleic acid target was carried out within each droplet using the high-performance T100™ Thermal Cycler (Bio-Rad). PCR products were then subjected to the QX200 Droplet Reader (Bio-Rad), which measures the fluorescence of each droplet using a two-color detection system. Raw data were analyzed using QuantaSoft™ software (Bio-Rad). Data were shown as a one-dimension plot with each droplet from a sample plotted on the graph of fluorescence intensity *versus* droplet number. The fraction of positive droplets was then estimated using a Poisson distribution model. Assays performed to optimize and validate the quantifi-

cation of *NPM1*-mutated transcript levels are described in the *Online Supplementary Appendix* (*Online Supplementary Methods*, *Online Supplementary Figures S2-S7*, *Online Supplementary Tables S2-S4*). For statistical analyses, overall survival and disease-free survival were estimated by the Kaplan-Meier method and compared by cause-specific hazard Cox models. Overall survival was measured from the date of diagnosis until death from any cause. Disease-free survival was measured from the date of complete remission until the date of relapse. Patients were censored at the time of allogeneic stem cell transplantation in first remission. A *P*-value <0.05 was considered statistically significant.

NPM1-type A mutation transcript levels in 28 AML samples were quantified using both RT-qPCR and droplet dPCR and produced concordant results, showing that dPCR could be considered as an alternative for monitoring type A mutations³ (Figure 1). Subsequently, 22 AML patients enrolled in the ALFA-0702 trial who achieved complete remission and harbored 16 different rare *NPM1* mutations were studied by droplet dPCR (*Online Supplementary Table S5*). Although the number of subjects was very small, AML patients with rare *NPM1* mutations who did not achieve a 4-log reduction of *NPM1*-based MRD in peripheral blood had a significantly shorter disease-free survival (3-year disease-free survival: 43.8% *vs.* 100%; *P*=0.004) (Figure 2A) as described for classical *NPM1*-type A, B and D mutations.⁶ The difference did not reach statistical significance for overall survival (3-year overall survival: 71.4% *vs.* 100%; *P*=0.065) (Figure 2B), perhaps due to low numbers. *FLT3*-ITD was found in one poor responder (ratio 0.95) and three good responders (ratios 0.4, 0.4 and 1.0). Interestingly, some studies have found that rare *NPM1* mutations (i.e., non-A/B/D) have different clinical or biological behaviors compared to classical *NPM1* mutations (i.e., type A, B or D).^{10,14} This could result from different amino-acid substitutions or accompanying alterations in commonly mutated genes such as *FLT3*, *DNMT3A* or *IDH1/IDH2*. In current practice, it can be assumed that the ability to monitor classical *NPM1* mutations by RT-qPCR in most laboratories could lead to earlier detection of relapses, better selection of patients with an indication for allogeneic stem cell transplantation, and easier administration of pre-emptive therapy. Although focused on a small subgroup of patients, our results extend those previously published by the ALFA group⁶ and suggest that a post-induction

NPM1-based MRD log reduction in peripheral blood greater than 4-logs defines a group of patients with a very low risk of relapse when treated with chemotherapy alone whatever the type of *NPM1* mutation. Additionally, this study highlights the robustness and accuracy of dPCR for detecting MRD in patients for whom standard MRD markers are not available.¹⁵ The dPCR assay reliably detected five copies of mutated *NPM1* transcript (the limit-of-detection assay was performed with type A, B and D transcripts). The detection limit was therefore 0.01% for a sample containing 50,000 copies of the housekeeping *ABL1* gene, which is equivalent to the RT-qPCR assay used in most laboratories. Thus, dPCR could be informative for the early detection of relapses and be used for MRD follow-up in patients. Considering its sensitivity and ease of use (especially the absolute quantification without the need for standard curves), dPCR may represent an alternative method equivalent to RT-qPCR for MRD monitoring of classical *NPM1*-type A, B and D mutations.

Auriane Lesieur,¹ Xavier Thomas,² Olivier Nibourel,^{1,3} Nicolas Boissel,⁴ Laurène Fenwarth,^{1,3} Stéphane De Botton,⁵ Elise Fournier,^{1,3} Karine Celli-Lebras,⁴ Emmanuel Raffoux,⁴ Christian Recher,⁶ Juliette Lambert,⁷ Céline Berthon,^{3,8} Arnaud Pigneux,⁹ Raphaël Itzykson,⁴ Pascal Turlure,¹⁰ Cécile Pautas,¹¹ Jacques Vargaftig,¹² Claude Preudhomme,^{1,3} Hervé Dombret⁴ and Nicolas Duployez^{1,3}

¹CHU Lille, Laboratory of Hematology, Lille; ²Hospices Civils de Lyon, Lyon-Sud University Hospital, Department of Hematology, Lyon; ³Univ. Lille, CNRS, Inserm, CHU Lille, Institut de Recherche contre le Cancer de Lille, UMR9020 – UMR-S 1277 - Canther – Cancer Heterogeneity, Plasticity and Resistance to Therapies, Lille; ⁴AP-HP, Saint-Louis Hospital, Department of Hematology, Saint-Louis Research Institute, Université de Paris, Paris; ⁵Gustave Roussy Institute, Department of Hematology, Villejuif; ⁶Toulouse Cancer University Institute, Department of Hematology, Toulouse; ⁷CH Versailles, Department of Hematology, Le Chesnay; ⁸CHU Lille, Department of Clinic Hematology, Lille; ⁹Bordeaux Haut-Lévêque University Hospital, Department of Hematology, Pessac; ¹⁰CHU Limoges, Univ. Limoges, Department of Hematology, Limoges; ¹¹AP-HP, Department of Hematology, Henri Mondor Hospital, Créteil and ¹²Curie Hospital, René Huguenin Hospital, Saint-Cloud, France

Correspondence: NICOLAS DUPLOYEZ
nicolas.duployez@chru-lille.fr

doi:10.3324/haematol.2020.260133

Received: May 20, 2020.

Accepted: November 16, 2020.

Pre-published: December 10, 2020.

Disclosures: no conflicts of interest to disclose.

Contributions: AL, ON, LF, EF, CPr and ND performed the molecular analyses; AL and ON designed the experiments; XT was the principal investigator of the ALFA-0702 trial; KCL ensured data management; XT, NB, SdB, ER, CR, JL, CB, AP, RI, PT, CPr, JV and HD provided samples and clinical data. AL and ND wrote the manuscript which was approved by all the authors.

Acknowledgments: the authors thank all Acute Leukemia French Association (ALFA) investigators and French Innovative Leukemia Organization (FILO) investigators who participated in the ALFA-0702 trial. The authors also thank Christophe Roumier and the tumor bank of Lille University Hospital (certification NF 96900-2014/65453-1) for handling, conditioning, and storing patients' samples. The work of all clinical research assistants is also acknowledged here.

References

- Döhner H, Estey E, Grimwade D, et al. Diagnosis and management of AML in adults: 2017 ELN recommendations from an international expert panel. *Blood*. 2017;129(4):424-447.
- Paietta E. Minimal residual disease in acute myeloid leukemia: coming of age. *Hematology Am Soc Hematol Educ Program*. 2012;2012:35-42.
- Schuurhuis GJ, Heuser M, Freeman S, et al. Minimal/measurable residual disease in AML: a consensus document from the European LeukemiaNet MRD Working Party. *Blood*. 2018;131(12):1275-1291.
- Grimwade D, Jovanovic JV, Hills RK, et al. Prospective minimal residual disease monitoring to predict relapse of acute promyelocytic leukemia and to direct pre-emptive arsenic trioxide therapy. *J Clin Oncol*. 2009;27(22):3650-3658.
- Jourdan E, Boissel N, Chevret S, et al. Prospective evaluation of gene mutations and minimal residual disease in patients with core binding factor acute myeloid leukemia. *Blood*. 2013;121(12):2213-2223.
- Balsat M, Renneville A, Thomas X, et al. Postinduction minimal residual disease predicts outcome and benefit from allogeneic stem cell transplantation in acute myeloid leukemia with *NPM1* mutation: a study by the Acute Leukemia French Association Group. *J Clin Oncol*. 2017;35(2):185-193.
- Svec D, Tichopad A, Novosadova V, Pfaffl MW, Kubista M. How good is a PCR efficiency estimate: recommendations for precise and robust qPCR efficiency assessments. *Biomol Detect Quantif*. 2015; 3:9-16.
- Palini B, Nicoletti I, Martelli MF, Mecucci C. Acute myeloid leukemia carrying cytoplasmic/mutated nucleophosmin (NPMc+ AML): biological and clinical features. *Blood*. 2007;109(3):874-885.
- Palini B, Mecucci C, Tacci E, et al. Cytoplasmic nucleophosmin in acute myelogenous leukemia with a normal karyotype. *N Engl J Med*. 2005;352(3):254-266.
- Alpermann T, Schnittger S, Eder C, et al. Molecular subtypes of *NPM1* mutations have different clinical profiles, specific patterns of accompanying molecular mutations and varying outcomes in intermediate risk acute myeloid leukemia. *Haematologica*. 2016;101(2): e55-e58.
- Gorelio P, Cazzaniga G, Alberti F, et al. Quantitative assessment of minimal residual disease in acute myeloid leukemia carrying nucleophosmin (NPM1) gene mutations. *Leukemia*. 2006;20(6):1103-1108.
- Ivey A, Hills RK, Simpson MA, et al. Assessment of minimal residual disease in standard-risk AML. *N Engl J Med*. 2016;374(5):422-433.
- Thomas X, de Botton S, Chevret S, et al. Randomized phase II study of clofarabine-based consolidation for younger adults with acute myeloid leukemia in first remission. *J Clin Oncol*. 2017;35(11):1223-1230.
- Koh Y, Park J, Bae E-K, et al. Non-A type nucleophosmin 1 gene mutation predicts poor clinical outcome in de novo adult acute myeloid leukemia: differential clinical importance of *NPM1* mutation according to subtype. *Int J Hematol*. 2009;90(1):1-5.
- Cilloni D, Petiti J, Rosso V, et al. Digital PCR in myeloid malignancies: ready to replace quantitative PCR? *Int J Mol Sci*. 2019; 20(9):2249.

Genome wide association study of silent cerebral infarction in sickle cell disease (HbSS and HbSC)

Silent cerebral infarcts (SCI) are common in patients with sickle cell disease (SCD). Up to 35% of children with HbSS will have an SCI by the age of 15 years, and this prevalence has been shown to increase linearly with age.¹ The exact nature of SCI is unknown, although they are probably small regions of ischemic damage detectable on magnetic resonance imaging (MRI). By definition, they do not cause overt neurological deficit. They have, however, been demonstrated to predict a lower intelligence quotient (IQ) and also carry a higher risk of large vessel territory ischemic stroke.² Established risk factors for SCI in patients with hemoglobin (Hb) SS include a lower baseline Hb, male sex and relative hypertension,³ but there is no consensus on the effect of HbF levels.³⁻⁶ Less is known about SCI in those with HbSC genotype, however, the prevalence in children has been reported at between 5.8-13.5%.^{7,8} We performed a retrospective analysis of 333 patients with HbSS and 76 patients with HbSC. We found SCI occurred far younger in HbSS, with a hazard ratio of 3.01 against HbSC for SCI, however, the prevalence of SCI in our HbSC cohort was unexpectedly high at 55%. We also showed that α thalassemia (AT) and female sex offered protection against SCI in patients with HbSS, but not HbSC. Additionally, we found no influence of glucose-6-phosphate dehydrogenase (G6PD) deficiency on SCI, and no influence of measured HbF levels, or genetic loci known to influence HbF levels, on SCI outcomes.

Patient data came from the South East London sickle gene bank (London, UK). Written informed consent was obtained through three approved study protocols (LREC 01-083, 07/H0606/165, and 12/LO/1610) and research conducted in accordance with the Helsinki Declaration (1975, as revised 2008). Genotyping data were established for 15 million variants using the Illumina Infinium MEGA chip and imputation using 1,000genome phase 3 data on the Michigan imputation server as described previously.⁹ AT was determined using single tube multiplex polymerase chain reaction (PCR) according to previously published methods.⁹ Clinical notes and neuroimaging results from the year 2000 onwards were reviewed for all patients. Evidence of SCI were determined by MRI using the accepted neuroradiological criteria³ and confirmed to have no correlating overt clinical event in the clinical notes. The age at which the first radiological evidence that an SCI had occurred was recorded. Controls were determined by MRI confirming the absence of any white matter hyperintensities. The age was defined by the most recent neuroimaging scan confirming this absence. Kaplan-Meier plots and Cox-proportionate hazard (coxPH) ratios were calculated in R 3.6.1. Linear mixed modeling was performed using genome-wide complex trait analysis (GCTA), with a genetic relatedness matrix to account for population structure. Age, sex, sickle genotype and AT were used as covariates. The threshold for genome wide statistical significance was set at 5×10^{-8} .

The cohort consisted of 333 patients with HbSS and 76 with HbSC genotypes. The average age was 35.8 years (yrs) (range, 11.4-78.1 yrs) in the HbSS cohort and 52.3 yrs (range, 17.6-84.2 yrs) in the HbSC cohort. Heterozygous AT ($\alpha\alpha/\alpha^{\beta\gamma}$) was detected in 130 (32%) of the total cohort, and homozygous AT ($\alpha^{\beta\gamma}/\alpha^{\beta\gamma}$) in 21 (5%). The prevalence of SCI in those with HbSC was equivalent to that seen in the SCA cohort (53.4% vs. 55%), although, as demonstrated in Figure 1A, these

Table 1. Results from linear mixed modelling on the influence of candidate variants reported to associate with silent cerebral infarcts (SCI) and variants known to significantly influence clinical HbF levels on SCI outcomes in all patients with sickle cell disease, and in those with HbSS genotype.

Gene	RS id	All patients	HbSS only
VCAMI	rs1041163	OR=1.08, $P=0.675$	OR=1.19, $P=0.413$
ADAMTS10	rs4275799	OR=0.91, $P=0.563$	OR=0.89, $P=0.511$
NOMI	rs887614	OR=0.99, $P=0.944$	OR=1.02, $P=0.919$
FRMD4A	rs3750882	OR=1.12, $P=0.456$	OR=1.07, $P=0.705$
CACNB2	rs2357790	OR=0.79, $P=0.081$	OR=0.76, $P=0.073$
BCL11a	rs6545816	OR=1.1, $P=0.529$	OR=1.04, $P=0.791$
BCL11a	rs1427407	OR=0.8, $P=0.159$	OR=0.85, $P=0.374$
BCL11a	rs11886868	OR=0.83, $P=0.215$	OR=0.89, $P=0.508$
HBS1L-MYB	rs9376090	OR=1.88, $P=0.347$	OR=2.31, $P=0.275$
HBS1L-MYB	rs66650371	OR=0.87, $P=0.674$	OR=0.89, $P=0.755$
HMIP	rs9399137	OR=0.87, $P=0.674$	OR=0.89, $P=0.755$
HMIP	rs9389269	OR=1.14, $P=0.714$	OR=1.18, $P=0.664$
HMIP	rs9402686	OR=1.2, $P=0.592$	OR=1.25, $P=0.549$
HMIP2b	rs9494142	OR=0.91, $P=0.684$	OR=0.91, $P=0.722$
HMIP2b	rs9494145	OR=1.01, $P=0.98$	OR=1.22, $P=0.593$
g(HbF)		OR=1.36, $P=0.466$	OR=1.08, $P=0.487$

RS id: reference single nucleotide polymorphisms identity; HbSS: hemoglobin SS; OR: overall response.

occurred at a much later age (average age 50.6 yrs vs. 25.7 yrs). CoxPH ratios showed a hazard ratio (HR) of 3.01 for SCI in patients with HbSS than those with HbSC.

Our cohort had a slight excess of females (245) to males (164). The Kaplan-Meier plots (Figure 1B) and coxPH ratios demonstrate that males carried a higher risk for SCI (HR=1.54, 95% Confidence Interval [CI]: 1.18-2.03, $P=0.0016$). Considering the two sickle genotypes individually, shown in Figure 2A and B, we found this to only be a risk factor in patients with HbSS (HR=1.86, 95%CI: 1.24-2.8, $P=0.002$), but not in those with HbSC (HR=0.77, 95%CI: 0.38-1.6, $P=0.465$). G6PD assay results were available for 321 of our cohort, including 36 with G6PD deficiency. Adding this as a covariate did not improve the model, and G6PD deficiency was not a statistically significant variable (HR=1.11, 95%CI: 0.67-1.8, $P=0.69$). We further tested this in just the male subgroup and reached the same conclusion.

AT is a known protective factor with respect to large vessel cerebrovasculopathy in SCD, however, its effect on SCI was not known. We report an overall protective influence (HR=0.77, 95%CI: 0.6-0.99, $P=0.038$) on SCI occurrence. Again, we found that this influence was only seen in those with HbSS (HR=0.74, 95%CI: 0.56-0.96, $P=0.026$), but not those with HbSC (HR=0.91, 95%CI: 0.50-1.7, $P=0.774$).

We also considered clinical measurements of HbF%. Methods of collection are detailed in a separate study.¹⁰ Three hundred fifty-nine patients had validated HbF measurements. The average HbF% in the HbSS cohort was 7.2% (n=292), and 1.9% (n=67) in those with HbSC. We found no association between HbF% and SCI outcomes, after adjusting for age, sex, and sickle genotype (overall response [OR]=0.80, 95%CI: 0.51-1.09, $P=0.126$).

We used our variant dataset to perform genome wide analysis on this patient cohort, using age at defined outcome, sex, sickle genotype and AT as covariates. We also included a genetic relatedness matrix to control for pop-

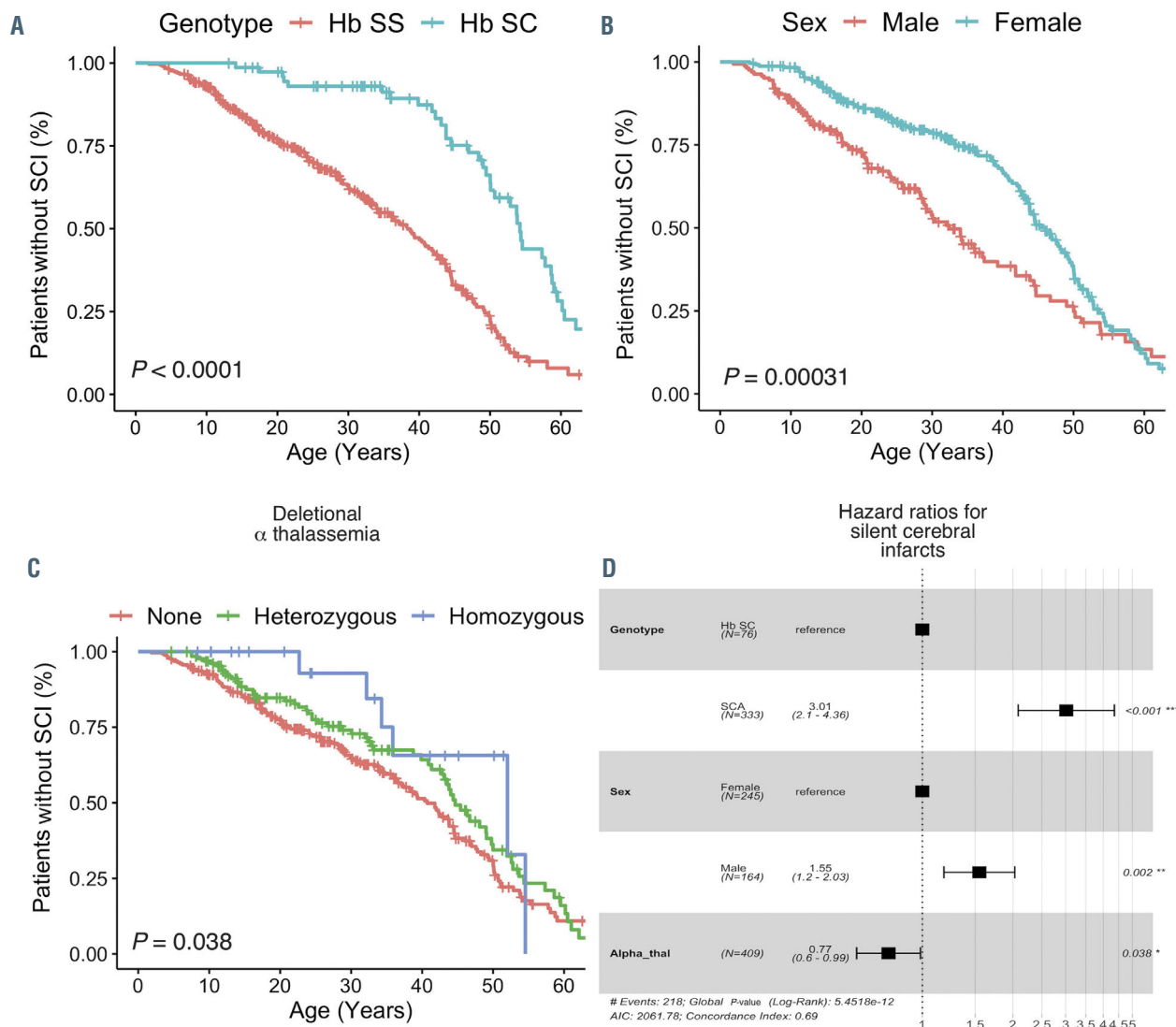


Figure 1. Survival analysis of factors affecting silent cerebral infarcts events in patients with sickle cell disease. (A) Kaplan-Meier plot comparing outcomes in hemoglobin (Hb) SS and HbSC genotypes. (B) Kaplan-Meier plot comparing outcomes in males and females. (C) Kaplan-Meier plots comparing outcomes with no α thalassaeemia (AT), heterozygous and homozygous deletional AT. (D) Forest plot of Cox-proportionate hazard ratios for the three factors affecting silent cerebral infarcts outcomes in patients with sickle cell disease.

ulation substructure and cryptic relatedness. The discovery cohort included 403 patients with full phenotype and covariate datasets. The λ_{GC} (0.986) and QQ plot (*Online Supplementary Figure S1A*) showed no evidence of genomic inflation. The Manhattan plot (*Online Supplementary Figure S1B*) did not show any variants approaching the threshold of statistical significance. The top five variant loci from the analysis are shown in the *Online Supplementary Table S1*. We used the summary statistics generated by this analysis to interrogate the association of five variants previously reported to affect SCI outcomes.¹¹⁻¹⁵ Additionally, we looked at the variants known to strongly influence HbF levels in sickle cell populations.¹⁴ No variants demonstrated an association with SCI at a nominal significance of $P < 0.05$ (Table 1). Additionally, we evaluated the HbF genetic prediction score, $g(HbF)$, which combines four markers to form a composite score of the genetic influence on HbF levels.¹⁰ This again did not show an association with SCI outcomes. We also confirmed all these negative findings in the HbSS cohort alone.

In this study, we have reviewed prevalence rates of SCI in patients with sickle cell disease and considered genetic risk factors that may influence their occurrence. We found the SCI prevalence in the HbSS cohort similar to that reported previously,¹ but additionally, report that the HbSC patients have a notably high prevalence, albeit at an older age. These data add to the rates reported in childhood studies^{7,8} and suggests that as with HbSS, there is a linear increase in prevalence with age. Moreover, although our HbSC cohort is small in size, our analysis suggests the risk factors are different to those in HbSS. We were unable to explore whether older age risk factors such as diabetes mellitus or hypertension were contributing to SCI risk in this older cohort.

We report, for the first time, the protective effect of AT against the development of SCI in patients with HbSS. A previous study failed to find an association, although this was a smaller study with less well defined neuroradiological criteria.¹⁵ This protective effect may be related to the higher steady state Hb levels associated with AT, which has previously been shown to confer a 2-fold protective

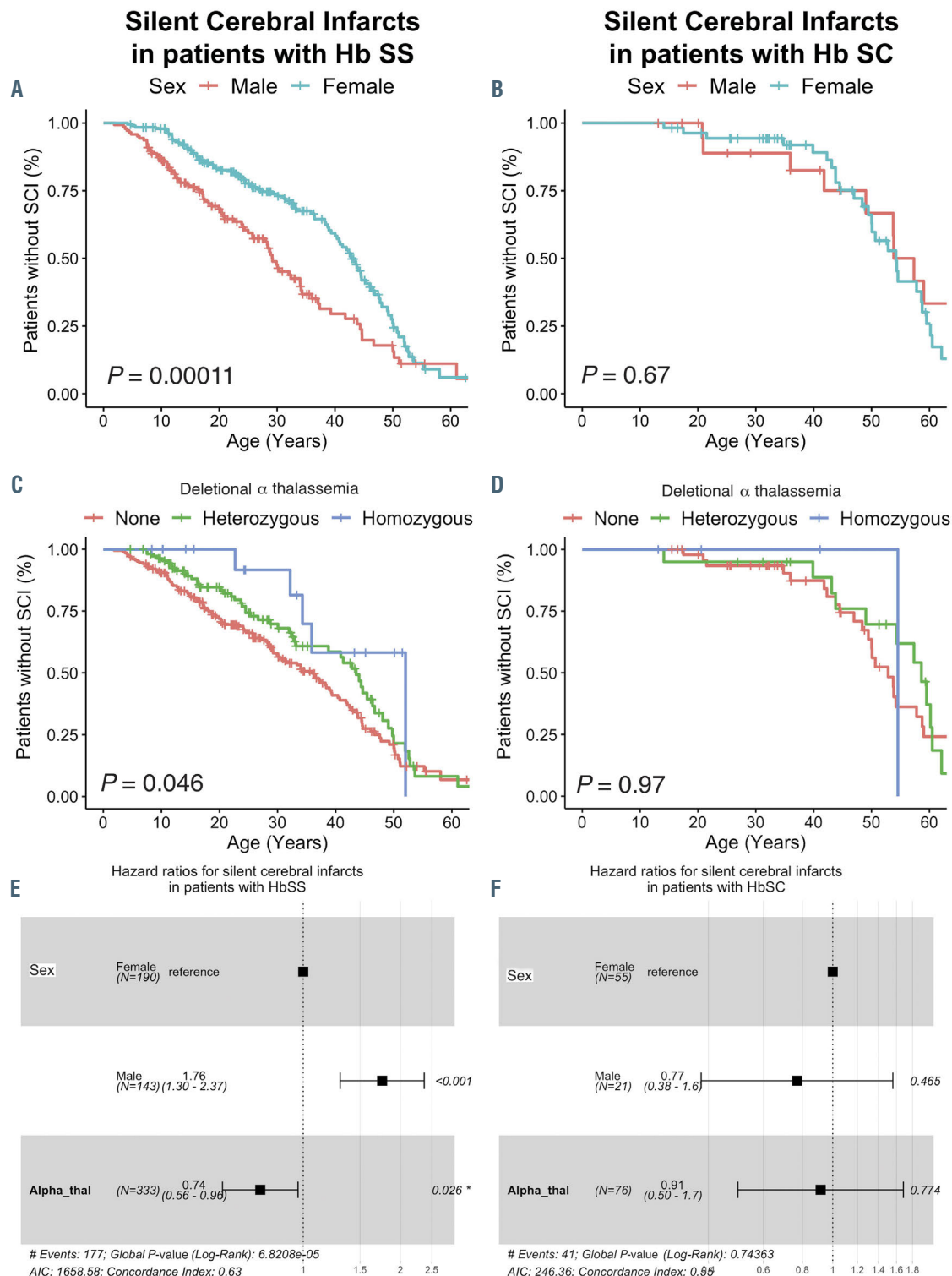


Figure 2. Survival analysis of factors effecting silent cerebral infarcts events in patients with HbSS and HbSC disease separately. (A) Kaplan-meier plot comparing outcomes in males and females in hemoglobin (Hb) SS. (B) Kaplan-meier plot comparing outcomes in males and females in HbSC. (C) Kaplan-meier plot comparing outcomes with no α thalassaemia (AT), heterozygous and homozygous of deletional α in patients with HbSS. (D) Kaplan-meier plot comparing outcomes with no AT, heterozygous and homozygous of deletional α in patients with HbSS. (E) Forest plot of the Cox-proportionate hazard ratios of the factors affecting silent cerebral infarcts (SCI) outcomes in patients with HbSS. (F) Forest plot of the Cox-proportionate hazard ratios of the factors affecting silent cerebral infarcts outcomes in patients with HbSC.

effect (<76 g/L vs. >86 g/L).³ However, there may also be an additional rheological benefit in the form of improved red blood cell deformability and reduced hemolysis reducing microinfarcts. Unfortunately, we did not have sufficient data on baseline Hb levels in this cohort to assess the interaction of AT and Hb on SCI.

Our study had some important negative findings. Some studies have found low HbF levels to be a risk factor⁴⁻⁶ for SCI, whereas others have not.^{3,15} In our cohort, we did not see any association of HbF% with SCI outcomes. We also did not see an association with the genetic modulators of HbF, nor the composite g(HbF) prediction score,¹⁰ suggesting genetic variation of HbF levels in our population of predominantly west African and Caribbean patients does not determine the risk of SCI. However, we did not consider the possible confounding influence of concurrent large vessel vasculopathy on SCI, which has been suggested to represent an alternative pathogenic mechanism of SCI.⁴ Additionally, although we confirmed the increased risk with male sex previously reported,³ we did not find any association of the X-linked condition G6PD deficiency. We also did not find a correlation with candidate variants previously identified. Finally, our own genome wide analysis also did not generate novel candidates, although it is possible that genetic associations might be found by larger studies.

In summary, our key findings are that co-inheritance of AT and female sex, but not elevated HbF%, provide protection against development of SCI in patients with HbSS. SCI are common and under recognised in patients with HbSC, and further studies are needed to better understand the prevalence rates and risk factors in this condition.

John N. Brewin,^{1,2} Helen Rooks,¹ Kate Gardner,^{1,3} Harry Senior,¹ Mrinmayi Morje,¹ Hamel Patel,¹ David Calvet,⁴ Pablo Bartolucci,⁴ Swee-Lay Thein,⁵ Stephan Menzel^{1#} and David C. Rees^{1,2#}

¹Kings College London, UK; ²Kings College Hospital, London, UK; ³Guys and St Thomas Hospital, London, UK; ⁴Henri Mondor Hospital, Paris, France and ⁵NIH, Bethesda, USA

[#]SM and DCR contributed equally as co-senior authors.

Correspondence:

JOHN BREWIN - john.brewin@kcl.ac.uk

doi:10.3324/haematol.2020.265827

Received: July 3, 2020.

Accepted: December 11, 2020.

Pre-published: December 23, 2020.

Disclosures: no conflicts of interest to disclose.

Contributions: JB, SM and DR designed the study; JB, HR, HS, MM, KG, SLT, PB and DC recruited patients and performed research; JB analyzed the data and wrote the manuscript. All authors reviewed and approved the manuscript prior to submission

References

1. Kassim AA, Pruthi S, Day M, Rodeghier M, et al. Silent cerebral infarcts and cerebral aneurysms are prevalent in adults with sickle cell anemia. *Blood*. 2016;127(16):2038-2040.
2. DeBaun MR, Kirkham FJ. Central nervous system complications and management in sickle cell disease. *Blood*. 2016;127(7):829-838.
3. DeBaun MR, Sarnaik SA, Rodeghier MJ, et al. Associated risk factors for silent cerebral infarcts in sickle cell anemia: low baseline hemoglobin, sex, and relative high systolic blood pressure. *Blood*. 2012;119(16):3684-3690.
4. Calvet D, Tuilier T, Mele N, et al. Low fetal hemoglobin percentage is associated with silent brain lesions in adults with homozygous sickle cell disease. *Blood Adv*. 2017;1(26):2503-2509.
5. Tewari S, Renney G, Brewin J, et al. Proteomic analysis of plasma from children with sickle cell anemia and silent cerebral infarction. *Haematologica*. 2018;103(7):1136-1142.
6. van der Land V, Mutsaerts HJ, Engelen M, et al. Risk factor analysis of cerebral white matter hyperintensities in children with sickle cell disease. *Br J Haematol*. 2016;172(2):274-284.
7. Guilliams P, Fields E, Hulbert L. Higher-than-expected prevalence of silent cerebral infarcts in children with hemoglobin SC disease. *Blood*. 2015;125(2):416.
8. Pegelow H, Macklin A, Moser G, et al. Longitudinal changes in brain magnetic resonance imaging findings in children with sickle cell disease. *Blood*. 2002;99(8):3014.
9. Brewin JN, Smith A, Cook R, et al. Genetic analysis of patients with sickle cell anemia and stroke before 4 years of age suggest an important role for APOE. *Circ Genom Precis Med*. 2020;13(5):531-540.
10. Gardner K, Fulford T, Silver N, et al. g(HbF): a genetic model of fetal hemoglobin in sickle cell disease. *Blood Adv*. 2018;2(3):235-239.
11. Bhatnagar P, Arking DE, Casella EB, Casella JF. Genome-wide association for silent cerebral infarction (SCI) in sickle cell disease: The silent infarct transfusion trial (SIT) cohort. *Blood*. 2009;114(22):3563.
12. Bhatnagar P, Barron-Casella E, Bean CJ, et al. Genome-wide meta-analysis of systolic blood pressure in children with sickle cell disease. *PLoS One*. 2013;8(9):e74193.
13. Hoppe C, Klitz W, Cheng S, et al. Gene interactions and stroke risk in children with sickle cell anemia. *Blood*. 2004;103(6):2391.
14. Thein SL, Menzel S. Discovering the genetics underlying foetal haemoglobin production in adults. *Br J Haematol*. 2009;145(4):455-467.
15. Kinney TR, Sleeper LA, Wang WC, et al. Silent cerebral infarcts in sickle cell anemia: a risk factor analysis. The Cooperative Study of Sickle Cell Disease. *Pediatrics*. 1999;103(3):640.

MK2 is a therapeutic target for high-risk multiple myeloma

Multiple myeloma (MM) is an incurable plasma cell malignancy characterized by heterogeneous genetic diversity. Although the development of proteasome inhibitors and immunomodulatory drugs combined with autologous stem cell transplantation (ASCT) have achieved advanced improvement for MM treatment, the majority of MM patients ultimately relapse.^{1,2} One hypothesis for relapse is the cytogenetic evolution of drug-resistant MM cells and the generation of more aggressively proliferative subclones over the patients' disease course. Recent studies support this hypothesis and demonstrate that the existence of intraclonal heterogeneity in MM and genome of high-risk patients with poor outcome and survival present more changes over the disease course.³ The progression of modern high-throughput genomic and proteomic analytical technique such as gene expression profile (GEP) and whole exome or genome sequencing combined with bioinformatic and bio-statistic approaches has aided the investigation of these MM clinical samples.^{4,5} Based on GEP analysis of sequential MM primary samples during the disease course, characterized by serial cycles of response, remission, and relapse combined with health donor control, our group identified a serial of genes including *NEK2*, *RARA2*, which induce MM proliferation and drug-resistance resulting in MM relapse and poor outcome.⁶

MAPKAPK2 (MK2), a major substrate of p38, is regulated through direct phosphorylation by p38 MAP kinase, and participates in many cellular processes such as stress and inflammatory responses, cell proliferation and gene expression regulation.^{7,8} To date, abnormality of MK2 is associated with a broad range of cancers, including glioblastoma, lung and bladder cancer.⁹ Intriguingly, p38-

MK2-Hsp27 signaling maintains survival of cancer stem cells,¹⁰ which is regarded as an obstacle of MM treatment and the resource for MM relapse in clinics suggesting MK2 is a promising therapeutic target in MM. However, MK2 has received little attention in MM.

In order to explore the role of MK2 in MM, we examined MK2 expression of normal plasma cells (NP) (n=22), monoclonal gammopathy of undetermined significance cells (MGUS) (n=44) and newly diagnosed myeloma patient plasma cells (n=351) using our GEP database collected from the National Institutes of Health Gene Expression Omnibus GSE2658 and the result showed significantly increased MK2 expression in MM cells compared to NP and MGUS cells (*data not shown*).¹¹ Following analysis of array-based comparative genomic hybridization (aCGH) data, GSE4452, collected from 67 MM patients indicated that the *MK2* locus was frequently amplified in MM patient samples relative to normal control (*data not shown*).¹² We further observed elevation of MK2 expression in high-risk MM patients compared to low-risk patients (Figure 1A). The expression of MK2 in the PR (high proliferation) and MS (MMSET translocation) groups, the worst two subgroups in MM patients, was dramatically elevated compared to the other six groups¹³ (Figure 1B). Upon correlation analyses of MK2 with clinical characteristics, MK2 expression performed as an independent factor associated with parameters like C-reactive protein at least 4.0 mg/L ($P<0.05$), chromosomal abnormalities (by G-banding) ($P<0.05$), and magnetic resonance imaging focal bone lesions, at least three lesions, which were acknowledged as a poor diagnosed markers in MM (*data not shown*).

We further tested *MK2* mRNA expression in MM patients from APEX trials which evaluated the response to standard therapies (bortezomib or dexamethasone).¹⁴ A pronounced elevation of average *MK2* expression was observed in the no-response treatment group compared

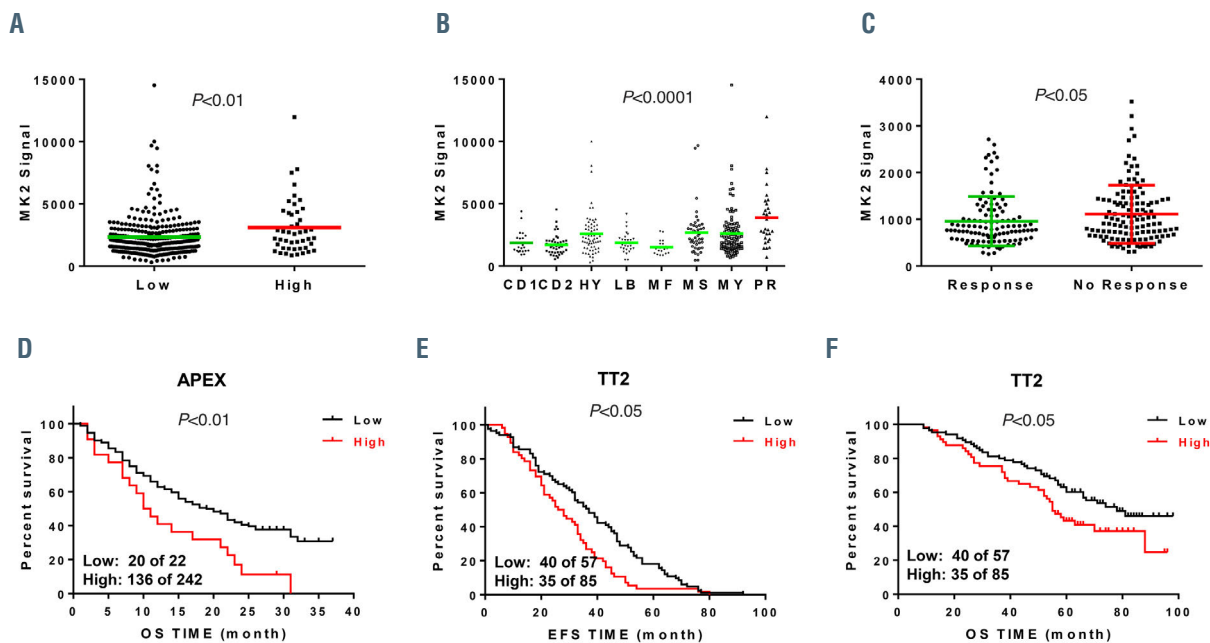


Figure 1. MK2 is a poor prognostic marker or a high-risk gene in multiple myeloma. (A) MK2 expression in the TT2 high and low group based 70-gene model. (B) A box-plot exhibited the average MK2 expression in eight multiple myeloma (MM) subgroups of the TT2 cohort. (C) A box-plot showed MK2 expression in patients categorized by unresponsive (No Response) or responsive (Response) to treatment with dexamethasone and/or bortezomib. (D) Kaplan-Meier analysis on the MM patients' survival in APEX cohort divided by different MK2 expression. (E and F) Kaplan-Meier curve on relapsed MM patients' event free survival (E) and overall survival (F) in the TT2 cohort divided by MK2 expression.

to the response group indicating that MK2 may lead to drug-resistance in MM (Figure 1C). The distinction of MM patients with MK2 was clinically relevant and patients with high-*MK2* expression had poor outcomes in the APEX cohorts (Figure 1D). Since the APEX cohort was comprised with relapsed MM patients, we also examined the patients who eventually relapsed in TT2 cohort. The results demonstrated that MM patients with higher *MK2* expression were associated with poor survival, event free survival and overall survival (Figure 1E and F). These findings from two independent cohorts suggest that increased *MK2* expression may lead to MM drug-resistance and relapse. Herein we propose that *MK2* is a poor prognostic marker or a high-risk gene in MM.

In order to determine if *MK2* plays a role as a high-risk gene in MM rather than a sequential phenomenon, we knocked down *MK2* expression in MM cells using lentiviral single hairpin RNA (shRNA) transfection. We first detected the protein expression levels of MK2 in MM cells by western blot and found that all the nine MM cell lines, XG1, CAG, ARP1, U266, OMP2, H929, MM.1S, 8226 and OCI-MY5, used in this assay ubiquitously expressed MK2 (*data not shown*). Then we down-regulated MK2 expression in ARP1 and OCI-MY5 cells by lentiviral shRNA particles. As shown in Figure 2A, MK2 expression was remarkably knocked-down in *MK2*-shRNA transfected MM cells (KD) compared to the control (Ctrl). In order to expose the effect of MK2 on MM cell growth, KD and Ctrl cells were cultured for 5 days and cell numbers were counted daily. *MK2*-KD MM cells exhibited a significantly lower cell growth rate than the Ctrl cells in both ARP1 and OCI-MY5 cells (Figure 2B), which was also verified by MTT assay (*data not shown*). The growth inhibition effect of *MK2*-shRNA was further confirmed by a clonogenicity assay. As shown in Figure 2C, *MK2*-KD cells generated ample reduction of

colonies relative to corresponding control cells. The decreased growth rate of *MK2*-KD cells was ascribed to increased apoptotic cell death by MK2 inhibition, and flow cytometry showed that Annexin V positive cells significantly increased after *MK2*-shRNA transfection for 48h (Figure 2D). These results suggest MK2 expression is important for MM cell growth *in vitro*.

We further extended our findings to an *in vivo* study and injected both ARP1^{KD} and ARP1^{Ctrl} cells subcutaneously into the opposite side flanks of each NOD scid gamma mouse (NSG) mouse (n=4). Tumor diameters were measured and recorded twice a week to examine the growth rate of the tumor cells. After 4 weeks, the tumors produced by ARP1^{KD} cells were visibly smaller than their corresponding ARP1^{Ctrl} counterparts. The average weight of ARP1^{KD} tumors (0.39 g) was 25% lower than the control tumors (1.55 g; Figure 2E). Time course regression analyses of growth rates exhibited that the ARP1^{KD} tumors volume significantly fell behind the ARP1^{Ctrl} control tumors (Figure 2F). These results indicate that genetic knockdown of *MK2* retards myeloma growth *in vivo*.

Inversely to the knockdown assay, we transfected MM cells with *MK2* CRISPR lentiviral activation particles,¹⁵ and verified success of the transfection by western blot assay which showed a visible elevation of MK2 expression in the lentiviral-transfected (OE) cells compared with control cells (WT) (Figure 3A). The trypan blue cell number counting assay demonstrated that ARP1 and OCI-MY5 *MK2*-OE MM cells presented a higher growth rate than their WT counterpart after 5 days of culture (*data not shown*). Next, a colony formation assay was employed and indicated that regardless of experimental conditions, *MK2*-OE cells generated more colonies than WT cells. Initially, *MK2*-OE cells formed a higher number of colonies than WT cells. In addition, compared with WT cells, the growth capability of *MK2*-OE cells treated

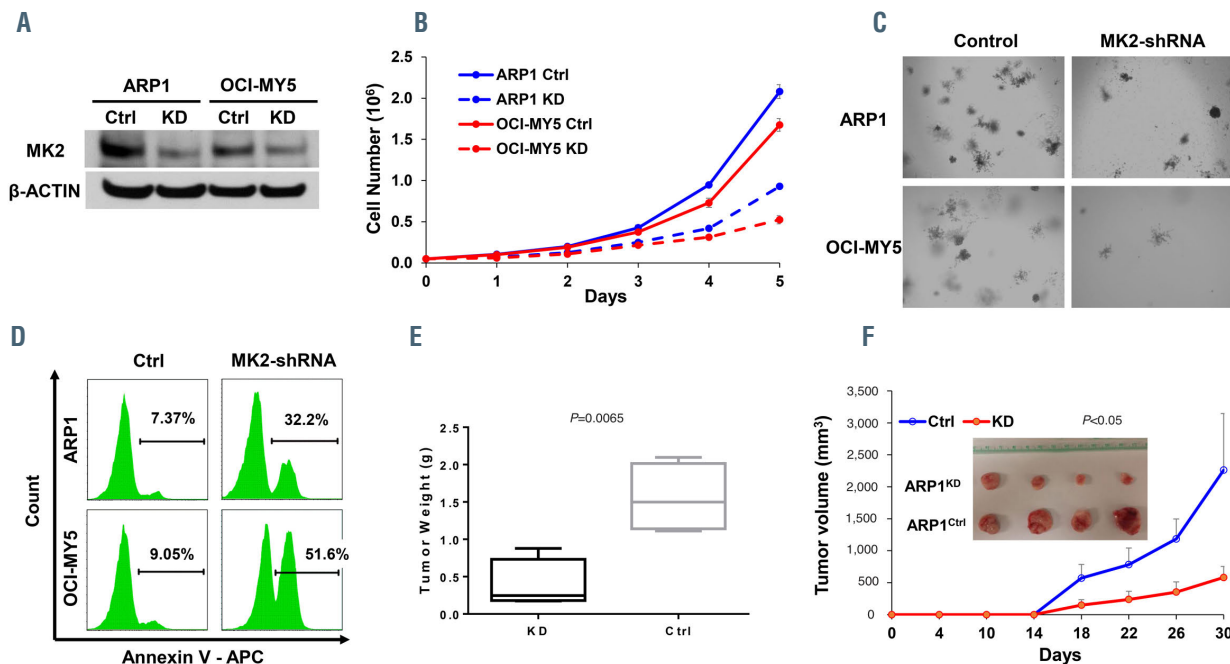


Figure 2. Decreased MK2 expression induces multiple myeloma cellular apoptosis and growth inhibition *in vitro* and *in vivo*. (A) MK2 expression in ARP1 and OCI-MY5 cells was measured by western blot after *MK2*-single hairpin RNA (shRNA) transfection. (B) Cell growth curve was drawn by trypan blue staining after observing ARP1 and OCI-MY5 *MK2*-knockdown (KD) and control (Ctrl) cells for 5 days. (C) Clonogenicity evaluation for the Ctrl and *MK2*-KD ARP1 and OCI-MY5 cells. (D) Flow cytometry for cellular apoptosis marker Annexin V in MM cells after *MK2*-shRNA lentivirus transfection for 48 hours. (E) Mean weight tumors derived from ARP1-Ctrl and ARP1-KD cells on day 30 post injection. (F) Tumor growth time course in NOD/SCID mice xenografted by ARP1-Ctrl and ARP1-KD cells in each flank respectively (n=4).

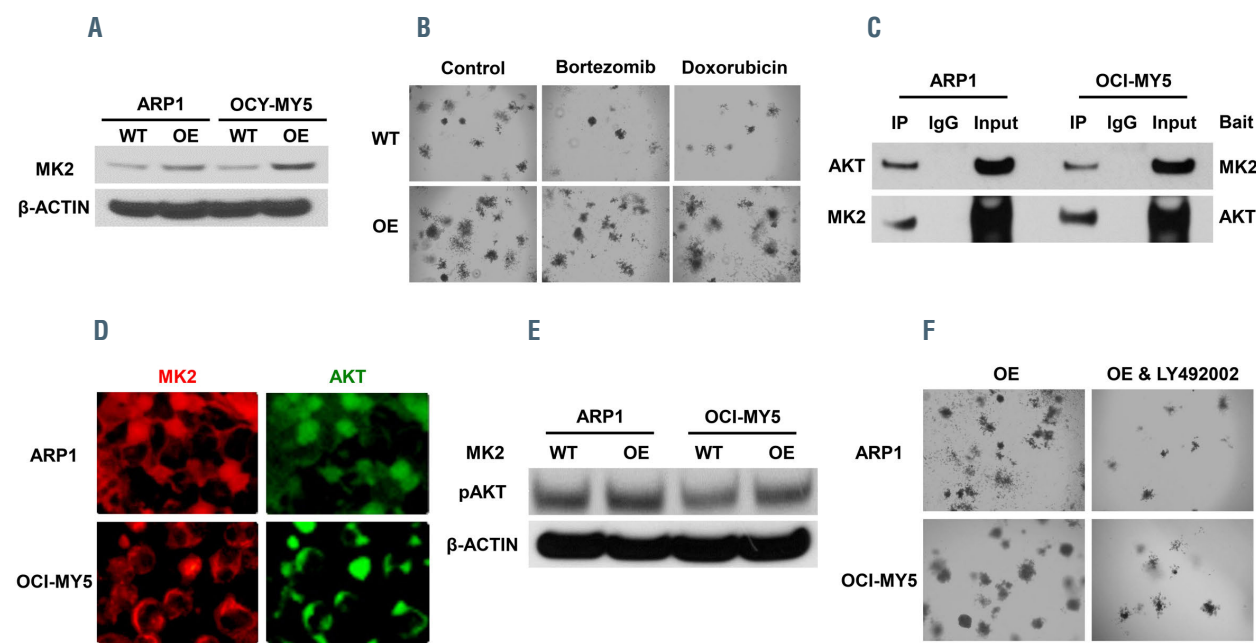


Figure 3. MK2 interacts with AKT to promote multiple myeloma progression. (A) Western blot assay on MK2 expression in ARP1 and OCI-MY5 wild-type (WT) and lentiviral-transfected (OE) cells. (B) Colony formation assay of ARP1 and OCI-MY5 MK2-WT and OE cells treated with or without bortezomib or doxorubicin. (C) Co-immunoprecipitation assay showed that MK2 interacted with AKT in MM cells. (D) Immunofluorescence staining on MK2, AKT and DAPI in ARP1 and OCI-MY5 cells. (E) Western blot assay on pAKT expression in ARP1 and OCI-MY5 MK2-OE cells treated with or without LY29002. (F) Colony formation of ARP1 and OCI-MY5 MK2-OE cells fed by medium in absence or presence of LY29002.

with bortezomib or doxorubicin was more prominent than that of *MK2*-OE cells without treatment (Figure 3B). Flow cytometric detection for Annexin V, a marker of apoptosis, illustrated the same trend, as treatment on cells with bortezomib (8 nM) or doxorubicin (100 nM) induced less death in the “OE” than “WT” samples (data not shown). These results support our proposal that MK2 promotes myeloma progression and drug resistance.

In order to analyze how MK2 mediates MM progression, a co-immunoprecipitation assay was performed to detect the down-stream target of MK2. We found that AKT could be immunoprecipitated by MK2 antibody. On the other hand, MK2 was pulled down using AKT antibody in both ARP1 and OCI-MY5 cells (Figure 3C). Further immunofluorescence study showed that the MK2 signal labeled by red color overlapped with green color representing the AKT signal (Figure 3D) in both ARP1 and OCI-MY5 cells. Both assays proved that MK2 directly bound with AKT in MM cells. As MK2 is a Ser/Thr protein kinase, we investigated whether MK2 could phosphorylate and activate AKT. Western blot results confirmed that pAKT(S473), the activated form of AKT, was up-regulated by MK2 overexpression compared to WT cells suggesting that MK2 phosphorylated AKT (Figure 3E). This interpretation was supported by the specific AKT phosphorylation inhibitor, LY490002, which overcame the MK2 activation induced MM cellular drug-resistance and profoundly suppressed clonogenicity in ARP1 and OCI-MY5 OE cells (Figure 3F). A plausible conclusion is, thus, that MK2 promotes MM progression through directly activating AKT. In addition, we also validated that MK2 inhibitor IV, a selective MK2 inhibitor had an inhibitory effect on MM cells both *in vitro* and in 5TGM1 MM mouse model (data not shown).

In summary, we first evaluated *MK2* expression in MM cells relative to normal control cells, and correlated *MK2* with MM patient outcomes in relapsed MM patients. We

also showed that *MK2* mediated MM cellular growth and drug-resistance. Finally, we disclosed that MK2 regulates MM progression through activating AKT signaling. Our findings indicate that MK2 acts as a novel clinical marker for high-risk myeloma. Targeting MK2 in combination with current therapies may improve effectiveness and long-term patient response to treatment.

Chunyan Gu,^{1,2,3*} Haibo Cheng,^{4,5*} Hongbao Yang,⁶ Yong Bian,⁷ Yaohui Wang,⁸ Yifen Zhang,⁸ Michael Pisano,² Gang Hu^{3#} and Ye Yang^{1,9,10#}

¹The 3rd Affiliated Hospital, Nanjing University of Chinese Medicine, Nanjing, China; ²Department of Pathology, School of Medicine, University of Iowa, Iowa City, IA, USA; ³School of Medicine and Life Sciences, Nanjing University of Chinese Medicine, Nanjing, China; ⁴The First Clinical Medical College, Nanjing University of Chinese Medicine, 210023, Nanjing, China; ⁵Jiangsu Collaborative Innovation Center of Traditional Chinese Medicine Prevention and Treatment of Tumor, Nanjing, China; ⁶Center for New Drug Safety Evaluation and Research, China Pharmaceutical University, Nanjing, China; ⁷Laboratory Animal Center, Nanjing University of Chinese Medicine, Nanjing, China; ⁸Department of Pathology, The First Affiliated Hospital of Nanjing University of Chinese Medicine, Nanjing, China; ⁹Key Laboratory of Acupuncture and Medicine Research of Ministry of Education, Nanjing University of Chinese Medicine, Nanjing, China and ¹⁰Internal Medicine, School of Medicine, University of Iowa, Iowa City, IA, USA.

*YY and GH contributed equally as co-first authors.

#CG and HC contributed equally as co-senior authors.

Correspondence:

YE YANG - yangye876@sina.com

GANG HU - ghu@njutcm.edu.cn

doi:10.3324/haematol.2017.182121

Received: October 7, 2017.

Accepted: March 14, 2018.

Pre-published: March 22, 2018.

Disclosures: no conflicts of interest to disclose.

Contributions: CG, GH and YY designed the project and wrote the manuscript; CG, HC and all other authors performed the experiments and interpreted the data.

Acknowledgments: the authors would like to thank Dr. Siegfried Janz, and Fenghuang Zhan from the University of Iowa for their scientific support.

Funding: this work was supported by National Natural Science Foundation of China 81770220, 81600177, 81670200, 81500166 (to CG & YY); National key research and development program—precision medicine sub-program 2016YFC0905900 (to YY); The 2016 outstanding youth fund of Jiangsu Province BK20160048 (to YY); Natural Science Foundation of Jiangsu Province BK20161041, 16KJB310009 (to CG); The Priority Academic Program Development of Jiangsu Higher Education Institutions for Chinese Medicine.

References

1. Bianchi G, Anderson KC. Understanding biology to tackle the disease: multiple myeloma from bench to bedside, and back. CA Cancer J Clin. 2014;64(6):422-444.
2. Barlogie B, Mitchell A, van Rhee F, Epstein J, Morgan GJ, Crowley J. Curing myeloma at last: defining criteria and providing the evidence. Blood. 2014;124(20):3043-3051.
3. Pawlyn C, Morgan GJ. Evolutionary biology of high-risk multiple myeloma. Nat Rev Cancer. 2017;17(9):543-556.
4. Holohan C, Van Schaeybroeck S, Longley DB, Johnston PG. Cancer drug resistance: an evolving paradigm. Nat Rev Cancer. 2013;13(10):714-726.
5. Bolli N, Biancon G, Moarii M, et al. Analysis of the genomic landscape of multiple myeloma highlights novel prognostic markers and disease subgroups. Leukemia. 2018;32(12):2604-2616.
6. Yang Y, Shi J, Tolomelli G, et al. RARalpha2 expression confers myeloma stem cell features. Blood. 2013;122(8):1437-1447.
7. Herranz N, Gallage S, Mellone M, et al. mTOR regulates MAPKAPK2 translation to control the senescence-associated secretory phenotype. Nat Cell Biol. 2015;17(9):1205-1217.
8. He J, Liu Z, Zheng Y, et al. p38 MAPK in myeloma cells regulates osteoclast and osteoblast activity and induces bone destruction. Cancer Res. 2012;72(24):6393-6402.
9. Li JY, Li RJ, Wang HD. gamma-secretase inhibitor DAPT sensitizes t-AUCB-induced apoptosis of human glioblastoma cells in vitro via blocking the p38 MAPK/MAPKAPK2/Hsp27 pathway. Acta Pharmacol Sin. 2014;35(6):825-831.
10. Lin SP, Lee YT, Wang JY, et al. Survival of cancer stem cells under hypoxia and serum depletion via decrease in PP2A activity and activation of p38-MAPKAPK2-Hsp27. PloS One. 2012;7(11):e49605.
11. Shaughnessy JD, Jr., Zhan F, Burington BE, et al. A validated gene expression model of high-risk multiple myeloma is defined by deregulated expression of genes mapping to chromosome 1. Blood. 2007;109(6):2276-2284.
12. Carrasco DR, Tonon G, Huang Y, et al. High-resolution genomic profiles define distinct clinico-pathogenetic subgroups of multiple myeloma patients. Cancer Cell. 2006;9(4):313-325.
13. Zhan F, Huang Y, Colla S, et al. The molecular classification of multiple myeloma. Blood. 2006;108(6):2020-2028.
14. Mulligan G, Mitsiades C, Bryant B, et al. Gene expression profiling and correlation with outcome in clinical trials of the proteasome inhibitor bortezomib. Blood. 2007;109(3):3177-3188.
15. Konermann S, Brigham MD, Trevino AE, et al. Genome-scale transcriptional activation by an engineered CRISPR-Cas9 complex. Nature. 2015;517(7536):583-588.

Breast dose matters

This high quality meta-analysis by Tromeur *et al.*¹ imparts great additional value to the recent Cochrane review on this topic of the evaluation of pulmonary embolism in pregnancy.² Specifically, it is quite impressive that both computed tomography pulmonary angiography (CTPA) and ventilation-perfusion (VQ) imaging have a pooled negative predictive value of 100% and the pooled rates on non-diagnostic results are comparable in this population.

We however differ regarding the maternal breast radiation exposure. There is an error in referencing Mitchell *et al.*³ in Table 4: the paper does not state the maternal effective doses at all for pregnant patients and the mean breast effective doses are incorrect. Mitchell *et al.*³ were able to reduce the mean breast dose from 7.64 mGy to 3.65 mGy utilizing a reduced 80 kV monitoring scan prior to the diagnostic scan. This paper does not give a dose range, thus approximately 50% of pregnant patients' breast dose was more than 3.65 mGy.³ Low-dose perfusion imaging as described by Tromeur *et al.*¹ utilizes 25% of a conventional perfusion dose, thus imparts 25% of the radiation to the maternal breast, maternal whole body and fetus: 0.16 mGy, 0.47 mGy and 0.02 mGy respectively.⁴ The CTPA maternal breast dose is at least 22 times higher than that of low dose perfusion imaging, and this is not insignificant given the increased breast mitotic rate during pregnancy. It is interesting that the short term breast cancer rate was not increased post CTPA. However, the majority of the CTPA patients were postpartum when the mitotic rate is normal, while the majority of patients who underwent VQ imaging were pregnant when the mitotic rate is increased.^{5,6} Limiting detection, screening has not yet begun for these cohorts.

We agree that the fetal dose of both CTPA and VQ are negligible, but given the at least 22-fold increase in breast dose for CTPA, low-dose perfusion imaging is preferred in the setting of a normal chest radiograph.

Renee M. Moadel,¹ Jean-Ju Sheen,²

Leonard M. Freeman¹ and Linda Broyde-Haramati¹

¹Montefiore Medical Center, Albert Einstein College of Medicine, Department of Radiology and ²Columbia University, Department of Obstetrics and Gynecology, New York, NY, USA.

Correspondence: RENEE M. MOADEL

rmoadel@montefiore.org

doi:10.3324/haematol.2019.219584

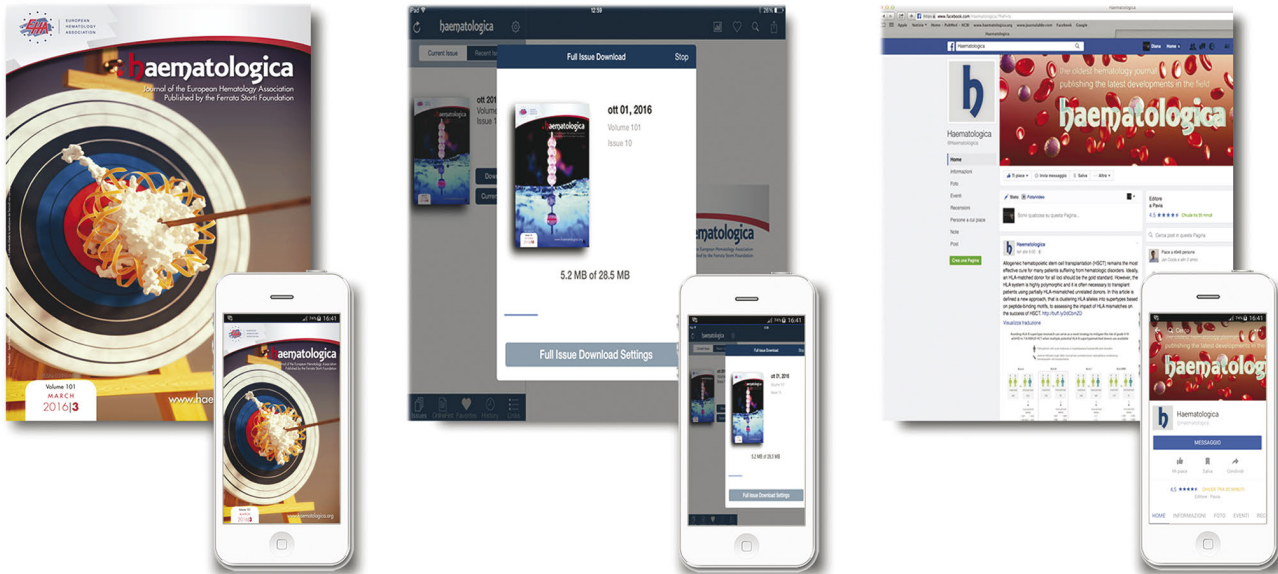
Disclosures: LBH is the spouse of a board member of Kryon, and LMF is on the advisory panel for Jubilant Draximage.

Contributions: all authors contributed to manuscript preparation.

References

1. Tromeur C, van der Pol LM, Le Roux PY, et al. Computed tomography pulmonary angiography versus ventilation-perfusion lung scanning for diagnosing pulmonary embolism during pregnancy: a systematic review and meta-analysis. *Haematologica*. 2019;104(1):176-188.
2. van Mens TE, Scheres LJ, de Jong PG, Leeflang MM, Nijkeuter M, Middeldorp S. Imaging for the exclusion of pulmonary embolism in pregnancy. *Cochrane Database Syst Rev*. 2017;1:CD011053.
3. Mitchell DP, Rowan M, Loughman E, Ridge CA, MacMahon PJ. Contrast monitoring techniques in CT pulmonary angiography: an important and underappreciated contributor to breast dose. *Eur J Radiol*. 2017;86:184-189.
4. Sheen JJ, Haramati LB, Natenzon A, et al. Performance of low-dose perfusion scintigraphy and CT pulmonary angiography for pulmonary embolism in pregnancy. *Chest*. 2018;153(1):152-160.
5. Battersby S, Anderson TJ. Proliferative and secretory activity in the pregnant and lactating human breast. *Virchows Archiv A Pathol Anat Histopathol*. 1988;413(3):189-196.
6. Burton KR, Park AL, Fralick M, Ray JG. Risk of early-onset breast cancer among women exposed to thoracic computed tomography in pregnancy or early postpartum. *J Thromb Haemost*. 2018;16(5):876-885.

RESEARCH, READ & CONNECT



We reach more than
6 hundred thousand readers each year

The first Hematology Journal in Europe

Impressions YTD

14,171,734

Digital Readers

4,908

Total Audience

558,982

Worldwide rank

7th

Impact factor

7.116

Total citations

10,831

 **haematologica**

Journal of the Ferrata Storti Foundation



haematologica – Vol. 106 n. 6 – June 2021 – 1511-1778